
European Seminar

OWEMES 2012
**Offshore wind and other
marine renewable energies
in Mediterranean and European seas**

Rome (Italy)
5-7 September 2012



ARTENERGY
PUBLISHING

10th EXPO
Eolica
MEDITERRANEAN



Italian National Agency for New Technologies,
Energy and Sustainable Economic Development



Proceedings of the European Seminar

OWEMES 2012

OFFSHORE WIND AND OTHER MARINE RENEWABLE ENERGIES
IN MEDITERRANEAN AND EUROPEAN SEAS

Rome - Italy

5-7 September 2012

Edited by Andrea Lazzari and Paola Molinas

(ENEA, Studies and Strategies Central Unit)

2013 ENEA
National Agency for New Technologies, Energy and
Sustainable Economic Development

Lungotevere Thaon di Revel, 76
00196 Roma

ISBN 978-88-8286-283-1



Proceedings of the European Seminar

OWEMES 2012

**OFFSHORE WIND AND OTHER MARINE RENEWABLE ENERGIES
IN MEDITERRANEAN AND EUROPEAN SEAS**

Rome

5-7 September 2012



ORGANIZERS

OWEMES Association
ENEA
ARTENERGY Publishing

SECRETARIAT

OWEMES Association
Via Antonio Serra 62 - 00191 Roma
Tel./Fax: +39 06 45426060

SPONSOR

GSE - GESTORE SERVIZI ENERGETICI

PATRONAGE

ANEV, ANIV, ATENA, CRIACIV, ES, EUROPEAN OCEAN ENERGY
ASSOCIATION,
EU SUSTAINABLE ENERGY CAMPAIGNE, IEA WIND, GWEC,
IEA OCEAN ENERGY SYSTEMS, IET

COLLABORATING ORGANIZATIONS

DIMA - Dpt. of Mech. & Aerospace Engineering, Rome University La Sapienza

STEERING COMMITTEE

Cosimo Caliendo, Min. Trasporti General Director - Italy *
Claudio Borri, CRIACIV Director - Italy
Bruno della Loggia, ATENA President - Italy
Luigi Fiorini, IET Italia - United Kingdom
Vittorio Gusella, ANIV President - Italy
Holttinen Hannele, IEA Wind - Finland
John Huckerby, IEA Ocean Chairman - New Zealand
Gerardo Montanino, GSE Director - Italy
Enzo Titone, REM Director - Italy
Simone Togni, ANEV President - Italy
Carlo Tricoli, ENEA - Italy
Giovanbattista Zorzoli, ISES Italia President - Italy
(* to be confirmed)

ORGANIZING COMMITTEE

A. Arena, ENEA
M. Bassetti, DIMA Univ. La Sapienza
S. Battistoni, ISES Italia
P. Carretta, ATENA Roma
D. De Leo, Art Energy Publishing
C. Del Bufalo, ENEA
F. Fontana, ENEA
G. Gaudiosi, OWEMES
L. Imperato, OWEMES
C. Padiglione, OWEMES
L. Pirazzi, ANEV
G. Riccucci, DIMA Univ. La Sapienza

TECHNICAL COMMITTEE

G. Arsuffi, ENEA - Italy
R. Barthelmie, Indiana Univ. - USA
C. Borri, CRIACIV - Italy
M. Burlando, Genoa Univ. - Italy
C. Casale, RSE - Italy
F. Cesari, Bologna Univ. - Italy
A. Corsini, Rome Univ. La Sapienza - Italy
G. Dalen, WPD - Sweden
A. Estanquerio LNEG - Portugal
A. Fiorentino, IEA-OES - Italy
M. Fiorini, IET Italia - Italy
G. Gaudiosi, OWEMES Association - Italy
S. George, EU-EOA - Belgium
A. Henderson, DONG Energy - United Kingdom
L. Imperato, Studio Rinnovabili - Italy
A. Lazzari, ENEA - Italy
C. Nath, GL-Group - Germany
F. Rispoli, Rome Univ. La Sapienza - Italy
F. Salvatore, INSEAN - Italy
G. Sannino, ENEA - Italy
F. Vorpahl, IWES Fraunhofer - Germany

Index of contents

Session 1: Wind Energy Resources	12
Chairmen: L. Imperato, M. Burlando	
<i>The Estimation of wind, wave and ocean current resources in the Mediterranean Sea for energy converters site selection</i> - N. Pinardi (CIRSA - Bologna Univ. (IT)), L. Torrisi, M. Ferri (CNMCA- Pratica di Mare, Rome (IT)), R. Archetti, A. Lamberti (DICAM - Bologna Univ. (IT)), M. Zavaratelli (CIRSA - Bologna Univ. (IT)), G. Coppini, M. Adani (INGV - Bologna Univ. (IT))	13
<i>Mediterranean Inshore Wind Resources: combining MCPs and CFD for marine resources quantification</i> - R.N. Farrugia, T. Sant (Institute for Sustainable Energy, Univ. of Malta, Triq il-Barrakki, Marsaxlokk (MT) and Department of Mechanical Engineering, Univ. of Malta, Msida (MT))	14
<i>Validation of an offshore wind atlas using the satellite data available at the coastal regions of Portugal</i> - R. Marujo, P. Costa, M. Fernandes, T. Simões, A. Estanqueiro (LNEG - Laboratório Nacional de Energia e Geologia, Lisboa (PT))	27
<i>The “Wind and Ports” Project for wind energy assessment and forecast: the case of the Port of Genoa</i> - M. Burlando, M. Tizzi, S. Navone, G. Solari (Dpt. of Civil, Environ. & Architect. Engineering, Genoa Univ. (IT)), G. Canepa (Port Authority of Genoa (IT))	36
Session 2: Marine Resource Simulation, Modelling	50
Chairmen: F. Cesari, A. Estanqueiro	
<i>An experimental test rig to simulate hydrodynamic forcing on floating offshore wind turbine platforms</i> - I. Bayaty, M. Belloli (Dpt. di Meccanica, Politecnico di Milano, Milan (IT)), S. Giappino (CIRIVE, Politecnico di Milano, Milan (IT))	51
<i>Italian Wind Atlas WebGIS and Technical-Economic Calculation Module</i> - L. Serri, D. Airoidi, C. Casale, E. Lembo, G. Stella (RSE Spa., Milan (IT))	61
<i>Using data assimilation in mesoscale numerical modeling to map offshore wind resource</i> - M. Fernandes, P. Costa, T. Simões, A. Estanqueiro (LNEG-Laboratório Nacional de Energia e Geologia, Lisboa (PT))	73
<i>Wave energy potential in the Mediterranean: the case of Pantelleria</i> - L. Liberti (ISPRA-Institute for Environmental Protection and Research, Rome (IT)), A. Carillo, G. Sannino (ENEA - Ocean Modelling Unit, Rome (IT))	81

Session 3: Wind Turbines Innovation	95
Chairmen: F. Vorpahl, G. Arsuffi	
<i>TPWind and European projects in offshore wind sector</i> - Manuela Conconi (European Wind Energy Association)	96
<i>An investigation of different offshore wind turbine jacket support foundation models designed for Central Mediterranean deep waters</i> - T. Gauci, T. Sant, M. Muscat, P. Mollicone, D. Camillieri (Dept. Mechanical Engineering, Univ. of Malta, Msida (MT))	116
<i>Design of a spar buoy for Offshore Wind turbines</i> - C. Romanò, E. Giorcelli, G. Mattiazzo, M. Raffero (DIMEAS - Dpt. Ingegneria Meccanica e Aerospaziale - Politecnico di Torino, Turin (IT))	129
<i>RAVE - Joint research at Germany's first offshore Wind Park Alpha Ventus</i> - E. Otto, M. Durstewitz, B. Lange, S. Pfaffel (Fraunhofer Institute for Wind Energy and Energy System Technology, Kassel (DE))	144
<i>Turbine foundation in intermediate waters: monopile versus jacket</i> - F.G. Cesari, F. Taraborrelli (DIENCA Dept., Bologna Univ. (IT)), T. Balestra (Tecon s.r.l., Assago-Milan (IT)), L. Milella (TRE SpA, Bari (IT))	158
Session 4: Turbines Dynamics, Access, Challenges	173
Chairmen: A. Henderson, G. Dalen	
<i>Impact of weather conditions on the windows of opportunity for operation of offshore wind farms in Portugal</i> - N. Silva, T. Simões, P. Costa, A. Estanqueiro (NLEG National Laboratory of Energy and Geology - Solar, Wind and Ocean Energy Unit, Lisboa (PT))	174
<i>Offshore challenges & Siemens solutions: learning from experience</i> - A.H. Woltmeijer (Siemens Energy Inc., Vejle (DK))	184
<i>Effects of fully nonlinear irregular wave forcing on the dynamic response of offshore wind turbine</i> - E. Marino, C. Borri (CRIACIV, Dept. Of Civil and Environmental Engineering, Florence Univ. (IT)), C. Lugni (CNR-INSEAN, Rome (IT))	199
Session 5: Wave Energy Resources	209
Chairmen: G. Sannino, A. Estanqueiro	
<i>Offshore Renewable Resources in the Mediterranean Area: the results of the ORECCA Project</i> - D. Airoidi, L. Serri, G. Stella (RSE Spa, Milan (IT))	210
<i>Wave energy exploitation in Italian seas: a feasibility study</i> - S. Bozzi (Dip. Di Bioingegneria, Politecnico di Milano, Milan (IT)), R. Archetti (DICAM, Bologna Univ. (IT)), G. Passoni (DIAR, Politecnico di Milano, Milan (IT))	221
<i>Extreme waves in the Central Mediterranean Sea for design of offshore wind farms and wave energy devices</i> - F. Arena, A. Carillo (ENEA - Ocean Modelling Unit, Rome (IT)), V. Laface, G. Malara, A. Romolo (Mediterranea University, NOEL Laboratory, School of Engineering, Reggio Calabria (IT)), G. Sannino (ENEA - Ocean Modelling Unit, Rome (IT))	230

Session 6: Wave Potential and Technology **244**

Chairmen: A. Corsini, F. Rispoli

Engineering design study of an innovative Hydrokinetic Turbine with on shore foundation **245**
- M. Amelio, S. Barbarelli, G. Florio, N.M. Scornaienchi (Mechanical Engineering Dpt. University of Calabria, Rende (IT)), A. Cutrupi, M. Sanchez-Blanco, G. Lo Zupone (Sintenergy “TechNest” Incubator, University of Calabria, Rende (IT))

Systemic performance of Wells turbines for small scale onshore wave energy converters **260**
- M. Bassetti, A. Corsini, A. Marchegiani, F. Rispoli, E. Tortora, E. Tuccimei (Dpt. of Mech. & Aerospace Engineering, Rome University La Sapienza, Rome (IT))

Roadmapping Ocean Energies for Portugal: a flexible strategy to manage the uncertainties **271**
- C.A. Silva, S. Matias (IDMEC/IST - Institute of Mechanical Engineering, Instituto Superior Técnico, Lisboa (PT)), A. Raventos (WAVEC - Wave Energy Center, Lisboa (PT))

Estimation of the wave energy potential on the offshore Mediterranean Sea and propagation toward a nearshore area **283**
- V. Vannucchi, L. Cappietti (Dip. di Ingegneria Civile e Ambientale - Florence Univ. (IT))

An integrated procedure for the design of a Wells turbine developed for Mediterranean operations **296**
- F. Arena (Mediterranea University, NOEL Laboratory, School of Engineering, Reggio Calabria (IT)), M. Bassetti, A. Corsini, G. Delibra (Dpt. of Mech. & Aerospace Engineering, Rome University La Sapienza, Rome (IT)), G. Faggiolati, S. Piccinini (Faggiolati Pumps S.p.A., Macerata (IT)), F. Rispoli (Dpt. of Mech. & Aerospace Engineering, Rome University La Sapienza, Rome (IT)), G. Romani (Faggiolati Pumps S.p.A., Macerata (IT)), A. Romolo (Mediterranea University, NOEL Laboratory, School of Engineering, Reggio Calabria (IT)), M. Ruggeri (Faggiolati Pumps S.p.A., Macerata (IT)), E. Tuccimei, P. Venturini (Dpt. of Mech. & Aerospace Engineering, Rome University La Sapienza, Rome (IT))

Session 7: Other Marine Renewable Energy and Environment issues **303**

Chairmen: C. Borri, M. Marcelli

Experimental study of the erosion in a sand bed caused by wakes behind tidal energy extraction devices **304**
- F. Fedoul, M. Obregon, J. Ortega-Casanova, R. Fernandez-Feria (Departamento Ingenieria Mecanica y Mecanica de Fluidos, ETS de Ingenieria Industrial, Universidad de Malaga, Málaga (ES))

Aperture Plasmonic Nano-antennas in Solar Energy Harvesting **315**
- D. Ramaccia (Department of Applied Electronics, ‘RomaTre’ University, Rome (IT)), S. Scanu, V. Piermattei (Laboratory of Experimental Oceanology and Marine Ecology, University of Tuscia, Civitavecchia (IT)), F. Bilotti (Department of Applied Electronics, ‘RomaTre’ University, Rome (IT)), M. Marcelli (Laboratory of Experimental Oceanology and Marine Ecology, University of Tuscia, Civitavecchia (IT)), A. Toscano (Department of Applied Electronics, ‘RomaTre’ University, Rome (IT))

<i>Small wind turbines applications in seaports: cost analysis and market potential in Italy</i> - D. Chiaroni, V. Chiesa, F. Frattini, R. Terruzzi (Dipartimento di Ingegneria Gestionale, Politecnico di Milano, Milan (IT))	319
<i>An e-Learning Platform for Off-shore Wind Energy Logistics and Infrastructures</i> - F. Fontana, E. Cosimi, G. Ponzio (ENEA, Rome (IT))	330
Poster Session	331
Chairmen: F. Cesari, A. Fiorentino	
<i>MOBI BUOY: Offshore Wind Measurements in the Sicily Channel</i> - D. Airoidi, C. Casale, E. Lembo, C. Rosito, L. Serri (RSE SpA, Milan (IT))	332
<i>A New Configuration of Vertical Axis Wind Turbine: towards the development of a highly distributed and efficient Wind Power Generation System</i> - M.R. Chiarelli (Dept. of Aerospace Engineering, Pisa Univ., Pisa (IT)), A. Massai (AM Engineering, Florence (IT)), G. Russo, D. Atzeni, F. Bianco (Dept. of Aerospace Engineering, Pisa Univ., Pisa (IT))	336
<i>New Way for Access and Maintenance of Offshore Wind Farms. The Use of Cableway to Reduce Cost and Improve accessibility. Comparison, Strengths and Limits of this Approach</i> - M. Grecchi (Altavia Milano srl (IT)), L. Meroni (Italtel S.p.A. (IT)), P. Betteto (Vemplast S.a.S. (IT))	352
<i>Levelised cost of electricity generated by offshore wind plant and other competing technologies: dynamic analysis using simulation theory</i> - M. Gaeta, M. Rao (ENEA, Unità Centrale Studi e Strategie, Rome (IT))	369
<i>TRITON - Wave Energy Converter</i> - R. Piccinini, M. Boffini (K.I. Energy, Busan (KR))	385
<i>Mapping Mediterranean Sea wind resource: state-of-the-art technologies for short term measurements and long term reference data</i> - M. Gianni, L. Imperato (Studio Rinnovabili S.r.l., Rome (IT))	386
<i>Wakes calculation in a offshore wind farm</i> - G. Crasto (WindSim AS, Tønsberg (NO))	392
<i>Overview of non destructive testing for composite materials</i> - C. Cappabianca (AIPND, Brescia (IT))	402
<i>PlasMare. Trattamento integrato eco-compatibile di Rifiuti Solidi Urbani su piattaforme navali</i> - S. Vacante (FINCANTIERI/CETENA, Genova (IT))	414
<i>New renewable energy source and its practical use in the Mediterranean and other European seas</i> - S. Goncharenko (Kimo-Business, Kiev (UA))	415
<i>Wave Energy Generation Difficulties solved by Eco Wave Power</i> - D. Leb (EcoWavePower, Tel Aviv (IL))	428
<i>A new device to produce electrical power from ocean waves: some applications to Italian coasts</i> - F. Arena*, A. Romolo*, A. Ascanelli, A. Viviano (Dept. of Mechanics & Materials, Reggio Calabria Mediterranea Univ. (IT) and *Wavenergy.it S.r.l., Reggio Calabria (IT))	453

<i>Ports for Offshore Wind Applications along the Tyrrhenian Coasts of Calabria and Sicily</i> - F.G. Cesari, F. Taraborrelli, D. Mostacci (DIENCA Dept., Bologna Univ. (IT)), L. Milella (TRE SpA, Bari (IT)), L. Pirazzi (ANEV (Rome (IT)))	454
<i>Italian Off-Shore Wave Energy Map, using Gauges and Numerical Model Data</i> – F.M. Carli, S. Bonamano (Laboratory of Experimental Oceanology and Marine Ecology, University of Tuscia, Civitavecchia (IT)), G. Stella, M. Peviani (RSE SpA, Seriate, Bergamo (IT)), M. Marcelli (Laboratory of Experimental Oceanology and Marine Ecology, University of Tuscia, Civitavecchia (IT))	467
Special Session: Mediterranean Marine Energy Technology Perspectives	477
Chairmen: A. Lazzari, C. Borri	
Presentations by:	
GSE: G. Montanino, <i>IT RES Support Mechanisms</i>	478
IEA Wind: W. Popko, F. Vorpahl (Fraunhofer Institute for Wind Energy and Energy System Technology IWES, Bremerhaven (DE)), J. Jonkman, A. Robertson (National Renewable Energy Laboratory, Golden, CO (US), <i>OC3 and OC4 projects - Verification benchmark exercises of the state-of-the-art coupled simulation tools for offshore wind turbines</i>	499
IEA OES: A. Brito e Melo, <i>Implementing agreement on Ocean Energy Systems</i>	504
MARINET: T. Lewis (Hydraulics and Maritime Research Centre, University College, Cork (IR), <i>Marine Renewables Infrastructure Network</i>	527
OMC: E. Titone, <i>Renewable and Fossil Resources: Opportunity for Synergy and Integration</i>	542
IET: M. Fiorini, <i>On the European Union Maritime Spatial Planning: are EU oceans and seas shrinking?</i>	547

PRESENTATION

European Wind Energy Association (EWEA) predicts a total wind energy installed capacity in 2020, equal to 230 GW including the increasingly important 40 GW offshore, that will generate 562 TWh/year in 2030 comparable with the 591 TWh/year onshore.

Offshore wind electricity generation in shallow waters is a mature and nearly cost competitive sector in Northern European seas, while applications are still at a very early stage in Mediterranean Seas characterized mostly by deep waters with significant potential.

Large size wind turbines on floating platforms in deep waters, by advanced design, new materials applications, grid integration, and with good operation and maintenance services are some of new technologies to be tested and deployed, while lowering the initial high costs.

The increasing interest of financial investors on marine renewable energies is a clear sign of development of a new “green” economy that can reduce negative effects of the actual global economic crisis.

OWEMES 2012 Proceedings will be a useful way to diffuse the technical results of the triennial European Seminar, the international meeting point in Italy, since 1994, of industries, researchers and other institutional organizations on offshore wind and other marine renewable energies.

Gaetano Gaudiosi
Executive Chair OWEMES
2012

Session 1: Wind Energy Resources

Chairmen: L. Imperato, M. Burlando

The Estimation of wind, wave and ocean current resources in the Mediterranean Sea for energy converters site selection - N. Pinardi (CIRSA - Bologna Univ. (IT)), L. Torrisi, M. Ferri (CNMCA- Pratica di Mare, Rome (IT)), R. Archetti, A. Lamberti (DICAM - Bologna Univ. (IT)), M. Zavaratelli (CIRSA - Bologna Univ. (IT)), G. Coppini, M. Adani (INGV - Bologna Univ. (IT))

Mediterranean Inshore Wind Resources: combining MCPs and CFD for marine resources quantification - R.N. Farrugia, T. Sant (Institute for Sustainable Energy, Univ. of Malta, Triq il-Barrakki, Marsaxlokk (MT) and Department of Mechanical Engineering, Univ. of Malta, Msida (MT))

Validation of an offshore wind atlas using the satellite data available at the coastal regions of Portugal - R. Marujo, P. Costa, M. Fernandes, T. Simões, A. Estanqueiro (LNEG - Laboratório Nacional de Energia e Geologia, Lisboa (PT))

The “Wind and Ports” Project for wind energy assessment and forecast: the case of the Port of Genoa - M. Burlando, M. Tizzi, S. Navone, G. Solari (Dpt. of Civil, Environ. & Architect. Engineering, Genoa Univ. (IT)), G. Canepa (Port Authority of Genoa (IT))

The estimation of wind, wave and ocean current resources in the Mediterranean Sea for energy converters site selection

N. Pinardi (*), L. Torrisi(**), M. Ferri(**), R. Archetti(***), A. Lamberti(***), M. Zavatarelli (*), G. Coppini(+) and M. Adani (+)

(*) *CIRSA, Univ. of Bologna*

(**) *CNMCA, Pratica di mare, Rome*

(***) *DICAM, Univ. of Bologna*

(+) *INGV, Sezione di Bologna*

A proper assessment of the wind regime is of fundamental importance in the wind farm design: it is necessary to characterize the wind climate in terms of the mean values, the frequency distributions for speed, direction and power density at different elevations (where the turbine will be installed). Similarly a good knowledge of wave and currents regimes is fundamental for the estimation of the sea energy resources.

Wind, waves and ocean current resources can be estimated nowadays with high resolution numerical models that use data assimilation to correct for models errors. The national meteorological service (CNMCA) and the GMES marine service provide wind, waves and currents data for the whole region of the Mediterranean Sea.

The paper aims to present the CNMCA and the GMES marine service data: the structure of the offshore wind, wave regimes and ocean currents will be described for an horizontal resolution of about 7 km. The seasonal signal of the wind and currents will be elucidated as well as the frequency spectra of the wind---wave and currents as well as the structure of their errors due to model inaccuracies. A preliminary estimation of the wind energy potential production in the Mediterranean sea will be evaluated based on the choice of the optimum aero generator at each site.

Mediterranean inshore wind resources: combining MCPs and CFD for marine resources quantification

R.N. Farrugia and T. Sant

Institute for Sustainable Energy, University of Malta, Triq il-Barrakki, Marsaxlokk MXK1531, Malta, & Department of Mechanical Engineering, University of Malta, Msida MSD2080, Malta, robert.n.farrugia@um.edu.mt, tonio.sant@um.edu.mt

Abstract – This work presents a fresh assessment of wind resources in an inshore coastal environment; focusing specifically on a site that has been shortlisted as a possible offshore wind farm location in Maltese territorial waters. Wind measurements conducted over the period November 2009 to October 2011 are sourced from a new wind mast installed at an onshore site close to the proposed offshore wind farm’s location. This study uses a combination methodology of Measure-Correlate-Predict (MCP) techniques in conjunction with commercial Computational Fluid Dynamics (CFD) software. MCP routines are conducted between a reference wind measurement station possessing a long-term time series of wind speed and direction records and the shorter-term new wind mast’s 80 metre level database; the latter playing the role of candidate site. This procedure was conducted to generate a long-term wind climatology for the specific measurement height above ground level at the candidate site. The resulting climatology was then used to calibrate the CFD software to generate an indicative wind resources map in a coastal environment in the central Mediterranean region.

1. Introduction

Offshore wind energy is perceived as a potential contributor to the Maltese island’s target to reach 10% of gross final consumption of energy from renewables by the year 2020 [1]. Wind energy conversion project feasibility is being investigated at a near shore offshore site. The islands are very densely populated and have a limited land area; factors that restrict the technical feasibility of large scale onshore wind projects [2]. One might think that an archipelago would have large expanses of available marine space for such technologies. However, the islands have deep seas to their south west with shallower waters to the north east [3, 4], naturally limiting the marine areas suitable for commercially-proven offshore wind turbine foundation technology. The existence of other coastal and marine activities will reduce further the theoretical technical potential. Development of commercially feasible fixed turbine foundation structures in deeper waters (30 to 50+ metres) or of floating support technologies would open up new boundaries in terms of the exploitable marine spaces and a possibly superior wind resource potential. Going further offshore would mitigate certain impacts, yet increase capital costs related to longer wind farm to grid-connection cabling routes and operation and maintenance expenses amongst others. The projects would also have to be large to benefit from economies of scale.

The Malta Resources Authority (MRA) is currently compiling information on near-shore offshore wind resources by means of an 80 metre wind monitoring mast that was installed at *Aħrax Point* on the island of Malta’s northern-most extremity in late 2009 (see Figure 1). Interest in wind resources in this region stems from the fact that an offshore marine reef and surrounding area is being considered as a candidate site for the near shore offshore wind farm. This site has been assessed as one of that could possess attributes suitable for the installation of marine-based wind turbines [5-11]. The reef itself, known as *Is-Sikka l-Bajda*, lies between 1.5 and 3.0 kilometres out at sea from the mast’s location.

The *Ahrax Point* mast is currently the highest wind monitoring structure on the archipelago. Apart from being instrumental in helping to investigate high level wind conditions in a coastal marine environment, its numerous sensors could also serve as a reference node for wind speed and direction behaviour within the lower boundary layer in the central Mediterranean region. Interest in offshore wind resources for wind energy harvesting has long been a theme in the Mediterranean basin and a number of studies have been conducted, or are underway in this respect [12, 13]. Fruition of one of a number of concepts for offshore wind farms in this quasi-landlocked sea would spearhead the technology, generate more interest, potentially serve as a catalyst for other projects, and spur growth of a project support infrastructure in the region. The paper presents results from a combined Measure-Correlate-Predict (MCP) and Computational Fluid Dynamics (CFD) analysis that is envisaged to explore longer-term wind resources off the north east coastline of the island of Malta. The source data measured at the candidate site (*Ahrax Point*) was extrapolated in the longer term by means of MCP techniques with another site at *Wied Rini*; in this case the latter acting as a reference site. The MCP-generated longer-term wind conditions at the *Ahrax Point* mast were subsequently used to calibrate CFD model runs that were envisaged to generate new estimates of local wind resources in the area surrounding the 80 metre mast; values that also help validate the combined MCP-CFD methodology performance with other studies for the offshore site.

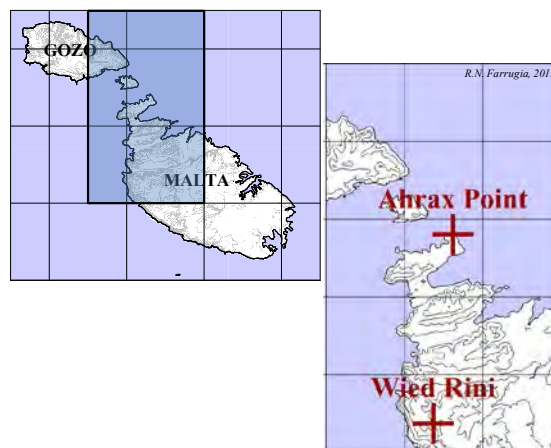


Figure 1: Schematics showing the location of the *Ahrax Point* and *Wied Rini* wind monitoring stations with respect to the Maltese archipelago.

2. Background

As always, wind resources are of critical importance to the economic viability of a wind project. This new study strives to use new wind data captured very close to the offshore site and at a height that is similar to the hub height of the modern offshore grade wind turbines. The MRA's wind monitoring station at *Ahrax Point* is located on a small promontory surrounded by water on three sides. The installation location itself may be considered to be at the northern-most tip on the main island of Malta. The wind monitoring structure that was planned and installed in late 2009 by Oldbaum Services Ltd. [14] consists of an 80 metre tubular mast with uniform cross-section. Instrumentation consists of wind speed and wind direction sensors, pressure, relative humidity and ambient temperature probes. The height of this structure and the variety of instrumentation at *Ahrax Point* is enabling the capture of information at a height above ground level that is to date unsurpassed in the local context [15, 16].

Research at the University of Malta's Institute for Sustainable Energy (ISE) and within the Department of Mechanical Engineering has also focused on the potential for wind power generation in Malta. Wind measurements have been undertaken at a number of local sites to generate more knowledge on local high level conditions and also on low level wind resources. One of the ISE's long standing wind measurement stations is that at *Wied Rini* on Malta's south west coast (see Figure 1). The site is at a high elevation by local standards (c. 200 m above mean sea level) and is exposed to the prevailing winds that dominate the central Mediterranean basin, although localised effects could also be present.

A disused lattice-type telecommunications tower is being used as a wind monitoring platform. The wind data from this location spanned over a number of years with measurement levels at 10 and 45 metres above the ground [17]. Recently the station was substantially upgraded in collaboration with the Ministry for Resources and Rural Affairs (MRRA) to also include other measurement points on the tower.

3. Methodology

3.1 The wind data

Wind speed and direction records were sourced from the 10 metre level in the case of the *Wied Rini* tower (see Figure 2) and from the 80 metre (speed) and 78.5 metre (direction) levels on the *Ahrax Point* mast (Figure 3). The time frames of the measurements used in this analysis are listed in Table 1. Data availability for *Wied Rini* over the full duration of measurements was 97.9%.

Direct comparison between the wind speed records captured at 80 metres at *Ahrax Point* and at 10 metres at *Wied Rini* indicates that the readings from the latter site are lower; as a direct and unavoidable consequence of the that site's lower monitoring level. Figure 4 shows the percentage difference between the measured monthly mean wind speeds at both locations over the 24 calendar month concurrent time frame, with the percentage difference defined as:

$$\left(\bar{U}_{M:WR10} - \bar{U}_{M:AP80} \right) / \bar{U}_{M:WR10} \quad (1)$$

where \bar{U}_M stands for the monthly mean wind speed value. Additional notation in the subscripts refers to the site and height in question.

Table 1: Table lists details relevant to the two wind data sources used in this study.

Site Name	Monitoring Height a.g.l. [m]	Duration Considered 10 minute averages
<i>Wied Rini</i>	10	December 1996-October 2011
<i>Ahrax Point</i>	80/78.5	November 2009-October 2011



Figure 2: The 10 metre level sensor cluster at Wied Rini which is being used as a source for the long-term ‘donor’ dataset is shown on the short supporting boom close to the tower.

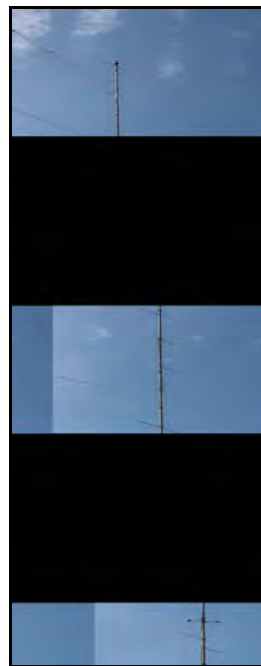


Figure 3: The 80 metre mast as installed at Ahrax Point. The wind speed and direction records come from the top-most mast level.

Inspection of the plot also indicates that the percentage difference between the monthly mean wind speeds decreases during the months exhibiting lower than average wind speeds; typically occurring during the hotter summer period. During the windier winter months, differences are more marked.

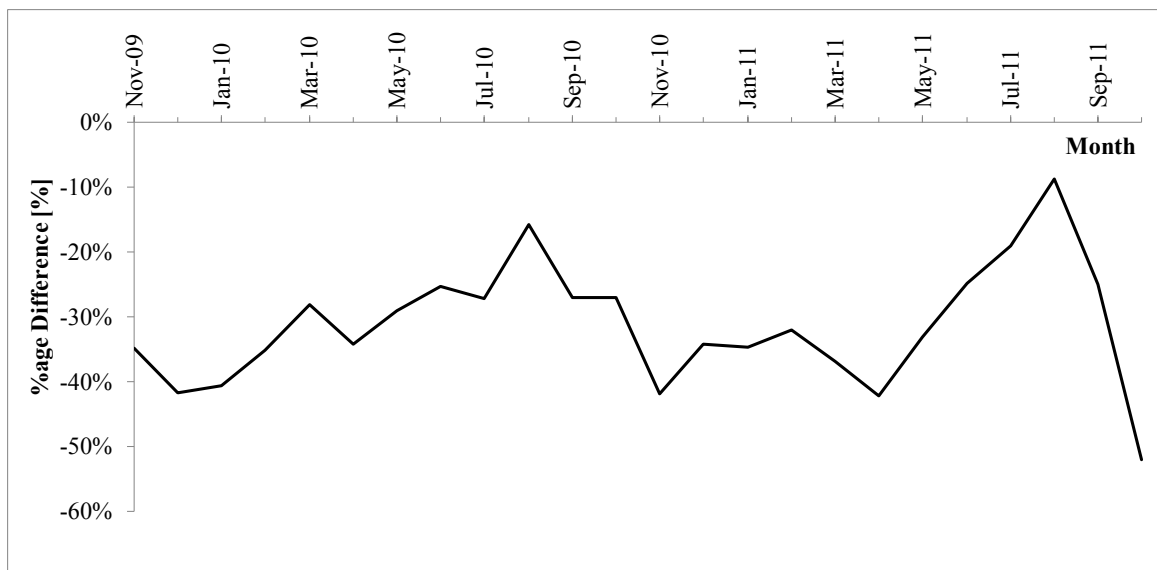


Figure 4: Percentage difference between monthly mean wind speed values measured at 10 metres at Wied Rini and at 80 metres at Ahrax Point.

3.2 Measure-Correlate-Predict (MCP) techniques

Whilst it is acknowledged that longer-term datasets will reduce the level of uncertainty in wind resource projections and turbine energy yield estimates, it is also clear that longer measurement programmes imply longer waiting times before the fruition of an actual project. Measure-Correlate-Predict (MCP) techniques have been devised as a stop-gap measure that enables longer-term projections of the site-specific wind resources at a candidate site, thus cutting down on the waiting times necessary to carry out longer-term wind assessments at the site of interest. In principle, MCP techniques strive to build a relationship between the candidate site (i.e. the site where the short-term measurements are being conducted to establish the viability of a wind project), and the reference site [18].

The *Wied Rini* long-term 10 metre level dataset was used in this MCP exercise to project long-term wind resources at *Ahrax Point*. The MCP techniques used in this study were those provided by the MCP module in the WindPRO™ [19] software. The MCP toolbox provided Linear Regression and Matrix MCP techniques amongst others.

One test involved assessing the percentage differences between the Linear and Matrix MCP-generated monthly mean wind speed values and the actual measured monthly means solely over the concurrent 24 calendar month period for 80 metres at *Ahrax Point* and as follows:

$$\left(\bar{U}_{MCP:AP80} - \bar{U}_{M:AP80} \right) / \bar{U}_{M:AP80} \quad (2)$$

where \bar{U}_M : stands for the measured monthly mean wind speed values and \bar{U}_{MCP} : for the MCP-generated monthly means. Once again, additional notation in the subscripts refers to the site and height in question.

Both Linear and Matrix MCP methodologies generated monthly means that track each other in similar fashion. The months when the percentage differences between the direct measurements at the two sites were lowest (refer to Figure 5) gave the largest differences between MCP-generated and the measured results. One hypothesis could be that the MCPs tended to overestimate the candidate site's wind resources during the calmer summer months, although this behaviour will need further investigation before some conclusion may be drawn.

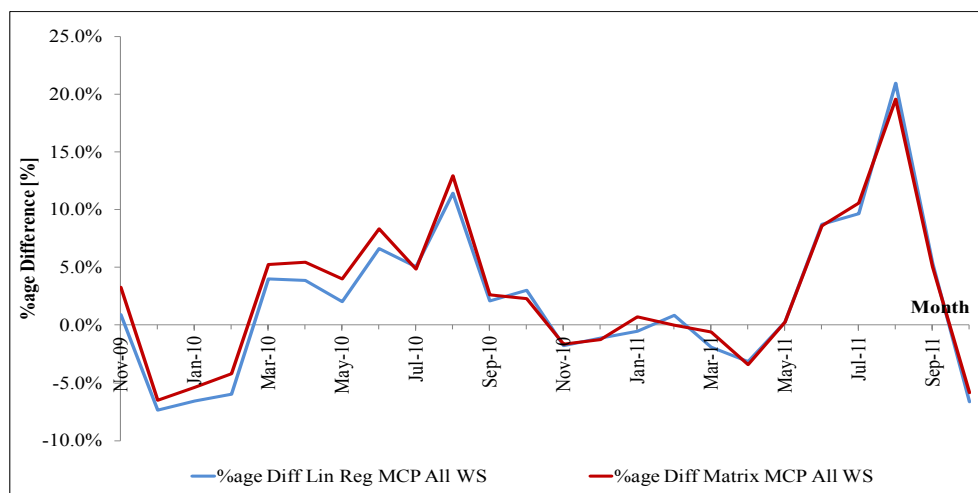


Figure 5: Percentage differences between WindPRO™ MCP-generated monthly means and the measured monthly values over the 24 calendar month concurrent measurement period.

The linear regression method was eventually selected as a basis for rebuilding the long-term meteorological time series at *Aħrax Point*. In the linear regression MCP technique, concurrent 10 minute average wind speed and direction records from the *Wied Rini* (10 metre level) were compared side-by-side with the *Aħrax* data captured at 80 metres above the ground. Regression was conducted on a 1 degree per sector analysis basis.

The resulting correlation coefficients (R values) and Standard Errors are displayed in radial plots for the 360 sectors (see Figures 6(a) and (b)). In general, the correlation coefficient is in excess of 0.8 indicating a reasonably good fit. Lower values are evident in the north and southerly sectors. Standard Errors are also higher for the south.

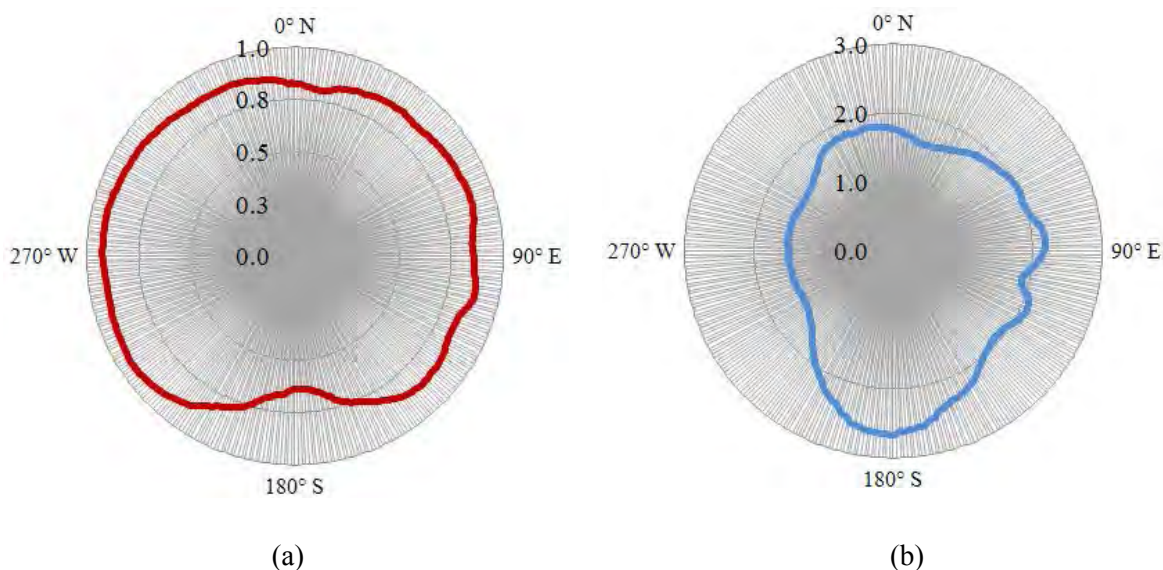


Figure 6: Radial plot showing (a) the correlation coefficients R , and (b) the Standard Errors, for the linear regression analysis between the two sites.

Once the linear relationship between the two sites had been built, the long-term data set at the reference site was scaled to reflect conditions at *Aħrax Point* over the full duration of the *Wied Rini* measurement programme. A meteorological time series consisting of 10 minute wind records was therefore generated for *Aħrax Point* over the period December 1996 to October 2011. Availability was the same as for the original reference site dataset.

As the intention of this current work was to generate longer-term projections of wind resources in the near shore coastal region off the north east coast of the island of Malta, this newly-generated representative time-series for *Aħrax Point* was then used as climatological input to the CFD models described in the next section.

3.3 The CFD modelling domains

3.3.1 Introduction

WindSim™ [20] is one of a number of CFD-based software programmes used to model wind flow over terrain. It is worth briefly describing the programme's layout in order to enable the reader to follow the technical terms used in the methodology descriptions.

The WindSim™ program consists of a number of inter-dependent modules. These enable the interfacing of topography and surface roughness features, wind flow fields that handle the CFD computations, a module enabling the insertion of climatologies and wind turbines, a module to generate wind resource maps and finally a part which enables calculation of wind turbine energy yield.

A computational domain was first designed within which the later modules carried out the computations. This required topography features, including height above mean sea level and surface roughness. The grid above the surface within which the CFD calculations were executed was also defined at this stage. The next stage involved the CFD computations. The programme solves the Reynolds Averaged Navier Stokes (RANS) equations through an iterative process using either a segregated or coupled solver that, once complete, is expected to achieve a converged solution monitored by means of a number of indicators. The measured or statistical climatologies were then fed into the domain, a technique that calibrates the model. Various results were computed including the inflow angle, x , y and z wind speed scalars and so on. Wind resource files within the domain were also generated. The final module permits calculation of energy yield using programme inbuilt or user-defined wind turbine power curves.

3.3.2 The Macro model domain

In the first run required for this study the topography covered an extensive or macro domain that was designed to encompass a large area around the islands; a strategy designed to also provide boundary conditions for later calculations that would zoom in on selected areas of interest. A reasonable buffer zone between the domain boundaries and the islands' landmass was retained to limit any potential blocking effects. The limits of the digital terrain model (DTM) referenced using a Universal Transverse Mercator (UTM) coordinate system (Zone 33 S) and the extents of the grid file with the respective resolutions are listed in Tables 2 and 3. The vertical resolution of the grid was variable, as the software distributes the cells closer to the surface with decreasing resolution as the height above the surface increases. The number of cells is almost 3,000,000. Figure 7(a) shows the extent of the macro domain with the island group and with height contours for the topography. Figure 7(b) shows a simple surface roughness map used in the computations.

Table 2: Extent of the Digital Terrain Model used in WindSim™ and dubbed the Macro domain.

x -min.	x -max.	y -min.	y -max.	x -extent	y -extent	Resolution
[m]						
420000.0	489984.0	3954000.0	3999972.0	69,984.0	45,972.0	180.0

Table 3: Extent of the data in the grid file (grid.gws) used in the calculations.

x -min.	x -max.	y -min.	y -max.	x -extent	y -extent	Resolution
[m]						
420000.0	489984.0	3954000.0	3999972.0	69,984.0	45,972.0	36.0

Table 4: Grid spacing and number of cells used in the Macro domain model.

	x	y	z	Total
Grid Spacing [m]	180.0	180.0	Variable	-
Number of Cells	388	255	30	2,968,200

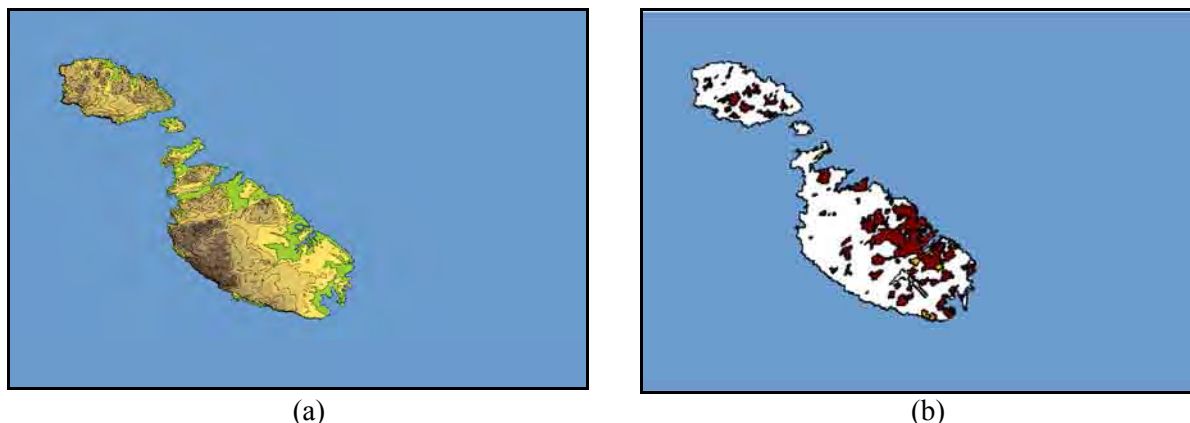


Figure 7: Screenshots from WindSim™ showing the extent of the Macro model domain used in the CFD simulations with (a) the topography file showing elevations above mean sea level and (b) the surface roughness map, both of which formed part of the DTM used in the CFD simulations module.

The default turbulence model was used, this being the standard $k-\epsilon$ model. The $k-\epsilon$ model may be classified as one of the eddy viscosity model types. A segregated solver was employed, with a standard air density default value of 1.225 kg/m^3 . A selection of screenshots from the software (shown as Figures 8 (a) to (d)) illustrates typical plots of the residuals values for various direction sectors. Convergence of all parameters under scrutiny occurs well before the 10,000 iterations were conducted. The variables being monitored are the residuals for the three velocity components U1, V1 and W1, KE - that represents the turbulent kinetic energy - and EP, the dissipation rate [20].

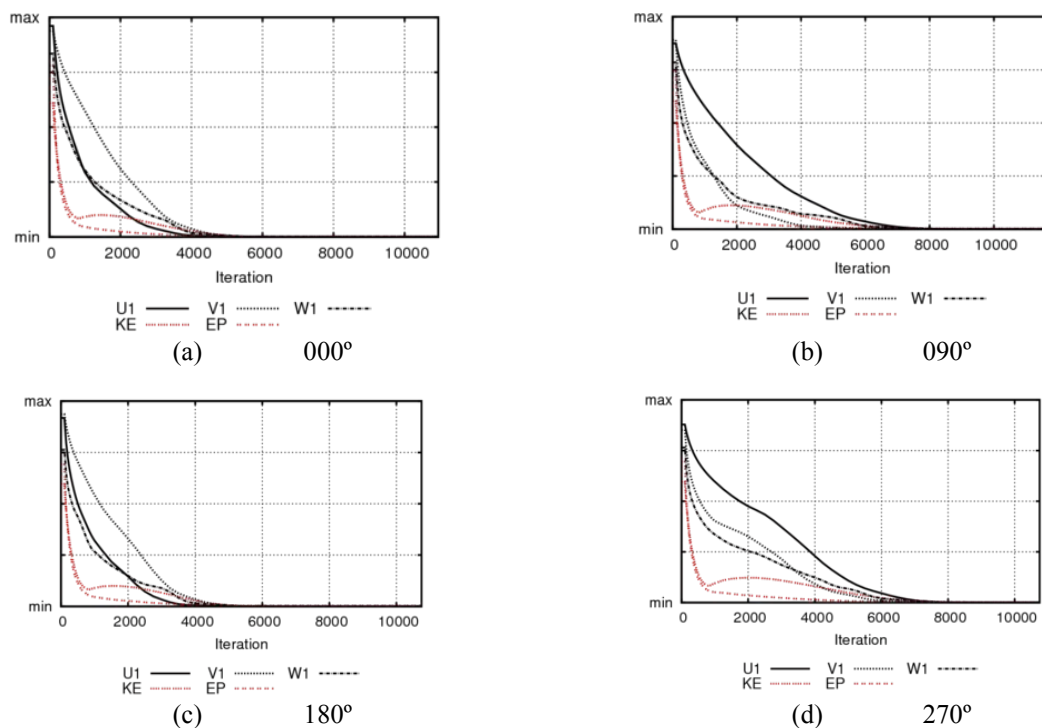


Figure 8: Typical convergence monitoring of residual values of key parameters; in this case showing results in the four cardinal direction sectors (images reproduced from WindSim™ screenshots).

The *Wied Rini* mean wind speed at 45 metres above ground level over a five year period (2003-2007) was 6.8 m/s [17]. Using *Ahrax Point* as a climatology object in the CFD model to generate wind resource maps at different levels above the ground yielded a long-term mean wind speed of between 6.7 and 6.8 m/s for a height of 45 metres at *Wied Rini*. The measured and computational results for the reference site are therefore very close.

Using CFD and MCP-generated wind resources at the same height as the *Ahrax Point* top level wind speed sensor (80 metres) resulted in a wind resource map over a wider marine area. Output data files containing x , y , z and mean wind speed values were converted using the Surfer® [21] mapping software to generate a grid file that allowed the data to be plotted and displayed as shown in Figure 9. This shows that wind speeds offshore are likely to be comparatively higher than in zones close inshore; as would be expected due to land shielding effects. The impact of the prevailing north westerly winds is reflected in the wind speed bands within the coastal zone to the leeward of the islands i.e. along the north east stretches of the coastline. Lower wind speed areas would also seem to extend further offshore to the south east of the islands. The lower wind speed area between the two main islands is also of interest and is presumably a result of the proximity of the three land masses that is being taken into consideration by the CFD model.

To date there are no offshore wind stations having measurement levels close to the hub height of modern wind turbines. Consequently, wind resources offshore can only be estimated using mathematical models and wind data from an onshore station such as the one at *Ahrax Point*. The domain size used in the Macro CFD modelling is very extensive and the operational characteristics of the CFD model have yet to be verified in the local context. Also, wind conditions at increasing distances from the mast could be subjected to localized effects. It is always recommended that wind resources at a prospective wind turbine installation site should be confirmed by site-specific wind measurements at the height of interest during the planning stages of a wind farm project.

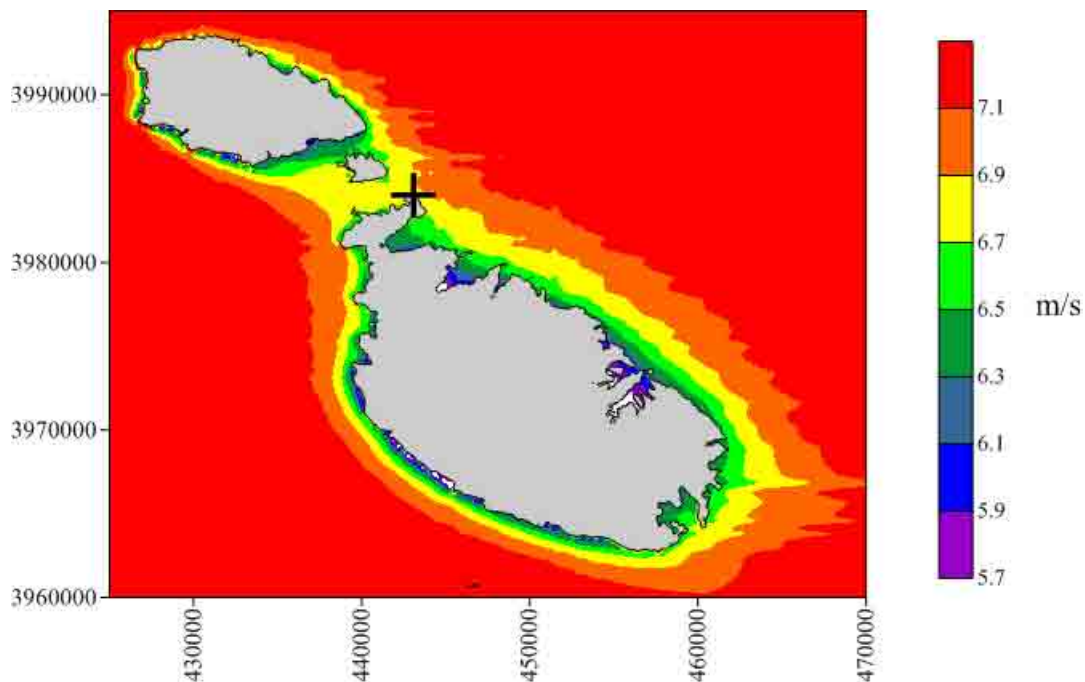


Figure 9: Mean wind speeds modelled for a height of 80 metres above the surface within the Macro domain. The location of the *Ahrax Point* mast is labelled with a marker.

3.3.3 The Micro model domain

The micro domain (Micro_01) was designed in order to enable a more detailed representation of wind conditions off the coast in the *Ahrax Point* area. The micro domain was selected from within the larger macro domain's grid file. In the case of the macro domain, boundary conditions at the inlet were set by the user and default values used for the velocity at the top of the boundary layer profile. Inlet conditions can either be fed to the model from a mesoscale model or from previously-generated results of a larger domain computation. In this case, the Micro domain was 'nested' within the macro domain to generate the wind fields. This process is expected to yield more accurate results within the area of interest. Another feature is the ability to incorporate a refinement grid within the Micro domain itself that re-distributes the computational mesh used in the CFD computations. This allows a more detailed grid in the area of interest, whilst relaxing grid resolution towards the micro model boundaries.

The Micro_01 model itself focused on the near shore offshore space in the vicinity of *Sikka l-Bajda* and a stretch of coastline between *Ċirkewwa*, *Ahrax Point* and *Mellieħa Bay*. These zones offer seas with depths of up to 30 metres that could support offshore wind turbines. The limits of the digital terrain models (DTM) and the extents of the grid files with the respective resolutions are listed in Tables 5 to 7. The resolution of the grid in the *x* and *y* directions was variable and ranged between minimum and maximum values as the refinement area option was utilised. The 30 cells in the *z* direction were also distributed with higher resolution closer to the surface. The segregated solver option was also used in this case. Figure 10 shows a comparison of the physical extents of the macro and micro domains.

Table 5: Extent of the data in the Macro domain grid file (grid.gws).

Macro domain						
x-min.	x-max.	y-min.	y-max.	x-extent	y-extent	Resolution
[m]						
420000.0	489984.0	3954000.0	3999972.0	69,984.0	45,972.0	36.0

Table 6: Extent of the Digital Terrain Model (DTM) extracted from the grid used in the Micro model runs.

Micro_01						
x-min.	x-max.	y-min.	y-max.	x-extent	y-extent	Resolution
[m]						
440000.0	450000.0	3980000.0	3990000.0	10,000.0	10,000.0	Variable

Table 7: Grid spacing and number of cells used in the Micro domain wind fields computations.

Micro_01				
	<i>x</i>	<i>y</i>	<i>z</i>	Total
Grid Spacing min. – max. [m]	13.0 - 209.2	13.0 - 209.2	Variable	-
Number of Cells	316	316	30	2,995,680



Figure 10: WindSim™ screenshot showing the extent of the Macro model and the Micro_01 domain.

The Mott MacDonald (2009) report [11] used nearby datasets compiled by the National Centre for Atmospheric Research (NCAR) [22] in conjunction with the European Wind Atlas and a WAsP [23] analysis to compute estimates for the wind resources at *Sikka l-Bajda*. Wind speeds at a height of 70 metres above surface over the reef area were estimated to be between 6.5 m/s and 7.5 m/s.

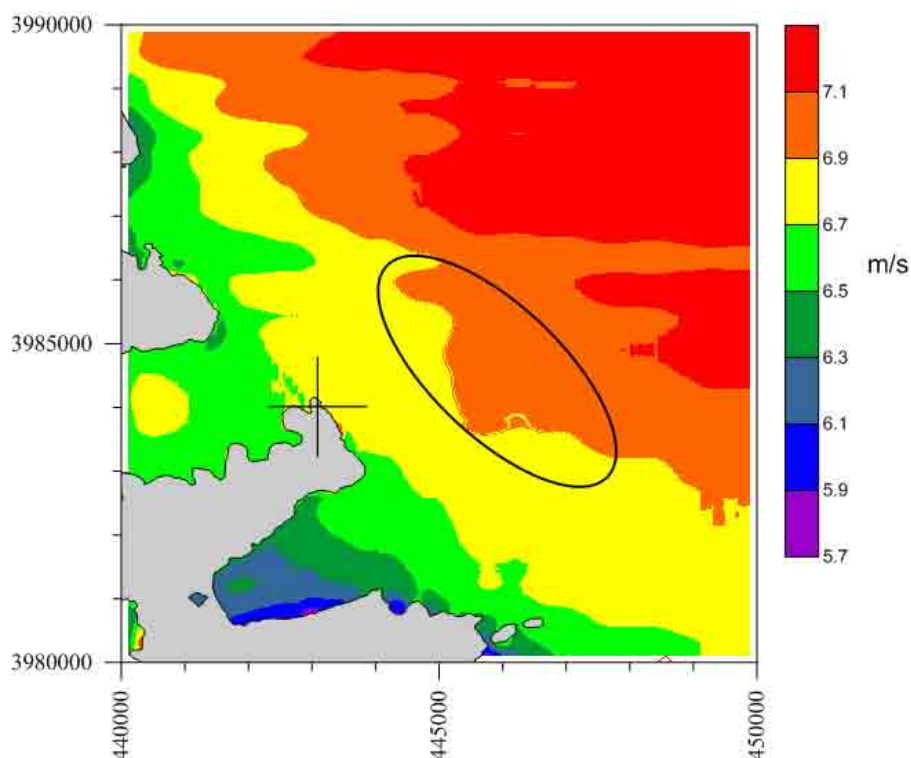


Figure 11: Wind resources map for 80 metres above the surface resulting from Ahrax Point's MCP-generated long-term climatology used as input to the CFD programme. The map shows the mast's location and the coastal area off Marfa Ridge also covering the approximate area of *Sikka l-Bajda* (denoted by an ellipse).

In this new study, wind resources were generated using WindSim's inbuilt wind resources module and the *Aħrax Point* MCP-generated long-term climatological time series for the 80 metre level. The Micro model enabled a more detailed analysis of the area in question. The same process of grid data file generation and import into the Surfer[®] software applies as explained earlier on. As in the previous case, wind speeds appeared to be lower close inshore, as would be expected for areas in the land 'shadow'.

In this new analysis (see Figure 11), the long-term mean wind speed over the reef at a height of 80 metres was estimated to range between 6.7 and 7.1 m/s. The range of values reconfirms earlier results. Future analytical work will seek to reassess this wind speed range for the reef area and its surroundings as more information becomes available and as the model inputs are refined further.

4. Conclusions

The main conclusions from this ongoing research work are as follows:

- An MCP analysis between onshore candidate and reference sites enabled the extrapolation of records from a new short-term measurement programme into a time series having the same time frames as the reference station dataset.
- Using the long-term time series as a climatology input to the CFD programme could enable a more accurate representation of the candidate site's longer-term wind speed characteristics.
- These preliminary results indicate that the combined MCP-CFD analysis is capable of generating reasonable estimates for wind resources and within the wind speed ranges reported in earlier work.
- The generation of a long-term time series at the candidate site will also enable a more detailed analysis of wind turbine performance by means of the CFD software tools.

Acknowledgements

The authors would like to acknowledge the support of the:

Ministry for Resources and Rural Affairs (MRRA), Floriana, Malta, for its support on the various wind monitoring initiatives.

Lands Department, Valletta, Malta.

Malta Resources Authority (MRA), Marsa, Malta, for providing the *Aħrax Point* data.

Oldbaum Services Ltd. and *Chillwind Ltd.* that installed the wind monitoring mast at *Aħrax Point*.

References

1. Malta's National Renewable Energy Action Plan as Required by Article 4(2) of Directive 2009/28/EC. Ministry for Resources and Rural Affairs (MRRA), Floriana, Malta, 2010.
2. R.N. Farrugia, M. Fsadni, E.A. Mallia and C. Yousif. Barriers and Incentives for the Widespread Application of Renewable Energy in Malta. In *World Renewable Energy Congress IX*, Florence, Italy, 2006.
3. D.W. Haslam. Mediterranean Sea - Maltese Islands - Malta, 2538: The United Kingdom Hydrographic Office, Taunton, United Kingdom, 1983.
4. D.W. Haslam. Mediterranean Sea - Maltese Islands - Ghawdex (Gozo), Kemmuna (Comino) and the Northern Part of Malta, 2537, The United Kingdom Hydrographic Office, Taunton, United Kingdom, 1983.

5. R.N. Farrugia and E. Scerri. Offshore Wind Potential of a Central Mediterranean Archipelago. In *Offshore Wind Energy in Mediterranean and Other European Seas Seminar (OWEMES 2000)*, Syracuse, Sicily, Italy, pp. 481-488, 2000.
6. R.N. Farrugia, J.J. Miles, B. Mast, D. VanLuvanee, T. Utt, and D. Perry. 'Sikka l-Bajda': A Case Study for Offshore Wind Power. In *Enemalta 25th Anniversary Conference on Energy and the Environment*, Mediterranean Conference Centre, Valletta, Malta, 2002.
7. R.N. Farrugia, M. Fsadni, E.A. Mallia, and C. Yousif. The Renewable Energy Potential of Malta. In *World Renewable Energy Congress IX*, Florence, Italy, 2006.
8. A Proposal for an Offshore Windfarm at Is-Sikka l-Bajda - Project Description Statement. Ministry for Resources and Rural Affairs (MRRA), Floriana, Malta, 2009.
9. R.N. Farrugia, A. Deidun, G. Debono, E.A. Mallia and T. Sant. The Potential and Constraints of Wind Farm Development at Nearshore Sites in the Maltese Islands. *Wind Engineering*, 34: pp. 12, 2010.
10. Strategy for Renewable Electricity Exploitation in Malta - Volume 1 - Renewable Energy Target. Mott MacDonald, Malta Resources Authority, Marsa, Malta, 2005.
11. Feasibility Study for Increasing Renewable Energy Credentials. Mott MacDonald, Malta Resources Authority, Marsa, Malta, 2009.
12. A. Lavagnini, A.M. Sempreviva and R.J. Barthelmie. Estimating the Wind Energy Potential Offshore in Mediterranean Areas. *Wind Energy*, 6: pp. 23-34, 2003.
13. A.M. Sempreviva, B. Furevik, F. Cheruy, R.J. Barthelemie, B. Jimenez and C. Transerici. Estimating Offshore Wind Climatology in the Mediterranean Area Comparison of QuickSCAT Data with Other Methodologies. In *Offshore Wind Energy in Mediterranean and Other European Seas 2006 (OWEMES 2006)*, Civitavecchia, Italy, 2006.
14. Oldbaum Services Limited, Stirling, United Kingdom.
15. R.N. Farrugia and T. Sant. Evaluation of the Wind Resources in a Central Mediterranean Island Using a Combination of Measurements and Modelling Techniques. In *TORQUE 2010: The science of making torque from wind*, Heraklion, Crete, Greece, 2010.
16. R.N. Farrugia, T. Sant, P. Mifsud, A. Cassola, G. Sant and M. Spiteri. High Level Wind Conditions at Prospective Wind Farm Sites on the Central Mediterranean Island of Malta. In *European Wind Energy Conference (EWEA) 2011*, Brussels, 2011.
17. R.N. Farrugia and T. Sant. Wied Rini II - A Five Year Wind Survey at Malta. *Wind Engineering*, 35: pp. 419-432, 2011.
18. T. Burton, D. Sharpe, N. Jenkins and E. Bossanyi. *Wind Energy Handbook*. John Wiley & Sons Ltd., U.K., 2004.
19. WindPRO™, Ver. 2.7. EMD International A/S, Aalborg Ø, Denmark, 2008.
20. WindSim™, Ver. 5.01.1. WindSim AS, Tønsberg, Norway, 1997 - 2010.
21. Surfer®, Ver. 10.5.560. Golden Software, Inc., Golden, Colorado, U.S.A., 1993-2011.
22. National Centre for Atmospheric Research (NCAR), Boulder, Colorado, U.S.A.
23. Wind Atlas Analysis and Application Program (WASP), DTU Wind Energy, Roskilde, Denmark.

Validation of an offshore wind atlas using the satellite data available at the coastal regions of Portugal

R. Marujo¹, P. Costa¹, M. Fernandes¹, T. Simões¹ and A. Estanqueiro¹

¹ National Laboratory of Energy and Geology, Estrada do Paço do Lumiar, 22 1649-038 Lisboa (Portugal), raquel.marujo@lneg.pt, paulo.costa@lneg.pt, miguel.fernandes@lneg.pt, teresa.simoese@lneg.pt, ana.estanqueiro@lneg.pt

Abstract – In this study a validation methodology for regional mesoscale model simulations when ingested with surface wind data inferred from satellite sources around Continental Portugal is evaluated. Observational wind data from a “quasi” offshore anemometric mast located in the Berlenga Island – near Peniche region – was used for the validation study. Satellite sources of wind data under assessment are the ones being used in the EC funded FP7 NORSEWInD project, such as the QuikSCAT and SAR. The validation study evolves 10 years of full wind data, starting in January 2000 to December 2009. The evaluation was performed in two different spatial validation approaches. Results from this study indicate that the wind satellite data has good quality to be assimilated on high resolution mesoscale model simulations particularly the ones concerned with long term behavior of the wind field near the coastal areas.

1. Introduction

Mesoscale model simulations are a very promising tool to characterize the wind flow and for the production of wind atlases for wind power studies. The output of these models consists on a group of several meteorological variables for different height levels on a grid that covers the area under investigation. Generally, the results provided by those models contain systematic errors that are not exclusively dependent on the physical parameterizations but are in fact influenced by the topography shape, the spatial resolution of the simulated grid, interpolation errors between observational and grid model points, among others. To interpret and characterize these errors a spatial statistical methodology, using the observational data as reference, was applied and evaluated.

The purpose of this work is to validate the wind field from a long term simulation provided by the WRF [1] mesoscale model, using spatial observational surface wind data from the QuikSCAT [2] satellite data for Portugal. The observational wind data from the satellite was given as input to two different spatial interpolation methodologies used for validation and evaluation of the quality of the simulated results, namely, the known Kriging interpolation method and a newer Composite interpolation method [3]. To evaluate the validation quality between each of the spatial interpolation schemes, a statistical analysis was then performed with the observational met mast tower installed at the Berlenga Island. Figure 1, depicts the area under study. The Berlenga Island is a small rocky island located about 10 miles away to the west coastal region of Peniche, in the vicinity of the Lisbon region.

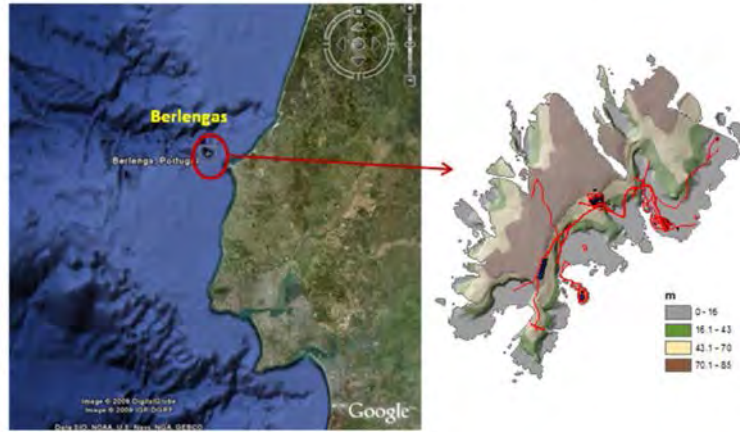


Figure 1: Island of Berlenga under the area of investigation.

The work developed in this study is in the scope of the validation research activities of the EU FP7 NORSEWInD project [4].

2. Spatial Interpolation Methodologies

The first procedure to validate the deviations between the winds predicted (WRF results) and observed (satellite data from QuikSCAT) was to compute the mean bias at each QuikSCAT location using the nearest WRF grid point:

$$\text{BIAS}(\mathbf{x}) = \frac{1}{N} \sum_{i=1}^N \text{Wind}_{\text{WRF}}(\mathbf{x}) - \text{Wind}_{\text{QuikSCAT}}(\mathbf{x}) \quad (1)$$

Where N is the total number of wind observations at each point along 10 years. A positive bias value indicates that the mesoscale model overestimates the wind whereas a negative bias implies an underestimation.

Next, a spatial deviation matrix was computed with the help of a spatial interpolation technique. Two different interpolation schemes were tested. Each one is described in the following sub-sections. The spatial deviation matrix should preserve the same area under investigation, the same spatial resolution and the same aspect 2D grid ratio between model grid and satellite data points.

After being built, this matrix will reflect the mean spatial deviations that represent the spatial validation or the uncertainty of the simulated wind fields. From the observational wind data placed in the study area, the quality of the interpolation method used for validation purposes will be inferred. This task will be done using the independent anemometric mast installed in Berlenga Island.

The quality of the spatial interpolation scheme can be inferred by evaluating the following statistical parameters, BIAS and MSESS (Mean square error skill score named here as SCORE) which is mathematically defined as:

$$\text{MSESS} = \frac{\text{MSE}_{\text{WRF}} - \text{MSE}_{\text{WRF}+\text{Deviation}}}{\text{MSE}_{\text{WRF}}} \quad (2)$$

Where MSE is defined as:

$$MSE(x) = \frac{1}{N} \sum_{i=1}^N [(\text{Wind}_{WRF}(x) - \text{Wind}_{\text{QuikSCAT}}(x))]^2 \quad (3)$$

And $MSE_{WRF+Deviation}$ means

$$MSE_{WRF+Deviation} = \frac{1}{N} \sum_{i=1}^N [(\text{Wind}_{WRF}(x) + \text{BIAS}(x))]^2 \quad (4)$$

The SCORE results will be represented in percentage (%). A value near 100% means the interpolation method for spatial statistical correction is perfect while a value near 0% means the mesoscale model and the statistical model are equivalent. A negative value indicates that the application of the correction will worsen the initial results.

2.1. Kriging interpolation method

Over the years, Kriging interpolation technique became an important spatial prediction tool in Geostatistics. It is a method that interpolates a value of a random field at an unobserved location based on the available surrounding measurements. The Kriging interpolation scheme is a best linear unbiased estimator (BLUE) that minimizes the spatial variance with a stochastic spatial function known as variogram. A simple formulation of this method can be expressed by:

$$z_0^* = z^*(x_0) = \sum_{i=1}^N \lambda_i z(x_i) \quad (4)$$

z_0^* : predicted value at x_0 ;
 λ_i : weight at location x_i ;
 d_i : distance between x_i and x_0 ;
 N : Number of sample values used in prediction;

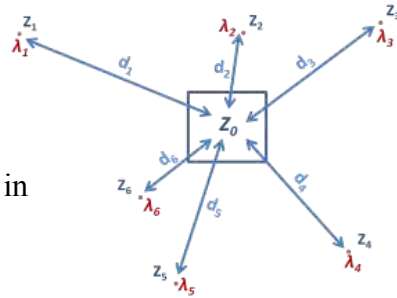


Figure 2: Weights of Kriging interpolation estimator.

More details about this spatial interpolator method can be found in [4, 5].

2.2. Composite method

The Composite method is a spatial interpolation tool developed by LNEG [6] where the deviation matrix is computed as a weighted linear combination of several data points. The linear coefficients associated to each grid point are calculated according to the inverse distance but applied to the nearest points. In this case, the distance is automatically computed via a radius of influence which depends on the spatial variance of the data.

3. Case Studies

The input data for testing both spatial interpolation schemes was:

- Ten years of wind data (2000-2009) from the WRF mesoscale model, at a height of 21 m with a spatial resolution of a 10x10Km.
- The available QuikSCAT points on the same simulation area, but extrapolated to 21 m a.g.l. with the wind power law (neutral stage) provided with an alpha coefficient of 0.104 which is common for the area under study.

Figures 3 and 4 displays the simulated wind field by WRF model and the QuikSCAT wind field, respectively.

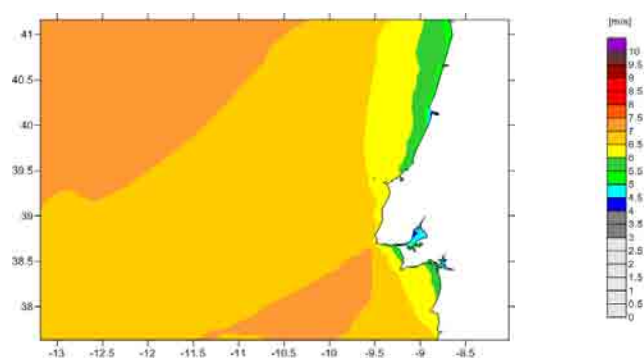


Figure 3: WRF mean wind field for the period between January 2000 and December 2009. ($h=21m$).

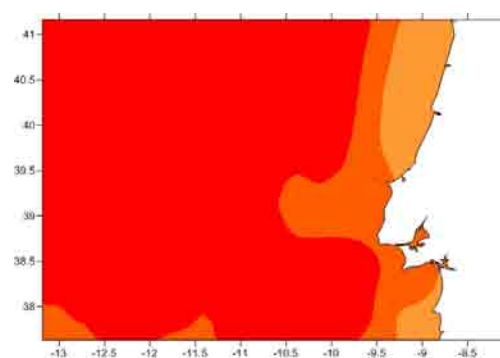


Figure 4: QuiKCAT mean wind field for the period between January 2000 and December 2009 (all data available for the area). ($h=21m$ after 10m extrapolation with the wind power law).

To demonstrate the usefulness of each interpolator method, two different case studies were performed.

3.1 Case study A

In this case, the grid presented in figure 3 with all the available QuikSCAT data points (figures 4 and 5) was used to perform the deviation matrix of the WRF field.

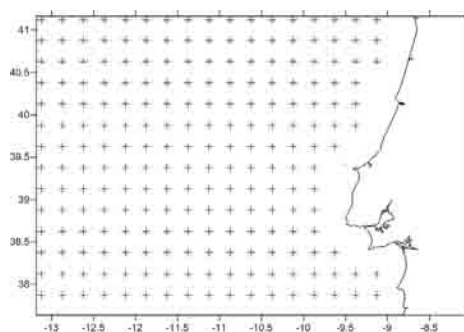


Figure 5: QuikSCAT available points at the simulated area – GRID 1.

The figures below show the deviation matrix and the final wind field for 219 QuikSCAT data points after the application of both interpolator methods (figures 6 and 7 with Kriging interpolator and figures 8 and 9 with the Composite method).

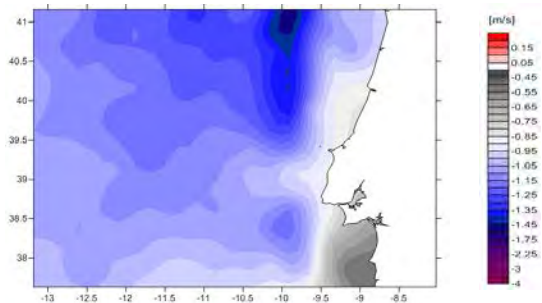


Figure 6: Deviation matrix performed with Kriging interpolation.

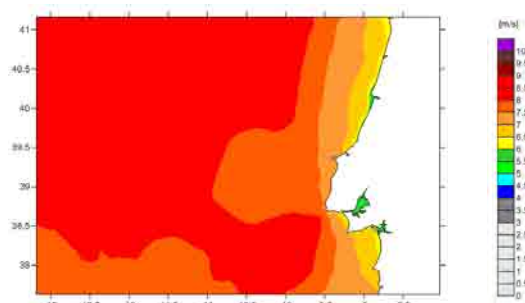


Figure 7: WRF+Deviation matrix with Kriging interpolation.

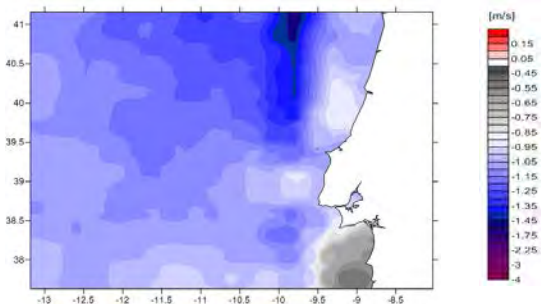


Figure 8: Deviation matrix performed with Composite method.

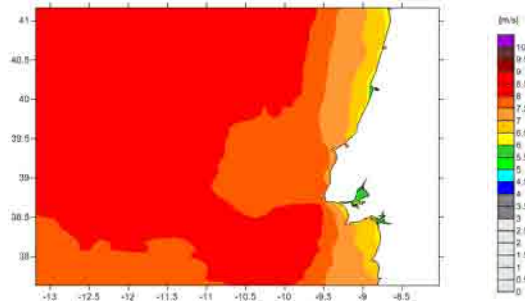


Figure 9: WRF+Deviation matrix with Composite method.

In figure 10 a plot of the spatial differences between both deviation matrixes is presented and table 1 represents the statistics obtained for three QuikSCAT data points identified in the figure.

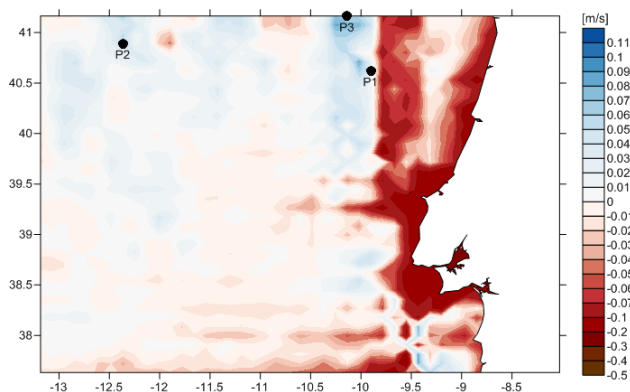


Figure 10: Difference between the deviation matrixes generated by the Composite and Kriging interpolation methods (Composite - Kriging).

Table 1: Bias between QuikSCAT points and model results (considering model results minus QuikSCAT).

		QuikSCAT	WRF	Kriging	Composite
P1	Wind speed (m/s)	8.04	6.75	8.15	8.11
	Bias (m/s)	-	-1.29	0.11	0.07
P2	Wind speed (m/s)	8.12	7.19	8.44	8.38
	Bias (m/s)	-	-0.94	0.32	0.26
P3	Wind speed (m/s)	8.01	6.79	8.32	8.27
	Bias (m/s)	-	-1.22	0.31	0.26

3.2 Case study B

Case study B is based on the application of two different grids (figures 11 and 12). These were obtained from a selection of ten available wind data points from QuikSCAT in order to compose a final deviation matrix. This approach can be useful when there is more than one source of satellite data unsynchronized in time or in spatial resolution (e.g. SAR satellite data).

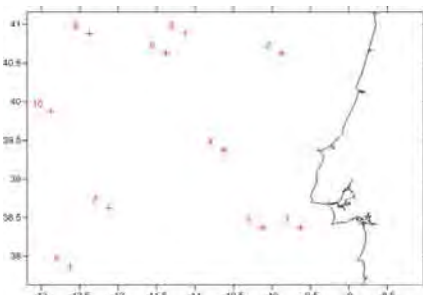


Figure 11: Ten QuikSCAT points inside the simulated area – GRID 2.

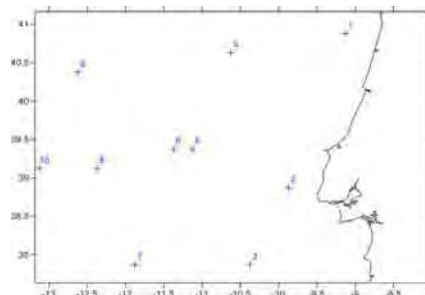


Figure 12: Ten QuikSCAT points inside the simulated area – GRID 3.

Following this idea, the results presented in figure 13 and 14, were obtained by averaging the two deviation matrices (as having two sources of different wind satellite data) created with Kriging interpolation scheme.

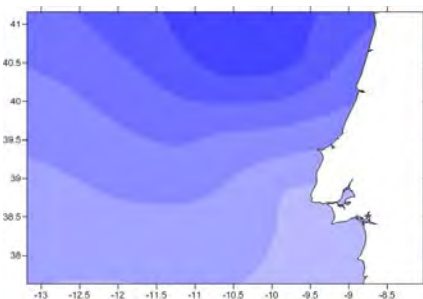


Figure 13: Final deviation matrix performed with Kriging interpolation method (two grids as input).

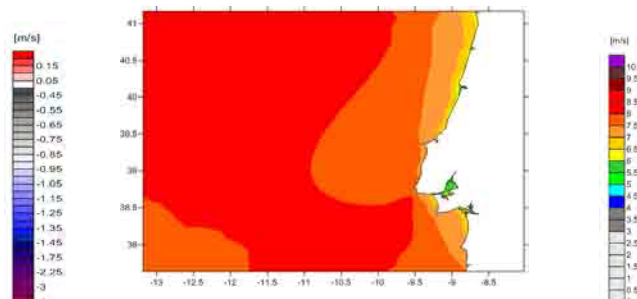


Figure 14: WRF+Deviation matrix with Kriging interpolation method (two grids as input).

For the Composite interpolation method the results were also assessed in a similar two step approach:

- First, the deviation matrix from each case (figures 11 and 12) using the selected data points was created.
- Secondly, the Composite method ingests the two deviation matrices and generates the final deviation matrix.

The following figures show the final deviation matrix on the left and the corrected wind field on the right.

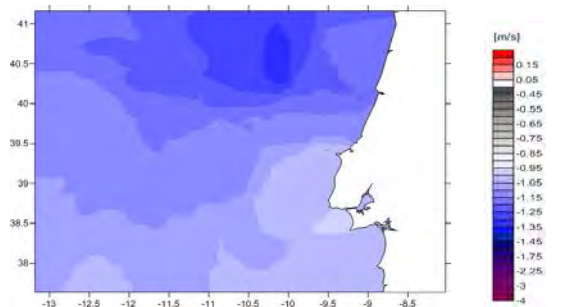


Figure 15: Final deviation matrix performed with Composite interpolation method (two grids as input).

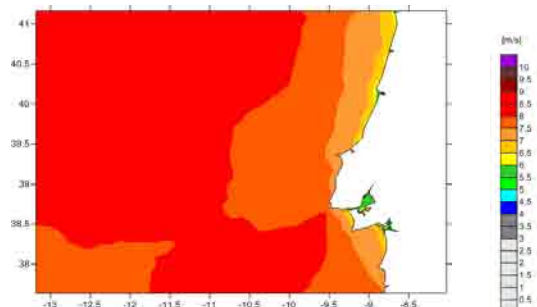


Figure 16: WRF+Deviation matrix with Composite interpolation method (two grids as input).

Figure 17 depicts the difference between the results from both deviation matrices (figure 13 and figure 15) and table 2 illustrates the obtained statistics for three QuikSCAT points identified in the figure.

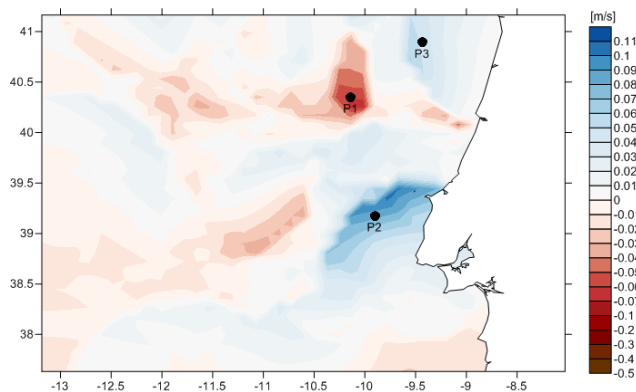


Figure 17: Difference between the deviations matrices from the Composite and the Kriging interpolation methods (Composite minus Kriging).

Table 2: Bias between QuikSCAT points and model results (considering model results minus QuikSCAT).

		QuikSCAT	WRF	Kriging	Composite
P1	Wind speed (m/s)	8.27	6.90	8.03	8.09
	Bias (m/s)	-	-1.37	-0.24	-0.18
P2	Wind speed (m/s)	7.77	6.83	7.78	7.70
	Bias (m/s)	-	-0.94	0.01	-0.07
P3	Wind speed (m/s)	7.58	6.46	7.69	7.64
	Bias (m/s)	-	-1.12	0.11	0.06

3.2 Evaluation

An evaluation of the validation quality provided by the two different spatial interpolation schemes is here presented. The independent wind data was taken from the anemometric mast located on Berlenga Island (see figure 1) which is operating since 2006. The anemometric tower is composed by an anemometer and a wind vane both installed at 20m (a.g.l.) and a second anemometer at 10m height (a.g.l.) corresponding to the meteorological reference height. An observational wind database from the simultaneous periods between the mast and the two model data inputs (QuikSCAT and WRF) was built in order to evaluate the spatial interpolator schemes. Table 3 shows the statistical validation results.

Table 3: Statistical validation results at anemometric mast point.

				Case A		Case B	
	WRF	QuikSCAT	Mast	Kriging	Composite	Kriging	Composite
Mean (m/s)	6.58	7.56	7.27	7.33	7.28	7.44	7.31
Bias (m/s)	-0.69	0.29	-	0.66	0.01	0.17	0.04
SCORE (%)	-	-	-	99.24	99.97	93.93	99.66

4. Conclusions

Two statistical interpolation schemes were used as a spatial validation technique to infer the uncertainties in the wind flow from the WRF mesoscale model results. A comparison of the Kriging interpolation method against the Composite method using two different case studies was performed. To interpret and characterize the spatial quality of both statistical schemes, some of the QuikSCAT satellite data was used as observational reference.

For case study A, the bias of the two methodologies at the selected points (table 1) shows that the Composite method has better performance on all studied cases. This hasn't been observed on case study B, where Kriging shows a better performance on the blue areas, depicted in figure 17, (which are represented by points P2 and P3 of table 2) and the Composite method shows a better performance on the red areas. Comparing all Kriging and Composite results it is noted that maximum bias values are always obtained by the Kriging interpolation method.

The performance of both statistical interpolator schemes is assessed via an independent anemometric mast for the period between 2006 and 2009. Results show a very similar behavior (scores between 99% - 100%) for both spatial methods when all the available reference data was used (case study A). On case study B, the Composite method has achieved a performance near 100% against the 94% of the Kriging method.

The high scores obtained with both statistical interpolator schemes enhance the fact that, inferred satellite wind data for the region around the meteorological mast of Berlenga has good quality. It is appropriate for assimilation studies on regional mesoscale models like wind atlases studies, offshore wind power prediction or even for characteristics studies of the long term wind behavior for the Atlantic coast of Continental Portugal.

5. Acknowledgements

The results and the meteorological and satellite data included in this study are part of the EU FP7 NORSEWInD project from which the authors are partners. The authors would also like to acknowledge the project ROADMAP WW (PTDC/SEN-ENR/105403/2008), FCT funded (Portuguese Foundation for Science and Technology).

References

1. W.C. Skamarock, J.B. Klemp, A time-split nonhydrostatic atmospheric model for weather research and forecasting applications, *J. Comp. Phys*, 227: 3465-3485, 2008.
2. Perry, K. L., et al. SeaWinds on QuikSCAT level 3 Daily, Gridded Ocean Wind Vectors. (JPL Seawinds Project) – Guide Document D-20335, version 1.1. Physical Oceanography DAAC, Jet Propulsion Laboratory, California Institute of Technology, October 1995. Document url: http://podaac.jpl.nasa.gov:2031/DATASET_DOCS/qscat_l3.html
3. <http://www.norsewind.eu>
4. Abramowitz, M., and Stegun, I. *Handbook of Mathematical Functions*, Dover Publications, New York, 1972
5. Cressie, N. A. C., *The Origins of Kriging*, Mathematical Geology, v. 22, p. 239-252, 1990.
6. P. Costa and A. Estanqueiro. A Methodology to Compute Wind Resource Grids in Complex Terrain Based on Multiple Anemometric Stations, EWEC, Madrid, 2003.

The “Wind and Ports” project for wind energy assessment and forecast: the case of the Port of Genoa

M. Burlando¹, M. Tizzi¹, S. Navone¹, G. Solari¹ and G. Canepa²

¹*Department of Civil, Chemical, and Environmental Engineering, University of Genoa, Via Montallegro 1, 16145 Genoa, Italy, massimiliano.burlando@unige.it, marco.tizzi@unige.it, solari@dicat.unige.it*

²*Port Authority of Genoa, Stazione Marittima, Ponte dei Mille, 16126 Genoa, Italy, g.canepa@porto.genova.it*

Abstract – The present paper arises from the successful experience of the European Project “Wind and Ports”, which mainly focused on the forecast of wind for the management and the safety of port areas. This project lasted 3 years and it involved 6 partners, i.e. the University of Genoa and the Port Authorities of Genoa, La Spezia, Livorno, Savona (Italy), and Bastia (France), with the aim of monitoring and predicting the wind in the main ports of the northern Tyrrhenian Sea for the operational security of port areas. The activities developed at each port within the context of this project consisted in the realisation of: an advanced in situ wind monitoring network; a wind velocity statistical analysis; a medium-term wind velocity forecast (0-3 days) system; a short-term wind velocity forecast (0-1 hour) system; a web-based GIS system realized to make the products of the project directly available to the end-users. Among several opportunities, all these products can be used as building blocks for further applications focusing on wind energy exploitation in coastal areas and in the near offshore. In particular, according to the project results, the statistical analysis has been used for the evaluation of the wind energy production and the efficiency of more than fifty different wind turbines in the Port of Genoa, and three different wind farms have been proposed adopting a small-size, medium-size, and large-size wind turbine. Further applications for predicting the wind energy at an operational level, which is important to promote the smart management of electrical grids, to allow the participation in the day-ahead electricity market, and to plan the maintenance of the wind turbines, are currently on-going and under validation.

1. Introduction

Seaport areas, in general, are very often exposed to wind velocities relatively higher than the surrounding inland, which is quite obvious because of the lower roughness of the sea with respect to land (see for example Wieringa, 1993, for some z_0 values of different terrain types). From the Italian Wind Atlas (<http://atlanteoelico.rse-web.it/viewer.htm>) it is evident that the Northern Italy is characterised by rather low mean annual wind speed values, except on top of the ridges and in coastal areas. Moreover, in the Northern Tyrrhenian, the former areas often belong to protected zones whereas the latter ones are usually considered of particular interest for tourism, so that the integration of wind farms into the territory is rather complicated. All these aspects make seaport areas very attractive for wind energy exploitation as they have relatively high wind potentials and, at the same time, wind turbines have limited impacts there because the big ports of the Northern Tyrrhenian are mainly industrial ports.

The original structure of the “Wind and Ports” project is depicted in the grey parts of Figure 1. The project is based on three tools as main input wind data (level A): historical databases obtained from long-period records of wind measurements; data from the Global Forecast System (GFS, see <http://www.emc.ncep.noaa.gov/index.php?branch=GFS>); wind data provided by monitoring networks installed in the port areas.

All this information is processed by means of different numerical models in order to derive the main products of the project (level B): a statistical characterisation of the port areas concerning current and extreme values; a medium-term wind forecasting system (up to 3 days ahead); a short-term wind forecasting system (up to 90 min ahead). A detailed description of the numerical modelling tools used in this project is beyond the scope of the present paper: only a brief description and references are included where needed. Finally, a web-based GIS system (level D) has been realised to make the aforementioned products available to the port operators. A short description of the project is provided in Section 2 of the present paper.

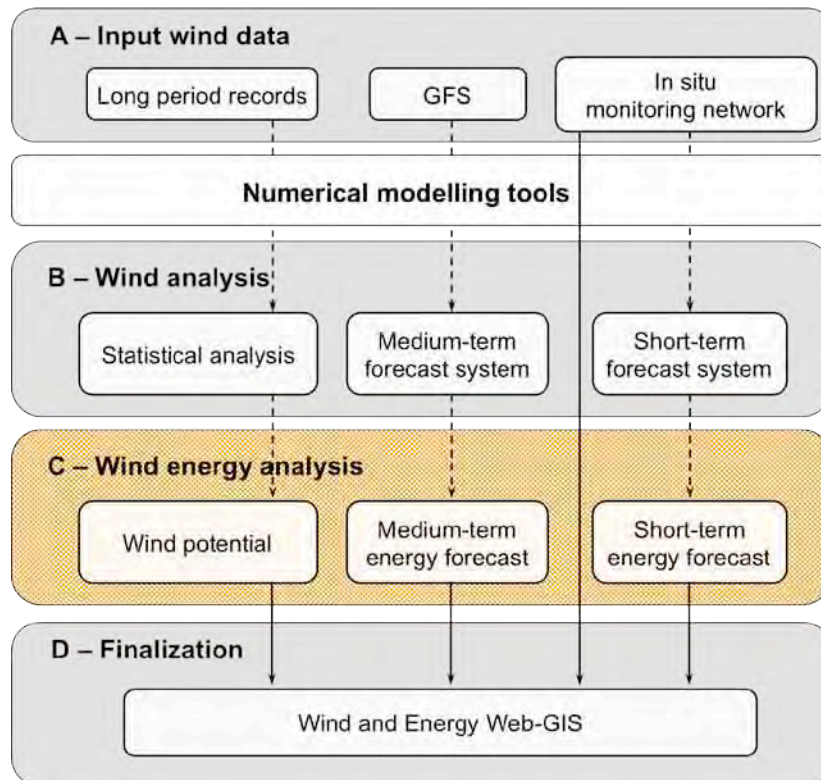


Figure 1: Scheme of the “Wind and Ports” project (grey) and the new module for wind energy analysis (yellow).

From the products of this project, further applications can be developed, for example concerning the realisation of a complete system for wind energy exploitation (level C). In particular, the statistical analysis performed during the project “Wind and Ports” may be used to design the wind farms in terms of wind potential evaluation and layout optimisation, whereas the forecast tools could be used for the management of the farm. At present, only the tool to calculate the wind potential has been implemented. This topic, which is also the focus of the present paper, is described in Section 3. The two forecast systems for medium- and short-term wind energy prediction are currently under development.

2. The “Wind and Ports” project

The main input wind data (level A of Figure 1) and the main products of the project (level B and level D of Figure 1) are described in the following Sections 2.1 and 2.2, respectively. The different numerical modelling tools used to obtain the aforementioned products are briefly described in the corresponding sections.

2.1 Input wind data

The project is based on three different kinds of wind data as input to the statistical analysis performed and to the numerical models used to realise the project's products (see Section 2.2). These input wind data consist of historical data bases obtained from long-period records of wind measurements (Section 2.1.1), wind data provided by the Global Observing System (GOS, <http://www.wmo.int/pages/prog/www/OSY/GOS.html>) of the World Meteorological Organization (Section 2.1.2), and wind data provided by the monitoring networks installed in the port areas (Section 2.1.3).

2.1.1 Long-period wind measurements

A set of 13 anemometric stations, shown in Figure 2, located in the surroundings of each port has been selected to obtain information about the wind climate of the port areas through their long-period records. Every station includes records of wind intensity and direction and, in some cases, of atmospheric pressure and temperature. The time series of the mean wind speed and direction have been corrected and analysed in order to determine the parent and extreme probability distributions at the anemometric sites and then they have been used to calculate some statistical wind maps over the port areas (see Section 2.2.1).



Figure 2: Map of the Northern Tyrrhenian Sea indicating the 13 long-term anemometric stations used to study the wind climatology of the 5 port areas.

2.1.2 Global Observing System data

Atmospheric measurements collected regularly every day at 00, 06, 12, and 18 UTC¹ all over the world are available to the international scientific community through the World Weather Watch programme of the World Meteorological Organization. These measurements consist of observations taken on land, at sea, in the air and in the outer space by means of facilities owned and operated by the Member countries of WMO.

¹ The Universal Time Coordinate (UTC) is the primary time standard adopted in meteorology. It is synonymous with Greenwich Mean Time (GMT).

The set of facilities and methods for making meteorological and other environmental observations on a global scale available in a standard form in support of the different needs of the scientific community constitutes the Global Observing System (GOS). All this information is then distributed and exchanged through the Global Telecommunication System (GTS), which is the communications and data management component of the World Weather Watch programme. Finally, meteorological analyses and forecast products based on these data are elaborated through the Global Data-Processing and Forecast System, which is organised on a three-level structure, i.e. global, regional, and national, and involves many different international institutions.

Among these, the National Centers for Environmental Prediction of the USA manages the Global Forecast System, which acquires data from GOS and runs its own global circulation model to forecast the state of the atmosphere up to 16 days ahead. Then, GFS provides initial and boundary conditions to run limited area models wherever one needs over the Earth. In the context of the project “Wind and Ports”, the meteorological model WRF is used as main tool for the medium-term wind forecast system (see Section 2.2.2), so that data from GOS is used indirectly through the operational chain made up of GFS-WRF.

2.1.3 *In situ monitoring networks*

Each port area has been equipped by a series of anemometers, suitably distributed in the most exposed zones, which makes up of 5 inter-connected local monitoring network facilities. Figure 3 shows the network of the instruments, which is constituted by 22 bi- or tri-axial ultrasonic anemometers (circles). Besides, 9 anemometers co-financed by the Port Authority of Genoa will be added soon (squares in Figure 3), leading to a network of 31 instruments in total.



Figure 3: Anemometer stations installed in the 5 port areas: financed by the project (yellow circles) and by the Port Authority of Genoa (yellow squares).

The positions of the instruments have been chosen in order to cover homogeneously the port areas and to register as much as possible undisturbed wind velocities. The instruments are generally mounted on high-rise towers or at the top of buildings, with particular attention to avoid local effects affecting the measures. The sampling rate of the anemometers is set to 10 Hz, with the exception of the anemometers installed in the Port of Bastia, which record at 2 Hz. Wind measurements are collected with a precision of 0.01 m/s and 1° for intensity and direction, respectively.

A set of local servers, placed in each port authority headquarter, receives the measures acquired by the anemometers in their own port area, and elaborates the basic statistics on 10 min periods. Then each local server automatically sends raw data and statistics to a central server at the University of Genoa.

It is worth noting that the wind data measured by the anemometers installed in the port areas will be statistically significant from a climatological point of view only after several years of recordings, so that these data cannot be used to elaborate statistical wind maps over the port areas. However, these data are fundamental for the short-term wind velocity forecast system (see Section 2.2.3) and their transfer in real time is crucial to update the system in order to make it really operational.

2.2 Products of the project

In the framework of the project “Wind and Ports”, three main products have been developed and delivered, based on the different kinds of wind input data described in Section 2.1.

These products consist of the statistical analysis of long-term anemometric records in order to obtain a statistical characterisation of the 5 port areas (Section 2.2.1), the realisation of a medium-term wind velocity forecast system (Section 2.2.2), and the realisation of a short-term wind velocity forecast system (Section 2.1.3).

2.2.1 Statistical analysis of the port areas

The time series of the 13 long-term anemometric stations selected in the surroundings of the Ports of Savona, Genoa, La Spezia, Livorno, and Bastia (Section 2.1.1) have been used to evaluate the (directional and non-directional) parent and extreme distributions within the aforementioned 5 port areas.

This result has been achieved through proper numerical tools that transfer, by means of a set of so-called transmission coefficients, the single-point anemometric information available at the long-term stations to the points of computational grids defined for each port with a horizontal resolution of 80 m (50 m for Bastia) and 10 different heights above the ground level (2, 5, 10, 15, 20, 30, 40, 50, 100, and 150 m AGL). In general, the evaluation of the transmission coefficients appropriate for reconstructing a wind field starting from a few points can be carried out through analytical, numerical or experimental methods. In this project, the coefficients have been evaluated by two numerical models, namely WINDS (Burlando et al., 2007) and an improved and extended version of the procedures introduced by the Engineering Science Data Unit (ESDU, 1993). Both these models take into account the high-resolution topography and roughness of the area under consideration. In particular, WINDS has been used mainly to obtain the transmission coefficients (see also Burlando et al., 2010, and Freda and Solari, 2010) to map the wind at given points into the wind at a different set of selected points, i.e. the computational grids of the 5 ports, while the revised version of ESDU has been used to derive the transmission coefficients that map turbulence intensity and gust peak.

Using these transmission coefficients the long-period time series have been transferred to the points of the port computational grids. Then, for each point of the computational grids, the parent population has been analysed and regressed by means of the hybrid Weibull model in directional and non-directional form. As far as the extreme wind velocities are concerned, the process analysis has been adopted to evaluate the corresponding extreme distributions (non-directional analysis only). Figure 4 shows an example of statistical maps, e.g. the mean annual wind speed and the wind speed corresponding to 50 years of return period, for the Port of Genoa at 50 m AGL. The maps are represented by means of coloured points in order to show the horizontal resolution of the grid points of the computational grid used for the Port of Genoa.

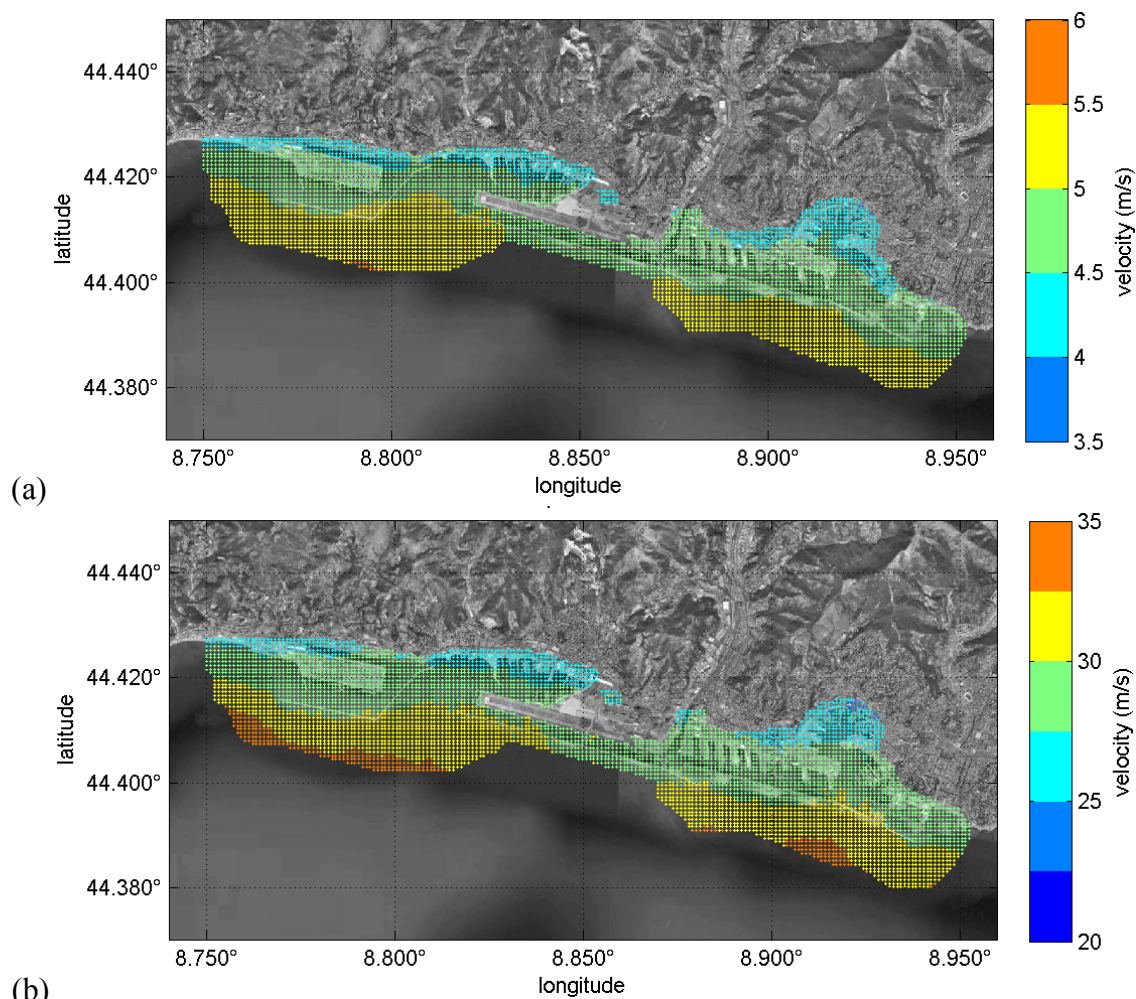


Figure 4: Statistical maps of the Port of Genoa at 50 m AGL: (a) mean annual wind speed; (b) wind speed corresponding to a return period of 50 years.

2.2.2 Medium-term wind velocity forecast system

The medium-term wind velocity forecast system is based on three different numerical models: the global circulation model of the Global Forecast System (already described in Section 2.1.2), the Weather Research and Forecasting model (WRF), and the WINDS model. This forecast system provides the user with wind forecasts up to +72 h ahead.

WRF is a next-generation mesoscale numerical weather prediction model, designed for operational forecasting as well as atmospheric research. Its solver integrates the compressible, non-hydrostatic moist Euler equations in flux form, which are conservative for scalar variables (Ooyama, 1990), formulated using a terrain-following hydrostatic-pressure vertical coordinate, as proposed by Laprise (1992). This meteorological model provides as prognostic variables also the two horizontal components and the vertical component of the wind velocity.

The diagnostic WINDS model is used to downscale the outputs of the larger-scale and lower-resolution numerical weather prediction model, i.e. WRF, to obtain higher-resolution wind fields onto the computational grids of the port areas.

The medium-term forecast system calculates the wind forecast, every day, from 00 UTC to +72 h with a time-step of 1 h, through 3 runs of WRF and 2 runs of WINDS. Each run provides the wind forecast over a smaller and smaller domain with increasing resolution.

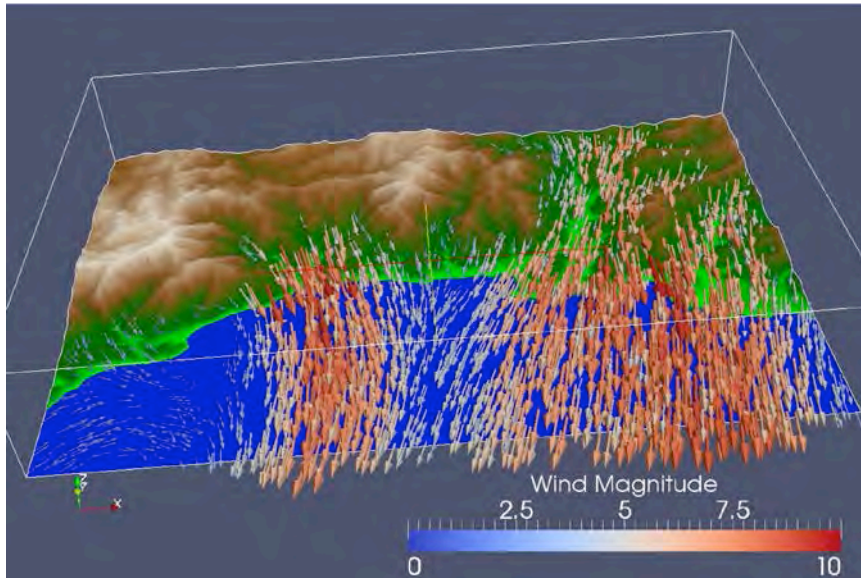


Figure 5: Three-dimensional wind field forecast obtained over the Port of Genoa by means of the coupled forecast system GFS-WRF-WINDS.

The largest domain of WRF covers all the Mediterranean Sea and the forecast is performed with the initial and boundary conditions of the GFS. Then, the second and third runs are performed over two additional grids with increasing horizontal resolution by means of a 2-way nesting technique. Finally, two runs of WINDS are performed by means of a 1-way nesting technique; the first run uses the boundary conditions from the finest-grid of WRF, whereas the second run uses the boundary conditions from the first run of WINDS. Figure 5 shows an example of the wind field forecast over the area of the Port of Genoa.

2.2.3 Short-term wind velocity forecast system

The short-term wind velocity forecast system is based, for each port area, on the data measured by the anemometers installed in the corresponding monitoring network (Section 2.1.3). This forecast is carried out by a two-step procedure: at first, short-term wind velocity forecasts are carried out at each anemometer of each port area; then, these results and the transmission coefficients (described in Section 2.2.1) are used to calculate the short-term wind velocity forecasts in the computational grids of each port.

The short-term wind velocity forecast procedure implemented for this project is founded on a fully probabilistic approach derived as an evolution of the one proposed by Freda et al. (2009). The forecast is based on a convenient conditional probabilistic model of the future values, given the wind speed at present. In particular, for each anemological station installed in the port areas, the wind speed at the forecast horizon $t_0 + n \Delta t$, where $\Delta t = 10$ min is the time between two subsequent mean wind velocity measurements and n is the number of time-steps, is evaluated based on the last wind speed values measured at time t_0 . The wind speed forecast is given in terms of a threshold that represents the maximum value expected in the forecast horizon with a given non-exceeding probability. For the “Wind and Ports” project, three forecast horizons, i.e. 30, 60, and 90 minutes, and three non-exceeding probabilities, i.e. 90%, 95%, and 99%, have been chosen. Further details on the probabilistic model can be found in Solari et al. (2012).

Analogously to the procedure adopted to transfer the anemometric records from the long-term stations to the computational grids of the port areas, the short-term wind velocity forecasts carried out at the anemometric stations of the monitoring networks are interpolated/extrapolated to the same computational grids by means of the transmission coefficients in order

to obtain short-term forecasting maps.

Figure 6 shows an example of the wind field forecast at 10 m AGL over the area of the Port of Livorno. Note that the difference between the higher wind speed values of the three anemometers in the northernmost part of the port area with respect to the values reported on the map is due to the fact that those anemometers are placed at heights much higher than 10 m AGL, which is the quote that the map refers to.

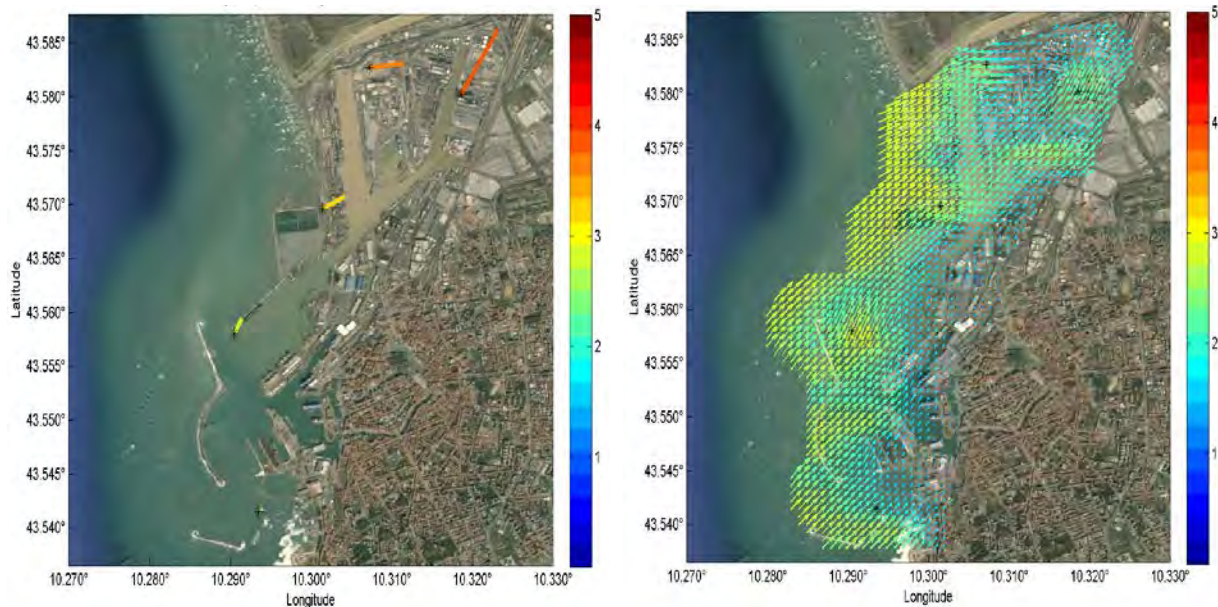


Figure 6: Wind field forecast at 10 m AGL over the area of the Port of Livorno: values of the wind speed and direction measured by the anemometers of the monitoring network (left); wind field forecast reconstructed from measurements (right).

3. Wind energy analysis of the Port of Genoa

The results provided by the project “Wind and Ports” can become the building blocks for further applications focused on wind energy exploitation in coastal and near-offshore areas. In particular, the results of the statistical analyses carried out for the Port of Genoa (as described in Section 2) can be exploited for the evaluation of the wind potential of that area and possible wind farms within it.

For this purpose, 51 different wind turbines have been considered, ranging from small to large size, with either vertical or horizontal axis (41 and 10 turbines, respectively). On the basis of the wind curve provided by the manufacturer, the turbine efficiency, the mean wind power and the annual energy potential have been evaluated for each turbine in every point of the computational grid defined for “Wind and Ports”. Section 3.1 provides a review of the main formulas for wind potential evaluation and presents the outcome for the Port of Genoa, together with a critical comparison between the results obtained for different wind turbines.

Moreover, three different wind farms have been proposed for a small-size, medium-size, and large-size wind turbine. The peculiarity of the Port of Genoa, which hosts an international airport within its territory, imposes a carefully study of urban regulations concerning the maximum height admitted under the area of airplane landing or take-off.

As an outcome, large-size turbines are allowed only in the western part of the port, whereas a favourable location for medium-size turbines is the central part of the port breakwater, in front of the airport runway; lastly, a wind farm with small-size turbines is proposed in the eastern part of the port, on the breakwater of the trade-fair marina.

For each wind farm different wind turbines and different configuration has been considered. It is worth noticing that the port breakwater is directed perpendicularly to the dominant wind directions, which correspond to the wind blowing from North and South-East, thus allowing the minimization of wind-turbines spacing (set to $4D$ here, D being rotor diameter). Section 3.2 presents a case study for the hypothetical wind farm with large-size wind turbines located on the Voltri breakwater, in the western end of the Port of Genoa.

3.1. Wind potential evaluation

As described in Section 2, a virtual long-term wind database has been obtained in every point of the port grid by transferring the long-term time series of the Genoa Airport. Then, statistical analyses have been carried out for each database. More precisely, the current-values distribution has been regressed by means of the hybrid Weibull model (Solari, 1996), which describes the probability density function (pdf) of the mean velocity as

$$f_v(v) = p_0 \delta(v) + (1 - p_0) \frac{k}{c} \left(\frac{v}{c} \right)^{k-1} e^{-\left(\frac{v}{c} \right)^k} \quad (1)$$

where p_0 is the probability of wind calms and k and c are the shape and scale parameters of the model.

The mean power density per unit area, ρ , is evaluated as

$$\rho = \frac{P}{A} = \frac{1}{A} \int_0^{\infty} \frac{1}{2} \rho A v^3 f(v) dv = \frac{1}{2} \rho c^3 \Gamma\left(\frac{k+3}{k}\right) \quad (2)$$

where P is the annual mean power of the wind, ρ is the air density, $f(v)$ is the velocity pdf described by the hybrid Weibull model (Eq. 1) and Γ is the Gamma function. The mean power density provides an estimate of the location of wind resource in the port area, i.e. a wind potential evaluation independent of the choice of a particular wind turbine. Figure 7 shows the map of the mean power density in the Port of Genoa at 50 m AGL. As expected, the power density of wind increases moving off the coast line. Moreover, higher values are observed in correspondence of some valleys in the western end of the port area (Leira and Cerusa Valleys), in the central part (Polcevera Valley) and in the eastern end (Bisagno Valley).

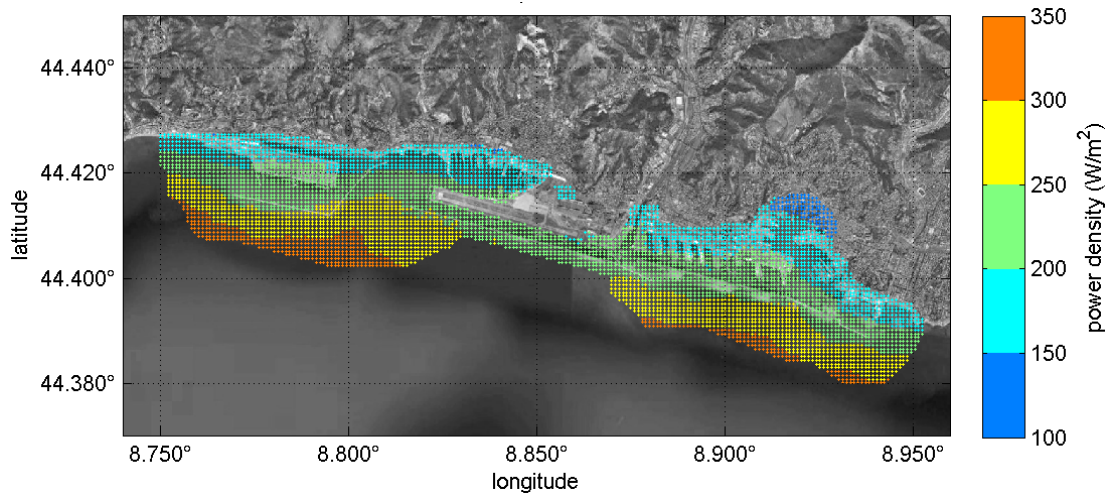


Figure 7: Mean power density in the Port of Genoa at 50 m AGL.

The evaluation of the wind potential associated to a particular wind turbine can be addressed by highlighting three different, however connected, aspects, i.e. turbine efficiency, operational mean power and annual energy.

The turbine efficiency, e , is defined as

$$e = \int_0^{\infty} \frac{P(v)}{P_{\text{rat}}} f(v) dv \quad (3)$$

where $P(v)$ is the power curve of the wind turbine and P_{rat} is its rated power. The turbine efficiency can assume values between 0 and 1 (when the turbine operates all the time at the nominal power), so that it gives a measure of the most suitable turbines for a particular site.

The operational mean power, \bar{P} , is defined as

$$\bar{P} = \int_0^{\infty} P(v) f(v) dv = P_{\text{rat}} e \quad (4)$$

Lastly, the mean annual energy, E , is defined as

$$E = T \int_0^{\infty} P(v) f(v) dv = T \bar{P} = T P_{\text{rat}} e \quad (5)$$

where T is equal to 1 year and is usually expressed in hours. Clearly, e , \bar{P} and E are proportional, the scale factors being P_{rat} between \bar{P} and e and T between \bar{P} and E .

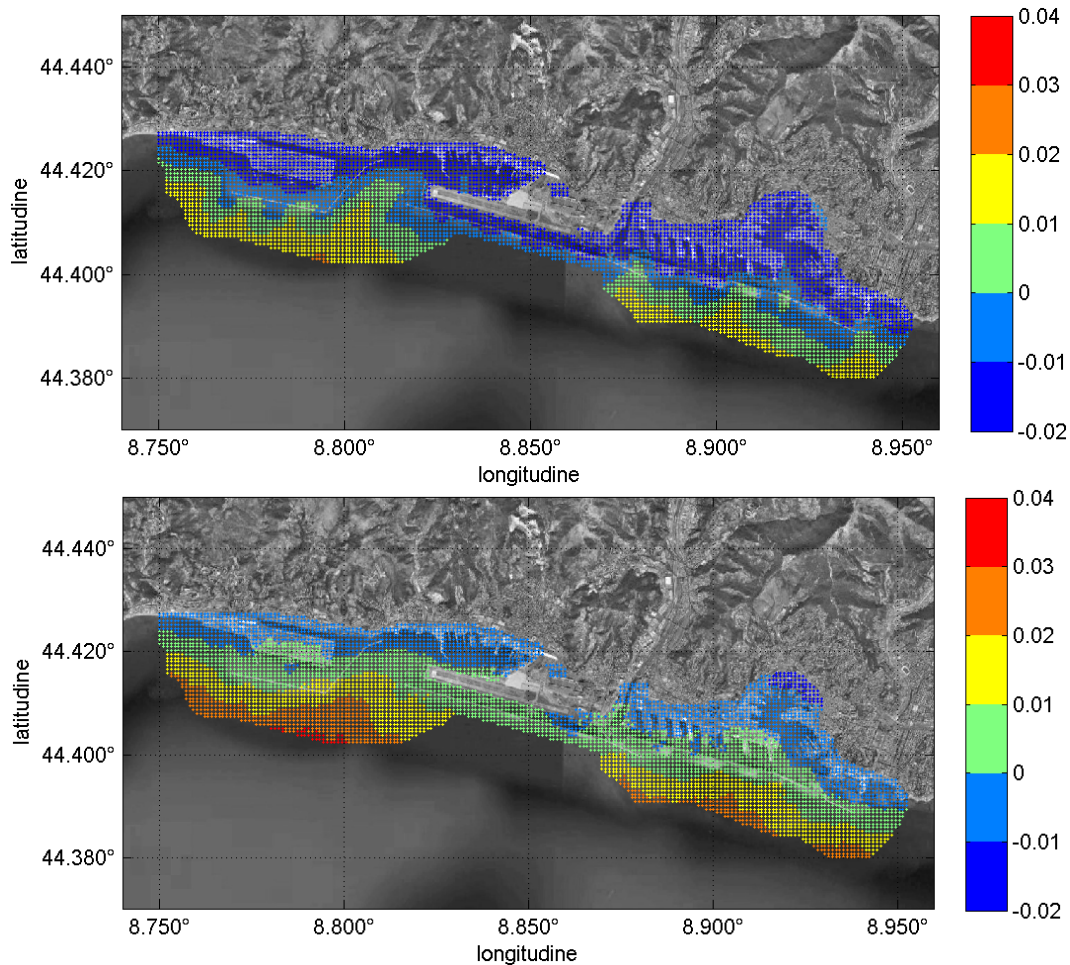


Figure 8: Efficiency difference between ENERCON E-33 and FALCON 600 W turbines at 10 m AGL (above) and at 50 m AGL (below).

The three quantities have been computed for each considered turbine in every point of the port computational grid, obtaining a series of maps of the wind potential of the Port of Genoa. A critical comparison between these maps allows a rational choice of the proper turbine in each area. As an example, Figure 8 shows two maps of the efficiency difference between two very different wind turbine, ENERCON E-33 (horizontal axis, $P_{rat} = 330$ kW) and FALCON 600 W (vertical axis, $P_{rat} = 0.6$ kW) at two different heights above ground level, i.e. 10 and 50 m AGL, respectively. The two maps show that the second turbine is more suited to an urbanized context (negative values correspond to higher efficiencies of the FALCON turbine), whereas the first one is more efficient only over the sea and the breakwater at 10 m, but over more than half of the area at 50 m AGL.

3.2. A wind-farm case study

Three wind farms have been proposed in the Port of Genoa, in three different areas of the port and with three different turbine sizes. The present section reports the case study of the wind farm hypothesized on the western end of the port breakwater in the Voltri area.

As anticipated, a proposal of possible wind farms in the Port of Genoa requires a combined study of several urban regulations together with the presented evaluation of wind potential. In particular, the presence of the airport in the central part of the port area imposes strict constraints on the maximum height admitted for any building in a large elliptic area surrounding the airport, as represented in Figure 9. Thus, large-size wind turbines are allowed only in both western and eastern ends of port domain (magenta and grey grids in the map); moreover, only the planned western breakwater end is suitable for a wind farm, because the eastern part has other urban constraints that do not allow a large wind farm to be built there. Besides, this is one of the windiest areas in the port.

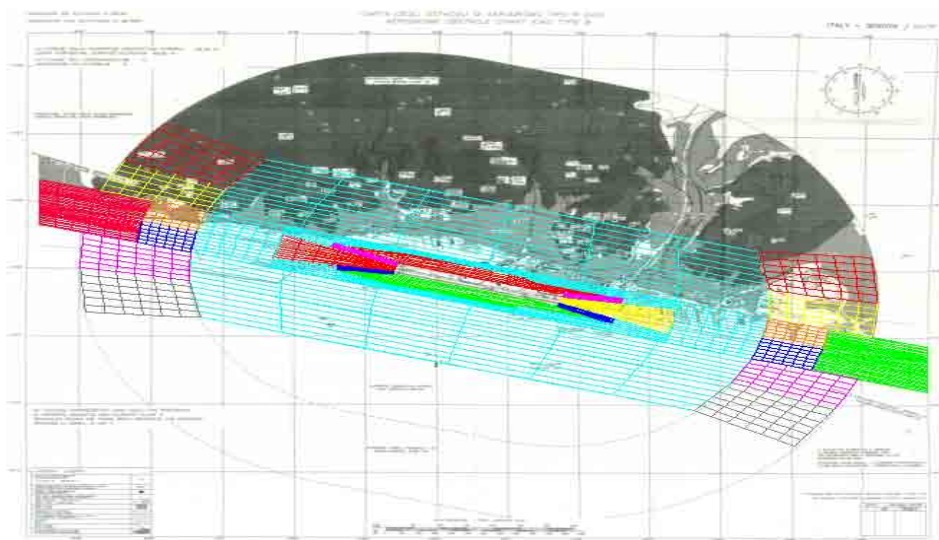


Figure 9: Maximum height admitted for the buildings surrounding Genoa airport (colour grids) and map of the main obstacles for airplane landing/take-off (grey background).

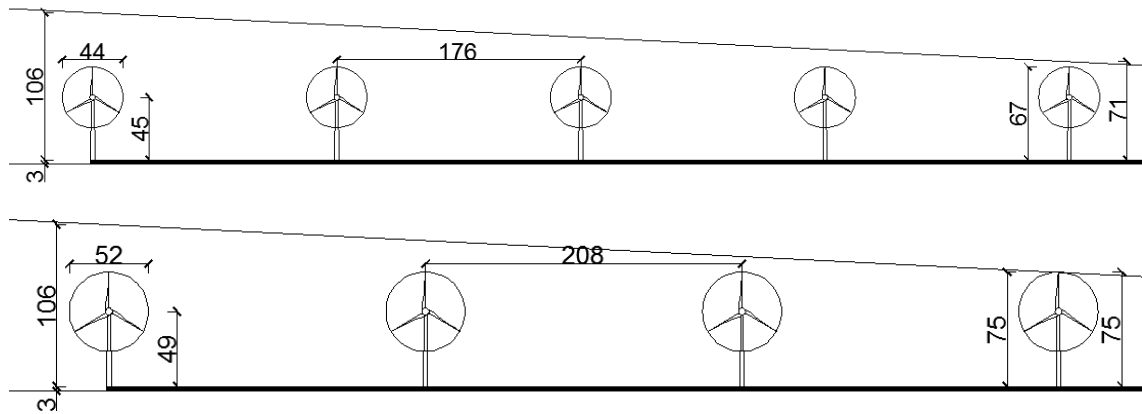


Figure 10: Two hypothetical configurations for a wind farm on the Voltri breakwater in the western part of the Port of Genoa: above, ENERCON E-44 turbines; below, VESTAS V52 turbines. The upper line is the maximum height admitted by the airport regulations.

The selected area is 1223 m long; there the maximum height admitted varies linearly from 70 to 106 m above the breakwater, which is 3 m above the sea level, as sketched in Figure 10.

A comparison between efficiency and annual energy production in the western end of the planned breakwater at 70 m above ground level has been carried out in order to evaluate the most efficient and the most productive wind turbines.

Table 1 provides a list of the first 6 turbines in both rankings. The two rankings are very different: the efficiency ranking presents small-size turbines in the first positions, due to the fact that their power curves are steeper for lower winds and the Weibull distribution in this area is characterised by high frequencies for wind velocities lower than 5 m/s.

For a more specific evaluation of energy production of the wind farm, we have chosen those wind turbines with an energy production larger than 1 GWh per unit (Table 1).

The spatial distance between wind turbines has been set to $4D$, and different configurations (even for the same turbine) have been considered depending on the rotor diameter, the hub height and the number of turbines.

Figure 10 presents two examples of hypothetical configurations.

Table 1: List of the 6 most efficient (left) and most productive (right) wind turbines on the western end of the Voltri breakwater in western part of the Port of Genoa.

Model	Efficiency [%]	Model	Energy [GWh]
S 343	49.5	GEV HP 1 MW	2.06
AV-7	43.6	ENERCON E-53	1.88
EOLICAR E 20 kW	34.4	V52	1.70
EOLICAR E 25 kW	31.0	ENERCON E-48	1.65
GARBI 150/28	31.0	ENERCON E-44	1.47
Mistral 1000 W	30.2	ENERCON E-33	0.71

Table 2: Ranking of all the turbine configurations considered for the wind farm proposed for the Voltri breakwater in the western part of the Port of Genoa. For each wind turbine, only the most productive configuration, in terms of rotor diameter, hub height and turbine number, is reported.

Model	Total annual energy [GWh]	Turbine number	Single-turbine annual energy [GWh]	Single-turbine efficiency [%]
E 44	7.02	5	1.40	17.8
V 52	6.41	4	1.60	21.5
E 48	6.22	4	1.55	22.2
GEV HP	4.00	2	2.00	22.8
E 53	3.64	2	1.82	25.9

The results for all the considered configurations are listed in Table 2.

Due to the lower hub height of ENERCON E-44, i.e. 45 m AGL, and the relatively small rotor diameter, i.e. 44 m, it is possible to install 5 wind turbines while satisfying both the constraints of maximum height admitted by the airport regulations and an inter-turbine distance of 4 rotor diameters. As the other wind turbines are larger than ENERCON E-44, the overall number of turbines in their wind farms has to be reduced, so that the total annual energy production is lower even if the annual energy produced by a single turbine is larger.

The final wind farm configuration, however, has to be chosen considering also other economical and environmental constraints that are not taken into account in the present analysis.

4. Conclusions

The present paper describes an application of the “Wind and Ports” project for wind energy exploitation. A statistical analysis has been performed for the evaluation of the wind energy potential of the Port of Genoa, taking into account more than 50 different wind turbines, both horizontal and vertical axis wind turbines. Three different wind farms have been proposed for a small-size, medium-size, and large-size wind turbine, respectively. However, only the larger-size wind farm has been described here.

Moreover, the medium- and short-term forecast systems, described in Section 2, could be used for predicting the wind energy at an operational level, which is important to promote the smart management of electrical grids, to allow the participation in the day-ahead electricity market, and to plan the maintenance of the wind turbines. However, the application of the two forecast systems for wind energy prediction has not been performed yet and it is under development.

The project “Wind and Ports” is very promising for the realisation of a complete system for wind energy exploitation, from the wind potential evaluation and layout optimisation to the operational management of the wind farms, and it is expected to become an important tool for the development of wind energy in these areas in the next future. Moreover, wind data acquired in these coastal areas will provide important information about the wind climate of the Northern Tyrrhenian Sea, which could be used to update the estimates of the Italian Wind Atlas as well as to provide new insights for floating or fixed offshore wind energy exploitation.

References

1. J. Wieringa. Representative roughness parameters for homogeneous terrain. *Boundary Layer Meteorol.*, 63: 323-363, 1993
2. M. Burlando, E. Georgieva and C.F. Ratto. Parameterization of the planetary boundary layer for diagnostic wind models. *Boundary Layer Meteorol.*, 125: 389-397, 2007.
3. M. Burlando, A. Freda, C.F. Ratto and G. Solari. A pilot study of the wind speed along the Rome-Naples HS/HC railway line. Part 1 — Numerical modelling and wind simulations. *Journal of Wind Engineering and Industrial Aerodynamics* 98: 392-403, 2010.
4. A. Freda and G. Solari. A pilot study of the wind speed along the Rome-Naples HS/HC railway line. Part 2 — Probabilistic analyses and methodology assessment. *Journal of Wind Engineering and Industrial Aerodynamics* 98: 404-416, 2010.
5. K.V. Ooyama. A thermodynamic foundation for modeling the moist atmosphere. *Journal of the Atmospheric Sciences* 47: 2580-2593, 1990.
6. R. Laprise. The Euler equations of motion with hydrostatic pressure as an independent variable. *Monthly Weather Review* 120: 197-207, 1992.
7. A. Freda, L. Carassale and G. Solari. A conditional model for the short-term probabilistic assessment of severe wind phenomena. In: *CD Proceedings of the 5th European and African Conference on Wind Engineering*, Florence, Italy, 2009
8. G. Solari, M.P. Repetto, M. Burlando, P. De Gaetano, M. Pizzo, M. Tizzi and M. Parodi. The wind forecast for safety management of port areas. *Journal of Wind Engineering and Industrial Aerodynamics* 104-106: 266-277, 2012.

Session 2: Marine Resource Simulation, Modelling

Chairmen: F. Cesari, A. Estanqueiro

An experimental test rig to simulate hydrodynamic forcing on floating offshore wind turbine platforms - I. Bayaty, M. Belloli (Dpt. di Meccanica, Politecnico di Milano, Milan (IT)), S. Giappino (CIRIVE, Politecnico di Milano, Milan (IT))

Italian Wind Atlas WebGIS and Technical-Economic Calculation Module - L. Serri, D. Airoidi, C. Casale, E. Lembo, G. Stella (RSE Spa., Milan (IT))

Using data assimilation in mesoscale numerical modeling to map offshore wind resource - M. Fernandes, P. Costa, T. Simões, A. Estanqueiro (LNEG-Laboratório Nacional de Energia e Geologia, Lisboa (PT))

Wave energy potential in the Mediterranean: the case of Pantelleria - L. Liberti (ISPRA-Institute for Environmental Protection and Research, Rome (IT)), A. Carillo, G. Sannino (ENEA - Ocean Modelling Unit, Rome (IT))

An experimental test rig to simulate hydrodynamic forcing on floating offshore wind turbine platforms

Bayati I.¹, Belloli M.² and Giappino S.³

¹*Dipartimento di Meccanica, 'Politecnico di Milano',
via La Masa 1, 20156 Milano, Italy, ilmas.bayati@mail.polimi.it*

²*Dipartimento di Meccanica, 'Politecnico di Milano',
via La Masa 1, 20156 Milano, Italy, marco.belloli@polimi.it*

³*CIRIVE, 'Politecnico di Milano',
via La Masa 34, 20156 Milano, Italy, stefano.giappino@polimi.it*

Abstract - The work presented in this paper reports the design and realization of a slider-crank based 2-DoF mechanism developed at Politecnico di Milano Wind Tunnel and devoted to simulate the motion of a floating wind turbine platform due to hydrodynamics forcing. As floating offshore wind farms are becoming objects of interest within the international scientific community, experimental tests have been increasingly demanding to support dynamics and structural numerical simulations; furthermore measurements on real prototypes are not negligible to validate complex prediction models because of the large amount of unknown and uncontrolled parameters. The motivation of this project must be investigated in the need of designing an experimental set-up to reproduce, in a fully controlled test environment, the combined effects of wind and hydrodynamic loads acting on a floating wind turbines.

1. Introduction

Offshore wind energy is increasingly focusing on deep water offshore wind turbines and particularly on floating platforms [11]. Different floating wind turbine platforms have been already preliminary designed in parallel with the study of their influence on the dynamics of “Megawatt Wind Turbines” [2], due to the combined effects of wave and wind loads on the structures. The development of highly complex simulation tools as multibody aero-servo-elastic codes allow to predict loads and frequencies of such structures, being a suitable guide for designers of megawatt floating wind turbines [7,8,9]. Nevertheless the need of a reliable validation of the above mentioned simulation codes requires the development of experimental campaigns in fully controlled test environment, in order to gather consistent information on the physics of such complex systems. Therefore scale models of floating wind turbines can be studied in facilities such as water tanks[1,3] or wind tunnels.

The latter has been chosen in this work (13.84 x 3.84 m Politecnico di Milano wind tunnel boundary layer test section) for its advantages in generating high quality wind profiles; the simultaneous hydrodynamic forces have been generated mechanically by a dedicated experimental rig.

2. Experimental Test Rig

Even if the real wave-structure dynamic interaction is surely more complex than that can be reproduced experimentally without testing the model in a water tank [1,3] in this work the design of a 2-DoF mechanism has been developed with the goal of creating a simple test rig but providing results physically understandable, being most of them not widely investigated yet. The test rig (Fig. 1) reproduces pitch/roll rotations and surge/sway displacements of a floating wind turbine scale model.



Figure 1: Wind turbine scale model on the test rig in the wind tunnel BL test section.

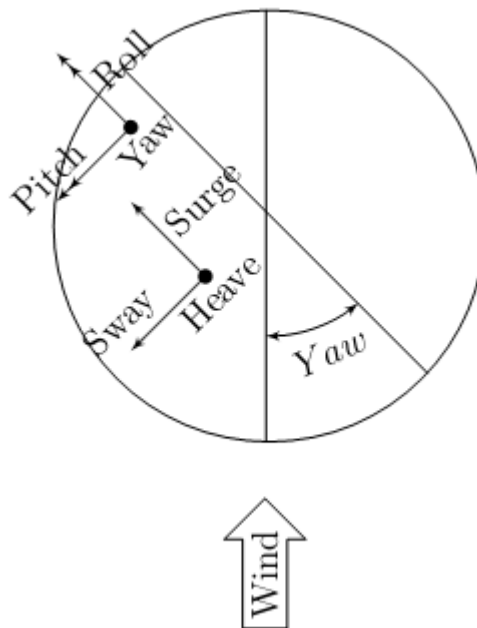


Figure 2: Top view sketch of wind tunnel turntable.

Such a mechanism has been mounted upon the turntable of the wind tunnel, that provides the possibility of rotating the wind turbine model with respect to the fixed wind direction, therefore different yaw angles can be investigated; more precisely yaw angles can vary statically within the experimental campaign when the tunnel is not blowing. In the Fig. 2 a self-explaining sketch of such a turntable is reported. Moreover pitch/surge and roll/sway coupled motions can be reproduced simply changing the configuration of the model with respect to the mechanism (Fig. 3).

3. Design Choices

The design choice of reproducing with such a mechanism some certain rotations and displacements instead of others is basically to place emphasis on the most influential movements of a floating wind turbine in terms of structural, dynamics and power aspects [10]; also the physics of wind-induced marine waves suggests that when wind appears over the free surface, water waves and turbulence are generated by shear stresses, more precisely turbulent diffusion promotes significantly mass and momentum transport beneath the interface between the water and air, significantly contributing on the generation of the wave itself. Consequently, the generated waves are typically co-aligned with the prevailing wind direction. This physical explanation can be consistently transposed to offshore environments where the floating wind turbines are operating. These aspects have greatly influenced the design of the 2-DoF mechanism, so that by setting the wind turbine model with the rotor shaft along the slider's lengthwise direction, as shown in the Fig. 1, the pitch and surge motions can be reproduced by the mechanism at issue. As previously said also different yaw angles can be investigated by rotating wind tunnel platform with respect to wind direction. Analyzing different yaw angles means considering particular environmental conditions where wave and wind direction are not perfectly aligned with respect to each other. The experimental rig also allows to provide hydrodynamic forcing responsible for sway and roll coupled motions, simply setting the wind turbine model perpendicularly with respect to the above mentioned configuration, see Fig. 3.

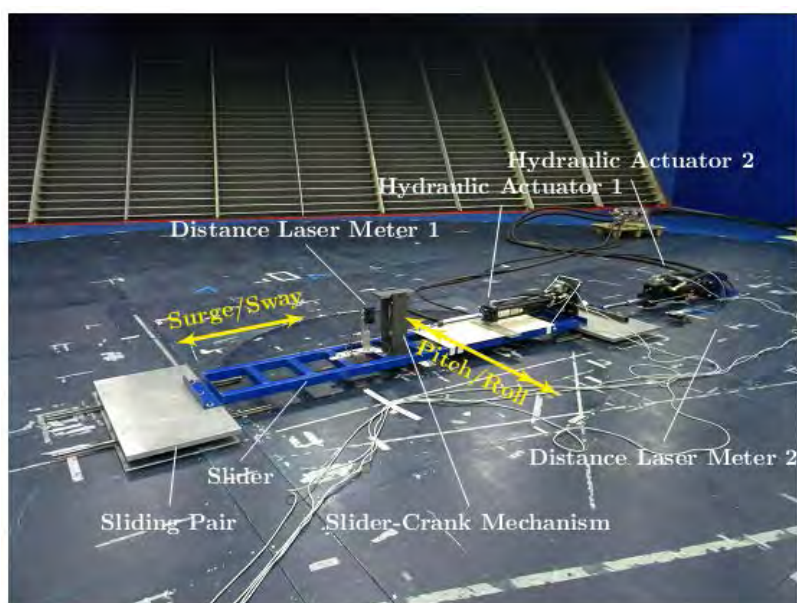


Figure 3: 2-DOF mechanism.

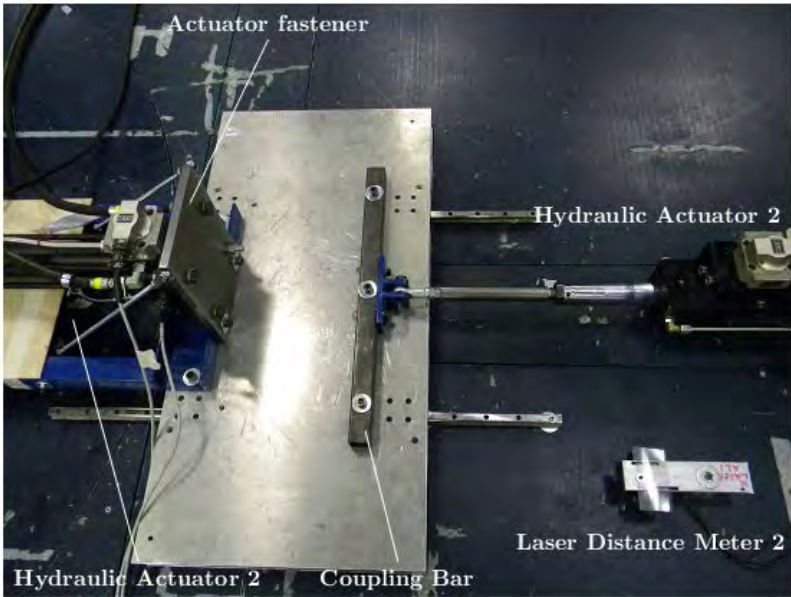


Figure 4: Details of the test rig.

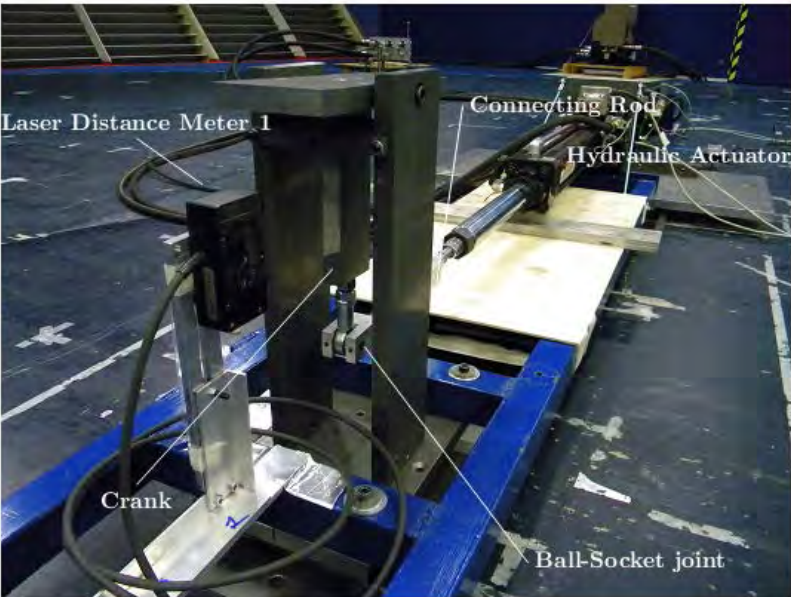


Figure 5: Details of the test rig.

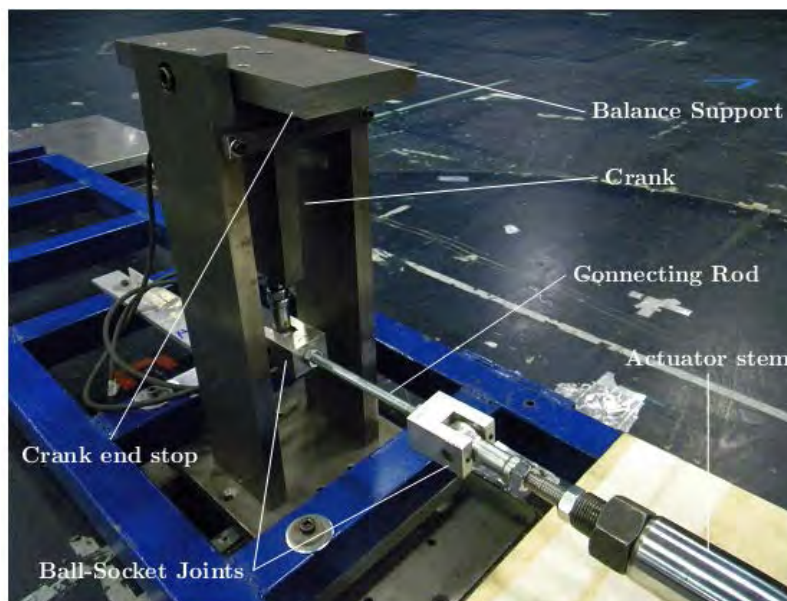


Figure 6: Details of the test rig.

3. Rig Components

In the Fig. 3 an overview of the main components of the mechanism are shown. The platform mainly consists of a long slider able to slide on a rail fixed to the ground. The linear displacement is provided by the MTS hydraulic actuator n° 2 (Tab. 2) providing the thrust to the slider by a coupling bar fixed on the slider plate, as shown in the Fig. 4. Another MTS hydraulic actuator (n° 1, Tab. 2) has been mounted upon the slider itself, bound to it by a fastening plate suitable for preventing the relative motion between the slider and the actuator due to inertial forces. The function of the latter actuator is to provide the rotation (pitch or roll) to the model. In order to convert linear displacement to rotation a slider-crank mechanism connected to the actuator and mounted upon the slider has been designed (Fig. 5, Fig. 6)

The slider of this mechanism is given by the actuator's stem, connected to the crank by connecting ball-socket joints and a connecting rod (Fig. 6); the ball-socket joints are suitable for bridging the inevitable misalignment between the slider and the crank. This obviously involves non-linearities in the kinematic chain of transmission, however this can be considered negligible in comparison with the displacements of the wind turbine nacelle. Moreover, as can it is shown in the Fig. 6, the excursion of the crank is limited by an end stop bar mounted for safety reasons, in order to prevent extreme rotations of the wind turbine model in cases of accidental wrong digital input signal by the control system of the actuators during the tests; a similar safety solutions has been developed for the linear stroke of the actuator n°1.

3.1 Measuring System

The wind turbine model is mounted upon this mechanism through a Ruag balance (Tab. 2) that it is in turn bound to the mechanism itself by an appropriate support, as shown in the Fig. 6 and Fig. 7. The coupling between the wind turbine tower and the balance is allowed by a shadow mask, ensuring the possibility of mounting the model in different configurations to provide surge/sway and pitch/roll motions, as previously mentioned.

Another balance (Ati, Tab. 2) has been installed in the nacelle (Fig. 7) in order to gather the aerodynamic forces acting on the rotor. Moreover the test rig involves two laser distance meters, as can be seen in Fig. 3 and Fig. 4, and two accelerometers mounted on the wind turbine nacelle. The laser distance meters consist in laser triangulation sensors M5L/50 and M5L/200 (see Tab. 2) to measure respectively the rotational and linear displacement. The signals coming from the laser acquisitions are fundamental for a correct phasing between the forces measured with balances and the displacements themselves, in the time domain, in order to avoid misunderstandings in the post-processing. Two capacitive accelerometers are also mounted on the turbine nacelle, one of them measures the accelerations along the shaft axis and the other one along the normal direction.

4. Wind Tunnel Validation Testing

For the sake of completeness in this section the results concerning a particular experimental configuration is reported. In the Fig. 7 a sketch regarding the surge motion investigation is shown. This experimental session has been carried out considering no yaw angular displacement between the wind tunnel platform and wind direction (see Fig. 2), so that the pure surge motion has been studied, being the wind direction parallel to the direction of the translational motion. The rotor angular velocity has been set to 16 rad/s for this test session. The rotor blade's length is 0.97 m.

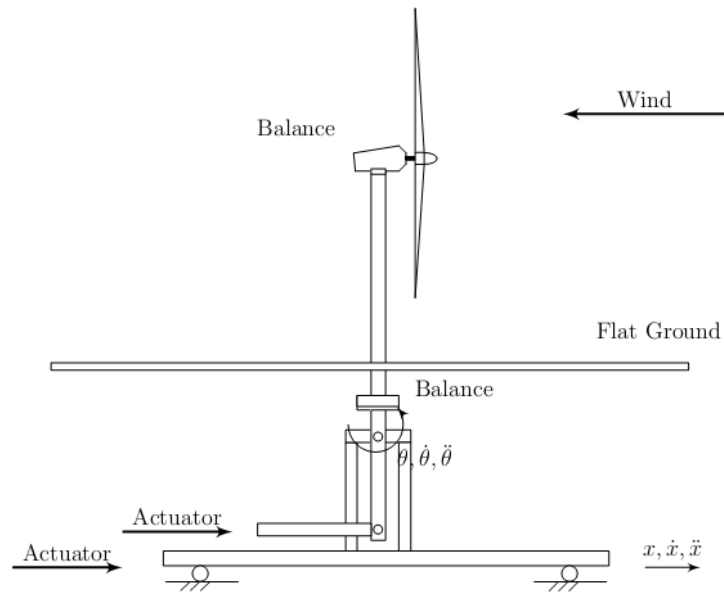


Figure 7: 2D-sketch of wind tunnel tests

Parameters	Units	Values			
Frequency (f)	[Hz]	0.2	0.4	0.6	1
Amplitude (A)	[mm]	10	20	40	80
Wind Speed (W)	[m/s]	4.5	5	5.5	6

Table 1: Characteristic values of the surge experimental campaign.

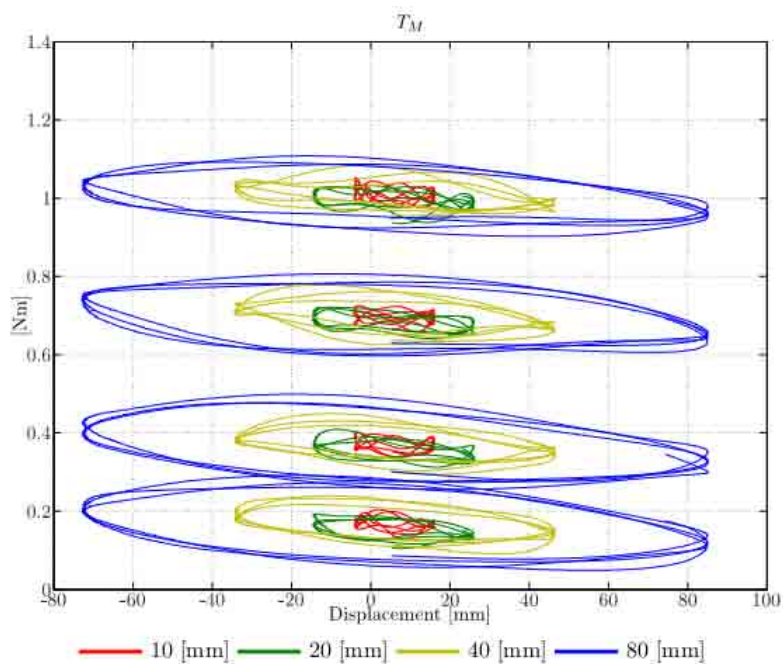


Figure 8: Motor torque for a sinusoidal imposed surge motion of 0.4 Hz at various amplitudes (Tab. 1).

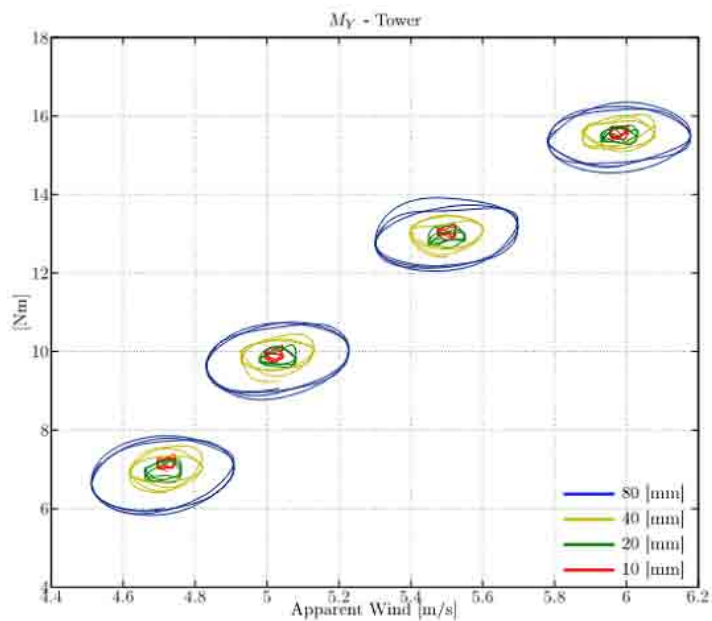


Figure 9: Torque at the base of the tower generated by drag force on the rotor: sinusoidal imposed surge motion of 0.4 Hz at various amplitudes as functions of apparent wind (Tab. 1).

Device	Full Scale	Sensitivity
Accelerometers	$\pm 20g \text{ m/s}^2$	100 mV/g
MTS Hydraulic Actuator n° 1	$\pm 125 \text{ mm}$	12.6 mm/V
MTS Hydraulic Actuator n° 2	$\pm 250 \text{ mm}$	25.4 mm/V
Laser M5L/50	$\pm 50 \text{ mm}$	2.5 mm/V
Laser M5L/200	$\pm 200 \text{ mm}$	10 mm/V

Table 2: Device data sheets.

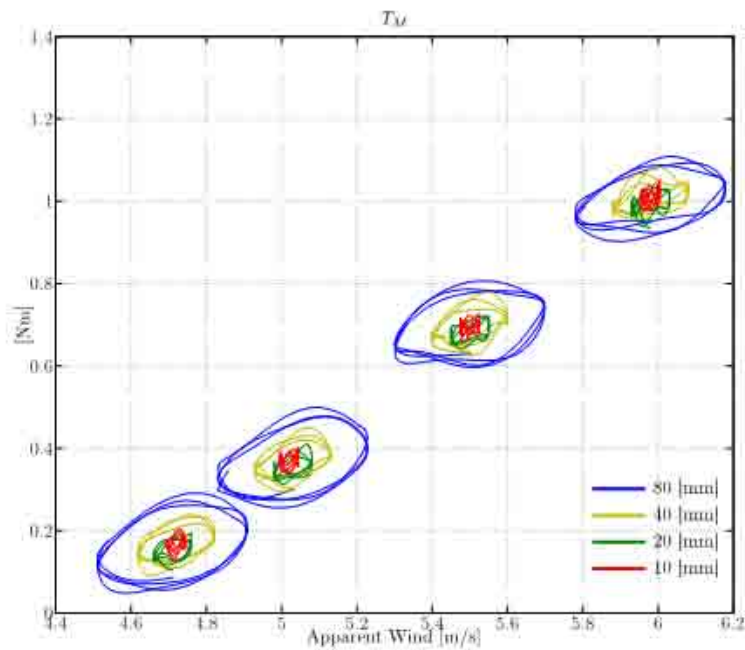


Figure 10: Motor torque for a sinusoidal imposed surge motion of 0.4 Hz at various amplitudes as function of apparent wind. (Tab. 1).

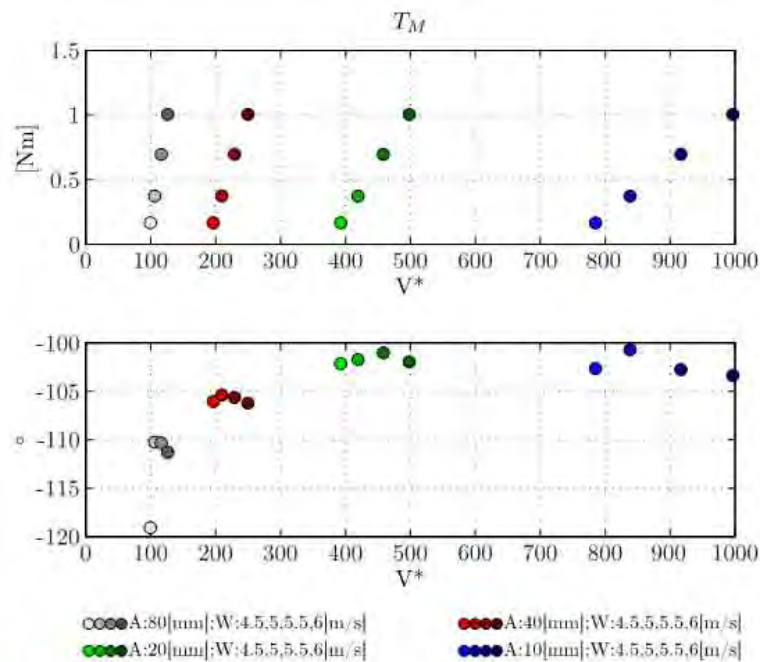


Figure 11: Motor torque: amplitudes and phases of frequency responses as functions of reduced velocity, for a sinusoidal imposed surge motion of 0.4 Hz (Tab. 1).

What can be easily appreciated from the Fig. 9 is a not linear relationship between the apparent wind acting on the blades and the generation of power in a floating wind turbine when a relative motion between the nominally laminar inflow and the generator itself occurs. These non-linearities are both connected, in terms of shape and slope, to the frequency and to the amplitude of the relative motion (see also Fig. 8)

In the Fig. 9 and Fig. 10 the forces have been plotted as functions of apparent wind, considering the contribution of both wind and platform motion speed: $v = w + \dot{x}$, where the terms are respectively the apparent wind velocity, wind velocity and the surge imposed motion velocity of the test rig. During the experimental campaign the parameters reported in the Tab. 1 have been widely investigated and the results have been conditioned by subtracting the forces coming from the related inertial "no-wind" measurements. This way the Fig. 8, Fig. 9 and Fig. 10 represent only the aerodynamic forces acting on the scale model. In the Fig. 11 the frequency responses of the motor torque have been represented, in terms of amplitudes and phases, as functions of reduced frequency V^* , where:

$$V^* = \frac{W}{fA}$$

Where W , f and A are respectively the wind speed, the frequency and the amplitude of the sinusoidal imposed surge motion. The Fig. 11 shows that by increasing the reduced velocity, the phase of the force, with respect to the corresponding displacement input, has mostly a quadrature component, so that the forces depending on the velocity of the fluid are mainly contributing on the aerodynamic forces, whereas the "in-phase" and "push-pull" components are negligible. This is consistent with the fact that increasing the reduced velocity deals with reducing the inertial mass-added effects.

5. Conclusion and Future Developments

The work presented in this paper shows the possibility of using a 2-DoF experimental rig to simulate the wave forcing on scale floating wind turbine platform within a wind tunnel facility. The experimental tests have been carried out in a wind tunnel boundary layer section of Politecnico di Milano, with the ability of a reliable control in the quality of the wind flow generated compared to other experimental facilities such as water tanks.

The results reported have shown non-linearities in the aerodynamic forcing on floating wind turbines due to hydrodynamic loads acting on the floating platform itself. This aspect can be investigated in further studies on the topic of the design of control system oriented to the minimization of dynamic effects of the floating platform on the power generation.

The surplus value of integrating this set-up with a "hardware-in-the-loop" real time system able to reproduce a platform motion consistently with wind and wave loads, allows to investigate more realistic test conditions; the test rig developed in this work can be improved by increasing the number of degrees of freedom.

Moreover this experimental rig can be used for specific wind turbine scale models to be preliminary tested in advance with respect to their final implementation, with the remarkable advantage of reproducing in a wind tunnel test session realistic wave and wind characteristics based on the statistical properties of the operating environment.

References

- [1] "Integrated Dynamic Analysis of Floating Offshore Wind Turbines," B. Skaare, T.D. Hanson, F.G. Nielsen, R. Yttervik, A.M. Hansen, K. Thomsen, and T.J. Larsen; European Wind Energy Conference, Milan, Italy, 2007.
- [2] Matha, D. Model Development and Loads Analysis of an Offshore Wind Turbine on a Tension Leg platform with a Comparison to Other Floating Turbine Concepts. NREL report NREL/SR-500-45891.
- [3] Cermelli C, Roddier D, Aubault A. Windfloat: a floating foundation for offshore wind turbines part ii: hydrodynamics analysis. OMAE2009-79231
- [4] S. Butterfield J. Jonkman W. Musial E.N. Wayman P.D. Scлавounos. Coupled Dynamic Modeling of Floating Wind Turbine Systems - Tech. rep. National Renewable Energy Laboratory, 2006.
- [5] F. Cheli G. Diana. Dinamica dei sistemi meccanici - Polipress 2010.
- Lugni C. Marino E. Borri C. Influence of wind-waves energy transfer on the impulsive hydrodynamic loads acting on offshore wind turbines Journal of Wind Engineering and Industrial Aerodynamics, 2011.
- [6] F.M Sinclair. Aerodynamic damping on offshore installation, a comparison of experimental measurements with theory - Journal of wind engineering and industrial aerodynamics, 1994.
- [7] J. Jonkman . Dynamics Modeling and Loads Analysis of an Offshore Floating Wind Turbine - Tech. rep. National Renewable Energy Laboratory, 2007.
- [8] J. Jonkman, S. Butterfield, W. Musial, and G. Scott Definition of a 5-MW Reference Wind Turbine for Offshore System Development. NREL/TP-500-38060
- [9] J. Jonkman. Definition of the Floating System for Phase IV of OC3. NREL/TP-500-47535
- [10] J. Jonkman Loads Analysis of a Floating Offshore Wind Turbine Using Fully Coupled Simulation. NREL/CP-500-41714.
- [11] S. Butterfield, W. Musial, and J. Jonkman, P. Scлавounos. Engineering Challenges for Floating Offshore Wind Turbines. NREL/CP-500-38776.

Italian Wind Atlas WebGIS and Technical-Economic Calculation Module

L. Serri, D. Airoidi, C. Casale, E. Lembo, G. Stella

RSE S.p.A., Via Rubattino 54, 20134 Milano (Italy),

tel. +39 02 39925285, fax +39 02 39925626, e-mail laura.serri@rse-web.it

Introduction

The Wind Atlas of Italy was developed by RSE in 2002 in collaboration with Genoa University and was updated in 2007 with the extension to offshore areas within 40 km from the coastline. It makes available 4 annual mean speed maps and 4 specific production maps at 25, 50, 75, 100 m a.g.l./a.s.l., with resolution of 1 km x 1 km, together with a map of the constrained areas. These maps have been implemented in a WebGIS application that allows public access to the stored information through Internet. In this application it is possible to navigate with standard zoom and panel functions on the map and also download the grid of the maps themselves. Through this application it is also possible to access and download the full dataset of wind measurements performed by RSE stations.

Moreover, an interactive technical-economic module can be activated in order to make technical and economic evaluations with reference to chosen wind turbine models installed at a given point starting from Wind Atlas data and/or user data. Since all these activities have been carried out within the framework of a national research project financed by the Research Fund for the Italian Electrical System under a contract agreement between RSE and the Italian Government, the WebGIS application has been built in Italian. More recently, however, an English version has also been implemented in order to address this product to an international context.

In the next chapters the methodology, the contents of the atlas and the principle functionalities of the WebGIS are described. Moreover two examples of the application of the technical-economical evaluation tool for one onshore and one offshore wind farm is reported. Lastly, a mention is done to the technical support (based on the information implemented in the wind atlas) given by RSE to Italian government in establishing regional targets for renewable energy production in order to share, among regions, the burdens ensuing from Italy's 17% target assigned by European Directive 2009/28/EC implementing the 20-20-20 policy of the EU ("Burden Sharing Decree").

1. Methodology and maps

A general atlas of Italy's wind resources has been developed by RSE in co-operation with the Department of Physics of the University of Genoa to provide local authorities and plant developers with a tool for singling out the best promising areas where the deployment of wind farms could be focused.

In the first work phase (2000-2002) the wind patterns all over Italy were simulated. A wind flow model (WINDS) was used to obtain preliminary wind maps from geostrophic wind data, taking into account orography and terrain roughness. These maps were validated by comparing wind speeds with those measured by 240 met stations. A full atlas (Atlante eolico dell'Italia) thus became ready, with maps of wind speed and specific energy production (MWh/MW).

In a second work phase (2006-2007), work was resumed to develop an improved, interactive version of the same atlas (ATLAEOLICO), including also offshore areas up to 40 km from the coastline. Wind data from another 176 stations were used to adjust the on-land wind estimates further.

Over the offshore areas, some more difficulty than on land was met in adapting the model maps, owing to the nearly complete lack of direct wind measures in the open sea.

Direct measurements were provided offshore only by few anemometers placed on buoys (which can be moored in shallow waters only) or mounted on oil drilling platforms in limited areas. Some indirect offshore wind speed estimates have also been considered, mainly coming from instruments (such as scatterometers) carried by satellites (such as the NASA satellite QuikSCAT) with a (quite low) accuracy varying with distance from the coast.

More recently, a map of the “Exclusion Areas” and a map of the “Existing Wind Plants” have been implemented.

2. The WebGIS and the Technical-Economical Evaluation Tool

Since 2007 the Italian Wind Atlas can be freely accessed through a WebGIS application [2] that allows an easy and wide distribution of research results and promotes the public participation. The WebGIS is an Internet based application that doesn't require any special software in order to be accessed by the final user and can be enriched with new information, data and results as soon as they are available.

More recently, an English version of this WebGIS has also been implemented in order to strongly enlarge its users addressing this product to an international context.

In Figure 1 the homepage of the interactive Wind Atlas of Italy is shown with an highlight to the main groups of functionalities.

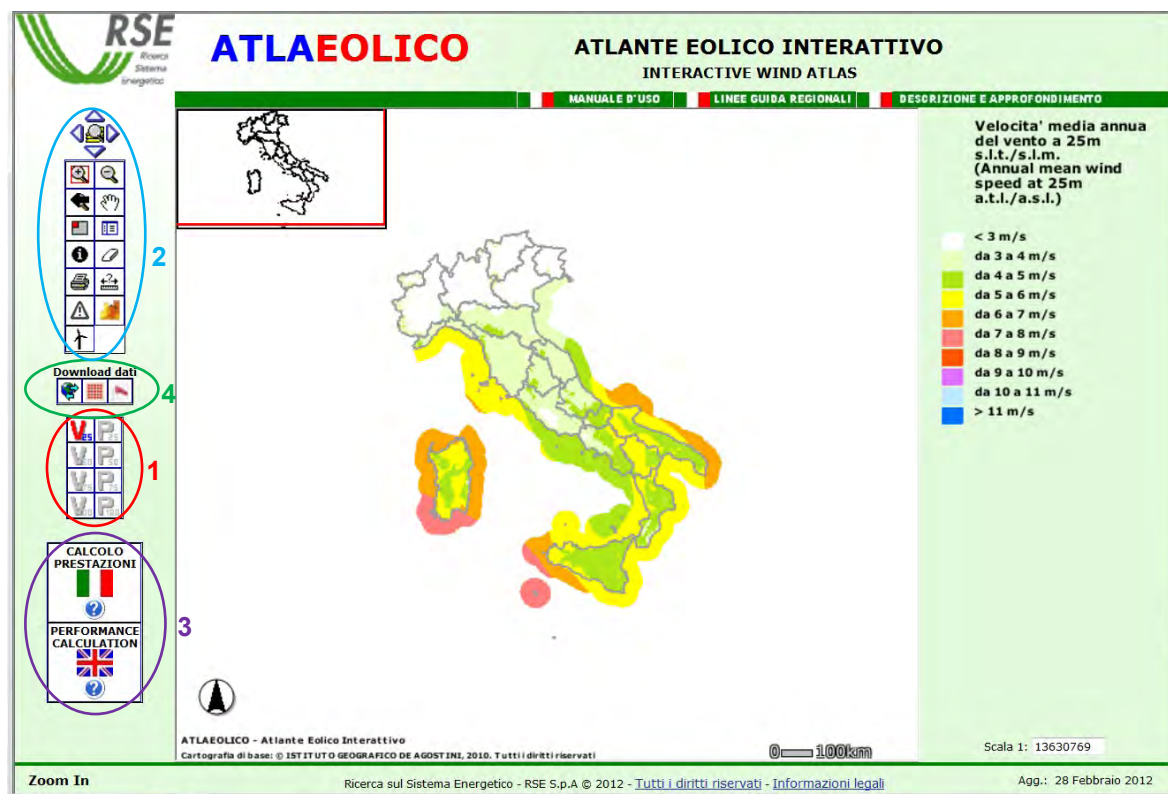


Figure 1: Image of the homepage of the WebGIS application of the Italian Wind Atlas. Main groups of information/functionality: 1) Wind Resource; 2) navigation tools + miscellaneous information; 3) technical-economical evaluation tool for wind farm evaluation; 4) download maps and data.

2.1 Wind Resource Maps

Annual mean speed and specific annual production maps at 25, 50, 75 and 100 m a.g.l./a.s.l. can be visualised through the buttons with “V” and “P”. The maps at 75 m a.g.l./a.s.l. are reported in Figure 2.

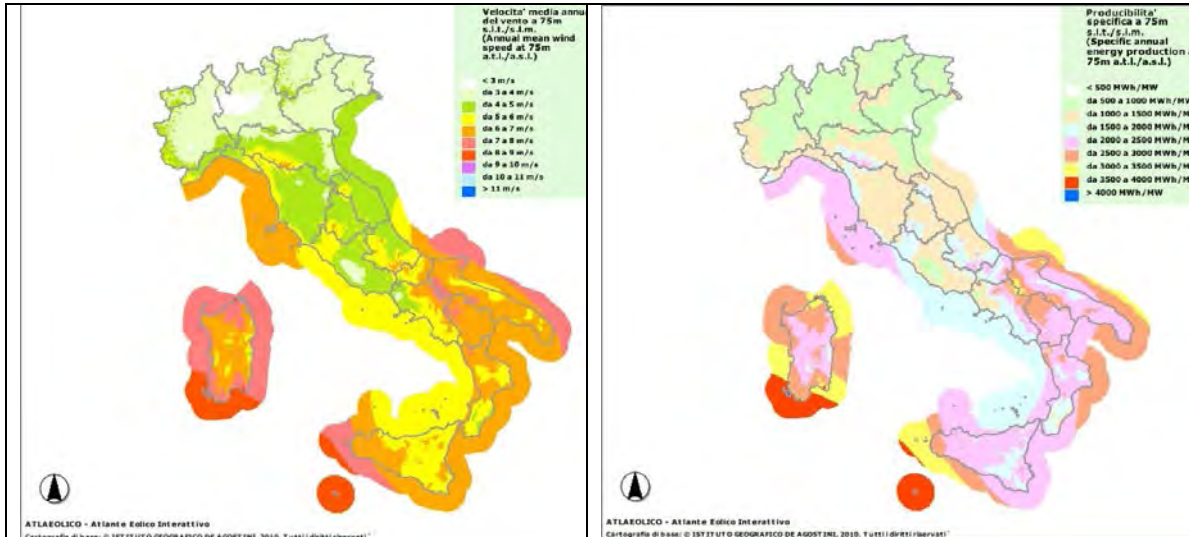


Figure 2: Annual mean speed (left) and specific annual production map (right) at 75 m a.g.l./a.s.l.

2.2 Miscellaneous Information

Exclusion area map (“warning symbol” button) has obtained combining different information: the slope of the terrain, the land use, the constrained mountain areas and the protected areas. This map has been built and used in the process of the regional distribution of the wind capacity among Italian region, see chapter 3. The installed wind capacity map has been aggregated by municipalities (“wind turbine” button) and can add information on the degree of deployment of wind energy in a given area (municipality/province/region). Municipality search tool (“yellow-orange buildings” button) is a speedy tool for finding a given municipality boundary. An image with information about the above mentioned items is shown in Figure 3 for the municipality of Volturino in Apulia Region.



Figure 3: Exclusion area map (shaded zones), installed wind capacity (blue circles), Volturino municipality boundary (red line) and Volturino plant (black arrow).

2.3 Technical-Economical Evaluation Tool: two study-cases

The technical-economical evaluation tool allows performing a preliminary cost analysis for a wind farm in a given site found clicking in a point of the map. It can be accessed through the “Union Jack” button for the English version. An instruction guide for this application can be accessed through the “?” button under the flag button.

The most of the data required for the calculation are already automatically uploaded from WebGIS database. For the other inputs, default values are suggested and already upload at the opening of the application.

The results of two case studies in Apulia Region are reported in the following: the first one is an onland wind farm corresponding to an already existing wind farm in Volturino (see Figure 3); the second one corresponds to a project of offshore wind farm in the Gulf of Manfredonia (see Figure 4).



Figure 4: Annual mean speed map at 75 m a.g.l./a.s.l. in the area of Manfredonia Gulf: offshore wind plant area (red dotted line) and Vieste measurement station (black arrow).

The Volturino and Manfredonia plants has already been investigated with WaSP commercial codes [4] starting from measured data. The Volturino plant has been investigated with Windfarm commercial code too [5]. In order to show the capability of the technical-economical evaluation tool, all the steps of the calculation have been reported for Volturino wind farm:

- The first input datasheet (Figure 5) summarizes the geographical information of the project.
- The second input datasheet (Figure 6) allows the user to choose the turbine model, the hub height and the turbine number (20 Vestas V47 turbine – rated power 660 kW – hub height 50 m).
- The power curve of the wind turbine is calculated for the selected site taking into account the actual air density (Figure 7).
- The wind resource data can be uploaded from the database of the Wind Atlas (as in this case) or inserted manually. In the central point of this plant the annual mean speed results 7,5 m/s and the k parameter 1,55 (Figure 8).
- Inputs concerning costs of the plant are required in the cost analysis datasheet 1 (Figure 9). In this case, only a small reduction of the infrastructure costs has been applied, all the other values are the default ones.

- Inputs concerning a number of different kind of percentage losses are required in the cost analysis datasheet 2 (Figure 10). Again, in this case default values have not been changed.
- In the same datasheet, the discount rate has to be indicated. Default value of 6 % has been chosen.
- Outputs are reported in the datasheet 2. The most relevant for Volturino wind farm are:
 - Gross Annual Energy Production (MWh): 40418
 - Gross Annual Energy Production (MWh): 34150
 - Levelled energykWh cost over the whole wind farm lifetime (c€/kWh): 8,6
 - Carbon dioxide avoided emissions (tons/year): 19124

A sensitivity analysis has been performed for this park regarding the kWh cost and the energy production.

About costs of energy, three kWh costs have been calculated varying the discount rate, see Table 1.

Discount rate (%)	kWh cost (c€/kWh)
5	8,0
6	8,6
7	9,1

Table 1: kWh cost variability for Volturino plant.

For the production variation, two other points on the wind map have been chosen near the one reported in Figure 5. The results are shown in **Table 2**.

Latitude	Longitude	Average mean speed (m/s)	K parameter	Gross AEP (MWh)	Net AEP (MWh)
1010841	4610145	7,5	1,55	40418	34150
1011846	4609775	7	1,54	36828	31117
1009836	4610039	7,9	1,55	43349	36626

Table 2: Wind resource and AEP for three points very close to Volturino wind farm.

Lastly, AEP evaluations are reported in **Table 3** together with the results obtained with WaSP and Windfarm code [6]. Very good agreement is found among the results taking into account that the WaSP and Windfarm simulation are based on in-situ measures whether the technical economical evaluation is based on the wind maps of the Wind Atlas of Italy.

Evaluation method	Gross AEP (MWh)	Net AEP (MWh)
Technical- economical tool	40418	34150
Wasp	38996	36112
Windfarm	40802	37551

Table 3: AEP evaluations with three methods for Volturino plant.


 PROJECT NAME		
INSERT THE PROJECT NAME IN THE CELL OPPOSITE	Volturino_case	
Site Universal Transverse Mercator (UTM) geographic coordinates	Time Zone (i.e. Fuso)	Fuso 32 UTM-WGS84
	UTM_EAST [m]	1010841
	UTM_NORTH [m]	4610145
Site location within the Italian territory	Municipality	VOLTURINO
	Province	FG
	Region	PUGLIA
Site altitude a.s.l. / Sea depth	[m]	650
Average air density at the site	[kg/m³]	1,15
Minimum site distance from electric infrastructure of possible connection point to the grid	[km]	17,229
HOME	GO TO THE NEXT SHEET	RESET
SITE DATA UPDATING		

Figure 5: Project input datasheet.


 WIND FARM CONFIGURATION		
Choice of the wind turbine model Pr : Rated Power ONS : on-shore model OFS : off-shore model <small>remark: for the model selection within the two indicated lists click on the box located above the chosen list and then select the wind turbine</small>	Wind turbine models with Pr <1000 kW <input checked="" type="checkbox"/>	Wind turbine models with Pr ≥1000 kW <input type="checkbox"/>
	<input type="button" value="Click on this button to see the power curve of the chosen turbine"/>	
	<input type="button" value="VESTAS V47 660 kW ONS"/>	<input type="button" value="REPOWER MM82"/>
Wind turbine rated power	660	[kW]
Wind turbine rotor diameter	47,0	[m]
Hub height that can be provided by the Manufacturer of the selected turbine model		
Select an option among the ones shown for the chosen wind turbine model	40	[m] → <input type="radio"/> option 1
	45	[m] → <input type="radio"/> option 2
	50	[m] → <input checked="" type="radio"/> option 3
	55	[m] → <input type="radio"/> option 4
	-	[m] → <input type="radio"/> option 5
Selected hub height	50	[m]
No. of wind turbine units of the wind farm	20	[-]
<small>insert the number ==></small>		
Overall rated power of the wind farm	13200	[kW]
HOME	GO BACK TO THE PREVIOUS SHEET	RESET
GO TO THE NEXT SHEET		

Figure 6: Wind farm configuration input datasheet.

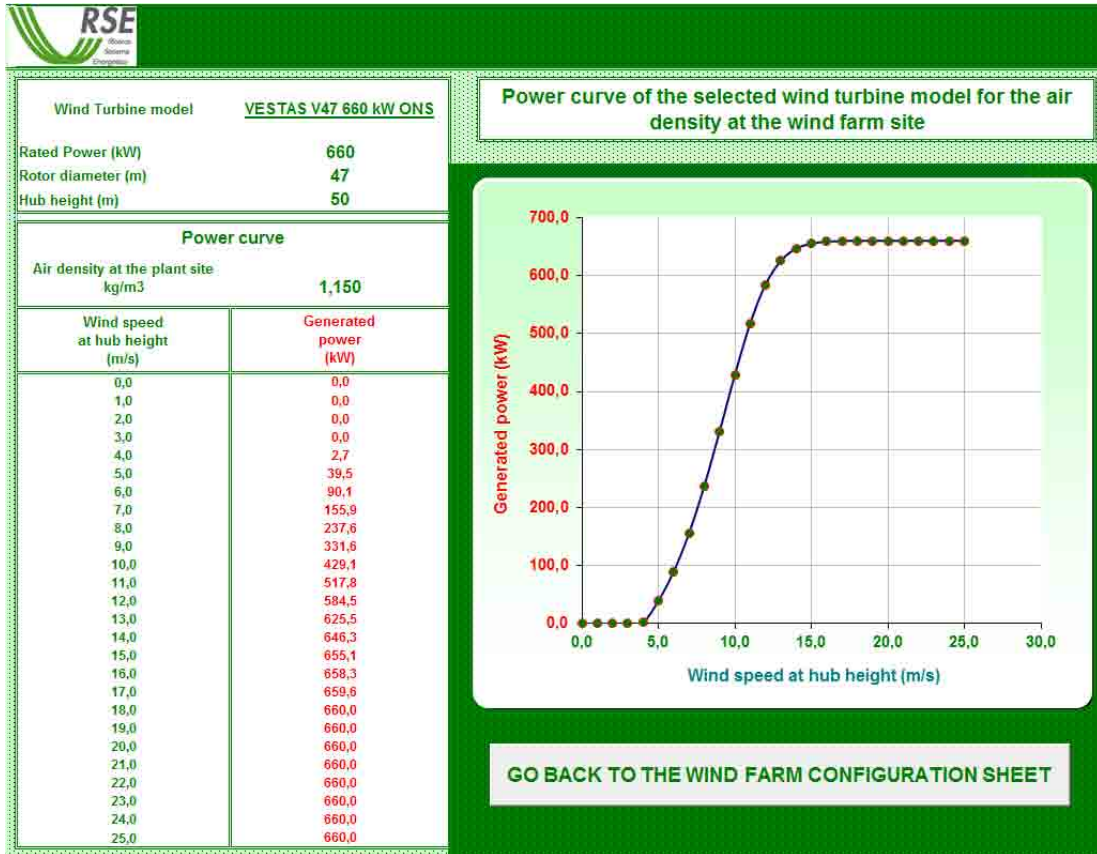


Figure 7: Power curve calculation datasheet.

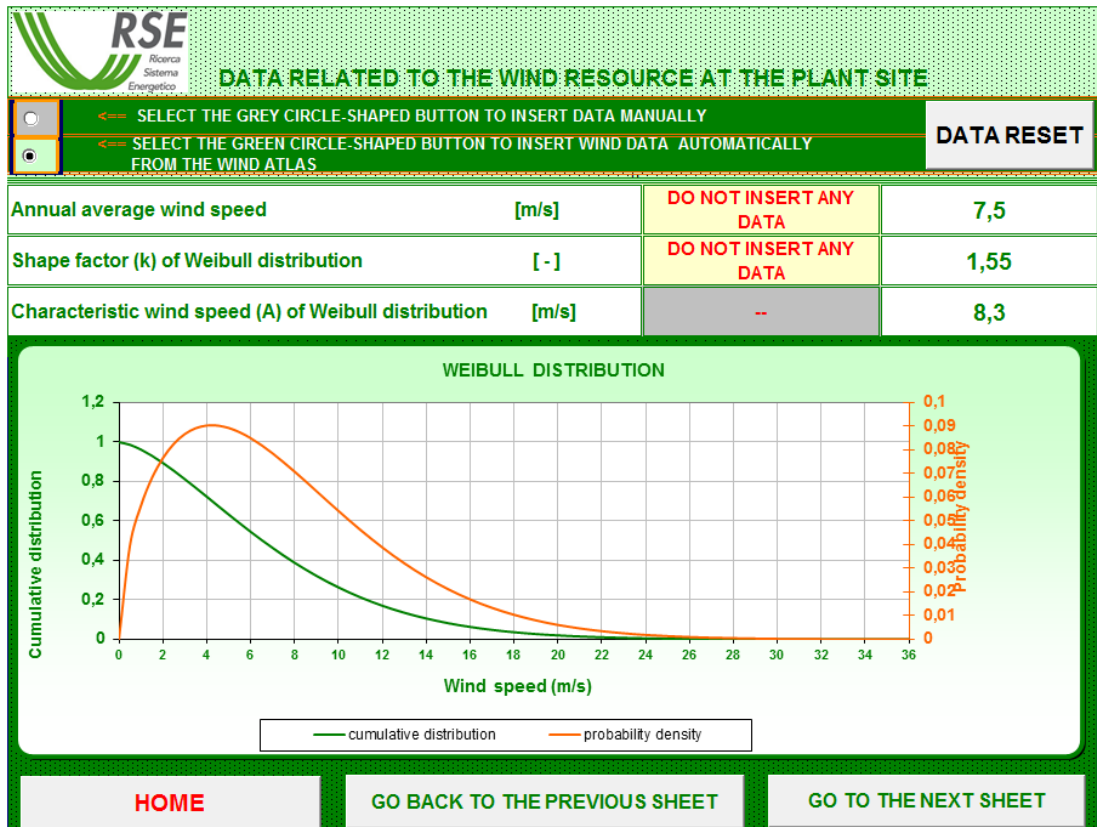


Figure 8: Wind resource input datasheet (from RSE Atlas).

PROJECT :		PROJECT NAME
Time parameters		
Starting year of the wind farm project (zero year) Remark: use the appropriate button to change the year		2012
Year of the project fulfilment (zero year + one)		2013
Wind farm lifetime [years]		20
Investment		
Specific capital cost (€ per installed kW) (typical values: onshore 1500-1800, offshore 2500-3000) [€/kW]		1500
Wind farm capital cost (without connection to the grid) [k€]		19800
Distance of the plant site from suitable electric infrastructure for connection to the grid [km]		17,229
Type of connection to the electric grid (MV cable, MV overhead line, HV cable, HV overhead line)		MV cable
Cost per kilometre of the connection to the electric grid [k€/km]		250
Cost of the infrastructure necessary for connection to the grid (MV bay, HV bay, HV/MV transformer, etc.) [k€]		2500
Overall cost for connection to the electric grid [k€]		6807
Overall wind farm cost [k€]		26607
Operation and maintenance (O&M)		
Annual fixed cost for O&M : in % of the overall investment cost (typical values are included within the range 1% - 3%) [%]		2,0
Variable cost for O&M (typical values are included within the range 0.5 - 1) [c€/kWh]		0,0
Annual allowance to landowners and/or local authorities: in % of the proceeds (typical values are included within the range 1.5 - 3%) [%]		1,5
Annual allowance to landowners and/or local authorities: annual fixed fee (typical values are included within the range 2 - 4) [k€/MW]		2,0
HOME GO BACK TO THE PREVIOUS SHEET GO TO THE NEXT SHEET RESET WITH DEFAULT VALUES		

Figure 9: Cost analysis (1/2) output datasheet.

PROJECT		PROJECT NAME
Technical parameters of the wind farm		
Selected wind turbine model		VESTAS V47 660 kW ONS
Rated power of the wind turbine model [kW]		660
No. of wind turbine units of the wind farm [-]		20
Overall rated power of the wind farm [kW]		13200
Gross annual energy production of the wind farm [MWh]		40418
Specific gross annual energy production of the wind farm [MWh/MW]		3062
Percentage value of the guaranteed generated power (typical value 95%) [%]		95,0
Annual availability index of the wind farm (typical values within the range 95-98%) [%]		97,0
Energy losses due to wake effect among the wind turbines [%]		5,0
Energy losses due to the electric connection within the wind farm (typical values within the range 2-3%) [%]		3,0
Annual availability index of the external electric grid (typical value 99.5%) [%]		99,5
Net annual energy production [MWh]		34150
Discount rate [%]		6,0
Levelised kWh cost over the whole wind farm lifetime [c€/kWh]		8,6
Avoided emissions		
Carbon dioxide (CO ₂) [tons/year]		19124
Nitrogen oxide (NO _x) [tons/year]		19
Sulfur AE dioxide (SO ₂) [tons/year]		50
Particulate [tons/year]		10
HOME GO BACK TO THE PREVIOUS SHEET RESET		

Figure 10: Cost analysis (2/2) and avoided emission output datasheet.

In the case of Manfredonia offshore wind farm, the input data are:

- Geographical: LAT:11003356, LONG:4642763, sea depth: 17 m, distance from shoreline: 11 km, distance from grid connection: 22.9 km;
- Wind farm configuration:72 Vestas V90 turbine – rated power 3000 kW – hub height 85 m;
- Wind resource (Wind Atlas): annual mean speed results 6,8 m/s and the k parameter 1,59;
- Costs: specific capital cost: 2900 €/kW, cost per kilometre of the electric connection: 950 k€/km (calculated according to suggestions in “?” - Instruction and Note), cost of infrastructure: 0 (this cost is included in cost per km in electric connection), all the other value are the default ones. The overall cost of the plant is about 3000 €/kW;
- Losses due to wake effects: 7.9 % (according to WaSP evaluation), all the other value are the default ones;
- The most relevant outputs for Manfredonia wind farm are:
 - Gross Annual Energy Production (MWh): 527040
 - Gross Annual Energy Production (MWh): 431711
 - Levelised energy kWh cost over the whole wind farm lifetime (c€/kWh): 16,4
 - Carbon dioxide avoided emissions (tons/year): 241758

Also in this case a comparison with the values of AEP obtained with WaSP code has been performed. The calculations with WaSP code have been based on the data measured by a wind station on a coastal site, Vieste (see Figure 4), more than 20 km far from the offshore site [6]. The results show again good agreement.

Evaluation method	Gross AEP (MWh)	Net AEP (MWh)
Technical- economical tool	527040	431711
Wasp	513458	472558

Table 4: AEP calculation with two methods for Manfredonia plant

2.4 Download of Maps and Data

Free download of the maps is allowed after registration. Maps can be downloaded in a printable PDF or RGB version (“world” button) as well as gridded data for GIS (“grid” button).

Moreover, the download of the complete historical series of measured wind data from RSE stations is accessible through the “flag” button. RSE wind measurement stations are installed in coastal, island and offshore sites, as described in [3] and shown in Figure 11.



Figure 11: Locations of RSE wind measurement stations (two in Ischia island). Green: operating; yellow: buoy -installation stage; blue: authorisation stage; red: authorisation process too long.

3. Applications of the Wind Atlas

3.1 Onshore and offshore wind potential evaluation

On the basis of the maps of the Wind Atlas of Italy several evaluations of onshore and offshore wind potential have been performed. The most refined evaluations have been obtained combining other information with the wind resource. Human settlements, land use, altitude, terrain slopes, ground roughness (vegetation etc.), environmental constraints (e.g. national parks) have been taken into account for the onshore evaluation as well as sea depth, distance from shore and presence of Marine Protected Areas for the offshore one. A method based on Geographical Information Systems was developed to make a selection of actually exploitable areas. Values of installed capacity density (typically 5 MW/ km² for onshore and 6,5 MW/ km² for offshore) were then assigned to selected areas on the basis of experience with the setting-up of existing plants, thus making out values of total capacities that could be installed. These theoretical capacity values were then reduced further by another screening which took into account less predictable aspects such as future renewable energy support policies, the likelihood that projects are granted building permits by local authorities, the willingness of land owners to make agreements for the setting-up of wind farms etc. This method led to estimated overall potentials up to about 10-12 GW onshore [1] and up to about 10,5 GW offshore (8,5 GW in deep waters where floating systems are expected to be installed) [3].

3.2 Regional Burden sharing

In spite of more than 6 GW of wind capacity has already installed at the half of 2011, most of which in the previous four years, each region has developed its own energy policy and plant permitting regulations with different choices about the energy mix. Only after summer 2011, the national government (technically supported also by RSE) has set out to establish regional

targets for renewable energy production in order to share, among regions, the burdens ensuing from Italy’s 17% target assigned by European Directive 2009/28/EC implementing the 20-20-20 policy of the EU.

With a methodology very close with the one described for the wind potential evaluation in the previous section. Combining the specific production map with the exclusion areas map, RSE has evaluated the available areas for an economical sustainable wind capacity installation setting a specific production threshold of 1750 MWh/MW. On the basis of this combined map the regional wind energy production targets (“Burden Sharing”) have been found, see Figure 12.

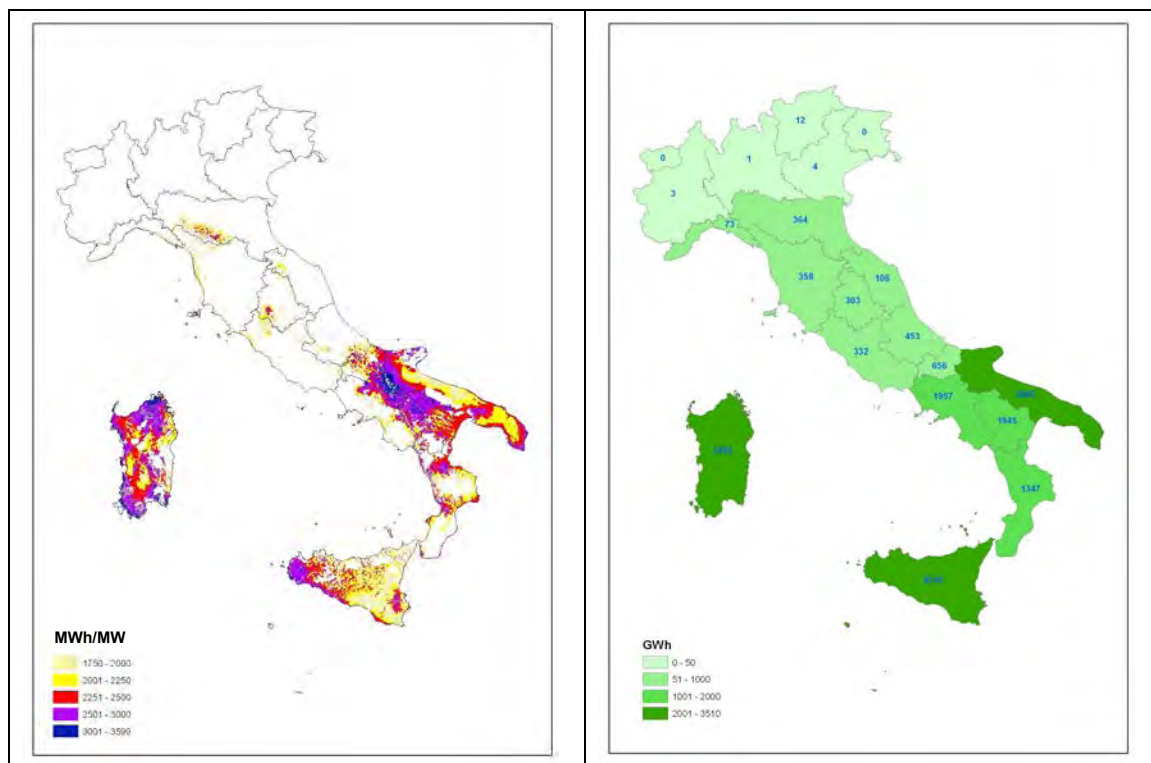


Figure 12: Available areas for an economical sustainable installation of wind capacity (left) and regional wind energy “Burden Sharing” (right)

In this connection, RSE has also started a research activity concerning the wind capacity already installed in Italy [8] with the aim of better understanding the characteristics and performance of the wind farms so far deployed and consequently improving its knowledge of the relevant issues. This knowledge will be very useful for supporting decision-makers at national and regional level in view of the future development of the wind sector in Italy up to 2020 and also beyond this date

4. Conclusions

The more recent version of the RSE Wind Atlas of Italy provides a full overview of wind resources all over the country, including an offshore strip up to 40 km from the coastline. This interactive version of this Atlas can be helpful to a number of users, from local authorities planning energy resource exploitation over their territory, to plant developers trying to single out areas suitable for more detailed siting of wind farms. Among others, users can also assess the feasibility and profitability of prospective wind farms at selected points on the wind maps.

The WebGIS of Wind Atlas (now with a new version in English) contains also a technical-economical module that allows a first evaluation of profitability of a wind farm in a given site.

Two examples have been reported: one for an onshore wind farm and the other for an offshore one, both located in Apulia region.

Moreover the application of the information implemented in the Atlas for the evaluation of the national and regional wind potential has been briefly described too.

The WebGIS of the Wind Atlas is a user-friendly way to disseminate knowledge and results about the wind resource in Italy both onshore and offshore. This application is enriched every year with new information and data. With more than 100 accesses every day from the beginning of 2007 is still one of the most popular product developed in the frame of the Research Fund for the Italian Electrical System. The English version here presented will address this product to an international context.

This work has been financed by the Research Fund for the Italian Electrical System under the Contract Agreement between RSE (formerly known as ERSE) and the Ministry of Economic Development - General Directorate for Nuclear Energy, Renewable Energy and Energy Efficiency stipulated on July 29, 2009 in compliance with the Decree of March 19, 2009

References

1. G. Botta, C. Casale, E. Lembo, S. Maran, L. Serri, G. Stella, S. Viani, M. Burlando, F. Cassola, L. Villa, C.F. Ratto, "The Italian Wind Atlas – Status and Progress", Proceedings of EWEC 2007, Milan, 7-10 May 2007
2. <http://atlanteolico.rse-web.it/viewer.htm>
3. D. Airoidi, C. Casale, E. Lembo, L. Serri, "Italian Offshore Wind Potential Evaluation through GIS Tools and Data", Offshore 2011, Amsterdam, 29th November-1st December 2011
4. www.wasp.dk
5. www.resoft.co.uk
6. C.L. Bossi, E. Lembo, L. Serri, D. Airoidi, "Eolico terrestre: affinamento delle conoscenze relative all'eolico installato tramite informazioni distribuite e simulazioni a scala locale", RdS report Prot. 12000405, 2012
7. E. Lembo, L. Serri, S. Alessandrini, G. Decimi, D. Ronzio, D. Airoidi, S. Sperati, "Raccolta ed analisi di dati sperimentali in aree marine. Studi sulla risorsa eolica offshore tramite applicazione di modellistica a scala locale e di modellistica meteorologica avanzata", RdS report Prot. 11000253, 2011
8. L. Serri, D. Airoidi, C. Bossi, C. Casale, E. Lembo, "6.5 GW of Installed Wind Capacity in Italy: Preliminary Results of a Statistical Study for the Support of Future Developments", EWEA2012, Copenhagen, 16-19 April 2012

Using data assimilation in mesoscale numerical modeling to map offshore wind resource

M. Fernandes^{1a}, P. Costa^{1b}, T. Simões^{1c} and A. Estanqueiro^{1d}

1) *Laboratório Nacional de Energia e Geologia I.P., Estrada do Paço do Lumiar, 22, 1649-038 Lisboa, Portugal.*

a) *miguel.fernandes@lneg.pt*, b) *paulo.costa@lneg.pt*, c) *teresa.simoies@lneg.pt*,

d) *ana.estanqueiro@lneg.pt*

Abstract – Observational surface wind data from QuikSCAT (QS) satellite and sea surface temperature (SST) data from GHRSSST Level 4 analysis have been ingested to an atmospheric mesoscale numerical model using a Newtonian relaxation assimilation technique. The mesoscale model WRF was used to map the wind resource at 90 m a.g.l. for the North Sea area. A model domain with a spatial resolution of 20x20 km was used to simulate a winter and a summer month, November 2008 and July 2009. The modeled wind results have been validated against observational data from the anemometric mast FINO1. A spatial improvement of the average wind field at 90 m a.g.l. from the observational data has been assessed. Each assimilated data source has shown a distinct impact. The QS assimilation had higher impact during the summer period while the SST assimilation during the winter period. Improvements of 5% and more were obtained from using data assimilation on the overall domain. Validation with the FINO1 anemometric mast shows improvements on the average vertical wind profile while error statistical parameters were only slightly improved.

1. Introduction

The offshore wind resource assessment is one of the primary key tools used by offshore wind farm promoters for decision making investments in offshore wind parks. In Europe, due to the renewable energy policies recently established by the European Commission (EU) for the wind sector, it is expected an interesting growth of offshore wind parks along the European coasts. To support the expected investments, wind research and industry partners in collaboration with the EU have created the FP7 NORSEWInD project (*Norsewind, 2008*) with the main purpose of delivering to the North, Baltic and Irish Sea areas high quality wind atlases for offshore wind resource assessment.

A Newtonian relaxation assimilation technique (*Stauffer and Seaman, 1990*) has been set up with the Weather Research and Forecasting (WRF) (*Skamarock and Klemp, 2008*) mesoscale model. The aim is to improve the regional wind atlases to be constructed for the areas of the NORSEWInD project. A model domain with a spatial resolution of 20x20 km was used to simulate a winter and a summer month, namely, November 2008 and July 2009. The QuikSCAT (QS) satellite surface wind data (*Perry et al., 1995*) and the sea surface temperature (SST) data from GHRSSST level 4 analyses (*Donlon C. et al., 2007*) were the observational sources ingested into the numerical model simulations.

The observational data from FINO1 anemometric mast, whose location is displayed in Figure 1, was used to perform point validation at 90 m a.g.l. The average vertical wind profile was computed for levels 33, 50, 60 and 90 m a.g.l.. An assessment of the spatial improvement of the average wind field at 90 m a.g.l. from the observational data was then performed.

2. Methodology

The WRF model was configured using 2 nested domains, a coarser (D1) with grid spacing of 100x100 km and a nested domain (D2) with 20x20 km using the parameterizations described in Table 1. The coverage area is displayed in Figure 1 which also points the location of FINO1 anemometric mast. Initial and boundary conditions were ingested into D1 from NCAR Reanalysis datasets (Kalnay *et. al.*, 1996) at a frequency of 4 times per day. These conditions were objective interpolated into D1 grid from the 2.5°x2.5° reanalysis grid spacing.

Table 1: WRF parameterization setup.

	D1	D2
Horiz. Res [km]	100	20
NX x NY	18x21	36x51
Vert. Levels	28	28
Micro-physics	WSM6	WSM6
LW radt.	RRTM	RRTM
SW radt.	Dudhia	Dudhia
Land-Surface	Noah	Noah
Surface	Eta	Eta
PBL	MYJ	MYJ
Cumulus	KF	KF

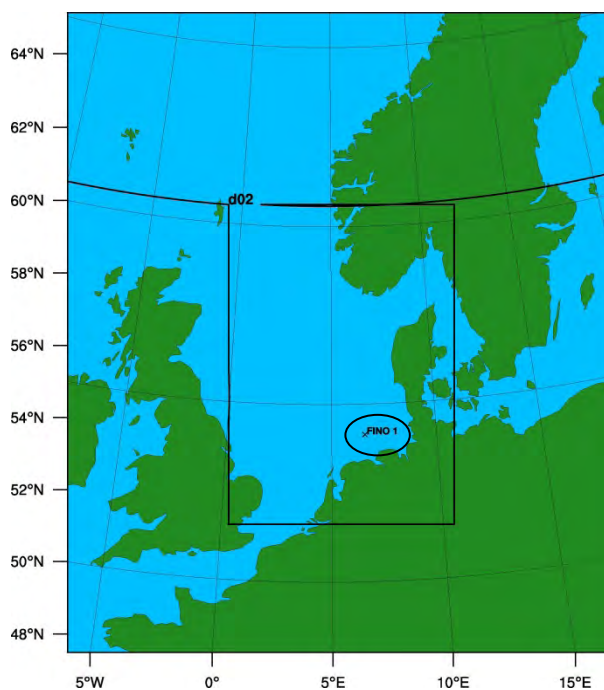


Figure 1: WRF domains setup and location of FINO1 anemometric station.

Three experimental runs were performed, a control run without data assimilation departing from a “cold” start via Reanalysis, a second run almost equal to the first but “warm” started with QS data assimilation and a third one “warm” started with SST data assimilation. The QS dataset is configured with a 0.25° gridded ocean surface wind vector field from daily ascending and descending satellite passes. It is a level 3 processed product and is nowadays freely available from PODACC-NASA’s website¹. A contour plot of the averaged QS sea wind speed and direction for each of the months under analysis is displayed in Figure 2.

The SST data used is a product from the Group for High Resolution Sea Surface Temperature (GHRSSST) Level 4 analysis produced daily on an operational basis but refined by the Danish Meteorological Institute for the North Sea area. This product is usually produced only once a day at 00h UTC. Figure 3 displays a plot of the monthly averaged SST for the study area.

¹<http://podaac.jpl.nasa.gov/>

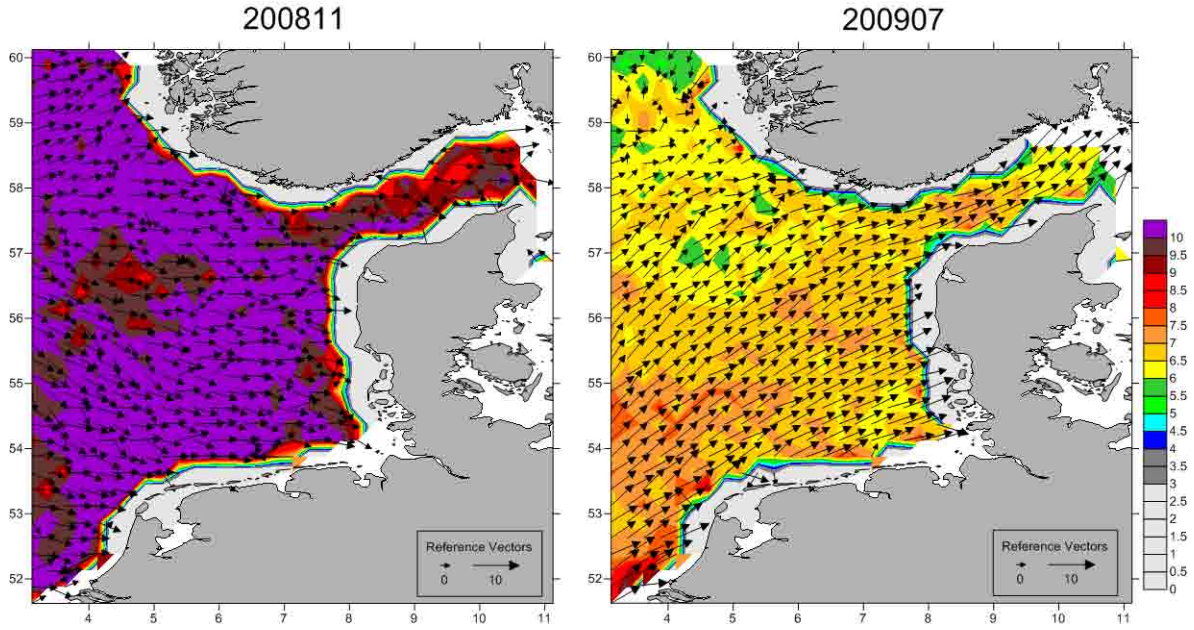


Figure 2: QuikSCAT monthly average wind speed and direction for the study area.

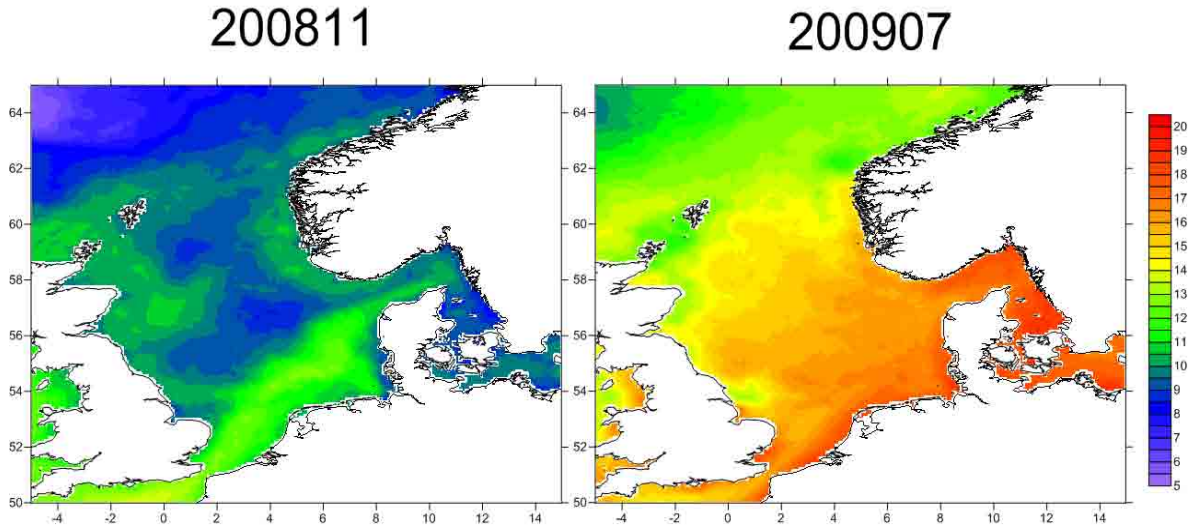


Figure 3: Averaged SST for November 2008 (on the left) and July 2009 (on the right) for the study area.

The FINO1 anemometric mast was chosen for point validation since it is one of the few offshore wind stations with available data at the study area for both months under analysis. A spatial improvement assessment (I_{WIND}) of the average wind speeds at 90 m a.g.l. was measured at each grid point by calculating the proximity of the assimilation run (AS) versus control run (CR) compared with QuikSCAT (QS) observations following equation (1).

$$I_{WIND}(\%) = 100 \times \frac{\|CR - QS\| - \|AS - QS\|}{\|CR - QS\|} \quad (1)$$

For the SST assimilation improvement (I_{SST}), only the comparison between the control (CR) and the assimilation run (AS_{SST}) was assessed. For this case, the SST improvement is expressed by the following equation:

$$I_{SST}(\%) = 100 \times \frac{\|CR\| - \|AS_{SST}\|}{\|CR\|} \quad (2)$$

3. Results

3.1 Validation against anemometric mast

Time series of wind data at ten-minute intervals were produced from WRF model at FINO1 to be comparable with wind data ten-minute averaged from the met mast. The main wind statistical parameters for both time series at 90 m (a.g.l.) were processed.

Results for November 2008 month are presented in Table 2, where OBS means FINO1 observational time series, WRF_NN is the control run, WRF_QS is QS assimilation run and WRF_SST is the SST assimilation run.

Table 2: Statistics for FINO1 point validation for November 2008.

		90 m a.g.l.			
		OBS	WRF_CR	WRF_QS	WRF_SST
WBL	AVG [m/s]	11.23	12.00	12.02	11.83
	STDEV [m/s]	4.53	4.43	4.20	4.40
	A [m/s]	12.62	13.46	13.45	13.20
	k	2.7	2.96	3.14	2.84
CORREL		-	0.83	0.83	0.84
WSPD	MAE [m/s]	-	2.07	1.99	1.95
	RMSE [m/s]	-	2.82	2.65	2.62
WDIR	MAE [°]	-	12.39	12.96	11.83
	RMSE [°]	-	17.14	18.10	16.48

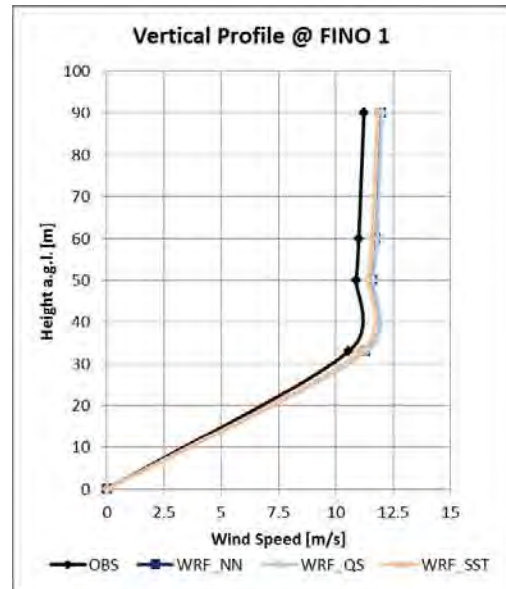


Figure 4: Average vertical wind profile at FINO1 for November 2008.

During the winter month, a correlation of 83% was obtained for all simulations with the WRF model predicting stronger winds than the observed, meaning that WRF for the winter period overestimated the winds from the common atmospheric transient weather circulation patterns that usually occurred at this time of the year. The assimilation of QS sea winds had a low impact on improving the simulated wind field at 90 m a.g.l. with slight improvements on both mean wind speed absolute error (MAE) and root mean square error (RMSE). With the assimilation of SST data, the wind flow errors have diminished allowing a closer approximation with the observational FINO 1 wind data.

This impact was observed at all levels of analysis as displayed in the vertical profile in Figure 4.

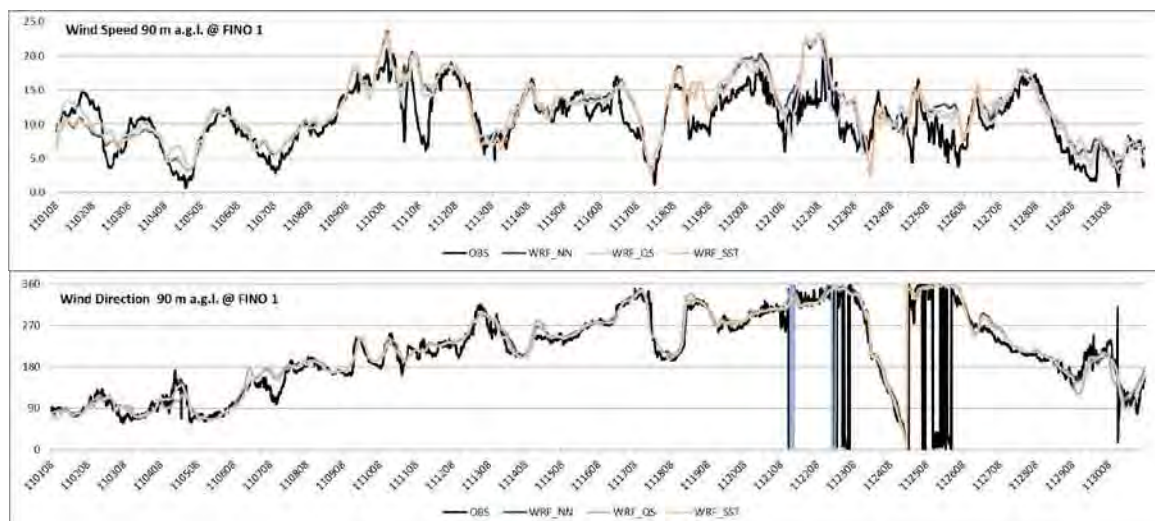


Figure 5: Time series of wind speed (above) and direction (below) for November 2008 at FINO1. Times series of observations (OBS), control run (WRF_NN), QS assimilation (WRF_QS) and SST assimilation (WRF_SST).

Figure 5 displays a plot of the time series for November 2008 month. The overestimation of wind speed by WRF model can be observed on several occasions. For wind direction, almost no changes can be observed between the three WRF simulation types. All of them were able to reproduce with success the observed wind direction.

A different behavior of the WRF model was observed for the summer month where the model has underestimated the wind speeds. Table 3 presents the same statistical validation parameters calculated for FINO1 local point.

Table 3: Statistics for FINO1 point validation for July 2009.

		90 m a.g.l.			
		OBS	WRF_CR	WRF_QS	WRF_SST
WBL	AVG [m/s]	8.60	8.46	8.40	8.44
	STDEV [m/s]	3.36	3.08	3.05	3.25
	A [m/s]	9.65	9.47	9.38	9.60
	k	2.71	2.99	3.02	2.66
CORREL		-	0.67	0.68	0.69
WSPD	MAE [m/s]	-	2.07	2.05	2.00
	RMSE [m/s]	-	2.62	2.59	2.63
WDIR	MAE [°]	-	19.98	23.93	19.35
	RMSE [°]	-	31.28	37.55	30.94

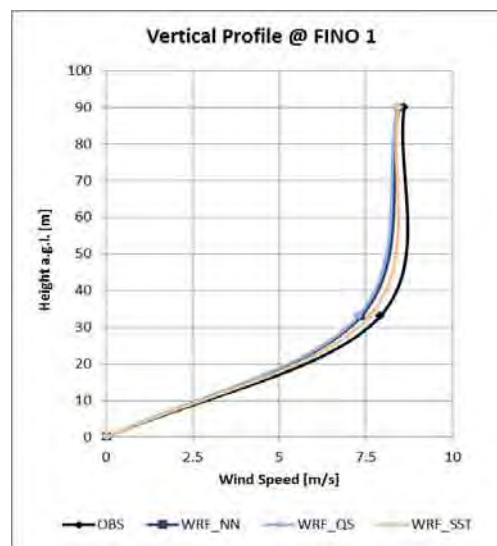


Figure 6: Average vertical wind profile at FINO1 for July 2009.

From Table 3, a correlation of about 68% was achieved by WRF model. The lower correlation value means that WRF running at 20x20 km spatial resolution could not represent well the thermal stratification phenomena activity in the North Sea area occurring in the summer months. Both assimilation runs and also the control run allowed approximately 1% of improvement on correlation when compared with observational values.

The average vertical profile displayed in Figure 6 (right side of Table 3) was only calculated for levels 33 m and 90 m (a.g.l.) due to inconsistencies on observations founded in levels 50 m and 60 m (a.g.l.). Simulation results with and without assimilating data have underestimated wind speeds on both levels. Nevertheless, this difference has diminished from the 33 m to the 90 m level.

Figure 7 presents the plots of the wind speed and direction time series for July 2009. There are several wind speed local maximums associated with episodes of strong transient stratification atmospheric phenomena coupled with local sea-breezes that WRF model was not able to reproduce with 20x20 km spatial resolution, reflecting this way the lower averages obtained. In an opposite case, the wind direction is generally well reproduced therefore reflecting the higher direction MAE and RMSE but with some exceptions by the QS assimilation run on some occasions due to the stratification phenomena.

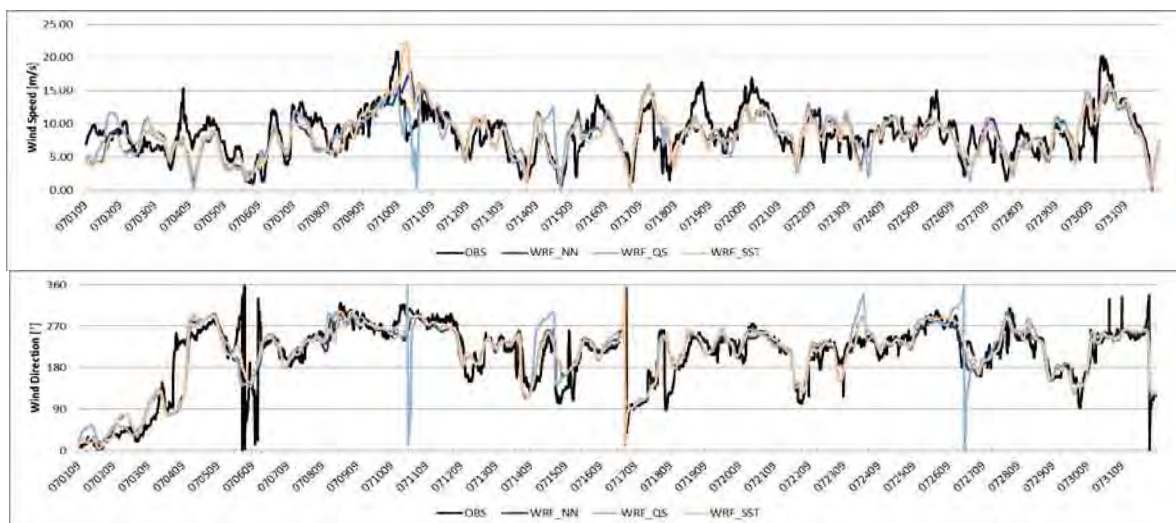


Figure 7: Time series of wind speed (above) and wind direction (below) for July 2009 at FINO1. Time series of observations (OBS), control run (WRF_NN), QS assimilation (WRF_QS) and SST assimilation (WRF_SST).

3.2 Spatial Improvement

A spatial analysis to assess a positive or negative impact of data assimilation when compared with the control run on the overall domain was assessed. Equation (1) was used to obtain the QS assimilation run performance and Equation (2) for the SST assimilation performance. Figure 8 displays the spatial performance for November 2008 month (winter) and Figure 9 for July 2009 (summer).

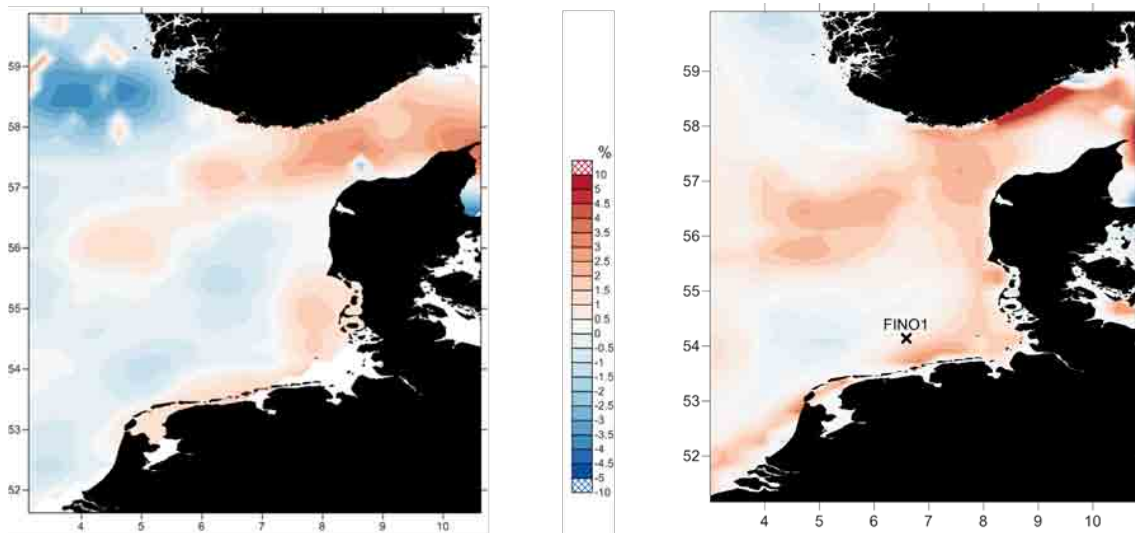


Figure 8: Spatial improvement for November 2008. QS assimilation performance on the left and SST assimilation performance on the right.

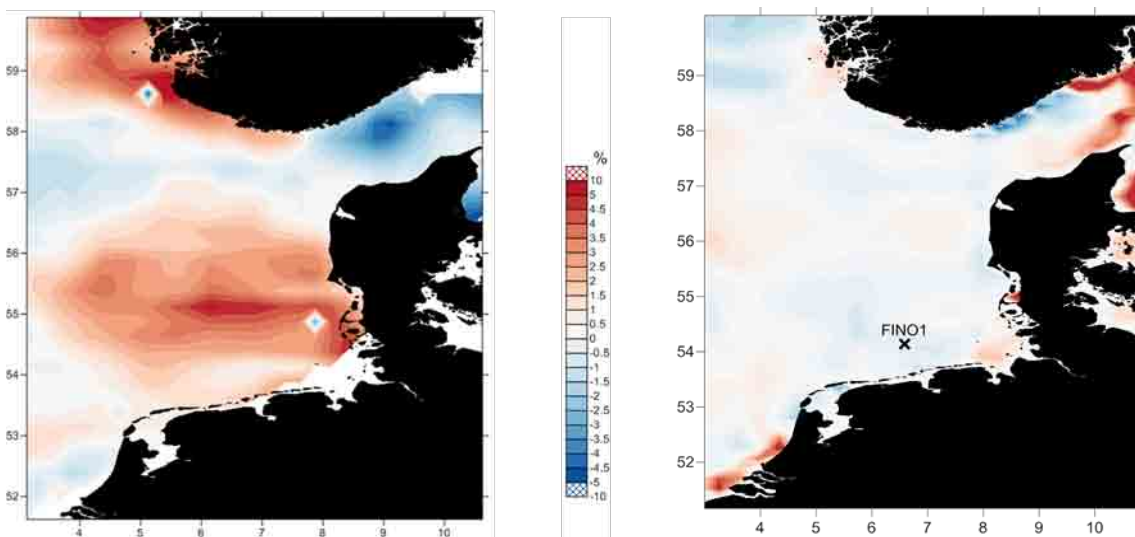


Figure 9: Spatial improvement for July 2009. QS assimilation performance on the left and SST assimilation on the right.

The QS assimilation had higher positive impacts during the summer month with large areas obtaining an improvement between 5 and 10%. The SST assimilation showed a higher positive impact during the winter month where large areas showed a positive impact, especially near the coast.

4. Conclusions

The Newtonian relaxation scheme used to assimilate the winds from the QuikSCAT and the SST from the GHRSSST databases has allowed improvements in the range of 5 to 10% for the summer period and from 3 to 5 % for the winter period.

During the winter, the SST data assimilated showed a higher positive impact while the QS assimilated data showed better results during the summer.

The point validation using met mast FINO 1 did not reflect the improvements displayed by the spatial analysis. This can be explained by the fact that FINO 1 dataset is part of the NCAR Reanalysis project assimilation cycles and therefore in a certain way this data is already “present” on the initial and boundary conditions ingested into the WRF model domain. Nevertheless, slight improvements on the MAE and RMSE were obtained due to the fact that QuikSCAT and GHRSSST databases have a better spatial resolution than NCAR’s Reanalysis project data. It should be noticed that the SST data assimilation has demonstrated ability to correct the vertical wind profile on both occasions, during the summer and winter cases.

Better results could be achieved if they were performed on better spatial resolutions. This work is currently being done for the purposes of the FP7 NORSEWInD project.

5. Acknowledgements

The results and the met mast data presented in this work are part of the EU FP7 NORSEWInD project from which the authors are partners. The authors would also like to acknowledge the project ROADMAP WW (PTDC/SEN-ENR/105403/2008), FCT funded (Portuguese Foundation for Science and Technology).

References

1. Donlon, C., I Robinson, K. S. Casey, J. Vazquez-Cuervo, E. Armstrong, O Arino, C. Gentemann, D. May, P. Le Borgne, J. Piolle, I Barton, H. Beggs, D. J. S. Poulter, C.J. Merchant, A. Bingham, S. Heinz, A. Harris, G. Wick, B. Emery, p. Minnett, R. Evans, D. Llewellyn-Jones, C. Mutlow, R. W. Reynolds, H. Kawamura, and N. Rayner, The Global Ocean Data Assimilation Experiment High-resolution Sea Surface Temperature Pilot Project, Bull. of the Amer. Meteor., 88 (8), 1197-1213, Aug, 2007.
2. Kalnay, E., M. Kanamitsu, R. Kistler, W. Collins, D. Deaven, L. Gandin, M. Iredell, S. Saha, G. White, J. Woollen, Y. Zhu, M. Chelliah, W. Ebisuzaki, W. Higgins, J. Janowiak, K.C. Mo, C. Ropelewski, J. Wang, A. Leetmaa, R. Reynolds, R. Jenne, and D. Joseph, 1996: The NCEP/NCAR 40-year reanalysis project. Bull. Amer. Meteor. Soc., 77, 437-471
3. NORSEWInD – Northern Seas Wind Index Database. Available at <http://www.norsewind.eu>.
4. Perry, K.L. et al.; SeaWinds on QuikSCAT level 3 daily, Gridded Ocean Wind Vectors; JPL Seawinds Project; California Institute of Technology; 1995.
5. Skamarock, W.C.; Klemp, J.B.; A time-split nonhydrostatic atmospheric model for weather research and forecasting applications, J. Comp. Phys, 227, 3465-3485; 2008.
6. Stauffer, D.R.; Seaman, N.L.; Use of Four Dimensional Data Assimilation in a Limited-Area Model. Part I: Experiments with Synoptic Scale Data, Monthly Weather Review, 118, 1250-1277; 1990.

Wave energy potential in the Mediterranean, the case of Pantelleria

L. Liberti¹, A. Carillo² and G. Sannino³

¹ *Institute for Environmental Protection and Research ISPRA, via Vitaliano Brancati 48, 00144 Rome, Italy, luca.liberti@isprambiente.it*

² *ENEA-Ocean Modelling Unit, via Anguillarese 301, 00123 Rome, Italy, adriana.carillo@enea.it*

³ *ENEA-Ocean Modelling Unit, via Anguillarese 301, 00123 Rome, Italy, gianmaria.sannino@enea.it*

Abstract – A wave energy atlas of the Mediterranean was obtained from a 10 years wave climate simulation at 1/16° resolution. The model was thoroughly validated using available satellite and buoy data. The most promising areas in terms of wave energy availability and seasonal variability were identified. Among the areas with the highest potential the Island of Pantelleria was selected to perform a more detailed small scale study. Wave energy potential around the island was calculated by running a high resolution 1/120° model nested in the Mediterranean model. An analysis of the results obtained by the two model was carried out for a location along the Pantelleria coastline. Significant differences between the distribution of wave energy obtained by the coarse and fine model were found especially near the coast.

1. Introduction

It is estimated that the contribution of ocean wave energy to renewable energy production will increase significantly in the next decades following the improvement in the technology of Wave Energy Converters (WECs) [1]. Currently a number of different WECs have been proposed and tested [2] but large scale commercial installations are not yet in operation.

Research on wave energy production is particularly active in countries bordering large oceans where the amount of available wave power is the highest. In Europe, countries located along the Atlantic Coast such as Ireland, Portugal, Spain, Norway and the UK are among the most committed to the development of wave energy converters [3].

While the amount of available wave energy is a crucial factor for the choice of a suitable location for wave energy extraction, high energy potential is usually associated to harsh wave climate during extreme events. Such conditions raise a number of technical issue that affect the design ad deployment of WECs. In calmer seas such as the Mediterranean, lower amounts of wave energy are normally available but many technical issues related to extreme sea climate could be more easily solved, possibly making wave energy production economically sound even in these areas.

Feasibility studies of wave energy plants require a detailed knowledge of the amount of available energy, its temporal and spatial variability and its distribution among different sea states. At present, an extensive and accurate estimation of wave energy for the Mediterranean sea is not yet available. In recent years, many authors presented global wave energy atlases, see for instance [4], [5], [6]. These atlases lack the spatial resolution required to correctly describe the wave energy distribution in small and semi enclosed basins as the Mediterranean. Wave energy atlases based on buoy measurements (see for instance [7]) are affected by gaps in the data series and describe the wave energy resource only locally.

Wave height and period show substantial spatial variations in enclosed seas where land obstructions deeply influence wave generation and propagation [8].

In these regions wave models represent the most important tool to assess wave energy distribution.

Currently a high resolution study of wave energy distribution in the Mediterranean appears to be lacking. For the purpose of providing high a resolution atlas of wave energy availability a 10 years simulation (2001-2010) of the wave climate in the Mediterranean was produced using the WAM model at $1/16^\circ$ resolution forced by the wind fields provided by the ECMWF.

In the present work the results from the model run were used to produce an atlas and a database of wave energy resource in the Mediterranean. Elaborations on the database were used to identify the most productive areas at a spatial scale not currently available in literature. At the same time, the database provides a starting point to perform higher resolution nested runs to describe wave climate in locations where the morphology of the coastline requires an even higher resolution to correctly catch wave energy spatial trends. As a sample application we present a high resolution study of the wave energy potential around the Island of Pantelleria located in the Sicily Channel which is among the most productive areas in the Mediterranean.

2. Model Description

Simulations were carried out using a parallel version of the WAM wave model Cycle 4.5.3 [9]. WAM is a third generation spectral wave model that solves the spectral action density balance equation without any assumption on spectral shape. Spectral action density $N(\sigma, \theta)$ is commonly used in spectral wave models in place of the spectral wave energy density $S(\sigma, \theta)$ which is not conserved in presence of currents. The two quantities N and S are related by the expression:

$$N(\sigma, \theta) = \frac{S(\sigma, \theta)}{\sigma} \quad (1)$$

where θ is the wave propagation direction and σ the relative frequency which is the wave frequency for an observer following the current.

The coarse grid model domain encompasses the entire Mediterranean Sea, from 5.50°W to 36.125°E of longitude and from 30.2°N to 45.825°N of latitude. The spatial domain was discretized using a regular grid of 667×251 nodes in spherical coordinates with a uniform resolution of $1/16^\circ$ in each direction, corresponding to a linear mesh size of 5-7 km.

The frequency and direction domains were discretized with 36 directional bins and 32 frequency bins starting from 0.06 Hz. The nested fine grid model domain consists is 61×61 cells centered around the Island of Pantelleria with has a uniform spatial resolution of $1/120^\circ$ (950-1150 m). The discretization of the directional wave energy density function is the same one used to the coarse model. The bathymetry of model cells was extracted from the General Bathymetric Chart of the Oceans (GEBCO) 30 arc-second gridded data set [10] as the average of the values falling in each computational cell. The model was driven by six-hourly wind fields obtained from ECMWF operational analysis (www.ecmwf.int) at uniform $1/4^\circ$ spatial resolution. Figure 1 shows the coarse model computational domain and bathymetry. The outline of the fine model grid is showed in Figure 9.

Wave climate simulations were performed for the period 2001-2010 extracting the integral wave parameters significant wave height (H_s), mean wave period (T_m), significant wave period (T_e) and mean direction (θ_m) every 3 hours. The nested fine grid model is forced at its external boundaries by the output from the coarse grid model and by the same wind fields.

3. Model Validation

The results of the Mediterranean model were validated using satellite and wave buoy measurements. Satellite radar altimeters provide indirect measurements of H_s in areas far from the coast where wave buoys are not usually found.

Satellite H_s measures were used to evaluate the overall performance of the model over the entire Mediterranean Sea; buoy measures were used to assess in more detail the model results near the Italian coast. Table 1 lists the satellites that were included in the validation. Figure 2 shows the satellite tracks over the Mediterranean where measures are periodically made. Satellite data was downloaded from the AVISO web site [11]. Outliers were removed following the method described by Queffelec and Bentamy [12] based on the statistical analysis of the differences between consecutive data points along the satellite tracks. The resulting H_s values were compared to model values extracted from the nearest model output in time, considering the grid cell containing the satellite point without temporal or spatial interpolation. Comparison between measured values and model output data series was carried out by evaluating common statistical indices. We included in our analysis the root mean square error (*rmse*), the bias between model and measures (*bias*), the scatter index (*si*) and the slope of the best fit line passing through the origin (*slope*).

Given a series of n model values y_i and corresponding measures x_i the indices are calculated as follows:

$$bias = \frac{1}{n} \sum_{i=1}^n (y_i - x_i) \quad (2)$$

$$rmse = \sqrt{\frac{1}{n-1} \sum_{i=1}^n (y_i - x_i)^2} \quad (3)$$

$$si = \frac{rmse}{\frac{1}{n} \sum_{i=1}^n (y_i)} \quad (4)$$

$$slope = \frac{\sum_{i=1}^n (y_i x_i)}{\sum_{i=1}^n (x_i x_i)} \quad (5)$$

Table 2 lists the statistics of the comparisons for each satellite. Values in the table show good agreement between model and satellite H_s with small biases not exceeding 0.15 m and best-fit lines with slopes above 0.9. Figure 3 shows the scatter plot of model and Jason-2 H_s over the entire Mediterranean. Given the large size of the dataset to display (242,766 points), model and satellite value pairs were grouped in square bins 0.25 by 0.25 m wide and areas corresponding to each bin were painted according to the number of value pair entries in the bin. Data dispersion around the 1:1 line is considerably small considering the overall number of samples.

Model results were further compared to buoy wave measurements collected by the Italian Wave Measuring Network (Rete Ondametrica Nazionale, RON) managed by Institute for Environmental Protection and Research (ISPRA). The network includes eight directional deep water buoys in operation since July 1989 recording significant wave height H_s , peak period T_p , mean period T_m and mean wave direction θ_m . Additional buoys were later added to the network. Until 2002, wave parameters were normally recorded every three hours.

During storms, when H_s exceeded a buoy-specific threshold, the recording rate was increased to 30'; in 2002 the measurement rate was set to 30' regardless of the sea state [13]. In the present work only three-hourly recorded data were taken into account in order to obtain a statistically homogeneous population. Buoys whose data record was considered too short were excluded from the analysis. Figure 4 shows the location of the RON buoys. Buoy measures were compared to model output extracted from the nearest computational node.

Figures 6 to 7 show the H_s scatter plots for selected buoys prepared following the same procedure described above for satellite data. Table 3 lists the values of the *bias*, *si*, *slope* and *rmse* for each buoy. Values in the tables suggest that the buoys can be grouped in three subsets depending on the level of agreement between model and buoy values. The results obtained at Alghero, Crotona, Cetraro and Capo Gallo buoys show very good agreement with the measurements with best-fit line slopes around the unity, biases of the order of centimeters and scatter indices below 0.4. For a second set of buoys including La Spezia, Ponza and Cetraro, the results appear to be still satisfactory but biases tend to be in the order of 0.1 m and best fit line slopes are below 0.9. H_s appears to be generally underestimated for the buoys located in the Adriatic Sea. This is probably due to the rather coarse resolution of the wind fields compared to the extent of the Adriatic Sea. H_s is also underestimated at the Catania buoy. This buoy is located in a sheltered position characterized by a mild wave climate, two factors that are known to contribute in reducing the model performance.

We further validated the wave model by comparing buoy and model average spectral period T_m which gives an broad estimate of the distribution of the wave energy density spectrum function $S(f, \theta)$ among the frequencies. In fact, as it will be shown, wave power flux is calculated from the significant wave period T_e , which is not directly available from the buoys measurements database. As shown in Table 4, the regression line slope is almost one for each buoy with the exception of Monopoli and Ancona where the model underestimates T_m and the *bias* is negative. For all the remaining buoys the model tends to overestimate the wave average period; where the regression line slope exceeds the unity, this trend is more marked at higher values of the period. The overestimation measured by the bias is relatively small. *Bias* values exceeding 0.5 s are found only at La Spezia. *Rmse* values are considerably higher than the ones obtained for H_s implying that model T_m values have higher dispersion. In any case, the absolute difference between buoy and model average period is less than 1 s in more than 70% of samples for all the buoys with the only exception of Catania.

4. Results

The Mediterranean model output was used to calculate the distribution of potential wave energy and to analyze its temporal variability. Following [14], in deep water, the available power flux per unit crest can be expressed as:

$$J = \frac{\rho g^2}{64\pi} T_e H_s^2 \quad (5)$$

where J is the energy flux in Watt per meter of wave crest, g is the gravity acceleration, ρ the sea water density assumed to be $\rho = 1025 \text{ kg/m}^3$, H_s the significant wave height and T_e the significant wave period. T_e represents the period of a sinusoidal wave having the same energy content of the sea state [15]. When the sea state is described by the spectral wave energy density function $S(f, \theta)$, T_e is given by the ratio between two moments of S :

$$T_e = \frac{m_{-1}}{m_0} \quad (6)$$

where the generic moment of S is given by:

$$m_n = \int_0^{2\pi} \int_0^\infty \sigma^n \cdot S(\sigma, \theta) d\sigma d\theta \quad (7)$$

Figure 7 shows a map of the available wave power flux per unit crest averaged over the entire simulation period 2001-2010 in the Mediterranean. The most productive area, with average values above 12 kW/m, is located in the western Mediterranean between the Balearic Islands and the western coast of Sardinia. The Sicily channel, off the north-western and southern Sicilian coasts, is also very productive with an average wave power flux per unit crest that reaches 9 kW/m. Slightly lower wave power appears to be available in central Mediterranean and southern Ionian Sea with average values not exceeding 8 kW/m near the coast. The western part of the Levantine basin exhibits similar values reaching almost 8 kW/m. The Adriatic sea, where average wave power does not exceed 3 kW/m, is one of the least productive regions. Similar values are observed in the most sheltered parts of the Ionian and Tyrrhenian between the mainland and Corsica and near the Messina Strait. The Aegean sea, despite its semi-enclosed configuration, appears to be more productive than the Adriatic Sea at least off the continental coast.

The results in Figure 7 show how, even in the relatively small Mediterranean basin, wave energy potential exhibits significant spatial gradients even at scales in the range 20-50 kilometers due to the combined effect played by land obstruction on wave propagation and on fetch length. This variability cannot be adequately described by lower resolution models or by local buoy measurements.

Seasonal distribution of wave energy also plays an important role in the selection of a specific site. In the Mediterranean, the winter and fall seasons are the most energetic while calmer sea states are normally observed during the rest of the year [12].

The wave power fluxes calculated by the model exhibit a similar trend.

Figure 8 shows the spatial distribution of seasonal average power flux in the Mediterranean for the entire simulation period. As expected, the winter months of December, January and February are the most productive followed by the autumn ones. Wave power spatial distribution follows approximately the pattern described for the yearly average. Some differences can be found in the Central Mediterranean, which appears to be especially energetic during the winter season and calm during the summer. The seasonal variation range tends to be smaller, in relative terms, in the Western Mediterranean and in the Sicily Channel compared to less productive areas.

From the results of the Mediterranean model appears that the Sicily Channel is one of the most promising areas for wave energy production both in terms of average availability and seasonal variability. Higher amount of wave energy is generally available near small islands located far from the main coastlines.

The Island of Pantelleria was chosen to perform an in-depth wave energy assessment. This island is located near the most productive areas within the Sicily Channel and, being more than 100 km far from the Sicily coast, needs to rely on local energy production. In order to describe in detail the wave energy potential around Pantelleria a very high resolution model was nested in the coarse model. Figure 9 shows the average wave power per unit crest distribution in the Sicily Channel and the location of the nested grid. It can be observed how wave energy potential tends to reach its maximum in the middle of the Sicily Channel just near the island.

Figures 10a and 10b show the average power flux obtained from the Mediterranean model and from the nested high resolution model around Pantelleria for the entire simulation period.

By observing the figures it appears that the main contribution to wave energy comes from waves propagating from N-NW.

The sheltering effect of the island results in a lower amount of available power in the S-SE coast. The main features of the wave energy distribution around the island are captured both by the fine and coarse model, however the high resolution model shows a systematic reduction of the available energy when approaching the coast in the most energetic section of the coastline. Near the northern and southern section of the island the finer details in the wave energy potential calculated by the high resolution result in higher energy potential near the coastline compared to the coarse model values. The shape of the low energy shadow area on the SW coast is also better resolved in the high resolution model.

In order to get some additional insight on the differences between the Mediterranean model and the high resolution nested model, the distribution of wave energy among sea states was analyzed in two points, one near shore and one about 10 km offshore, along the most productive area (see Figure 10 b). The offshore point falls approximately at the center of the coarse model cell placed at the NW corner of the island. Figures 11 and 12 show the distribution of wave energy among sea states.

The scatter plot at lower left panel of the figures represents the distribution of yearly average energy in terms of T_e and H_s , evaluated over the 10 years period. The contribution to the total energy given by an individual sea state described by T_e and H_s are classified in rectangular intervals defined by a 0.25 s wide interval for T_e and 0.25 m wide interval for H_s and the corresponding rectangle is colored according to the total energy. Lines of constant power are drawn on the scatter plots to highlight wave power variability. On the upper and right panels of each scatter plot two histograms shows the distribution of average yearly wave energy over T_e and H_s respectively. In each histogram a red line represents the cumulated percentage of total energy available in terms of T_e and H_s . Red markers are placed every 10th percentile on the cumulated line. In the upper-right panel a rose diagram describes the directional distribution of average yearly energy over 30° wide direction bins. Each concentric circle represents 20% contribution to the total wave energy.

Looking at Figures 11 and 12 it appears that the amount of available wave power is reduced by more than 20 %, from 6.7 kW/m to 5.2 kW/m, from the offshore location to the near shore one. The distribution of wave energy among sea states for the two locations is very similar with a slight increment at the near shore location in the fraction associated to sea states with high period and low wave heights. Directional distribution of incoming wave energy is much more concentrated around the NW direction near the coast (80%) compared to the offshore location (only 60 %).

The differences between the results of the two models tend to become less significant when moving to the open sea. In fact, the average wave power measured at the offshore point is almost the same value obtained from the first active cell NW of Pantelleria in the coarse model (6.8 kW/m).

As most wave energy converters are expected to be placed near the coastline where they are more easily connected to the power grid, it is extremely important to have a reliable description of wave energy from high resolution models.

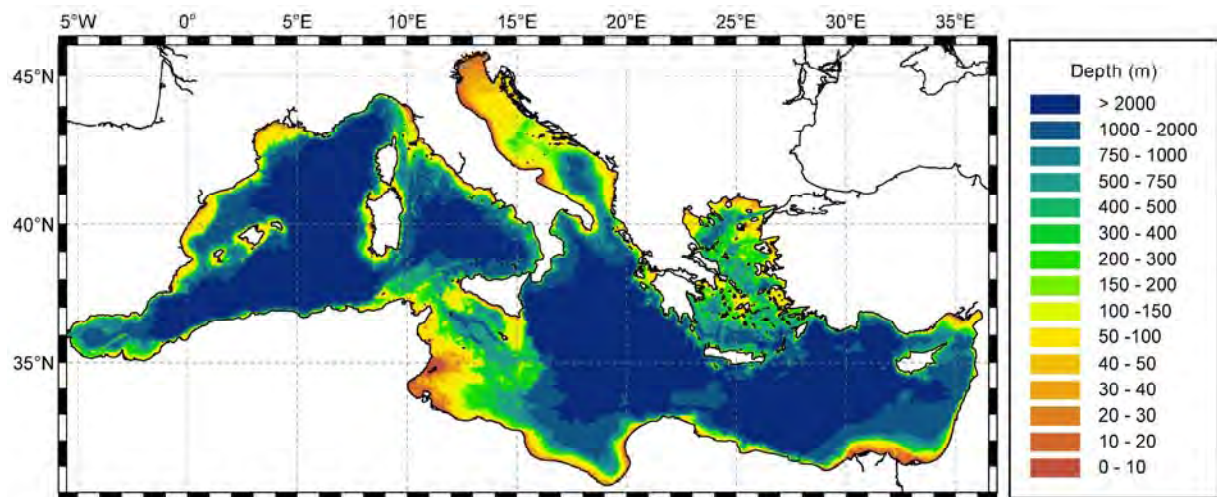


Figure 1: Mediterranean model domain and bathymetry.

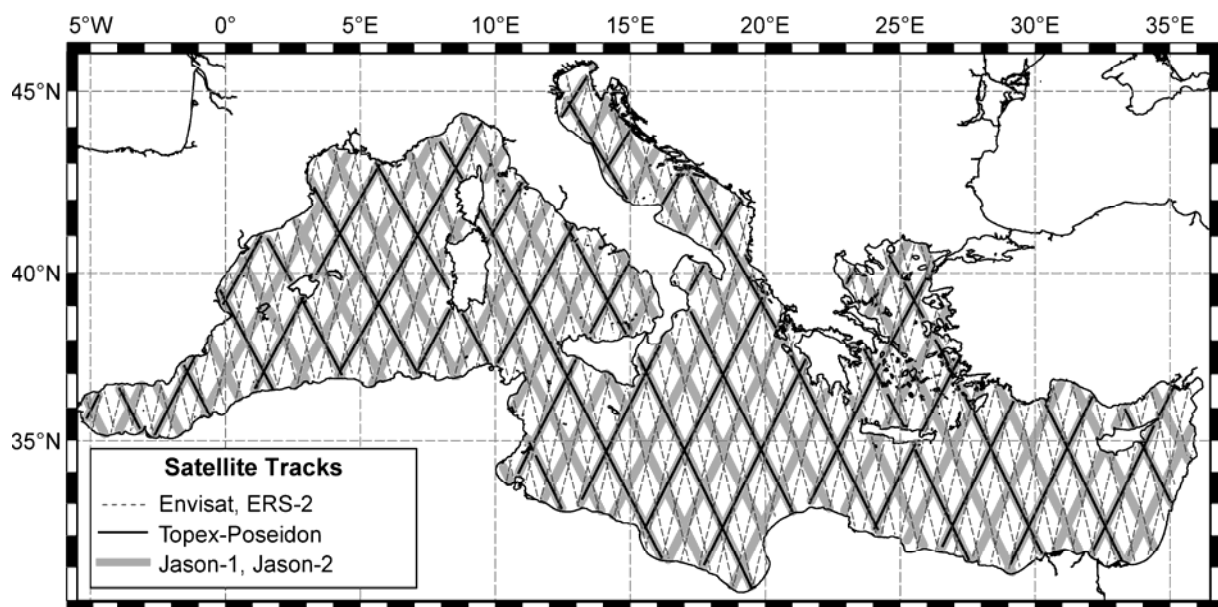


Figure 2: Tracks of Satellites performing radar altimeter measurements over the Mediterranean between 2001 and 2010.

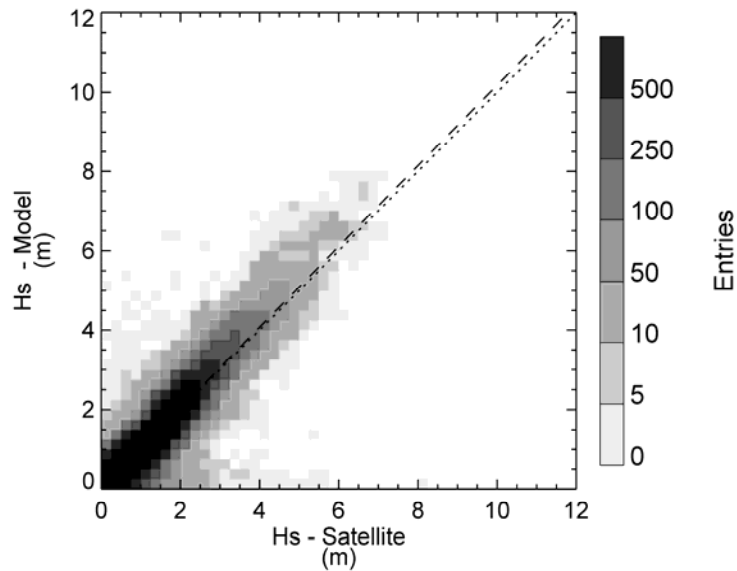


Figure 3: Scatter plot of model vs. Jason-2 H_s for the entire Mediterranean. Dashed line is the best-fit line between model and satellite data points.

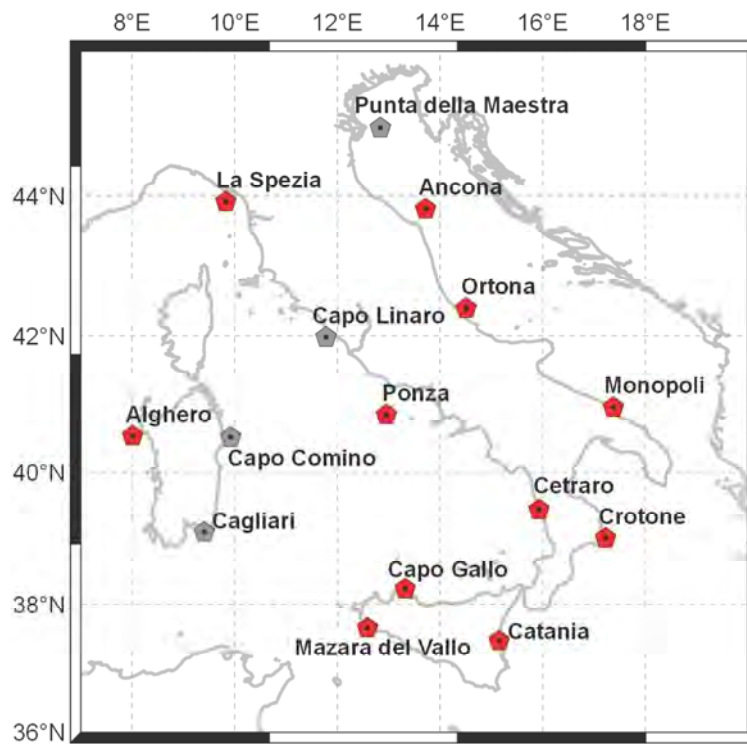


Figure 4: Locations of wave buoys of the Italian Wave Measuring Network (Rete Ondametrica Nazionale, RON). Red symbols indicate buoys included in model validation.

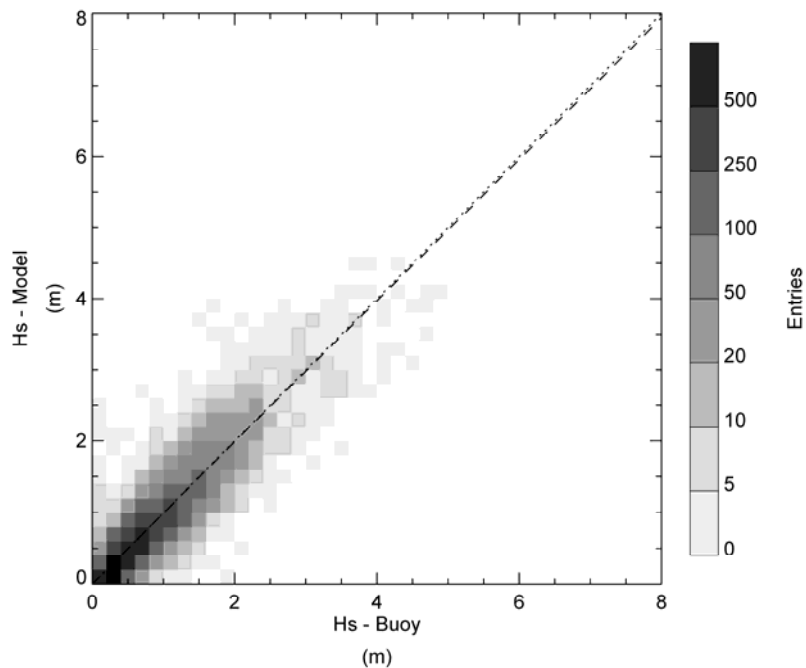


Figure 5: Correlation between buoy and model H_s at Crotona. Dashed line is the best-fit line between model and buoy data points.

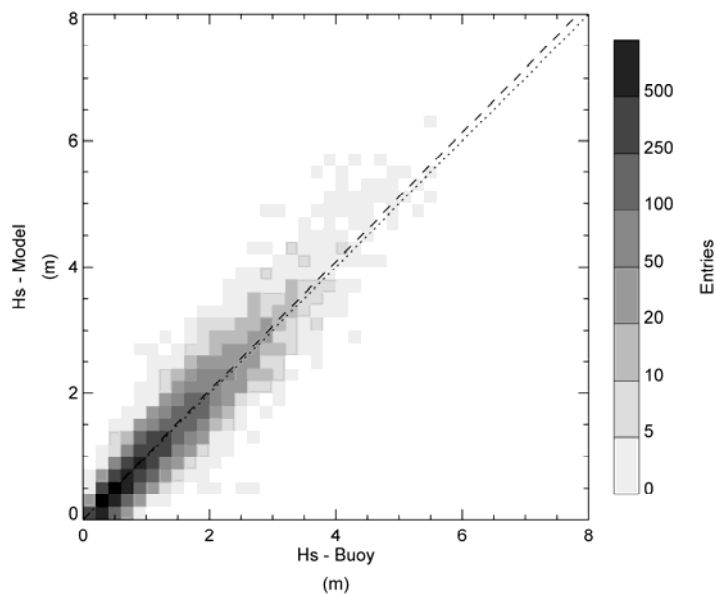


Figure 6: Correlation between buoy and model H_s at Mazara del Vallo. Dashed line is the best-fit line between model and buoy data points.

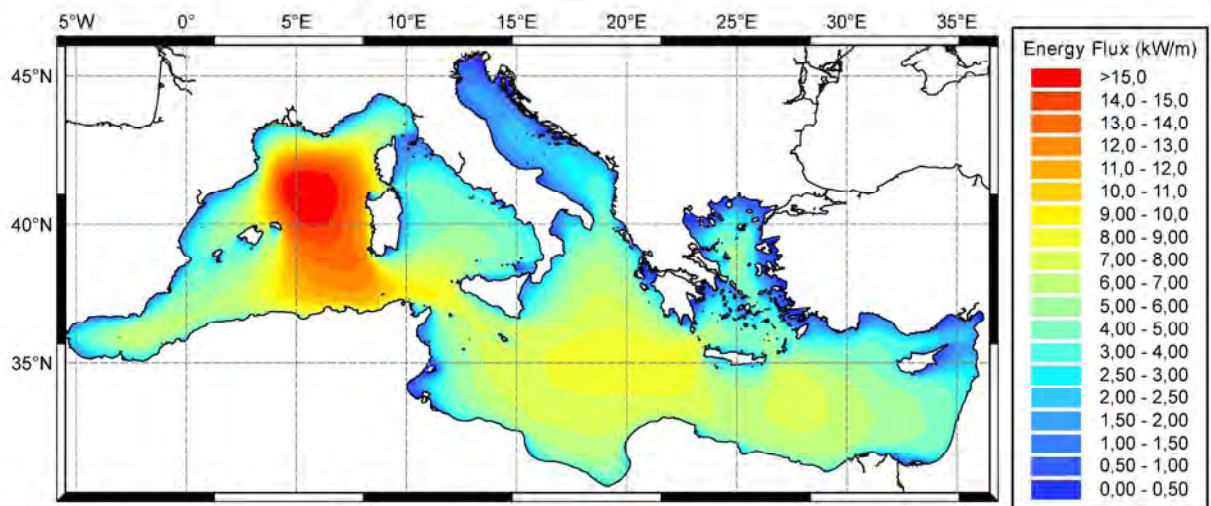


Figure 7: Average power flux per unit crest distribution in the Mediterranean between 2001 and 2010.

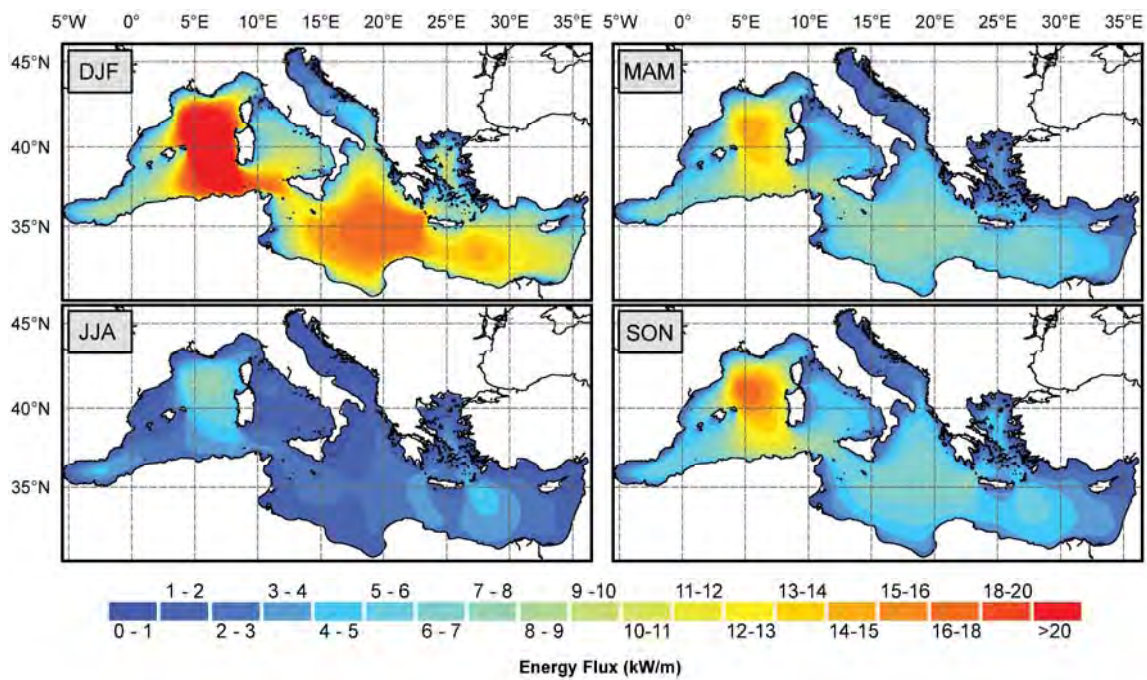


Figure 8: Average seasonal distributions of wave power flux per unit crest in the Mediterranean between 2001 and 2010. DJF: December, January, February; MAM: March, April, May; JJA: June, July, August; SON: September, October, November.

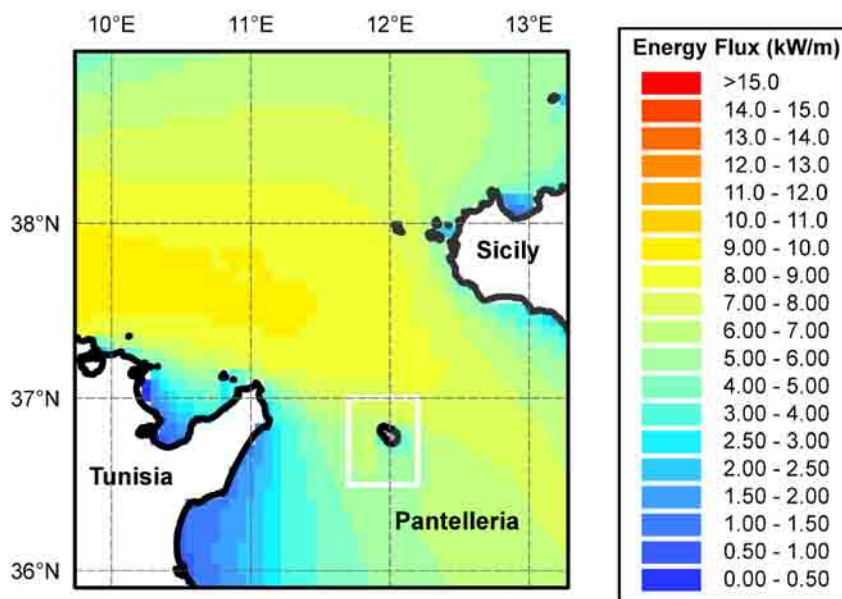


Figure 9: Average wave power flux per unit crest in the Sicily Channel between 2001 and 2010. White rectangle marks the outer limits of the nested model computational domain.

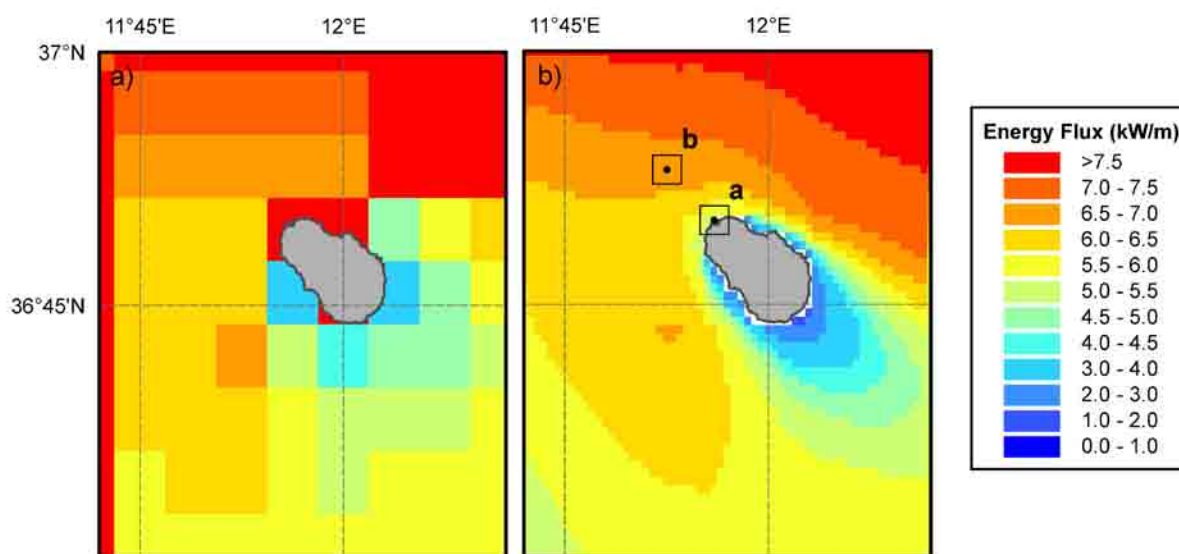


Figure 10: Average wave power flux per unit crest around Pantelleria between 2001 and 2010. a) Mediterranean model results b) High resolution results.

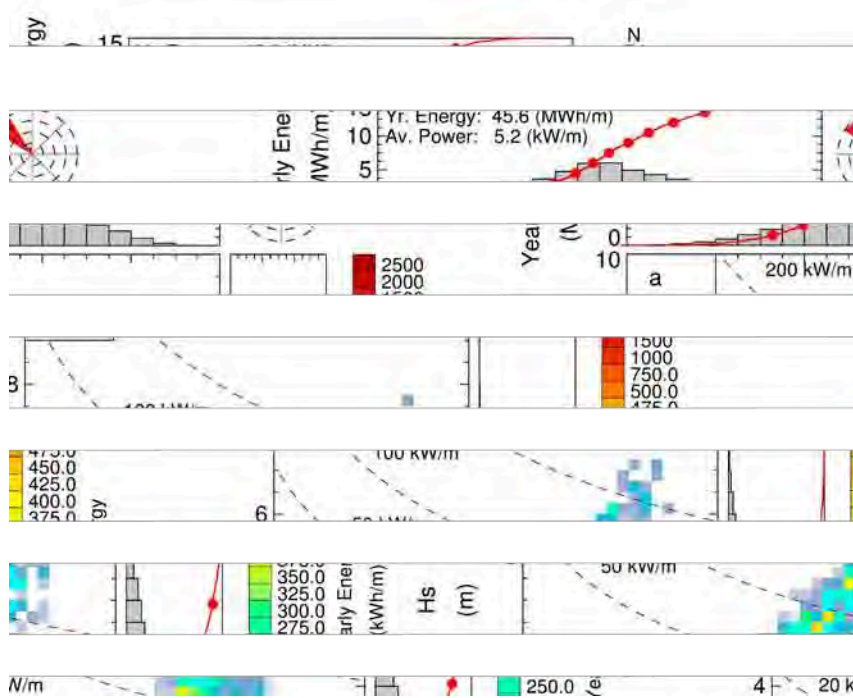


Figure 11: Distribution of wave energy among sea states for the entire simulation period at location a) as reported in Figure 10.

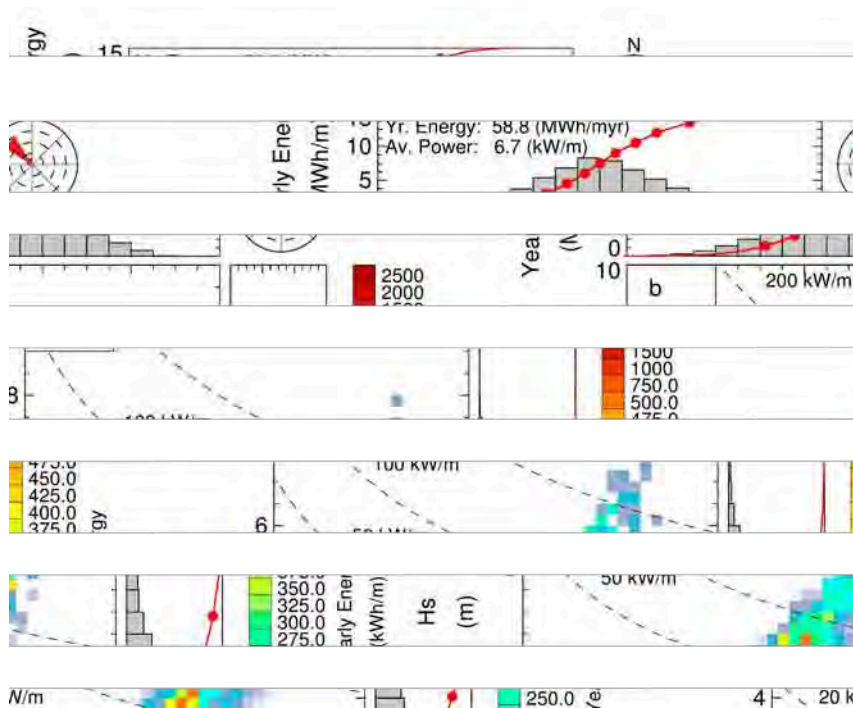


Figure 12: Same as Figure 11 for location b) as reported in Figure 10.

Table 1: Characteristics of satellites used for model validation.

Satellite	Repeat Cycle (days)	Track Separation at the equator (km)	Period Considered
Topex-Poseidon	10	315	Jan. 2001 - Oct. 2005
Jason-1	10	315	Jan. 2002 - Dec. 2010
Jason-2	10	315	Jun. 2008 - Dec. 2010
Envisat	35	80	Oct. 2002 - Oct. 2010
ERS-2	35	80	Jan. 2001 - Dec. 2006 Jan. 2008 - Dec. 2010

Table 2: Statistics of satellite and model significant wave height (H_s) comparison for the entire Mediterranean.

Satellite	Samples	Bias (m)	Rmse (m)	Slope	Si
Topex-Poseidon	457,000	-0.128	0.331	0.912	0.279
Jason-1	910,133	-0.028	0.362	0.979	0.304
Jason-2	242,766	0.024	0.366	1.018	0.303
Envisat	695,768	-0.141	0.385	0.921	0.310
ERS-2	363,336	-0.011	0.426	0.962	0.400

Table 3: Statistics of buoy and model significant wave height (H_s) comparison.

Buoy	Samples	Bias (m)	Rmse (m)	Slope	Si
Alghero	15,283	-0.005	0.311	0.985	0.278
Ancona	10,212	-0.214	0.361	0.725	0.477
Catania	12,549	-0.178	0.308	0.747	0.501
Crotone	14,962	0.004	0.276	0.993	0.374
La Spezia	10,952	-0.011	0.426	0.962	0.400
Mazara del Vallo	15,323	0.013	0.257	1.022	0.253
Ortona	12,786	-0.150	0.284	0.753	0.460
Ponza	14,479	-0.103	0.273	0.892	0.328
Monopoli	15,641	-0.124	0.307	0.836	0.427
Cetraro	16,630	-0.070	0.241	0.897	0.341
Capo Gallo	9,001	0.019	0.255	1.040	0.339

Table 4: Statistics of buoy and model wave average spectral period (T_m) comparison.

Buoy	Bias (s)	Rmse (s)	Slope	Si
Alghero	0.230	0.791	1.032	0.172
Ancona	-0.349	0.959	0.883	0.240
Catania	0.142	1.163	0.996	0.274
Crotone	0.206	0.805	1.031	0.207
La Spezia	0.506	1.049	1.107	0.257
Mazara del Vallo	0.195	0.780	1.030	0.177
Ortona	0.063	0.718	0.992	0.198
Ponza	0.035	0.646	0.993	0.160
Monopoli	-0.327	1.017	0.877	0.257
Cetraro	0.156	1.009	1.004	0.223
Capo Gallo	0.307	0.925	1.048	0.225

9. Acknowledgements

The altimeter products were produced by CLS Space Oceanography Division and distributed by AVISO, with support from CNES. We are grateful to the CRESCO supercomputing facilities located at ENEA (<http://www.cresco.enea.it>).

References

1. Association EOE: Oceans of energy European Ocean Energy Roadmap 2010-2050. Tech. Rep.; European Ocean Energy Association; 2010.
2. AFDO. Falcão AFDO: Wave energy utilization: A review of the technologies. In *Renewable and Sustainable Energy Reviews*, vol. 14(3), pp, 899–918, Elsevier, 2010.
3. IEA. Implementing agreement on ocean energy systems. Tech. Rep.; IEA; 2010.
4. A. M. Cornett: A global wave energy resource assessment. In *Proceedings of the 18th International Offshore and Polar Engineering Conference*, Vancouver, BC, Canada. 2008.
5. S. Barstow, G. Mørk, L. Lønseth, JP. Mathisen: World waves wave energy resource assessments from the deep ocean to the coast. In: *Proceedings of the 8th European Wave and Tidal Energy Conference*, Uppsala, Sweden. 2009.
6. G. Mørk, S. Barstow, A. Kabuth, M. T. Pontes: Assessing the global wave energy potential. In: *Proceedings of the 29th International Conference on Ocean, Offshore Mechanics and Arctic Engineering*, 2010.
7. D. Vicinanza, L. Cappiotti, V. Ferrante, P. Contestabile: Estimation of the wave energy in the Italian offshore. In: *Journal of Coastal Research*, 64(12), pp. 613–617, 2011.
8. L. Cavaleri, L. Bertotti: Accuracy of the modeled wind and wave fields in enclosed seas. In: *Tellus A*, 56(2), pp 167–175, 2004.
9. H. Günther, A. Behrens: The WAM model validation document version 4.5.3. Tech. Rep.; *Institute of Coastal Research Helmholtz-Zentrum Geesthacht (HZG)*, 2011.
10. GEBCO.<http://www.gebco.net/data and products/gridded bathymetry data/>;
11. Aviso. <ftp://ftp.aviso.oceanobs.com/pub/oceano/AVISO/>, 2011.
12. P. Queffelec, A. Bentamy: Analysis of wave height variability using altimeter measurements: Application to the Mediterranean sea. In: *Journal of Atmospheric and Ocean Technology* 24 (12), pp. 2078–92, American Meteorological Society, 2007.
13. S. Corsini, L. Franco, R. Piscopia, R. Inghilesi: L’atlante delle onde nei mari italiani - Italian wave atlas. Tech.Rep.; APAT (ISPRA), 2004.
14. R. Waters, J. Engström, J. Isberg, M. Leijon: Wave climate off the Swedish west coast. In *Renewable Energy*, 34(6), pp. 1600–1606, 2009.
15. G. Iglesias, R. Carballo: Wave energy resource in the Estaca de Bares area (Spain). In *Renewable Energy*, 35(7), pp. 1574–1584, 2010.

Session 3: Wind Turbines Innovation

Chairmen: F. Vorpahl, G. Arsuffi

TPWind and European projects in offshore wind sector - Manuela Conconi (European Wind Energy Association)

An investigation of different offshore wind turbine jacket support foundation models designed for Central Mediterranean deep waters - T. Gauci, T. Sant, M. Muscat, P. Mollicone, D. Camillieri (Dept. Mechanical Engineering, Univ. of Malta, Msida (MT))

Design of a spar buoy for Offshore Wind turbines - C. Romanò, E. Giorcelli, G. Mattiazzo, M. Raffero (DIMEAS - Dpt. Ingegneria Meccanica e Aerospaziale - Politecnico di Torino, Turin (IT))

RAVE - Joint research at Germany's first offshore Wind Park Alpha Ventus - E. Otto, M. Durstewitz, B. Lange, B. Lange, S. Pfaffel (Fraunhofer Institute for Wind Energy and Energy System Technology, Kassel (DE))

Turbine foundation in intermediate waters: monopile versus jacket - F.G. Cesari, F. Taraborrelli (DIENCA Dept., Bologna Univ. (IT)), T. Balestra (Tecon s.r.l., Assago-Milan (IT)), L. Milella (TRE SpA, Bari (IT))

TPWind and European projects in offshore wind sector

Manuela Conconi

European Wind Energy Association

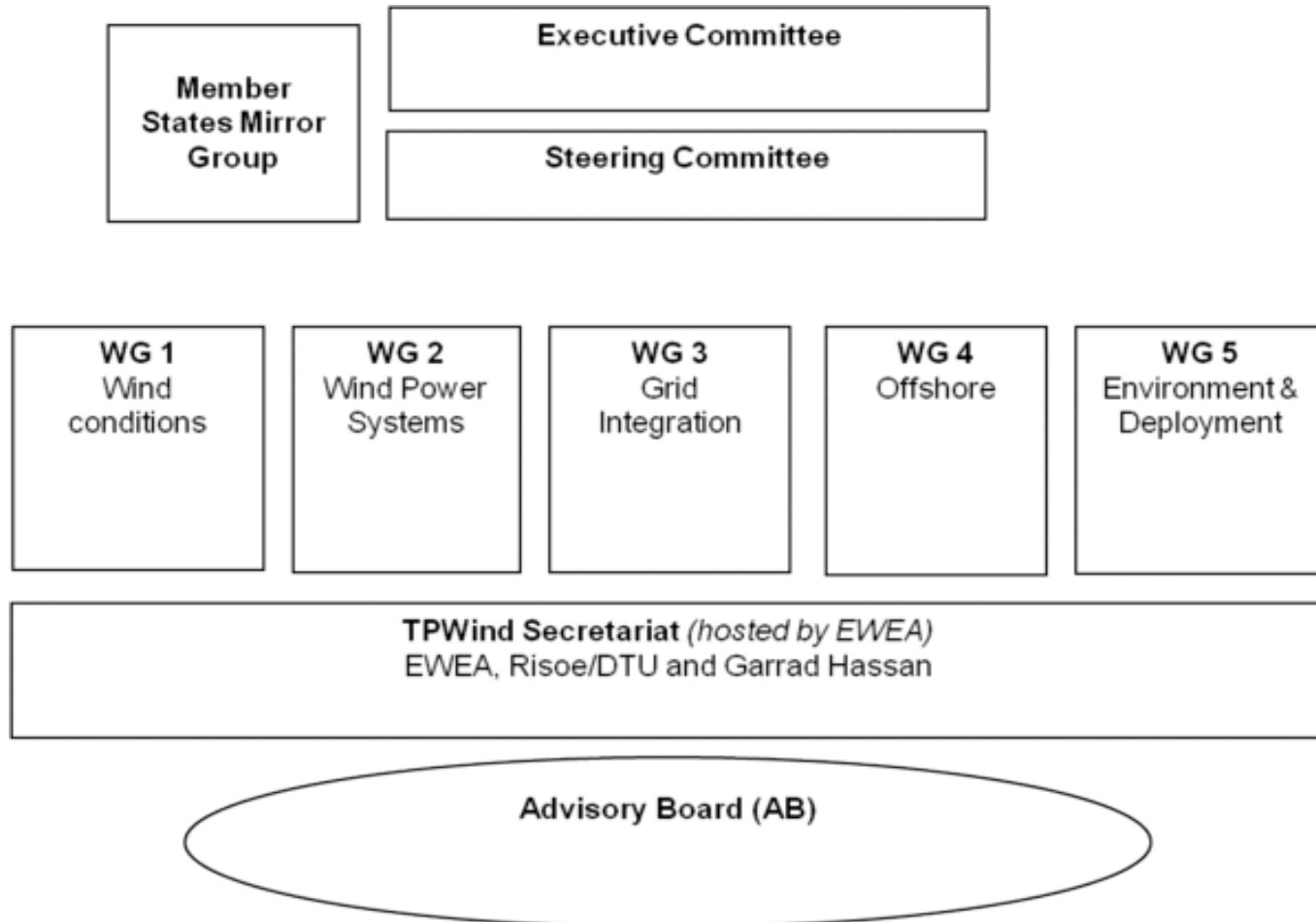


TPWind and European projects in offshore wind sector

Manuela Conconi



TPWind structure (www.windplatform.eu)



The EWI – European Wind Initiative

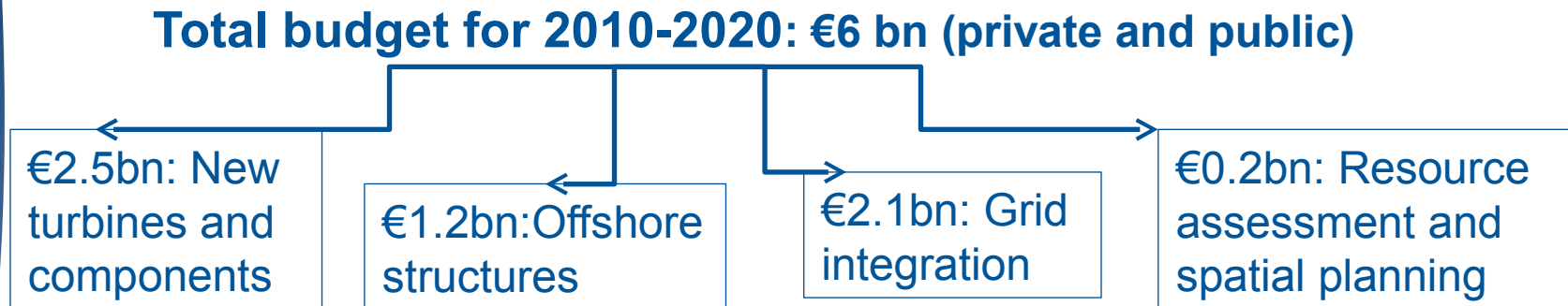
- Aim: improved and increased public funding for wind energy R&D
- One of the goals of the EU Strategic Energy Technology Plan (SET-Plan), was to launch European Industrial Initiatives (EIs), i.e. Programmes for fostering R&D in 8 strategic energy sectors:

Wind	Bio-energy
Solar	Energy efficiency
Nuclear	Smart grids
CCS	Hydrogen and fuel cells

The EWI is rooted in the SET-Plan, a 2007 blueprint for the development of low-carbon technologies, and it was produced by TPWind in cooperation with EU Institutions and Member States

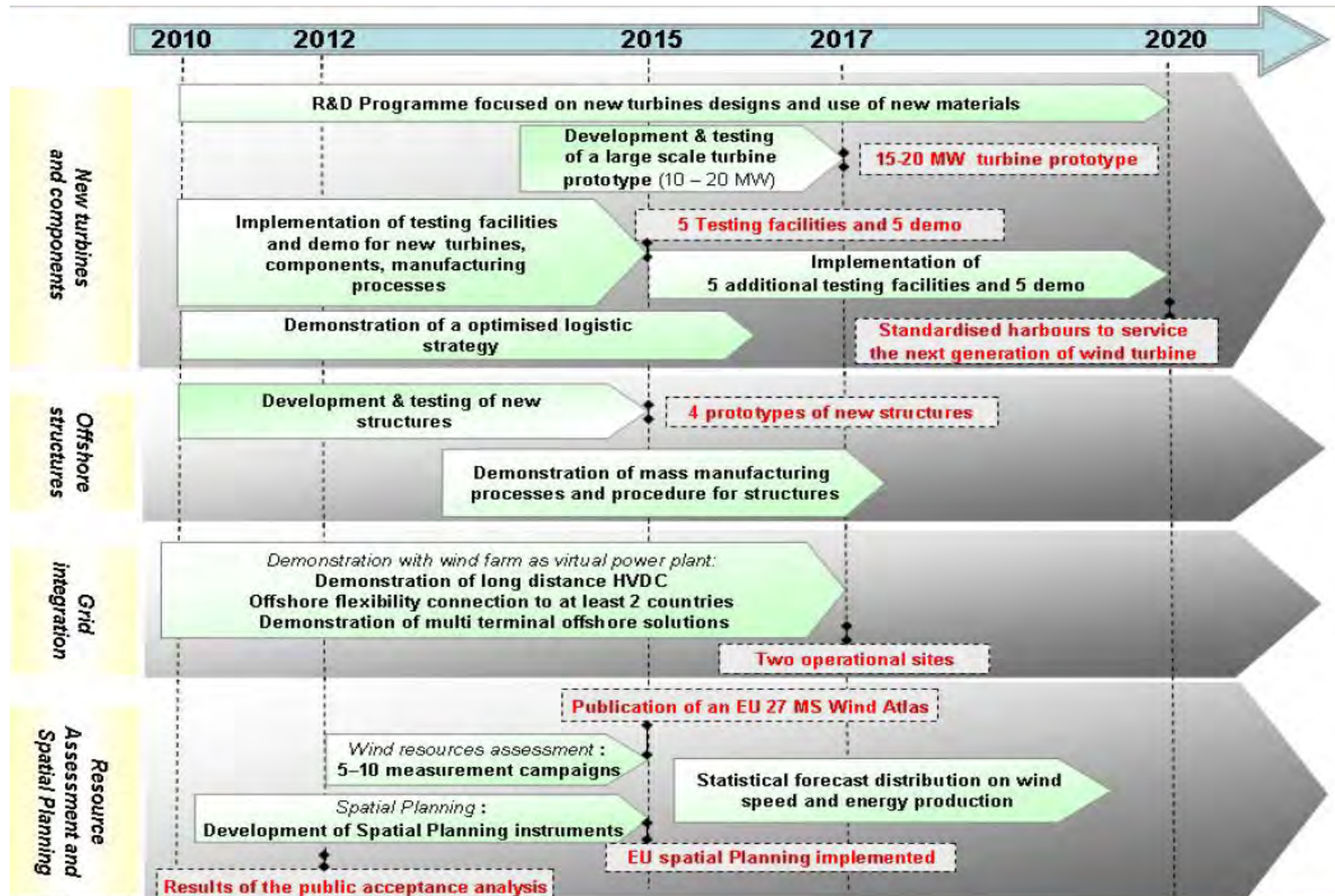
The EWI - structure

- Published in 2009 (EC Communication: “Investing in the development of low carbon technologies”)
- Launched in 2010
- Wind energy R&D funding : 2010 – 2020 period
- 3-years Implementation Plan
- Implemented by TPWind, EU institutions and Member States





The EWI: overview

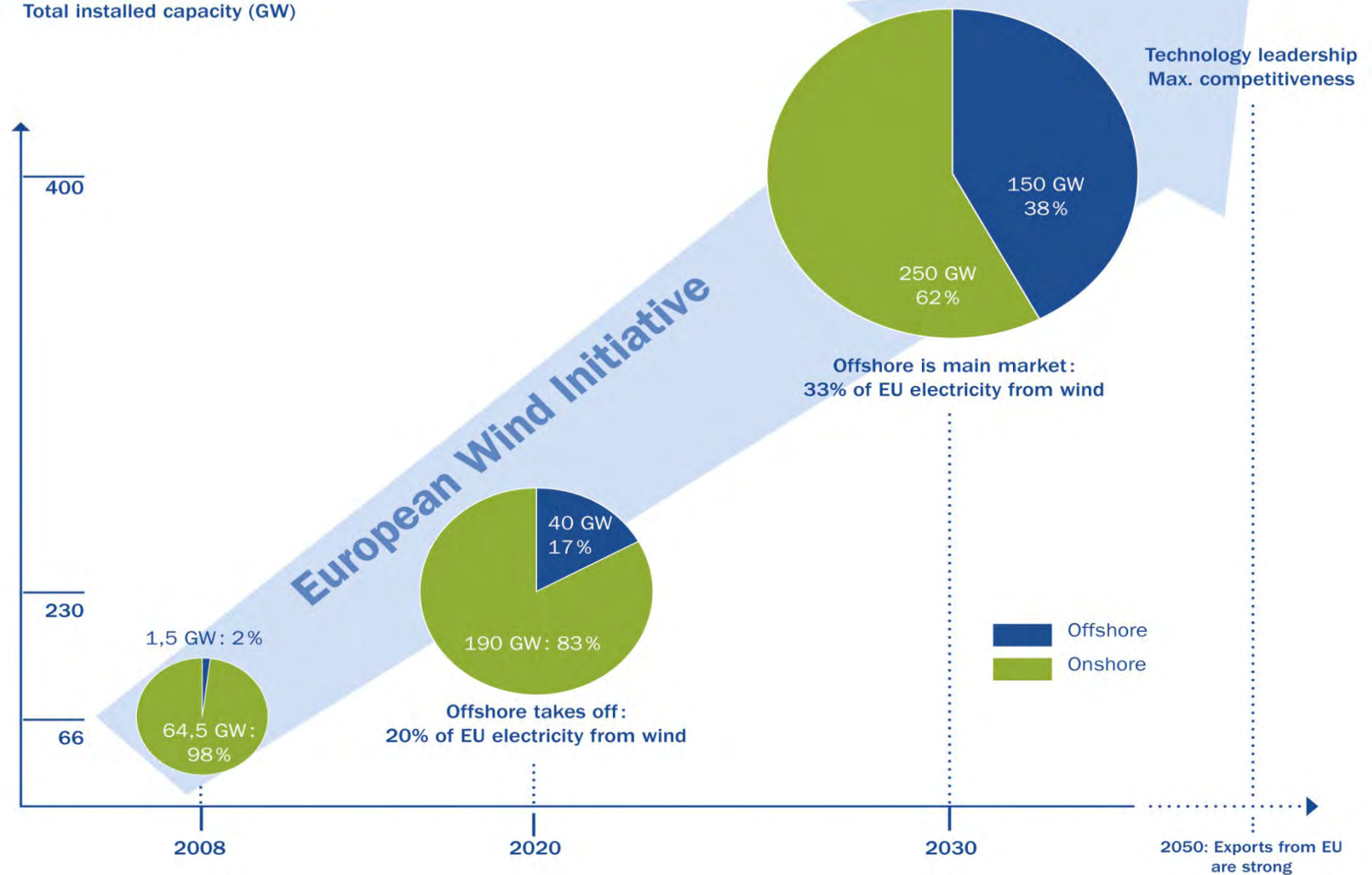




The EWI: expected impact on the sector

Sustained European technology leadership

Total installed capacity (GW)



2011 offshore wind power market

- 235 new offshore wind turbines installed, worth some €2.4 billion
- 866 MW in total – 17 MW less than 2010
- Nine wind farms were fully completed and grid connected in 2011
- Three experimental floating concepts were erected, one of which was a full scale grid connected concept.
- 87% of new capacity was added in the UK

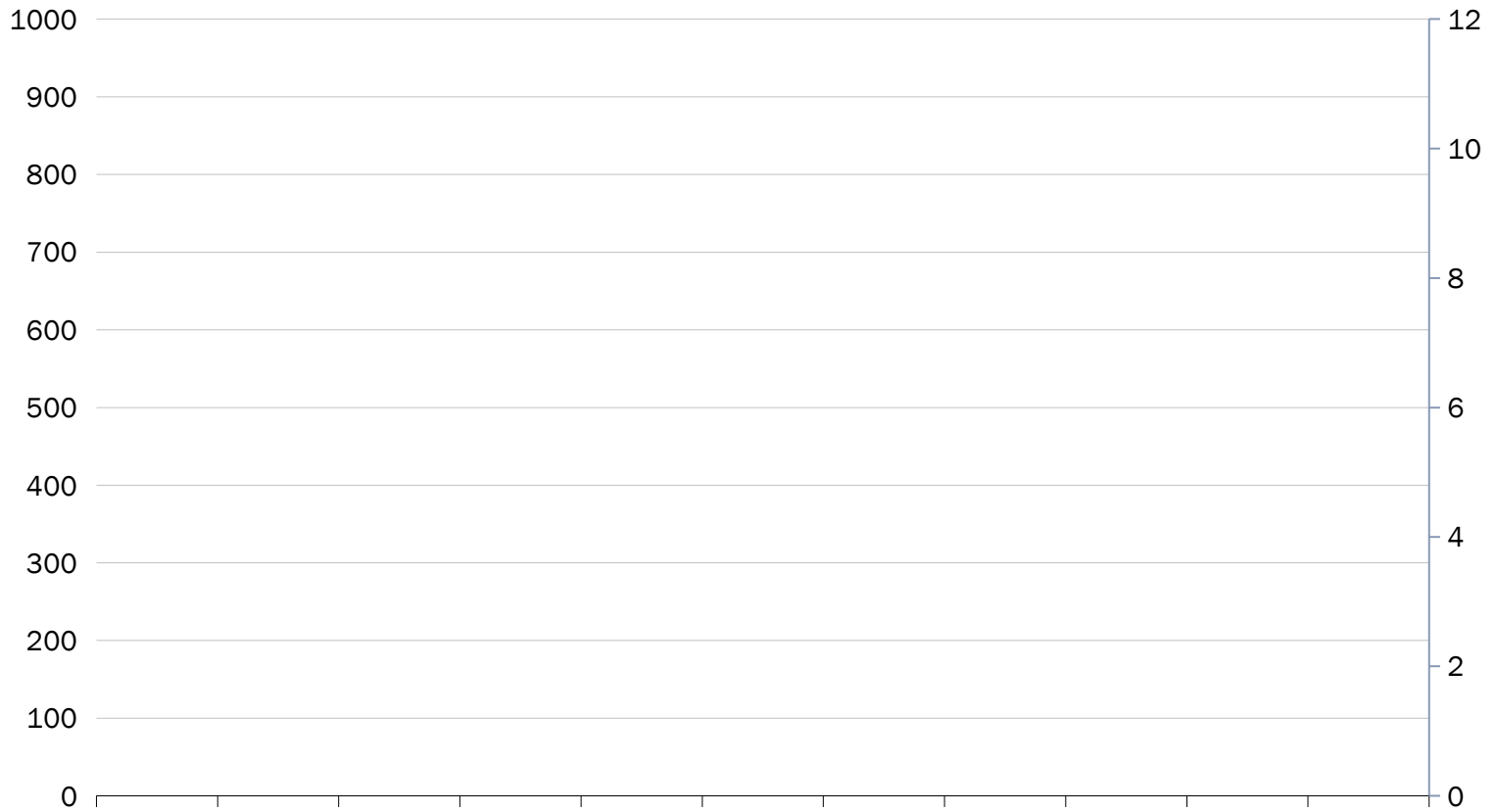
Market outlook: 2012 and beyond

- Bringing cumulative capacity in Europe to **4,336 MW** (30/06/2012)
- 132 new offshore wind turbines,
- 523.2 megawatts (MW) fully grid connected in Europe in the first six months of 2012.
- 50% increase compared to the same period in 2011 (when 348.1 MW were installed). →
- 13 wind farms under construction 3,762 MW

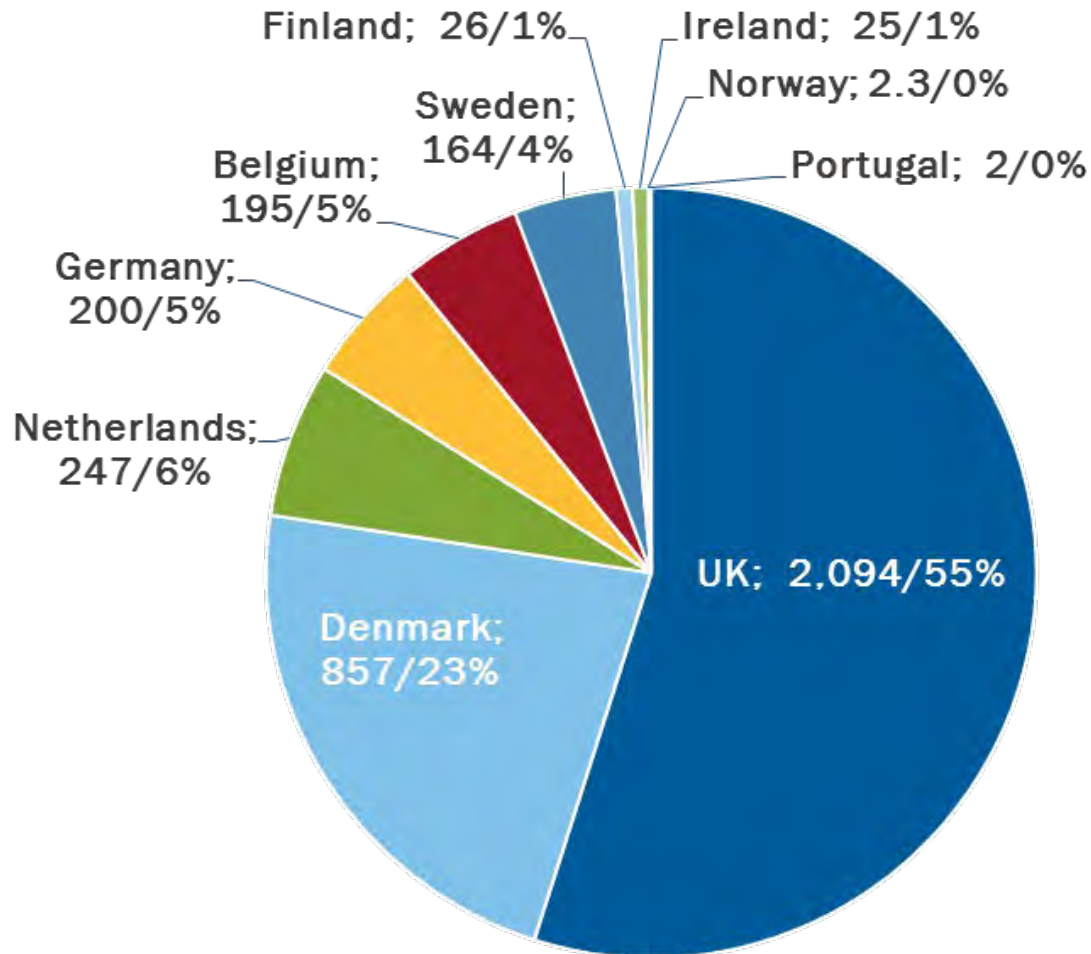
Cumulative and annual offshore wind installations (MW)

Annual

Cumulative



Installed capacity: Share of 2011 installations (MW/%)

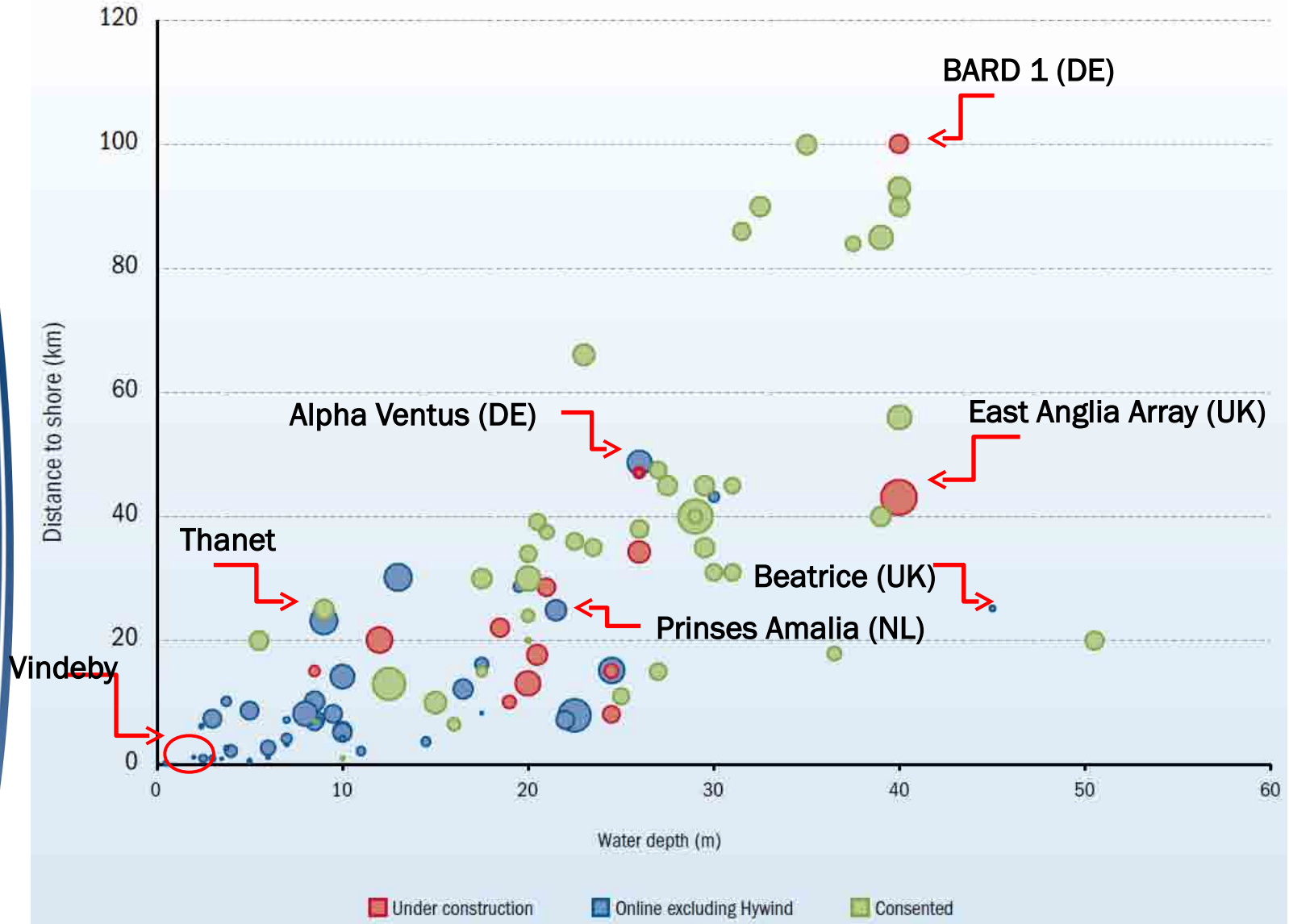


Offshore wind energy market in the EU 2011 – 2020 (MW)

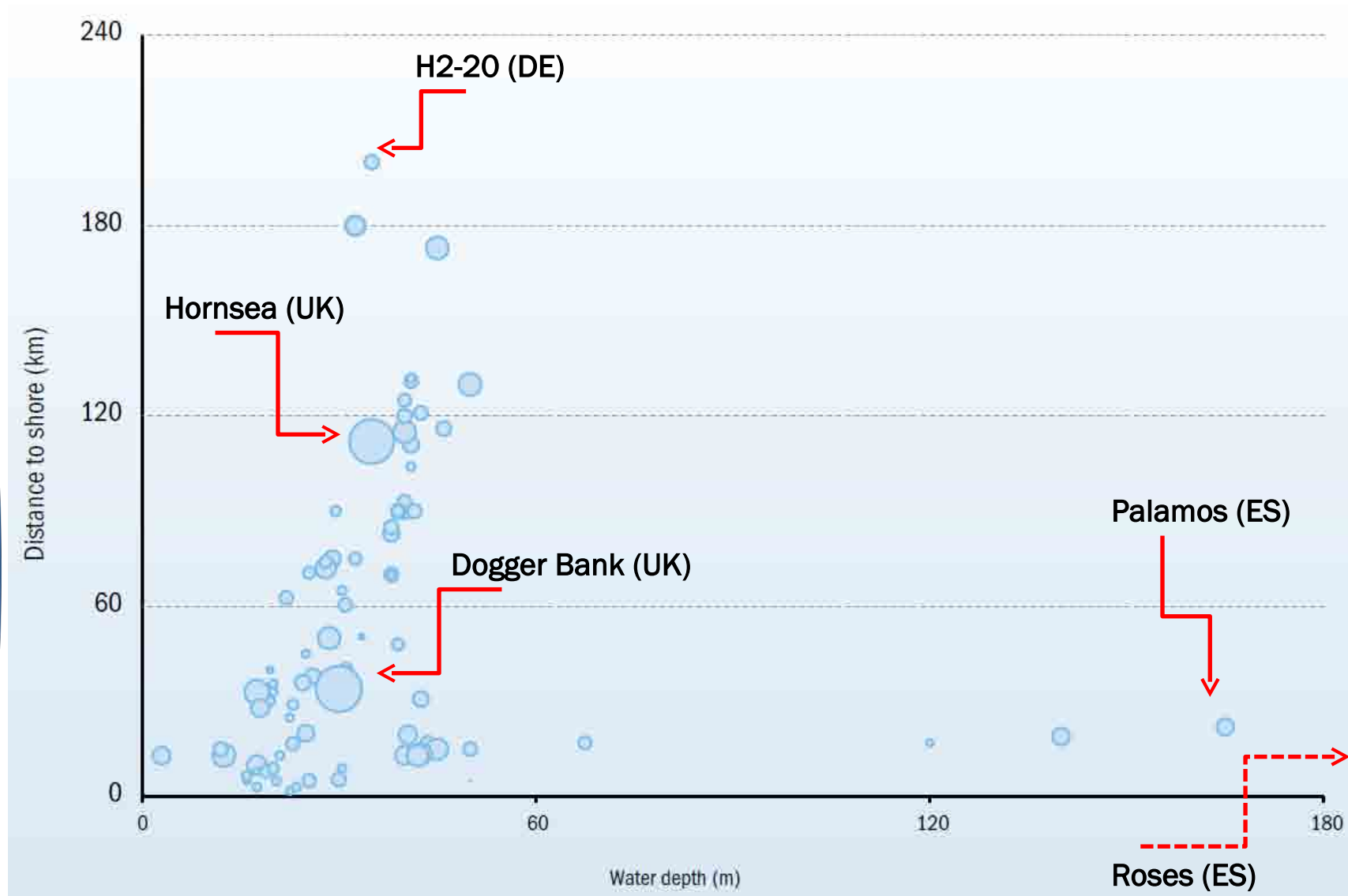


- 2012: annual installations of around 1.4 GW
- 2020: annual installations of 6.9 GW
- 2020: cumulative installations of 40 GW

Distance and water depth of wind farms



Distance and water depth of wind farms



EU offshore projects (I)

ORECCA

- **Coordinated Action**
- **Knowledge sharing on offshore renewable energy conversion platforms**
- **Coordinator : Fraunhofer - IWES**
 - ▶ **Off-shore Renewable Energy Conversion platforms**
 - ▶ Grant agreement number: 241421
 - ▶ 18 months – March 2010 to August 2011
 - ▶ 28 partners from 11 different countries
 - ▶ Total budget: 1,797,870 €
 - ▶ Max. EC contribution: 1,599,032 €
 - ▶ Website: www.orecca.eu



EU offshore projects (II)

MARINA platform

MARINA Platform

- **Multipurpose floating platform**
- **Potential combination wind-ocean energy**
- **Coordinator : Acciona Energia S.A.**
 - ▶ **MArine Renewable INtegrated Application Platform**
 - ▶ Collaborative Project
 - ▶ Grant agreement number: 241402
 - ▶ 54 months – January 2010 to June 2014
 - ▶ 17 partners from 12 different countries
 - ▶ Total budget: 12.761.220€
 - ▶ Max. EC contribution: 8.708.660€
 - ▶ Website: www.marina-platform.info



EU offshore projects (III) - DEEPWIND

DEEPWIND

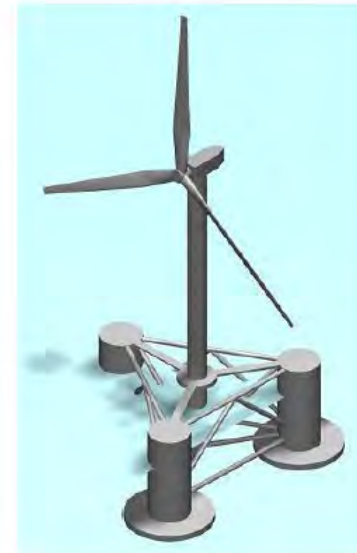
- **FET- Collaborative**
- **Future Deep Sea Wind Turbine Technologies**
- **Coordinator : DTU-RISOE (DK)**
 - ▶ **Vertical Axis Floating Wind Turbine**
 - ▶ Grant agreement number: 256769
 - ▶ 48 months – October 2010 to September 2014
 - ▶ 12 partners from 6 different countries
 - ▶ Total budget: 4,178,234 €
 - ▶ Max. EC contribution: 2,992,438 €
 - ▶ Website: www.deepwind.eu



EU offshore projects (III) - HiPRwind

HiPRwind

- **Large-Scale Collaborative**
- **High Power, high Reliability offshore wind technology**
- **Coordinator : FhG-IWES (DE)**
 - ▶ **Floating wind energy system**
 - ▶ Grant agreement number: 256812
 - ▶ 60 months – November 2010 to October 2015
 - ▶ 19 partners from 9 different countries
 - ▶ Total budget: 19,831,585 €
 - ▶ Max. EC contribution: 11,021,621 €
 - ▶ Website: www.hiprwind.eu

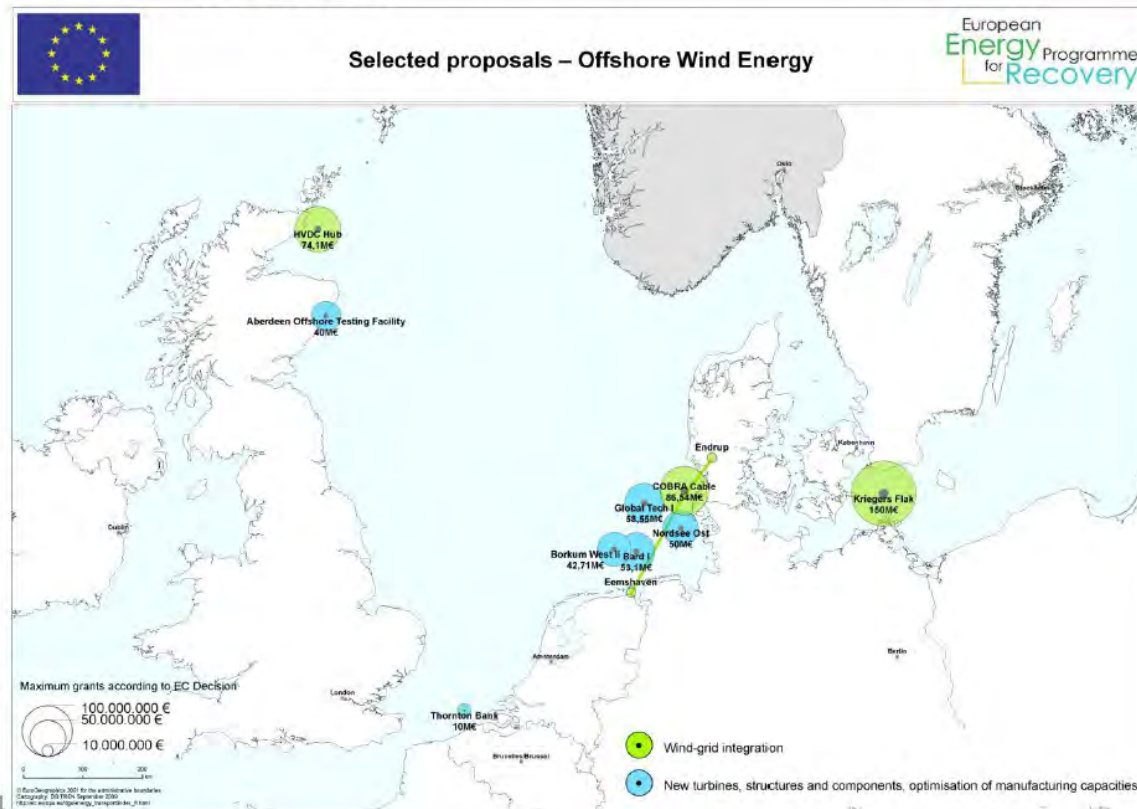




Recovery Plan Offshore Wind Energy

Recovery Plan Offshore Wind Energy: (2009-2010)

- **Grid integration of offshore wind energy (315 M €)**
 - **New turbines, structures, components, optimisation of manufacturing (250 M €)**
- TOTAL: 565 M€**



03/2011

Thank you

www.windplatform.eu

www.ewea.org

mco@ewea.org

An investigation of different offshore wind turbine jacket support foundation models designed for Central Mediterranean deep waters

T. Gauci¹, T. Sant, M. Muscat, P. Mollicone and D. Camillieri

Dept. Mechanical Engineering, University of Malta, Msida MSD 2080 Malta,

¹thomas.gauci@um.edu.mt, Tel.: (+356) 2340 2032, (+356) 79370423

Abstract – The trend for improving the cost effectiveness of offshore wind turbines is to maximise wind turbine size while minimising support structure costs. Minimising the support structure costs in deeper waters is undoubtedly more challenging. Studies have shown that the type of foundation model used at the base of the support structure has a significant influence on the overall design result. Two foundation models are studied independently: the pinned foundation and the rigid foundation. The effect of the foundation type on the modeled overall support structure characteristics, are investigated. The objective of this study is to produce an optimised jacket design for a 70 metre water depth in the central Mediterranean region. The study shows that different foundation types influence the internal loads of the individual jacket members and consequently affect the structure's natural frequencies. The final result shows that the jacket structure with a pinned foundation design was 43.6 tonnes lighter than its rigid counterpart.

1. Introduction

Current offshore wind energy is significantly more expensive than onshore wind energy [1]. A main contributing factor to the expense of offshore wind is the requirement of relatively expensive support structures and their foundations. This requirement is a necessity due to the harsher weather conditions at sea and the larger and more expensive infrastructure required for installation and maintenance.

Regardless of these challenges, offshore wind technology as a whole is advancing at an accelerating rate due to the large energy potential available in this environment. Increasing research efforts and continuous advancements in offshore technology are increasingly being made.

The main technology drivers today are to increase the cost effectiveness of offshore wind energy by increasing turbine size and reducing substructure costs. This will enable project developers to exploit offshore areas in deeper waters located more distant from the coast where consenting is less difficult.

Malta, an island in the central Mediterranean region, is almost totally dependent on imported fossil fuels. A secure and more sustainable energy system will require diversification of the energy supply, with a greater share met by alternative technologies. Under the new energy package for Europe, Malta is bound to supply 10 % of its final energy consumption from renewable energy sources by 2020 and at the same time reduce the green house gas emissions by 20% of the 1990 levels [1]. Wind energy may contribute a significant proportion to the country's renewable energy mix.

Given Malta's geographical land restriction (a total of 300 km² including built up areas), there is increased interest to develop wind farms at sea. Given the availability of large territorial waters, Malta's theoretical offshore wind potential is enormous. To date most offshore support structures for wind turbines have been commissioned for shallower waters in the North Sea, the deepest being the Beatrice project [2] at an installation water depth of 45 m.

The more benign conditions of the Mediterranean Sea require a tailor made design and analysis for the Maltese region. A considerable large area with transitional depth range (50-70 m) is available in the South East Offshore Zone (SEOZ) of the Maltese Islands. This area includes Hurd Bank. No doubt that the depth limit of 70 m requires a challenging design solution in terms of costs and installation requirements. On the other hand, when compared to those in the North Sea, the milder climatic factors around Malta are expected to reduce the load bearing demand on the support structure and facilitate the installation and maintenance work.

This study proposes an optimisation design process of a jacket structure in which 2 different foundation types at the base of the structure were modeled independently. An investigation of the effect of the different foundation type on the final design was carried out. The ultimate objective of this work was to investigate an optimal modeling design process to improve the feasibility of jacket structures in central Mediterranean deep waters. Rigid foundation designs allow well established installation technology to be implemented for bottom mounted structures in a marine environment. In shallow waters this is a practical approach, but may prove impractical in deeper waters due to excessive material use and more complex sea-bed preparation work. A pinned foundation for a bottom mounted structure in a marine environment makes the design more compliant to wave and wind action. This form of foundation design requires a gravity based design which avoids any form of pile driving or pre drilling but requires extensive sea bed preparation that could prove costly in deep waters.

2. Background on Offshore Wind Turbine Support Structure Design

An offshore wind turbine structure is subject to a large range of complex and non-linear environmental conditions. Design of an offshore support structure is carried out in compliance with international offshore standards of design. Offshore standards provide principles, technical requirements and guidance for design, construction and in-service inspection of offshore wind turbine structures. The support structure design within this study is in compliance with the DNV-OS-J101 [3] and the IEC 61400-1 [4] standards.

The design process of an offshore support structure starts with the assessment of all potential sites and support structure concepts. This first step includes establishing the conceptual design including the foundation (piled, gravity based or grouted), the sub structure (monopile, tripod, jacket or floating), the materials required and the optimal manufacturing and installation processes. In the initial stages of the design process, information about the turbine to be supported as well as site data (metocean data, geophysical and geotechnical data) is collected to be able to define the minimum overall height and the base width of the substructure. Following this, the design load cases acting on the support structure are established. A natural frequency analysis is undertaken to identify the critical frequencies of the entire system that will lead to resonance during the operation of the rotor. This analysis is followed by an ultimate load analysis and a fatigue analysis.

3. Design Basis

For this project the substructure design was carried out on the basis of the available data for the SEOZ site. A report [5] which described the evaluation of the bathymetric, wind, wave and geological conditions of the South East Offshore Zone (SEOZ) was compiled for this study. Figure 1 shows the Maltese islands including the indicated SEOZ site. The SEOZ is located between 5 and 14 km from the nearest shoreline and covers an area of approximately 55 km². This site has the potential to generate 770 Gigawatt hours per annum, equivalent to 16% of the predicated energy consumption for Malta in 2020.



Figure 1: The South East Offshore Zone (SEOZ) outlined for the area having a maximum sea depth of 70 m.

On the basis of this site evaluation report [5], the parameters given in Table 1 were established. Since the maximum sea depth at the SEOZ site is 70 m, it was decided to design the substructure for this water depth. [6]. The various design parameters were established in accordance with the DNV and IEC standards [3, 4].

Turbine	NREL	5 MW
Wind	Annual average wind speed	7.5 m/s
	IEC wind turbine class	III
	Turbulence intensity class	B
	50 year extreme wind speed	37.5 m/s
Wave	Significant wave height	6.8 m
Bathymetry	Water depth	70 m
Water Levels	Maximum still water level	+1 m
	Minimum still water level	-1 m
Sea Bed	Geology	Hard limestone (Globigerina/Upper Coralline Limestone)[12]

Table 1: Site condition design parameters [5].

The design was based on the NREL 5 MW reference wind turbine model. Table 2 displays the main parameters of the NREL turbine as specified in [6].

Turbine parameter	Value	Unit
Rated Power	5.0	MW
Rotor Diameter	126	m
Mass of rotor and nacelle	350	tonne
Cut- in wind speed	3	m/s
Rated Wind speed	11.4	m/s
Cut- out wind speed	25	m/s
Nominal rotor speed	12.1	rpm
Lower bound rotor speed	6.9	rpm
Upper bound rotor speed	12.1	rpm

Table 2: Turbine Parameters [6].

4. Design Methodology

The design methodology adopted in this study consisted of two design phases; the preliminary design phase and the detailed design phase. Figure 2 illustrates a simple flow chart of the two-phase approach and the -processes involved in each phase.

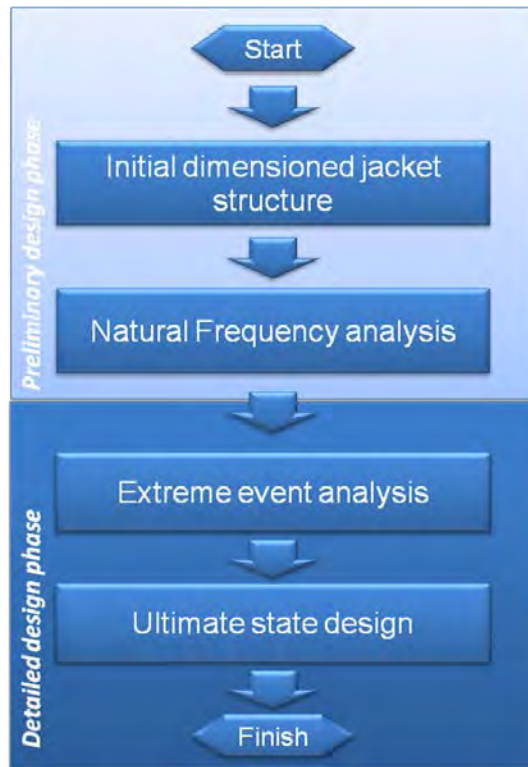


Figure 2: Two phase design methodology flowchart.

In the preliminary design phase, the initial configuration of the overall jacket structure was defined following the guidelines of the DNV standard [3]. This involved the determination of the transition piece elevation, the top and base widths, as well as the number of x-bracings. The base width of the jacket structure was determined by performing a natural frequency analysis exercise, which is the second process in the preliminary design phase.

The detailed design phase involved the extreme event analysis and the ultimate state design. In the extreme event analysis load cases were simulated on the modeled structure to evaluate the extreme loading on the structure. The load cases were set up in accordance with the DNV standard [3]. The simulation of the individual load cases was performed using GH Bladed [7], which is an industry standard tool for the integrated design of wind turbines. The tool models the combined static and dynamic loads acting on the entire wind energy converter resulting from the wind, waves, gravity and inertia.

Ultimate state design, being the final design process, involved the optimisation of the jacket structure. Optimisation of each member was carried out using the NORSOK [8] standard. This design process was repeated for the two different foundation types, i.e. the rigid and pinned foundation types. The results are shown in section 5 of this paper. Sections 4.1 - 4.4 in turn describe in further detail each design process illustrated in figure 2.

4.1 Initial dimensions for the jacket structure

In this first design process the main concept was to utilize a four legged offshore jacket structure for a 70 m water depth up to 15.1 m above mean sea level (MSL). Therefore the jacket structure required being 85.1 m in height. This required the definition of the number of X-bracings and diameter-to-thickness ratios (D/t) for every member in the structure. D and t represent the diameter and thickness of a tubular structural member respectively.

The NORSOK standard [8] sets some geometric restrictions. Figure 3 illustrates a typical Jacket K-joint detail with associated components labeled in red. According to the NORSOK standard [8] the angles between the brace and the leg must exceed 30° , the gap for a simple K-joint should be larger than 50 mm and that the D/t ratio should be less than 120 for any tubular member used in the design.

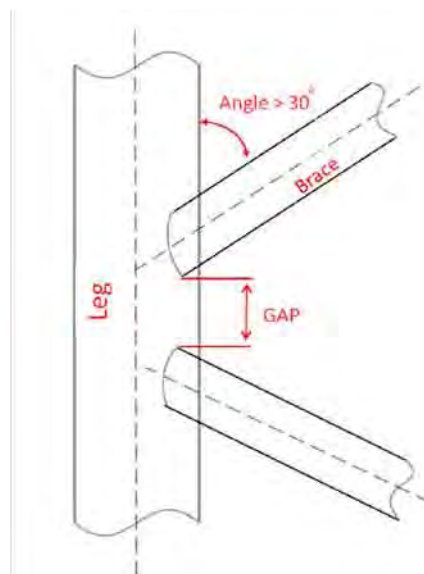


Figure 3: K-joint detail adapted from NORSOK Standard [8].

Preliminary drawings were prepared to determine the number of X-bracing levels that the jacket tower would have. The objective was to satisfy the NORSOK [8] standard while using the minimum number of X-bracings. Based on the Upwind reference Model[9], four levels of X-bracing were chosen. Similarly the Upwind reference model[9] is the result of a tailor made design process developed for a 50 m water depth subject to the Dutch North Sea climate. The angle between the leg and bracing was then incrementally increased from 30° upwards in steps of 1°, until the structure satisfied the design requirements set by the same NORSOK standard [8]. The outcome was a four legged jacket structure with four levels of X-bracing that have a 35° angle between the leg and the bracing.

With the initial dimensions defined, a parametric geometric model was set up in the finite element software ANSYS [10] and the base width varied in order to obtain the x,y,z co-ordinates of the key points that define the jacket structure geometry for different sized models. The parametric study gave an indication of the position of the members and joints that were ultimately modeled in GH Bladed [7]. Figure 4 displays three complete jacket structure models with different base widths of 20 m, 16 m and 12 m. The geometry configurations of these three jacket structures satisfy the geometric constraints of the NORSOK standard [8]

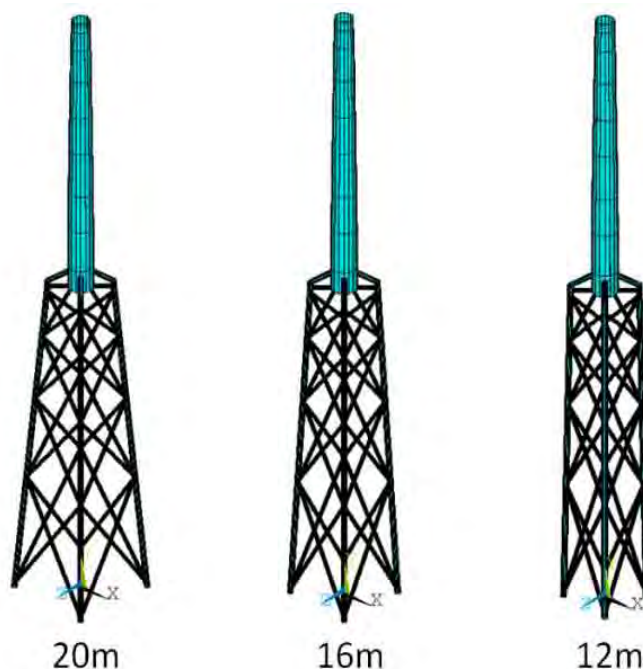


Figure 4: Three complete structure models with different base widths generated in ANSYS [10].

4.2 Natural frequency Analysis

This design process consisted of a parametric study in which the 1st natural frequency of multiple models was found as a function of varying jacket base width. This process was carried out through the use of GH Bladed [7]. The base width of a jacket structure has a significant effect on the total mass and stiffness of the structure that ultimately influences the natural frequency of the structure. The aim of this process was to optimise weight while ensuring that the natural frequency does not coincide with that of the turbine rotor.

The fundamental natural frequencies necessary to be avoided in wind turbine support structure design, are the rotor rotational frequency (1P) and the blade passing frequency which is equal to 3P in the case of a three bladed rotor. These frequency ranges of the reference NREL 5 MW [6] wind turbine were found to be equal to 0.115-0.202 Hz and 0.345-0.606 Hz, respectively. Therefore a workable envelope of frequency range was determined to be between 0.222-0.31 Hz. A 10 % safety margin was added to these limits to account for any discrepancy in calculations. Figure 5 indicates the workable frequency envelope with an X located between the 10 % safety margins. The target natural frequency for the support structure was defined to be **0.29 Hz**. This was chosen closer to the upper limit of the workability envelope because as reported in [11] when the 1st natural frequency of the structure lies closer to the 1P frequency range, higher damage due to fatigue is experienced.

The base width of the jacket design was incrementally increased in steps of 2 m from 12 m to 20 m. All other dimensions were kept constant. A modal analysis was carried out in GH Bladed [7] on each complete support structure model including the rotor nacelle assembly, the wind turbine tower and the jacket substructure. In this way the 1st natural frequencies of the analyzed models were extracted. Table 3 shows the model support structures that satisfy the workable envelope shown in figure 5. In addition to this, Table 3 also shows the predicted mass of each model based on assumed member diameters of 0.8 m and 1.2 m, as well as wall thicknesses of 20 mm and 50 mm for the X-braces and main legs respectively [9]. The predicted model masses were computed through the use of GH Bladed [7].

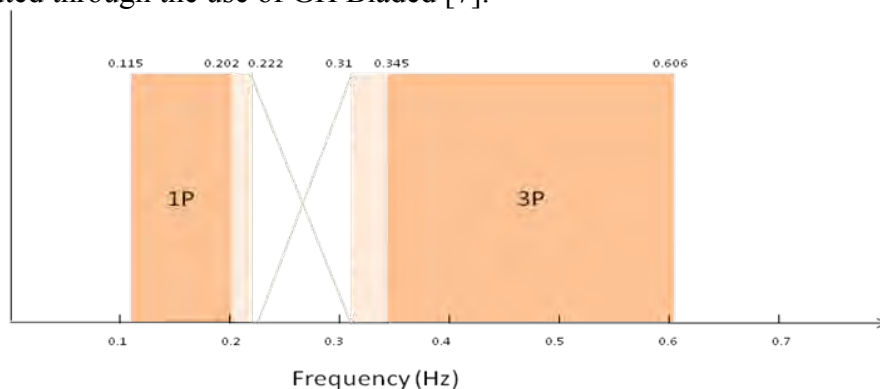


Figure 5: Workable natural frequency envelope.

Base width [m]	1st natural frequency [Hz]	Mass [tonnes]
12	0.264	512.71
14	0.277	516.326
16	0.288	520.245
18	0.297	524.534
20	0.305	529.131

Table 3: Model base widths with corresponding 1st support structure natural frequency and mass.

Figure 6 shows how the 1st natural frequency and mass of the jacket structure varies with the increasing base width for the selected models. The quasi-linear relationship displayed by the curves in figure 6 was found to be similar to those presented in the Upwind report [11]. As previously established, the design target natural frequency for the support structure was selected to be 0.29 Hz. Based on this, the preliminary design jacket structure with base width 16 m having a natural frequency of 0.288 (Hz) and a mass of 520.245 tonnes was selected for further analysis.

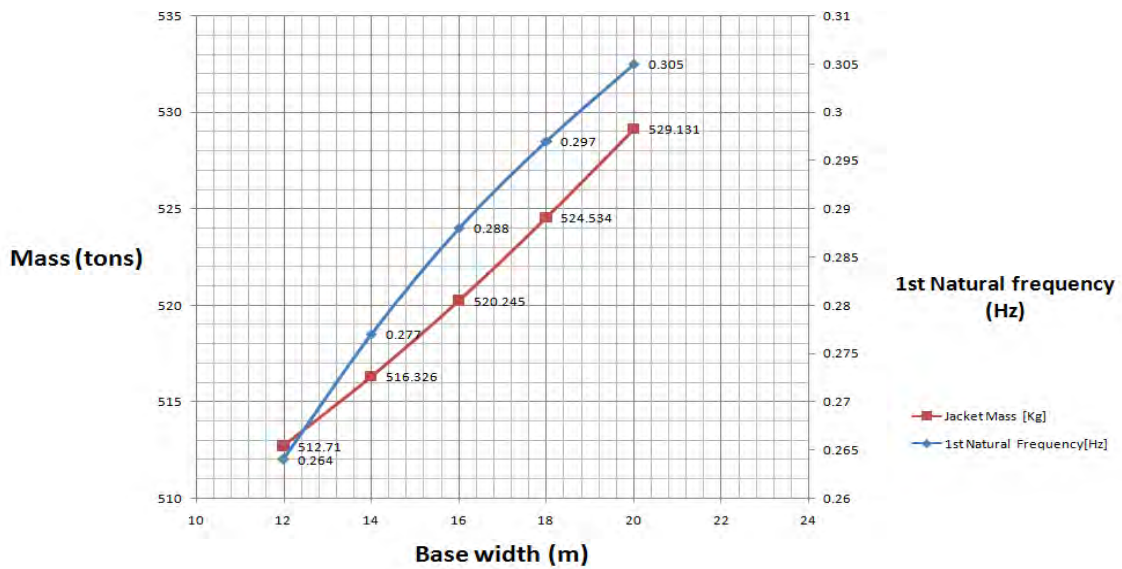


Figure 6: Total Mass and 1st natural frequency plotted against base width with a rigid foundation.

4.3 Extreme event analysis

The aim of the extreme event analysis was to evaluate the extreme loading on the support structure through simulation of a number of design driving load cases. This process was carried out separately for jacket structures with rigid and pinned foundations. A design load case group was set up consisting of three main design driving load cases. These design load cases (DLC's) are known to produce the worst loading scenario (extreme loading) on the support structure [11]. The set up of the environmental and wind turbine parameters of the DLC's were done according to the DNV standard [3]. Simulations included both aerodynamic and hydrodynamic analysis. The following load cases [11] were included for the analyses:

- a. DLC 1.3 - power production with extreme turbulence model (ETM)
- b. DLC 1.4 - power production with extreme coherent gust with change of direction (ECD)
- c. DLC 6.2a - parked rotor with loss of electrical network connection with extreme wind model (EWM)

Simulations in GH Bladed [7] of the above load cases were carried out on the jacket support structure model taking the base width equal to 16 m as determined during the natural frequency analysis process. The maximum and minimum values for the six components of the load vectors (Fx, Fy, Fz, Mx, My and Mz) acting at the rotor hub centre (90 m amsl) were derived.

Figure 7 illustrates the 6 component vectors derived at the hub height through GH Bladed [7].

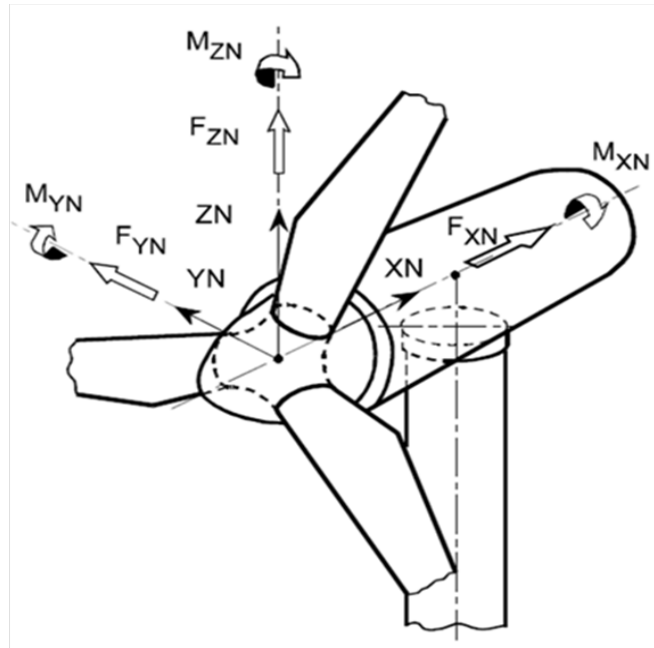


Figure 7: Six component vectors evaluated at the hub height through GH Bladed [7].

When modeling the rigid foundation, all degrees of freedom at the four foundation nodes at the base of support structure were fully fixed. For the pinned foundation the three rotational degrees of freedom (θ_x , θ_y , θ_z) at the four foundation nodes of the modeled structure were free to rotate while Δx , Δy , Δz were fixed

4.4 Ultimate State design

The objective of the ultimate state design process was to optimise the members of the jacket structure to withstand the extreme loading evaluated in extreme event analysis. Ultimate state design was achieved through dimensioning the jacket members to satisfy structural integrity checks according to the NORSOK design standard [8]. Member stability check equations included the combination of tension, compression, bending, shear and hoop stresses.

Optimisation of the jacket structure was achieved by carrying out a member optimisation design cycle (MODC). The procedure MODC was carried out through the use of the finite element software ANSYS [10]. Figure 8 illustrates the operational sequence of the MODC procedure.

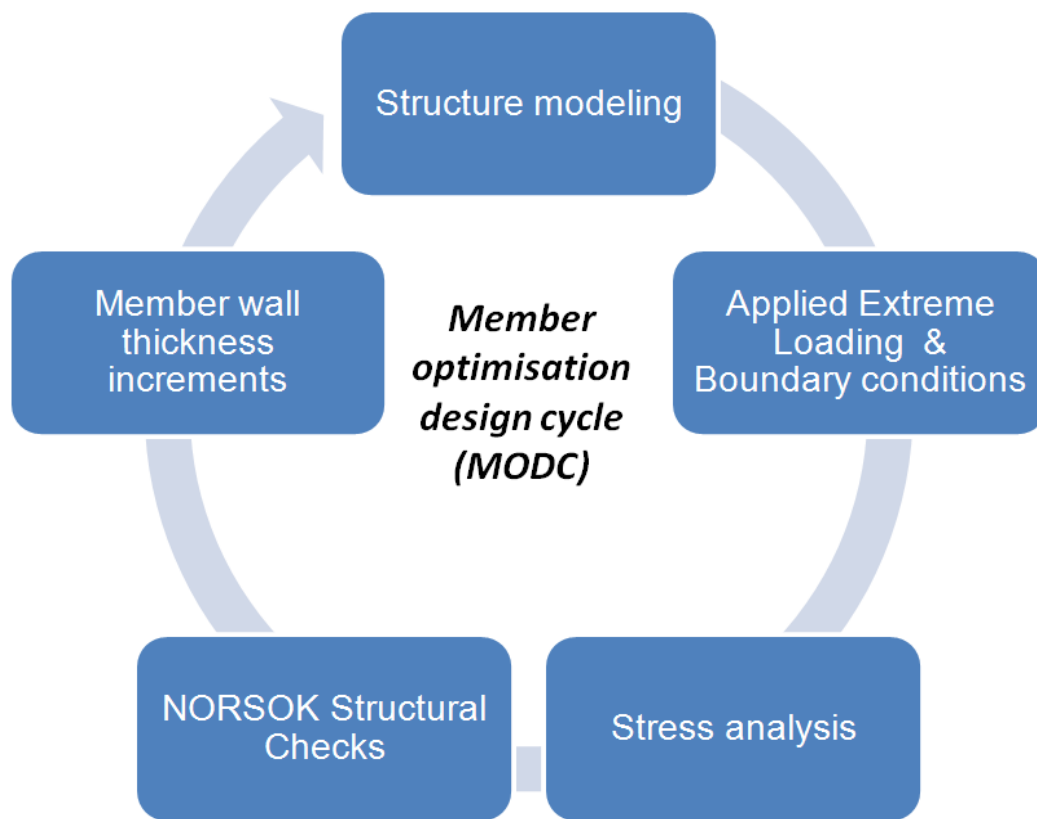


Figure 8: Member optimisation design cycle (MODC).

The MODC procedure was initiated with the element support structure having the initial dimensions established in the preliminary design phase. BEAM 188 was used for modeling of the support structure in ANSYS. The model included the jacket structure, the transition piece and the wind turbine tower. A mesh convergence study was carried out which showed that 20 mesh divisions per element gave rise to sufficient accuracy and convergence while reducing the computational time for stress analysis to be carried out. The buoyant force was accounted for by determining an apparent density and applying it to the submerged part of the structure. The boundary conditions at the foundation nodes of the jacket model were then applied. The MODC procedure was repeated for both a fixed foundation and for a pinned foundation. The extreme loading combinations evaluated in the extreme event analysis were applied at the hub centre of the support structure. Following the applied extreme loading combinations at the hub centre, a stress analysis was carried out. Combinations of axial, compression bending, shear and torsion stresses were evaluated for each member within the jacket structure.

Structural checks according to the NORSOK design standard [8] for each member were then carried out. Checks per member were carried out against the stresses computed from the ANSYS simulations. If a selected member failed to satisfy all checks then the member is deemed to have failed compliance with the NORSOK standard [8]. Members that fail to comply had their wall thickness increased by increments of 0.5 mm. The cycle then repeated itself with the re-modeling of the support structure incorporating the changes in the newly dimensioned members.

The optimised cycle was repeated until all members satisfied all the required equations. The final result was an optimised jacket structure design for a 70 metre water depth that satisfied the structural integrity checks of the NORSOK design Standard [8].

5. Foundation modeling design results

The following results describe comparatively the final optimised jacket designs as a result of the adopted design methodology.

Table 4 compares the resulting jacket member design dimensions for the two different modeled foundations. Figure 9 illustrates a side view of the jacket design with labeled sections that have tabulated results in table 4.

		Rigid	Pinned
X-bracing (mm) Wall thickness (mm)	Level 1	8	9
	Level 2	7	8
	Level 3	7	8
	Level 4	10	9
Main Leg (mm) Wall Thickness (mm)	Top Section	35	30
	Middle Section	33	28
	Lower Section	35	30
Natural frequency (Hertz)	Support structure	0.293	0.286
Masses (tonnes)	Jacket	399.2	355.6
	Transition Piece	72.1	72.1
	Tower	229.9	229.9
	Total	701.2	657.6

Table 4: Jacket design with rigid and pinned foundations - wall thicknesses and weightings.

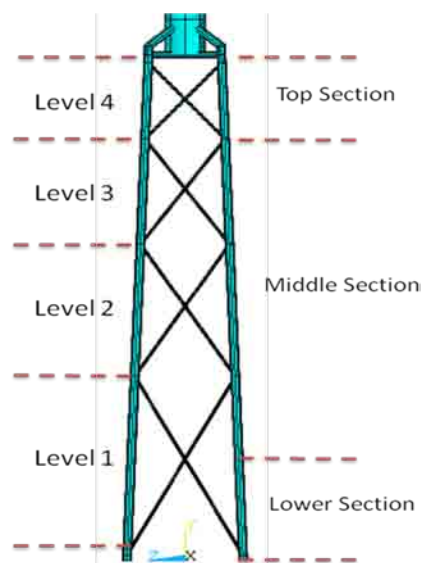


Figure 9: Jacket design Layout.

It is seen that modeling of the pinned foundation resulted in a jacket design weight of 355.6 tonnes. This is 43.6 tonnes lighter than the jacket design modeled with a rigid foundation. The main factor contributing to the weight discrepancy is the overall 5 mm wall thickness difference in the main supporting legs of the two jacket designs. Results from the modal analysis carried out in GH-Bladed [7] on the final jacket designs shows 0.009 Hz difference in the 1st natural frequency of the jacket structures which causes a relatively significant shift of 10 % within the operable natural frequency envelope. This difference is a cause of the 43.6 ton weight difference between the two jacket designs.

Both final designs have a natural frequency that satisfies the target natural frequency envelop described in section 4.2.

Similar to the final design seen in the Upwind project [11], both designs resulted in a wall thickness increase for the x-bracing and main legs at the foundation and transition piece intersection. This result was expected at the foundation because essentially the structure is a cantilever model with the largest reaction forces at the foundation. The increased thickness nearer to the transition piece intersection may be due to the reaction forces due to the acting secondary cantilever foundation for the wind turbine and tower.

Further, the pinned foundation jacket design has a more even distribution of wall thickness throughout the x-bracing members. This may be due to the more compliant nature of the pinned foundation design resulting in a more even distribution of stress throughout the structure.

6. Conclusion

A tailor made design methodology for an optimised jacket design suited for a 70 m water depth was described. An investigation comparing jacket structures with rigid and pinned foundations was carried out.

The following main conclusions could be drawn from this study:

- The weight of the jacket structure design with pinned foundations was found to be 43.6 tonnes lighter than that with rigid foundations (355.6 tonnes instead of 399.2 tonnes).
- The modeled rigid and pinned foundation designs had a support structure 1st natural frequency of 0.293 Hz and 0.286 Hz respectively. Both values satisfy the established natural frequency envelope in order to avoid resonance at 1P and 3P excitation frequencies.
- The optimised jacket design with pinned foundations was found to have a more evenly distributed wall thickness throughout the x-bracing when compared to that with rigid foundations.

7. Further work

The effects of fatigue on the joints of a jacket structure are significantly dependent on the support structures natural frequency. This necessitates further work to study the effects of different foundation modeling types on a completed fatigue assessment of the support structure. Fatigue state design according to the DNV standard [3] will be used to ensure that the structure will have sufficient resistance against fatigue failure.

Following the fatigue assessment, further study on the installation procedure is necessary to conclude on the overall feasibility of the rigid or pinned foundation design.

8. Acknowledgments

The study was financially supported by the Malta Council for Science and Technology (R&I-2009-003).

9. References

1. Malta's National Renewable Energy Action Plan as Required by Article 4(2) of Directive 2009/28/EC. 2010, Ministry for Resources and Rural Affairs Floriana, Malta.
2. M. Seidel, D. Gosch. Technical Challenges and Their Solution for the Beatirce windfarm demonstrator project in 45 m water depth, Conference Proceedings DEWEK, Wilhelmshaven, 2006.
3. Det Norske Veritas, DNV-OD-J101 Offshore Standard, Design of Offshore Wind Turbine Structures, 2007.
4. International Electrotechnical Commission, IEC 16400-3, Design requirements for offshore wind turbine, 2006.
5. Deep Offshore Wind Project: Evaluation of the site Bathymetric, Wind, Wave and Geological Condition at the South East Offshore Zone. Unpublished report, University of Malta 2011.
6. J. Jonkman, S.Butterfield, W.Musial and G.Scott. Definition of a 5- MW reference wind turbine for offshore system development, Colorado, 2009.
7. GH Bladed Version 4.1, Garrard Hassan and Partners Ltd, Bristol, Licensed to the University of Malta.
8. NORSOK N-004, Design of steel structures, Norway, 2004.
9. Naveen Kumar Vemula, Wybren de Vries, Tim Fischer, Andrew Cordle, Björn Schmidt. 'Design solution for the Upwind reference offshore support structure', UPWIND project 2010
10. ANSYS Version 11.0 Ansys Inc, Canonburg, PA (Research Academic License University of Malta)
11. Upwind Vries, Wybren de. Support structure concepts for deep water sites. , UPWIND project, 2011.
12. Zammit, Dane. A preliminary assessment of the long-term prospects for offshore wind farms in Maltese territorial waters. MSc Dissertation, University of Malta . 2010.

Design of a spar buoy for Offshore Wind turbines

C. Romanò¹, E. Giorcelli², G. Mattiazzo³ and M. Raffero⁴

¹*Dipartimento di Ingegneria Meccanica e Aerospaziale, 'Polito' University,
Corso Einaudi 40, 10129 Torino, Italy, carlo.romano@polito.it*

²*Dipartimento di Ingegneria Meccanica e Aerospaziale, 'Polito' University,
Corso Einaudi 40, 10129 Torino, Italy, ermanno.giorcelli@polito.it*

³*Dipartimento di Ingegneria Meccanica e Aerospaziale, 'Polito' University,
Corso Einaudi 40, 10129 Torino, Italy, giuliana.mattiazzo@polito.it*

⁴*Dipartimento di Ingegneria Meccanica e Aerospaziale, 'Polito' University,
Corso Einaudi 40, 10129 Torino, Italy, mattia.raffero@polito.it*

Abstract - Offshore wind Energy demonstrated to be one of the most promising technologies for growing electric energy demand worldwide. The main objective of this research was to conceive a floating offshore structure for supporting wind turbines. The Mediterranean Sea is characterized by deep water, especially in the western area, from Italy towards Spain, and this makes floating support structures desirable, since in deep water they are cheaper than bottom fixed piles [1]. An aerodynamic, electric and mechanic model was developed and tested against experimental results of laboratory and wind tunnel tests on a small scale wind turbine, demonstrating its reliability, so it was used to determine actions on the floater and a first concept design was performed using commercial software for marine structures analysis. Further steps in this process will include integration of the turbine model with hydrodynamic calculations, as well flume, tank and open sea tests for the designed floater.

1. Introduction

Interest in renewable energy has been continuously growing during the latter years, even more after acceptance of Kyoto protocol by the most developed states, and due to an increasing sensibility of people in environmental matters. Wind energy demonstrated to be one of the most promising technologies in this field, since it's the closest to reach the so called "grid parity", that means that the cost per kilowatt produced by wind is closer and closer to the cost of the same energy produced by traditional fossil fuels. [1] The research in wind energy field has lead to continuous improvements in turbines performance, cost lowering and safety of the systems. One of the main problems of wind turbines is their size, that causes a strong visual impact, and for this reason often people unwillingly accept, or firmly oppose, wind parks where they live. One possible solution is to set wind farms in open sea, which is also a valuable solution for production efficiency, since in that environment the wind is more constant and stronger respect to land [2].

In northern Europe many offshore wind farms are working nowadays, and this confirms offshore wind power as a good technical solution for renewable energy harvesting. Up to now the offshore wind option for the Mediterranean countries has not been fully considered even though about 2000 MW offshore wind power plants have been installed in North European Countries in water depth up to 30 m on gravity and monopile foundations. The offshore wind data indicate that the Mediterranean offshore wind energy could be in the same range of onshore wind, 165 TWh/year (5 % of 2030 forecast Mediterranean electric energy demand) of which 80 TWh/year at water depth below 30 m and 85 TWh/year at water depth from 30 up to 200 m [3].

Placing wind turbines in open sea nevertheless implies serious difficulties in design and manufacturing of wind turbines themselves, and also for supporting structures, that must be safe and lasting in a challenging environment. Waves loading and salinity are only two examples of the issues that have to be faced when designing a support structure for an offshore wind turbine. The Mediterranean Sea is characterized by deep water, especially in the western area, from Italy towards Spain [4], and this makes floating support structures desirable, since in deep water they are cheaper than bottom-fixed structures. [5]

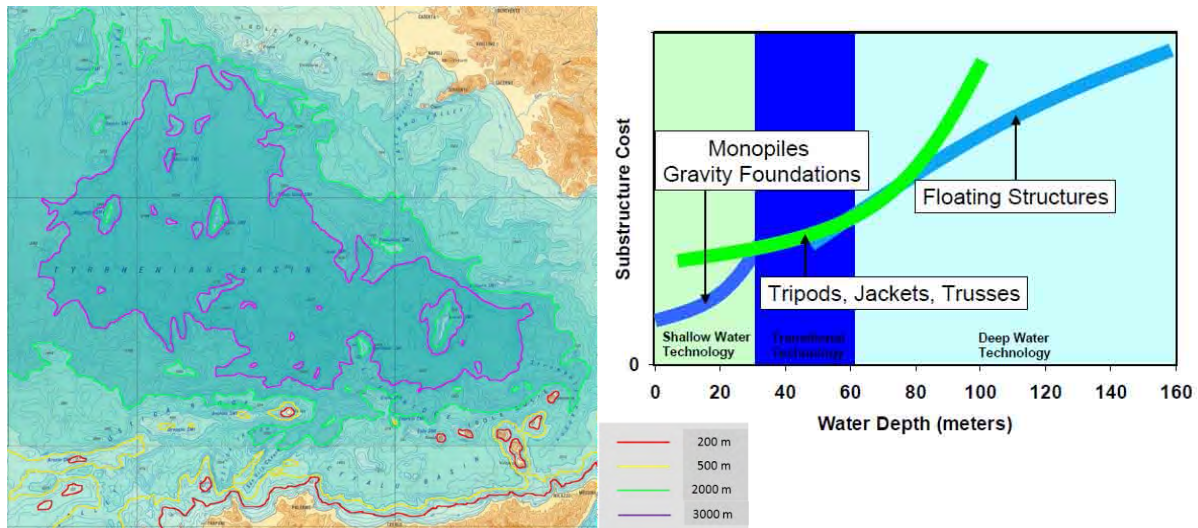


Figure 1: Western Italy coast bathymetric map and cost analysis for offshore structures [5].

2. Nomenclature

V	Voltage
I	current
R_s	stator resistance
L_{eq}	equivalent inductance
Z_{eq}	equivalent impedance
λ_m	magnetic flux
ω	electric frequency
R_{est}	Resistive load
E	electro motive force
ψ	permanent magnet flux
θ	angle between magnetic flux and real axis of electric system
φ	phase angle between current and voltage
ρ	mass density of fluid
g	gravitational acceleration
m	mass of body
D_V	displaced volume

3. Method of Approach

The physics of a floating win turbine is complex, and involves aerodynamics, hydrodynamics, mechanics, soil mechanics, wave-structure interaction and electric power generation, just to list some. A multi physics approach is desirable to define which phenomena are coupled to other, and to give a first description of the problem.

The main objective is to limit the floater’s motions, in order to let the turbine work properly: in fact even small pitching motions give the rotor a strong variation of apparent incident wind speed, especially in the case of large offshore turbines. The main problem is to determine which forces act on the floater, due to the wind turbine operation: To gather this information, an aerodynamic, electric and mechanic model was developed and tested against experimental results of laboratory and wind tunnel tests on a small scale wind turbine, demonstrating its reliability, so it was used to determine actions on the floater and a first concept design was accomplished.

4. Coupled model

A coupled aerodynamic and electrical model, suitable to simulate wind power generators regardless of their dimensions, was developed, and its general layout is presented in *Figure 2* . Since a small wind turbine was disposable for experimental test, [6] the model was set to simulate this particular device, and a test campaign on the real device was performed to verify model predictions. Wind conditions are requested as an input, and the system gives voltage, electric current, shaft torque, axial force and rotational speed of blades as an output. This model has a multi-disciplinary basis like many other codes developed in the last years [7], [8] but was intentionally kept simple in order to have a quick and easy tool for preliminary design, that is a different purpose if compared to literature high-complexity codes [9] [10] [11]. A more complex model could be used, if necessary, in a second step of the design process, in order to achieve more detailed results and more information about the system’s behavior.

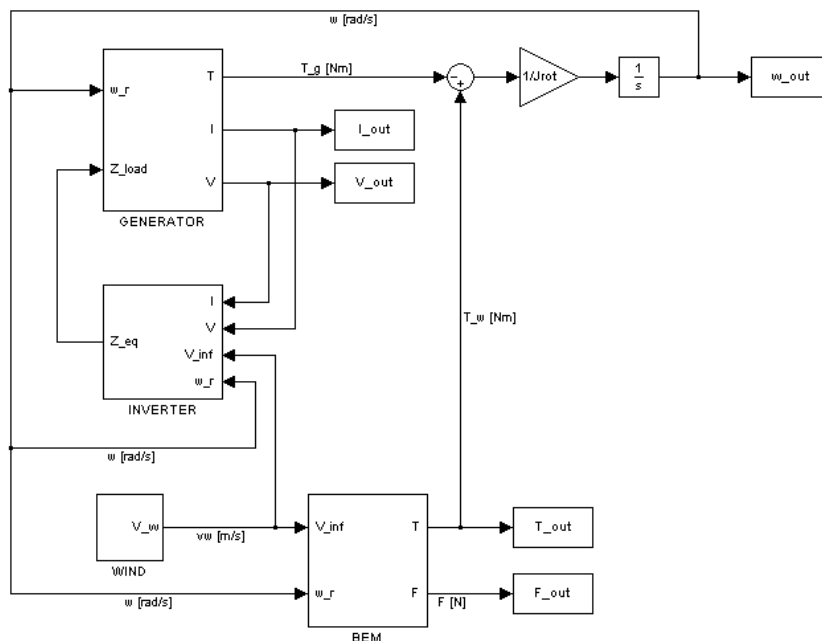


Figure 2: Model Layout.

The aerodynamics module is based on classical Blade Element Momentum theory (BEM), with Glauert and Prandtl corrections, while the electrical module is based on a simple electric representation of the generator. The two modules run at the same time, exchanging data thus taking into account interactions between electric phenomena, aerodynamic and mechanical behavior.

The electric part of the wind power system is made of an electric generator, a diode bridge and an inverter, that connects the generator to the grid and fits the output power to grid requirements.

In order to simulate a system of this kind with high accuracy, complex and time-consuming models of components and control laws are necessary, and for a gross evaluation of system performances this does not lead to appreciable improvement in results. If we suppose a fast electric dynamics, if compared to aerodynamic and mechanical ones, we can neglect high order electric effects, thus extremely simplifying calculations.

4.1 Electric model

The electric model is intended to take into account the effects of the generator and its load in regime conditions. To avoid excessive computational resources, a simplified approach was chosen. The electric generator is modeled as an equivalent circuit [12], [13], [14]; a variable resistive load was also implemented in the model. Since the electrical system is supposed to be balanced, only one phase quantities are computed, then the output power will be three times the one computed by the algorithm. This model, coupled with the aerodynamic one, was run to forecast the turbine's behavior during regime wind tunnel tests.

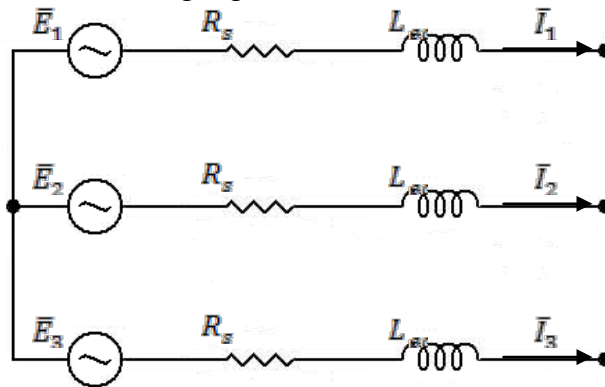


Figure 3: Generator equivalent circuit.

Let the system parameters be

$$\begin{cases} L_{tot} = L_{sq} + L_{load} \\ C_{tot} = C_{pfc} + C_{load} \\ R_{tot} = R_s + R_{load} \end{cases}$$

Hence the circulating current per phase in the equivalent circuit can be expressed as follows

$$\bar{I} = \frac{\bar{E}}{\bar{Z}_{tot}} = \frac{\bar{E}}{R_{tot} + i \left(\omega L_{tot} - \frac{1}{\omega C_{tot}} \right)} \quad (1)$$

Where the electro motive force (emf) is due to the permanent magnets flux ψ

$$\bar{E} = i\omega\bar{\psi} = i\omega e^{i\theta} \quad (2)$$

With θ indicating the angle between magnetic flux and real axis of electrical system, calculated as integral of the angular velocity. The voltage applied on the external load can be obtained by the formula

$$\bar{V} = \bar{I}\bar{Z}_{load} \quad (3)$$

Where

$$\bar{Z}_{load} = R_{load} + i \left(\omega L_{load} - \frac{1}{\omega C_{load}} \right) \quad (4)$$

Since we suppose a pure resistive load, the terms L_{load} and C_{load} can be neglected, as the power factor correction capacity of the electric machine can be. The electric power output of the generator, in case of pure resistive load, is expressed by the formula:

$$P_e = 3VI \quad (5)$$

The mechanical input power, coming from the blades, is higher, and the difference can be ascribed mainly to friction, Joule losses and core losses.

$$P_m = 3EI\cos\varphi + C_0(\omega)\omega \quad (7)$$

The total output power dispersed above the resistive load will be considered equal to the power given by the generator. The generator parameters given by the documentation of the constructor were verified with tests in the laboratory.

4.2 Aerodynamic model

The aerodynamic model is based on the classical Blade Element Momentum theory (BEM), with Prandtl tip and hub loss factors and Buhl correction for axial induction factor. [15],[16] The Blade Element Momentum method couples the momentum theory with the local events taking place at the blades. A stream tube enclosing the rotor is discretized into annular elements of height dr , as shown in *Figure 4*. The lateral boundary of these elements consists of streamlines; in other words there is no flow across the elements. The different control volumes are assumed to be independent, hence each strip can be treated separately and the solution at one radius can be computed before solving for another radius. At the end of the process the weighted contribution of each section is assembled, in order to provide mechanical power produced by the turbine, thrust force and shaft torque.

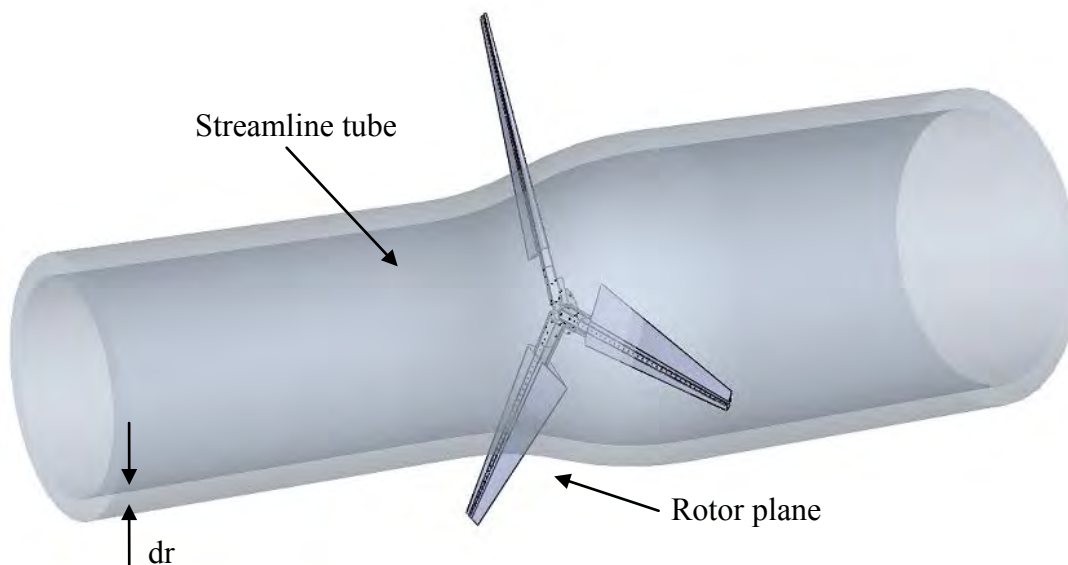


Figure 4: Streamlines tube in Blade Element Momentum theory.

In each blade section aerodynamic forces are due to the relative velocity between blade and air: with respect to the wing case, the wind turbine blade is rotating, thus the relative velocity is the combination of wind velocity vector, rotational velocity vector, and in case tower velocity. The wake downstream the turbine is characterized by rotation, hence the velocity triangle at the trailing edge is different from the one at the leading edge; moreover, the velocity field behind the turbine is different from the incoming velocity field.

Two coefficients a , axial induction factor, and a' , tip loss factor, were defined [15], [16], to take into account the wake effect. The practical consequence is that rotational velocity and incoming wind speed are modified by these factors, thus changing local angles on the blade. This artifice permits to treat the problem like an ideal rotating wing inside a potential flow field. With these assumptions, aerodynamic lift and drag is calculated for each section of the blades.

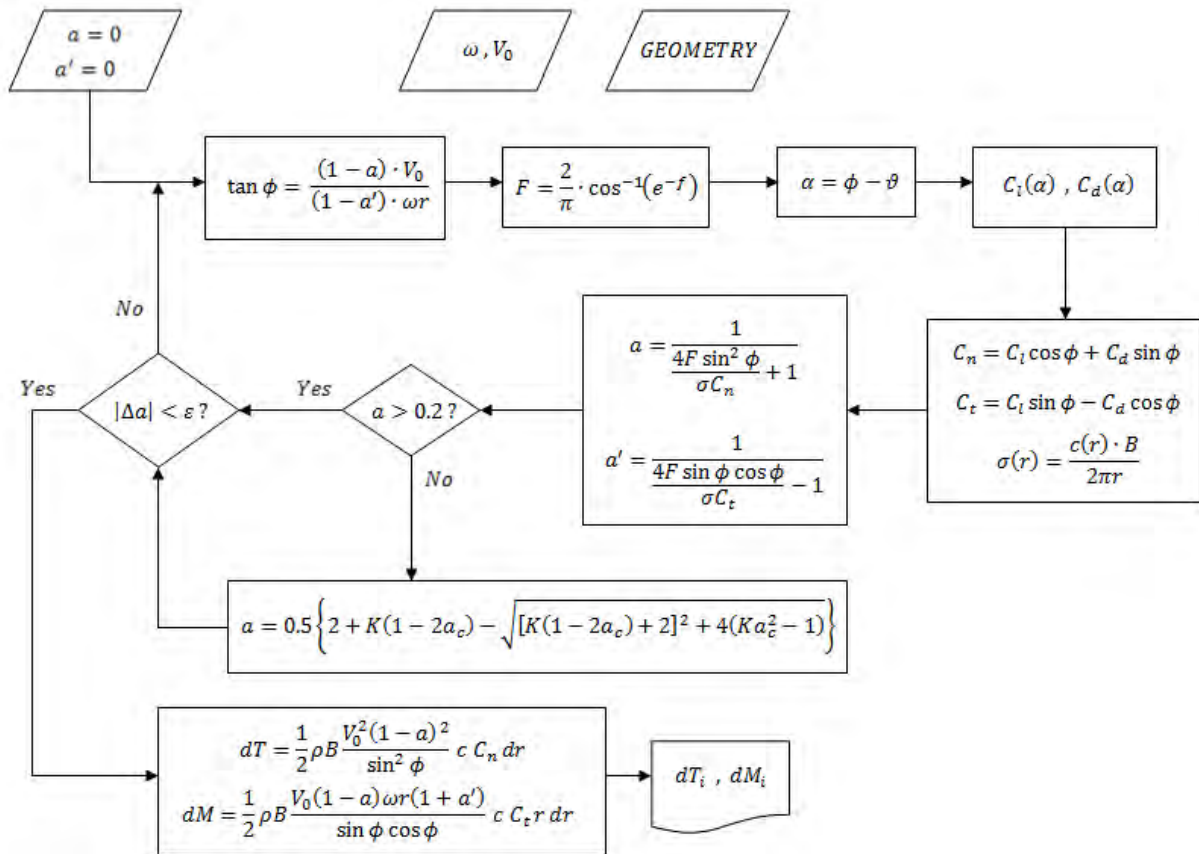


Figure 5: BEM algorithm flowchart.

The algorithm implemented can be summarized as the flow chart in Figure 5 shows.

In the developed model, rotational speed is given by the electrical-mechanical module. The major limit of the BEM based models is that they are useful if aerodynamic coefficients of blades are well known, but for a first draft of a wind turbine, generally there is no need to design the airfoil from scratch. On the contrary these kind of models require few computational resources if compared to more complex systems, like CFD's. In the code presented here, the Prandtl and Glauert corrections are active even in post-stall conditions, since this strategy demonstrated to be more reliable in predictive calculations. [17].

5 Experimental tests

The authors had a small scale wind turbine disposable for testing [18], so the model was run with these system parameters, and some predictive calculations were performed. A test rig was built inside the laboratory and the electric generator was characterized.

Errore. L'origine riferimento non è stata trovata.

The prime mover is a three phase, 4 kW electric motor, speed controlled by an inverter. A torque meter plus a phonic wheel are the instrument for mechanical parameters measurements. The generator can be loaded with a pure resistive variable load or a grid connected inverter. For early tests, and later for wind tunnel tests, it was chosen to apply a pure resistive variable load, since the main objective of the study is the mechanism to convert flow kinetic energy to electric; and not to satisfy grid requirements, the inverter behavior is not of interest in this particular case, while the regulation of the resistive load is easier. Analog control of the prime mover and data acquisition were realized a National Instruments card connected to a PC.

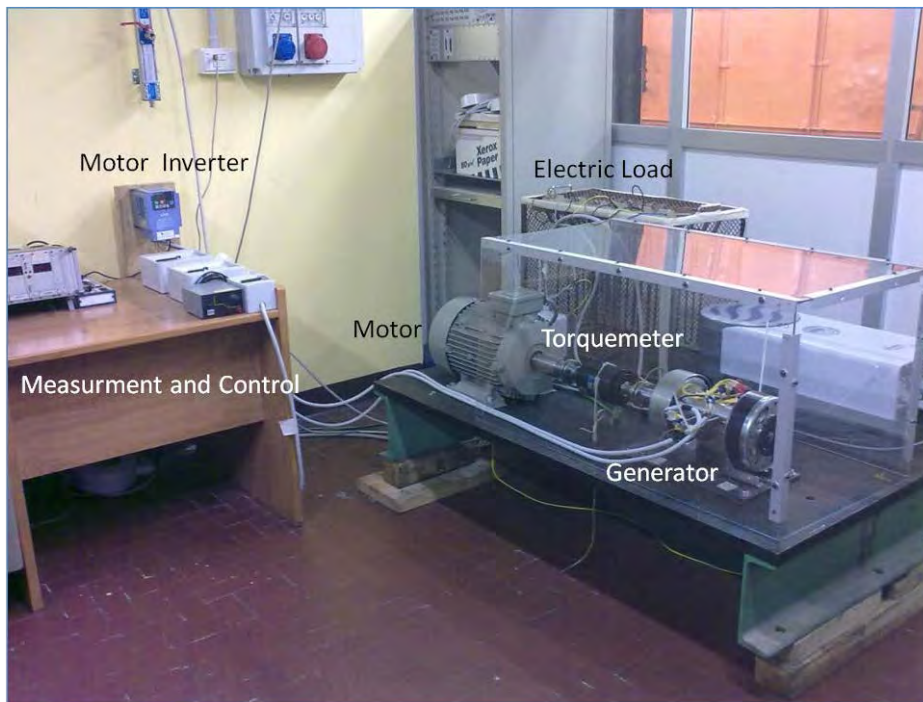


Figure 6: Test rig.

Controls and acquisition interface are located far from the rig, in order to keep the user safe in case of malfunctioning. Figure 6 shows the realized test rig.

Afterwards a series of experimental tests was performed in order to evaluate model reliability. These tests were divided in two different sets: a first test of the electric part of the turbine on a test rig at Politecnico di Torino, and a series of tests in the wind tunnel of Centro Ricerche FIAT. Figure 7 and Figure 8 summarize laboratory test results, and show comparison between the results of experimental and numerical characterization of the electric generator.

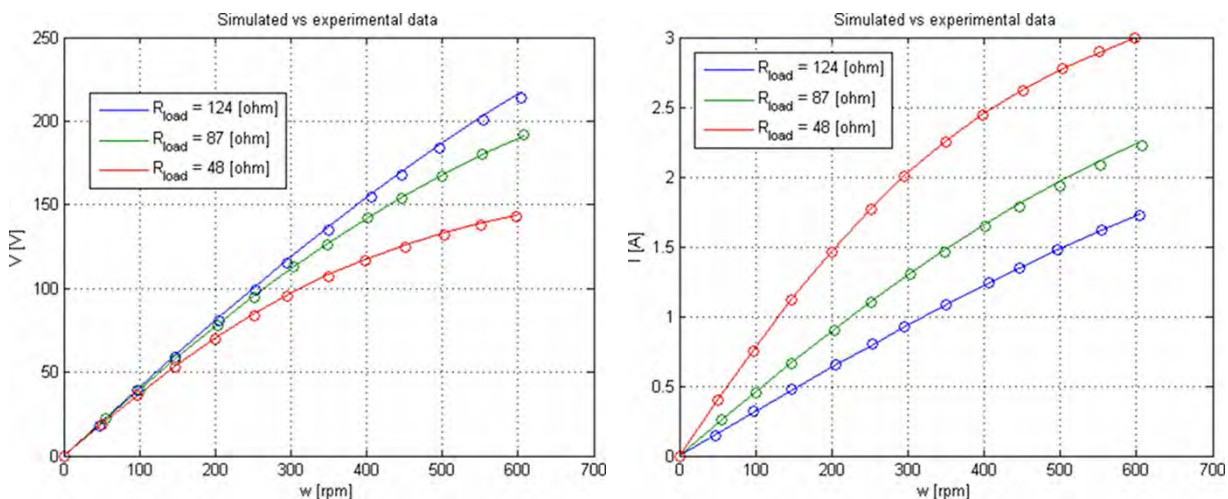


Figure 7: Voltage and current comparison, model vs experimental data.

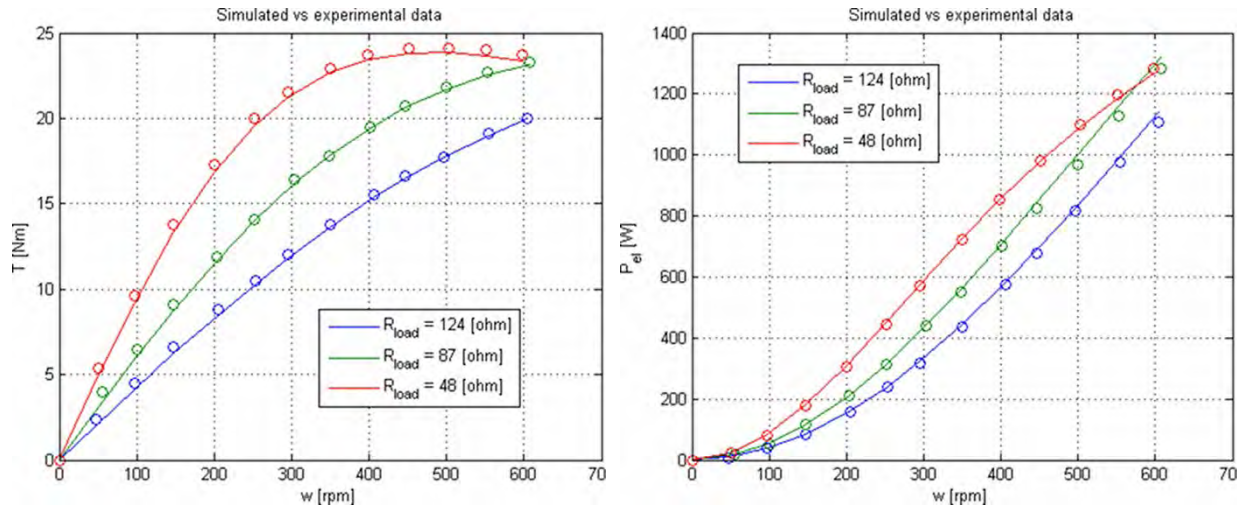


Figure 8: Torque and Power comparison, model vs experimental data.

Experimental and simulation data are in very good agreement both varying angular speed of the rotor and the load resistance.

In the Wind tunnel the complete system was tested at different wind speeds; the electric load consisted in a variable array of resistors, plus a fixed resistor of about 30 Ohms, capable to dissipate the whole power generated by the wind Turbine. Electric quantities were measured with shunt resistors and a couple of load cells gave axial force and torque acting on the turbine as an output (Figure 9).

After the system was completely known, the forces acting on the tower completely determined, and the aero-electro-mechanical model validated, the desired inputs for the floater design were available.

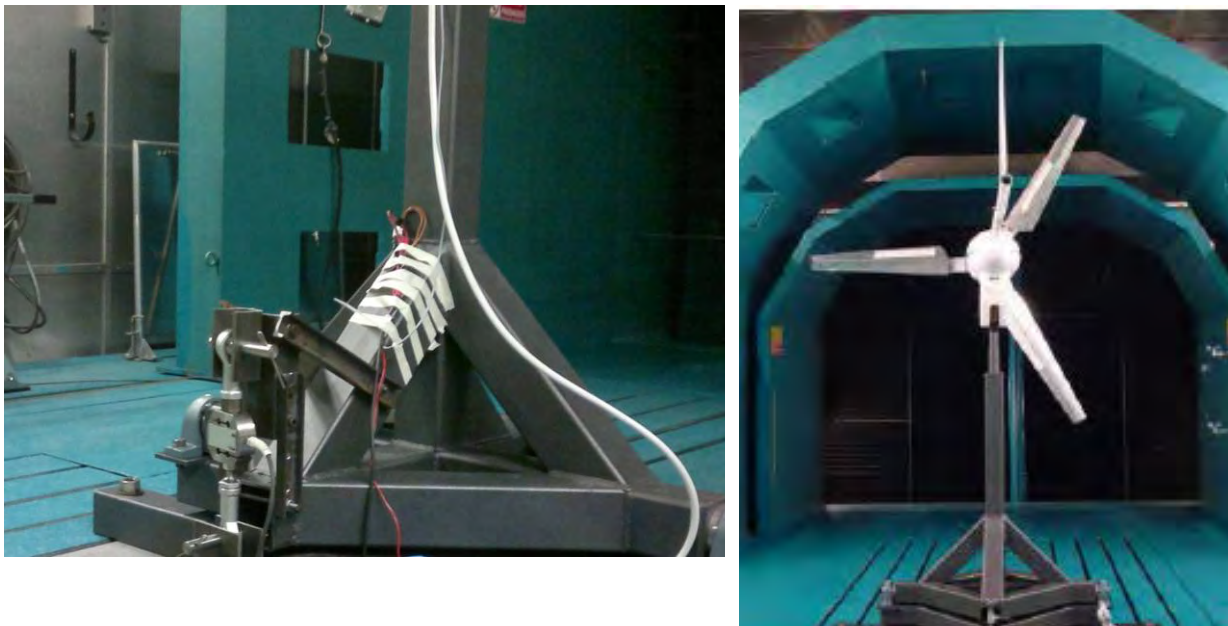


Figure 9: Wind Tunnel tests, from left to right the axial force measurement load cell and the system inside the wind tunnel.

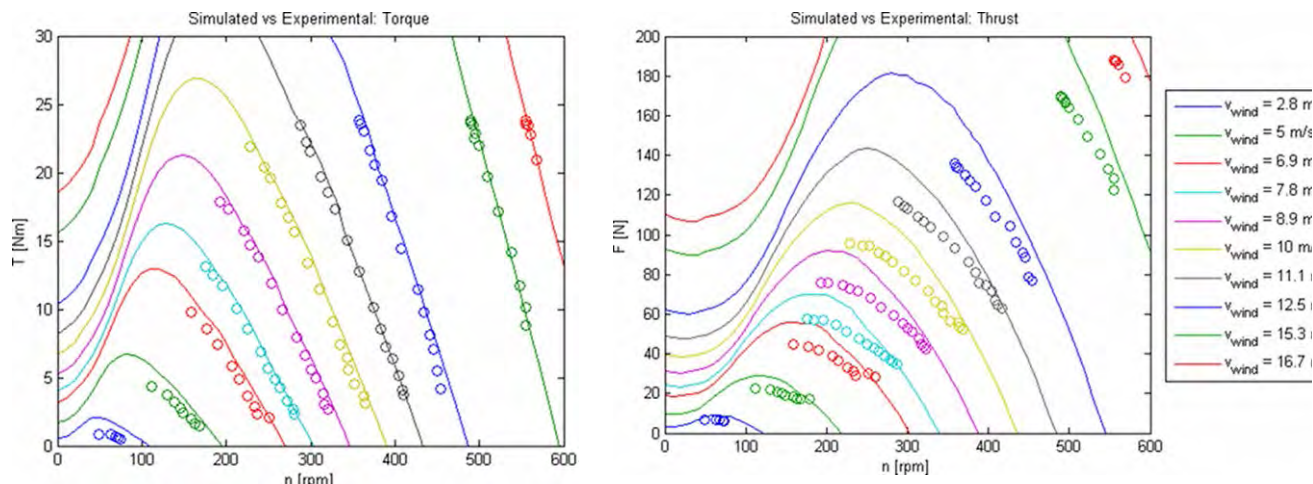


Figure 10: Experimental vs modeling results (aerodynamic-electric model).

Figure 10 shows the comparison between experimental results in wind tunnel tests and the calculation outputs of the coupled model. Both thrust and torque show a good agreement with experimental data; only thrust is slightly over estimated, and this could be due to the fact that the blades aerodynamic profile, is close to a NACA 2412, but is not exactly the mentioned one; because of the construction technique.

This fact leads to some differences in torque and thrust coefficients. The error in estimation is anyway acceptable, and solvable with wind tunnel airfoil characterization.

Finally, a power curve was built, both with calculated and experimental data.

The comparison is shown in Figure 11.

BEM indicates mechanical power available at generator’s shaft, SIM the simulated mechanical power, including torque saturation, and EXP is the experimental curve obtained with wind tunnel tests.

Adding coupling with electro-mechanical model contributes to improve experimental data fitting in simulations.

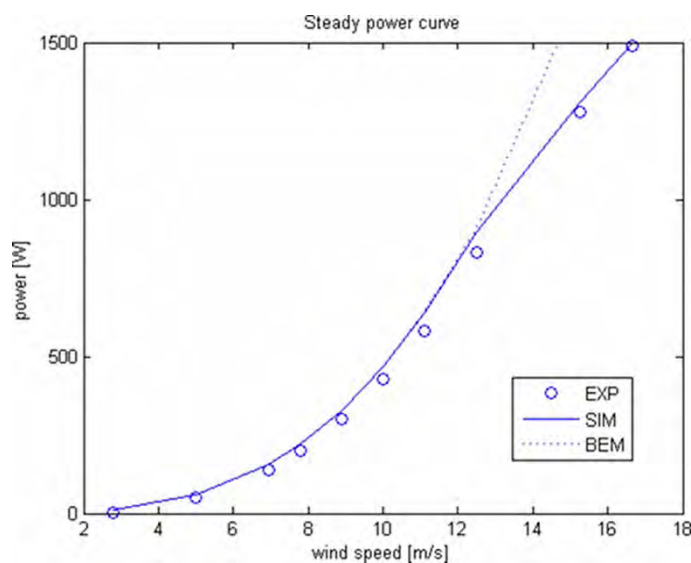


Figure 11: Steady power curve comparison, experimental and simulated.

6 Floater design method

In order to design a suitable floater for a given wind turbine, using data coming from the model that estimate forces acting on the basement, a method involving hydrostatics, hydrodynamics and coupled modeling has to be used .

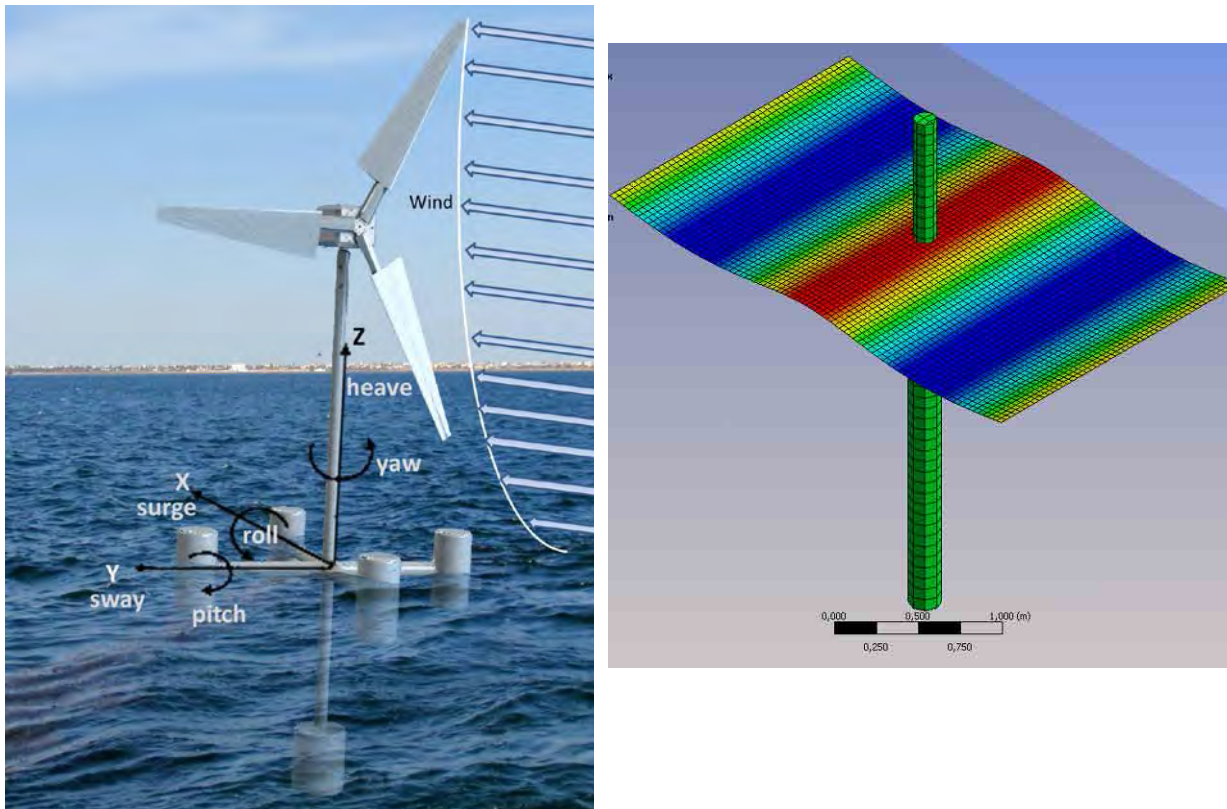


Figure 12: Problem schematics and concept solution.

There are three main principles of stabilization in floaters design: buoyancy, mooring lines and ballast. [19] None of these principles can exist alone in a floater, and none of them has nowadays demonstrated superiority above the others from both economic, feasibility and reliability point of view. The authors decided to implement the design of a spar buoy, which has its main stabilization effect in the ballast, and seems to be the most technologically reliable, despite a slightly higher cost with respect to the tension leg platform, that appears to be a highly cost-effective floater concept for wind turbines. A good proof of reliability of spar buoy concept is the Hywind project. [20] The design process is based on defining a suitable floater for a 3 kW rated power turbine. The result can be used as proof of concept and up scaled to define floaters for bigger turbines [21].

First of all, a static floating stability calculation has to be performed, in order to obtain righting moments on the floater, and then a dynamic analysis can be performed to estimate the system's behavior in waves.

For static floating stability the spar floater can be assumed as slender cylinder in water, then the main motions that should be analyzed are heave, pitch and roll. Since the floater is axial symmetric, only one rotational equilibrium will be examined.

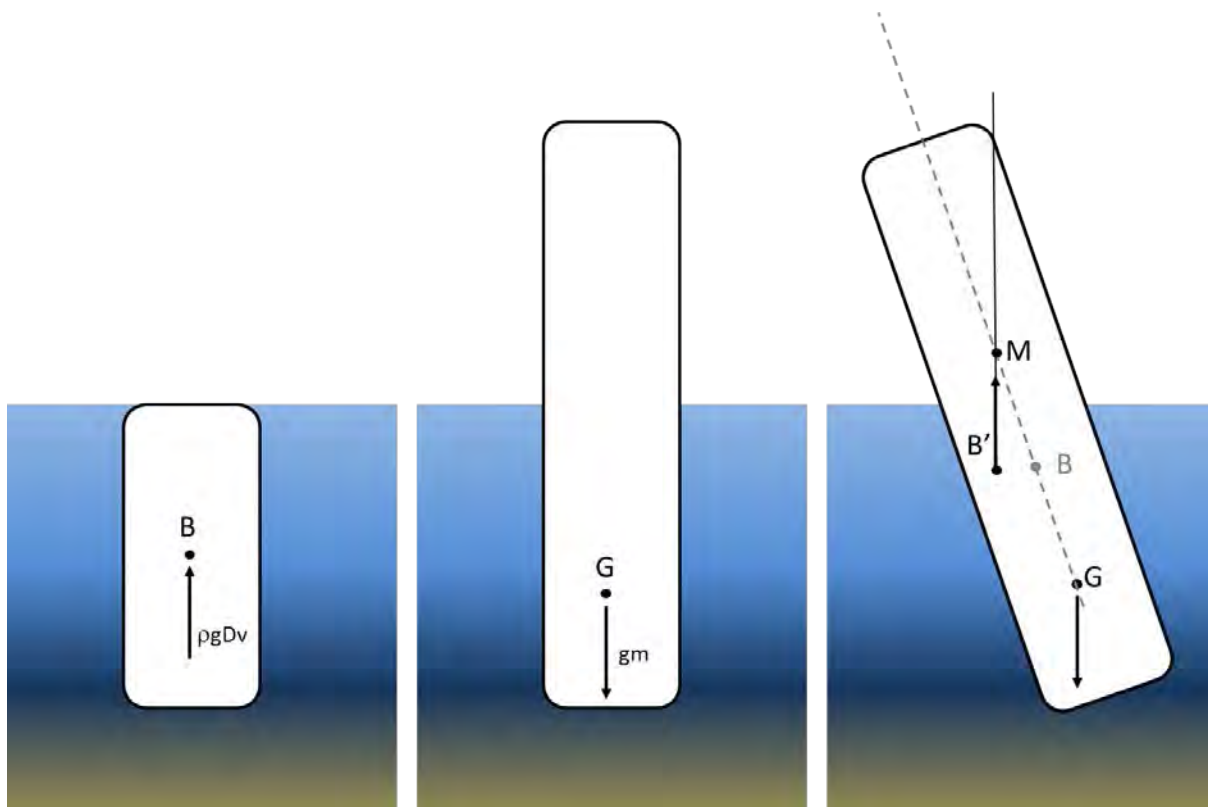


Figure 13: Static floating stability.

The vertical equilibrium is granted by buoyancy force, that is the vertical up thrust that the structure experiences due to the displacement of the fluid [22] Archimedes principle states the vertical equilibrium between buoyancy and gravity forces

$$\rho g D_v = gm \tag{8}$$

where ρ is the mass density of fluid, g is gravitational acceleration, m the total mass of body and D_v the displaced volume.

Let metacenter be the point of intersection between the lines through the buoyant forces at zero heel angle and at a small heel angle. It is known from theory that to have stable equilibrium the metacenter should be above the center of mass: in this case it will follow that the structure naturally tends to the initial position in case of disturbance of its rest conditions.

A static stability curve can thus be calculated for each floater, thus identifying the maximum angle for which the structure will naturally tend to reposition in the undisturbed position in case of external forcing, like wind on the turbine. External forcing in this case is given by thrust force on the wind turbine.

From a dynamics point of view, body motions in waves in the frequency domain are of great interest, since they gave a quick idea of body response to wave input. Usually the first harmonics of motion are of interest. Frequency domain response is also useful to perform time domain simulation using the convolution technique [23], [24]. The linearized problem of a body moving in waves can be solved by superposition of two phenomena: free oscillation of the cylinder in still water and body restrained in waves. [22]

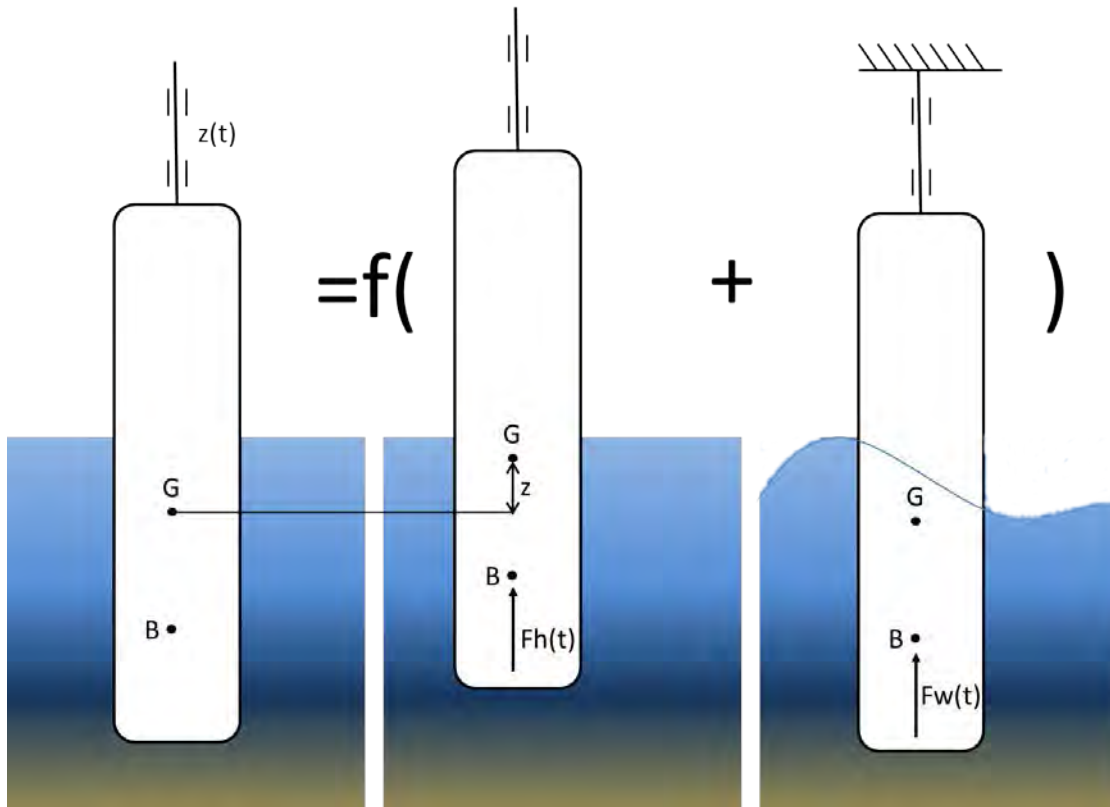


Figure 14: Heaving cylinder in waves as superposition of forces due to free decay and restrained body in waves.

The equation of motion will assume the form

$$(M + A)\ddot{X} + B\dot{X} + KX = F_h + F_w \quad (9)$$

Where M is the mass matrix of the body, A the added mass matrix, B the damping matrix and K the equivalent stiffness matrix, that is obtained from static floating stability calculations. The term F_h represents hydro mechanical loading, induced by oscillations of the rigid body moving in still water, and F_w represents wave loading, due to the waves acting on the restrained cylinder. The amplitude response of the floater motion is called RAO, or Response Amplitude operator. Some literature good practice suggests, when starting from scratch, to use the following empirical proportions to design a floater for the wind turbine [25] [26]:

$$\left\{ \begin{array}{l} \text{draft} = \frac{3}{2} \text{ tower height} \\ \text{tower height} = \frac{3}{2} \text{ rotor diameter} \\ \text{ballast mass} \cong 10 \text{ to } 20 * \text{ nacelle mass} \end{array} \right.$$

With these assumptions, some preliminary calculations have to be performed, in order to achieve a first dimensioning of mass distribution and floater displacement:

The first dimensioning is performed in order to establish a mass distribution that allows the floater to bear the wind turbine and the tower, and to have the center of gravity in a position that grants static stability in water, then a frequency response analysis has to be performed in order to forecast a mass distribution that allows also dynamic stability.

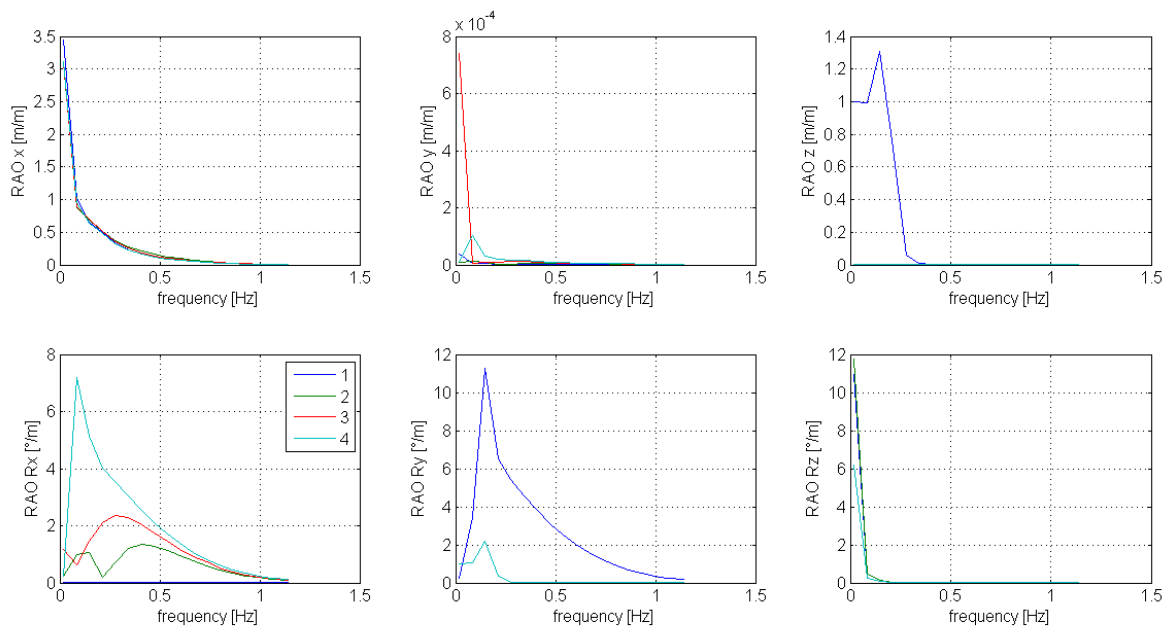


Figure 15: Dynamic response of the floater.

This information will drive the design of the shape of the floater. A concept design of a floater for a 3 kW wind turbine (shown in Figure 12) was performed.

Frequency domain calculations indicate that in most degrees of freedom the floater has a natural frequency below 0.15 Hz, the wave frequency representative of the selected reference site (Pantelleria Island, representative wave is 6-7 s peak period and 1.1 m significant wave height), hence different mass distribution and center of gravity positioning were compared (Figure 15).

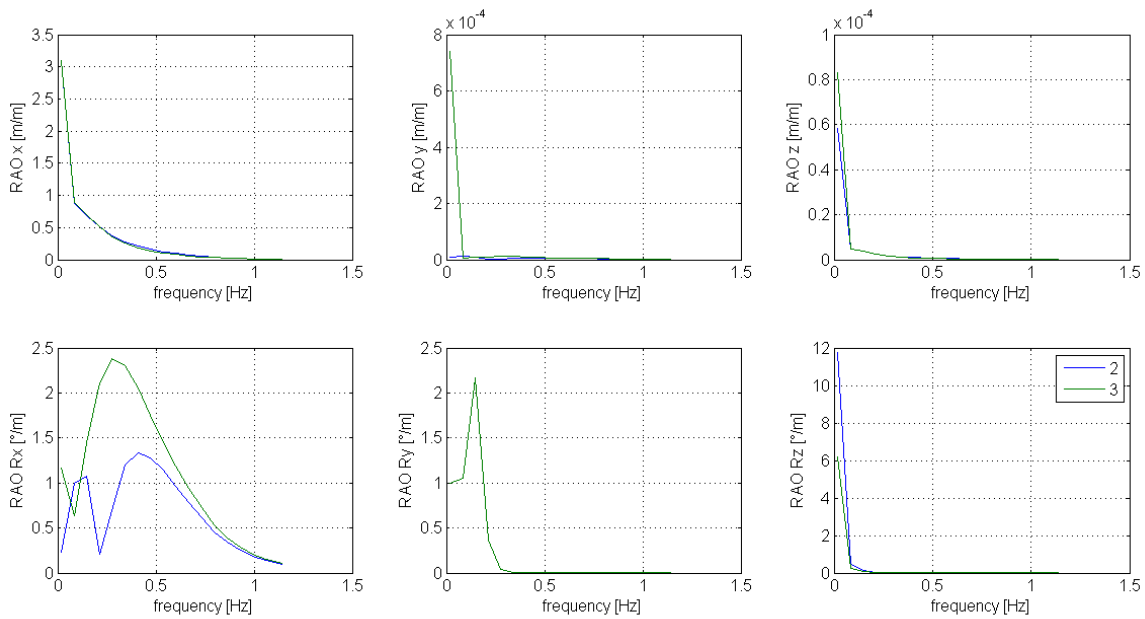


Figure 16: Most suitable floater choice.

As expected, the heave and pitch motions are the most solicited by wave loading. From these first results, it comes out that solution number 2 is the best among the analyzed cases (*Figure 16*).

A more detailed study of this solution has hence to be done: first of all a sensitivity analysis to the whole wave spectra of reference site will be performed; consequently a series of time domain coupled simulations is needed: in this step effects of wave loading and forces coming from the tower, gyroscopic effects due to the pitching motion coupled to rotor motion and mooring lines effects have to be evaluated all together, in order to have a realistic forecast of the systems behavior.

Discussion and conclusions

An aerodynamic, electric and mechanic model was developed and tested against experimental results of laboratory and wind tunnel tests on a small scale wind turbine. Experimental activity demonstrated that the mathematical model is reliable, since results of calculation matched well with experimental data, both in laboratory and wind tunnel tests. The developed model was used to determine expected maximum actions on the floater and a first concept design was performed using commercial software for marine structures analysis.

Outputs of the design are encouraging; in fact the conceived floater is suitable for the reference site sea conditions. Further steps in this process will include integration of the turbine model with hydrodynamic calculations, as well flume, tank and open sea tests for the designed floater.

References

1. C. Romanò et al., Experimental Methodologies for the measurement of wind turbines performance, *Proceedings of the ASME 2010 10th Biennial Conference on Engineering Systems Design and Analysis*, ESDA2010 July 12-14, 2010, Istanbul, Turkey
2. Randi A. Arinaga, Kwok Fai Cheung. Atlas of global wave energy from 10 years of reanalysis and hindcast data *Renewable Energy* 39(2012) 49-64
3. Gaetano Gaudiosi and Claudio Borri, Offshore wind energy in the Mediterranean countries, *Revue des Energies Renouvelables SMEE'10 Bou Ismail Tipaza* (2010) 173 – 188
4. <http://www.naturamediterraneo.com> accessed on February 2012
5. W.Musial, S. Butterfield and B., Ram Energy from Offshore wind, *Offshore Technology Conference Houston Texas* May 1-1 2006
6. www.deltatronic.it accessed on November 11, 2011
7. J. Jonkman et al., “Offshore Code Comparison Collaboration within IEA Wind Task 23: Phase IV Results Regarding Floating Wind Turbine Modeling”, NREL, April, 2010
8. J.G. Schepers “Verification of European Wind Turbines Design Codes”, EU-JOULE Project Final Report, May 2002
9. Jason M. Jonkman, Marshall L. Buhl Jr., “Fast User’s Guide”, technical report, NREL, 2005
10. <http://www.gl-garradhassan.com> accessed on October 12, 2011
11. Torben Juul Larsen, Anders Melchior Hansen “How 2 HAWC2, the user's manual”, technical report
12. Olivieri L., Ravelli E., “Principi ed applicazioni dell’Elettrotecnica”, vol II Cedam Padova 1990 ISBN: 8813191243

13. Ferraris L., "Macchine Elettriche", clut – Torino 2003, ISBN 88-7992-179-7
14. Krause P. C., Analysis of Electric Machinery. New York: McGraw-Hill, 1994
15. Martin O. L. Hansen, "Aerodynamics of Wind Turbines", Earthscan 2008, ISBN 978-1-84407-438-9
16. Glauert, H. (1935), "Airplane propellers", in W. F. Durand (ed) Aerodynamic Theory, vol 4, Division L, Julius Springer, Berlin
17. Tangler, J., Kocurek, J. D., "Wind Turbine Post-Stall Airfoil Performance Characteristics Guidelines for Blade-Element Momentum Methods", proceedings of the the 43rd AIAA Aerospace Sciences Meeting and Exhibit Reno, Nevada January 10–13, 2005
18. Deltatronic International, "Dtwind 1.5 technical report", technical report, 2008
19. Butterfield, S.; Musial, W.; Laxson, A. Feasibility of Floating Platform Systems for Wind Turbines, *Global Windpower 2004 Conference Proceedings (CD-ROM)*, 28-31 March 2004, Chicago, Illinois. Washington, DC: American Wind Energy Association; Omni Press; NREL Report No. PO-500-36049
20. www.statoil.com accessed on January 2012
21. R.P.L. Nijssen et al., The Application of scaling rules in up-scaling and marinisation of a wind turbine *European Wind Energy Conference and Exhibition (EWEC)*, Copenhagen, Denmark, July 2001
22. J.M.J. Journèe and W.W. Massie, Introduction in Offshore Hydromechanics *Delft University of Technology* March 2001
23. J.M. Jonkman and P.D. Sclavonious, Development of Fully Coupled Aeroelastic and Hydrodynamic Models for Offshore Wind Turbines *Proceedings of the ASME Wind Energy Symposium, Reno, Nevada* January 10-12 2006
24. J.M Jonkman and M.L. Buhl, Development and Verification of a Fully Coupled Simulator for Offshore Wind Turbines. *Proceedings of the 45th AIAA Aerospace Sciences meeting and Exhibit, Wind Energy Symposium*, January 8-11 2007
25. Scлавounos, P., Tracy, C., and Lee, S., Floating offshore wind turbines: Responses in a seastate pareto optimal designs and economic assessment. *Department of Mechanical Engineering Massachusetts Institute of Technology*. 2007
26. Matha D., Model development and loads analysis of an offshore wind turbine on a tension leg platform, with a comparison to other floating turbine concepts. *Technical report, NREL*. 2010

RAVE – Joint research at Germany’s first offshore wind park alpha ventus

Eva Otto, Michael Durstewitz, Bernhard Lange, Sebastian Pfaffel

Fraunhofer Institute for Wind Energy and Energy System Technology, Department Energy Meteorology and System Integration, Königstor 59, 34119 Kassel, Germany, eva.otto@iwes.fraunhofer.de, michael.durstewitz@iwes.fraunhofer.de, bernhard.lange@iwes.fraunhofer.de, sebastian.pfaffel@iwes.fraunhofer.de.

Abstract – Twelve 5 megawatt wind turbines of the first German offshore wind park “alpha ventus” were built in 2009 under genuine offshore conditions. Alpha ventus will gather fundamental experience with a view to future commercial use of offshore wind power in Germany. The research initiative RAVE – Research at alpha ventus – accompanies the construction and operation of alpha ventus to attain a broad basis of experience and expertise for future offshore wind parks. RAVE joins together the scientific activities of the turbine manufacturers and a multitude of research institutes. The research initiative is supported by the Federal Ministry for the Environment, Nature Conservation and Reactor Safety (BMU) following a resolution by the German Parliament. Coordinator is the Fraunhofer Institute for Wind Energy and Energy System Technology IWES.

1. Introduction

In the foreseeable future wind energy will make the biggest contribution to the growth of renewable energy in the electricity sector in Germany. Offshore technology as well as wind farm repowering will gain in importance as a result.

The Federal Government's “Strategy of the German Government on the use of offshore wind energy” aims at an offshore wind power capacity of 20-25 gigawatt by the year 2030 – approximately 15 % of the German electricity demand (BMU 2002).

The first German offshore wind farm alpha ventus is a project by the consortium Deutsche Offshore-Testfeld- und Infrastruktur GmbH & Co. KG (DOTI), a joint venture between the energy utilities EWE, E.ON and Vattenfall Europe. DOTI has leased the rights for the site, located 45 km north of the Island of Borkum, from the Stiftung Offshore-Windenergie (Offshore Wind Energy Foundation). Twelve wind turbines manufactured by AREVA Wind and Repower Systems (Figure 1), with a hub height of ca. 90 m, a rotor diameter of 116 m respectively 126 m, and a capacity of 5 megawatt each, should deliver electricity for about 50,000 households.

The alpha ventus test and demonstration project initiated the utilization of wind energy in the North and Baltic Seas. The construction of the transformer station and laying of the undersea cable were completed in 2008. The installation of the twelve wind turbines, which was planned for 2008 originally, had to be postponed due to unfavorable weather conditions until 2009.

In comparison to other operating offshore projects alpha ventus is located much further from the land, and in greater water depth (Figure 2).

Furthermore the researchers of the German research initiative RAVE – Research at alpha ventus – carry out various measurements and investigations to further promote Germany’s know how in this field.

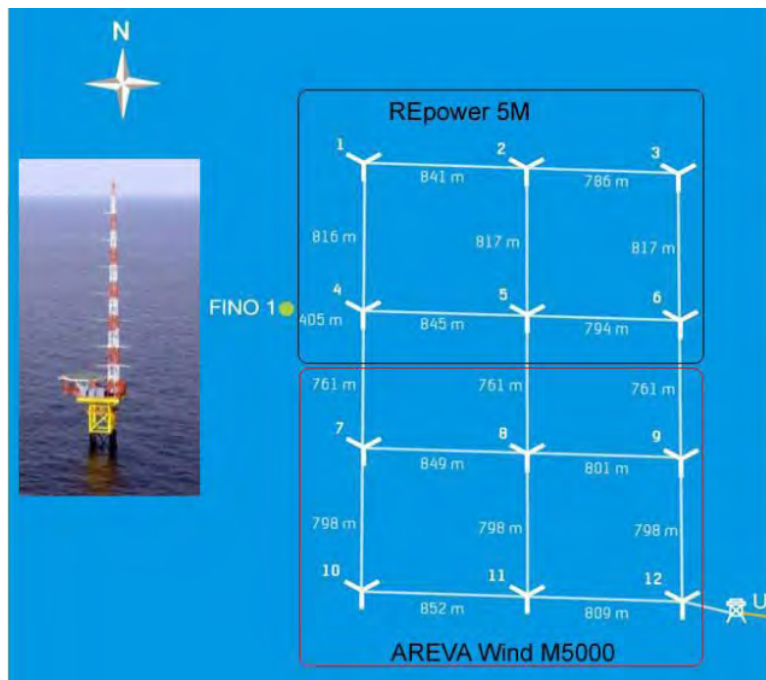


Figure 1: Layout of alpha ventus. The German research platform FINO1 is situated at short distance.

Since the start of the initiative in 2007 the main research focus has been mainly on cost reduction, increase in profit, advancing the availability of wind energy generators, improving technologies for the construction of offshore wind energy, ecological accompanying research as well as technical optimization of wind energy generators with regard to ecological impact. The 25 ongoing and already completed projects lay the foundations for improving the offshore capability of multi megawatt wind parks and contribute to the environmental compatibility of offshore wind energy utilization. In particular, it has been demonstrated that research into offshore wind energy requires interdisciplinary co-operation as knowledge from so many different disciplines is required (www.rave-offshore.de).

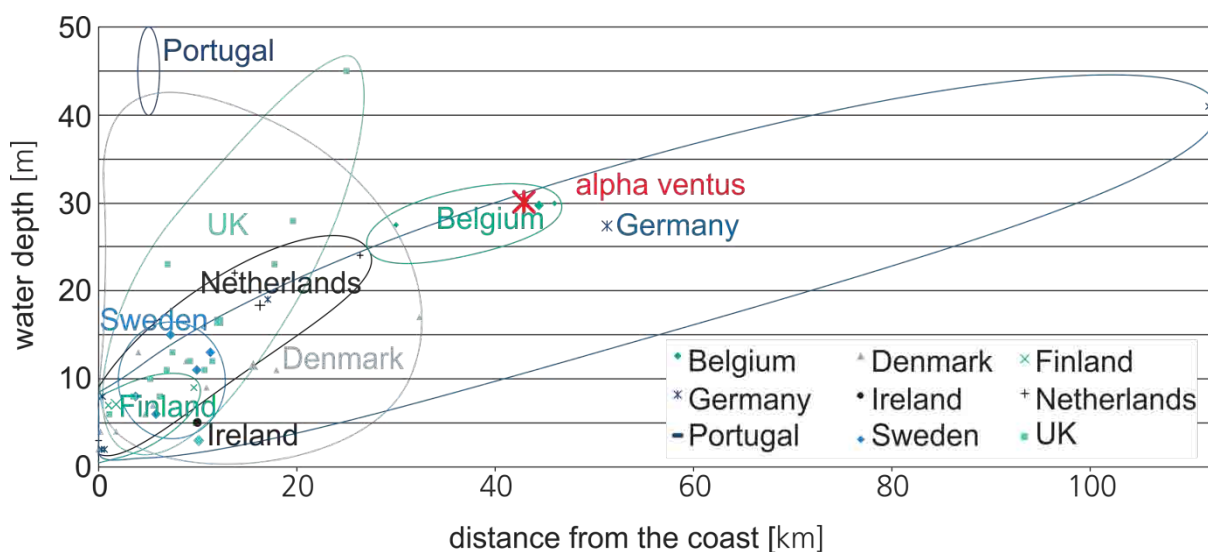


Figure 2: Water depth and distance from the shore of offshore wind farms in different European countries – alpha ventus is highlighted in red; Status 12/2011 (Fraunhofer IWES 2011).

2. Organizing the Research Cooperation and Measurements

2.1 RAVE Coordination Project

The objective of the RAVE Coordination project is to network the currently 25 individual RAVE projects and to represent them. In order to use synergies and improve quality of results, the collaboration is based on a balanced concept. The organizational coordination is achieved by the RAVE steering committee.

Moreover, international cooperation is supported through RAVE delegates in the European Wind Energy Technology Platform (TPWind) and through cooperation within the International Energy Agency Implementing Agreement for Co-operation in the Research, Development, and Deployment of Wind Energy Systems (IEA Wind).

In addition, RAVE Coordination is responsible for public relations. Experiences and results originating from RAVE research activities are presented to scientists, students, investors, politicians, and the general public. In order to reach a broad forum, RAVE Coordination has organized and carried out the RAVE International Conference 2012 in May 2012 in Bremerhaven, Germany (www.rave2012.de).

2.2 RAVE Measurement Service Project

For RAVE research projects comprehensive measuring data are indispensable. The RAVE Measurement Service Project has the goal to carry out measurements and to coordinate the data demand of the individual RAVE projects as a service for all involved institutes, authorities and companies. Load conditions, operational noise, noise emissions during the installation, meteorological, oceanographic and geological data are the main measurement parameters.

Additional measuring instruments are installed on the turbines AV7 and AV8 (AREVA Wind M5000), on AV4 and AV5 (REpower 5M), on the alpha ventus transformer platform, the onshore transformer station, and at various other positions in the waters of the alpha ventus test field (Figure 3).

Data from a total of about 1,200 measuring points are recorded and processed, and are available for accredited RAVE researchers in the RAVE data base.

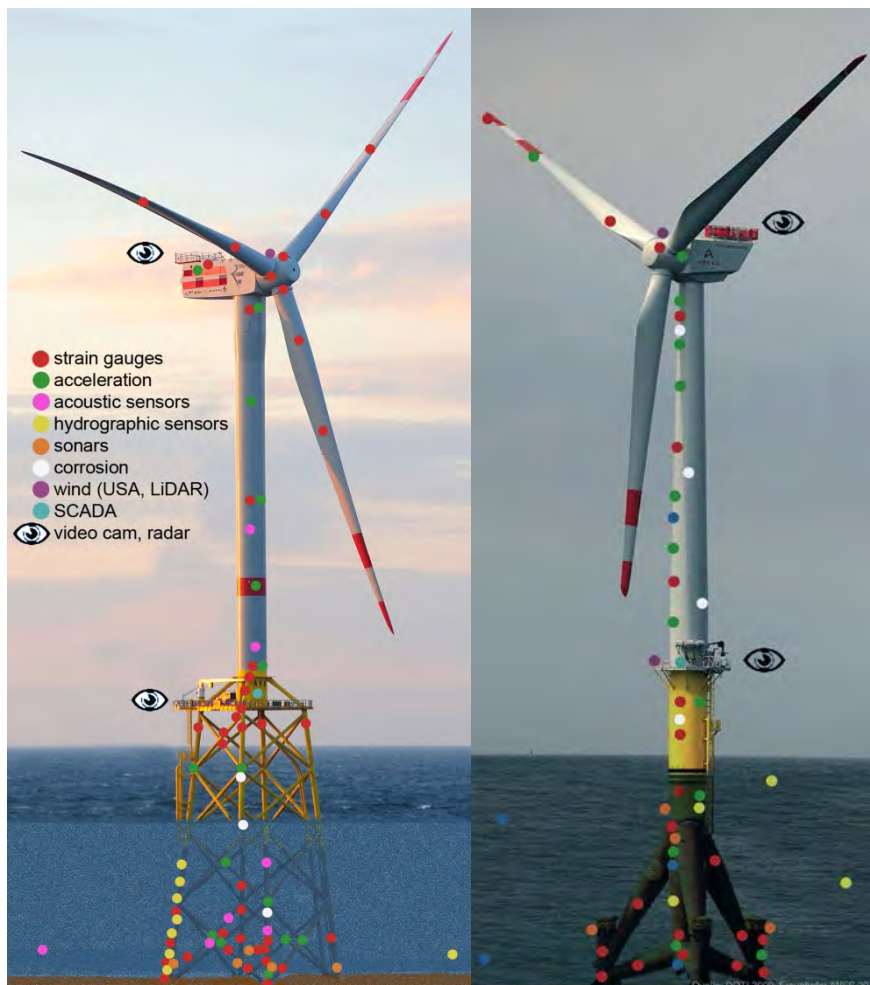


Figure 3: Sketch of Repower 5M (AV4; left) and AREVA Wind M5000 (AV7; right) offshore wind turbine in the alpha ventus test field. Markings on the structure and in the water indicate locations and type of instrumentation used for the RAVE measurements.

3. Research Activities

3.1 Research on foundation and construction

Two steel foundations are used at the alpha ventus wind park. The AREVA Wind turbines use a “tripod”-concept as a support structure. The Repower turbines are mounted onto a “jacket”-foundation, which uses as many similar parts as possible (Figure 4).

The project RAVE Foundations analyzed the effects of wind, waves and operations on different foundation types (monopile, tripod, jacket, etc.). Its follow-up project RAVE Foundations Plus shall investigate research and testing procedures for foundation monitoring and data evaluation suitable for offshore wind turbines.

A further subsidiary project, RAVE Gigawind alpha ventus, intends to improve the supporting structure through an integrated dimensioning concept and to develop it into a commercially mass-producible item. The RAVE Geology project investigates the seabed and particularly its suitability for offshore constructions.

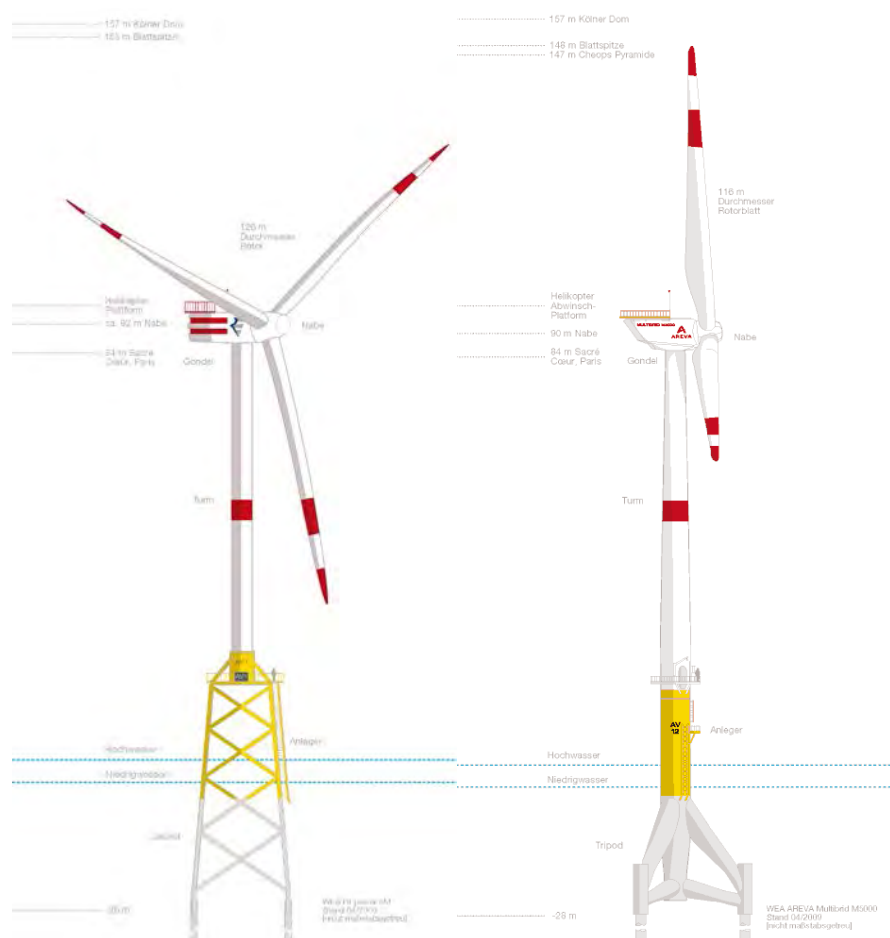


Figure 4: Sketch of REpower 5M with a jacket foundation (left); AREVA Wind M5000 with a tripod.

3.2 Research on technology and monitoring

Before the construction of offshore wind parks can take-off on a larger scale, it is imperative to incorporate the experience and knowledge gained from the planning, construction and operation of the alpha ventus test site into further developing and optimizing the technology. Therefore, further rotor blade development is the focus of the RAVE REpower Blades project while the interdependency of the overall system is analyzed by the RAVE REpower Components project. The improvement of selected components is pursued by the RAVE AREVA Wind M5000 Improvement project. In RAVE OWEA, key aspects of reliable design and operation of offshore wind turbines are being verified. The project RAVE LIDAR (Light Detection And Ranging) investigates the application of modern wind measurement techniques to offshore turbines as well as potential improvements to operations management.

Additionally, the completed monitoring project RAVE Offshore~WMEP has recorded and interpreted essential operation data to enable the determination of such matters as the influence of particular meteorological conditions, energy revenues, energy production, downtimes, electricity production costs, availability, maintenance and grid connection issues as well as other key performance indicators.

Two new cooperation partners have recently joined the RAVE initiative. The project RAVE TUFFO investigates the impact of turbulent humidity fluxes on the static stability of the marine boundary layer. RAVE UFO measures and analyzes climatological environmental parameters and their influence on the components of wind energy turbines.

3.3 Research on grid integration

The energy from offshore wind parks must first be brought to land using subsea cables. The high-performance connections on land are used to transport the generated electricity to load centers where much electricity is needed. In the RAVE Grid Integration project, strategies for the integration of offshore wind energy into the power grid are being developed and implemented. The aim is to reduce balance energy and the provisions for reserve power with the help of newly developed offshore wind power prediction systems while at the same time ensuring the high availability and the safety of the grid.

3.4 Research on environment

The goal of the complementary ecological research in the RAVE Ecology project is to gain extensive knowledge of the impacts of construction and operation conditions on the marine environment, for example, on benthos, fish, resting birds, migratory birds and marine mammals. The main focus of the RAVE Geology project is to pursue the acquisition and evaluation of the sediment dynamical processes (scour) and overall sand movement in order to obtain reliable information for the design basis of the offshore constructions and the liquefaction behavior of the upper seabed. In the RAVE Operational Noise project the underwater sound propagation of the operational noise of the wind turbines under various boundary conditions as well as the overall noise stress for sea life and particularly sea mammals are being determined. The RAVE Hydro Sound project is investigating measures of noise reduction during the construction phase through pumping air bubbles into the water. The safety of submarines will be enhanced in the RAVE Sonar Transponders project through the technical integration of sonar transponders in the overall wind park design.

4. Conclusions

For the deployment of wind generators at sea, proven systems engineering and management must be adapted to the harsh environment. Not only appropriate foundations, encapsulations for the nacelles and materials with long-term stability have to be developed but also the safe and economical integration into the electrical grid has to be realized.

We have to face the special challenges of offshore wind energy and find affordable solutions. In the next few decades only wind and bio-energy will be able to make significant contributions to the electricity energy supply; thus slowing down the dramatic increase of CO₂ concentration in the atmosphere. If the world-wide electricity demand continues to grow at 2.5% p. a. and wind and bio-energy generation grow at 20% p. a., together with hydropower, which is already widely exploited in Europe, they will theoretically be able to supply world electricity needs by 2030. Only with uninhibited growth over time will solar energy be able to make an appreciable contribution. After significant growth in this sector, solar energy will be able to supplement water and bio-energy, which are limited for reasons of sustainability, and solar energy will offer a long term and almost inexhaustible potential.

Initially, however, global consideration will be given to the appreciable contribution hydropower and wind energy can make to electricity generation, as such technology provides the greatest CO₂ prevention benefits. Due to competitive production costs, it also equates to the lowest possible cost of CO₂ prevention. With current mean electricity production costs of 8 ct/kWh and optimally of 4 ct/kWh on land, wind energy is close to being competitive when compared to conventional power stations and fully competitive with future low CO₂ emitting power plants. Offshore wind generation is expected to be initially twice as high.

5. Overview of RAVE research projects

Project	Main research questions	Status
Foundation and Support Structures		
<p>RAVE – GIGAWIND alpha ventus ForWind – Leibniz Universität Hannover</p> <p>Holistic design concept for offshore wind turbine support structures on the base of measurements at the offshore test site alpha ventus</p>	<ul style="list-style-type: none"> ▪ How can offshore wind turbine support structures be improved in order to become an economic, mass-produced product? ▪ What are the real and individual load on an offshore wind turbine and how can they be measured and observed? ▪ How can the life time of offshore structures be extended? ▪ Which changes in the sea bed are expected from driven piles? 	<i>completed</i>
<p>RAVE – Foundations BAM – Federal Institute for Materials Research and Testing</p> <p>A practical design and monitoring procedure for foundations of offshore wind turbines under cyclic loads.</p>	<ul style="list-style-type: none"> ▪ How accurate are predictions about the long-term behavior of the turbine's foundation? ▪ What is the influence of the pore water pressure on the pile's resistance? ▪ How is the pile affected by the combination of cyclic lateral and vertical loads? 	<i>completed</i>
<p>RAVE – Foundations Plus BAM – Federal Institute for Materials Research and Testing</p> <p>Procedures for foundation monitoring and data evaluation suitable for offshore wind turbines</p>	<ul style="list-style-type: none"> ▪ Determination of the actual resistance characteristics of a pile foundation out of measured data ▪ Adaption of measuring devices to the requirements of offshore conditions ▪ Development of an assessment method for the foundation monitoring based on monitoring data ▪ Development of a standard for the application of the so-called Observational Method for Offshore foundations 	<i>ongoing</i>

Turbine Technology and Monitoring		
<p>RAVE – REpower Components REpower Systems SE</p> <p>Further development of offshore wind turbine components with respects to costs, longevity and servicing conditions</p>	<ul style="list-style-type: none"> ▪ Can modern offshore turbines fulfill future grid requirements that are comparable with conventional power plants? ▪ Can new control methods reduce mechanical loads on the turbine resulting in lower material input without cutting down the energy yield? ▪ Attainment of a high level of transparency for offshore wind power plants by means of a new generation SCADA system? 	<i>completed</i>
<p>RAVE – REpower Blades REpower Systems SE</p> <p>Development of an innovative, performance-optimized and cost-efficient rotor blade for offshore wind turbines</p>	<ul style="list-style-type: none"> ▪ How can higher aerodynamic efficiency be achieved? ▪ Can the planned innovations increase the economic efficiency? ▪ Will advanced production technology contribute to such improved results? 	<i>completed</i>
<p>RAVE – AREVA Wind M5000 Improvement AREVA Wind GmbH</p> <p>Further development, construction and testing of the M5000 wind turbine under offshore conditions</p>	<ul style="list-style-type: none"> ▪ The technical behavior of the AREVA Wind M5000 in an offshore environment will be monitored. The main question is whether any necessary adjustments must be made. ▪ Is it possible for the complete remote control system and the analysis of data to be carried out via a new SCADA system? ▪ Can the planned innovations increase the economic efficiency? 	<i>ongoing</i>
<p>RAVE – LIDAR Stuttgart Wind Energy, University of Stuttgart</p> <p>Further development of LiDAR wind measuring techniques for offshore applications</p>	<ul style="list-style-type: none"> ▪ What are the possible applications of LIDAR technology in the offshore wind energy industry? ▪ How does power curve assessment with ground and nacelle based LIDAR systems compare to standardized measurements with cup anemometers? ▪ What is the behavior of wind turbine wakes in an offshore environment and how can the wake wind field be measured with LIDAR technologies? ▪ Which loading reduction can be achieved with LIDAR supported control based on inflow wind field measurements? 	<i>completed</i>
<p>RAVE – LIDAR II ForWind – University of Oldenburg</p> <p>Further development of LiDAR wind</p>	<ul style="list-style-type: none"> ▪ How can a robust and cost-efficient nacelle-based lidar system be demonstrated for power performance measurement and control of wind turbines? 	<i>ongoing</i>

<p>measuring techniques for offshore applications</p>	<ul style="list-style-type: none"> ▪ How can the power performance of wind turbines inside wind farms be assessed and monitored using nacelle-based wind measurements? ▪ How can nacelle-based wind measurements be employed for predictive turbine control facilitating gust compensation and optimization of energy yield? 	
<p>RAVE – OWEA ForWind – University of Oldenburg</p> <p>Verification of offshore wind turbine technology with focus on atmospheric conditions, turbine behavior and load cases in offshore environment</p>	<ul style="list-style-type: none"> ▪ What is the effect of specific atmospheric conditions in offshore environments on the power curve of wind turbines? Can power curves be measured offshore with sufficient accuracy using LIDAR technology? ▪ How do airflows in wind farms behave and interact? How does operation in the wake of other turbines affect a wind turbine’s loading in an environment with very low ambient turbulence? ▪ Are state of the art simulation models and tools appropriate for predicting wind turbine behavior and loading for offshore applications? How much can results be improved by integrated analysis if complex foundations are involved? ▪ How should an efficient, robust, and durable load monitoring system for offshore wind turbines appear and how can it help to improve wind turbine performance? ▪ How can turbulence parameterization in numerical regional weather models for entire coastal regions like the southern North Sea be improved? 	<p><i>completed</i></p>

<p>RAVE – Offshore-WMEP Fraunhofer IWES</p> <p>Monitoring of the offshore wind energy deployment in Germany with focus on energy production, availability, service concepts, external conditions etc.</p>	<ul style="list-style-type: none"> ▪ What energy yield can be achieved and what does offshore wind energy cost? ▪ What is the effect of specific offshore conditions on equipment and on the operation and performance of wind turbines and what are the main differences to onshore systems? ▪ What are the fluctuations of feed-in caused by the variation of wind speeds and how is availability affected by extreme wind conditions? ▪ What are the advantages and/or disadvantages of different system concepts, different concepts of installation, maintenance strategies, and different grid-connection concepts? 	<p><i>completed</i></p>
<p>RAVE – UFO fk-wind - Institute for Wind Energy at the University of Bremerhaven</p> <p>Measurement and analysis of climatological environmental parameter and their influence on components of wind energy turbines.</p>	<ul style="list-style-type: none"> ▪ Measurement and analysis of climatological environmental parameter and their influence on components of wind energy turbines. ▪ Detection of salt deposit, humidity, temperature and microorganisms. 	<p><i>ongoing</i></p>
<p>RAVE – TUFFO Karlsruhe Institute of Technology (KIT)</p> <p>Investigation of the impact of turbulent moisture fluxes on the turbulence in the marine boundary layer.</p>	<ul style="list-style-type: none"> ▪ Investigates the impact of turbulent moisture fluxes on the turbulence in the marine boundary layer. ▪ Due to the presence of the sea surface, these fluxes tend to destabilize the atmospheric stratification and to increase the turbulence intensity. 	<p><i>ongoing</i></p>
<p>Grid Integration</p>		
<p>RAVE – Grid Integration Fraunhofer IWES</p> <p>Development of strategies and tools for the effective integration of offshore wind power into the electricity supply system</p>	<ul style="list-style-type: none"> ▪ Which wind power forecast models are needed for offshore wind farms? ▪ Which numerical weather prediction models will be used to achieve the best wind power forecasts? ▪ How can offshore wind farms be operated almost as conventional power plants? ▪ How to model fluctuating wind power? 	<p><i>completed</i></p>

Environment		
<p>RAVE – Ecology BSH – Federal Maritime and Hydrographic Agency</p> <p>Research on the impact of offshore wind parks on marine environment and evaluation of BSH's Standard for Environmental Impact Assessments</p>	<ul style="list-style-type: none"> ▪ Will marine mammals and passage migrant birds continue using the wind farm area as habitat? ▪ What impacts will noisy construction work and the operational phase have on marine mammals and fish? ▪ What changes in the habitats of benthic organisms and fish species are to be expected close to the foundations? How far does the influence of the artificial hard substrate extend? ▪ How do migratory birds react to the rotating, lighted turbines? Will there be collisions and evasive movements? 	<i>ongoing</i>
<p>RAVE – Operational Noise Flensburg University of Applied Sciences</p> <p>Assessment of the operational underwater sound immission of offshore wind turbines under varying boundary conditions</p>	<ul style="list-style-type: none"> ▪ How loud are single 5 MW offshore wind energy converters in the water? ▪ What amount of underwater noise does the alpha ventus wind farm produce? ▪ How do weather and tide conditions influence underwater noise production and propagation? ▪ What is the shape of the transfer-function between tower vibration and underwater noise? 	<i>completed</i>
<p>RAVE – Hydro Sound ForWind – Leibniz Universität Hannover</p> <p>Evaluation of sound reduction measures to minimize impacts on the marine environment</p>	<ul style="list-style-type: none"> ▪ Concept design and development of a layered bubble curtain close to the foundation of an offshore wind turbine of type AREVA Wind M5000 ▪ Testing and subsequent evaluation of the operation of the layered bubble curtain under offshore conditions and meeting the requirements of pile driving procedures, which are necessary to install the foundations ▪ Assessment of the tide's influence on the noise mitigation efficiency of the bubble curtain ▪ Investigation of the influence of the ram energy level on the noise mitigation efficiency of the bubble curtain 	<i>completed</i>

<p>RAVE – Sonar Transponder ForWind – Leibniz Universität Hannover</p> <p>Investigation of sonar transponders for offshore wind farms as acoustic warning systems to submarines and integration into an overall technical concept</p>	<ul style="list-style-type: none"> ▪ Which mounting position is most suitable for the sonar transponder? To answer this question, the topology of both the foundation and the whole wind park has to be taken into account. ▪ How can hydro-sound propagation of the far field be calculated taking into consideration the topology of the foundation, water depth, bathymetry, and entry of air bubbles? ▪ What diffraction and interference effects are possible when one or more transponders are activated? ▪ How can the impact on marine mammals be minimized? 	<p><i>completed</i></p>
<p>RAVE – Acceptance Martin Luther University Halle-Wittenberg</p> <p>Assessment of the social acceptance of offshore wind energy utilization by residents and tourists in four coastal regions on the North and Baltic Sea</p>	<ul style="list-style-type: none"> ▪ How distinct is the acceptance of offshore wind power, and what factors influence this? ▪ What effects do offshore wind farms have on tourism and the local economy? ▪ What measures can be employed to solve or avoid conflicts between residents, operators, and public authorities? 	<p><i>ongoing</i></p>
<p>RAVE – Geology / Oceanography BSH – Federal Maritime and Hydrographic Agency</p> <p>Analyzing impacts of offshore wind farms to the marine environment</p>	<ul style="list-style-type: none"> ▪ Determination of scour depths and scouring dynamics ▪ Influence of offshore wind turbines on the overall sediment dynamics at an offshore wind farm ▪ Characterization of impacts of sediment dynamical processes on geotechnical properties and benthic organisms of the upper seabed ▪ Continuous oceanographic observations ▪ Provision of oceanographic measurement data for all RAVE-projects ▪ Analysis of interactions between offshore structures and the marine environment 	<p><i>ongoing</i></p>

Cross-sectional projects		
RAVE – alpha ventus alpha ventus consortium DOTI operator of alpha ventus	<ul style="list-style-type: none"> ▪ Planning, construction and operation of a 60 MW pilot offshore wind farm for test and research purposes 	<i>completed</i>
RAVE – Coordination I Fraunhofer IWES Organizing research collaboration	<ul style="list-style-type: none"> ▪ Organizational coordination ▪ Scientific coordination ▪ Conceptual design of measurements and instrumentation with RAVE partners ▪ Representation of the RAVE-initiative ▪ RAVE related PR activities 	<i>completed</i>
RAVE – Coordination II Fraunhofer IWES Continuation of the research collaboration	<ul style="list-style-type: none"> ▪ Organizational coordination ▪ Scientific coordination ▪ Development of measurement concept with research partners ▪ Representation of the RAVE-initiative ▪ RAVE related PR activities and dissemination of research results 	<i>ongoing</i>
RAVE – Measurement Service Project BSH – Federal Maritime and Hydrographic Agency Technical coordination of RAVE research measurements	<ul style="list-style-type: none"> ▪ Technical coordination of RAVE research measurements ▪ Implementation of measurement concept ▪ Installation and technical realization of measurements ▪ Operation, maintenance and inspection of gauges ▪ Logistics 	<i>ongoing</i>

Appendix

For further information on RAVE and all individual research projects, visit:

www.rave-offshore.de

For presentations of research results at the RAVE International Conference 2012, visit:

www.rave2012.de



RAVE is funded on the base of an act of the German Parliament by



supervised by



and coordinated by



References

1. Federal Ministry for the Environment, Nature Conservation and Nuclear Safety (BMU). Strategy of the German Government on the use of offshore wind energy, 2002, available at http://www.bmu.de/english/renewable_energy/downloads/doc/3389.php
2. Fraunhofer-Institut für Windenergie und Energiesystemtechnik IWES. Windenergie Report Deutschland 2011, 2012, available at: <http://www.windmonitor.de>

Turbine foundation in intermediate waters: monopile versus jacket

F.G. Cesari¹, F. Taraborrelli, T. Balestra², L. Milella³

¹*DIENCA Dept., University of Bologna, via Dei Colli n.16 – 40100 Bologna, Italy, cesfranco@libero.it*

²*TECON, Palazzo F3, Assago Milano), tullio.balestra@teconsrl.it*

³*TRE SpA, Bari, luigi.milella@tozziholding.com*

Abstract - The search, for a better productivity in wind energy generation, pushed towards offshore sites with very good wind conditions, so to reach high sea depth. These sites, so said “intermediate waters”, fall in the -30 m -50 m depth range, which appears as an extreme limit for economical acceptance of substructures fixed to the sea bed. The range of “deep waters” could be up to 75/100 m (or more). The study has been concentrated on a complex system made by wind turbine-foundation - approximately for a 3 MW wind generator- and two different substructure configuration, a monopile supporting structure and a three/four legged jacket as used in the platforms for oil/gas extraction. The preliminary design analysis is based on site data typical of the Adriatic Sea in order to identify, the general dimensions and weight in compliance with some essential technical specifications. Particular attention has to be paid to compare the stress response of the two type of substructure, the monopile and the jacket.

1. Some introductive considerations

An important engineering challenge of today, and a vital one for the future, should be the development of any alternative sources of energy in respect of plants using fuel from Carbon cycle. This is a firm priority either in the UE or especially in Italy setting a target electricity from renewable sources by 2020.

A central component to this commitment will be to harvest electrical power from industrial sector with vast energy reserves as the offshore plants particularly through wind turbines. Much technology transfer can be gained from onshore experience, which supplies a lot of ‘green energy’ to the population, but in condition to provoke some objections on aesthetic and visual grounds. By locating the turbines offshore it has been also possible to install larger wind farms than those onshore, as happens in many Northern European countries.

It should be advantageously evident that, by moving offshore, larger structures can be installed allowing a much greater power output. It should be noted that offshore winds are not necessarily stronger, but are usually more consistent and with intensity less dissipated by liquid surface of the sea. There are also large tracts of seabed that are not used for other purposes (except temporarily for fishing) and may be suitable for hosting wind farms.

If the on shore wind turbines are too much invasive for the landscape, those offshore can reduce the visual pollution by moving them far from the coast. The distance and the orientation play a great role on the acceptance by population, displacing too the site towards sea zones not located in front of crowded coasts.

There is significant pressure, however, to put wind turbines offshore, where they will be out of sight, as explained conveniently by the data form the Tables 1 and 2, which consider in effect only offshore plants. For each site is indicated the type of foundation and the main characteristics of them.

Table 1: Wind farms equipped by different supporting structures.

Structural configuration	Examples	Use	Notes
Monopile	Arklow (Ireland); Barrow (UK); Blyth (UK); DanTysk (DE); Egmond aan Zee (NL); Greater Gabbard (UK); Gunfleet Sands (UK); Horns Rev 1&2 (DK); Kentish Flats (UK); Lely (NL); London Array (UK); Lynn & Inner Dowsing (UK); North Hoyle (UK); Rhyl Flats (UK); Robin Rigg (UK); Scroby Sands (UK); Utgrunden (SE);	Shallow to medium water depths	<p>a. Made from steel tube, typically 4-6-8 m in diameter;</p> <p>b. Installed using driving and/or drilling method;</p> <p>c. Transition piece grouted onto top of pile;</p>
Jacket	Alpha Ventus (Repower, 6 turbines), DE; Beatrice Windfarm (Moray Firth), UK; Ormonde (UK); EnBW Baltic 2 (41 turbines over 80), DE;	Medium to deep water depths	<p>a. Made from steel tubes welded together, typically 0.5-1.5 m in diameter;</p> <p>b. Anchored by driven or drilled piles, typically 0.8-1.2 m in diameter;</p>
Tripod	Alpha Ventus (Multibrud turbines), DE; Bard Offshore 1, DE;	Medium to deep water depths	<p>a. Made from steel tubes welded together, typically 1.0-5.0 m in diameter;</p> <p>b. Transition piece incorporated onto centre column;</p> <p>c. Anchored by driven or drilled piles, typically 0.8-2.5 m in diameter;</p>
Gravity base	Ayos Kemi (FI); Lillgrund (SE); Middelgrunden (DK); Nysted (DK); Thornton Bank Phase 1 (BE); Tuno Knob (DK); Vindeby (DK);	Shallow to medium water depths	<p>a. Made from steel or concrete;</p> <p>b. Relies on weight of structure to resist overturning, extra weight can be added in the form of ballast in the base;</p> <p>c. Seabed may need some careful preparation;</p> <p>d. Susceptible to scour and undermining due to size;</p>
Floating/ submerged structures	Hywind (Norway); Tricase (IT)	Very deep water depths	<p>a. Still under development;</p> <p>b. Relies on buoyancy of structure to resist overturning;</p> <p>c. Motion of floating structure could add further dynamic loads to structure;</p> <p>d. Not affected by seabed conditions.</p>

Source: Wind Energy with integration

Table 2: Overview of available offshore wind turbines. Source: EWEA 2009 with integrations.

	Power Output [MW]	Manufacturer	Concept	Rotor diameter [m]
BARD 5.0	5	Bard engineering	Variable speed (Gearbox)	122
Multibrid	5	Areva	Variable speed ld.	116
Repower	5/6	Repower	Variable speed ld.	126
Siemens SWT	3,6	Siemens	Variable speed ld.	107/120
Vestas	3	Vestas	Variable speed ld.	90/112
Nordex N90	2,5	Nordex	Variable speed ld.	80
GE 3.6	3,6	General Electrics	Variable speed ld.	111
GE 4.0	4	GE (Scanwind)	Direct Drive (no gearbox)	110
Darwind	5	XEMC	Direct Drive (no gearbox)	115

2. Wind condition suitable areas for offshore wind farm

A clear understanding of the load-transfer mechanisms, from turbine to foundation and from it to the soil, leads to increased confidence in the overall design. As comes from the structural chain the foundation has to sustain all loads that may be applied, particularly during normal and extreme environmental conditions. If so does not happen, the principal consequence could occur should be the financial loss. It will be a very negative result for an offshore plant, if the structure fails (unlike other offshore applications where loss of life is the primary concern, because fortunately no people remain onboard of turbine during the operation).

Essential for wind farm is a certain number of factors, affecting in a positive sense the selection of site, as main quantities of site (maximum wind speed, wave heights, currents, soil properties, etc.), distance from coast and urban centres, sufficiently favourable bathymetric lines, limits going from peripheral areas around the site, biocenotic parameters affecting the sea bed, general environmental conditions due to alieutic and bird life characteristic in the zone interested by plant, good logistic infrastructures as roads, railways net, motorways, airports for transportation, efficient and ample harbours and protective havens, etc.

Combining these information with those from bathymetry – depth of seabed must be not major than 30-40 m – available areas reduce further on; in fact areas in the Otranto channel and in the Sicily strait must be excluded. Exclusion of the Sicily strait is due also to reasons of sea biology. Considering areas in the Adriatic Sea just above selected, at a distance from the coast not lower than 3 miles and a depth of the seabed lower than 50 m, it's reasonable to consider the seabed having a ripple shape.

Each site, however, may require different engineering strategies, depending on the soil conditions, such as sand density and depth to the clay stratum, as well as the strength of the underlying clay.

The following sections will discuss some structural and foundation systems that might be employed for offshore wind turbines in intermediate waters. They may not be suitable for every site, but the development and testing of competing strategies will help to drive down the cost.

3. Wind Farms suitable for offshore sites

A negative aspect for offshore turbine could arrive from the environmental (wind and wave) loadings. They are particularly significant on the massive bodies, leading to greater forces in the large structure than those that would occur onshore.

To support the wind turbine and to ensure a sufficient connection with the ground a specific structure, i.e. the foundation (Figure 1), has to be envisaged also for transferring the forces from the wind converter and all aerial components (like tower and outside sea foundation) to the surrounding soil. This is a critical part of the design of a wind-turbine structure.

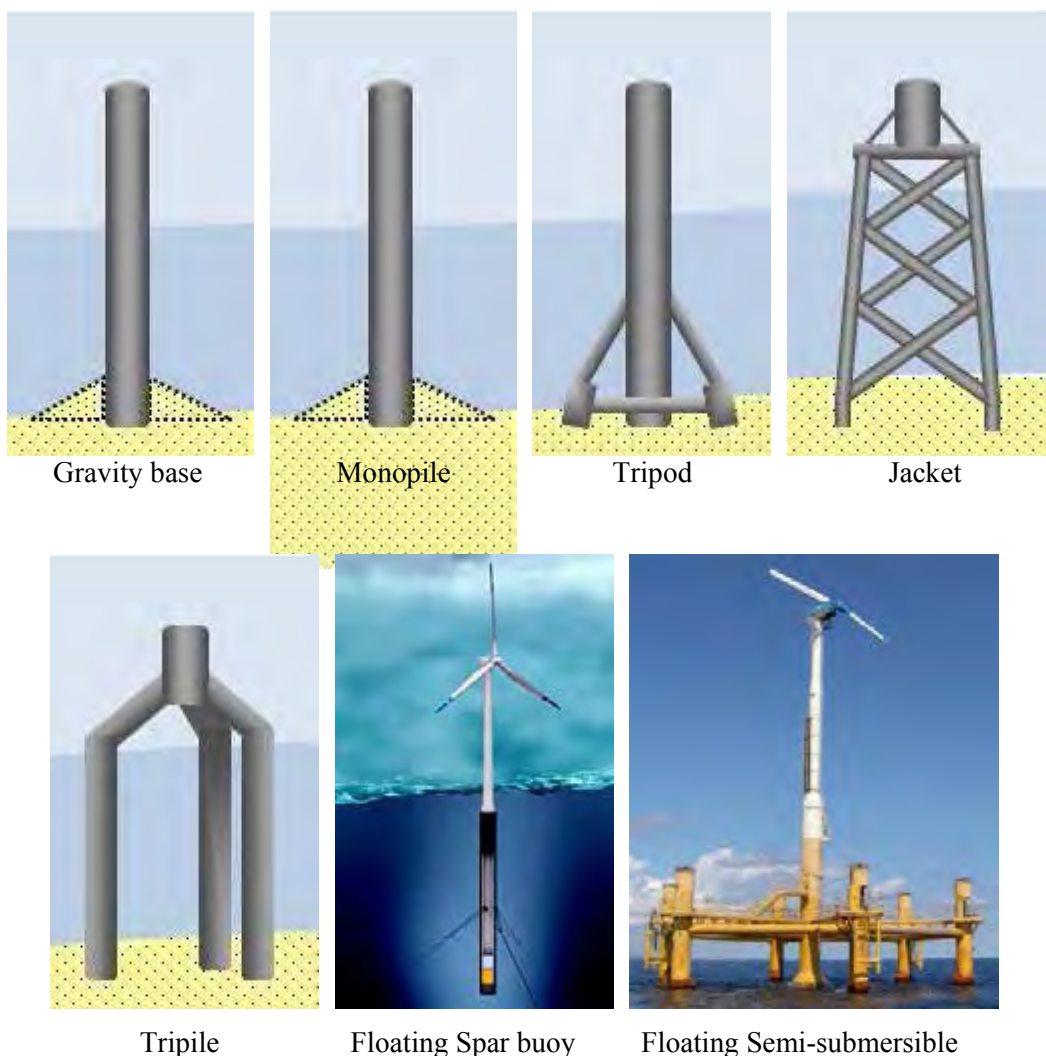


Figure 1: Available substructure concepts for offshore wind turbines (source: www.offshorewind.de and EWEA, 2009).

4. Applicable foundation depending on water depth

Required performance of the foundation is depending on the wind turbine power (vertical loads, horizontal loads, max. deflection, dynamic constraints) as the seabed depth.

Following the indications from the Table 1 the identification of the type of foundation versus water depth are:

- Shallow water: monopole (Figure 1);
- Intermediate water: jackets or tripod (Figure 1);
- High water: floating structure (Figure 1).

The range of water depths where the monopile and jackets can be compared is between 25 and 30 m.

This paper presents the comparison between monopile and jacket in 30 m water depth. The installation site is supposed to be in Southern Adriatic Sea, where the seabed is made of soft sand on the top, with layers of silt and clay. The considered site environmental and soil condition have been derived by the data relevant to a number of gas production platforms installed in the vicinity.

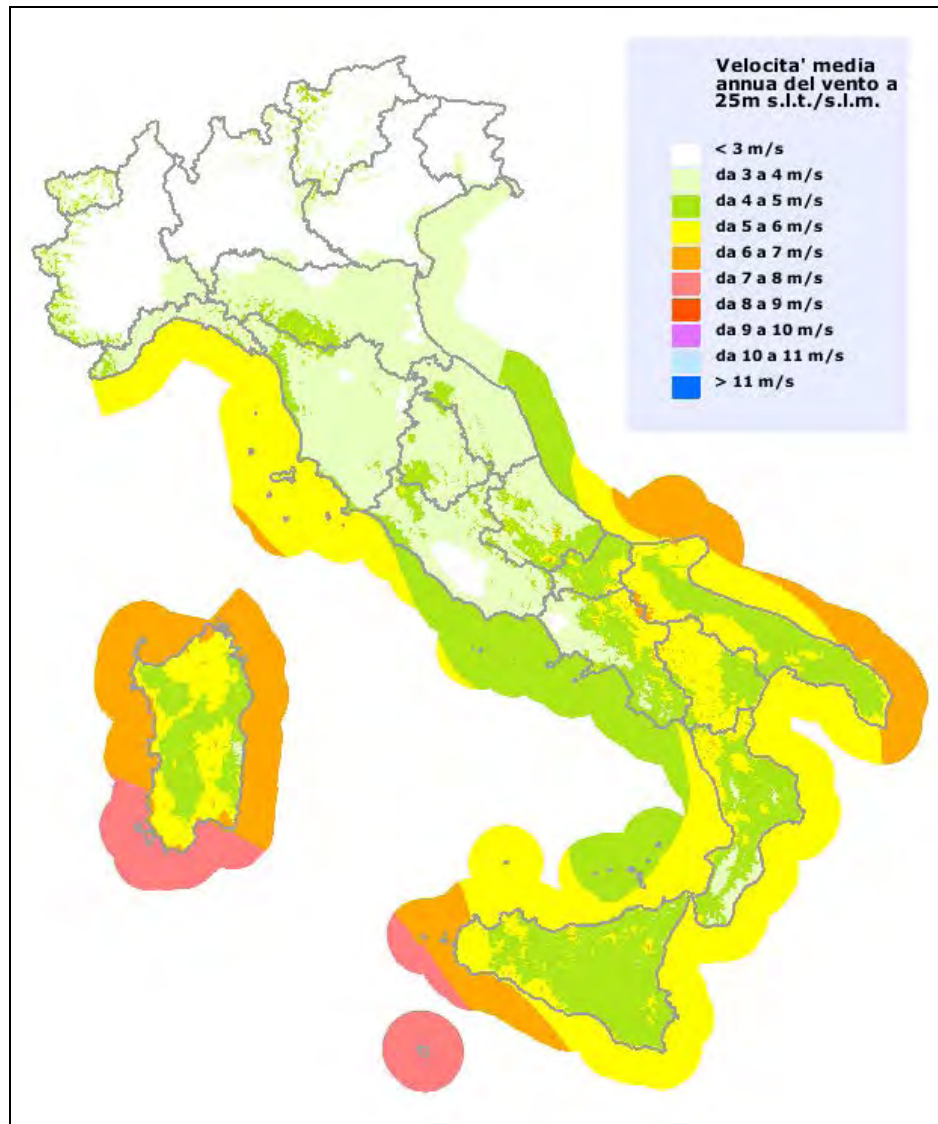


Figure 2: Italy wind map (Interactive wind atlas, CESI-Univ. di GE).



Figure 3: Turbine monopile substructure in english windfarms: Arklow Bank (a) and Burbo Bank (b).

The wave and current data are below reported:

- *Operating condition:*

Wave height = 10.3 m

Wave Period = 9.7 sec.

current profiles through water depth for 1-year return period:

Elevation from midline = 0.0 m

Current speed = 0.86 m/s

Elevation from midline = surface

Current speed = 0.41 m/s

- *Storm condition:*

Wave height = 10.3 m

Wave Period = 9.7 sec.

current profiles through water depth for 100-years return period:

Elevation from midline = 0.0 m

Current speed = 0.81 m/s

Elevation from midline = surface

Current speed = 0.51 m/s

Considering these data for sea conditions we try to compare the structural behaviour of monopile with that of jacket.

5. Loading conditions

The loads are determined by wind pressure on all the aerial components (nacelle, tower and the part of substructure over the sea level) and wave loads under it. All of them are obviously cyclic in nature. The worst loading case is usually when the turbine is operating in moderate winds while the sea is in an extreme state.

The combination of extreme sea and wind states is generally not critical, as the blades are fluttered during extreme winds to reduce the blade load and therefore the probability of blade damage.

Generally speaking the foundation substructure is subjected to a certain state due to maximum vertical load, V , which depends by the turbine power. The maximum horizontal load, H , and applied overturning moment, M , on the foundation would be substantial compared with the vertical load. For a 5/6 MW turbine, the applied loading situation could be described as follows $H \sim 4$ MN (at the maximum) and $M \sim 80/120$ MN m (or equivalent to the horizontal load being often applied 30 m above the base). In the case of a 3 MW the respective loads could be of the order of 1.200 kN for horizontal actions and 3.500 kN for vertical direction and 52.000 kNm for bending moment. The foundation must be designed to resist these loads adequately.

Typically, the maximum operational wind load would be approximately 1 MN or something more, as previously noted. This would be applied at the hub (say 90/100 m above the sea floor) and would be relatively constant over a long time period. The current and wave loads might be *ca.* 1 MN. These are applied at a much lower level, depending on the depth of water (say 10 m) and cycle at periods of *ca.* 10 s, considerably faster than the wind loads. This combination of loads translates to a resultant horizontal load of 2 MN with a resultant moment of 100 MN m. This is an unusual loading case as the ratio of moment to horizontal load is fluctuating rapidly with time, rather than remaining constant as would be more typical in offshore design. Furthermore, the wave direction may not be coincident with the prevailing wind direction. Therefore, the loads (moment and horizontal) acting on the foundation may not be coincident. Note that the wind force contributes *ca.* 25% of the horizontal load but *ca.* 75% of the overturning moment, because it is applied at such a high level.

6. Monopile substructure

The monopile is a large diameter steel pile with open end embedded in the sea bed (Figure 4). This is the simplest structure that can be used for supporting the wind turbine and is therefore the preferred one in shallow water.

For increasing water depths the performance of the monopile significantly decreases also because the required pile size is more dictated by dynamic consideration than by strength requirement. The largest installed monopiles reach up to 6 m diameter and 150 mm wall thickness

The monopiles have been extensively adopted in water depth up to 20-25 m. More than 70% of the world's offshore wind turbines are supported by monopoles (as explained in Table 1). For higher water depths the need of avoiding too high natural period requires heavy and large piles making this substructure configuration less attractive.

Depending on soil condition, monopiles can be installed by driving with conventional hammers or with vibratory hammers, or, in case of rock, lowered in a predrilled hole and grouted.

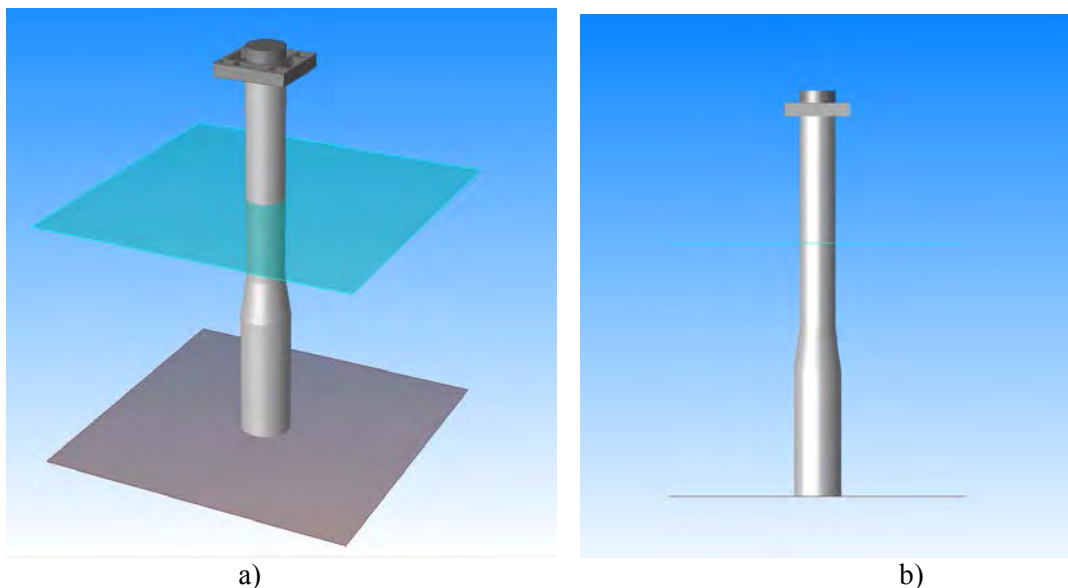


Figure 4: Scheme of the monopile in the overall representation (a) and its upperst member (b).

To actually support the wind turbine column it is necessary installing on top of the monopile a transition piece (Figure 5). The transition piece includes a suitable working platform and can be adjusted in order to recover the out of level of the monopile head.

The characteristics and the performance of a monopile supporting a 3 MW turbine in 30 m water depth are briefly summarized below.

Monopile characteristics

- Lower section diameter x wall thickness [mm]: 6000 x 80
- Upper section diameter x wall thickness [mm]: 4500 x 80
- Estimated weight [ton]: 500
- Overall wave and current load (see Table 3).



Figure 5: Transition piece in a functional representation (a) and during installation (b).

OWEMES 2012

Table 3: Wind and wave actions.

LOAD CASE CENTER REPORT *****

LOAD CASE	LOAD LABEL	RELATIVE TO STRUCTURAL ORIGIN											
		***** X - DIRECTION *****				***** Y - DIRECTION *****				***** Z - DIRECTION *****			
		FORCE (KN)	X (M)	Y (M)	Z (M)	FORCE (KN)	X (M)	Y (M)	Z (M)	FORCE (KN)	X (M)	Y (M)	Z (M)
9	WINX	53.41	0.00	0.00	15.48	COUPLE	0.00	0.00	0.05	0.00			
10	WINY	COUPLE	0.00	0.00	0.02	53.41	0.00	0.00	15.48	0.00			
11	WOPA	1895.02	0.00	0.00	-9.09	0.00				2403.58	0.00	0.00	-29.61
12	WOPB	1339.98	0.00	0.00	-9.09	1339.98	0.00	0.00	-9.09	2403.58	0.00	0.00	-29.61
13	WOPC	0.00				1895.02	0.00	0.00	-9.09	2403.58	0.00	0.00	-29.61
14	WSTA	2560.22	0.00	0.00	-8.09	0.00				2745.01	0.00	0.00	-25.09
15	WSTB	1810.35	0.00	0.00	-8.09	1810.35	0.00	0.00	-8.09	2745.01	0.00	0.00	-25.09
16	WSTC	0.00				2560.22	0.00	0.00	-8.09	2745.01	0.00	0.00	-25.09
17	OPJA	2748.43	0.00	0.00	-0.73	250.00	0.00	0.00	18.00	-596.42	0.00	0.00	209.88
18	OPJB	1766.59	0.00	0.00	-2.60	2120.09	0.00	0.00	0.84	-596.42	0.00	0.00	209.88
19	OPJC	-250.00	0.00	0.00	18.00	2748.43	0.00	0.00	-0.73	-596.42	0.00	0.00	209.88
20	STJA	3487.34	0.00	0.00	-1.24	250.00	0.00	0.00	18.00	-254.99	0.00	0.00	481.85
21	STJB	2288.93	0.00	0.00	-2.73	2642.43	0.00	0.00	0.04	-254.99	0.00	0.00	481.85
22	STJC	-250.00	0.00	0.00	18.00	3487.34	0.00	0.00	-1.24	-254.99	0.00	0.00	481.85

- natural vibration mode:

MODE	FREQ. (CPS)	GEN. MASS	EIGENVALUE	PERIOD (SECS)
------	-------------	-----------	------------	---------------

Table 4: Displacements and rotations at interface with wind turbine column.

JOINT NUMBER	LOAD CASE	SACS-IV SYSTEM			JOINT DEFLECTIONS AND ROTATIONS		
		***** CENTIMETERS *****	***** CENTIMETERS *****	***** CENTIMETERS *****	***** RADIANS *****	***** RADIANS *****	***** RADIANS *****
		DEFL (X)	DEFL (Y)	DEFL (Z)	ROT (X)	ROT (Y)	ROT (Z)
0000	OPJA	13.4579086	1.8402334	-0.0559689	-0.0005011	0.0035153	0.0017688
	OPJB	8.3486910	15.7133245	-0.0559689	-0.0047696	0.0021519	0.0017688
	OPJC	-1.8853749	20.5626049	-0.0559689	-0.0062724	-0.0005080	0.0017688
	STJA	16.7134418	1.8833305	-0.0507187	-0.0005077	0.0042176	0.0017688
	STJB	10.6542339	18.1470528	-0.0507187	-0.0052860	0.0026487	0.0017688
	STJC	1.9277980	23.9942646	-0.0507187	-0.0070010	-0.0005145	0.0017688

7. Jacket foundation

The jacket (Figures 6-7) is the typical type of structure used in the Oil industry for supporting the offshore drilling and production facilities. It is a very efficient structure since combines a high strength without attracting high wave and current loads due to its transparency.

The jacket concept is therefore adopted also for supporting wind turbines in water depths where the monopile results not suitable. The jacket can be made by three or four tubular legs and is secured to the soil by open end driven steel piles.



*Figure 6: Alpha Ventus German wind farm
(the last two lines consist of 6 Repower on braced substructure).*

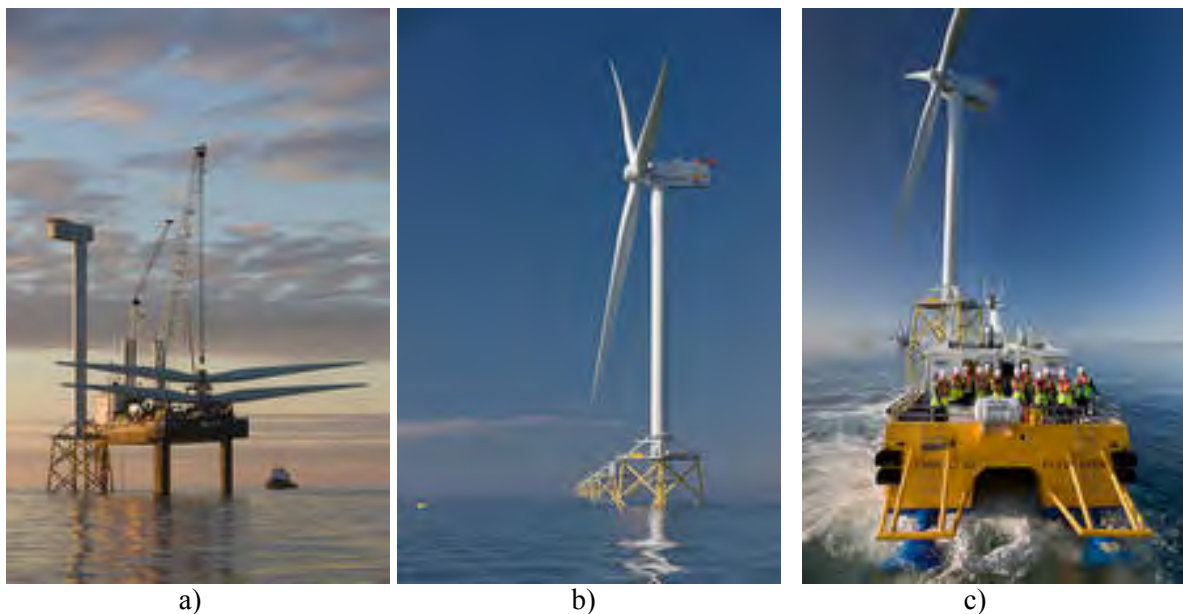


Figure 7: Installation of rotor (a), sequence of braced substructures (b) and during an inspection (c) at Ormonde wind farm

In the standard installation process the piles are driven through the jacket legs (main piles) or through suitable sleeves (skirt piles) and therefore are installed after the jacket. In offshore wind farm, where the structure to be installed are numerous up to hundreds, the post-piling technique is no more convenient. It is actually advisable (and this is what happens) pre-installing all the piles and provide the jacket with suitable pins protruding from jacket bottom frame. Once the piles are in position the jackets can be lowered and stabbed onto the piles. The connection between piles and jacket can be done by grouting or by alternative technique like swaging or other quick coupling technique.

The overall advantage of jacket concept is well suited to large site with varying conditions:

- accommodating to varying soil condition by different pile penetration to evaluate the
- insufficient resistance of subground soil;
- increased foot print around the foundation pile;
- little sensitivity to large wave;
- limited dynamic amplification of loads to high stiffness to be introduced in the structure;
- cover large variation in water depth by cantilevering pipes with use the same jacket; modifying geometry, base dimensions, etc.

The structural design allows deriving the best performance by

- simple geometry and standard members for easy production;
- little sensitivity to scour and sand wave;
- little sensitivity to fatigue by proper design of tubular joints and tower/jacket junction.

The characteristics and the performance of a jacket supporting a 3MW turbine in 30 m water depth are briefly summarized below.

- Bottom dimension [m]: 15.5 x 15.5
- Top elevation [m]: 4.3 x 4.3
- Estimated weight: 350 t
- Overall wave and current load (see Table 5):

Table 5: Wave and current load

***** SEASTATE LOAD CASE CENTER REPORT *****

RELATIVE TO STRUCTURAL ORIGIN

LOAD CASE	LOAD LABEL	***** X - DIRECTION *****				***** Y - DIRECTION *****				***** Z - DIRECTION *****			
		FORCE (KN)	X (M)	Y (M)	Z (M)	FORCE (KN)	X (M)	Y (M)	Z (M)	FORCE (KN)	X (M)	Y (M)	Z (M)
10	WINX	78.86	0.13	0.00	12.40	COUPLE	0.00	0.00	0.00	COUPLE	0.00	0.00	0.00
11	WINY	COUPLE	0.00	0.00	0.00	78.89	0.13	0.00	12.41	COUPLE	0.00	0.00	0.00
12	WOPA	2436.88	0.76	0.00	-6.76	COUPLE	0.00	0.00	0.00	-1520.45	-0.80	0.00	2.91
13	WOPB	1715.03	0.43	0.05	-6.84	1716.77	0.49	0.01	-6.82	-1437.82	-0.61	-0.66	3.35
14	WOPC	COUPLE	0.00	0.00	0.00	2471.14	0.47	0.00	-6.91	-1482.07	0.19	-0.96	3.26
15	WSTA	3704.61	0.61	0.00	-6.99	COUPLE	0.00	0.00	0.00	-1444.81	-1.36	0.00	2.63
16	WSTB	2568.12	0.50	0.17	-6.83	2569.10	0.58	0.10	-6.81	-1459.90	-0.78	-0.99	2.59
17	WSTC	COUPLE	0.00	0.00	0.00	3682.52	0.42	0.18	-7.01	-1487.03	0.26	-1.46	2.56
18	OPJA	3315.74	0.56	0.00	-0.33	249.95	0.00	-0.60	18.01	-4910.37	-0.25	0.01	9.96
19	OPJB	2159.63	0.35	0.04	-1.87	2514.90	0.34	0.01	0.94	-4827.76	-0.18	-0.19	10.21
20	OPJC	-249.98	0.34	-0.12	18.00	3350.03	0.35	0.00	-0.51	-4872.07	0.06	-0.28	10.12
21	STJA	4692.31	0.49	0.00	-1.95	249.95	0.00	-0.65	18.01	-4834.61	-0.41	0.01	9.99
22	STJB	3089.46	0.42	0.14	-2.88	3443.98	0.44	0.08	-0.73	-4849.75	-0.24	-0.29	9.95
23	STJC	-249.80	0.82	-0.15	18.01	4670.27	0.34	0.15	-1.95	-4877.02	0.08	-0.44	9.90

• natural vibration mode:

MODE	FREQ. (CPS)	GEN. MASS	EIGENVALUE	PERIOD (SECS)
------	-------------	-----------	------------	---------------

Table 6: Displacements at interface with wind turbine column.

		SACS-IV SYSTEM JOINT DEFLECTIONS AND ROTATIONS					
		***** CENTIMETERS *****			***** RADIANS *****		
JOINT NUMBER	LOAD CASE	DEFL (X)	DEFL (Y)	DEFL (Z)	ROT (X)	ROT (Y)	ROT (Z)
0000	OPJA	3.7953069	0.4741629	-0.4230556	-0.0001790	0.0022588	0.0005751
	OPJB	2.4803462	3.6397674	-0.4174730	-0.0072780	0.0015114	0.0006964
	OPJC	-0.4798325	4.6653228	-0.4320154	-0.0101138	-0.0001794	0.0007723
	STJA	5.2686253	0.4971353	-0.4303799	-0.0001815	0.0020937	0.0005867
	STJB	3.5766344	4.7162137	-0.4253824	-0.0072036	0.0014313	0.0007816
	STJC	-0.4980296	6.0989008	-0.4432429	-0.0099965	-0.0001794	0.0008925

8. Conclusive remarks on structural aspects

Due to both installation and maintenance costs, the installation of offshore wind farms in “deep waters” is not always economically acceptable. A specific area in the southern Adriatic Sea has been considered for the installation of a wind farm. The study has been concentrated on a complex system made by metallic foundation-wind turbine, but the monopile substructure doesn't offer a good solution for the problem of supporting turbine.

Comparing the data from Tables 4 and 6 the displacements of monopile are larger than those of jacket. Along the axis X the displacement for monopile is 3 times of that for jacket (16, 7 cm against 5.2 cm). For the axis Y the discrepancy is increased to 6 times approximately (23, 9 cm and 4.6 cm). Instead on the axis Z is the contrary, 0.055 cm for monopile and 0.44 cm for jacket. Similar response is evident for the regime of the rotations.

This means that the monopile is considerably more elastic than the jacket.

Another property has to be added to those already discussed before. A well-known and proven versatile offshore structure can be adapted to mass fabrication and installation in offshore wind:

- at deeper water, jacket foundations will be competitive;
- jacket foundations adapts well to large sites with different soil conditions and water depths;
- standardised production of jacket sections and transition piece is required;
- mass production of identical tubular joints for K-joint and X-joint connections;
- cost per kilo for the jacket is the key to success.

References

1. Eggen, A.O., Heggset, J., Gjerde, O., Valland, A. and Nona^os. Deep sea offshore windturbine technology. Operation and maintenance – state-of-the-art study. *Restricted report, SINTEF, Trondheim L.M. 2008.*
2. European Wind Energy Technology Platform - TPWind Strategic Research Agenda - Market Deployment Strategy from 2008 to 2030. *2008*
3. Gerdes, G, Tiedemannm A and Zeelenberg, S. Case Study: European Offshore Wind Farms - A Survey for the Analysis of the Experiences and Lessons Learnt by Developers of Offshore Wind Farms. *2006.*
4. Sharples, M and Sharples, B.J.M. Damage and Critical Analysis of Accidents to Assist in Avoiding Accidents on Offshore Wind Farms on the OCS. *Report prepared for Minerals Management Service, Department of the Interior, US. Project No. 633, Contract M09PC00015. 2010.*
5. Vattenfall. Horns Rev Offshore Wind Farm Annual Status Report for the Environmental Monitoring Programme. *2005.*

Session 4: Turbines Dynamics, Access, Challenges

Chairmen: A. Henderson, G. Dalen

Impact of weather conditions on the windows of opportunity for operation of offshore wind farms in Portugal - N. Silva, T. Simões, P. Costa, A. Estanqueiro (NLEG National Laboratory of Energy and Geology - Solar, Wind and Ocean Energy Unit, Lisboa (PT))

Offshore challenges & Siemens solutions: learning from experience – A.H. Woltmeijer (Siemens Energy Inc., Vejle (DK))

Effects of fully nonlinear irregular wave forcing on the dynamic response of offshore wind turbine - E. Marino, C. Borri (CRIACIV, Dept. Of Civil and Environmental Engineering, Florence Univ. (IT)), C. Lugni (CNR-INSEAN, Rome (IT))

Impact of weather conditions on the windows of opportunity for operation of offshore wind farms in Portugal

N. Silva^{1a}, T. Simões^{1b}, P. Costa^{1c} and A. Estanqueiro^{1d}

¹*Solar, Wind and Ocean Energy Unit - National Laboratory of Energy and Geology, Estrada do Paço do Lumiar, 22 1649-038 Lisboa (Portugal)*

1a) narsilva@gmail.com, 1b) teresa.simoed@lneg.pt, 1c) paulo.costa@lneg.pt, 1d) ana.estanqueiro@lneg.pt

Abstract – Several obstacles and challenges are present in the construction and development of offshore wind farms. Two important issues of concern are the atmospheric and oceanic conditions that difficult the access to those wind parks. A window of opportunity is a timeframe when weather and sea conditions are acceptable for certain work task in the development, construction and operation/maintenance of the offshore wind park. This study identifies typical time-size periods of windows of opportunity to access three offshore Portuguese maritime regions. The accessibility conditions also take into account the system type transportation method for local access, namely, rubber boat, boat with OAS or helicopter.

1. Introduction

In recent years there has been a growing awareness and environmental education in society. In fact, the concerns regarding the environment, particularly climate change have been very present in people lives. The most relevant evidence was the Kyoto Protocol (1997) or more recently the Copenhagen Summit (2009) on which were appointed and settled political/economic issues for the environmental benefit of the European Union. The evidence that endogenous production of energy (renewable) reduces the external dependence of imported fuels has significantly grown in society, particularly during the most recent years when the wind energy production has featured an expressive increase [1].

Currently, one of the most promising wind development areas in Portugal are the offshore wind parks [2]. However, there are several obstacles and challenges for the deployment of these wind farms. The “expertise” transition from land to the marine environment will need to deal with a harsher environment for operations, higher costs and also with the accessing impact for visiting the wind farm according to the weather and oceanic patterns.

The construction and maintenance operations should only be conducted in safe weather conditions: dependent on the wind speed, sea swell and visibility [3]. This dependence should not be neglected since a low profitability of the wind farm can occur when the strategy to manage the wind farm for repairing or installing materials is not appropriate.

The availability of a wind farm, defined as the percentage of time when there are technical conditions for the production of electricity, is a function of the accessibility to the wind park [4]. Figure 1 shows the relation between the availability of the wind park and its accessibility conditions. An increase of the distance to shore implies a decrease of the availability due to lower accessibility conditions to the wind farm [5].

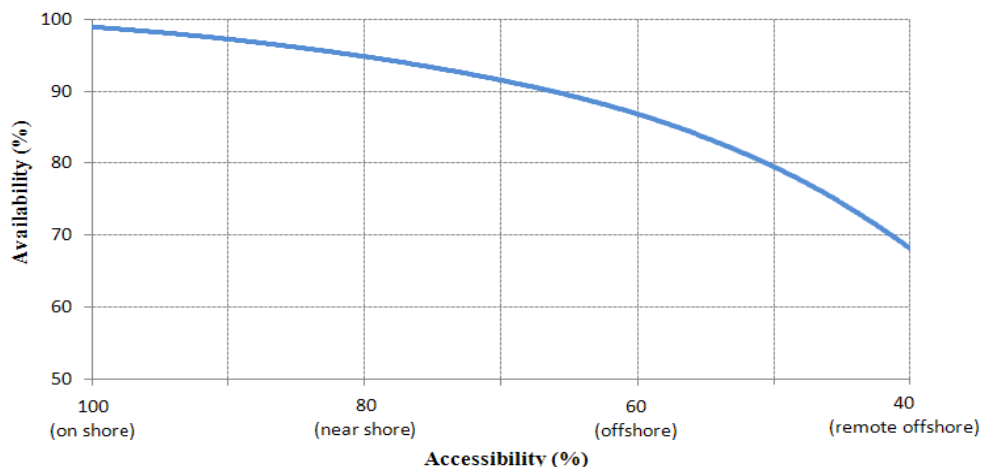


Figure 1: Graphical representation of the availability of a wind farm as a function of the accessibility by boat (adapted from [5]).

2. Methodology

2.1. Data

Three cases studies for Continental Portugal were chosen to illustrate the developed methodology. Figure 2 depicts each of the three sites and Table 1 their respective coordinates.



Figure 2: Graphical representation of the three case studies around the western coastal regions of Continental Portugal.

Table 1: Site locations for the cases studies.

Site	Distance to the coast (km)	Depth (m)	Polar Coordinates	
			Longitude	Latitude
1	2	30	-8.9°	41.8°
2	9	38	-8.8°	41.2°
3	5	38	-9.4°	39.2°

The oceanic and atmospheric data used in this study was generated and supplied by the Danish company ConWxApS. This company is dedicated to the prediction of weather and sea conditions using numerical models (IRIE and WaveWatch III v.3.14) [6]. Simulated hourly data was provided for the three sites (table 1), covering an almost uninterrupted period of 10 years, ranging from 03 January 2000 to 31 December 2009. The wave data covers the period between 03 January 2000 and 03 January 2009. The simulated parameters available were:

- Significant wave height
- Waves period
- Waves direction
- Wind speed at 10 meters
- Wind speed at 100 meters
- Wind direction

The simulated wind data was compared with the Offshore Wind Atlas developed by LNEG [7] while the wave data was compared with the Portuguese Wave Atlas– *ONDATLAS* [8]. On both cases there's an underestimation of the data provided by the ConWxApS company. Table 2 and 3 show the correction factors used on both cases.

Table 2: Average wind speeds obtained with both models and the correction factor.

Site	Wind speed at 100 meters (m/s)		
	IRIE Model	Offshore Wind Atlas	Correction Factor
1	5.73	7.68	1.34
2	6.43	7.39	1.15
3	6.51	7.53	1.16

Table 3: Significant wave height obtained with both models and the correction factor.

Site	Significant wave height (m)		
	WaveWatch III	ONDATLAS	Correction Factors
1	1.16	2.01	1.73
2	1.24	2.00	1.61
3	1.35	2.13	1.58

Statistical methods are commonly presented in literature as the best tools for analyzing the behavior of wind and waves via their probabilistic behavior, using a probability distribution function. The best distribution function to describe wind speed [9] and significant wave height [10] is the Weibull distribution. The distribution of windows of opportunity can also be represented by a Weibull distribution [11]. Equation (1) shows the Weibull distribution function and equation (2) its cumulative form

$$f(x) = \begin{cases} \frac{k}{A} \left(\frac{x}{A}\right)^{k-1} \cdot \exp\left[-\left(\frac{x}{A}\right)^k\right], x \geq 0 \\ 0, x < 0 \end{cases} \tag{1}$$

$$F(x) = 1 - \exp\left[-\left(\frac{x}{A}\right)^k\right] \tag{2}$$

The parameters A and k on equations (1) and (2) represent, respectively, the scale factor (same unit than variable x) and the shape factor (non-dimensionless).

An exceedance probability $P(x)$ can also be obtained or the length of the windows of opportunity by applying the following equation:

$$P(x) = 1 - F(x) \tag{3}$$

2.2 Windows of opportunity determination

As mentioned above due to adverse weather conditions an offshore wind farm may be inaccessible during a certain period of time or even if the accessibility is guaranteed its length may not allow performing specific tasks. However the accessibility in the wind park does not only depend on the weather and sea conditions, but also on the type of access system [12].

Typically the access to wind turbines in an offshore wind farm can be accomplished through a simple rubber boat. Although, sometimes the use of a helicopter or boats prepared with offshore access system (OAS) is necessary. The access system types are also dependent on meteorological and oceanic conditions which are presented in Table 4 [13].

Table 4: Limit values for visiting offshore wind farms by access system type.

Access system	Maximum significant wave height (m)	Maximum wind speed (m/s)
Rubber boat	1.5	10.0
Boat with OAS	2.5	12.0
Helicopter	-	20.0

It is also important to mention that the main activities concerned with the construction/maintenance/operating of the wind parks have a security criteria based on wind speed. Table 5 shows the maximum wind speeds allowed for the most frequent work tasks performed in offshore wind farms [11, 14].

Table 5: Limit values for task performance.

Maximum wind speed (m/s)	Task
5.0	Climbing met masts
7.0	Inspection of the tower and blades
12.0	Climbing to the rotor
17.0	Working inside the nacelle

In this work, the determination of the windows of opportunity starts by defining a maximum wind speed V_{max} and a maximum significant wave height $H_{s,max}$ according to the values presented in tables IV and V. If the wind speed and the significant wave height at a certain time are below V_{max} and $H_{s,max}$ then there is a window of opportunity. Otherwise, the weather conditions are adverse, not allowing the access to the offshore area. If the length of the window of opportunity ($T_{window\ of\ opportunity}$) is lower than the time required to perform a task (T_{need}) then the task cannot be performed. In fact, the task shall only be performed when $T_{window\ of\ opportunity}$ is greater or equal than T_{need} . Figure 3 depicts on a diagram the processes related to the determination of an adequate window of opportunity for a specific task (table 5).

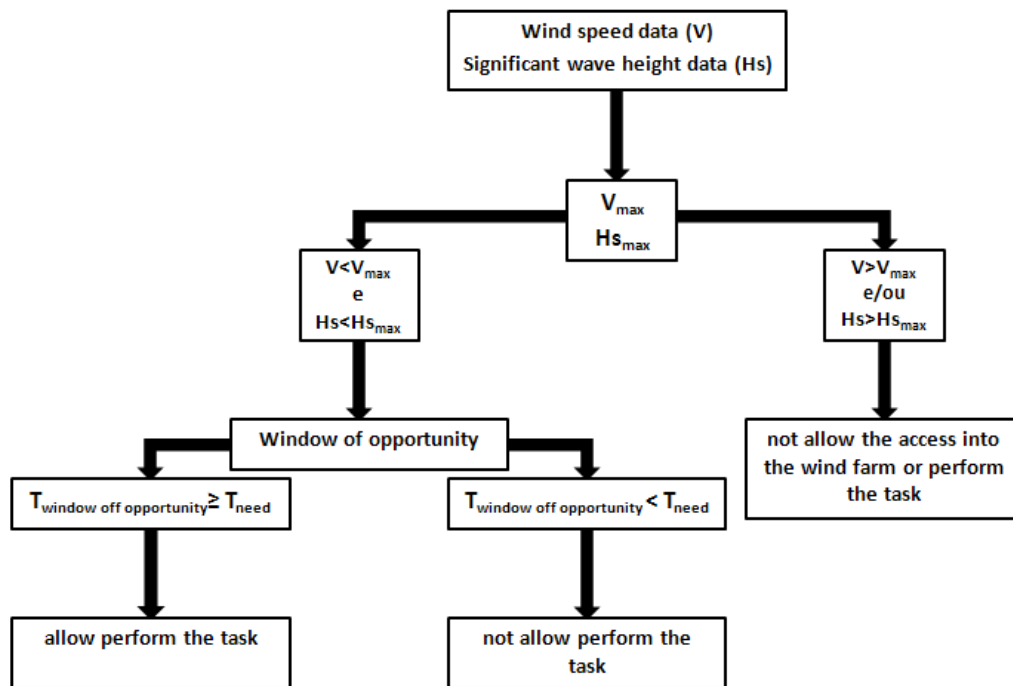


Figure 3: Flow diagram to inspect a window of opportunity.

For the Portuguese coastal areas, and taking into account the wind and ocean variability in these areas, the maximum values V_{max} and $H_{s,max}$ for each of the three regions under analysis can be taken as $V_{max}=12\text{m/s}$ and $H_{s,max}=2.5\text{m}$ for any season.

A simulation scenario is displayed in Figure 4, considering all July months from the 10 year data period and transportation access by boat with OAS capacity. It shows the climatological wind of opportunity for July where the abscissa represents hours from 00h UTC day 1. The green line corresponds to the typical period of window of opportunity and the red one the waiting time (periods where the weather or sea conditions don't allow the access to the offshore wind farm).

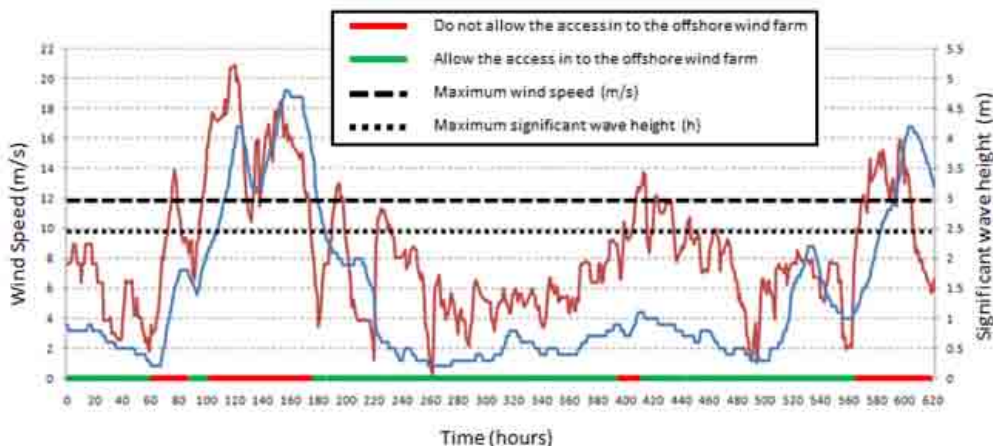


Figure 4: Mean representation of windows of opportunity for the month of July (10 years of simulated data). The three study areas are considered.

3. Results

For each of the three study sites, a climatological scenario was produced for the average spring, summer, autumn and winter seasons. Since, in Portugal, the Windfloat prototype – a newer offshore technology for fluctuating turbines is now installed around site nr. 2 for test site performance, the results hereafter will only be summarized for this site.

The graph presented in figure 5 shows the average accessibility (%) for site 2 throughout the period under analysis by access system type.

In table 6 the representative statistics are included.

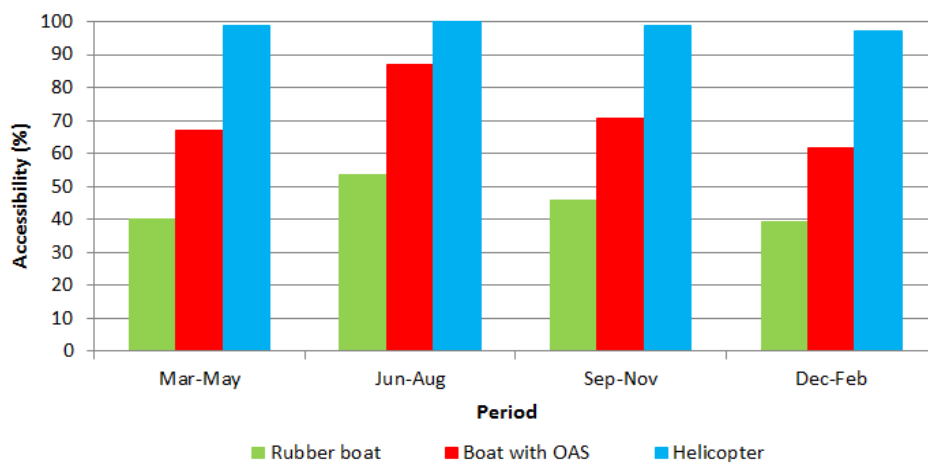


Figure 5: Average Accessibility throughout the analyzed period by method of access (Site 2).

Table 6: Statistics of the windows of opportunity (Site 2).

Access system		Length of the windows of opportunity	
		Hours	Days
Rubber boat	Average	49	2
	Maximum	513	21
	Minimum	1	0
Boat with OAS	Average	97	4
	Maximum	1047	44
	Minimum	1	0
Helicopter	Average	467	19
	Maximum	4579	190
	Minimum	1	0

The cumulative probability density function and the exceedance probability for the length of the windows of opportunity are depicted in figures 6 to 8 according to each access system type.

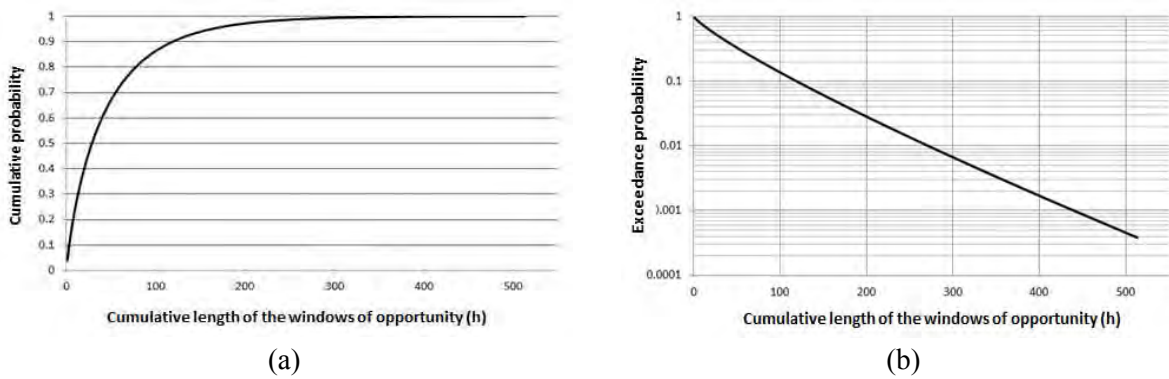


Figure 6: Graphs of (a) Cumulative probability and (b) Exceedance probability of the length of the windows of opportunity using a rubber boat as an access system type (Site 2).

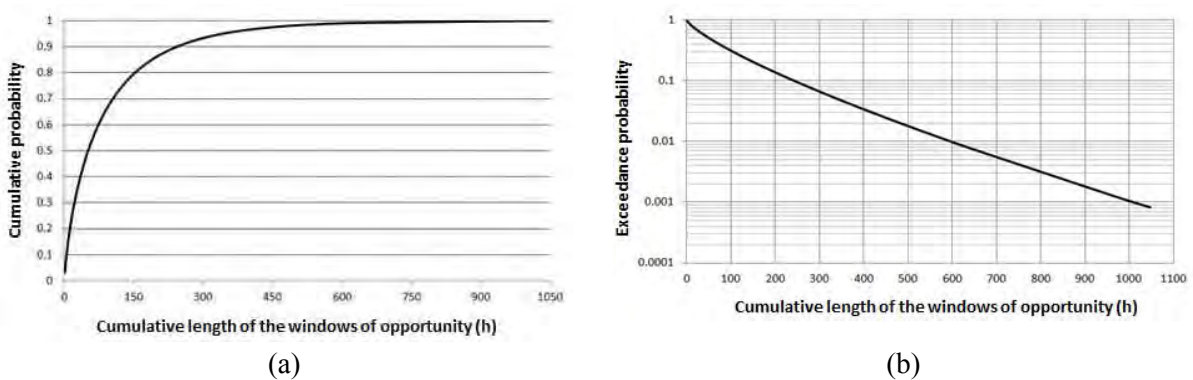


Figure 7: Graphs of (a) Cumulative probability and (b) Exceedance probability of the length of the windows of opportunity using a boat with OAS as an access system type (Site 2).

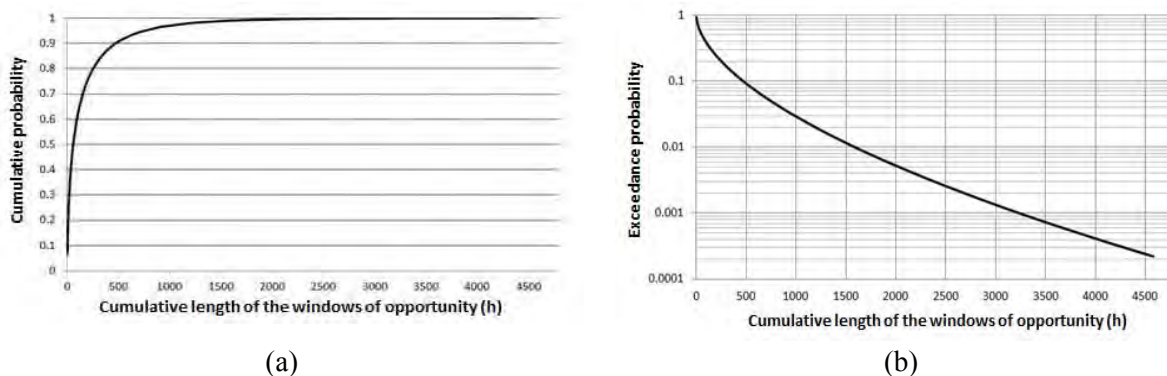


Figure 8: Graphs of (a) Cumulative probability and (b) Exceedance probability of the length of the windows of opportunity using a helicopter as an access system type (Site 2).

The following tables distinguish the performance probability of the most important the construction and maintenance tasks to perform in offshore wind farms.

Table 7: Performance probability of several tasks of construction and maintenance in offshore wind farms, for a rubber boat as the access system (Site 2).

Task	Condition		Height (m)	Perform. proba. of tasks (%)
	V_{max}	$H_{S_{max}}$		
Climbing met masts	5.0	1.5	10	29.4
			100	22.4
Tower and blade inspection	7.0		10	39.4
			100	33.5
Climbing to the rotor	12.0		10	45.2
			100	44.9
Working inside the nacelle	17.0		10	46.1
			100	45.4

Table 8: Performance probability of several tasks of construction and maintenance in offshore wind farms, for a boat with OAS as the access system (Site 2).

Task	Condition		Height (m)	Perform. proba. of tasks (%)
	V_{max}	$H_{S_{max}}$		
Climbing met masts	5.0	2.5	10	37.3
			100	28.4
Tower and blade inspection	7.0		10	53.2
			100	44.1
Climbing to the rotor	12.0		10	72.1
			100	69.1
Working inside the nacelle	17.0		10	75.6
			100	72.5

Table 9: Performance probability of several tasks of construction and maintenance in offshore wind farms, for a helicopter as access system (Site 2).

Task	Condition		Height (m)	Perform. proba. of tasks (%)
	V_{\max}	$H_{s_{\max}}$		
Climbing met masts	5.0	-	10	41.2
			100	31.3
Tower and blade inspection	7.0		10	60.8
			100	49.7
Climbing to the rotor	12.0		10	92.9
			100	84.6
Working inside the nacelle	17.0		10	98.3
			100	99.2

4. Conclusion

In the present study, a methodology to evaluate the length of the windows of opportunity for visiting offshore wind parks in Portugal was accessed. Three sites were studied. In this article, only the results from site ID 2 were analyzed due to the presence of the offshore Windfloat technology that was recently deployed near that site.

According to the simulated results, it was found that the most favorable periods for accessing the site is the summer period with an availability between 80-90% when using boats with OAS technology, while the lowest accessibility was found for the winter season with an average ~60% availability for the same boat technology.

When a helicopter is used, no seasonal variation is present and therefore the accessibility is close to 100% throughout the year. The length of the windows of opportunity, when comparing rubber boats with other access system types, increases in about 23 days for boats with OAS and in about 169 days for the helicopter case. As an example we can consider 100 hours as the necessary length of the opportunity to access the offshore wind park.

From graphics 6, 7 and 8 we conclude that the exceedance probability is 16% for a rubber boat, 31% for a boat with OAS and 39% for the helicopter as the access system.

The results obtained for site 2 are very promising for accessing the offshore WindFloat technology for site's maintenance, testing and resistance purposes. For other sites, namely, site ID 1 and site ID 3, the simulated results are very similar to the ones here illustrated although these haven't been described here.

Overall, Portugal appears to have promising conditions for offshore site maintenance strategies, with acceptable sizes of the windows of opportunity which is an important factor in favor of the offshore wind farm deployment on the western coastal regions.

References

1. EWEA, 2010.
http://ewea.org/fileadmin/ewea_documents/documents/statistics/EWEA_Annual_Statistics_2010.pdf, consultado em Fevereiro 2011.
2. Costa P., T. Simões, A. Estanqueiro, 2010 “Sustainable Offshore Wind Potential in Continental Portugal”. Workshop on Oceans as a Source of Energy, Sede da Ordem dos Engenheiros/Academia de Engenharia, Lisbon.
3. Bussel, G. J. W. e A. R. Henderson, 2001. State of the art and technology trends for offshore wind energy: operation and maintenance issues. European Wind Energy Conference (EWEC), Brussels.
4. Prins, R., 2001. Offshore access – the key to offshore wind farm efficiency. European Wind Energy Conference (EWEC), Brussels.
5. Bussel, G. J. W., 2002. Offshore wind energy, the reliability dilemma. International Conference, Berlin, pp. 2-6.
6. ConWx, 2010. Meteoceanhindcast system – Introduction to hindcast system, 15 pp.
7. Costa, P., P. Miranda e A. Estanqueiro, 2006. Development and validation of the portuguese wind atlas. European Wind Energy Conference (EWEC), Athens.
8. Wind Wave Atlas for Portugal - ONDATLAS, pp. 8-11, 37-40, 150-153. Produced by INETI, 2003
9. Yilmaz, V. and H. ErayÇelik, 2008. A statistical approach to estimate the wind speed distribution. DogusUniversitesi, 9(1),pp. 122-132.
<http://journal.dogus.edu.tr/13026739/2008/cilt9/sayi1/M00195.pdf>, available at June 2010.
10. Holthuijsen, L. H., 2007. Waves in oceanic and coastal waters. Cambridge. Cambridge University Press, 405 pp.
11. Rademakers, L. W. M. M. e H. Braam, 2002. O&M aspects of the 500 MW offshore wind farm at NL7. DOWEC Project, n° 10080, rev 2.
http://www.ecn.nl/fileadmin/ecn/units/wind/docs/dowec/10080_002.pdf, available at August 2010.
12. Prins, R., 2001. Offshore access – the key to offshore wind farm efficiency. European Wind Energy Conference (EWEC), Brussels.
13. Bussel, G. J. W e W. A. A. M. Bierbooms, 2003. Analysis of different means of transport in the operation and maintenance strategy for the reference DOWEC offshore wind farm. Wind Engineering, v. 27, n° 5, pp. 381-392.
14. McMillan, D. e Graham Ault. 2007. Towards qualification of condition monitoring benefit for wind turbine generators. Wind Engineering v. 31, n° 4, pp. 267-285.

Offshore challenges & Siemens solutions: learning from experience

A.H. Woltmeijer

Siemens Energy Inc., Vejle (DK)



Offshore Challenges & Siemens Solutions

- Learning from experience

Content

-  **Siemens Wind Power Offshore**
-  **Offshore Challenges**

Siemens Wind Power offshore facts

More than 20 years of experience

Installed base: > 800 turbines with > 2.4 GW capacity

Sold more than 2000 WTGs (6.8 GW)

No. 1 in offshore wind power ¹.

Our turbines from the first offshore wind power plant are still up and running

Unsurpassed reliability and performance: A proven 20+ year product lifetime and 95% real availability

1. Megawatts commissioned, EWEA, January, 2012

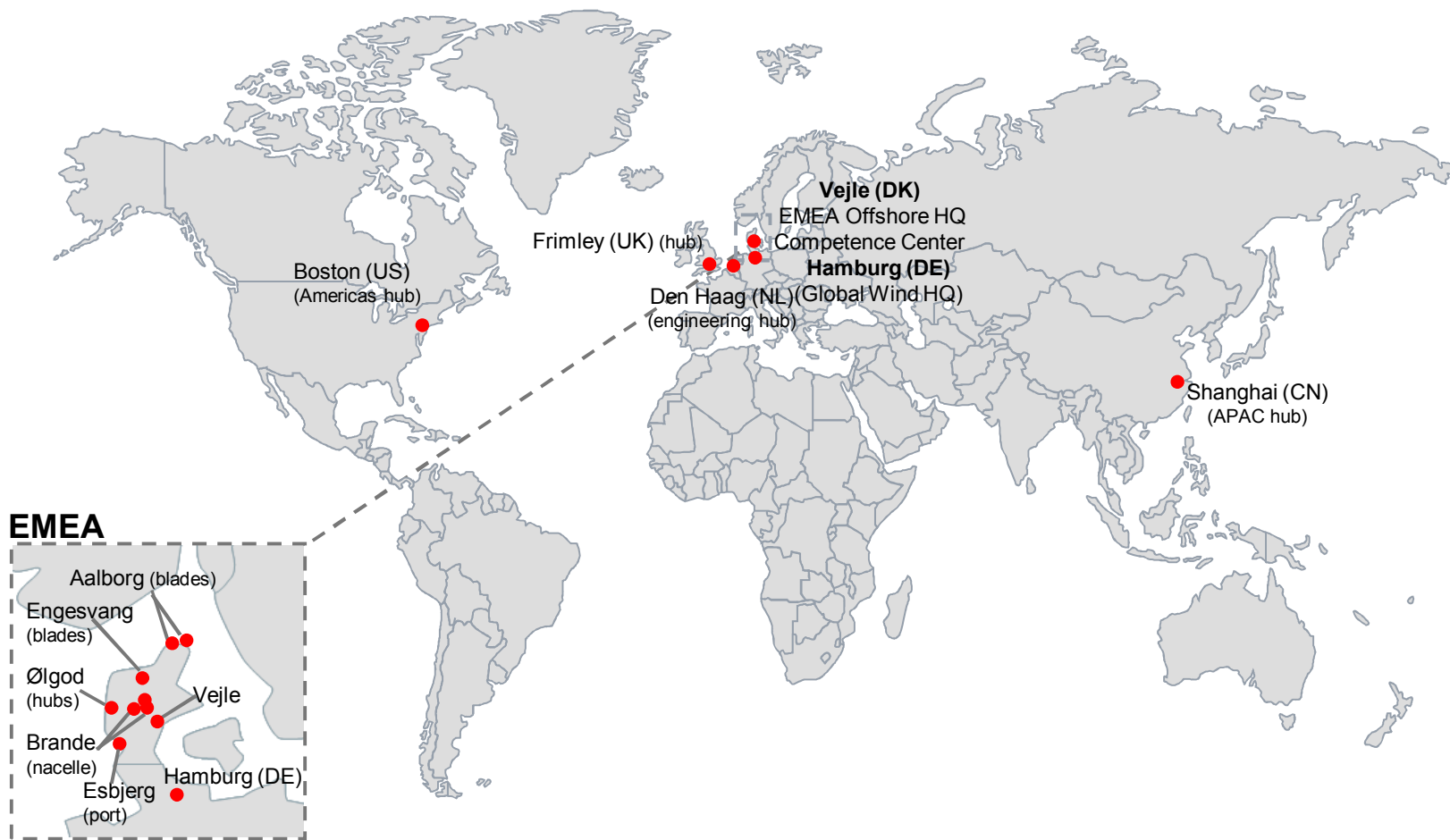
20 years of experience in offshore

<p>World's 1st offshore wind power plant 1991</p>  <p>Vindeby 5 MW</p>	<p>World's 1st offshore wind power plant w/ MW turbines 2000</p>  <p>Middelgrunden 40 MW</p>	<p>World's largest offshore wind power plant in operation 2003</p>  <p>Nysted 166 MW</p>	<p>World's largest offshore wind power plant in installation 2009-10</p>  <p>Greater Gabbard 504 MW</p>	<p>World's largest wind power market entered in China 2011</p>  <p>Rudong Intertidal Huge potential</p>	<p>World's largest offshore wind power plant ever contracted 2012</p>  <p>London Array 630 MW</p>
---	--	---	---	--	--

Our performance

- Leading market share and number one in offshore ¹
- Industrialized offshore wind power (from 5 MW to 630 MW wind power plants)
- Market entry into the Asia Pacific region

Offshore presence worldwide



Market leader in offshore with > 2.4 GW installed*

Burbo Banks, UK
→ 25 x SWT-3.6-107 (2007)

Lynn / Inner Dowsing, UK
→ 54 x SWT-3.6-107 (2008)

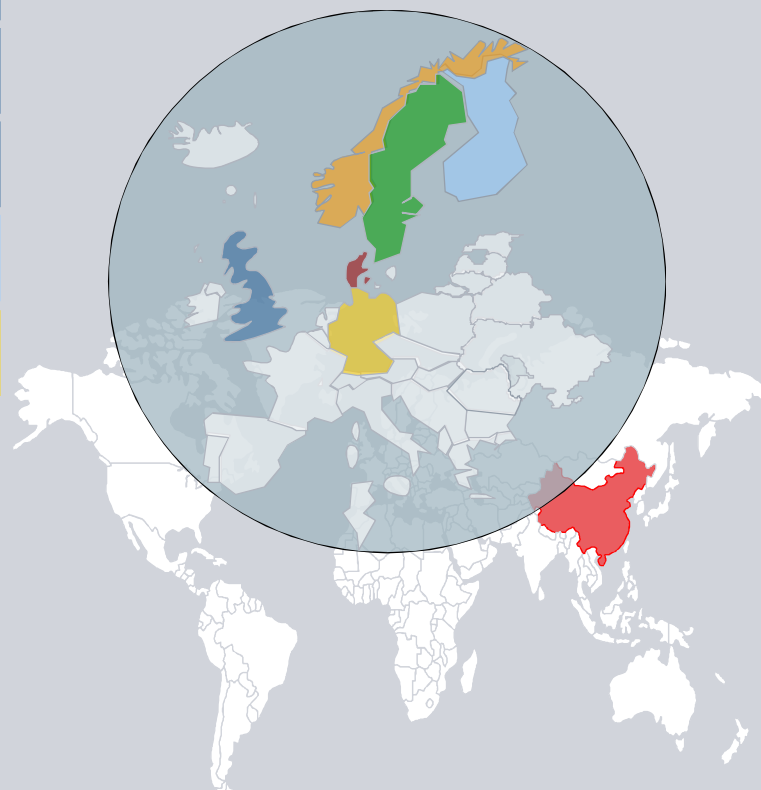
Gunfleet Sands, UK
→ 48 x SWT-3.6-107 (2009)

Rhyl Flats, UK
→ 25 x SWT-3.6-107 (2009)

Pori, FIN
→ 1 x SWT-2.3-101 (2010)

EnBW Baltic I, DE
→ 21 x SWT-2.3-93 (2010)

Rudong Intertidal, CHN
→ 21 x SWT-2.3-101



Vindeby, DK
→ 11 x 0.45 MW (1991)

Middelgrunden, DK
→ 20 x SWT-2.0-76 (2000)

Samsø, DK
→ 10 x SWT-2.3-82 (2002)

Rønland, DK
→ 4 x SWT-2.3-93 (2002)

Rødsand/Nysted, DK
→ 72 x SWT-2.3-82 (2003)

Frederikshavn, DK
→ 1 x SWT-2.3-82 (2003)

Horns Rev II, DK
→ 91 x SWT-2.3-93 (2009)

Rødsand II, DK
→ 90 x SWT-2.3-93 (2010)

Lillgrund, SE
→ 48 x SWT-2.3-93 (2007)

Hywind, NO
→ 1 x SWT-2.3-82 (2009)

*commissioned

Many projects under installation and to come...

Greater Gabbard, UK

→ 140 x SWT-3.6-107

Sheringham Shoal, UK

→ 88 x SWT-3.6-107

London Array, UK

→ 175 SWT-3.6-120

Walney, UK

→ 51 x SWT-3.6-107

→ 51 x SWT-3.6-120

Lincs, UK

→ 75 x SWT-3.6-120

Gwynt Y Mor, UK

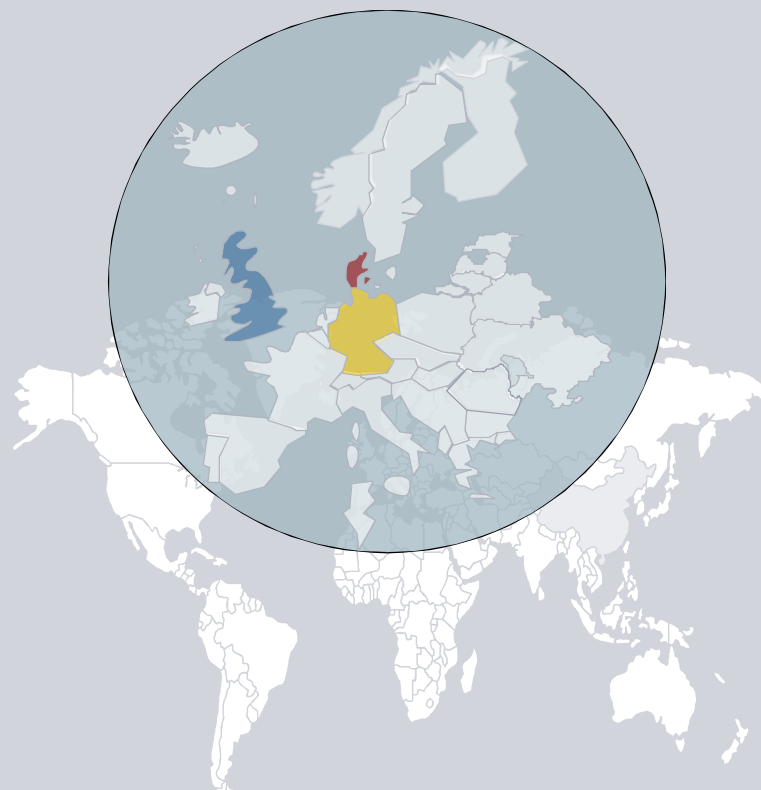
→ 160 x SWT-3.6-107

West of Duddon Sands, UK

→ 108 x SWT-3.6-120

Teesside, UK

→ 27 x SWT-2.3-93



Anholt, DK

→ 111 x SWT-3.6-120

EnBW Baltic 2, DE

→ 80 x SWT-3.6-120

Borkum Riffgat, DE

→ 30 x SWT-3.6-107

DanTysk, DE

→ 80 x SWT-3.6-120

Borkum Riffgrund 1+2, DE

→ 178 x SWT-3.6-120

Meerwind Süd Ost, DE

→ 80 x SWT-3.6-120

Amrumbank West, DE

→ 80 x SWT-3.6-120

The SWT-3.6-107 wind turbine is an experienced offshore workhorse for rough site conditions

Technical data



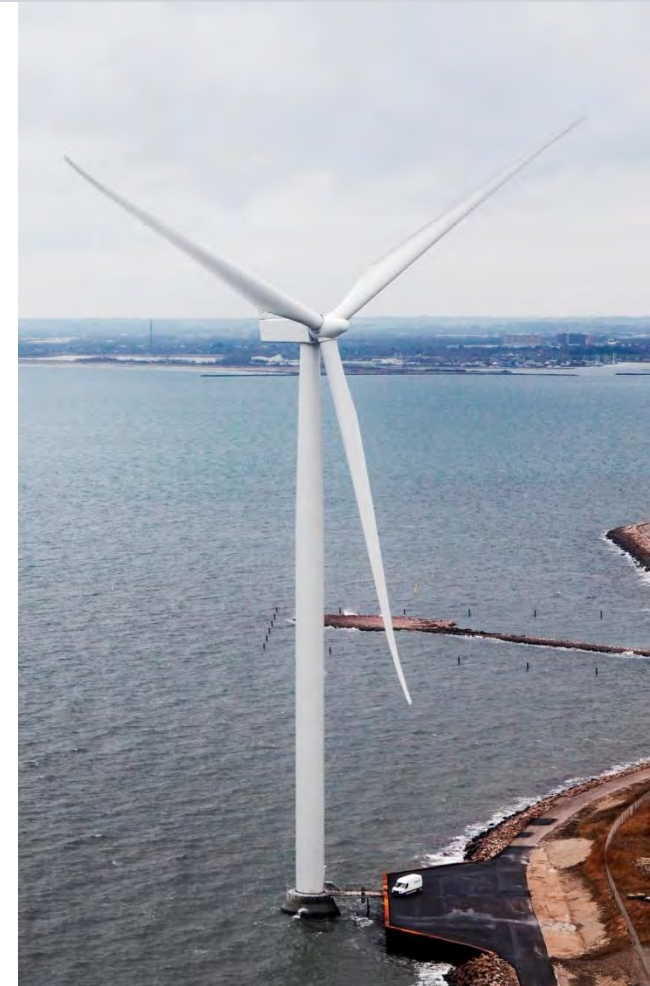
IEC Class:	IA
Rotor diameter:	107 m
Blade length:	52 m
Swept area:	9,000 m ²
Hub height:	site specific
Power regulation:	pitch regulated, VS
Annual output at 8.5 m/s:	14.2 GWh ¹⁾
Blade weight:	15.9 tons
Rotor weight:	92.5 t
Nacelle weight:	136 t
Tower weight (IEC IA):	Site specific
Serial production:	2006
Units ordered for offshore:	621 ²⁾
Units installed offshore:	380 ²⁾

1. Power curve (revision 1) 2. June 2012

SWT-3.6-120: Swept area increased by 25.5% to 11,300 m², compared to SWT-3.6-107

Technical data

IEC Class:	IA
Rotor diameter:	120 m
Blade length:	58,5 m
Swept area:	11,300 m ²
Hub height:	Site specific
Annual output at 9 m/s	16,793 MWh
Rotor weight:	98 t
Nacelle weight:	142 t
Tower weight:	Site specific
Prototype installed:	2009
Serial production:	2010
First installed offshore:	2011
Units ordered for offshore:	1021 units ¹⁾
Units installed offshore:	54 units ¹⁾



Content

- ▶ Siemens Wind Power Offshore
- ▶ **Offshore Challenges**

Offshore wind is in a steep development phase

	1990s	2000s	Present	2020+
Countries with offshore wind	3	7	11	20+
Avg. wind farm / project size	6 MW	90 MW	~ 350 MW	>500 MW
Avg. yearly installed capacity	3 MW	230 MW	~ 3.000 MW	6.000 MW
Significant manufacturers	2	3	6-7	>8
Avg. turbine size	< 0.5 MW	3 MW	5 - 6 MW	>7 MW
Avg. rotor diameter	37 m	98 m	120-130 m	180-240 m
Avg. water depth	5 m	15 m	~ 30 m	Up to 200 m
Customers	Scandinavian utilities	European utilities	Utility and non-utility investors; European developers	Utility and non-utility investors; Large international consortia and developers

Offshore wind power projects: Now and tomorrow

2007

Lillgrund Wind Farm

- **48 wind turbines** (110MW)
- Water depths: **4-13 m**
- Distance to shore: **6-9 km**
- Avg. Wave height: **0.9 m**



2012

Sheringham Shoal Wind Farm

- **88 wind turbines** (316.8 MW)
- Water depths: **14-23 m**
- Distance to shore: **23 km**
- Avg. Wave height: **1.1 m**



2013

Dan Tysk Wind Farm

- **80 wind turbines** (288 MW)
- Water depths: **23-31 m**
- Distance to shore: **70 km**
- Avg. Wave height: **1.1 m**



Challenges in the offshore business

Optimize technology for larger projects, farther offshore



Optimize installation technology and secure vessels

**REDUCE
LCOE**

Industrialize logistics



Apply experience gained to new markets

Learning from the past to ensure future success



Experience

Optimized processes across the complete project life cycle make Siemens a stable, reliable, and trustworthy business partner



Reliability



Collaboration



Innovation



Service

Effects of fully nonlinear irregular wave forcing on the dynamic response of offshore wind turbine

E. Marino¹, C. Borri² and C. Lugni³

¹*CRIACIV c/o Dep. of Civil and Environmental Engineering, University of Florence, Via di Santa Marta, 3 – 50139, Firenze, Italy, enzo.marino@dicea.unifi.it*

²*CRIACIV c/o Dep. of Civil and Environmental Engineering, University of Florence, Via di Santa Marta, 3 – 50139, Firenze, Italy, dir-criaciv@dicea.unifi.it*

³*CNR-INSEAN - National Research Council, Via di Vallerano, 139 - 00128, Rome, c.lugni@insean.it*

Abstract – In this paper we present an extension of the capabilities of a numerical model recently developed by the authors for the simulation of fully nonlinear waves and their interaction with offshore wind turbines. The novelty of the present contribution lies in the extension of the above global model also to less severe environmental conditions, permitting accounting for the effects of nonlinear hydrodynamics (from weakly to fully nonlinear) for a wider range of environmental conditions.

The main facts that will be shown in the paper are: i) the presence of steep nonbreaking waves, significantly influences the structural response; ii) breaking waves induced by nonlinear interactions may hit the turbine tower causing impulsive loading contributions. For both cases much emphasis will be placed on the dangerous resonant effect that higher-frequency loads induce on the structural response.

1. Introduction

The worldwide offshore wind energy sector is still not fully flourishing due to the significant increase of cost caused by the substructure. Thus, when cost reduction, as well as structural safety, becomes the core of modern design approaches, more accurate simulation tools, capable of capturing the effects of complex environmental conditions on large multi-megawatt wind turbines, are strongly required.

A novel numerical package capable of predicting the nonlinear loads acting on offshore wind turbines exposed to severe sea states has been recently proposed in Marino (2011), Marino et al. (2011a,b).

The model reproduces the structural response by coupling a fully nonlinear wave kinematic solver with a hydro-aero-elastic simulator of the entire system. Due to the large number of simulations required to set up a suitable probabilistic model for the design loads extrapolation, the main goal of the proposed simulation scheme was the enhancement of the model accuracy without penalizing the computational time. The computational efficiency is guaranteed by a domain decomposition strategy such that the fully nonlinear numerical wave solver is invoked only on special sub-domains where highly nonlinear waves, such as breaking waves, are expected. The effects on the structural response of the impulsive wave loads associated with plunging breakers (Wienke and Oumeraci, 2005) was the main concern.

The novelty of the present contribution is the extension of the above global model also to less severe environmental conditions, when, at least according to the linear wave theory, no breaking waves are detected. In particular, we will show that: i) the presence of steep nonbreaking waves, generating from sea state n°6 (SS6) on, significantly influences the

structural response; ii) breaking waves induced by the nonlinear waves interactions may occur even if they are far to be predicted by the linear criterion.

With this improvement, the numerical package permits now accounting for the effects of nonlinear hydrodynamics (from weakly to fully nonlinear cases) given a wider range of environmental conditions. For the sea states classification we refer to Faltinsen (1990).

2. Model description

The global numerical framework is based on the coupling between the NREL open source software FAST (Jonkman, 2005) for the hydro-aero-elastic simulation and the potential flow models (linear and fully nonlinear) used to predict the wave loads acting on the turbine substructure.

The simulation scheme starts with the definition of the environmental parameters - mean wind speed, significant wave height and peak spectral period. An irregular sea is then reproduced in the time domain through a linear spectral approach. A zero-crossing analysis of the free surface elevation at the wind turbine location permits selecting only those waves marked by a steepness higher than a fixed threshold value ka_{\min} . In correspondence of these selected events, critical time instants t_{b_i} can be identified as follows

$$t_{b_i} = t_{up}(1) + \sum_{h=1}^{i_b-1} T(h) + T(i_b)/4 \quad (1)$$

where t_{up} contains the up-crossing time instants, \bar{T} is the vector collecting all the periods contained in the free surface time series, whose elements are: $T(h) = t_{up}(h+1) - t_{up}(h)$, and i_b is the vector index corresponding to the wave steepness exceeding the threshold value. Each of these time instants t_{b_i} , along with the spatial location of the wind turbine, defines the central point of a time-space sub-domain

$$\Omega_i = [x_t \pm \delta x_t] \times [t_{b_i} - \delta_1 t_{b_i}, t_{b_i} + \delta_2 t_{b_i}] \quad (2)$$

on which the fully nonlinear solver is called for a more refined simulation. In Eq.(2), x_t denotes the turbine location, δx_t , $\delta_1 t_{b_i}$ and $\delta_2 t_{b_i}$ the spatial and temporal radii of the i -th sub-domain, respectively. Note that, while it is assumed a symmetric spatial sub-domain, unsymmetrical radii are necessary for the temporal domain.

2.1 Fully nonlinear water wave problem

The two-dimensional problem governing the propagation of gravity waves is formulated assuming the potential theory. For an inviscid fluid in irrotational flow, the potential function $\phi(t, p)$ describes the velocity field at the time instant t in each point p belonging to the spatial domain $\Omega(t)$, i.e. $\bar{v}(t, p) = \nabla\phi(t, p)$.

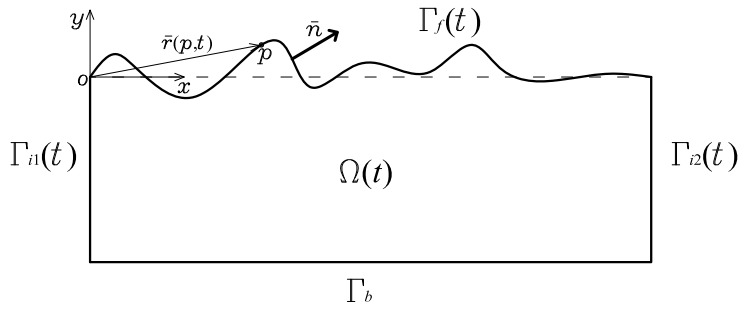


Figure 1: Two-dimensional domain of the time-dependent Laplace equation.

For incompressible fluid, mass conservation leads to the Laplace equation valid in the whole field

$$\nabla^2 \phi(p, t) = 0 \quad \forall p \in \Omega(t) \quad (3)$$

The two-dimensional domain $\Omega(t)$ is bounded by four boundaries – inflow Γ_{i1} , bottom Γ_b , inflow Γ_{i2} , and free-surface $\Gamma_f(t)$. See Figure 1.

A higher-order boundary element method (HOBEM) is used to discretize Laplace equation. Eq.(3) is first transformed into a boundary integral equation, then discretized into a number of quadratic boundary elements Brebbia (1998), Wrobel (2002). For more details about the implementation of the HOBEM see Marino (2011).

For the time integration a 4th-order Runge-Kutta algorithm is implemented. The free surface time-dependent potential problem is solved by means of a 2-step mixed Eulerian-Lagrangian scheme. We remark that, in the solving scheme, the analytic linear solution plays a twofold role: it is used to initialize the solver by providing the free surface elevation and the velocity potential on the free surface, it is used to provide Neumann boundary conditions (involved in the Eulerian step) on the upstream and downstream boundaries during the simulation.

2.2 On the transition between the linear and fully nonlinear models

The inflow sections and the free-surface regions close to them need particular care from the theoretical and numerical point of view. In those regions, indeed, initial and boundary conditions of the fully nonlinear solver come from the linear theory, resulting in a theoretical inconsistency. Therefore, temporal and spatial ramp functions, as well as numerical damping zones, are required to avoid numerical instabilities rising due to the transition from the linear (Eulerian description) to nonlinear (Lagrangian description) solution and vice-versa (Dommermuth, 2000). The reader may refer to Marino et al. (2012) for a comprehensive description and validation of the adopted transition scheme.

After a sensitivity analysis carried out on several ramp shapes, it turned out that for both temporal and spatial domains a cosine function assures satisfactory transitions. We indicate with L_{rmp1} and L_{rmp2} the portions of $\Omega_t = [x_t \pm \delta x_t]$ where the spatial ramp function applies, and with T_{rmp1} and T_{rmp2} the intervals on $\Omega_x = [t_{b_i} - \delta_1 t_{b_i}, t_{b_i} + \delta_2 t_{b_i}]$ where the temporal ramp is used. For the validation of the numerical solver, as well as for the calibration of the ramp functions parameters used in the global domain decomposition strategy, we refer to Marino et al. (2012).

3. Baseline turbine model

The turbine model is the NREL “5-MW Reference Wind Turbine for Offshore System Development” (Jonkman, 2009). A fixed-bottom monopile substructure is assumed to be located in a 20 m water-depth site. Some gross parameters of the model are listed in Table 1.

Table 1: Selected parameters of the baseline wind turbine model.

Rating Power	5 MW
Hub Height	90 m
Rated Wind Speed	11.4 m/s
Rotor Mass	110 t
Nacelle Mass	240 t
Tower base and pile diameter	6 m
Tower top diameter	3.87 m
Pile length (and water depth)	20 m
Pile mass	190 t

4. Applications

Here we focus on the application of the proposed numerical scheme to analyze the effects of the nonlinear hydrodynamics on the structural response by reproducing two sea states with increasing severity. In particular, according to the sea states classification proposed in Faltinsen (1990), we present results regarding SS6 and SS7. See Table 2.

Table 2: Parameters characterizing SS6 and SS7.

Sea state	SS6	SS7
U	24 m/s	26.5 m/s
H_s	5.0 m	7.5 m
T_p	12.4 s	15 s

SS6 is characterized by a mean wind speed U at the hub height around 24 m/s. Notice that with this wind condition the turbine would be still in power production. On the contrary, during the SS7 the turbine is parked. However, for the sake of simplicity, in this context we assume for both cases a parked configuration.

Table 3 reports the parameters adopted to set up the sub-domains and the ramp functions. Normally, these parameters are sea state-dependending. However, for SS6 and SS7 a unique set of parameters can be assumed assuring the same accuracy, see Marino et al. (2012) for convergence study. In the table, λ and τ indicate the mean wavelength and the mean wave period, respectively.

Table 3: Mean wavelength and wave period, sub-domain size, and ramp functions parameters for both simulation of SS6 and SS7.

Sea state	SS6	SS7
λ [m]	126.32	170.66
τ [s]	10.37	13.27
$\delta x_t = 3\lambda$ [m]	378.95	256
$\delta_1 t_{b_i} = 14T_p$ [s]	173.60	210
$\delta_2 t_{b_i} = 6T_p$ [s]	74.40	90
$L_{rmp1} = L_{rmp2} = 1\lambda$ [m]	126.32	85.33
$T_{rmp1} = 8T_p$ [s]	99.20	120
$T_{rmp2} = 4T_p$ [s]	49.60	60

During 1-hour simulation of SS6, the steepness threshold value $ka_{\min} = 0.15$ is exceeded five times. Events with steepness lower than this threshold are not selected as not particularly relevant in this context.

For the simulation of SS7, the steepness threshold is brought to $ka_{\min} = 0.18$. This permits placing more emphasis on the contribution given by steeper waves. Moreover, some of the selected events may be waves breaking against the turbine tower. In these sub-domains, the code capability of reproducing fully nonlinear events in a Lagrangian manner, permits accounting also for the impulsive loading contribution caused by the plunging breakers. The steepness threshold value for the SS7 is exceeded 5 times, and on sub-domains 2, 4 and 5, waves break against the turbine tower. (All the three breaking waves are plunging type). On the remaining two sub-domain 1 and 3, likewise all the five cases of SS6, steep nonbreaking waves are registered.

4.2 System response

In terms of structural response, the effects of the nonlinear hydrodynamic contributions are evaluated by comparing the response obtained using the proposed model with the one obtained with the plain linear wave theory. In Figure 2-5, comparisons are made on free surface elevation (top subfigure), then, from top to bottom, on the tower-base shear force in the direction of wind and waves, tower-base overturning bending moment, and (bottom subplot) tower-top fore-aft displacement.

It is known that when offshore structures are interested by the passage of steep waves, potentially dangerous resonant phenomena may be triggered. In particular, the ringing phenomenon deserves much care due to its burst-like characteristics. The ringing phenomenon is primarily ascribable to the presence of a high-frequency secondary load cycle (SLC) that causes a vibration at the resonance frequency of the system. The ringing vibration mechanism produces high stress levels in only few oscillations – a strong transient behaviour whose decay depends on the system damping. The secondary load cycle depends on a number of factors. Apart from the local wave steepness, which needs to be sufficiently high to trigger ringing vibration, SLC occurrence depends on the shape of the structure, the location of its centre of mass, flow conditions, etc. However, it exhibits some peculiar characteristics: it appears approximately around one quarter-one half local wave period later the main peak, and causes a sudden transient oscillating response. Refer to Chaplin et al. (1997), Grue and Huseby (2002), Kurtis and Kareem (1998) for a detailed description of the phenomenon.

In the experiments of Chaplin et al. (1997), the KC number ($\pi H_s/D$) was in the range of 3-10, and an inertia regime was assumed. The same for Grue and Huseby (2002), where ringing

was observed for KC numbers in the range of 4-6. Moreover, with respect to the $(k\eta_m, kR)$ plane, where k is the wave number, η_m the maximum wave elevation and R the cylinder radius, they reported that secondary load cycles appear in the range (0.2-0.4, 0.1-0.3).

The KC numbers of our simulations are 2.6 and 3.9 for SS6 and SS7, respectively. Thus, for both cases the inertia contribution is the dominating term in the Morison equation. In addition, we stress that the first tower natural frequency of our system is about 0.35 Hz (see Agarwal and Manuel 2009), then the ratios structure frequency to wave frequency are 4 and 5 for SS6 and SS7, respectively.

Thus, having verified that flow conditions, forcing regime, wave steepness, wave number, as well as the ratio structure natural frequency to wave frequency of our simulations are comparable with those characterizing the experiments of Chaplin et al. (1997), Grue and Huseby (2002), some ringing phenomena are expected in our simulations.

4.2.1 Response to SS6

If we look at third (from top) subplot of Figure we see that right after the peak at 255 s ca., a SLC occurs (note its total absence in the linear response in the above subplot). In correspondence of this SLC, a strong transient vibration is triggered in the tower-top displacement, see the bottom subplot of Figure 2. Furthermore, the same SLC may be responsible for the peak (in the force) at 301 s which is higher than the previous ones even though the difference between the nonlinear and linear free surface elevation is less pronounced than before (see top subplot). The force at the passage of the steep wave at 301 s is not marked by its own SLC, it just overlaps an ongoing oscillation (onset at 255 s). This seems to be an amplification of the structural response. In fact, the time history of the top displacements reveals that a resonance in the motion of the tower is prolonged over several periods.

Response on the sub-domain 3 of 5 is reported in Figure 3. A quite clear SLC appears at ca. 2375 s. As in the previous case, and in well agreement with the experimental results cited above, tower-top motion undergoes a sudden vibration at this instant. Higher harmonics are also well recognized in the bending moment, see fifth sub-plot (from top) of Figure 3.

4.2.2 Response to SS7

Moving to SS7, we present results regarding sub-domains 1, 2 and 5. Events 2 and 5 are characterized by plunging breaking waves, while the first event is a case of steep nonbreaking wave. In Figure 4 the nonlinear events 1 (nonbreaking wave) and 2 (breaking wave) are shown. For the nonbreaking wave case, it is interesting to note the presence of a similar response pattern as in the SS6 above. Indeed, we firstly observe that approximately at 745 (first sub-domain) a SLC takes place. We stress its total absence in the linear case and that right in correspondence of it an high-frequency vibration of the structure begins (see bottom subplot of Figure 4). Moreover, around 820 s, a more pronounced SLC is observed and an even stronger transient is triggered in the tower-top displacement and tower-base bending moment.

The second event is characterized by the impact that takes place at 1117 s ca., Figure . An important fact arises: we note that, before the impact, during the wave steeping, a number of SLCs occur until they culminate in extremely high-frequency loads at the impact. Further, these SLCs gradually diminish until they disappear at around 1200 s. These SLCs, see for example the one at 1150 s, cause additional amplification of the tower motion and the effects keep propagating for several periods, see bottom subplot of Figure 4.

Finally, in Figure 5, the response on the sub-domain 5 is shown. On this sub-domain, a very strong impact occurs at 3168.5 s. Before this impact, however, we note that at 3090 s ca., a steep nonbreaking wave causes very high-frequency loads which generate transient oscillations of

the system. Moreover, from this instant on, and up to the impact, a series of higher and higher-order loading cycles are clearly distinguishable.

We point out that the impact, caused by a plunging jet-type breaking wave, produces effects very similar to those experimentally observed by Welch et al (1999), (cf. Fig. 3 and Fig. 11 of the cited paper with our displacements and bending moments). It is also worth mentioning that both the KC number and the ratio first structure natural frequency to wave frequency of our simulations are in the same range of the experiments performed by Welch et al. (1999).

5. Concluding remarks

We have presented a novel numerical model capable of accounting for the effects of random nonlinear waves on offshore wind turbines. The most noteworthy feature of the proposed numerical scheme lies in the domain decomposition technique on which it is based. It is known that to set up reliable probabilistic model, a large number of simulations are necessary when the interest is the assessment of the design loads. Our model permits considering from weakly up to fully nonlinear waves effects with a relatively small computational effort, mainly due to the domain decomposition strategy.

The main results that arise from the application of the proposed model are that, from SS6 on, the effects of nonlinear wave contributions significantly influence the structural response. Moreover, the model reveals that, in these environmental conditions, employing the standard linear wave theory to reproduce random seas would lead to dangerous inaccuracies. We have shown that significant peaks in the system response (tower-base force and bending moment as well as tower-top displacements) would be underestimate causing unacceptable prediction. But, even more important, it has been demonstrated that very important resonant phenomena, such as ringing, can be captured only when nonlinear contributions are accounted for.

In the very end, we spend a word of caution about the assessment of the ringing phenomenon. Although remarkable similarities appear between our numerical results and the typical ringing response observed in literature, a better understanding is needed about the role of the lumped mass at the top of the tower (RNA assembly) - we recall that in all the mentioned experiments it was always the case of a homogeneous cylinder - and about the effect of the full-field turbulent wind with the machine in operation. These further investigations will be addressed in a specific work in preparation.

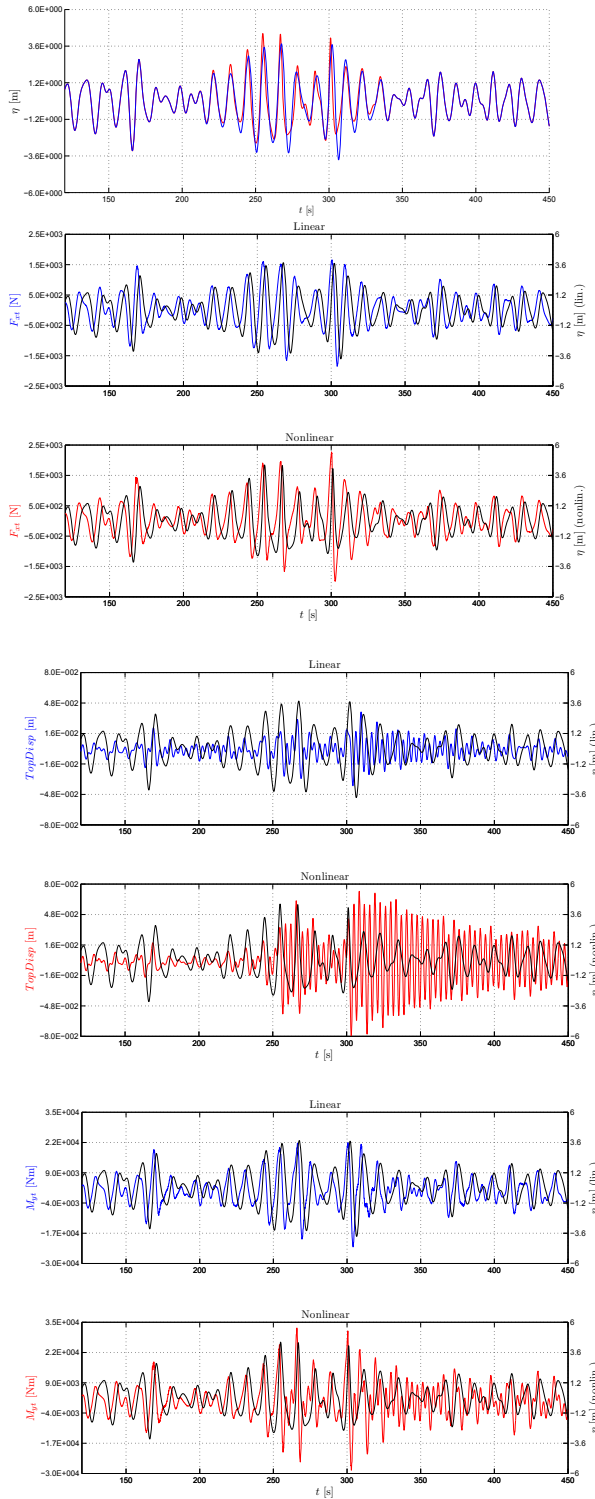


Figure 2. SS6. Sub-domain 1 of 5. Linear (blue) and nonlinear (red) free surface elevation comparison (top figure) and corresponding tower-base shear force F_{xt} , tower-base overturning moment M_{yt} , tower-top displacement $TopDisp$.

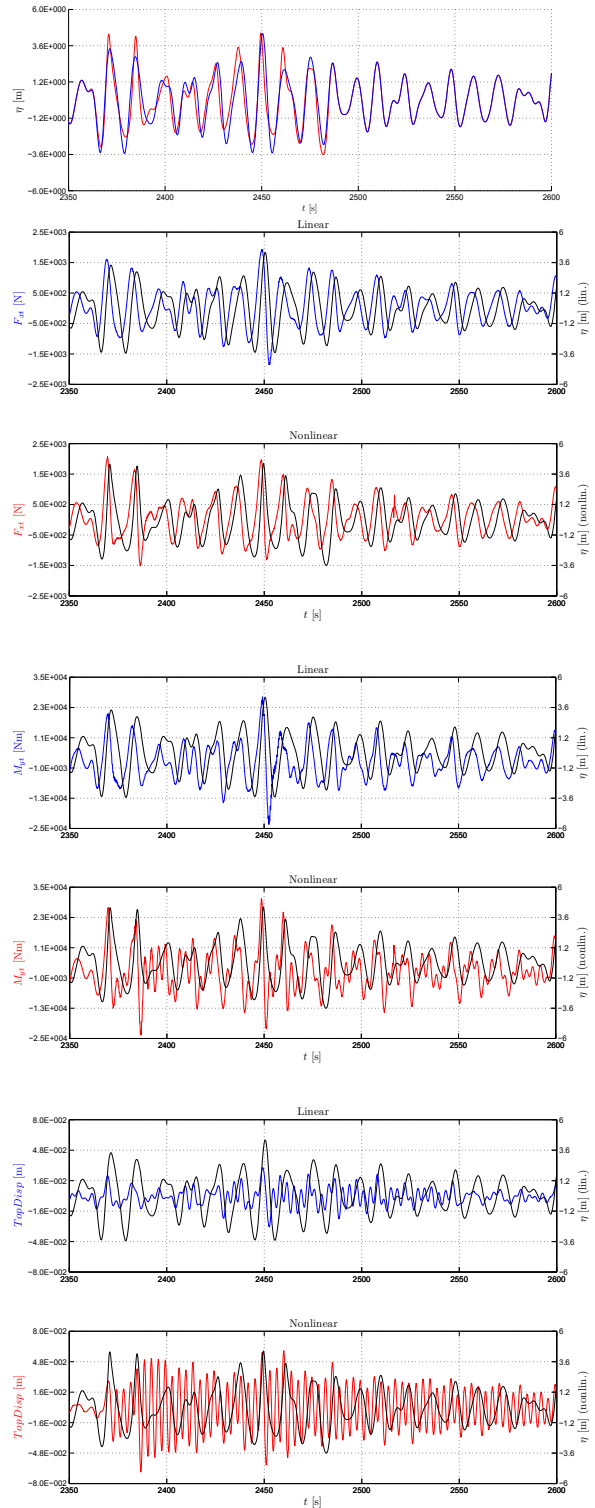


Figure 3. SS6. Sub-domain 3 of 5. Linear (blue) and nonlinear (red) free surface elevation comparison (top figure) and corresponding tower-base shear force F_{xt} , tower-base overturning moment M_{yt} , tower-top displacement $TopDisp$.

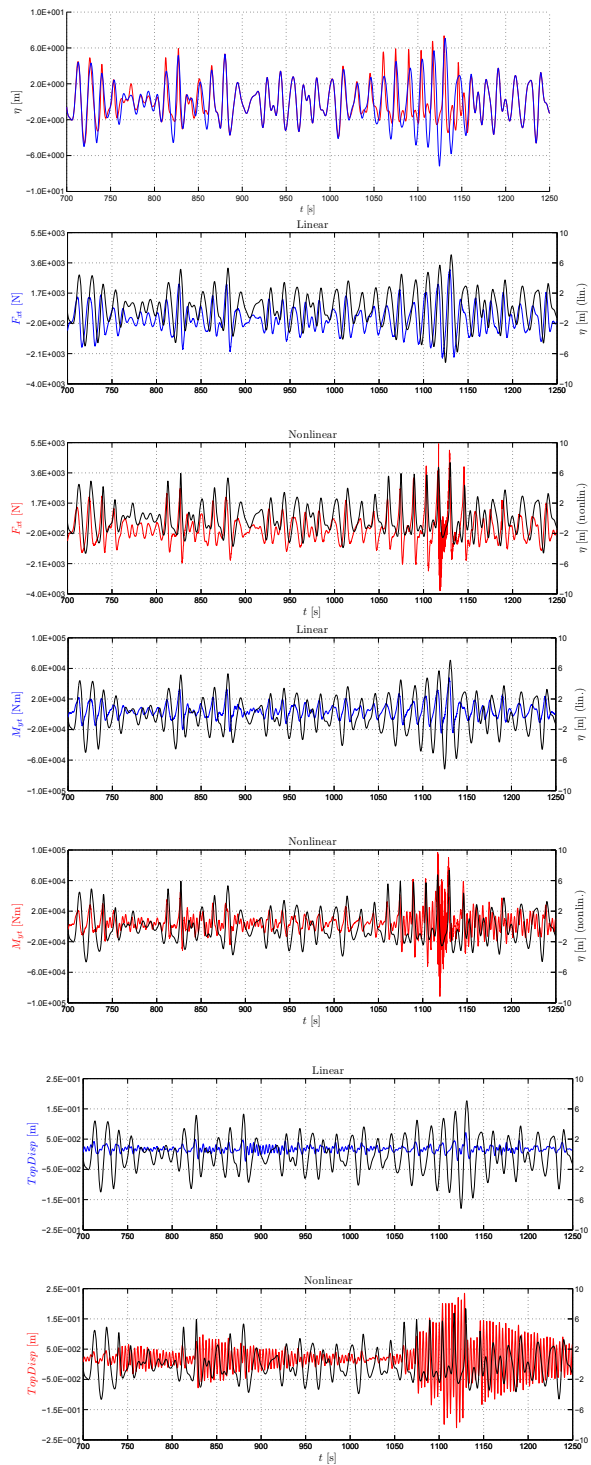


Figure 4. SS7. Sub-domains 1 and 2 of 5. Linear (blue) and nonlinear (red) free surface elevation comparison (top figure) and corresponding tower-base shear force F_{xt} , tower-base overturning moment M_{yt} , tower-top displacement $TopDisp$.

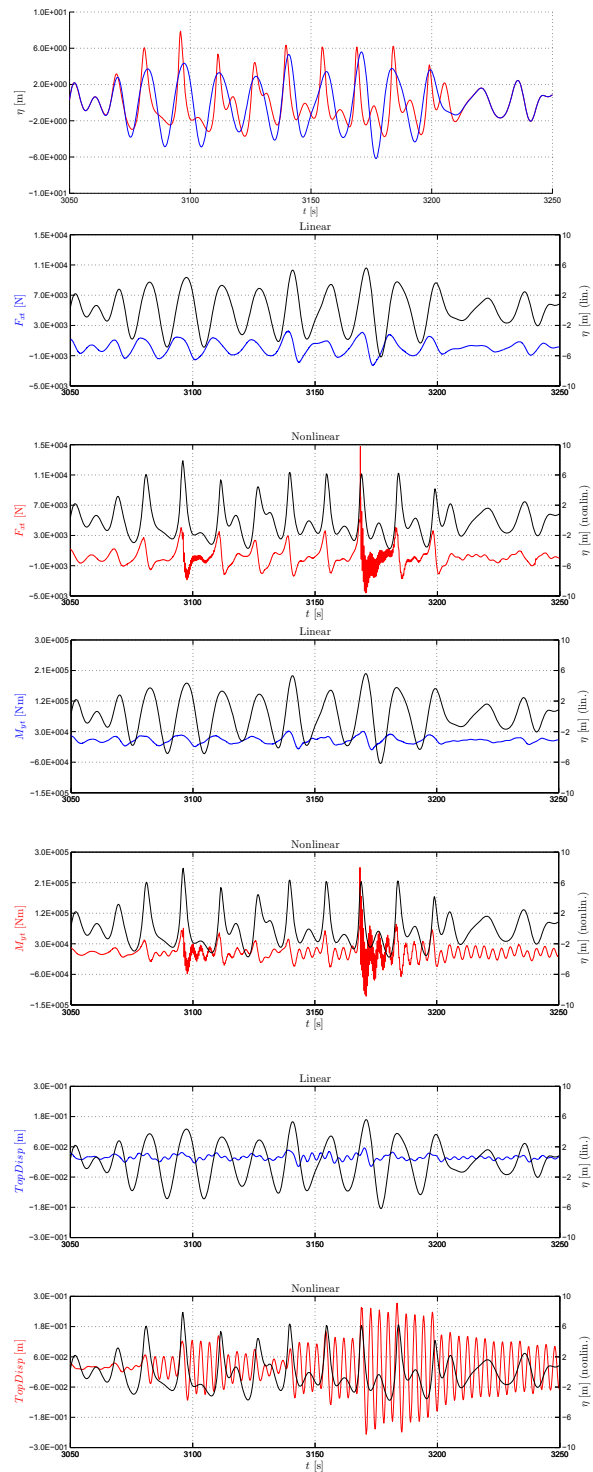


Figure 5. SS7. Sub-domain 5 of 5. Linear (blue) and nonlinear (red) free surface elevation comparison (top figure) and corresponding tower-base shear force F_{xt} , tower-base overturning moment M_{yt} , tower-top displacement $TopDisp$.

References

1. Agarwal, P., Manuel, L. 2009. Simulation of offshore wind turbine response for long-term extreme load prediction. *Engineering Structures*, 31(10), 2236-2246.
2. Brebbia, C., Dominguez, J. 1998. *Boundary Elements, An Introductory Course*, WIT Press, Boston, Southamton.
3. Chaplin, J. R., Rainey, R. C. T., & Yemm, R. W. 1997. Ringing of a vertical cylinder in waves. *J. Fluid Mech.* (1997), vol. 350, pp. 119–147.
4. Dommermuth, D. 2000. The initialization of nonlinear waves using an adjustment scheme, *Wave Motion*, 32, 307-317.
5. Faltinsen, O.M., 1990. *Sea Loads and on Ships and Offshore Structures*. Cambridge Press.
6. Grue, J., Huseby, M. 2003. Higher-harmonic wave forces and ringing of vertical cylinders. *Applied Ocean Research*, 24(2002), 203-214.
7. Marino E. 2011. *An Integrated Nonlinear Wind-Waves Model for Offshore Wind Turbines*, FUP, Firenze University Press.
8. Marino, E., Borri, C., Peil, U. 2011a. A fully nonlinear wave model to account for breaking wave impact loads on offshore wind turbines. *Journal of Wind Engineering and Industrial Aerodynamics*, 99(4), 483-490.
9. Marino, E., Borri, C., Lugni, C. 2011b. Influence of wind–waves energy transfer on the impulsive hydrodynamic loads acting on offshore wind turbines. *Journal of Wind Engineering and Industrial Aerodynamics*, 99(6-7), 767-775.
10. Marino, E., Borri, C., Lugni, C. 2012. A novel numerical strategy for the simulation of irregular nonlinear waves and their effects on the dynamic response of offshore wind turbines (to appear).
11. Jonkman, J.M., Buhl Jr., M.L. 2005. *FAST User's Guide*, NREL/EL-500-29798.
12. Jonkman, J., Butterfield, S., Musial, W., Scott, G. 2009. Definition of a 5-MW reference wind turbine for offshore system development. Technical Report, NREL.
13. Kurtis R. Gurley, and Ahsan Kareem. 1998. Simulation of Ringing in Offshore Systems under Viscous Loads. *Journal of Engineering Mechanics*, 124(5), 582--586.
14. Wienke, J., Oumeraci, H. 2005. Breaking wave impact force on a vertical and inclined slender pile-theoretical and large-scale model investigations. *Coast. Eng.* 52, 435-462.
15. Welch, S., Levi, C., Fontaine, E., Tulin, M. P. 1999. Experimental Study of the Ringing Response of a Vertical Cylinder in Breaking Wave Groups. *International Journal of Offshore and Polar Engineering*, 9(4), 276-282.
16. Wrobel, L.C., 2002. *The Boundary Element Method. Volume I. Applications in Thermo-Fluids and Acoustics*. Wiley.

Session 5: Wave Energy Resources

Chairmen: G. Sannino, A. Estanqueiro

Offshore Renewable Resources in the Mediterranean Area: the results of the ORECCA Project - D. Airoidi, L. Serri, G. Stella (RSE Spa, Milan (IT))

Wave energy exploitation in Italian seas: a feasibility study - S. Bozzi (Dip. Di Bioingegneria, Politecnico di Milano, Milan (IT)), R. Archetti (DICAM, Bologna Univ. (IT)), G. Passoni (DIAR, Politecnico di Milano, Milan (IT))

Extreme waves in the Central Mediterranean Sea for design of offshore wind farms and wave energy devices - F. Arena, A. Carillo (ENEA - Ocean Modelling Unit, Rome (IT)), V. Laface, G. Malara, A. Romolo (Mediterranea University, NOEL Laboratory, School of Engineering, Reggio Calabria (IT)), G. Sannino (ENEA - Ocean Modelling Unit, Rome (IT))

Offshore Renewable Resources in the Mediterranean Area: the Results of the ORECCA Project

D. Airoidi, L. Serri, G. Stella

RSE S.p.A., Via Rubattino 54, 20134 Milano (Italy),

tel. +39 02 39925283, fax +39 02 39925626, e-mail davide.airoidi@rse-web.it

Introduction

ORECCA (Off-shore Renewable Energy Conversion platforms – Coordination Action) has been a project founded by EC in the frame of the Seventh Framework Program (FP7). It started in March 2010 and ended in August 2011. The goals of the ORECCA project have been the creation of a framework for knowledge sharing and the developing of a roadmap for research activities in the context of offshore renewable energy that are a relatively new and challenging field of interest. In particular, the project has stimulated collaboration in research activities leading towards innovative, cost efficient and environmentally benign offshore renewable energy conversion platforms for wind, wave and other ocean energy resources, for their combined use as well as for the complementary use such as aquaculture e.g. biomass and fishes and monitoring of the sea environment. Within the ocean energy sector, the ORECCA Project is confined to wave energy and tidal stream energy devices.

For offshore renewables sector, installation and operation costs are still very high. The combined deployment of different offshore renewables for energy production can optimise the use of the infrastructures such as ports and grid connections and can improve the quality of the power produced. Moreover the combined use of the same marine area can reduce the possible conflicts with “traditional” uses of the sea such as fishery and navigation.

The overall marine area considered in the project is very wide: from Azores to Black Sea and from Iceland to Canaries. The information collected about the offshore renewable resources, bathymetry, EEZ, distance from shore, MPA, ports and offshore renewable plants in all European waters has been implemented in a GIS (Geographical Information System) and has been used for qualitative-quantitative evaluations. A WebGIS application, sponsored by RSE, has been developed in order to publish spatial data and results on internet.

After an introduction to the concept of offshore renewable energy conversion platform, a focus on offshore renewable resources (wind, wave and tidal) and their possible combined deployment in the Mediterranean area is reported. Lastly the perspectives of future development are presented.

1. Off-shore Renewable Energy Conversion platforms

Offshore platforms are a well-known concept in the Oil&Gas sector. A lot of solutions have been found, tested and are now currently used. Offshore renewable energy platforms represent a “wedding” between offshore platforms and devices for production of energy from offshore renewable sources, namely offshore wind and ocean energy. Within the ocean energy sector, the ORECCA Project is confined to wave energy and tidal stream energy devices.

These are the main outstanding points to be stressed:

- The EU renewable energy targets for 2020 and the international policies look at renewable energy as a high challenge for the future, and in the long term scenarios of offshore renewable energy deployment will become more and more important because of their very huge potential, see Table 1.

Offshore wind	European target [1]	350 GW
	International target [2]	1150 GW
Ocean energy	European target [3]	188 GW
	International target [4]	748 GW

Table 1: 2050 Offshore Wind and Ocean Energy Targets.

- Offshore energy production is a relatively new field. Offshore wind is the more advanced sector, even if offshore-dedicated turbines and floating systems are still at the study/development stage. In the tidal stream energy sector reasonable consensus exists on horizontal axis turbines, but no commercial devices are yet available, while a large number of devices are under various stages of development. In the wave energy sector there are a large number of different devices at various stages of development, based on a number of different principles.
- Commercially existing offshore renewable energy plants are today only wind farms with fixed foundations. A number of prototypal floating wind systems, as well as wave and tidal devices, are at different development stages. Only two combined devices are installed at sea at the moment: a 30 kW combined wave and tidal vertical axis device by Ecofys [5] and wind and wave Poseidon 37 combined platform. Floating Power Plant has constructed a 37 m model for a full offshore test. On 14th June 2010 Poseidon was towed back to the test site in Onsevig to commence Test Phase 2, which will provide valuable data required for the next phase, the commercial design phase [6].
- Costs and problems of sea installations are very high and the economic returns on investments in the renewable energy sector still need incentives to be sustainable and competitive (this holds even for onshore installations!). Cost reduction is the key factor for development and this process can be significantly helped by large-scale deployment of offshore renewable energy plants.

The basic idea of combined platforms and synergies is oriented to the optimisation of the ratio costs/benefits. More devices or activities allow getting more economical returns, while the use of common structures (i.e. platforms) and infrastructures (i.e. grid connection) allows to reduce costs. Moreover, combined multipurpose platforms will definitely optimize the competition of ocean uses as long as the same infrastructures and devices are being used for multiple aspects such as logistics and infrastructures, creating a number of jobs. This can be useful for increasing the social acceptance of this kind of technology, which is actually one of the obstacles in the developing of offshore renewable technologies. In the near future, it is not foreseen that multipurpose platform concepts will be financially feasible without incentives as should hopefully happen with the single offshore renewable energy technologies. However, it is very important, already at this early stage of development, to analyse possible synergies existing in the whole offshore energy sector. Synergies can be very different, i.e. sharing the same sea area among different technologies and/or other activities such as aquaculture or desalination (reducing competition of ocean uses [7]) and sharing the same platform among different energy conversion devices and/or activities such as offshore logistic hubs or sea monitoring.

Specifically, the assembly made up of various devices co-mounted on the same platform has been defined as a combined platform.

The combined platforms have been classified into two major categories named “Offshore Hybrids” and “Energy Islands” according to the following definitions:

- 1) OFFSHORE HYBRIDS: floating or fixed platforms using wind energy converters combined with an additional wave and/or tidal energy device. A significant example is the evolution of the Ecofys C-energy prototype that combines the three technology;
- 2) ENERGY ISLANDS: multipurpose platforms, generally very big, that utilize many possible sources of renewable energy from the ocean, i.e. wind, solar, wave, sea current, tidal current and biomass energy. Moreover, due to the available space on the platform, combination with other activities and/or functionality is suggested. One of the first proposed significant examples is the KEMA Energy Island, which combines wind energy production with an inverse offshore pump accumulation station on an offshore island [8].

2. Offshore renewable resources in the Mediterranean area

In the frame of ORECCA Project, information has been collected about resources (wind statistics, wave spectra, ocean currents, temperatures..), bathymetry, seabed morphology and geology, existing and planned use - marine spatial planning, environmental conditions (marine life, habitats, ecosystems), competing other uses such as navigation routes, regulatory, financial and legislative framework. The geographically distributed information has been implemented in a GIS project and used for evaluation of possible scenarios of development and deployment of offshore renewable resources also in combination. This GIS project has been furthermore implemented in a WEBGIS application. According to [9], WEBGIS is “a complex system with access to the Internet, for capturing, storing, integrating, manipulating, analysing and displaying data related to locations without the need of having proprietary GIS software”. The ORECCA WebGIS allows the sharing of information and the results of ORECCA project among the community and set up an example of “geographical platform” at European level (RSE that has been a partner of the ORECCA project, has supported the implementation of ORECCA WebGIS after the end of the project¹).

In Figure 1 is shown the homepage of this WebGIS application. Most of the images reported in the next sections are created through the WebGIS.

2.1 Characteristics, sea depth and offshore plants

The area of the Mediterranean and Black Sea is the crossroad among three continents, with many cultures, lifestyles and countries at very different stages of development. In its waters mankind has learned to navigate, and along its shores Western civilization was born. It is well known for its mild climate, beautiful landscapes and hospitable countries full of historical and artistic heritage that have made tourism widespread. Fishery and navigation are widely diffused too. From the physical point of view, the Mediterranean and Black Sea basins feature rather homogeneous characteristics as far as geomorphology, meteorology, climate and environment are concerned. Nevertheless, the actual degree of knowledge of their energy resources and peculiar environmental aspects is currently less advanced than on other areas, such as for instance the North Sea, where the largest number by far of existing offshore wind plants have so far been installed.

¹ This work has been financed by the Research Fund for the Italian Electrical System under the Contract Agreement between RSE (formerly known as ERSE) and the Ministry of Economic Development - General Directorate for Nuclear Energy, Renewable Energy and Energy Efficiency stipulated on July 29, 2009 in compliance with the Decree of March 19, 2009

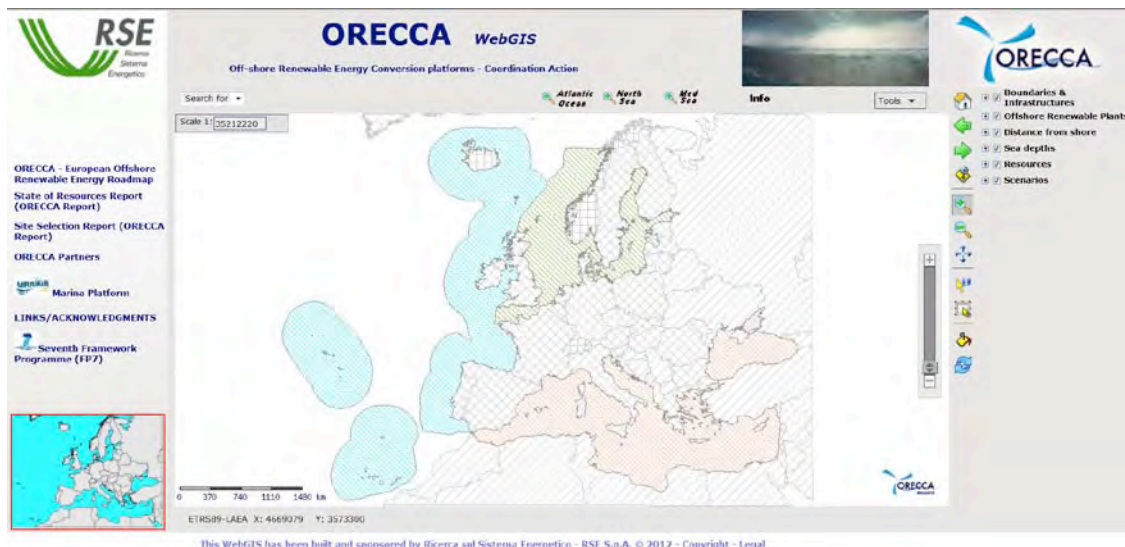


Figure 1: ORECCA WebGIS homepage (www.orecca.eu).

In general, the Mediterranean and Black Sea basins are less rich in either wind or wave or tidal resources (as to tides, the resource may even be deemed negligible). Furthermore, the areas with shallow waters suitable for currently available conversion systems based on fixed foundations are limited in number, as shown in Figure 2. In particular, this figure shows bathymetry classes defined in accordance with the technologies that are fit for given sea depths: for 0-30 m water depth (“shallow waters”) fixed foundations based on mono-piles or gravity foundations can be installed. For 30-50 m water depth (“transitional waters”) jacket, tripod or suction bucket foundations or concrete foundations can be installed. For deeper waters, floating systems have to be used. These systems are still at the prototype stage and the wide diffusion of this technology is deemed to take place from 2020 to 2030. At present only two prototypes have been installed and water depths up to 700 m are reported as suitable at least for floating mono-column wind turbine supports [10]. Most of the wind farms with floating wind turbines currently under consideration are to be located in water depths around 200 m [11].

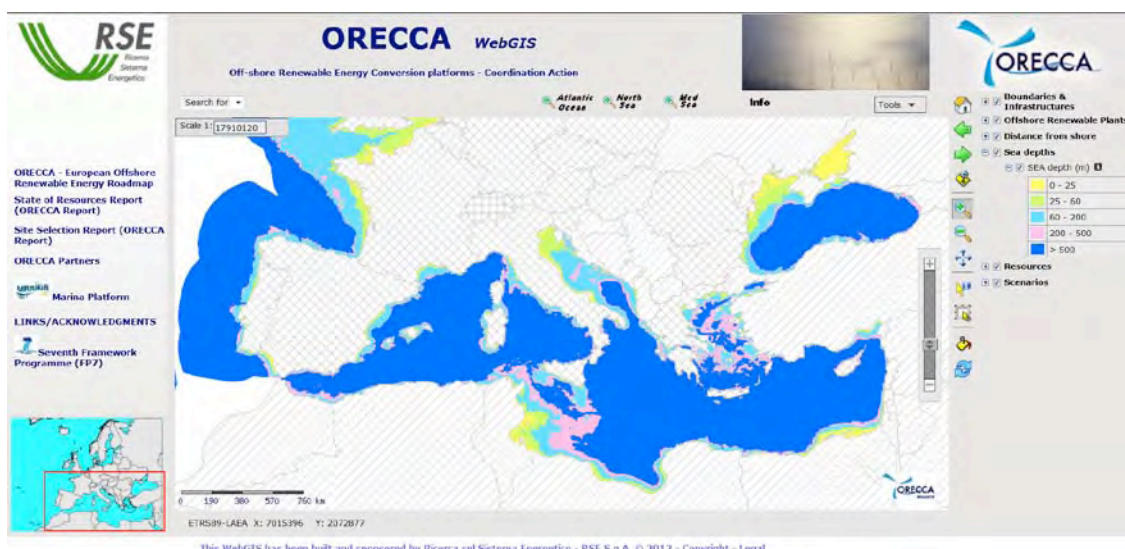


Figure 2: Sea depth.

In spite of all its setbacks, the Mediterranean Sea basin appears in principle as an interesting area for developing offshore renewable energy sources, for two main reasons. On the one hand, extreme environmental conditions are here less harsh than in oceans and other European seas, which could favour the development of dedicated, less “robust” and consequently less expensive conversion devices. On the other hand, it is estimated that energy demand will grow at the fastest rate right in North African countries according to a report by Observatoire Méditerranéen de l’Energie (OME) [12], much of the forthcoming increase in energy demand is expected to take place in the South Mediterranean countries. The overall energy demand of the Mediterranean countries is expected to grow by 1.5% per year on average, reaching 1426 Mtoe in 2030. Through 2030, the North countries are expected to lose some of their share to the South, whose share will account for over 42% of energy demand as compared to its current 28%.

The Mediterranean offshore wind potential has been investigated since 1992 [13]. A recent study makes an evaluation of 10 % electricity contribution coming from offshore wind installations by 2030 [14]. More than 90 offshore wind farms totalling about 20 GW of capacity are under consideration in this area [11], see Figure 3. The half is in area with water depth greater than 60 m where floating farms are expected.



Figure 3: Wind plants at different stage of the authorisation process.

A mention has to be given also to two prototypes tested for some time in Italian waters:

1. the BlueH floating wind turbine off the coast of the Apulia Region near Tricase [15];
2. the Kobold turbine by Ponte di Archimede driven by sea current in the Strait of Messina [16].

Studies for a common approach for the development of ports [17] and for the Maritime Spatial Planning for better development of offshore renewable energies [18] for this region are in progress.

2.2 Wind Resource and Scenario

Although the need for better information on offshore wind resources over the area of the Mediterranean and Black Sea has long been acknowledged [19], and several studies on this subject have already been performed, at present it is still generally agreed that the level of uncertainty and resolution of currently available wind maps [20] should be improved

considerably, especially with a view to evaluating the likely amount of energy that could be produced from wind.

Moreover, many of these available wind maps refer to heights above sea level that are lower than the rotor hub heights of most wind turbines today set up at offshore wind farms.

The main issue of the Mediterranean and Black sea area is fundamentally the lack of direct measurements of offshore wind. The number of wind measuring buoys at present in operation is around twenty, see Figure 4, and many of these buoys have been laid down at sea only recently. Furthermore, most buoys have been concentrated along the coasts of northern countries in the Mediterranean area, i.e. Spain, France, Italy and Greece, and along the coasts of Turkey in the Black Sea. RSE has recently installed a buoy in the Sicily Channel.

Like for all offshore areas, offshore measurements of wind speed and direction over the Mediterranean and Black Sea have also been carried out by the QuikSCAT satellite [21] for 10 years (from 1999 through 2009) and make it possible to draw up homogeneous wind maps of large areas with 0.25° resolution. These maps have already been made ready for the Mediterranean basin as well [22] and used as wind resource database in the ORECCA project. It should be borne in mind that measures taken from satellites by means of scatterometers do have rather high uncertainties (up to 2 m/s) especially in closed basins such as the Mediterranean Sea and, even more, the Adriatic Sea or the Black Sea. In addition, the numbers of measures are fewer in sea areas closer to coasts, which are, on the other hand, of more interest in view of possible installation of offshore wind farms. For these reasons the wind resource map considered in the ORECCA project misses the information in a buffer of 25 km from shoreline. In order to perform a scenario for the future technically and economically sustainable development, the wind resource has been



Figure 4: Offshore wind measuring buoys.

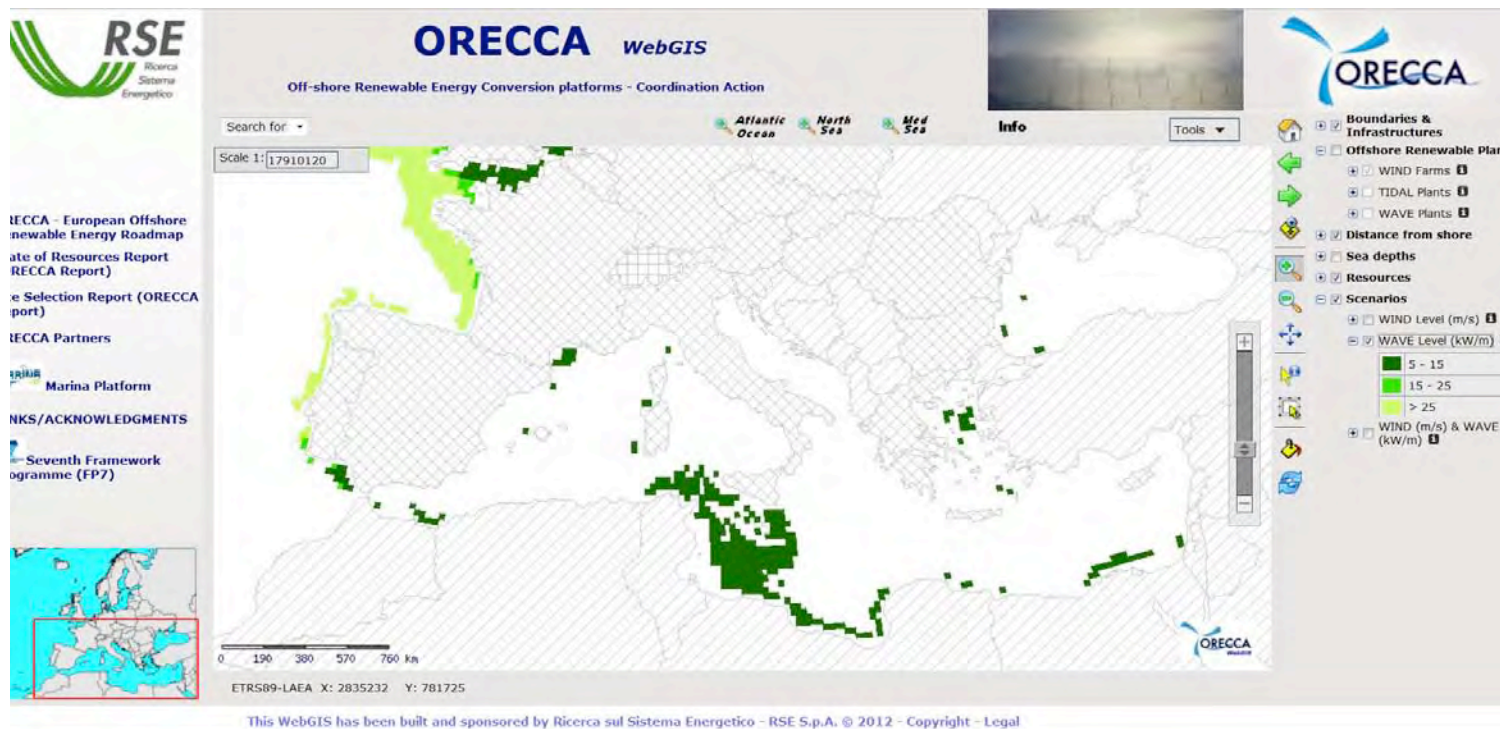


Figure 6: Wave resource scenario.

2.4 Tidal Current Resource

With regard to tides and tidal currents in the Mediterranean and Black Sea basins, the general opinion is that these resources cannot give significant contributions to energy production, with few exceptions in those areas, such as the Strait of Gibraltar, the Strait of Messina, the area of the Bosphorus and the Dardanelles, where the particular shapes of surrounding land and sea bottom are capable of accelerating water masses, as found in the selection of tidal site in Europe performed by ITPower, see Figure 7.



Figure 7- Tidal stream sites.

2.5 Combined scenarios for wind and wave

Areas suitable for installation of offshore multipurpose platforms for energy production from wind and wave resource in combination have been found crossing wind and wave resource scenarios. The result is a six level scenario according to the following combination growing in energy content (v = mean annual wind speed @10 m a.s.l, W_p = annual mean wave power):

1. Level 1: $6 \text{ m/s} \leq v < 8 \text{ m/s}$ & $5 \text{ kW/m} \leq W_p < 15 \text{ kW/m}$
2. Level 2: $6 \text{ m/s} \leq v < 8 \text{ m/s}$ & $15 \text{ kW/m} \leq W_p < 25 \text{ kW/m}$
3. Level 3: $6 \text{ m/s} \leq v < 8 \text{ m/s}$ & $W_p \geq 25 \text{ kW/m}$
4. Level 4: $v > 8 \text{ m/s}$ & $5 \text{ kW/m} \leq W_p < 15 \text{ kW/m}$
5. Level 5: $v > 8 \text{ m/s}$ & $15 \text{ kW/m} \leq W_p < 25 \text{ kW/m}$
6. Level 6: $v > 8 \text{ m/s}$ & $W_p \geq 25 \text{ kW/m}$

The resulting map is reported in Figure 8.

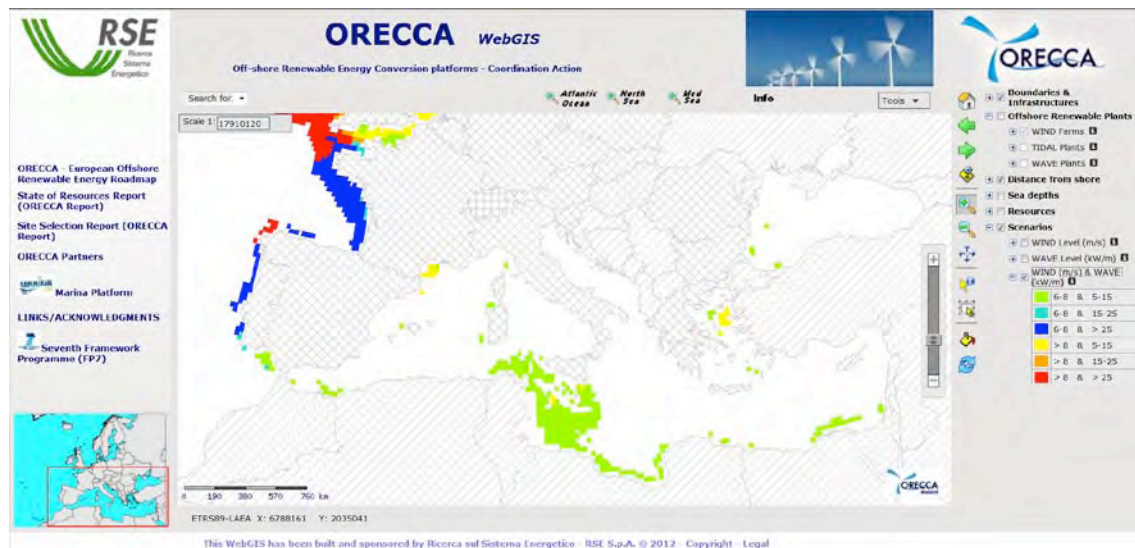


Figure 8: Combined wind and wave scenario.

As expected, the combined scenario for the Mediterranean area has low energy content mainly due to the wave energy content. Two reminders have to be done: information in the first 25 km from the shoreline is missing. In this area this buffer corresponds more or less to all the shallow waters, so the six level scenario is actually a scenario for deep waters deployment in a medium-long term temporal scenario. In spite of the “low” energy content of the wave resource, small, light, modular and “low cost” devices could be developed and addressed to this area for a sustainable deployment.

3. Conclusions and perspectives

The general concepts emerged for the offshore renewable resources in the Mediterranean area can be summarized in the following points:

- More knowledge is in general needed about all the items that could influence the development of offshore renewable energy resources in the Mediterranean Sea and moreover in the Black Sea. In particular direct offshore measurements of wind, wave, current and salinity gradient are needed to reduce the uncertainty of present estimates

of power contents and consequently expected energy production. This is a key issue in this area where resources are less than in the other European Seas and maybe extra cost reductions of offshore energy production costs should be considered in order to reach the economic sustainability.

- Moreover other accurate, updated and complete information about uses of the sea, social and environmental issues (such as maps of the uses of the sea, maps of *Posidonia* beds, indicators of tourism and landscape sensitive areas, archeological sites etc...) are needed for better understanding the possible conflicts and barriers.
- Three concepts have emerged about technologies, combined platforms and synergies:
 - Less resource means also (in general) less harsh extreme conditions. This allows for simpler design, as well as smaller and lighter devices, thus reducing the costs for construction, installation and maintenance. Smaller devices could also be suitable for the deployment of wave power. New approaches and designs are suggested to match resource peculiarities.
 - Floating devices installed in waters with depth greater than 50-70 m, at a minimum of 10 km from shore, allow to obtain the best synergies among higher resources (at least for wind), landscape issues and tourism (low visual impact), environmental issues (no *Posidonia* thrives in deeper waters and, more generally, biodiversity is poorer).
 - The most “promising” synergies for the Mediterranean areas are the combination of wind devices and aquaculture and the combination of wave devices and breakwaters. Investigation is suggested also in the field of offshore solar energy.
- The demonstration of a socially, economically and environmentally sustainable floating system (for wind and maybe for combined technology) is seen as a key step for driving public funding towards the support of research in this area and also for encouraging public/private investors to develop the infrastructure needed for large scale deployment of this technology (ports, shipyards, vessels etc.).
- Environmental issues have to be taken into account with reference to the EU Guidance Document for Wind Energy developments and Natura 2000. Peculiarities of species and biodiversity in this area may not yet be well known. Research projects are ongoing. Mitigation measures have to be investigated and found (where necessary and if possible) as regards the species and peculiarities of this area.
- Conflicts for the uses of the sea have to be well understood and considered. Best practices can be imported from other areas.
- The authorization process is now very complex in almost all the countries: clear, simple authorization processes with 1-stop shops with defined timing frames is needed also in order to attract investors.
- Clear, honest and pervasive communication is strongly needed.
- An original approach dedicated to this area is strongly suggested.

For complete information about the results of the ORECCA Project and for accessing the “ORECCA European Offshore Renewable Energy Roadmap” go to www.orecca.eu .

References

- [1] “Pure Power - Wind energy targets for 2020 and 2030”, A report by the European Wind Energy Association - 2009 update, November 2009
- [2] <http://www.carbontrust.co.uk/news/news/press-centre/2011/Pages/offshore-wind-gg.aspx>
- [3] “Oceans of energy - European Ocean Energy Roadmap 2010-2050”, a publication of the European Ocean Energy Association, Brussels, 2010
- [4] “Energy [r]evolution - A SUSTAINABLE WORLD ENERGY OUTLOOK” Greenpeace International, European Renewable Energy Council (EREC), June 2010, ISBN 978-90-73361-90-4
- [5] <http://www.c-energy.nl/>
- [6] www.floatingpowerplant.com
- [7] F. Neumann, “Ocean Energy as Ocean Space Use – Only Conflicts or Also Synergies?”, in OES-IA, Annual Report 2009
- [8] W.W. de Boer, F.J. Verheij, D. Zwemmer, R. Das, “The Energy Island – An Inverse Pump accumulation Station”, EWEC 2007, Milan, Italy, 7-10 May 2007
- [9] M. Painho, M. Peixoto, P. Cabral, R. Sena, “WebGIS as a teaching tool“, <http://proceedings.esri.com/library/userconf/proc01/professional/papers/pap910/p910.htm>
- [10] www.statoil.com
- [11] www.4coffshore.com
- [12] OME, “MEDITERRANEAN ENERGY PERSPECTIVES 2008”
- [13] G. Gaudiosi, ‘Offshore Wind Energy Potential in Mediterranean’, ENEA-Italy, World Renewable Energy Congress, Reading -UK 1992
- [14] Gaudiosi, C. Borri, “Offshore wind energy in the Mediterranean countries”, *Revue des Energies Renouvelables SMEE’10 Bou Ismail Tipaza* (2010), 173 – 188.
- [15] www.bluehusa.com/
- [16] www.pontediarchimede.it/language_it/
- [17] Maria Helena Martins et Ana Filipa Prata , «European Union, a whole new world of challenges to Mediterranean ports», *Cahiers de la Méditerranée [En ligne]* , 80 | 2010 , mis en ligne le 15 décembre 2010, Consulté le 06 mai 2011. URL : <http://cdlm.revues.org/index5223.html>
- [18] www.seaenergy2020.eu/
- [19] A.M. Sempreviva, R.J. Barthelmie, G.Giebel, G. B. Lange; A. Sood, “Offshore wind resource assessment in European seas, state-of-the-art. A survey within the FP6 POW'WOW coordination action project”, 2007 European Wind Energy Conference and Exhibition, Milan 2007
- [20] The Medatlas Group: Gaillard P., P. Ravazzola, Ch. Kontolios, G. A. Athanassoulis, Ch. N. Stefanakos, Th. P. Gerostathis, L. Cavaleri, L. Bertotti, M. Sclavo, E. Ramieri, L. Dentone, C. Noel, C. Viala, J.-M. Lefevre (2004): “Wind and Wave Atlas of the Mediterranean Sea”
- [21] <http://manati.orbit.nesdis.noaa.gov/datasets/QuikSCATData.php/>
- [22] B.R. Furevik, A. M. Sempreviva, L. Cavaleri., J.M. Lefèvre, C. Transerici, “Eight years of wind measurements from scatterometer for wind resource mapping in the Mediterranean Sea”, *Wind Energ.* (2010), DOI: 10.1002/we
- [23] www.oceanor.com

Wave energy exploitation in Italian seas: a feasibility study

S. Bozzi¹, R. Archetti² and G. Passoni³

¹Dipartimento di Bioingegneria, Politecnico di Milano, Piazza Leonardo da Vinci 32, 20133 Milano, Italy, silvia.bozzi@polimi.it

²Dipartimento di Ingegneria Civile Ambientale e dei Materiali, Università di Bologna, Viale Risorgimento 2, 40136 Bologna, Italy, renata.archetti@unibo.it

³Dipartimento di Ingegneria Idraulica, Ambientale, Infrastrutture viarie, e Rilevamento, Politecnico di Milano, Piazza Leonardo da Vinci 32, 20133 Milano, Italy, giuseppe.passoni@polimi.it

Abstract – In this paper the feasibility of wave energy exploitation off the Italian coasts is investigated. At this aim, the energy production is estimated considering two of the most promising offshore technologies: the AquaBuOY device and the Pelamis device. The hypothetical wave farms are installed at two of the most energetic sites off the Italian West Mediterranean coast: Alghero and Mazara del Vallo. The Pelamis device provides the highest annual energy production with 8% capacity factor at both sites. Higher capacity factors can be obtained by scaling the devices in order to have the maximum power output for the typical wavelength of the investigated sites. At Alghero the optimal scaling of the devices is 1:2 and 1:2.5 for Pelamis and AquaBuOY, respectively, and it allows to increase the capacity factors up to 15%. If such devices could accommodate this downscaling, their performance in energy conversion could become economically attractive also for Italian seas.

1. Introduction

Early in the last decade many efforts have been focused on the estimation of the wave energy potential off the coasts of the global oceans, in order to provide a basis for wave energy exploitation (a recent review on wave energy resource characterization can be found in Pontes, 2002). In Europe, an Atlas has been created (Pontes, 1998), which contains detailed wave climate and wave energy statistics at 85 points distributed along the European coastline and in the Mediterranean an atlas of wind and wave energy sources has been published (Medatlas Group, 2004).

A first estimate of the wave power levels along the Italian coasts has been done by Filianoti (2000) analyzing 11-year wave data for 8 locations off the Tyrrhenian, Adriatic and Ionic coasts. Recently this study has been updated, considering an 18-year wave measurement period and has been extended to 7 further offshore locations (Ferrante et al., 2010).

The estimates of average annual wave power show that the most energy rich areas of the global oceans occur in moderate to high latitudes. In the northern hemisphere the highest energy levels are along the western coasts of Europe, situated at the end of the long, stormy fetch of the Atlantic Ocean. The average annual wave power, which is usually expressed as power per unit length of wave crest (or shoreline direction), increases from about 40 kW/m off the Portugal coast up to 75 kW/m off the British Isles and then decreases to 30 kW/m off the northern part of the Norwegian coastline (Brook, 2003).

In the southern hemisphere the most energetic areas are located off Southern Chile, South Africa and off the south and south-west coast of Australia and New Zealand (Falcão, 2010).

In the Mediterranean basin, the average annual wave power varies between 4 and 12 kW/m, the highest values occurring in the area of the south-western Aegean Sea which is

characterized by a relatively long fetch and high wind energy potential (Clément et al., 2002). Italy is characterized by two main wave climates: the western coastline is exposed to high waves coming mostly from the II and III quadrants while the waves on the eastern coasts are milder and come mainly from the north (Piscopia, 2002). As a result the average annual wave power is around 2 kW/m off the Adriatic coast and between 3 and 5 kW/m off the Tyrrhenian coast (Ferrante et al., 2010). The most energetic sites are a number of offshore island and specific locations around Sicily and Sardinia, where the average annual wave power can reach 10 kW/m (Clément et al., 2002).

During recent years a great variety of technologies has been proposed to capture energy from waves. They are usually classified by either the principle of operation or the geometry of the device or the primary location (onshore, nearshore or offshore). A widely used classification is based on the horizontal size and orientation of the device. If the horizontal physical dimension is much smaller than the wavelength of the incident waves, the WEC is called point absorber (Budal and Falnes, 1975). On the contrary, they are called attenuators and terminators if they have a horizontal extension which is comparable with typical wavelength of the waves from which they are designed. Attenuators are aligned along the prevailing wave direction while terminators are positioned perpendicularly to the dominant direction of the incident waves. A more comprehensive classification system has been proposed by Hagerman (1985) and further modified and updated by Brook (2003). It classified the wave energy conversion technologies on the basis of the energy extraction method (heave, surge, pitch, yaw or combined modes), the type of absorber (rigid, flexible or free surface), and the type of reaction point (inertial structure, sea-floor anchors or fixed structures) and the primary location of the device. The first generation devices were mostly located on the shoreline or near-shore and were typically based on the method introduced by Masuda (1981), named oscillating water column (OWC). They have the advantage of easier installation and maintenance and they do not require deep-water mooring or long underwater electric cables. However, the shoreline devices experience a much less energetic wave regime. On the contrary the most recent wave energy technologies (also named third generation devices) are located offshore to exploit the more powerful wave regime available in deep waters (> 40 m depth). They are typically oscillating bodies, either floating or fully submerged, which provide a large power output either by a single device of large physical dimensions or by small modular devices deployed in arrays. The offshore devices face problems due to mooring, access for maintenance and need of long underwater electrical cables.

In this work a feasibility study of wave energy exploitation in Italian seas is carried out. The energy production of two of the most promising wave energy converters is estimated for two of the most energetic sites off the Italian West Mediterranean coast. The paper is organized as follows: in the first section we characterize the wave energy resource along the Italian coasts. In the second section we describe the wave energy converters considered for this analysis. Then we estimate the energy production of the hypothetical wave farms and we calculate the scale of the devices which would maximize their capacity factors at the study sites. Finally, in the last section some conclusions are drawn.

2. Wave Energy Resource

In order to study the feasibility of wave energy exploitation off the Italian coasts, the two most promising locations off the Italian coasts, where wave measurements and statistics are available were selected; the sites are Alghero, on the western coast of Sardinia and Mazara del Vallo, on the Sicily Strait (Figure 1).

Wave data were collected by the directional wave buoys of the Italian wave network (details on the locations and wave data are available at www.telemisura.it).

The wave climate of Alghero estimated from historical data over a period of several years is shown in Figure 2.

Based on 17-years measurement of wave statistics (significant wave height and peak period, APAT, 2004), the potential wave energy at these locations was estimated. For each recorded sea state (every three hours or every half-hour when storm peak wave height exceeded the threshold of the station) the wave power per unit of wavefront length was calculated by the following formula:

$$P = \frac{1}{64\pi} \rho g^2 H_s^2 T_e \quad (1)$$

where ρ is the seawater density (1025 kg/m^3), g is gravity, H_s is the significant wave height and T_e is the energy period, i.e. the ratio between the spectral moment of order -1 and of order zero. The energy period of a sea state is equivalent to the period of a single sinusoidal wave that would have the energy of a sea state.

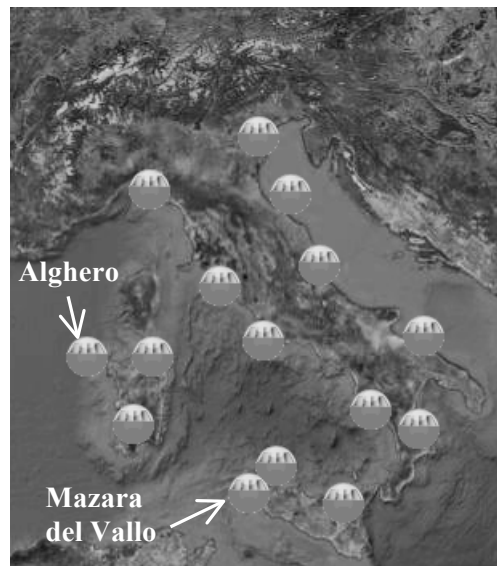


Figure 1: Location of wave buoys of the Italian wave network and case study locations

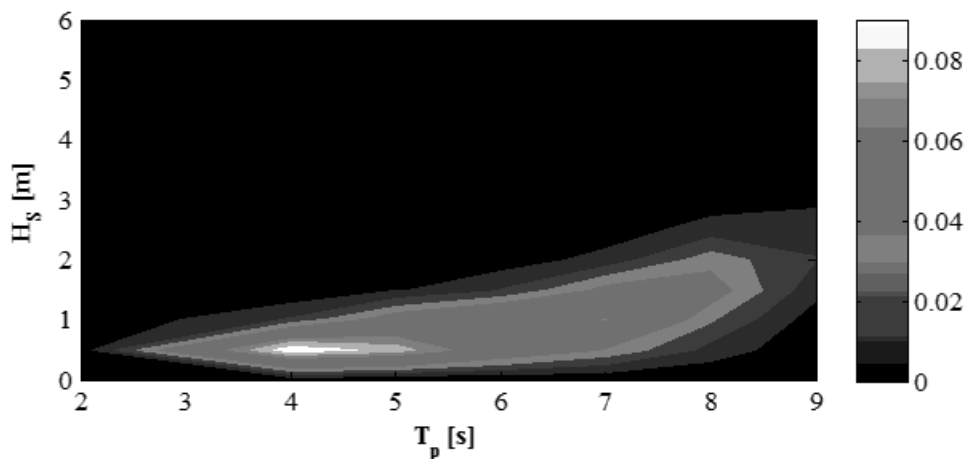


Figure 2: Probability of occurrence of sea states at Alghero.

The spectral moment m_{-1} was calculated assuming a JONSWAP spectrum (Hasselmann, 1973) for the sea state and adopting the shape parameters provided by the atlas of Italian seas for the two locations (APAT, 2004).

The resulting average annual wave power is 9.5 kW/m for Alghero and 3.9 kW/m for Mazara del Vallo, confirming results by Ferrante et al. (2010) and Clément et al. (2002).

3. Wave Energy Converters

The energy production off Alghero and Mazara was estimated considering two of the most promising offshore wave energy converters: the Pelamis device and the AquaBuOY device. The Pelamis wave energy converter, created by Ocean Power Delivery Ltd. of Edinburgh, Scotland (Ocean Power Delivery, 2000), is a semi-submerged, articulated structure composed by four cylindrical sections linked with hinged joints and aligned with wave direction. The wave-induced motion of these joints (either by heaving or swaying) is resisted by hydraulic rams, which pump high-pressure oil through hydraulic motors driving the electrical generators. A single Pelamis device is 120 m long and 3.5 m in diameter and has a power output of 750 kW. Several devices can be connected together and linked to shore through a single seabed cable. A full-scale prototype was tested in Scotland in 2004 and then in 2008 a set of three devices was deployed off the northern coast of Portugal at a 50 m depth, making it the world's first commercial wave farm.

The AquaBuOY is a technology developed by Finavera Renewables Inc. (AquaEnergy Group, 2002). The AquaBuOY device is a floating buoy mounted above a piston contained inside a tube, open on both ends, with a hose pump attached to each end. As the buoy oscillates, the hose pumps produce a flow of pressurized water that drives a Pelton turbine, connected to a generator. Each 40-ton AquaBuOY has a rated power of 250 kW. The device is modular and can be scaled from a small cluster of hundreds of kilowatts to a large power plant of several hundred megawatts.

A well-established method to assess the performance of the wave energy converters is based on the so-called power matrices. These are bivariate matrices indicating the power output of a device as a function of significant wave height and wave period. A distinct pair of H_S and T_p is referred to as an energy bin. Wave energy companies have published power matrix for their devices as a concise way to present its performance in real sea states. The AquaBuOY power matrix (Weinstein et al., 2004), used in the presented analysis is shown in Figure 4a. The Pelamis power matrix (Pelamis, 2008) is presented in Figure 5a.

4. Energy Production

Electricity production (in kWh) was calculated by multiplying the expected power output (in kW) of a sea state (defined by H_S , T_p) by its occurrence (in hours). It should be noted that using discrete energy bins introduces some errors, so interpolation was needed to estimate the device performance for the sea states registered at the studied sites. For each $H_S - T_p$ pair the energy production was estimated by a bilinear interpolation of the values provided by the power matrices.

Over the 17-years period between 1990 and 2007 the annual energy output (AEO), i.e. the mean annual energy production, of the Pelamis device is 556 MWh at Alghero and 296 MWh at Mazara del Vallo (Table 1). The annual energy production of the AquaBuOY wave energy converter is 184 and 80 MWh at Alghero and Mazara del Vallo, respectively. In both locations the WEC providing the highest energy production is the Pelamis wave energy converter. The AquaBuOY device generates 3 times less energy than Pelamis at both sites but it is characterized by a more constant energy production along the studied period.

Table 1: Characteristics and performance of AquaBuOY and Pelamis devices at Alghero and Mazara del Vallo.

	Alghero		Mazara	
	AquaBuOY	Pelamis	AquaBuOY	Pelamis
Rated power [KW]	250	750	250	750
Annual energy output [MWh]	184	556	80	296
Full load hours [h]	735	741	320	395
Capacity factor [%]	8%	8%	4%	5%

The performance of the devices can be better expressed in terms of full load hours and capacity factors. The full load hours are calculated as the mean annual production divided by the rated power of the wave energy converter. The capacity factor (or load factor) is the ratio of the full load hours and the 8766 hours of the year and so it indicates the percentage of the time in a year during which the device is running at its maximum power.

The capacity factors of AquaBuOY and Pelamis at Alghero are both equal to 8% while at Mazara del Vallo the hypothetical wave farms of AquaBuOY and Pelamis would have capacity factors of 4% and 5%, respectively. As a result of the different wave climates of the two sites, in Alghero the capacity factor is approximately twice the one in Mazara.

The estimated capacity factors are low compared to the ones obtained for the same wave energy converters in other offshore locations in Europe and America (ref). One of the reasons is that the AquaBuOY and Pelamis devices are designed to reach the maximum power for long wave conditions typical of oceanic coastlines and randomly found in Italian seas.

In the Mediterranean Sea, the wave climate is characterized by high waves and high persistence of storms, but not by long wave conditions. For example, by comparing the map of probability of occurrence of sea states at Alghero (Figure 2) with the AquaBuOY and Pelamis power matrices (Figure 4a and 5a) it can be noticed that the best performance of the WECs is obtained for sea states with very low percentage of occurrence.

These results indicate that the WECs considered in this study are oversized with respect to local wave climate and that a more efficient energy conversion can be obtained by scaling the devices in order to have the maximum power output for the typical wavelength of the investigated sites. In locations such as the Mediterranean Sea as well as the Canada West Coast and the USA East Coast smaller wave energy converters with lower power outputs would be more suitable, as suggested by Dalton et al. (2010).

At the study sites we calculated the annual energy output and the consequent capacity factor for AquaBuOY and Pelamis of different dimensions to find out the geometric scales of the devices maximizing the capacity factors. For each dimension of the two WECs the associated power matrix was estimated according to Froude similarity. Froude scaling laws imply that if the geometric scale is λ , the time scale is $\lambda^{-0.5}$ and the power scale is $\lambda^{3.5}$.

Figure 3 shows the capacity factors as a function of scale for the hypothetical wave farms of AquaBuOY and Pelamis at Alghero and Mazara del Vallo.

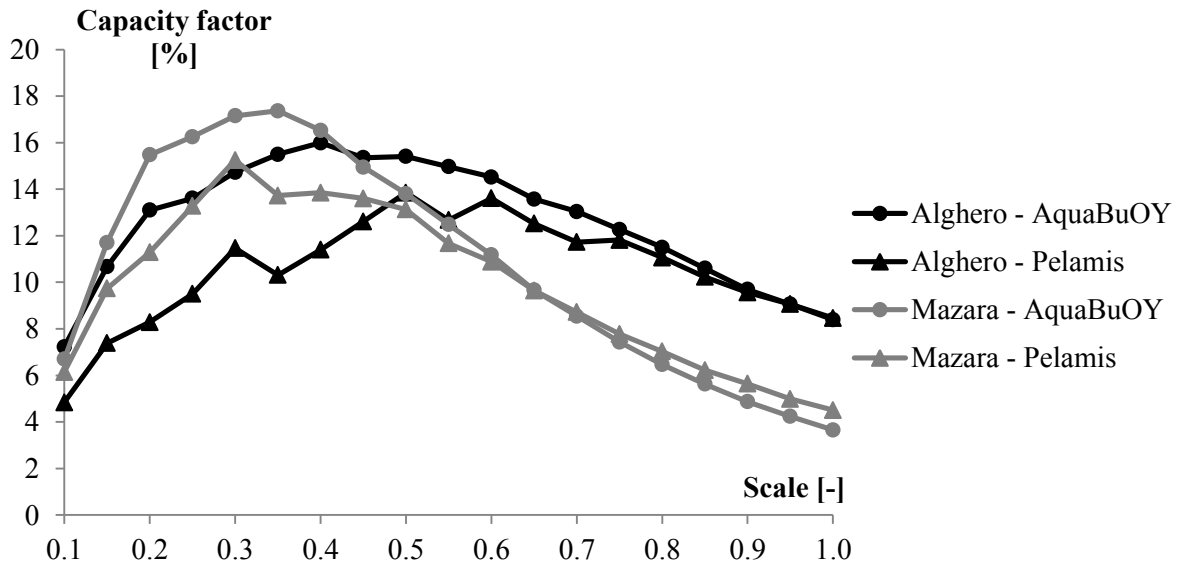


Figure 3. Capacity factors of AquaBuOY and Pelamis at Alghero and Mazara del Vallo for different device dimensions

The capacity factors reach their maxima for geometric scales in the range 0.3-0.5. The characteristics and performance indices of the optimal devices are reported in Table 2.

At Alghero the optimal geometric scales are 0.4 and 0.5 for AquaBuOY and Pelamis, respectively. These reduced WECs would have respectively a rated power of 66 kW and 10 kW, an annual energy production of 80 MWh and 14 MWh and a capacity factor of 16% and 14%. At Mazara del Vallo the highest capacity factors are obtained for smaller devices ($\lambda = 0.35$ and $\lambda = 0.3$ for AquaBuOY and Pelamis, respectively) than in Alghero due to the less energetic wave climate of the site.

Nevertheless, if such devices were downscaled their performance in energy conversion would be better than in Alghero and comparable with the one of the hypothetical wave farms considered by Dalton et al. (2010) in USA and Canada. In Mazara del Vallo the capacity factors of the AquaBuOY and Pelamis devices reduced to approximately 1/3 of their original dimensions would be 17% and 15% respectively. These devices would have respectively a power output of 6 kW and 11 kW and a mean annual energy production of 10 MWh and 15 MWh.

Table 2. Characteristics and performance of the downscaled AquaBuOY and Pelamis devices at Alghero and Mazara del Vallo.

	Alghero		Mazara	
	AquaBuOY	Pelamis	AquaBuOY	Pelamis
Scale [-]	0.4	0.5	0.35	0.3
Rated power [KW]	22	66	6	11
Annual Energy Output [MWh]	30	80	10	15
Full load hours [h]	1350	1213	1521	1336
Capacity factor [%]	15%	14%	17%	15%

Figure 4 and 5 show the power matrices of the full size AquaBuOY and Pelamis (top figures) and of the same devices reduced in size by approximately 1/3 (bottom figures). Axes limits are kept equal to show the effect of the downscaling. It can be noticed that the reduction of the device dimension allows capturing the short wave energy which would otherwise be lost with the full scale WECs.

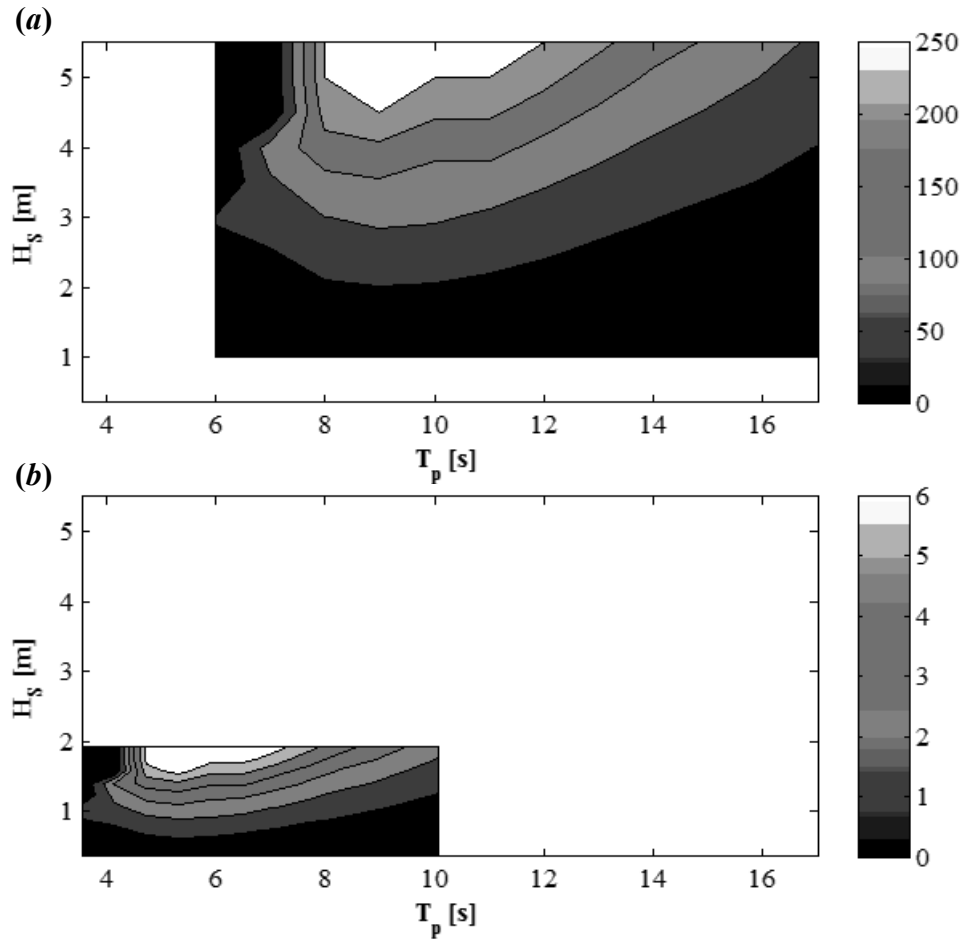


Figure 4. (a) Power matrix of the full scale AquaBuOY, (b) Power matrix of the AquaBuOY, scaled to obtain the maximum capacity factor at Mazara ($\lambda = 0.35$).

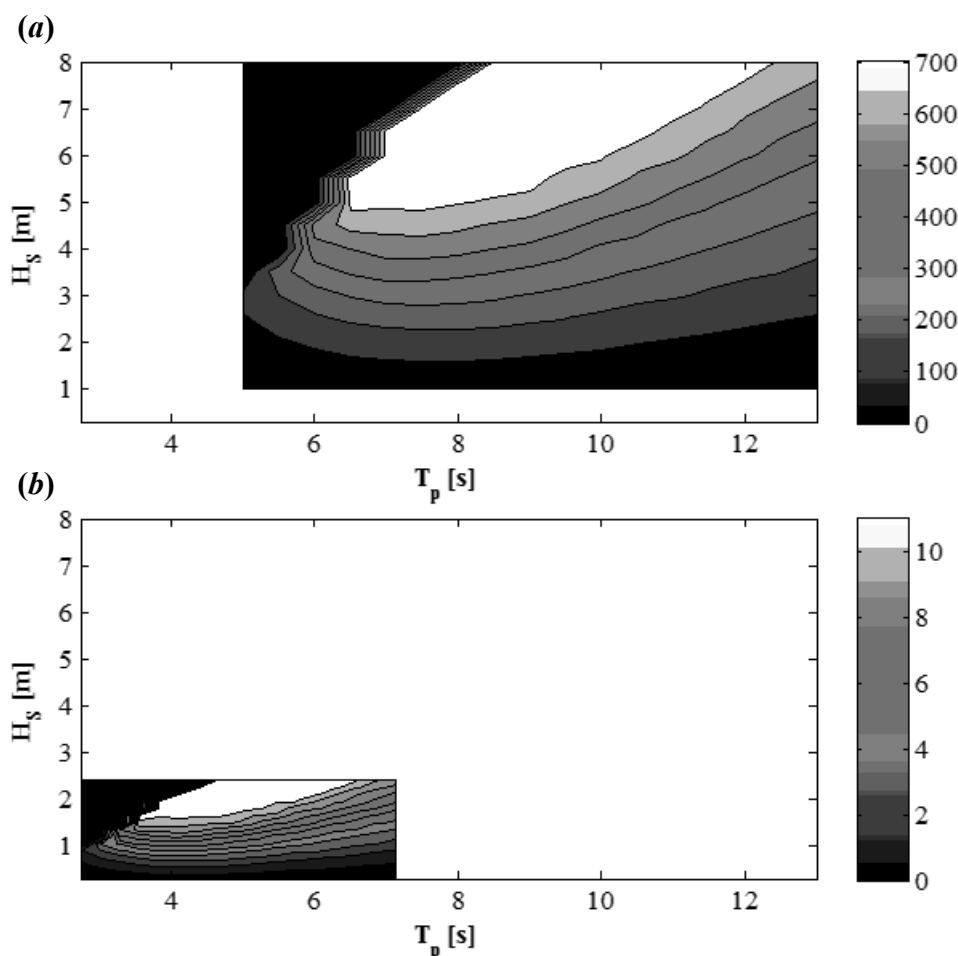


Figure 5. (a) Power matrix of the full scale Pelamis, (b) Power matrix of the Pelamis, scaled to obtain the maximum capacity factor at Mazara ($\lambda = 0.3$).

5. Discussion and conclusions

Wave energy exploitation has significantly advanced in Europe over the last two decades and many wave energy converters (WECs) are now at the end of the development stage while others are currently being deployed.

The wave energy potential along the Italian coasts is lower than in the Atlantic sites, but it could be anyway attractive if site-specific devices were properly tailored. In fact, the Tyrrhenian Sea shows an interesting energy potential: a number of offshore island and specific locations around Sicily and Sardinia have an average annual wave power of the order of 10 kW/m.

The lower wave energy off the Italian coasts, compared with the Atlantic ones, does not exclude Italy from exploiting energy from marine renewable resources. It just indicates that deploying classic marine energy converters would not be a cost effective investment at the current state of WEC technology development. Nevertheless, after proper scaling of the devices, their performance in energy conversion could become appealing also for Italian wave climates. In fact, by a site-specific downscaling of the devices their capacity factors become of the same order of magnitude of those calculated for hypothetical wave farms in USA and Canada (Dalton et al., 2010), showing that the most Italian energetic sea sites can be exploited for wave energy production, as well. These results have been obtained by Froude scaling of two of the most promising and documented wave energy devices. New findings may arise from more detailed investigations on dynamical models of some PTO devices in their proper parameter space as recently done by Gomes et al. (2012) for the OWC technology.

References

1. M.T. Pontes, L. Cavaleri and D. Mollison. Ocean waves: energy resource assessment. *Marine Technol. Soc. J.*, 36: 42–51, 2002.
2. M.T. Pontes. Assessing the European wave energy resource. *Trans ASME J. Offshore Mech. Arct. Eng.*, 120: 226–31, 1998.
3. Medatlas Group. *Wind and wave atlas of the Mediterranean Sea*, 2004.
4. P. Filianoti. La disponibilità di energia ondosa su varie aree del pianeta. *Proceedings of the XXVII Congress of Hydraulics and Hydraulics Facilities*, Paper in Italian language, 2000.
5. V. Ferrante, D. Vicinanza, P. Contestabile and L. Cappiotti. Potenzialità dell'energia ondosa lungo le coste italiane. *Proceedings of the XXXII Congress of Hydraulics and Hydraulics Facilities*, Paper in Italian language, 2010.
6. J. Brooke. Wave Energy conversion. *Elsevier Ocean Engineering Book Series*, 2003.
7. AF de O. Falcão. Wave energy utilization: A review of the technologies. *Renewable and sustainable energy reviews*, 14: 899–918, 2010.
8. A. Clément, P. McCullen, AF de O. Falcão et al. Wave energy in Europe: current status and perspectives. *Renewable and sustainable energy reviews*, 6: 405-431, 2002.
9. R. Piscopia, R. Inghilesi, A. Panizzo, S. Corsini and L. Franco. Analysis of 12-year wave measurements by the Italian wave network. *Proceedings of the 28th ICCE Conference*, pp. 121-133, 2002.
10. K. Budal and J. Falnes. A resonant point absorber of ocean-wave power. *Nature*, 256: 478-479, Corrigendum in 257: 626, 1975.
11. G. Hagerman. Wave power. In *Encyclopedia of Energy Technology and the Environment*, (Edited by A. Bisio and S.G. Boots), pp. 2859-2907, John Wiley & Sons Inc., 1995.
12. Y. Masuda, Y. Miyazaki, O. Yamada et al. Wave power generator assembly, *U.S. Patent N. 4405866*, 1981.
13. APAT. *Atlante delle onde nei mari italiani - Italian wave atlas*, Roma, 2004.
14. K. Hasselmann, T.P. Barnett, E. Bouws et al. Measurements of wind-wave grow and swell decay during the Joint North Sea Wave Project (JONSWAP), *Ergaenzungsheft zur Deutschen Hydrographischen Zeitschrift Reihe, A8*, 12, 1973.
15. Ocean Power Delivery. <http://www.oceanpd.com>, 2000.
16. AquaEnergy Group, 2002. <http://www.aquaenergygroup.com>
17. A. Weinstein, G. Fredrikson, M. J. Parks and K. Neislen. AquaBuOY – the offshore wave energy converter: Numerical modeling and optimization. *Ocean Energy Conference*, Aqua Energy Ltd, 2004.
18. Pelamis. Ocean energy. <http://www.pelamiswave.com>, 2008.
19. G.J. Dalton, R. Alcorn and T. Lewis. Case study feasibility analysis of the Pelamis wave energy converter in Ireland, Portugal and North America. *Renewable Energy*, 35: 443–455, 2010.
20. R.P.F. Gomes, J.C.C. Henriques, L.M.C. Gato and AF de O. Falcão. Hydrodynamic optimization of an axisymmetric floating oscillating water column for wave energy conversion. *Renewable Energy*, 44: 328-339, 2012.

Extreme waves in the Central Mediterranean Sea for design of offshore wind farms and wave energy devices

F. Arena¹, A. Carillo², V. Laface³, G. Malara⁴, A. Romolo⁵ and G. Sannino⁶

¹ *Mediterranea University, NOEL laboratory, School of engineering, Loc. Feo di Vito, 89122 Reggio Calabria, Italy, arena@unirc.it*

² *ENEA - Ocean Modelling Unit, via Anguillarese 301, 00123 Rome, Italy, adriana.carillo@casaccia.enea.it*

³ *Mediterranea University, NOEL laboratory, School of engineering, Loc. Feo di Vito, 89122 Reggio Calabria, Italy, valentina.laface@unirc.it*

⁴ *Mediterranea University, NOEL laboratory, School of engineering, Loc. Feo di Vito, 89122 Reggio Calabria, Italy, giovanni.malara@unirc.it*

⁵ *Mediterranea University, NOEL laboratory, School of engineering, Loc. Feo di Vito, 89122 Reggio Calabria, Italy, aromolo@unirc.it*

⁶ *ENEA - Ocean Modelling Unit, via Anguillarese 301, 00123 Rome, Italy, gianmaria.sannino@enea.it*

Abstract – This paper proposes the analysis of extreme waves in the Mediterranean Sea, for design of sea structures, including supports for offshore wind farms and wave energy devices. Input data are significant wave heights H_s given by buoys data and by a numerical simulation performed on the Mediterranean Sea between 2001 and 2009, with a third generation ocean wave model.

Extreme waves are modeled by applying the Equivalent Power Storm (EPS) model, which represents any actual storm by means of two parameters. The former gives the storm intensity, and is equal to the maximum significant wave height during the actual storm; the latter represents the storm duration. The structure of the storms depends upon a power law, with a λ exponent: for $\lambda = 1$ we have triangular storms (Boccotti, 2000; Arena & Pavone, 2006, 2009), for $\lambda = 2$ parabolic storms, for $\lambda = 0.5$ cusp storms and so on (Fedele and Arena, 2010).

The EPS model is applied for calculating the return period of a sea storm in which the maximum significant wave height exceeds a fixed threshold. This analysis is proposed for some storms recorded in any considered location. Then the significant wave height is calculated for several values of the return period. These values are required for the design of devices used as support of wind farms, or for production of electrical power from wave energy.

1. Introduction

The design of offshore wind farms and of wave energy devices involves the characterization of the wave climate and of extreme events at a certain location. Such analysis allows for the estimation of the sea state used for the structural design. Further, it plays a key role in the design of any wave energy device, since optimization of energy harvesting characteristics is highly dependent on a reliable estimate of the wave energy available at that location.

The wave climate investigation requires two fundamental steps: wave data measurements, from which significant wave heights and peak spectral periods are calculated, and long-term statistical analysis of the data. It is emphasized that, in the context of wave energy devices, such analysis is fundamental for calculating energy related quantities. Indeed, the mean annual electric energy produced by the plant or the mean downtime, that is the time interval in which the device is not working, can be estimated only by long-term statistical analysis.

Several methods are available in the open literature for calculating long-term statistics. For instance, the Annual Maxima and the Peak Over Threshold (Guedes Soares and Scotto, 2001) models are widely employed in the calculation of extreme sea states. In this paper, the Equivalent Power Storm (EPS) (Fedele and Arena, 2010) model is used in conjunction with field measurements for estimating the return values associated to a certain significant wave height threshold (for estimating the return period of the event, given a fixed threshold of significant wave height) and the mean persistence of the significant wave height over a certain threshold in a sea storm. The EPS model is a generalization of the ETS (Equivalent Triangular Storm) model proposed in the eighties by Boccotti (1986). The key idea of the model is that a certain storm can be replaced by an ideal storm, which is equivalent to the real one in a specified probabilistic sense. Boccotti considered a triangular storm, which is fully characterised by only two parameters: the height and the base of the triangle (Arena & Pavone, 2006, 2009). Fedele and Arena (2010) have utilized an ideal storm represented by a power law function. The usefulness of the method is related to the empirical observation, based on the processing of hundreds of storms, that the probability distribution of the maximum expected wave heights are well interpreted by this model (Boccotti, 2000). Therefore, it provides a way for producing ideal storms which are probabilistically equivalent to the real ones.

Starting from the EPS concept, it is possible to define an ideal sea as the counterpart of a real sea. That is, since a real sea is a sequence of storms, an ideal sea is a sequence of EPSs equivalent to the real ones. In doing so, the mathematical treatment of the problem is highly simplified and the statistical properties are preserved, because each EPS is probabilistically equivalent to a related real storm.

The objective of this paper is to analyse Mediterranean storms by the EPS model. The analysis is performed from the perspective of energy related devices. Thus, the return values and the mean persistence are determined in order to provide an estimate of the downtime. Such an analysis is mandatory during the design of any device. Indeed, return values and downtime are connected, respectively, to the mean number of times per year in which the device must be deactivated and to the mean time duration, in a storm, in which the device must be deactivated for preserving the safety of the plant.

In the first part of the paper, wave measurements are presented. Data are provided by a WAM model and by RON (Italian buoys network) measurements. Then, the mathematical background of the EPS model is introduced. The recorded data are used in conjunction with the EPS model for estimating the afore-mentioned quantities. Finally, concluding remarks highlight the main results of this analysis.

1. Wave data

1.1 Third order generation ocean wave model for the Mediterranean Sea

A wave climatology based on a ten years long simulation has been performed using WAM model (Wave prediction Model, WAMDI-Group 1988). WAM is a third generation wave model which solves the wave transport equation explicitly without any presumptions on the shape of the wave spectrum. Simulations were produced using WAM Cycle 4.5.3 over a domain covering the entire Mediterranean Sea, from 5.50°W to 36.125°E of longitude and from 30.2°N to 45.825°N of latitude. The domain was discretized with a regular grid of 667x251 nodes in spherical coordinates with a uniform resolution of 1/16° in each direction, corresponding to a linear mesh size of 5-7 km. By extending the computational domain over the entire Mediterranean Sea, the wave climate along the Italian coast takes into account both

local wave generation and propagation from distant areas.

Model bathymetry has been calculated from the General Bathymetric Chart of the Oceans (GEBCO) 30 arc-second gridded data set by averaging the depths of data points falling in each computational cell. The directional wave energy density spectrum function has been discretized using 36 directional bins and 32 frequency bins starting from 0.06 Hz with relative size increments of 0.1 between one frequency bin and the next. The simulation has been performed for the period 2001-2010. The model has been forced with six hourly wind fields obtained from the ECMWF operational analysis interpolated at the resolution of $\frac{1}{4}^\circ$.

1.2 RON network

The “Rete Ondametrica Nazionale” (RON) is the reference network for the collection of wave data all around Italy. The network works by means of 15 buoys capable of providing both wave height and direction of propagation. The data are freely available via the ISPRA institute (Istituto Superiore per la Protezione e la Ricerca Ambientale), which gives time series of significant wave height H_s , peak spectral period T_p , average period T_m and dominant wave direction θ obtained by processing the wave data. In this study only the significant wave height H_s is used.

Four locations are considered for the analysis: Alghero, located on the West coast of Sardinia; La Spezia, in the North of Italy; Ponza, in the center of Italy; and Cetraro, in the South of Italy (Fig. 1). These buoys have been chosen as they are placed in the most favourable location for wave climate.

Available data span over various time intervals, as buoys were installed at different times. Table 1 summarizes data availability for each buoy. It is seen that at least 10 years are available. Such time duration is adequate for the application of the ETS model and is sufficient for the calculation of the pertinent parameters (see next paragraph).



Figure 1: Location of the analysed points from the RON buoys and the WAM model.

Table 1: Data availability.

Location	First available data	Last available data
RON - Alghero	01-July-1989	05-April-2008
RON - Cetraro	01-January-1999	05-April-2008
RON - La Spezia	01-July-1989	31-March-2007
RON- Ponza	01-July-1989	31-March-2008
WAM – Genoa	01-January-2001	31-December 2009
WAM – Pantelleria	01-January-2001	31-December 2009
WAM – South-West Sardinia	01-January-2001	31-December 2009
WAM - Civitavecchia	01- January-2001	31-December 2009

The sampling time of the significant wave height is not constant. Specifically, first data were recorded every three hours, while last data were recorded every thirty minutes. Thus, the significant wave heights were filtered in order to keep a homogeneous set of data with 3-hours sampling time.

2. Mathematical background: long-term statistics by the equivalent power storm model

2.1 Probability distribution of significant wave height

Consider $P(H_s > h)$ the probability that, in a sea state, the significant wave height is greater than a fixed threshold h at a certain location. Such probability is determined from wave data and, then, fitted by assumed theoretical distributions. Several distributions are available in the open literature, such as the log-normal distribution by Jasper (1956), the Weibull distribution by Battjes (1970) or combinations of various models as proposed by Haver (1985). The choice of a model is determined by the capability of fitting field data. In this paper, the two-parameter Weibull is considered, given by

$$P(H_s > h) = \exp\left[-\left(\frac{h}{w}\right)^u\right]. \quad (1)$$

The parameter u is a shape parameter. It controls significant wave height values at various probability levels. The parameter w is a scale parameter. In a probabilistic sense, the larger w is, the larger wave heights are at the location. They are determined by fitting significant wave height data at a location. This distribution is widely used for modelling data obtained in the Mediterranean Sea (Boccotti, 2000), in the Atlantic and Pacific Oceans (Guedes Soares, 1986; Arena, 2004; Arena and Pavone, 2006, 2009; Fedele and Arena, 2010).

2.2 Equivalent Power Storm model

A sea storm is a sequence of sea states in which the significant wave height H_s is above a certain, constant, threshold H_s' and does not fall above it for a certain time interval Δt (Boccotti, 2000). The values of the threshold H_s' and of the time interval Δt depend on the characteristics of the recorded sea states and, thus, on the location under study. Boccotti (2000) has proposed the following values: $H_s' = 1.5\bar{H}_s$ (being \bar{H}_s the mean significant wave height obtained by the wave data) and $\Delta t = 12\text{h}$.

The mathematical modelling of a sea storm is quite cumbersome. It involves the modelling of a non-stationary process, which is known, in a statistical sense, only by sets of discrete points. The points are the significant wave height values calculated from buoy measurements. The simplification introduced by Fedele and Arena (2010) is based on the replacement of the time history of the real, recorded, storm by the following ideal time history:

$$h(t) = a \left[1 - \left(\frac{2|t - t_0|}{b} \right)^\lambda \right], \quad t_0 - b/2 \leq t \leq t_0 + b/2 \quad (2)$$

which is a power law (with $\lambda > 0$) function of time. It is seen that by posing $\lambda = 1$, the classical ETS model (Boccotti 2000) is recovered. If $\lambda = 2$ the equivalent storm has a parabolic shape. If $\lambda = 0.5$ the equivalent storm is a cusp.

The parameters a and b are, respectively, the height and the duration of the EPS. The time instant t_0 is the time instant of the maximum significant wave height of the real storm. The height a is assumed equal to the maximum significant wave height of the storm. The duration b is calculated in order to guarantee the equality of the maximum expected wave height of the real storm and of the EPS. The maximum expected wave height is given by equation

$$\bar{H}_{\max} = \int_0^\infty P(H_{\max} > H) dH, \quad (3)$$

where $P(H_{\max} > H)$ is the exceedance probability of H_{\max} . Specifically, $P(H_{\max} > H)$ is given by (Borgman, 1973)

$$P(H_{\max} > H) = 1 - \exp \left\{ \int_0^D \frac{\ln \{ 1 - P[H | H_s = h(t)] \}}{\bar{T}[h(t)]} dt \right\}, \quad (4)$$

being D the storm duration, $h(t)$ the significant wave height time history, \bar{T} the mean zero up-crossing wave period and $P(H | H_s = h)$ the exceedance probability of the crest-to-trough wave height, given $H_s = h$. Eq. (4) reduces, by substitution of eq. (2), to

$$P(H_{\max} > H; a, b) = 1 - \exp \left\{ \frac{b}{\lambda a} \int_0^a \frac{\ln \{ 1 - P(H | H_s = h) \}}{\bar{T}(h)} \left(1 - \frac{h}{a} \right)^{1/\lambda - 1} dh \right\}. \quad (5)$$

Despite the fact that the equality involves only first order moments, in practice the exceedance probabilities $P(H_{\max} > H)$ of the real storm and of the ideal one are quite close to each other. In this regard, the parameter λ can be chosen via a best fit of the tail of the distribution.

2.3 Prediction of the severest operational conditions: return values and mean persistence over the threshold

Consider a wave energy device which operates until a certain significant wave height h is reached. In this context, the return period $R(H_s > h)$ of a storm in which the maximum significant wave height is greater than h and the mean persistence $\bar{D}(h)$ of the significant wave height over h define key quantities for the evaluation of critical operational conditions. $R(H_s > h)$ was derived by Fedele and Arena (2010). It is given by equation

$$R(H_s > h) = \frac{1}{\int_h^{\infty} \frac{a}{\bar{b}(a)} G(\lambda, a) da}, \quad (6)$$

where $\bar{b}(a)$ is the mean base-height regression, which relates the mean value of the bases b to the heights a of the EPSs and $G(\lambda, a)$ is a function related to the probability density function of the EPS heights. The expression of $\bar{b}(a)$ is derived from strictly empirical arguments, as it is highly dependent on the location under examination. Analysis of several data has shown that the mean base-height regression formula

$$\frac{\bar{b}(a)}{b_{10}} = K_1 \exp\left(K_2 \frac{a}{a_{10}}\right), \quad (7)$$

provides a good estimation of $R(H_s > h)$, where K_1 and K_2 are location-dependent parameters and a_{10} and b_{10} are the mean values of the heights and of the duration of the 10N strongest storms in the considered location, with N the number of years of available data. The function $G(\lambda, a)$ is defined as

$$G(\lambda, a) = \begin{cases} \left. \frac{\sin(\pi / \lambda)}{\pi / \lambda} \int_1^{\infty} \frac{d^2 P(H_s > z)}{dz^2} \right|_{a,x} (x - a)^{-1/\lambda} dx; & \text{if } \lambda > 1 \\ \frac{d^2 P(H_s > a)}{da^2}; & \text{if } \lambda = 1. \\ \left. \frac{(-1)^n a^n \sin(\pi \mu)}{n! \pi \mu} \int_1^{\infty} \frac{d^{n+2} P(H_s > z)}{dz^{n+2}} \right|_{a,x} (x - 1)^{-\mu} dx; & \text{if } \lambda = (n + \mu)^{-1} < 1 \end{cases} \quad (8)$$

By definition of return period (6), the mean number of times per year in which critical operational conditions occur, is given by

$$N(H_s > h) = \frac{1}{R(H_s > h)} = \int_h^{\infty} \frac{a}{\bar{b}(a)} G(\lambda, a) da, \quad (9)$$

The calculation of the persistence $\bar{D}(h)$ complements eq. (9) by estimating the mean time duration in which the significant wave height is larger than h in the storms where the maximum

significant wave height is larger than h . The analytical calculation of $\bar{D}(h)$ is straightforward. Indeed, it is given by (Boccotti, 2000)

$$\bar{D}(h) = R(H_s > h)P(H_s > h). \quad (10)$$

Since a wave energy converter is designed for working in a certain significant wave height range, the mean persistence renders an estimate of the mean “downtime”. That is, the mean time interval in which the device does not operate because of the occurrence of the extreme sea states.

3. Results and discussion

3.1 The wave climate at some location in the Italian sea

First of all the data of the buoys of the RON Italian network have been processed for the location of Alghero, Ponza, Cetraro, La Spezia. In addition the wave climate at location of Genoa, Pantelleria, Civitavecchia and South-West of Sardinia has been analysed through the data of the WAM (WAVE prediction Model, WAMDI-Group 1988).

For all the locations, the probability distribution $P(H_s > h)$ has been calculated through the available data, evaluating the distinctive parameters u and w of the site. In Figure 2, the $P(H_s > h)$ are represented in a Weibull plot, where the data (dots) shows a linear trend. The parameters u and w of Eq. (1) for the examined locations are given in Table 2, confirming that the West coasts of Sardinia is characterized by the strongest wave conditions in the Italian seas, since they are distinguished by the highest values of the w parameter. Then, Pantelleria and Ponza are identified by an intense wave climate and Genoa by the lightest one. In addition, the u parameter of the $P(H_s > h)$ gives a measure of the difference of sea wave heights at different level of probability of exceedance. This difference at a certain site is greater as u is larger. For the considered points the u parameter is almost homogeneous.

Afterwards, the sea storms of all the locations have been analysed. The highest storms for the points considered through the WAM are illustrated in the Figure 3. For these sites, the EPS model has been applied and the results are shown in the same figure for $\lambda=1$ (equivalent triangular storm), $\lambda=0.75$, $\lambda=2$ and $\lambda=3$. Considering all the sea storms, the base-height regression for an examined location has been evaluated. This analysis has been carried out for all the considered calculation points of the RON buoys and of the WAM. The regressions are shown in Figure 4 by assuming the heights and the bases of the sea storms normalized, respectively, to a_{10} and b_{10} . A large dispersion of the bases with respect to the b_{10} value is observed for lower height, with a convergence of b/b_{10} to 1 for greatest a/a_{10} . The parameters of the regression (Eq. 7) are given in Table 2. The results confirm the behaviour highlighted through the distribution of the significant wave height at a location. The West coasts of Sardinia are characterized by the most intense storms, with greatest a_{10} parameter.

Table 2: Parameter of the $P(H_s > h)$ distribution and of the base-height regression (Eq. 7) of the sea storms

RON	u	$w(m)$	$a_{10}(m)$	$b_{10}(hours)$	k_1	k_2
Alghero	1.105	1.236	5.6	75	1.309	-0.35
Cetraro	0.903	0.568	3.3	69.3	0.903	0.032
Ponza	1.126	0.833	3.7	72	1.071	-0.13
La Spezia	1.007	0.698	3.6	74.25	0.997	-0.1
WAM	u	$w(m)$	$a_{10}(m)$	$b_{10}(hours)$	k_1	k_2
South-West Sardinia	1.138	1.22	5.21	102.39	1.162	-0.18
Civitavecchia	1.013	0.595	3.18	77.14	1.336	-0.34
Pantelleria	1.151	1.069	4.51	95.81	0.957	0.059
Genoa	0.963	0.481	2.7	80.8	1.228	-0.25

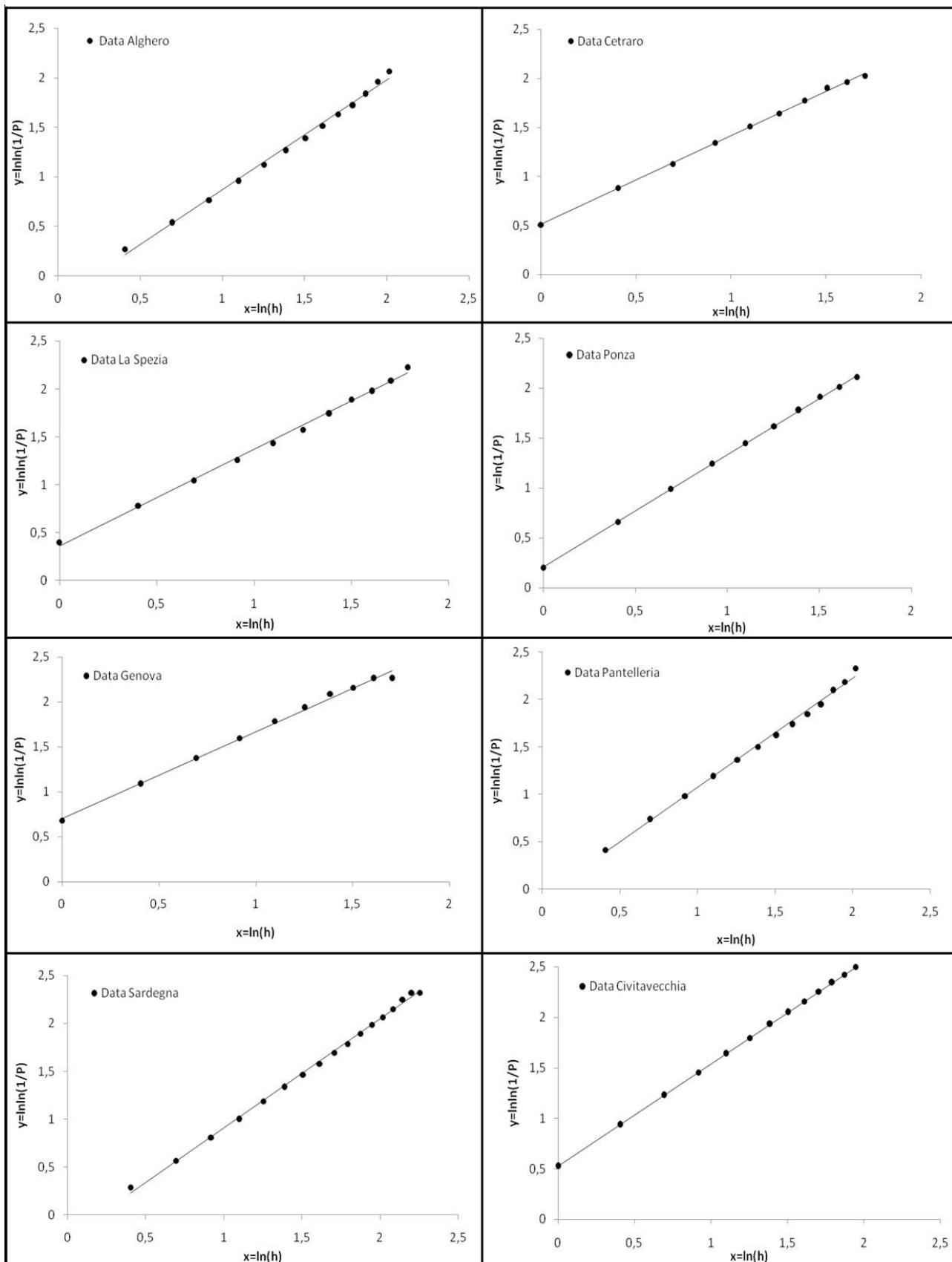


Figure 2: The significant wave height distribution $P(H_S > h)$ for the examined location along the Italian coasts.

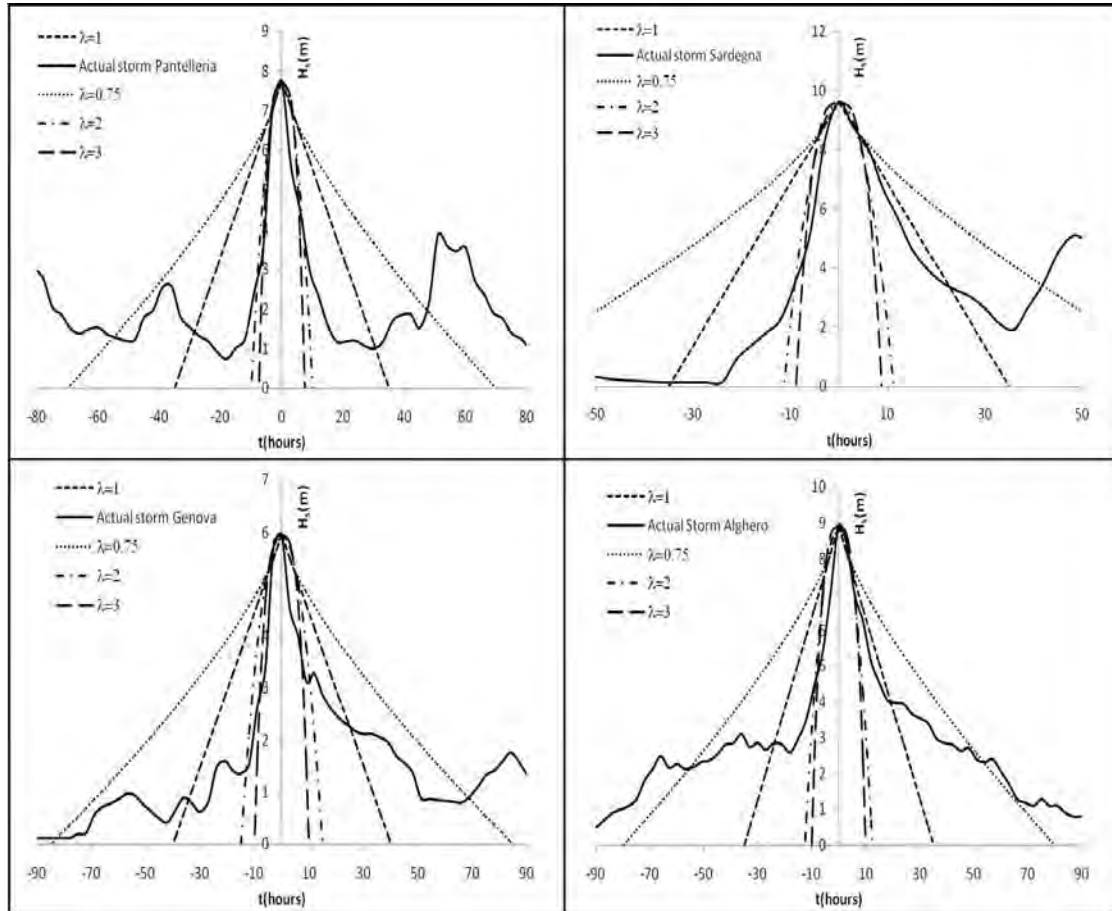


Figure 3: Actual storm (evaluated through the WAM) and the relative EPS storm for the some location along the Italian coasts.

3.2 The return values and mean persistence over the threshold for the Italian sea

Figures 5 and 6 show the return period $R(H_s > h)$ in the considered location through the RON buoys and the grid of the WAM. Moreover, Table 3 gives the threshold of significant wave height for fixed value of $R(H_s > h)$ and the related persistence $\bar{D}(h)$.

Considering lower threshold of return period $R(H_s > h)$, the data of RON buoys processed for the examined locations gives significant differences only for Alghero, characterized by the highest values of H_s at any value of return period. Those are the working conditions for a device or any type of structure at a fixed location.

In Alghero, every 1 year in average a storm with maximum significant wave height greater than 7.2 m is realized. This value of significant wave height is overcome for about 9.5 hours. In La Spezia the threshold of maximum significant wave height will be 4.7 m for the same return period. Through the analyses of WAM data the differences among different locations are greater at every value of return period, confirming the Sardinia the heaviest sea. The persistence over a threshold are greater than those achieved through the data of the RON at any threshold.

Considering higher threshold of return period $R(H_s > h)$, like 100 year, which can be assumed for the design of the structure, the value of the extreme significant wave height in the most severe sea storm is quite different among all the locations. The most intense events with return value of 100 years will occur in the west coast of Sardinia, and in Cetraro and Pantelleria.

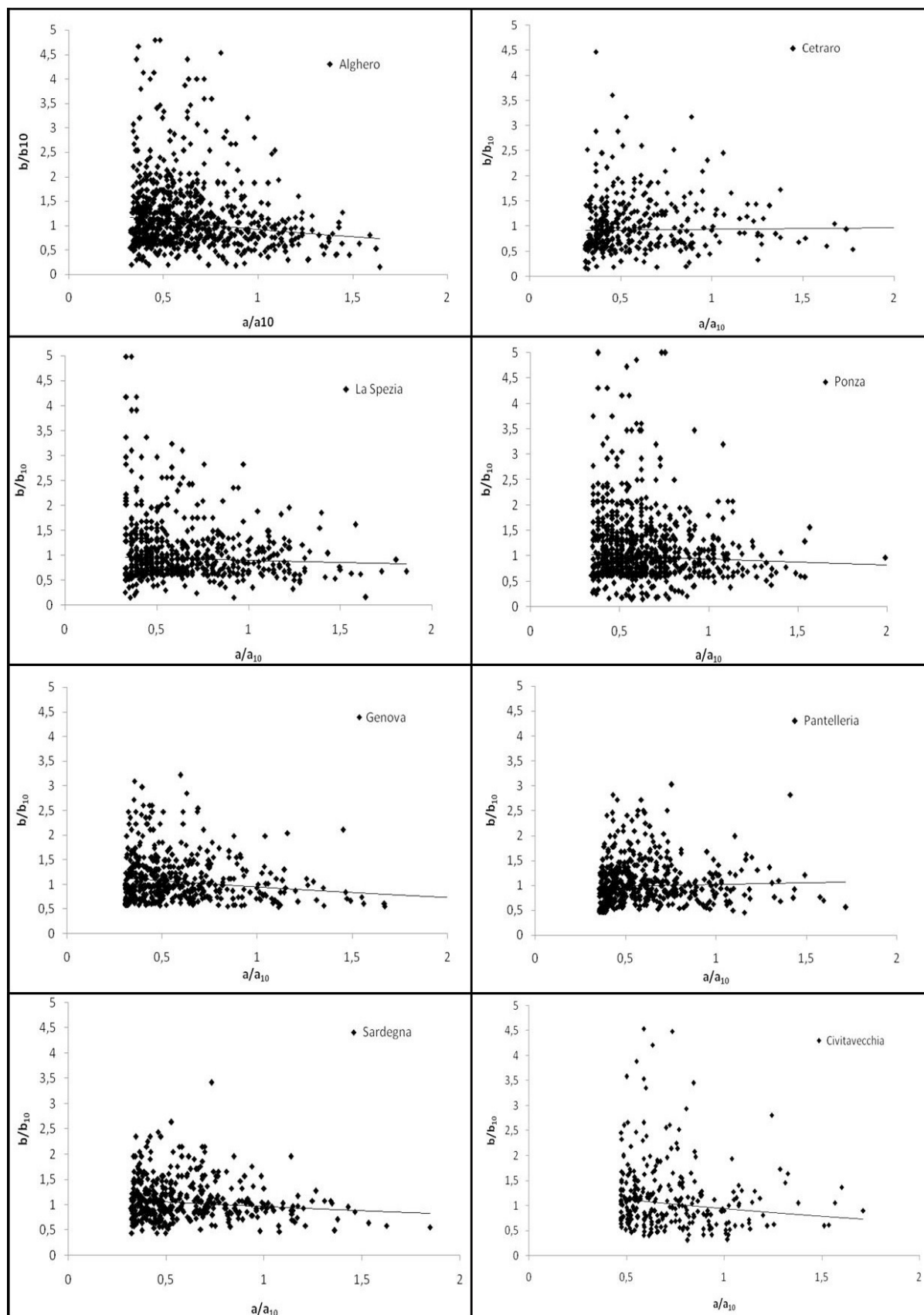


Figure 4: Normalized bases versus normalized height of the highest sea storm in the time of observation (Table 1) for the examined location along the Italian coasts.

Table 3: Significant wave height for fixed threshold of the return period $R(H_s > h)$ and the relative $\bar{D}(h)$

Data	$R(H_s > h) = 1 \text{ year}$		$R(H_s > h) = 5 \text{ years}$	
RON	$h(R) [m]$	$D(h) [\text{hours}]$	$h(R) [m]$	$D(h) [\text{hours}]$
Alghero	7.15	8.35	8.86	6.49
Ponza	4.70	7.82	5.79	6.10
Cetraro	4.80	9.10	6.27	6.94
La Spezia	4.74	9.01	6.01	6.96
WAM	$h(R) [m]$	$D(h) [\text{hours}]$	$h(R) [m]$	$D(h) [\text{hours}]$
Civitavecchia	3.97	9.45	5.03	7.31
Genova	3.48	10.42	4.50	8.00
Sardinia	6.42	11.66	8.00	8.99
Pantelleria	5.59	10.66	6.92	8.25

Data	$R(H_s > h) = 10 \text{ years}$		$R(H_s > h) = 100 \text{ years}$	
RON	$h(R) [m]$	$D(h) [\text{hours}]$	$h(R) [m]$	$D(h) [\text{hours}]$
Alghero	9.57	5.91	11.87	4.49
Ponza	6.24	5.56	7.70	4.24
Cetraro	6.91	6.26	9.03	4.58
La Spezia	6.55	6.31	8.32	4.73
WAM	$h(R) [m]$	$D(h) [\text{hours}]$	$h(R) [m]$	$D(h) [\text{hours}]$
Civitavecchia	5.48	6.64	6.96	5.00
Genova	4.93	7.24	6.35	5.39
Sardinia	8.64	8.15	10.72	6.16
Pantelleria	7.47	7.49	9.22	5.68

4. Conclusions

In the paper the long-term analysis is proposed for waves in the Mediterranean Sea. The results are useful for design of wave energy devices as well as for wind farms, when extreme waves are required to determine the extreme loads. The analysis has been done by considering data from Italian buoys network and data from numerical simulation in the Mediterranean Sea.

The Equivalent Power Storm (EPS) model has been applied, which represents any actual storm by means of two parameters, characterizing the intensity and the duration of the storm. For different values of the return period R , the return value of significant wave height has been calculated. It is useful for design condition, if the largest values of R are considered (for example 100 years) and for operational condition ($R=1, 5$ and 10 years). In both conditions, an additional parameter has been calculated, which gives the mean time in which the significant wave height remains over a fixed threshold (in the storms in which that threshold is exceeded).

The latter may be representative of the downtime, if the threshold of significant wave height is fixed equal to the maximum value that may be accepted for maintaining of operational condition of the devices.

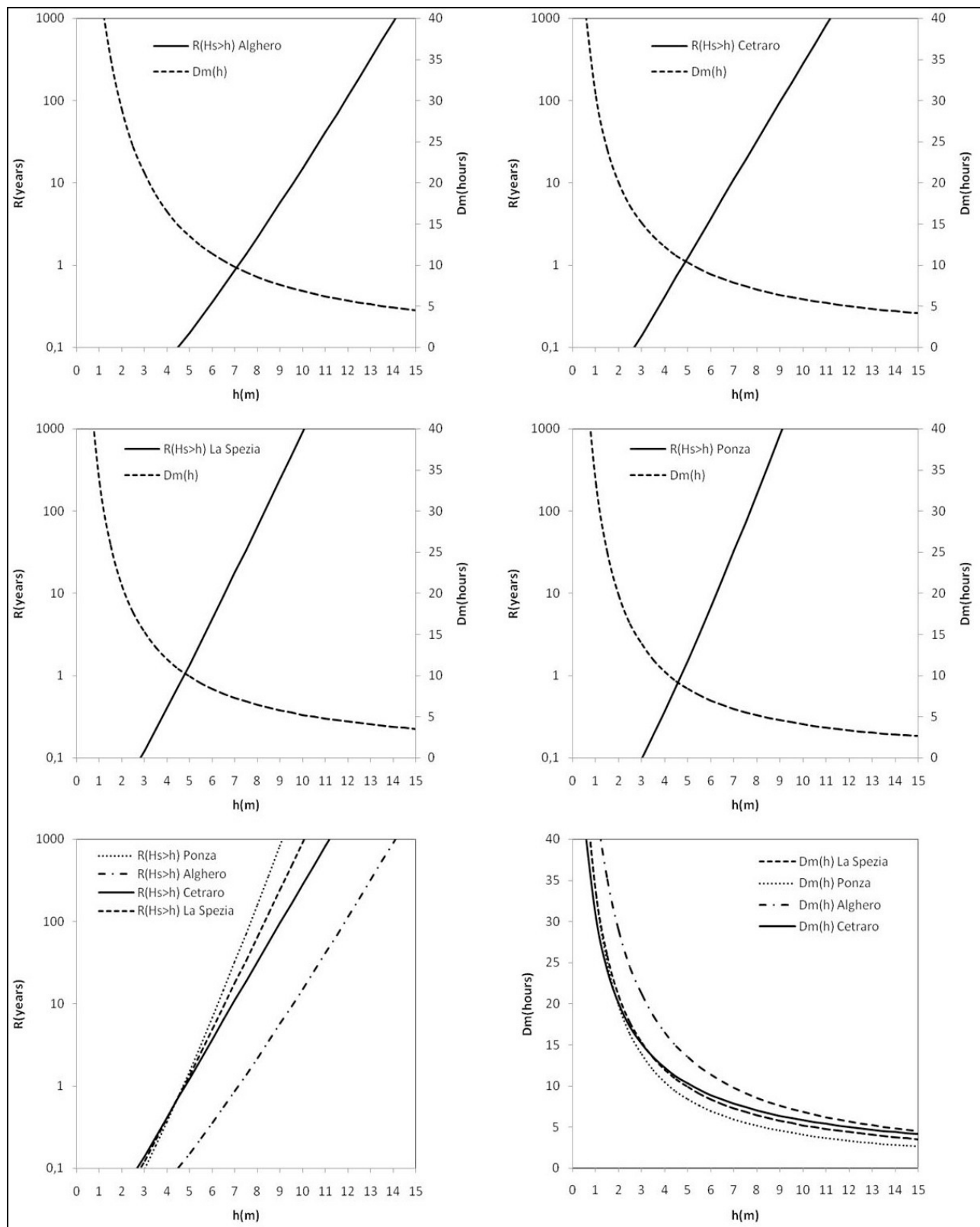


Figure 5: The return period $R(H_S > h)$ and the persistence $\bar{D}(h)$ for the examined Italian RON buoys.

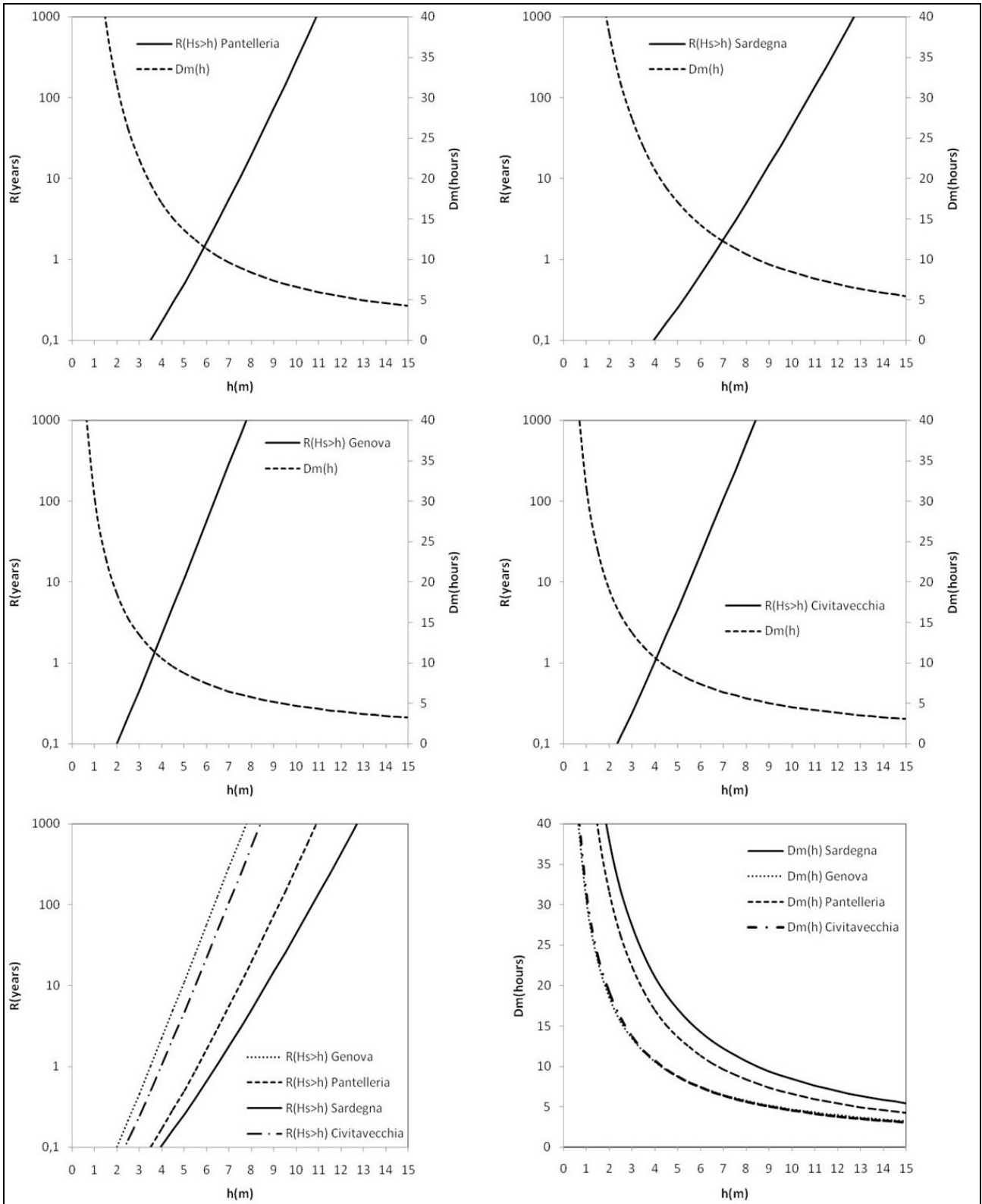


Figure 6: The return period $R(H_S > h)$ and the persistence $\bar{D}(h)$ for the examined Italian location analysed through the WAM model of third generation.

References

1. F. Arena. On the prediction of extreme sea waves. In *Environmental Sciences and Environmental Computing Vol. 2* (Edited by P. Zannetti), pp. 1-50, The EnviroComp Institute, 2004.
2. F. Arena and D. Pavone. Return period of nonlinear high wave crests. *J. Geophys. Res.*, 111(C08004), 2006.
3. F. Arena and D. Pavone. A generalized approach for long-term modelling of extreme crest-to-trough wave heights. *Ocean Modelling*, 26(3-4): 217-225, 2009.
4. J.A. Battjes. Long term wave height distribution at seven stations around the British isles. Wormley, National Oceanographic Institute, *Report A44*, 1970.
5. P. Boccotti. On coastal and offshore structure risk analysis. *Excerpta of the Italian Contribution to the Field of Hydraulic Engineering* 1: 19-36, 1986.
6. P. Boccotti. *Wave mechanics for ocean engineering*. Oxford, England: Elsevier Science, 2000.
7. L.E. Borgman. Probabilities for highest wave in hurricane. *J. Waterw., Harbors Coastal Eng. Div. Amer. Soc. Civ. Eng.* 99: 185-207, 1973.
8. F. Fedele and F. Arena. Long-Term Statistics and Extreme Waves of Sea Storms. *J. Phys. Oceanogr.*, 40: 1106–1117, 2010.
9. C. Guedes Soares. Assessment of the uncertainty in visual observations of wave height. *Ocean Engineering* 13(1): 37-56, 1986.
10. C. Guedes Soares and M. Scotto. Modelling uncertainty in long-term predictions of significant wave height. *Ocean Engineering* 28: 329-342, 2001.
11. S. Haver. Wave climate off northern Norway. *Applied Ocean Research*, 7(2): 85-92, 1985.
12. N.H. Jaspers. Statistical distribution patterns of ocean waves and of wave induced stresses and motions with engineering applications. *Transactions Society Naval Architects and Marine Engineers*, 64: 375–432, 1956.

Session 6: Wave Potential and Technology

Chairmen: A. Corsini, F. Rispoli

Engineering design study of an innovative Hydrokinetic Turbine with on shore foundation

- M. Amelio, S. Barbarelli, G. Florio, N.M. Scornaienchi (Mechanical Engineering Dpt. University of Calabria, Rende (IT)), A. Cutrupi, M. Sanchez-Blanco, G. Lo Zupone (Sintenergy “TechNest” Incubator, University of Calabria, Rende (IT))

Systemic performance of Wells turbines for small scale onshore wave energy converters -

M. Bassetti, A. Corsini, A. Marchegiani, F. Rispoli, E. Tortora, E. Tuccimei (Dpt. of Mech. & Aerospace Engineering, Rome University La Sapienza, Rome (IT))

Roadmapping Ocean Energies for Portugal: a flexible strategy to manage the uncertainties

- C.A. Silva, S. Matias (IDMEC/IST - Institute of Mechanical Engineering, Instituto Superior Técnico, Lisboa (PT)), A. Raventos (WAVEC - Wave Energy Center, Lisboa (PT))

Estimation of the wave energy potential on the offshore Mediterranean Sea and propagation toward a nearshore area -

V. Vannucchi, L. Cappietti (Dip. di Ingegneria Civile e Ambientale - Florence Univ. (IT))

An integrated procedure for the design of a Wells turbine developed for Mediterranean operations

– F. Arena (Mediterranea University, NOEL Laboratory, School of Engineering, Reggio Calabria (IT)), M. Bassetti, A. Corsini, G. Delibra (Dpt. of Mech. & Aerospace Engineering, Rome University La Sapienza, Rome (IT)), G. Faggiolati, S. Piccinini (Faggiolati Pumps S.p.A., Macerata (IT)), F. Rispoli (Dpt. of Mech. & Aerospace Engineering, Rome University La Sapienza, Rome (IT)), G. Romani (Faggiolati Pumps S.p.A., Macerata (IT)), A. Romolo (Mediterranea University, NOEL Laboratory, School of Engineering, Reggio Calabria (IT)), M. Ruggeri (Faggiolati Pumps S.p.A., Macerata (IT)), E. Tuccimei, P. Venturini (Dpt. of Mech. & Aerospace Engineering, Rome University La Sapienza, Rome (IT))

Engineering design study of an innovative hydrokinetic turbine with on shore foundation

M. Amelio¹, S. Barbarelli¹, G. Florio¹, N. M. Scornaienchi¹, A. Cutrupi²,
M. Sánchez-Blanco², G. Lo Zupone²

¹*Mechanical Engineering Department, University of Calabria, Ponte P. Bucci street, Cube 44/C, Rende (CS), Italy, s.barbarelli@unical.it*

²*Sintenergy "TechNest" Incubator – Vermicelli Square, University of Calabria, 87036 Arcavacata (Rende, CS), Italy, a.cutrupi@sintenergy.it*

Abstract – Tidal currents are a resource of great potentiality and not yet fully explored. Several efforts have been made to exploit these resources, but the costs associated to the deployment of tidal plants in marine environments are usually too high. The aim of this work is to present a system able to handle with the above mentioned problems, through the development of a particular hydrokinetic turbine design. In previous works, the authors described a basic turbine configuration achieving interesting performances, although some operational inconveniences were detected, reason why those problems have been faced and the solution optimized and redesigned. As a result, a new design of the turbine is proposed, consisting of a double rotor spinning in opposite directions in order to balance the induced mechanical torque. From preliminary evaluations related to the Messina Strait tidal cycles (Punta Pezzo site, RC, Italy), a single 12 m diameter turbine can supply a power of about 500 kW with a peak current speed of 3 m/s and deliver up to 450 MWh/year.

1. Introduction

There are several ways to harness the energy from renewable sources like wind or water, mainly converting the kinetic flow energy into electrical power [1-8].

The main challenges are: high efficiency and low environmental impact, with reasonable costs. Due to their significant dimensions, the wind turbines have a significant visual impact. In order to reduce this disadvantage, the offshore installations are more often implemented [5], but a good cost/benefits ratio is actually achieved only in shallow waters, not too far from the coast. A convenient alternative is to shift the attention from wind to water, in order to take advantage of the higher fluid density allowing higher power outputs with smaller size turbines.

These turbines can be interesting for a number of reasons:

- lower visual impact, since they are installed underwater and just buoys and/or floating structures are visible, also to ensure a safe navigation;
- reduced risk for fauna: the low rotational speed and number of blades, together with large diameters, allow the fishes and marine species to pass through;
- predictability of tidal currents speeds and ranges (seasonal intensity and directions) are easy and definitely available, unlike the wind resources;
- exploitation of the sea energy resource, due to its predictability, may provide an electrical output of better quality, as to be able to balance against the irregularity of wind power.

In literature many examples of marine turbines are present. To date, these turbines are yet under investigation [6] mainly by fluid dynamic calculations and modeling.

The state of the art in this field is today at an experimental stage and only a few devices have been assembled and tested in real conditions.

The main challenges are to improve their efficiency and reduce the costs. For the first goal, each solution, depending on the turbine type (horizontal or vertical axis) or geometry (Kobold [7], Darrieus [8]) chosen, could be optimised by the theoretical efforts described above and by the possible test in appropriate scale.

The second goal is harder to achieve: the installation of traditional off-shore devices is considerably expensive, time consuming and requires high skilled personnel. The installation of on-shore systems is significantly cheaper, simpler and faster.

In previous works [9-11] a turbine moored to the coast by a steel rope was introduced. Its peculiarity was the use of a deflector which reduces the various hydrodynamic forces involved into a single tensile stress along the rope. Such machine was useful for sites with right bathymetric profile, and high current speeds. Many sites around the world are characterized by the presence of water currents with velocities greater than 3 m/s [3-4]. The proposed installation is however intended for working at Punta Pezzo, in the Messina Strait.

In this paper a further development of this machine is described involving a different torque balancing system together with a visual impact reduction.

2. Single Rotor Tidal Machine: Operating Principle

In previous works [9-11], an innovative tidal machine, able to operate in a power plant whose foundation was placed directly on the coast, has been set up. In the two following sections the main steps summarizing the machine characteristics and its design procedure will be deployed.

2.1 Description of the system

The system has been set up in a simple way considering the possibility to operate with a turbine moored to the coast by a steel rope.

Fig. 1 and 2 show the main views of the single rotor machine. It is moored to the shore by a tensile cable led by a rigid rod. The equilibrium is ensured by a deflector connected to the stator. The forces acting on the deflector (L_r lift and D_r drag) and (T) due to the rotation of the turbine combine in a resultant that tightens the rope (see Fig. 1).

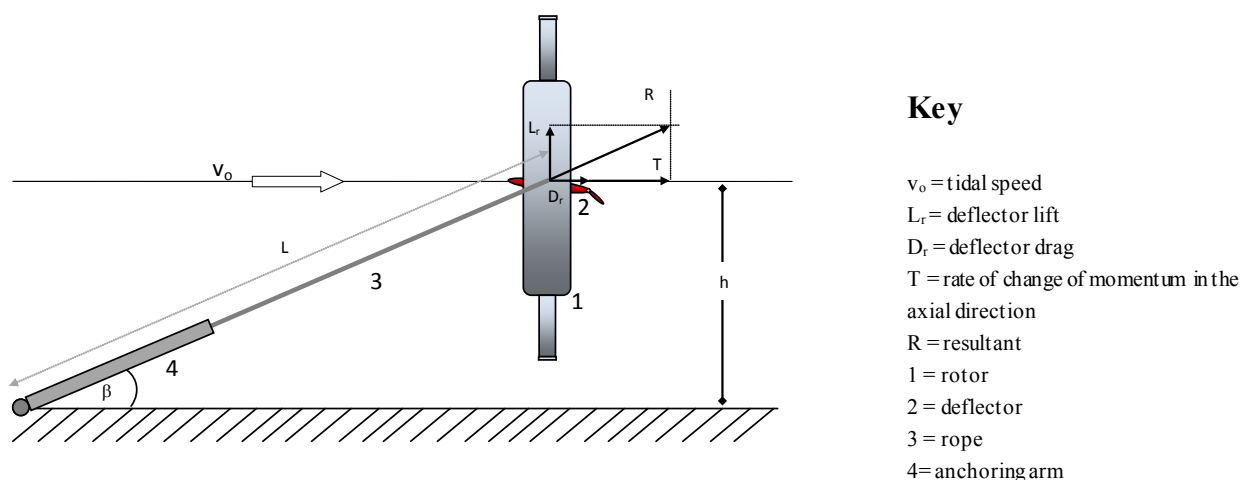


Figure 1: Scheme of the prototype, showing the balance of forces.

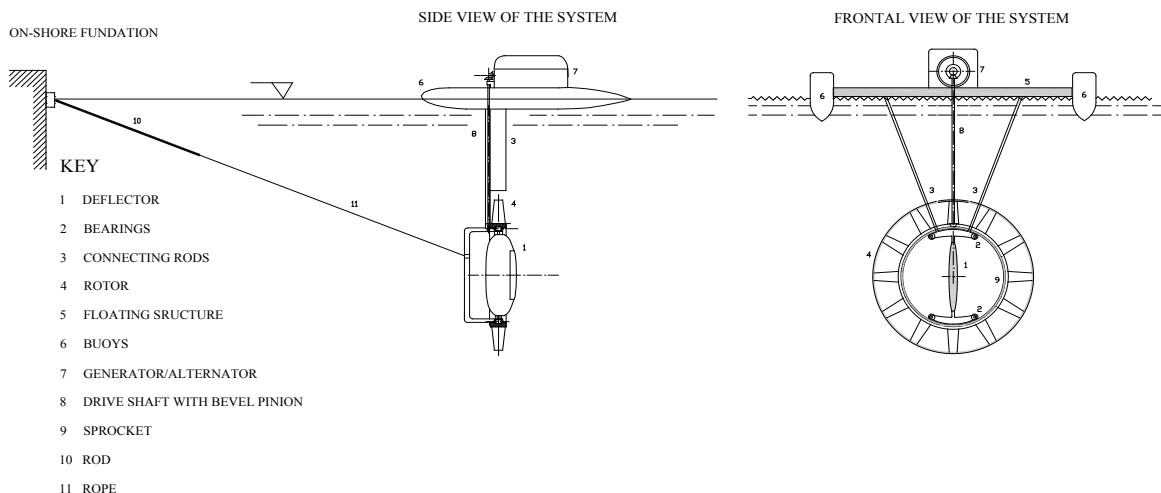


Figure 2: Scheme of the prototype, showing side and frontal views.

Figure 2 shows the overall machine design (frontal & side views). The torque acting on the turbine rotor is fully counterbalanced by the effect of a buoyant system. The buoyant system is connected to a floating structure which hosts the generator/alternator. The rotational motion is driven to the generating device by a drive shaft with a bevel pinion connected through a sprocket. In addition, a rigid frame (see Fig. 2) has been implemented in order to connect the rope to the turbine vertical diameter and ensure the vertical equilibrium.

The turbine weight and the sustaining effect of the buoyant system produce a stabilizing momentum opposing to the one developed by the blades' thrust. The vertical deviation has been estimated in an angle of few degrees, which would have not significant effects for the energy conversion.

The system has been designed to work in sites where the current periodically changes direction. When a tide inversion occurs, a special device rewinds the rope, so that the turbine moves from position 1 (see Fig. 3) to the positions 2 and 3 without changing the angle β_1 : it allows the rod to rotate, so the turbine passes through the positions 4 and 5. Finally the rope is released, so the machine, passing to the position 6, finds a new equilibrium in position 7, with an angle β_2

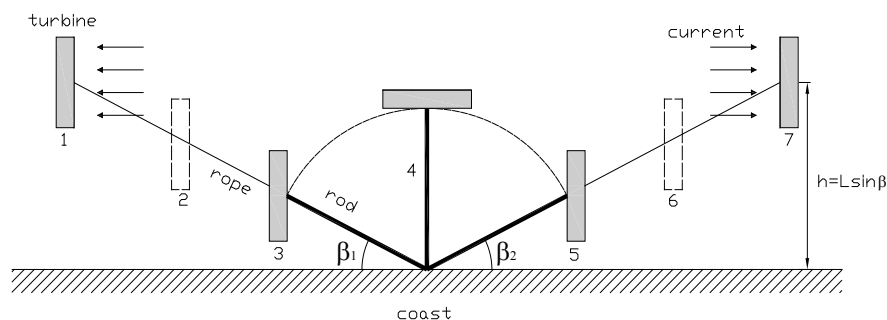


Figure 3: Turbine equilibrium positions varying with the motion of tides.

2.2 Previous results

In order to design machines able to provide hundreds of kW it is necessary to choose values of diameters between 10 and 20 m and to ensure that the turbine works at variable rotational speed and, then, at constant values of λ .

According to the Betz theory [12-15] and assuming that the turbine always works at its best operating condition (input and output speed equal respectively to $2/3 - 1/3$ of the unaltered flow velocity v_o), the forces mentioned in paragraph 2.1 can be calculated through the following equations:

$$T = \rho A_{rot} v(v - v_2) = \frac{4}{9} \rho A_{rot} v_o^2 \quad (1)$$

$$D_r = \frac{1}{2} \rho C_D \left(\frac{2}{3} v_o \right)^2 A_{Defl} \quad (2)$$

$$L_r = \frac{1}{2} \rho C_L \left(\frac{2}{3} v_o \right)^2 A_{Defl} \quad (3)$$

In the previous equations A_{Defl} indicates the deflector area, A_{rot} the blade disc area, C_L the lift coefficient and C_D the drag coefficient.

The resultant assumes the angle β with reference to the coast (see Fig. 1). This angle characterizes the system because it never changes, but it depends only on geometrical parameters.

The equilibrium equation is given by:

$$(T + D_r)L \sin(\beta) = L_r L \cos(\beta) \quad (4)$$

Through the equations (1), (2) and (3) the equilibrium equation becomes:

$$\left[\frac{4}{9} \rho A_{rot} v_o^2 + \frac{1}{2} \rho C_D \left(\frac{2}{3} v_o \right)^2 A_{Defl} \right] \tan(\beta) = \frac{1}{2} \rho C_L \left(\frac{2}{3} v_o \right)^2 A_{Defl} \quad (5)$$

Finally, introducing in eq. (5) the deflector efficiency E and developing the rotor area A_{rot} , the position angle β depends only on the geometrical parameters as shown in the next equation.

$$2 \frac{\pi}{4} D_e^2 \left(1 - \frac{D_i^2}{D_e^2} \right) \tan(\beta) = C_L A_{Defl} \left(1 - \frac{\tan(\beta)}{E} \right) \quad (6)$$

The position angle β is an important design parameter since it allows to set up the turbine internal diameter (D_i), the disc area A_{rot} and then, together with other factors, the power P of the turbine once the external diameter D_e is fixed (see eq. 7).

$$P_e = \eta_e \eta_m C_p(\lambda) A_{rot}(\beta) \rho \frac{v_o^3}{2} \quad (7)$$

The power curves, related to 4 different current velocities, of a turbine with an external diameter equal to 12 m and a C_p coefficient equal to 0,48 change with the β angle as shown in Fig. 4.

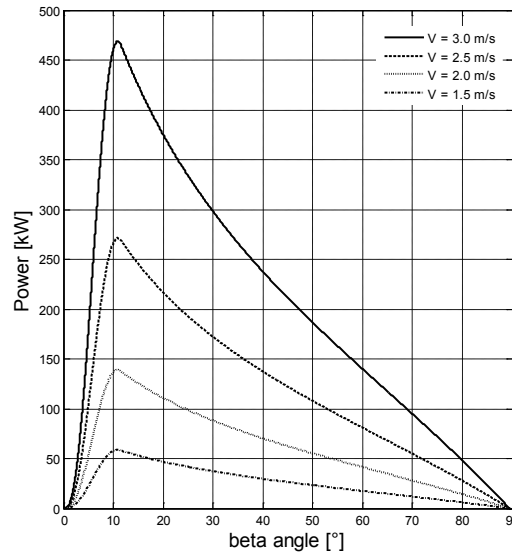


Figure 4: Power curves.

The optimal angle associated with the maximum power, is always 11° regardless from the considered velocity range.

The blades design defines the rotor geometry. For this purpose an appropriate blade profile, the value of the tip speed ratio λ and the number of blades z must be chosen. Once the latest parameters are set up, through the relations of optimal blade design (8), (9), (10), (11) it is possible to obtain the variation along the radius r of two main parameters: the chord c and the angle of attack β_p [15]:

$$c = \frac{1}{z} \cdot \frac{\pi D_e}{\lambda C_{lb}} \cdot \frac{8/9}{\sqrt{\frac{4}{9} + \lambda^2 \mu^2 \left[1 + \frac{2}{9\lambda^2 \mu^2} \right]^2}} \quad (8)$$

$$\beta_p = \phi - \alpha_p \quad (9)$$

where the factors ϕ and μ are expressed by the equations (10) and (11):

$$\phi = \arctg \left(\frac{2/3}{\lambda \mu \left(1 + \frac{2}{9\lambda^2 \mu^2} \right)} \right) \quad (10)$$

$$\mu = \frac{2r}{D_e} \quad (11)$$

At this point it is necessary to choose the tip speed ratio λ value and the number of blades z .

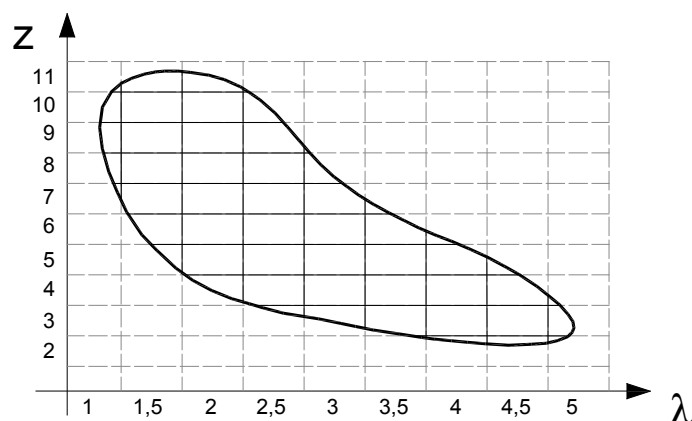


Figure 5: Application chart.

For this purpose, the turbine application chart, shown in Fig. 5, [10-11] is useful to calculate the best values of λ , z . The area surrounded by the black line is defined considering that:

1. very high values of λ indicate too thin blades unable to resist the stresses acting on them;
2. very low values of λ indicate an excessive overlapping of the blades profiles placed around the hub;
3. the number of blades z must be greater than 2;
4. a higher number of blades z is profitable (and then allowed) only if it generates incomes higher than the costs.

The area shown in Fig. 5 is discretized in a finite number of cells by changing λ with steps of 0,5.

To calculate the system energy output it is necessary to know the speed distribution of the streams in the considered site. According to the data supplied in 2008 [16], the hourly current speeds distribution for the Punta Pezzo site has been deduced, and shown in Fig. 6.

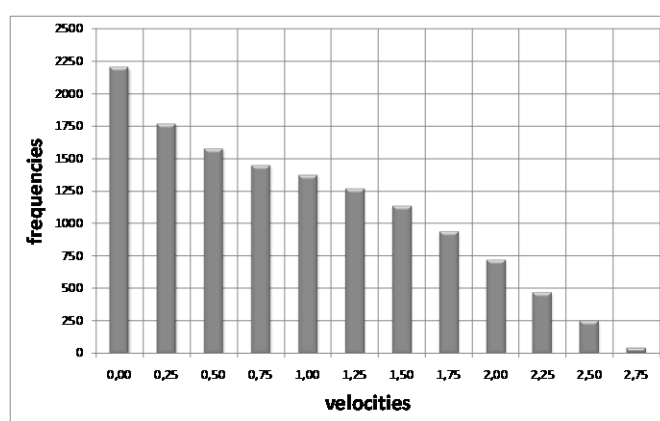


Figure 6: Hourly currents speeds distribution.

Now it is possible to calculate cell by cell, the C_p [14] value and the $V_{startup}$ value [10-11], depending on λ and z (see Figs. 7a and 7b).

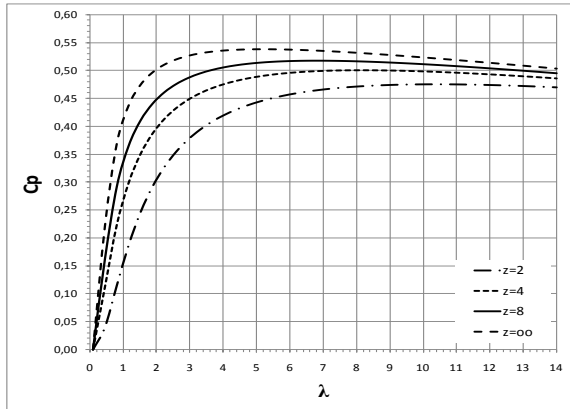


Figure 7a: C_p curves.

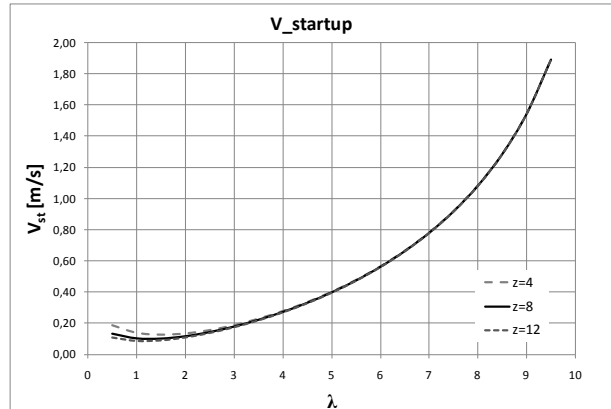


Figure 7b: Cut in velocities.

For each class of velocity represented in Fig. 6, it is possible to calculate the cubic average speed, by considering only values greater than $V_{startup}$, and the turbine power as indicated in equation 7.

The energy output yearly produced for any given configuration (λ, z) , can be calculated by summing the energy of all the velocity classes v_i displayed in Fig. 6:

$$\sum_{\text{year}} P(v_i) \Delta t_i = \frac{1}{2} \rho \eta_e \eta_m C_p(\lambda, z) \sum_{\text{year}} v_i^3 \Delta t_i \quad v_i \geq v_{\text{startup}}(\lambda, z) \quad (12)$$

The cell producing the best energy output (among those displayed in the application chart) fixes the design parameters λ, z .

3. Double Rotor Turbine Outline

The new machine (see scheme in Fig. 8) is arranged by a circular stator implementing two rotors (inside and outside). The two rotors blades are designed in order to allow:

- the same rotation speed but in opposite directions;
- the same torque acting on each rotor.

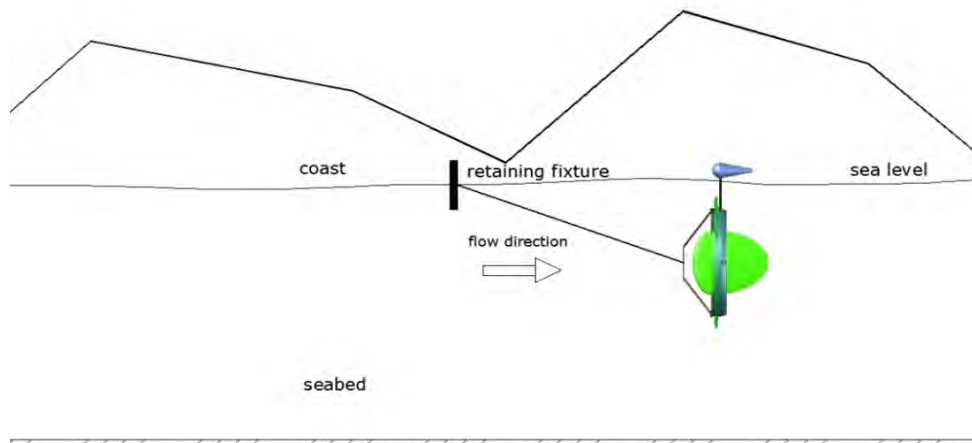


Figure 8: Working scheme.

Architecture of the machine

The two rotor implementation allows a balanced system working without any torsional effects. The compact stabilizer keeps the machine in vertical position at a constant level from the sea surface, as shown in Figs. 9 and 10.

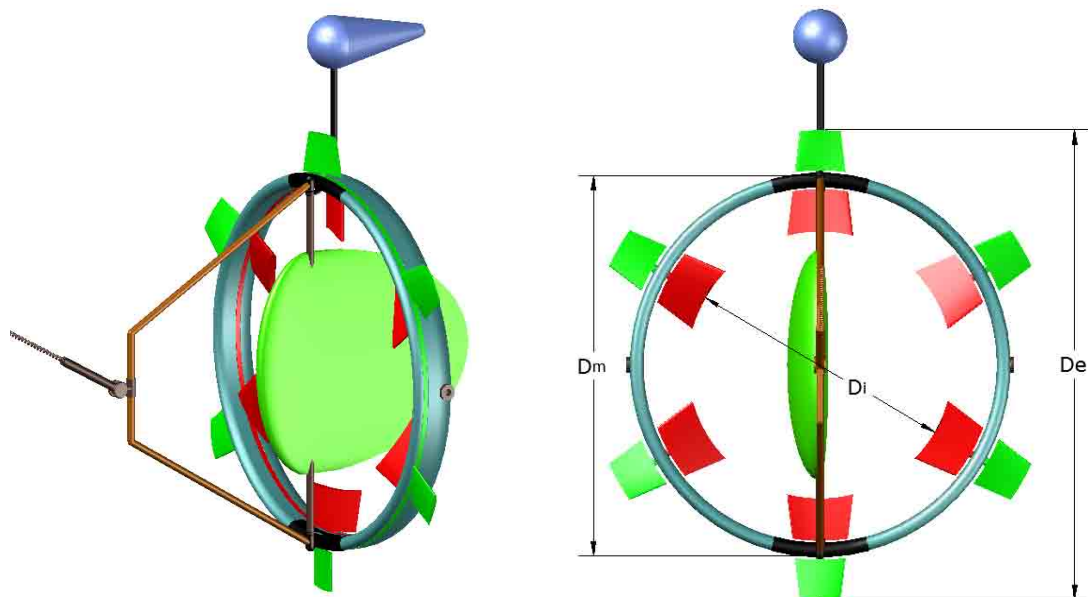


Figure 9: Views of the new turbine.

1. stator
2. inside rotor
3. inside rotor blade
4. outside rotor
5. outside rotor blade
6. level stabilizer
7. level stabilizer support
8. retaining systemstator connector
9. deflector support
10. retaining systemconnector
11. deflector
12. retaining to rope connector fixture

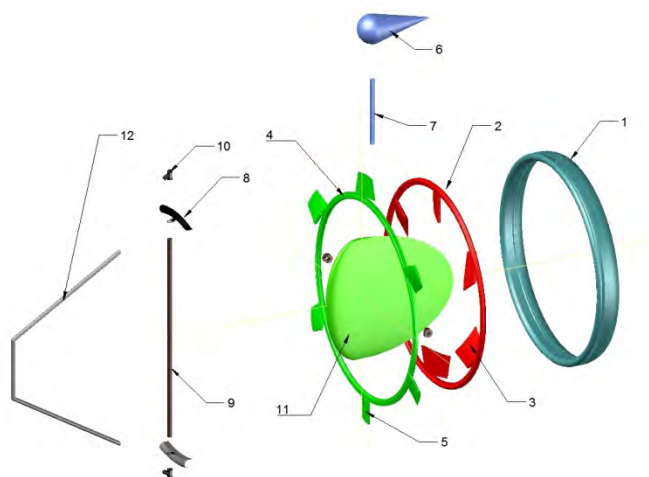


Figure 10: Main parts of the turbine.

Inside each rotor there are several permanent magnets, coupled with their respective coils located inside the stator, which movement will generate the magnetic field needed for producing electricity (see Fig. 11).

Improvements compared to the old configuration

Several features have been developed and implemented for this new machine:

1. the stabilizing system is now easier and lighter, without any widefloating structure (suspended by buoys), as shown in Fig. 2, but just a simple level stabilizer (see Figs. 8, 9);
2. no mechanical devices are now needed to convert mechanical energy into electrical one: a permanent magnet generator is implemented directly on the machine (see Fig. 11);
3. no mechanical transmission, no pinions or gearboxes needed to transfer the motion for producing electrical energy, and, consequently, no mechanical losses are present. The electrical energy produced is driven to the inverter by cables.

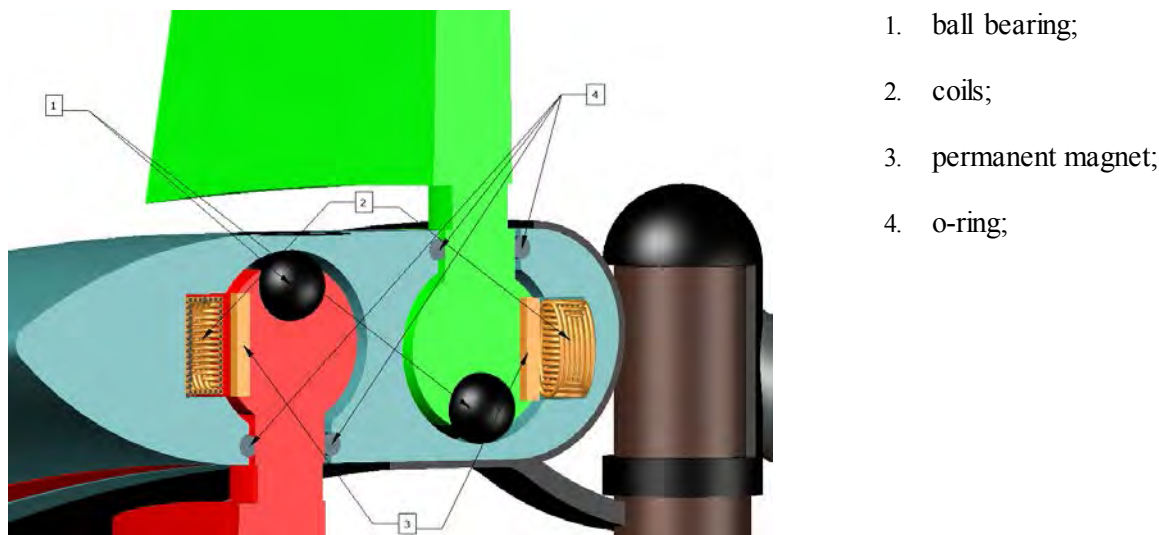


Figure 11: Permanent magnet generator.

3.1 Rotors dimensioning

The calculus procedure is the same defined in the previous works [10-11]. However, in this specific case the turbine is arranged by two rotors working together to achieve a better equilibrium. Each rotor is designed with the equations (8), (9), (10), (11) once the parameters λ and z are fixed. Therefore those parameters for both the rotors are to be considered.

Determination of the tip speed ratios λ_1, λ_2

In order to design the rotors it is necessary to fix some criteria. With the aim to have two electrical generators rotating at the same speed and considering the mechanical balance above described, the main criteria are as follows:

- the rotors must rotate at the same speed in opposite direction;
- the torques acting on the rotors must be the same.

Therefore the powers developed by the two rotors are the same. In the following equations the above criteria are deployed:

$$P_1 = P_2 \quad (13)$$

$$\frac{1}{2} \rho C_p(\lambda_1) A_1 v_0^3 = \frac{1}{2} \rho C_p(\lambda_2) A_2 v_0^3 \quad (14)$$

$$C_p(\lambda_1) A_1 = C_p(\lambda_2) A_2 \quad (15)$$

The power coefficient expression comes from the vortex cylinder theory combined with the Prandtl's theory [15]:

$$C_p \cong \frac{16}{27} \left[\exp(-0,3538 \cdot \lambda^{-1,2946}) - \frac{\lambda}{E_p} \left[1 - \frac{0,93}{z \sqrt{\lambda^2 + 0,445}} \right] \right]^2 \quad (16)$$

By combining equations (15) and (16) and developing the blades areas A_1 and A_2 :

$$\left[\exp(-0,3538 \cdot \lambda_1^{-1,2946}) - \frac{\lambda_1}{E_p} \left[1 - \frac{0,93}{z_1 \sqrt{\lambda_1^2 + 0,445}} \right] \right]^2 \cdot \frac{\pi(D_e^2 - D_m^2)}{4} = \left[\exp(-0,3538 \cdot \lambda_2^{-1,2946}) - \frac{\lambda_2}{E_p} \left[1 - \frac{0,93}{z_2 \sqrt{\lambda_2^2 + 0,445}} \right] \right]^2 \cdot \frac{\pi(D_m^2 - D_i^2)}{4} \quad (17)$$

Considering that:

$$\frac{\lambda_1}{\lambda_2} = \frac{\frac{u_1}{v_0}}{\frac{u_2}{v_0}} = \frac{\frac{\pi n D_e}{\pi n D_m}}{\frac{D_e}{D_m}} \quad (18)$$

or developing with respect to the intermediate diameter D_m :

$$D_m = \frac{\lambda_2}{\lambda_1} D_e \quad (19)$$

and taking into account the design diameter ratio:

$$\frac{D_i}{D_e} = r \quad (20)$$

or :

$$D_i = r D_e \quad (21)$$

the equation (17) becomes:

$$\left[\exp(-0,3538 \cdot \lambda_1^{-1,2946}) - \frac{\lambda_1}{E_p} \left[1 - \frac{0,93}{z_1 \sqrt{\lambda_1^2 + 0,445}} \right] \right]^2 \cdot \frac{\pi D_e^2 \left(1 - \frac{\lambda_2^2}{\lambda_1^2} \right)}{4} = \left[\exp(-0,3538 \cdot \lambda_2^{-1,2946}) - \frac{\lambda_2}{E_p} \left[1 - \frac{0,93}{z_2 \sqrt{\lambda_2^2 + 0,445}} \right] \right]^2 \cdot \frac{\pi D_e^2 \left(\frac{\lambda_2^2}{\lambda_1^2} - r^2 \right)}{4} \quad (22)$$

Once the value of λ_1 (external rotor), the blades number z_1 and z_2 , the external diameter D_e , the internal diameter D_i and thus the ratio r are fixed, through the last equation it is possible to calculate the value of λ_2 (internal rotor).

The couple of values of λ , z , through the equations (8-11), determines the design of the blades for each rotor.

The input of the design procedure is then: the tip speed ratio of the external rotor λ_1 , the number of blade z of each rotor (normally chosen $z_1=z_2$), the external diameter D_e , the diameter ratio r which depends on the position angle β .

The external diameter D_e is a free parameter: it is chosen according to the possibility to install the turbine near the coast in deep waters. For the choice of the internal diameter it is necessary to calculate the power curves shown in Fig. 4: the best power implies an optimal position angle β and then an optimal diameter ratio D_i/D_e (see eq. 6).

Finally on the application chart of the double rotor machine it is possible to look for the cell producing the maximum energy output and so to determine the blade design parameters (λ, z) .

4. Results

The turbine design starts from the choice of the parameters (λ, z) on the application chart (see Fig. 12).

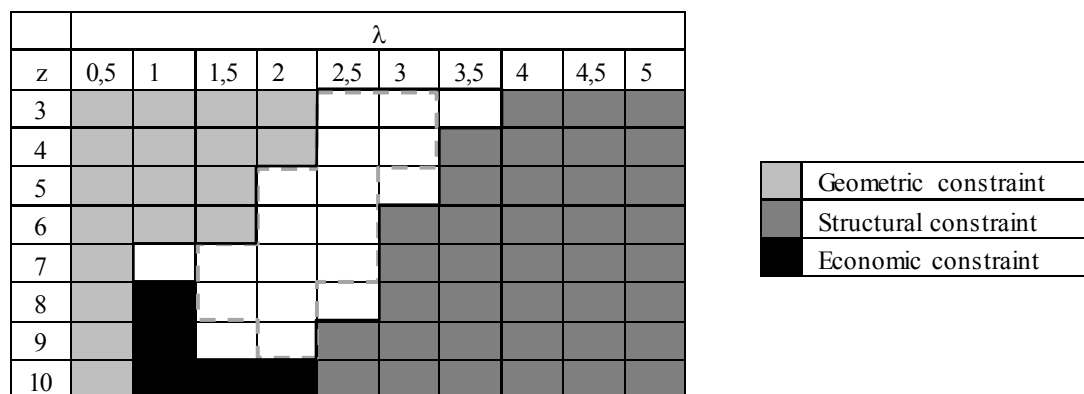


Figure 12: Application chart double rotor turbine.

The above mentioned constrains (geometric, structural and economic) cancel the inadmissible configurations (λ, z) .

In this chart [17], the geometric constrain is fixed by considering that:

- the chord variation occurs without excessive gradient between the blades tip related to the internal rotor and the blades hub related to the external rotor;
- only a difference of 0,3 meters between the two chords above can be allowed.

The structural constraint defines a knock out area for all configurations (λ, z) inducing stresses on the blades higher than the admissible limits for a given material.

The economic constraint is deduced by evaluating if the costs increase required for producing one more blade, involving a higher energy output, is covered by higher incomes.

The chart is drawn up by considering the operating cells of both rotors. The black lines surround the white cells of the external rotor while the dashed gray lines surround the white cells of the internal rotor (see Fig. 12). It is necessary to determine the best energy output among the cells pertinent to the internal rotor and among the cells pertinent to the external rotor.

The energy output is calculated cell by cell by integrating in a year the value of the power $P(v)$ relative to the speed ranges of the considered site,

$$E(\lambda, z) = \int_{year} P(v) dt \quad v \geq v_{startup} \tag{23}$$

The tidal velocities change with the time t according to the following harmonic series [16]:

$$V(t) = A_1 \text{sen} \omega_1 t + A_2 \text{sen} \omega_2 t + A_3 \text{sen} \omega_3 t + A_4 \text{sen} \omega_4 t + A_5 \text{sen} \omega_5 t + A_6 \text{sen} \omega_6 t + A_7 \text{sen} \omega_7 t + A_8 \text{sen} \omega_8 t \quad (24)$$

where the values A_i and ω_i depend on the chosen site. The calculus of the integrate (23) is done by considering values of velocity greater than the turbine startup velocities which depend on the values (λ, z) as shown in Fig. 7.

Fig. 13 shows the energy output level curves obtained for the Calabrian site of Punta Pezzo, located in the Messina Strait. Each curve represents a specific energy level per unit of blade area. The curves are useful to point out the best values (λ_1, z_1) for the external rotor.

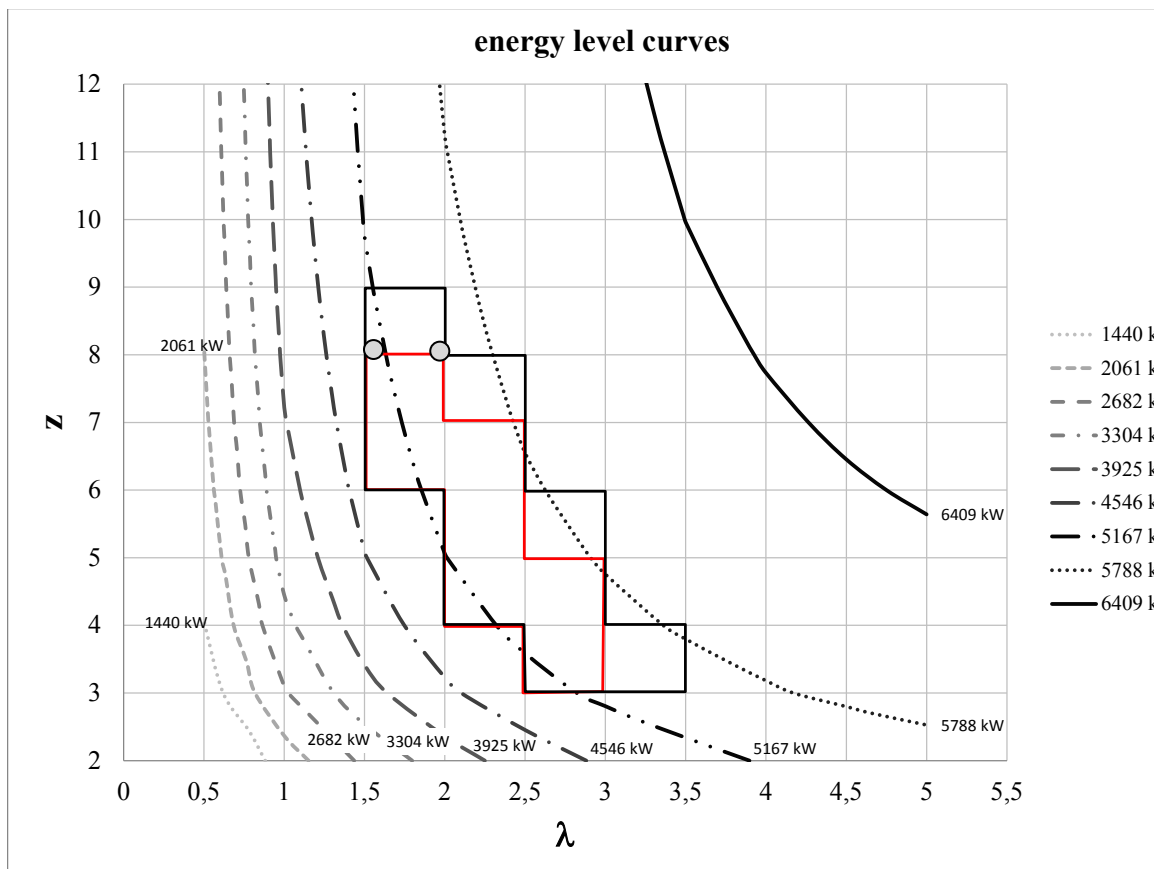


Figure 13: Contour plot.

Obviously the value of λ_2 (internal rotor) depends on the value of λ_1 (external rotor) according to the equation (22). Then, by imposing the same number of blades ($z_1 = z_2$) it is possible to determine the optimal energy output of the whole machine.

In Fig. 13 these values are highlighted. The best value of λ_1 (external rotor) is equal to 2.5 and the best number of blade z_1 is equal to 7. The energy output related to this configuration is 5996 kWh/m². Therefore the values for the internal rotor are: $\lambda_2 = 2, z_2 = 7$ with an energy output of 5685 kWh/m².

Once the value of C_p is known, regarding to the best configuration above calculated, it is possible to draw the power curves by changing the position angle β .

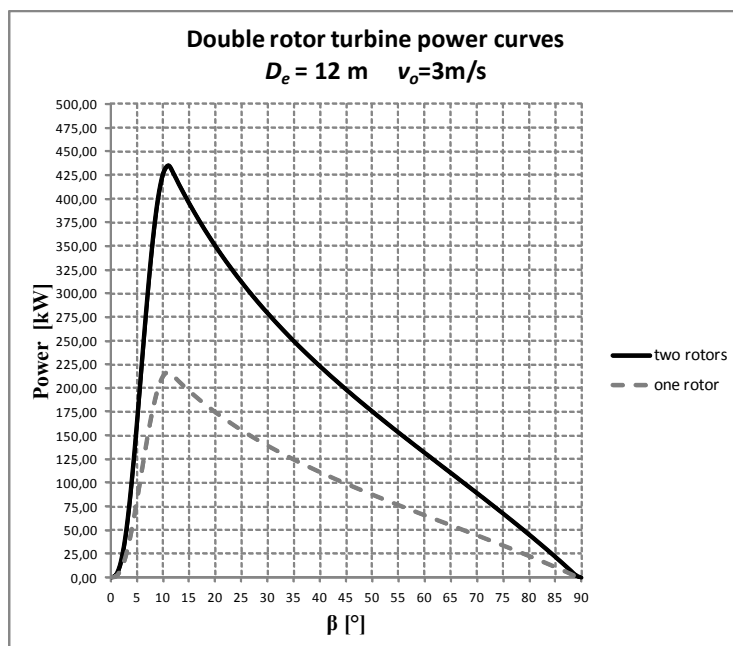


Figure 14: Power curves.

Fig. 14 shows the power curves of the two rotors (internal and external) by considering an overall turbine dimension of 12 m. The area of each rotor is calculated by estimating the intermediate and internal diameter according to equations (19) and (21). In this last figure it is possible to see that the maximum value, corresponding to a power of 430 kW, is obtained for a β equal to 11° . The optimal value of β allows to calculate the diameter ratio r , and then the internal diameter D_i and the value of each disc area. Table 1 reports the main parameters related to the turbine focused in this work.

Table 1: Design parameters.

Parameter	Symbol	value
external diameter	D_e	12,00 m
intermediate diameter	D_m	9,73 m
internal diameter	D_i	6,63 m
external rotor area	A_e	38,74 m ²
internal rotor area	A_i	39,83 m ²
external rotor tip speed ratio	λ_1	2,5
internal rotor tip speed ratio	λ_2	2
external rotor number of blades	z_1	7
internal rotor number of blades	z_2	7
position angle	β	11°

The plant to be installed with the parameters above is able to produce 464.000 kWh/year with an economical revenue of 150.000 €/year. By considering an initial investment of 700.000 € the payback time is equal to 5 years.

5. Conclusions

An important step in the development of a tidal kinetic machine prototype has been achieved. Unlike the first model the new turbine is lighter, easier to operate and it doesn't need an excessive maintenance. The operating principle is the same as the previous configuration: the turbine is moored to the shore by an extensible steel rope and it can reach an equilibrium condition thanks to the presence of a central deflector able to convert all the forces acting on the turbine into a single resultant force aligned with the rope.

The implementation of the two rotors is an innovative element that allows equilibrium in the vertical plane by counterbalancing any torsion effect.

In addition, the built-in permanent magnet generator eliminates further complexity. This way, the system becomes simpler, with even lower environmental impact and requiring fewer economic resources for its implementation and maintenance.

Further studies will be carried out for improving mechanical features such as bearings, seals, materials, connections and so on.

Anyway, the energetic evaluation relative to a pilot plant at the pier of Punta Pezzo (strait of Messina – Italy) does not change substantially referred to the one carried out in the previous work. The energy output is estimated around 464.000 kWh/year with annual incomes of 150.000 € and payback time of 5 years.

References

1. Esteban Miguel, Leary David. Current developments and future prospects of offshore wind and ocean energy. *Appl Energy* 2012;90:128–36. doi:10.1016/j.apenergy.2011.06.01. ISSN 0306-2619.
2. Khan MJ, Bhuyan G, Iqbal MT, Quaicoe JE. Hydrokinetic energy conversion systems and assessment of horizontal and vertical axis turbines for river and tidal applications: a technology status review. *Appl. Energy* 2009; 86(10):1823–35. ISSN 0306-2619. doi:10.1016/j.apenergy.2009.02.017.
3. Rourke Fergal O, Boyle Fergal, Reynolds Anthony. Tidal energy update 2009. *Appl Energy* 2010;87(2):398–409. ISSN 0306-2619. doi: 10.1016/j.apenergy.2009.08.014.
4. Coiro DP. Energia Pulita dalle correnti marine: aspetti scientifici, tecnologici ed economici Proceedings of Energie alternative e buone pratiche ambientali. In: Tuttambiente3, manifestazione Mareamico symposium, June 23–25, 2006, Lucca, Italy.
5. M. Dolores Esteban, J. Javier Diez, Jose S. López, Vicente Negro. Why offshore wind energy. *Renewable Energy*, Volume 36, Issue 2, February 2011, Pages 444–450.
6. Fergal O. Rourke, Fergal Boyle, Anthony Reynolds. Marine current energy devices: Current status and possible future applications in Ireland. *Renewable and Sustainable Energy Reviews* *Renewable and Sustainable Energy Reviews*, Volume 14, Issue 3, April 2010, Pages 1026-1036.
7. Coiro, D.P. and Nicolosi, F. Numerical and Experimental Tests for the Kobold Turbine. Proceedings of SINERGY Symposium, November 1998 Hangzhou, People's Republic of China.
8. Kiho, S., Shiono, M., & Suzuki, K. (1996). The power generation from tidal currents by darrieus turbine. *Renewable Energy*, 9(1-4 SPEC. ISS.), 1242-1245.

9. Amelio M., Barbarelli S., Florio G., Scornaienchi N. M., Cutrupi A., Interdonato A. Turbina Innovativa per il Recupero di Energia dalle Correnti di Marea con Deflettore Centrale e Braccio Meccanico Collegato al Litorale. Proceedings of “65° Congresso Nazionale ATI” Symposium, 13-17 September, 2010, Chia Laguna Resort - Domus De Maria - (Cagliari) – Italy.
10. Amelio M. , Barbarelli S. , Florio G. , Scornaienchi N. M. , Cutrupi A. , Minniti G. , Sanchez Blanco M. Innovative Tidal Turbine with Central Deflector for the Exploitation of River and Sea Currents in On-Shore Installations. Proceedings of ICAE 2011 (International Conference on Applied Energy), Perugia, 16-18 Maggio, 2011.
11. Amelio M. , Barbarelli S. , Florio G. , Scornaienchi N. M. , Cutrupi A. , Minniti G. , Sanchez Blanco M. Innovative Tidal Turbine Exploiting River and Sea Currents in On-Shore Installations. Proceedings of 66° Congresso Nazionale ATI, University of Calabria - Rende (CS), 5-9 settembre, 2011.
12. John D. Anderson. Fundamental of Aerodynamics. McGraw Hill Higher Education; 4th edition 2006.
13. Ira H. Abbott. A.E. von Doenhoff. Theory of Wing Sections: Including a Summary of Airfoil Data [Paperback]. Dover Books on Physics, first edition 1949.
14. Rodolfo Pallabazzer. Sistemi Eolici. Rubbettino Editore, first edition, 2004.
15. Tony Burton, David sharpe, Nick Jenkins, Ervin Bossanyi. Wind Energy Handbook. Wiley. First edition 2001.
16. Istituto Idrografico Della Marina. Tavole di Marea 2008.
17. Osso Roberto, 2012 “Revisione della Geometria di un Prototipo di Turbina Marina Idonea per Impianti On Shore”, Mechanical Engineering Department, University of Calabria Degree Thesis, *work in progress*.

Systemic performance of Wells turbines for small scale onshore wave energy converters

M. Bassetti¹, A. Corsini¹, A. Marchegiani¹, F. Rispoli¹, E. Tortora¹ and E. Tuccimei¹

¹Dipartimento di Ingegneria Meccanica e Aerospaziale, 'Sapienza' University, Via Eudossiana 18, I00184 Roma, Italy, marco.bassetti@uniroma1.it, alessandro.corsini@uniroma1.it, andrea.marchegiani@uniroma1.it, franco.rispoli@uniroma1.it, eileen.tortora@uniroma1.it, esmeralda.tuccimei@uniroma1.it

Abstract – Ocean wave energy is a renewable source which is potentially able to be harnessed for conversion into electrical power grid. In the number of the technologies proposed in the last decades, the Oscillating Water Column (OWC) is to be considered as the most mature solution as demonstrated by the numerous plants operating around the world. Although there are no size parameters affecting the OWC rated power, the size of the on-duty plants is usually about 0.5 MW. This circumstance is due to the definition of a design standards developed for particular open-ocean sea conditions (i.e. specific power level of 30 - 40 kW/m of wave crest). When looking at the Mediterranean sea states, the lower wave energy content demands for a small-scale rating of the conversion system and for a revisited design concept.

To this end, this work is aimed at comparing the performance of different self rectifying air turbines designed by applying two-dimensional semi-empirical analyses. The base-line design solution is that of the monoplane Wells turbine without inlet and outlet guide vanes. This standard has been compared against a newly designed turbine configuration advocating the use of blade sweep as a mean to extend the stall-free operations

The paper, finally, assess the performance of the designed small-scale OWC devices by using transient simulation of the energy conversion chain from wave to wire in a Mediterranean minor island site. The TRNSYS framework is proposed as an effective tool to simulate the integration wave-related non deterministic power contribution to existing energy systems and networks.

1. Introduction

In the wide range of existing renewable energy sources, the wave energy production technologies have had a great boost during the last thirty years. Among them, the technology of Oscillating Water Columns (OWC) is well advanced, but the specific conditions of the Mediterranean Sea and other factors, impose utilization constraints that require further research and testing [1]. The wave energy features have an extremely high dependency on space (such as sea bathymetry and sea-swell direction) and time parameters, although patterns of seasonal variation can be recognized. As a consequence, to identify the best location to deploy a wave energy farm, it is needed an accurate wave energy potential study [2].

One of the most promising self-rectifying air turbine for pneumatic-mechanical energy conversion in an OWC device is Wells turbine, invented by A.A. Wells in 1976 [3], since it maintain constant the sense of rotation, when airflow changes its direction.

The Wells turbine, during his working, is subjected to an oscillating mass flow rate, which varies between zero and a maximum value, which in turns has an extremely large variation from wave to wave and with sea conditions.

In particular, the sea wave typical of the Mediterranean Sea, taken as base line in this study, are characterized by small specific energy level, less than of the ocean waves. In this situation, the Wells turbine presents problems both at low flow rate, negative output power and above a critical value for the onset of the blade stall.

In previous works [4,5] was presented a method to improve the resistance to stall of the turbine, extending the operative margin [6], and based on the adoption of a modification of the blade profile, called compound sweeping. The use of a sweep angle of the blades deliberately controls the lift distribution along the span producing an improvement on the turbine performance.

Several studies on the modification of the blade profile have been carried out in the past [7,3,8]. The paper illustrates a simplified OWC model implemented in the TRNSYS [9] simulation framework, in which the methodology correlates the power output of the system with the geometry (swept compound) adopted for to improve the resistance to stall of the blade stacking line of the Wells turbine, and also with thermodynamic and wave parameters.

The influence of the geometry of the turbine blades on the power output of the OWC device is investigated.

In the open literature several mathematical approaches have been proposed to model the hydrodynamic of an OWC system, covering a wide range [10,11]. Remarkable contributions have been provided by the Instituto Superior Tecnico of Lisbon that established the analytical background in modelling the OWC hydrodynamics and pneumatic conversion forced by a monochromatic wave in the time domain [12], or by random waves in the frequency domain [13,14].

The sea-state data set used in this study were derived from the APAT national wave meter on-line database [15] and taken from [2], in which the available wave energy content is determined on different time periods, summarized in the Table 1. In particular these data referred to the wave buoy located 1.3 km far from Punta della Guardia, in the south coast of Ponza, on a sea depth of 100 m.

The data set with hourly distribution was extended to represent a typical annual behaviour.

Table 1: Ponza buoy characteristics and data [15].

	Month	H _s [m]	T _p [s]	T _m [s]	Dir [°N]	E _w [MJ/m]	P _w [kW/m]
Buoy model Datawell directional wavec MKI Position: 40°52'0.1''N 12°56'60''E Water depth: 100 m	Jan	0.9	7.3	4.1	201.8	2 563.6	2.9
	Feb	0.9	4.8	3.5	160.1	1 896.5	2.4
	Mar	0.6	5.7	4.0	238.9	950.0	1.1
	Apr	0.9	5.7	4.0	212.3	2 612.5	3.0
	May	0.6	5.1	3.8	229.6	1 256.4	1.4
	Jun	0.4	4.5	4.1	223.8	340.6	0.4
	Jul	0.7	5.3	4.5	254.5	1 480.7	1.7
	Aug	0.8	5.4	4.7	235.6	2 413.8	2.7
	Sept	0.7	5.5	4.1	219	1 760.8	2.0
	Oct	0.6	4.8	4.3	173.3	960.1	1.1
	Nov	0.6	5.1	4.5	213.7	1 040.0	1.2
	Dec	1.0	5.9	4.6	186.7	3 596.8	4.0

In Fig. 1 are shown the wave characteristics of the sea state of Ponza referring to the year 2003, and there is represented the wave energy distribution over a year.

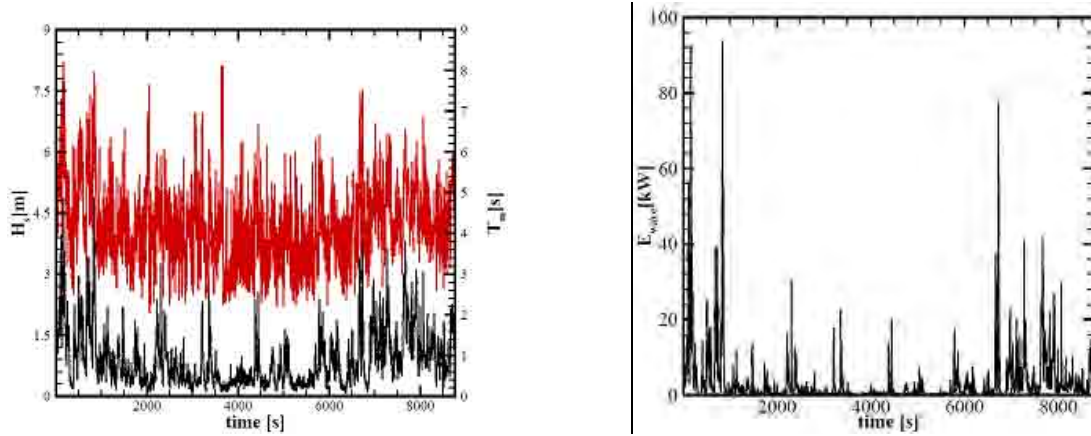


Figure 1: Wave period and amplitude of the sea state of Ponza island in 2003 (left), wave energy during a year (right).

2. Design of Wells turbine

2.1 Correction methodology for sweep angle

In order to extend the operative margin of the Wells turbine and to optimize its aerodynamic performances for applications like Mediterranean Sea, the configuration of the blades can be changed introducing the concept of sweep angle, which has had different definitions in the open literature, spanning from the sweep of airplane wings to those of turbomachinery blades.

Raghunathan [3] defined a sweep angle for the Wells turbine: a blade section at a given radius that is downstream of the adjacent blade section at lower radius has a positive sweep (backward) and when it is upstream sweep is negative (forward). On the base of this meaning, we have adopted the definition of the sweep as the angle between the radial direction and the leading/trailing edge at each blade section [16]: the equivalent sweep angle is the mean value between these two values.

On the base of this sweep definition also a straight blade with constant chord presents a sweep angle variable along the blade span, decreasing from the hub to the tip and it is the same at leading edge and at trailing edge if the mean chord line has the radial direction.

The sweep angle modifies the circulation because the perpendicular component of the relative velocity at the leading edge changes and consequently also the Mach and Reynolds numbers change, as:

$$M_{SW} = M_{USW} \cos \lambda_{EQ} \quad (1)$$

$$Re_{SW} = Re_{USW} \cos \lambda_{EQ} \quad (2)$$

consequently the lift coefficient is reduced: the equation (3) explains the relationship between the stacking line geometry and the spanwise distribution of the circulation [16].

$$\frac{C_{L_{SW}}}{C_{L_{USW}}} = \cos \lambda_{EQ} \quad (3)$$

Consequently, the sweep angle modifies also the drag produced on the blade [4], that can be written as [17]

$$C_D(z) = C_{Di}(z) + \psi(z) \cdot \frac{C_L^2(z)}{a} + C_{Df} \quad (4)$$

where C_{Di} is the local induced drag which is obtained from the relation

$$C_{Di}(z) = \frac{C_L(z)}{\Omega} \cdot \left(\beta(z) - \frac{C_L(z)}{a} \right) \quad (5)$$

and C_{DF} measures the form drag and skin friction, i.e., the viscosity effects. The coefficient

$$a = 2\pi \cdot \cos \lambda_{EQ} \cdot \sqrt{\frac{AR}{2 \cdot \cos \lambda_{EQ}}} = \pi \cdot \sqrt{2AR \cos \lambda_{EQ}} \quad (6)$$

is the lift slope whereas

$$\psi(z) = \sqrt{\left\{ 1 + \left(2\pi \cdot \frac{tg \lambda_{EQ}}{\lambda_{EQ}} \cdot z \right)^2 \right\}} - 2\pi \frac{tg \lambda_{EQ}}{\lambda_{EQ}} z \quad (7)$$

is the interpolation function and

$$\Omega = 2 - \sqrt{\frac{AR}{2 \cos \lambda_{EQ}}} \quad (8)$$

is the downwash factor.

C_{LUSW} and C_{DF} are carried out *via* Xfoil 6.94 [18] at each section in which the turbine blade is divided and the correction due to the presence of sweep angle is implemented. Xfoil is an interactive program mostly used for the design and analysis of 2D subsonic isolated airfoils and it is a public domain by Drela and Youngren [18,19] and the 3D blade geometry was derived by stacking 2D blade section data using these viscous analysis options.

Based on this consideration, each blade section is considered as an isolated aerofoil and the lift and drag forces can be resolved into the axial and tangential force components, that the relative coefficients (C_{ax} and C_{θ}) [20] read as:

$$C_{ax0} = C_l \cos \beta_1 + C_d \sin \beta_1 \quad (9)$$

$$C_{\theta 0} = C_l \sin \beta_1 - C_d \cos \beta_1 \quad (10)$$

The total turbine torque and power generated by the Wells turbine with the sweep correction described over are:

$$C_{\theta} = \frac{T}{\rho_a h l z r_{mid} \frac{(U_{mid}^2 + v_{ax}^2)}{2}} \quad (11)$$

$$C_{ax} = \frac{\Delta p Q}{\rho_a h l z v_{ax} \frac{(U_{mid}^2 + v_{ax}^2)}{2}} \quad (12)$$

2.2. Turbine configurations

For the turbine design it is necessary to impose some operative parameters, sea wave period and the time varying law for the volume flow rate. The requirements on rotational speed and casing diameter are driven by the need for a compact unit. Others choices have to be done regarding the turbine dimensions, as hub to tip ratio, number of blades, blade chord, tip clearance [21,22]. The design parameters of the turbine considered in this study are summarized in the Table 2 and they are the same for straight and swept compound configurations.

According to sweep definition, for this investigation the straight blade presents a backward sweep angle that decreases linear from 16.88° at the hub to 7.3° at the tip.

The swept compound blade geometry [4] has been obtained by prescribing, as given in Fig. 3(a), the sweeping forward of those blade sections in the span fraction (from the hub to midspan) where is required an increase of the circulation, and the sweeping backward of the the blade approaching the tip in presence of a spanwise reducing circulation. The value of the sweep angle decrease from 17.94° at the hub to 12.87° at 0.3 span fraction; in the 0.3-0.5 span fraction interval the angle varies from 11.74° to 10.79° ; from midspan to tip the angle decreases from 35.71° to 26.62° .

Table 2: Design parameters of Wells turbine.

Turbine Characteristics			-
D	Casing Diameter	0.75	m
	Blade Profile	NACA0015	-
n	Angular velocity	3600	rpm
χ	Hub-to-Tip Ratio	0.43	-
σ	Blade Solidity	0.4 (st) / 0.7 (sw)	-
Z	Blade Count	7	-
l	Blade Chord	0.095 (st) / 0.101 (sw)	m
p_{cr}	Critical pressure	3158	Pa
P_{nom}	Nominal Power	15	kW

Fig. 2 shows the shape of the two blade configurations considered in this investigation and the corresponding power curves.

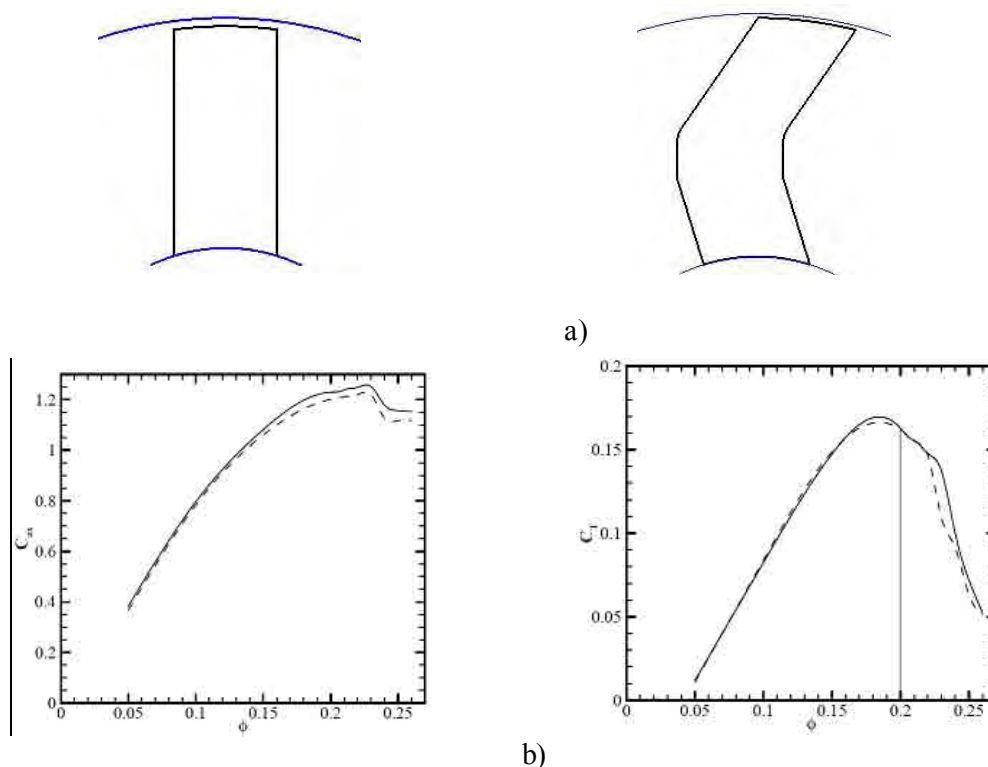


Figure 2. a) Straight and swept compound blades; b) Characteristic curves, power (left) and torque (right). Solid line: straight blade, dashed line: swept blade.

3. Transient model of wave energy conversion

In this investigation is used the TRNSYS software simulation to evaluate the productivity of a device installed on Ponza Island in the Mediterranean Sea and to evaluate how the power output of the plant depends from the geometry of the turbine blades.

TRNSYS [9] is a transient systems simulation program with a modular structure and each module contains a mathematical model for a system component.

The TRNSYS engine calls the system components with a specified sequence based on the input file and iterates until the system of equations is solved. For the present study the TRNSYS model of the OWC power converter is made by three original components developed to simulate, respectively, the OWC chamber and the two configurations of the Wells turbine. The chamber component requires as input the sea state characteristics, like wave period and amplitude, and computes the magnitude of the instantaneous air pressure evolution in time, which is communicated to the turbine component for the evaluation of its performance.

3.1. Hydrodynamic equations model of the OWC

In the pneumatic energy conversion model introduced in the TRNSYS framework the hypothesis taken as baseline are: idealized adiabatic and reversible filling-discharge processes [23], the air considered as a perfect gas and the thermodynamic state within the chamber assumed uniform for all the time.

As first proposed [24], the air pressure fluctuation in the OWC chamber is approximated by means of a simplified algebraic law depending on the chamber geometry (a,b,h,V₀), the air thermodynamics (p_a, ρ_a, γ) (Tab. 3) and the wave quantities (A,T,ω,k). This function reads [24] as:

$$p(t) \cong p_{FT} f_{wave} f_{chamber} = \frac{2b\omega A \sin(ak) / k}{\sqrt{\left(\frac{2\mu b\omega \sin^2(ak)}{g\rho_w k} + \frac{K}{\rho_a}\right)^2 + \left(\frac{\omega V_0}{\gamma p_a}\right)^2}} \cdot \frac{0.05a + 0.45}{0.079T_m + 0.4223} \quad (13)$$

It is worth noting that in (13) there is a dependence by the wave period T_m only, instead for characterizing the chamber geometry it was used the chamber length a.

Table 3. Thermodynamic values of the air.

Thermodynamics			-
p _a	Atmosferic pressure	101325	Pa
ρ _a	Air density	1.25	kg/m ³
ρ _w	Water density	1025	kg/m ³
γ	Specific air ratio	1.4	-

In order to correlate the pressure inside the chamber and the power output of the system, it may write [13]:

$$\Pi = f_p(\Psi) \quad (15)$$

where

$$\Psi = \frac{P}{\rho_a n^2 D^2} \quad (16)$$

$$\Pi = \frac{P}{\rho_a n^3 D^5} \quad (17)$$

are dimensionless coefficients of pressure, power and flow-rate respectively, while D is the outer turbine rotor diameter, n its rotational speed, P the power output and \dot{m} the mass flow rate.

The variable ρ_a is the reference density computed as the stagnation density at the turbine entrance [23].

Into the OWC chamber model has been used the (13) for evaluating the pressure inside the chamber.

The function f_p in (13) depends on the geometry of the turbine, but not on its size and rotational speed. For these reasons, in the present work f_p is approximated with a second-order polynomial:

$$\Pi = c_1\Psi^2 + c_2\Psi + c_3 \quad (18)$$

in which the coefficient c_1 , c_2 , c_3 are depending by the blade configuration, straight and compound swept [4] blades, and by the region in which the turbine is working, pre-stall, stall and post-stall regions. For obtaining these coefficients the correction due to the presence of the sweep angle was introduced in the computation of the power of the turbine and consequently in the power output of the OWC device. The power-pressure curve, from which the coefficients (Tab. 4) of the (18) are taken, is shown in Fig. 3.

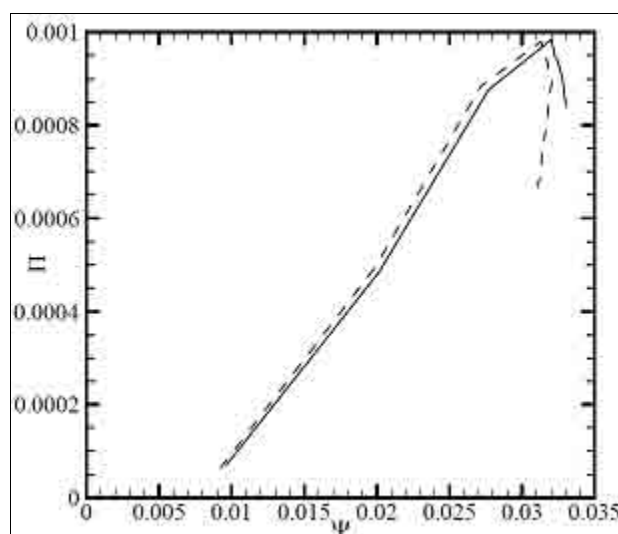


Figure 3: Pressure-Power curve; solid line: straight blade, dashed line: swept blade.

Table 4: Coefficients for different family of Wells turbine.

	<i>Straight blade</i>			<i>Swept blade</i>		
	Pre-stall region	Stall region	Post-stall region	Pre-stall region	Stall region	Post-stall region
c_1	0.6878	-39.305	-175.3	0.7166	-27.082	-84.111
c_2	0.019	2.3727	11.316	0.0197	1.6065	5.2242
c_3	-0.0002	-0.0347	-0.1817	-0.0002	-0.0228	-0.0801

3.2. The test case of Ponza island

The TRNSYS OWC model is used to evaluate the productivity of a device installed on Ponza Island in the Mediterranean Sea, with the data presented in the Fig. 1 and Tab. 1.

In the Table 5 are summarized the input data, the sea reference conditions and the dimensions of the chamber used for the TRNSYS simulations.

Table 5: Input data: OWC chamber dimensions and wave reference conditions.

Sea Conditions			(units)
H_s	Significant Height	1.1	m
T	Period	5	s
Q	Max Volume flow rate	8.2	m ³ /s
H	Water depth	50	m
Chamber Characteristics			-
A	Chamber length	4	m
B	Chamber width	2	m
V_0	Chamber Volume	16	m ³

4. Results

The performance of the two Wells turbines are summarized in Table 6: the power available with the swept blade is slightly reduced with respect to the straight blade. Table 7 and Figure 5 show, instead, the rise of productivity with swept blade especially with low wave power, typical condition of Mediterranean Sea. This fact can be seen also in pressure-power curve (Figure 4) where swept blade curve has a bigger power coefficient than the straight blade at the same pressure coefficient before stall.

Table 6: Power output for straight and Swept blade.

	P_{max} (kW)	P_{av} (kW)	η
Straight blade	17.61	6.52	0.89
Swept blade	16.28	6.52	0.87

Table 7: Productivity at different power levels.

	Energy up to 10% P_{nom} (kWh)	Duty time up to 10% P_{nom} (hours)	Energy up to 35% P_{nom} (kWh)	Duty time up to 35% P_{nom} (hours)	Energy up to 50% P_{nom} (kWh)	Duty time up to 50% P_{nom} (hours)
Straight blade	56555.41	5357	52011.33	3941	48043.24	3325
Swept blade	56506.87	5463	52038.07	4050	48220.88	3448

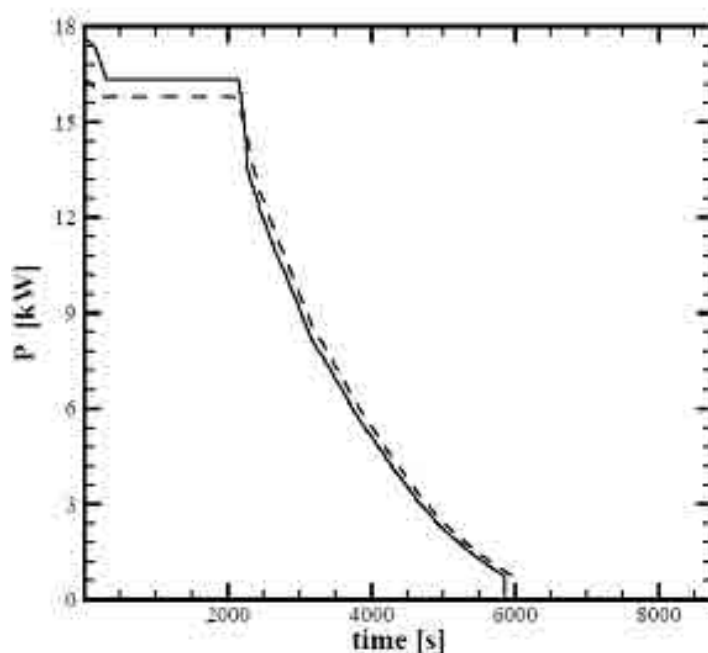


Figure 4: Frequency distribution of power output for straight (solid line) and swept (dashed line) blade.

5. Conclusion

A model for OWC device coupled with a Wells Turbine was developed.

The hydrodynamic model of the pneumatic conversion of the wave motion into the pressure inside the chamber of an OWC was described, correlating it with the power output of the device. The corresponding equations implemented in a TRNSYS program were also shown.

A stand alone power system located in the island of Ponza is taken as a test case, to simulate and evaluate the different productivity of an OWC coupled with the two different Wells turbines considered. The results of this study show that though the Wells turbine with straight blades has a higher power output, the swept compound turbine presents a longer duty time that is more useful for a stand-alone application like the test case considered, in particular for the sea state conditions characterized by a low energy density like the Mediterranean Sea.

Acknowledgements

The authors acknowledge Italian Environment Protection Agency (APAT) for providing the sea wave states data and are indebted to Eleonora Marro for helping with wave data analyses and also to Stefano Minotti for contributing to the study of the different configuration of Wells turbine.

Nomenclature

- A Chamber length, m
- B Chamber width, m
- AR Aspect ratio
- C_{ax} Power coefficient
- C_{θ} Torque coefficient
- C_L Lift coefficient of a blade

C_D Drag coefficient of a blade
 C_d Drag coefficient of an aerofoil
 C_l Lift coefficient of an aerofoil
 D Outer diameter of the rotor, m
 H_S Significant height of the wave, m
 k wave number
 l blade chord, m
 n rotational speed
 \dot{m} mass flow rate, kg/s
 p pressure, Pa
 P power output, W
 Q volume flow rate, m³/s
 r radius, m
 T Wave period, s
 Z Number of blades

Greek symbols

β_I incidence angle
 χ hub to tip ratio
 λ_{EQ} equivalent sweep angle
 ρ density
 σ blade solidity
 η efficiency

Subscripts and superscripts

a Air
 av Average
 ax Axial
 θ Tangential
 0 Isolated aerofoil
 max Maximum
 mid Midspan
 nom Nominal
 sw Swept
 usw Unswept

References

- [1] A-OES Annual Report 2006.
- [2] A. Corsini, E. Marro, F. Rispoli, E. Tortora. Space-time mapping of wave Energy conversion potential in Mediterranean Sea states. *Proc. ASME-ATI-UIT Conference on Thermal and Environmental Issues in Energy Systems*. 2010.

- [3] S. Raghunathan. The Wells air turbine for wave energy conversion. *Prog. Aerospace Sci.* vol. 31, pp. 335-386. 1995.
- [4] A. Corsini, F. Rispoli, E. Tuccimei. Development of air turbines for small power OWC. *EWTEC Proceedings*. Southampton (UK), September 2011.
- [5] A. Corsini, A. Marchegiani, S. Minotti, F. Rispoli. On the use of blade sweep in Wells turbines for low power generation. *Proc. ICAE*, Perugia, 2011.
- [6] E.N. Jacobs, K.E. Ward, R.M. Pinkerton. The characteristics of 78 related airfoil sections from tests in the variable-density wind tunnel. *NACA Report no. 460*, 1933.
- [7] M.T. Pontes. The ocean: an inexhaustible renewable energy source?. *European Conference*, Galway (Ireland), 2004.
- [8] T.H. Kim, T. Setoguchi, K. Kaneko, S. Raghunathan,. Numerical investigation on the effect of blade sweep on the performance of Wells turbine. *Renewable Energy*, vol. 25, pp. 235-248, 2002.
- [9] S.A. Klein, W.A. Beckam, JW Mitchell, J.A. Duffie, NA Duffie, TL Freeman, JC Mitchell, JE Braun, BL Evans, JP Kummer, RE Urban, A Fiksel, JW Thornton, NJ Blair, PM Williams, DE Bradley. TRNSYS –A Transient System Simulation Program. Version 15.1. Solar Energy Laboratory, University of Wisconsin, Madison, 2000.
- [10] A.Brendmo, J.Falnes, P.M.Lillebekken. Linear modelling of Oscillating Columns including viscous loss. *Applied Ocean Research*, pp.65-75, 1996.
- [11] Y.M.C. Delauré, A. Lewis. 3D hydrodynamic modelling of fixed oscillating water column wave power plant by a boundary element methods. *Ocean Engineering*, Vol.30, pp.309-330, 2003.
- [12] A.F. de O. Falcão, P.A.p. Justino. OWC wave energy devices with air flow control. *Ocean Engineering*, pp.1275-1295, 1999.
- [13] A.F. de O. Falcão, R.J.A. Rodriguez. Stochastic modelling of OWC wave power plant performance. *Applied Ocean Research*, pp.59-71, 2002.
- [14] A.F. de O. Falcão. Control of an oscillating-water-column wave plant for maximum energy production. *Applied Ocean Research*, pp.73-82, 2002.
- [15] National Environment Protection Agency (APAT). Sea wave database. Available from: www.idromare.it.
- [16] J. Vad. Effects of sweep and spanwise changing circulation applied to airfoils: a case study. *Journal of Computational and Applied Mechanics*, vol. 5, n. 2, pp. 383-400, 2004.
- [17] D. Kuchemann. A simple method for calculating the span and chordwise loading on straight and swept wings of any given aspect ratio at subsonic speeds. *Ministry of Supply, Aeronautical Research Council Report and Memoranda n. 2935*, 1956.
- [18] M. Drela, H. Youngren (2001) XFOIL 6.94 User Primer. [Online]. Available: http://web.mit.edu/drela/Public/web/xfoil/xfoil_doc.txt.
- [19] The XFOIL 6.94 website. [Online]. Available: <http://web.mit.edu/drela/Public/web/xfoil/>
- [20] S.L. Dixon and C.A Hall. Fluid Mechanics and Thermodynamics of Turbomachinery. 6th ed., Butterworth-Heinemann, Elsevier, Usa, 2010.
- [21] T. Heath, T.J.T. Whittaker, C.B. Boake. The design, construction and operation of the LIMPET wave energy converter (Islay, Scotland). Proceeding *4th European Wave Power Conference*. 4th-6th, December 2000, Aalborg (Denmark), paper B2.
- [22] A.F. De O. Falcão. The shoreline OWC wave power plant at the Azores. *Proceedings of the Fourth European Wave Energy Conference*, Aalborg (Denmark) Paper B1, 2000.
- [23] A.F. de O. Falcão, P.A.p. Justino. OWC wave energy devices with air flow control. *Ocean Engineering*. pp.1275-1295, 1999.
- [24] A. Corsini, F. Rispoli. Modeling of wave energy conversion with an Oscillating Water Column device. *OWEMES conference*, 2006.

Roadmapping Ocean Energies for Portugal: a flexible strategy to manage the uncertainties

C.A. Silva¹, S. Matias¹, A. Raventos²

¹*IDMEC/IST – Institute of Mechanical Engineering, Instituto Superior Técnico
Av. Rovisco Pais, 1, 1049-001 Lisbon, Portugal, csilva@dem.ist.utl.pt*

²*WAVEC – Wave Energy Center*

Av. Manuel da Maia, n° 36, r/c Dto., 1000-201 Lisboa

Abstract – Roadmaps have been an important policy instrument to promote the development of clean energy technologies, as it is the case of marine energies in the last 5 years. However, most of the roadmaps have missed their own proposed goals, due to a lack of sensitivity analysis to uncertain parameters, reducing their effectiveness as a policy mechanism.

This paper presents a new threefold methodology to develop technology roadmaps that are flexible enough to deal with the uncertainties by: 1) assessing the uncertainty of different parameters and its impact on roadmaps; 2) analyzing different scenarios corresponding to different combinations of uncertain parameters; 3) monitoring the progress of the roadmap using a list of key indicators and automatically update it according to the scenarios previously defined.

The methodology was applied to development of a flexible strategy to aid policy makers to promote marine energies in Portugal, contributing for the country low carbon energy strategy and the economic development.

1. Introduction

Portugal is today one of the European and world leaders on electricity production using renewable resources. The 51% share in 2010 corresponded to the 4th place in EU-27 [1], mostly due to hydro and wind resources. But the government is aiming to achieve 60% in 2020 [2], following the European strategy for energy and to attain this goal, it is necessary to diversify the renewable resources portfolio for electricity production.

From the set different renewable resources for electricity production, marine energies (wave, tide and offshore wind) have a large potential of application in Portugal. All together, these energy resources may contribute with at least 20 TWh/year of electric energy, which represents 40% of the actual consumption [3]. Over the last 30 years, Portugal has been on the front edge of marine energies research and development: the first wave power plant (400 kW) in the world that was connected to the distribution grid was built in 1999, the CAO central in Pico, Azores; the first wave power plant (2.25 MW) in the world selling electricity to the grid was in operation for few months in 2009 in Aguçadoura; and the first deep offshore 2MW wind platform has been in operation in Aguçadoura also since November 2011.

Figure 1 presents some pictures of these experimental installations in Portugal.

This has been the result of having more than 30 R&D institutions developing activities in all different areas of the system: resource mapping, environmental impact, plant design, production system design, materials, control systems, grid connection. In the beginning of 2009, these institutions have launched a collaborative network to increase synergies in order to maintain Portugal in the forefront of marine energy systems, not only in terms of research, but mostly to push the developments to the industry and the market.

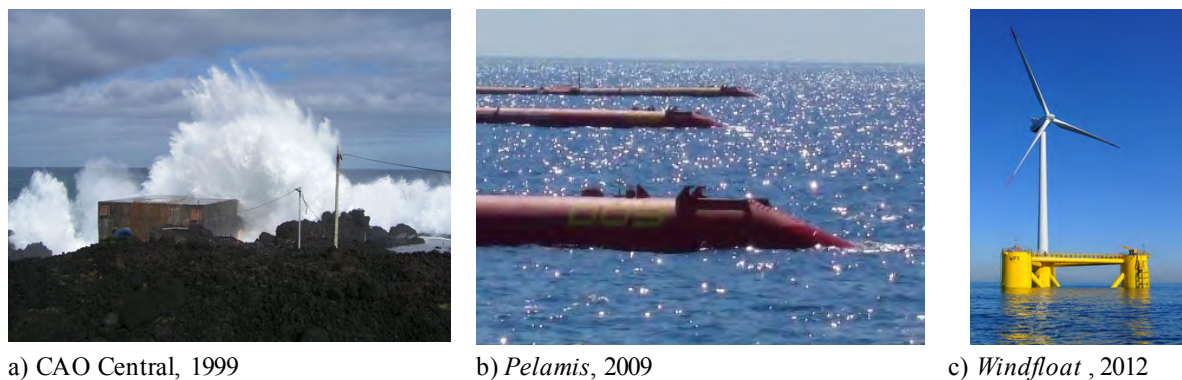


Figure 1: Experimental marine energy installations in Portugal.

And to accomplish this vision, one of the first tasks was to define a common national strategy – a roadmap - that indicated the research, industrial and policy guidelines to promote the leadership of Portugal in the utilization of marine energies for electricity production.

Other European countries have already defined their own agenda in this field for the next decade. United Kingdom published a strategic roadmap [4] that aimed for the deployment of competitive 2GW of generation power using marine energies. This will be achieved through an aggressive action plan matching R&D, policy making and funding collection. However, the plan is rather generic. It does not discuss the uncertainties around the different dimensions (technical, commercial and political) and their impact on the roadmap implementation; it does not consider ways to assess its implementation; it does not provide alternatives pathways in case the implementation is not done according to initial expectancies.

This has been already observed on other roadmaps for deployment of renewable energy resources. See for example the roadmap for offshore wind [5] or the roadmap for distributed generation [6] or the roadmap for photovoltaic systems [7]. The goals are usually clear, but the guidelines to get there are always very generic. These roadmaps always indicate that they are dynamic and should be updated (and have been) but never present any methodology to really cope with the uncertainties around the implementation.

The objective of this paper is to introduce a novel design methodology of roadmaps for renewable and clean energy systems that includes uncertainty management, monitoring and update tools. The methodology has been applied to the development of a roadmap for the marine energies in Portugal, which is of great relevance for the country's social and economic development.

2. Roadmapping: a literature review

Roadmaps are defined as the views of a group of stakeholders on how to get where they want to go in order to achieve their desired objective. It is usually a visual aid that links research programs, development programs, capability targets, and requirements [8]. This practice was initially developed by Motorola more than two decades ago [9], but is now applied by companies, academia and governments [8].

Over the last decade, several roadmaps have been presented to foster the renewable energy resources deployment. The objective of these roadmaps, usually promoted by governmental agencies, is to present guidelines for technological, industrial, market and policy actions that promote the development of non mature technologies and bring them into the market. As examples for Europe, we have the offshore wind [5], the distributed generation [6], the photovoltaic [7], and more recently the wave and tide [4] and the hydrogen [10].

In the US case, one of the most representative roadmap is the one from California State for all renewable energies technologies [11]. All these roadmaps set objectives and milestones for the implementation of renewable energy resources, usually within a 10 to 15 years horizon.

As described in those documents, the methodology used to design those roadmaps consists of defining the present situation, build new visions, analyze the gap between the present state and the visions and finally define an action plan. The visions are based on assumptions and preferences that often describe “wishful thinking” scenarios, discussed on regular meetings and workshops with academia, government and industry stakeholders.

In order to analyze the gap between these visions and the present state, these scenarios can be analyzed in detail by a smaller number of reference stakeholders [4]. Both [4] and [10] describe also an extensive modeling of both technological and socio-economic aspects of the consensus scenario using MARKAL/TIMES tool [12]. This can be complemented with a preliminary uncertainty analysis, considering different degrees (lower and upper bound) of achievement of some of the objectives and measures to accomplish them [9]. The roadmap design usually ends with a discussion of a draft document and approval of changes which define the final action plan.

The typology and methodology applied to design those roadmaps follow a standard technique and therefore presents the same issues: the difficulty of maintaining and update a roadmap; and the lack of customization to particular conditions [13]. The discussed roadmaps do not present any comments around the uncertainties of the proposed plans; do not foresee follow up methodologies to check on the implementation progress of the roadmaps; and do not propose alternative strategies in case the milestones are not achieved in time. And the probability of failing the roadmap is high, as it can be already observed by comparing the objectives of older roadmaps and the present status of deployment.

In 2010, the International Energy Agency released a guide of best practices for designing and implementing roadmaps of renewable technologies that indicates the need to monitor the implementation and the need to perform cyclic reviews to achieve the best implementation [14]. In terms of marine energy technologies, two important documents have been released over the last two years ([15][16]), but none of the documents describes uncertainty, scenario analysis, monitoring indicators nor review strategies.

This paper presents a new threefold methodology to develop technology roadmaps that are flexible enough to deal with the uncertainties by: 1) assessing the uncertainty of different parameters and its impact on roadmaps; 2) analyzing different scenarios corresponding to different combinations of uncertain parameters; 3) monitoring the progress of the roadmap using a list of key indicators and automatically update it according to the scenarios previously defined. This approach is discussed in the following sections in details, applied to the development of the roadmap for marine energies in Portugal.

3. Uncertainty assessment

Roadmaps do not analyze the uncertainties of the proposed plans and not propose alternative strategies plans in case the milestones are not achieved in time, thus, the probability of failing roadmap goals is very high, as it can be observed in Figure 2 by comparing the objectives of older roadmaps ([7],[17]) and the present status of deployment of the corresponding technologies [18].

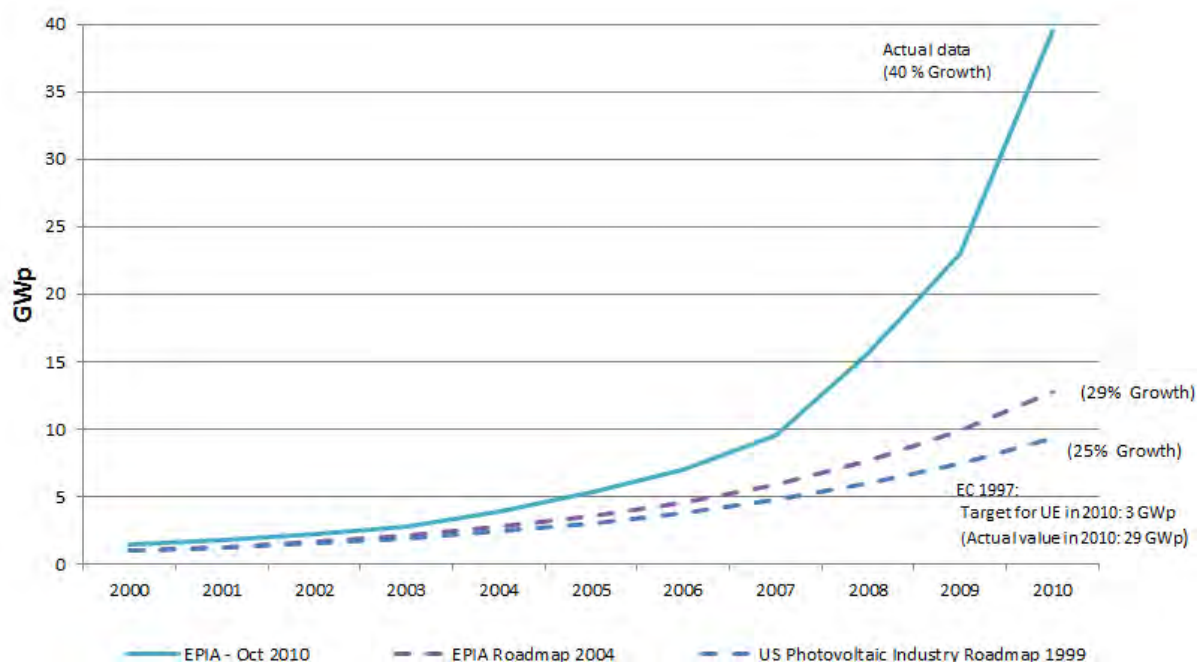


Figure 2: PV growth: Cumulative Installed Capacity Worldwide Estimates vs. Actual Data.

To understand the main parameters uncertainties in the roadmap design, we reviewed the roadmaps from the last decade of solar PV systems enumerated in Table 1.

Table 1: Roadmaps of PV systems from the last decade.

Title	Author	Origin	Date
PV Industry Roadmap	USA PV Industry	USA	1999
Solar Electric Power	USA PV Industry	USA	2001
The Australian PV Industry Roadmap	Australian BCSE	Australia	2004
EPIA Roadmap PV	EPIA	EU	2004
A Vision for Photovoltaic Technology	European Commission	EU	2005
A Roadmap for Photovoltaics: Research in the UK	UK Energy Research Centre - UKERC	UK	2007
Solar Photovoltaic Energy	IEA	World	2009
Trends In Photovoltaic Applications	IEA	World	2009
Unlocking the Sunbelt Potential of Photovoltaics	EPIA	World	2010
PV Status Report	European Commission	EU	2010
Solar Generation 6	EPIA	World	2010

All these roadmaps use the following indicators to describe the technology's evolution:

- Cumulative installed capacity (GW) and Produced electricity (MWh);
- Public/private R&D funding (€);
- Feed-In-Tariffs (€/MWh);
- Levelized Cost of Electricity (€/kWh);
- Technology efficiency.

The analysis of the different roadmaps described in Table 1 showed that certain indicators had large variations from the estimated, such as the cumulative installed capacity (growth rate), or the LCOE. The uncertainty around these parameters could have been reduced if these parameters and others that directly influence them (e.g. R&D investments, capital investments (CAPEX) and feed-in tariff) had been closely monitored and updated [19].

As for the technology efficiency, though the evolution has been slower for the PV technology than previously anticipated, it did not affect significantly the deployment of the technology, as the cumulative installed capacity grew more than estimated.

As a conclusion, it is essential to monitor closely the cumulative installed capacity, the investment in R&D and the Feed-in-Tariffs in order to be able to update the roadmap evolution.

5. Scenario design

Portugal's National Plan for Renewable Energies [20] sets a target of 60% of electricity from renewables in 2020, which is expected to represent 31% of the final demand, in order to comply with the EU2020 strategy [2]. In this plan, the marine energies such as waves and offshore wind are expected to have some contribution by 2020 - 250 MW and 180 MW respectively - while the onshore wind capacity is expected to be 8 GW and solar PV 1GW.

As the objective of the Portuguese roadmap is to contribute to define a long-term strategy for the marine energies, we developed evolution scenarios until 2050. As marine energies will be competing with the other established energies, in particular fossil fuels, we used the IEA Energy outlook scenarios fuel prices estimations for 2050 [21]: the IEA Ref that considers that access to energy will increase; and the IEA 450 that considers that the planet's temperature will only increase 2 °C due to the stabilization of the CO₂ greenhouse gas emissions to 450 ppmCO₂ equivalent. These costs are presented in Table 2 and Table 3.

Table 2: Fuel and CO₂ prices estimations.

Prices	IEA Ref				IEA 450 ppm			
	2010	2015	2030	2050	2010	2015	2030	2050
Coal (k€/TJ)	2,1	2,1	2,5	2,8	2,1	2,0	1,5	1,5
Gas (k€/TJ)	6,5	6,5	9,1	13,6	6,5	6,5	7,1	7,1
CO ₂ (k€/t)	0,02	0,043	0,054	0,54	0,02	0,05	0,11	0,11

For the investment costs of the different technologies, we considered the IEA estimations and two additional scenarios specifically for the marine energies: the WAVEREF and the WAVEOPT. These costs are presented in Table 3.

To estimate the evolution of the different energy mix for electricity generation in Portugal until 2050, we use the TIMES model [12], which provides a technology rich basis for estimating energy dynamics over a long-term, multiple period time horizon. It is usually applied to the analysis of the entire energy sector, but may also applied to study in detail single sectors, as the

electric in this case to project the optimal energy mix that minimizes the total discounted system cost up to 2050, choosing among different energy technologies for the four different scenarios, the combination of the two scenarios of evolution of fuel and CO₂ prices (IEAREF and IEA450) and the two scenarios for marine energies Investments and O&M Costs (WAVEREF and WAVEOPT).

Table 3: Investments and O&M Costs estimations.

Costs	WAVEREF				WAVEOPT			
	2010	2015	2030	2050	2010	2015	2030	2050
Investment (€/kW)								
Coal	1571	1434	1298	1163	1571	1434	1298	1163
Gas	616	581	546	513	616	581	546	513
Wind Onshore	1217	985	864	820	1217	985	864	820
Wind Offshore	2516	1614	1319	1319	2516	1614	1319	1319
Wave	5680	2777	1793	1266	2933	19226	1263	1007
Solar PV	3420	1539	1026	684	3420	1539	1026	684
O&M (€/kW/y)								
Coal	31,4	28,7	26	23,3	31,4	28,7	26	23,3
Gas	12,3	17,4	16,4	15,4	12,3	17,4	16,4	15,4
Wind Onshore	24,3	29,5	25,3	24,6	24,3	29,5	25,3	24,6
Wind Offshore	50,3	48,4	39,6	39,6	50,3	48,4	39,6	39,6
Wave	113,6	83,3	46	38	78,7	57,8	34,4	30,2
Solar PV	68,4	15,4	8,8	6,8	68,4	15,4	8,8	6,8

The results are presented in Figure 3 for each of the 4 scenarios.

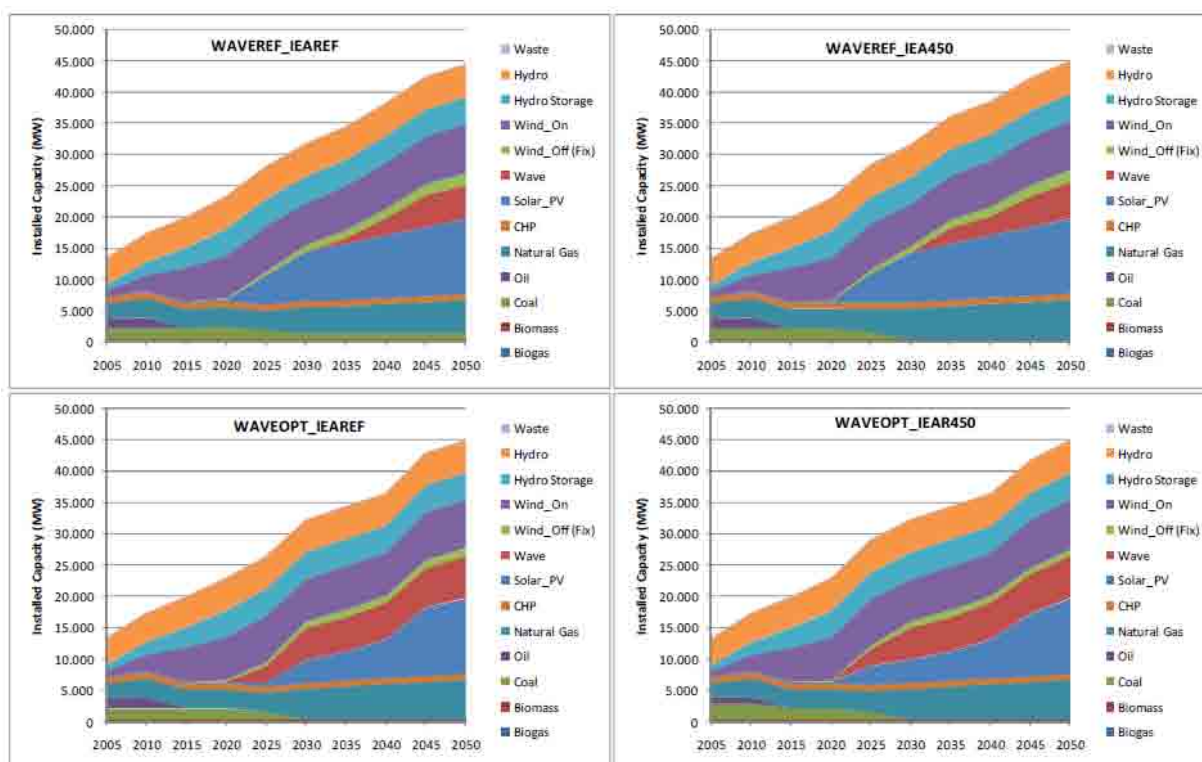


Figure 3: Installed capacity in Portugal for the different scenarios.

The first important result is that coal becomes a non-competitive option by 2020 in the IEAREF scenario and even before in the IEA450 scenario (due to the higher costs of CO₂). Notice that CCS (carbon, capture and storage) technologies were not considered. Gas, however, remains as a competitive option up to 2040, but only to cover peaks in demand. Looking at the renewable resources, onshore wind is the clear winner from 2005 to 2025 (where it reaches its upper bound of installed capacity) together with large hydro that it is always competitive but limited in capacity.

In all scenarios, solar PV is the most competitive technology by 2050 with its maximum capacity and production reached in all scenarios. In any case, the model considers the installation of all technologies as the model considers some dynamics regarding the seasonal and daily variability of the resources and all the resources become complementary. Thus, it is not surprising to see almost 45 GW of installed capacity in 2050 (more than 3 times the capacity in 2005), but relying in renewable resources will certainly lead to an overcapacity of the system, which does not mean necessarily a higher cost, as the model minimizes the total cost of the system.

Wave energy results show that for all scenarios the installed capacity is between 5 and 6.7 GW in 2050, representing a share between 18 to 23% of the electricity demand. This is the second largest share of renewable electricity, only after solar PV (with a share of electricity of 23.3% in 2050) and in front of wind onshore (with 18%). However, this is due to the fact that wind onshore and solar PV are limited to 8 GW and 12 GW respectively in 2050 and the rest of the capacity is attributed to wave (limited to 6.7GW) and wind offshore (limited to 2 GW). Wave energy becomes more competitive than coal and gas between 2020 and 2030 depending on the scenario.

The WAVEREF and WAVEOPT scenarios show significant different projections for wave energy. In the WAVEREF scenario, wave energy only becomes competitive in 2030 with an increasing capacity reaching more than 5 GW in 2050. However from this point on, wave energy rapidly increases its capacity and production and becomes more competitive than offshore wind in 2045. In the optimistic scenario however, wave becomes competitive already in 2020 and reaches its upper boundary of capacity of 5 GW in 2030 and 6.7 GW in 2050.

There is little difference between the IEA Reference and 450 scenarios, except for the case of coal that maintains some marginal capacity in the WAVEREF_IEAREF scenario with lower CO₂ prices, while in all the others disappears in 2030.

6. Monitoring and update

In this section, we present the software tool that has been developed to develop the roadmap for marine energies in Portugal – the *RoadMapping Tool*. The main objective of this application is to build scenarios, monitor and update a technological roadmap automatically. In particular, we want to design a strategy to achieve the 2020 goal of having 250 MW installed capacity of wave energy [20].

On a first stage, the user provides a set of technological data, including initial conditions, historical data and target values that allow building the various economic scenarios for the technology evolution, using growth rate and learning curve to forecast different indicators.

The *RoadMapping Tool* will then monitor these indicators and re-estimate the forecasted values when they start to diverge from the required targets, showing what is required to achieve them. In this way, the application is able to automatically update the roadmap and overcome eventual uncertain events.

The application considers three main scenarios simultaneously: the Reference scenario which is the one that describes the expectations from the stakeholders; the Forecast (Max) scenario

which describes the optimistic view where all the favorable conditions are met; and the Forecast (Min) scenario that describes the most pessimistic view where all the worst conditions are met. All three scenarios can be described by any set of parameters defined by the user regarding fossil fuel prices, deployment of renewable energy technologies, a set of defined targets for installed capacity, etc.

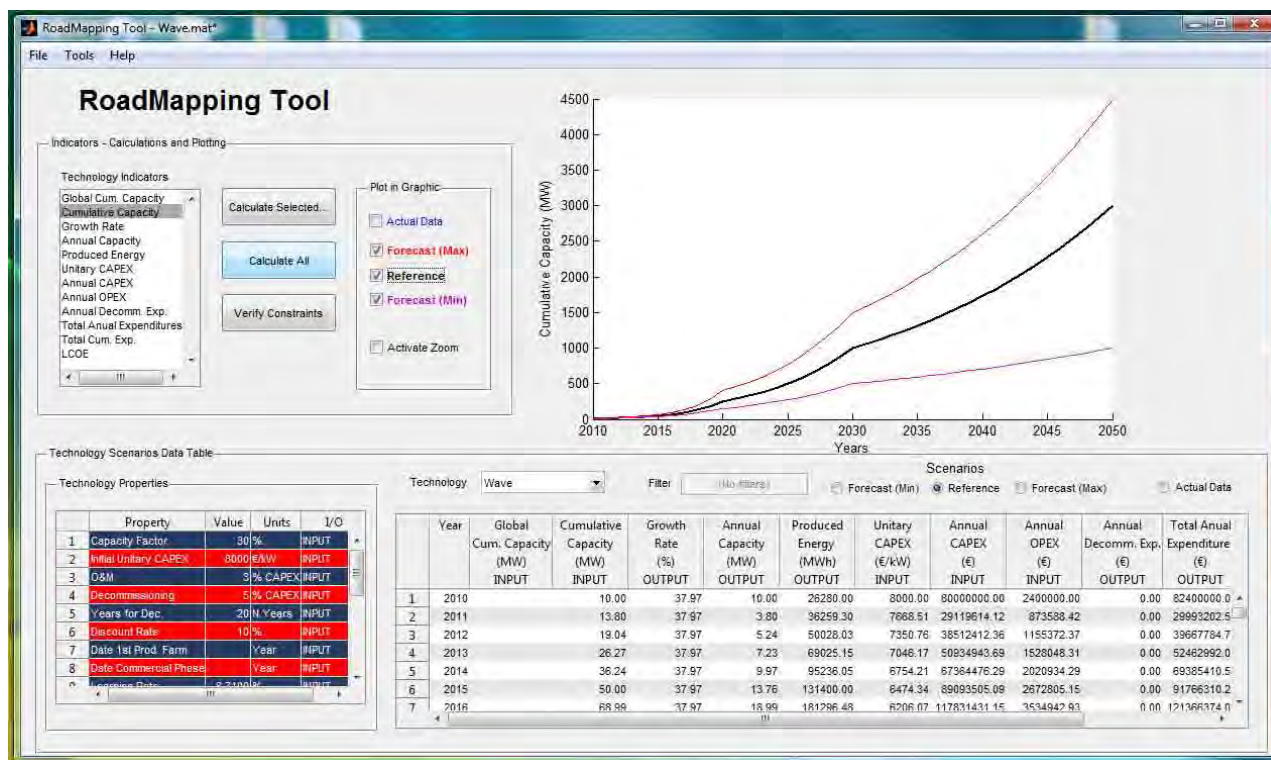


Figure 4: The Roadmapping Tool applied to marine energy technologies in Portugal until 2050.

As a result, the tool presents the evolution of a series of socio-economic and technical indicators which are of primary importance in the construction of the roadmap, and dependent of many variables, including the roadmap scope and target. These indicators include the Cumulative Capacity, Growth Rate, Annual Capacity, Produced Energy, Unitary CAPEX, Annual CAPEX, Annual OPEX, Annual Decommissioning Expenditures, Total Annual Expenditures, Total Cumulative Expenditures, LCOE and R&D Expenditures.

6.1 - Initial Conditions and Assumptions

The initial year is considered to be 2012, with a current capacity is 4,2 MW (prototype installations). The other initial conditions and assumptions that have been made are presented in Table 4. Decommissioning costs are not presented since the time period for this roadmap is too short for decommissioning operations (less than 20 years).

The learning rate was calculated based on the main cost centers for wave energy installations as described in [22]. The weight on the final cost is assumed to be the same as for the final learning rate, which is 8,71%.

For the Forecast (Min) and Forecast (Max) scenarios (optimistic and pessimistic scenarios), the only varying parameters were the learning rate and the installed capacity targets for 2020. The considered values are describes in Table 4 and Table 5.

Table 4: Initial Conditions and Assumptions for the three Scenarios.

	Scenarios		
	Forecast (Min)	Reference	Forecast (Max)
Installed Capacity (MW)	100	250	250
Initial Unitary CAPEX (Eur/kW)	8000	8000	8000
Capacity Factor (% CAPEX)	30	30	30
O&M CAPEX (% CAPEX)	3	3	3
Discount Rate (%)	10	10	10
Learning Rate (%)	6.61	8.71	10.74

Table 5: Wave Energy Cost Centers, Respective Weights and Learning Rates for the three scenarios.

Cost Center	Weight (%)	Learning Rate (%)		
		Forecast (Min)	Reference	Forecast (Max)
Installation	6	6	8	10
O&M	28	10	12	15
Station Keeping	5	10	12	15
Structure	30	6	9	10
Power Take-off	21	5	7	9
Grid Connection	10	1	1	3

6.2 Results

The figures below show the results considering different indicators. Regarding the cumulative capacity and the growth rate (see Figure 5), the results show that to achieve the 2020 target, a very high growth rate has to be achieved (67%), even if we consider the pessimistic scenario where only 100 MW are installed (49%). This corresponds to an annual installation capacity between 5 to 10MW per year until 2015 (in all scenarios) that has to more or less double every year in the Reference scenario (20, 40, 80 MW), which is extremely hard to envisage today. Considering that the prototypes that have been installed are typically less than 1 MW, this would correspond roughly to the installation of 10 prototypes a year until 2015 expecting that one of it proved to be a technology breakthrough and enter commercialization after 2015.

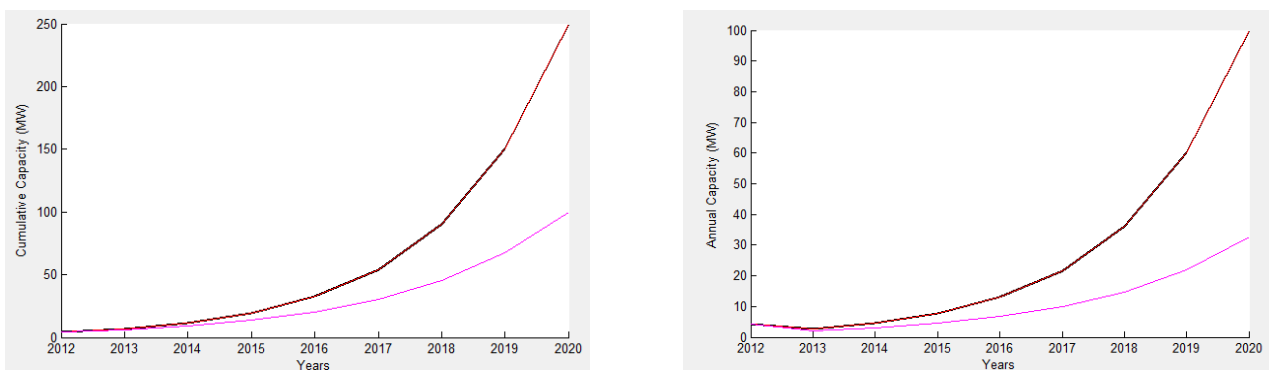


Figure 5: Cumulative capacity and annual capacity.

Regarding the unitary CAPEX, shown in Figure 6, this would mean that in the optimistic scenario it must be reduced by half and at least 25% on the pessimist scenario.

In any case, these numbers are 2 to 3 times greater than the ones considered for the WAVEREF scenarios in section 5. Scenario design for 2020, which means that even considering a certain complementarity between PV systems and Wave systems in terms of resource variability, if by 2030 the waves are not competitive, it may be that the window of opportunity for this type of energies is closed.

In terms of annual CAPEX, this represents investments in the order of magnitude of few dozen millions of euros over the next three years (and hundreds until 2020, even in the pessimist scenario), which under the current financial crisis is also hard to foresee. In terms of OPEX, these would correspond to 5-15 million Euros in 2020.

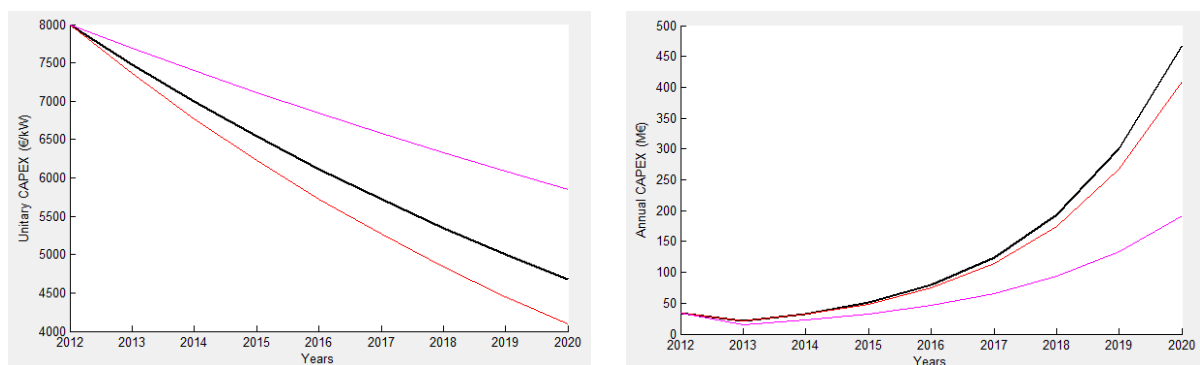


Figure 6: Unitary CAPEX and annual CAPEX.

Finally, as shown in Figure 7, the total cumulative investment to achieve the 2020 goal would represent 1200 to 1400 million Euros over the next 8 years (considering the Reference or the Optimistic scenario) and at least 600 million to achieve the pessimist scenario (100 MW of installed capacity only). In any scenario, the LCOE would be around 800€/MWh in 2020, which is an extremely high value compared to other renewable resources and even with the generous existing feed-in-tariff in Portugal for this type of technology (260€/MWh), it will be extremely difficult to find investors for the projects beyond prototype testing.

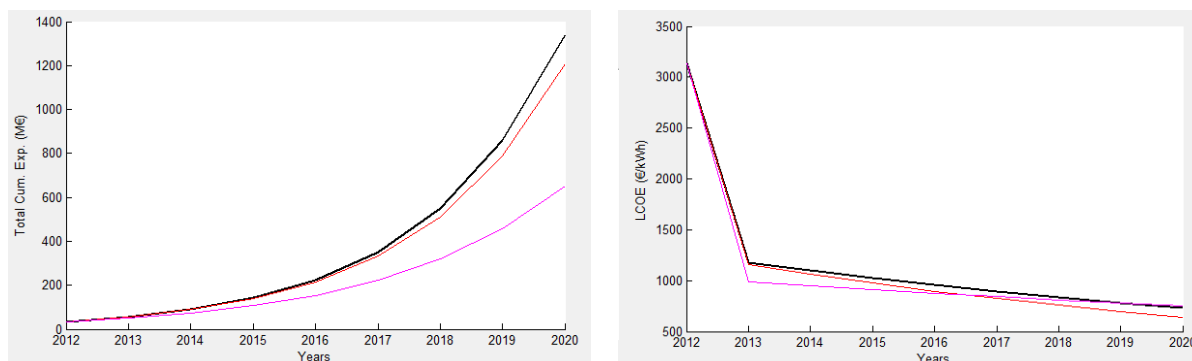


Figure 7: Total cumulative investment and LCOE.

7. Discussion and Conclusions

The results presented in the previous section show that the objective of achieving the goal of installing 250MW of wave systems for electricity generation in Portugal at 2020 is extremely hard to achieve, even considering the most optimistic scenarios regarding uncertain events, for a variety of technical and economic reasons discussed in detail as follows.

First, it would require that until 2015, a constant rate of 10 prototype projects up to 1 MW would be installed every year. The latest prototype launched in Portugal in 2012 consists of 3 machines of 100 kW each [23], we are already far from achieving such a rate over the next three years.

Then, and even considering that a series of prototypes was installed over the next three years and considering further that one of this prototypes would prove to be the technological breakthrough required to start developing commercial solutions the investment costs would be still very high, albeit a generous feed-in-tariff is available in Portugal for this type of technology. Under the deep financial crisis that Europe is living today, it is very unlikely that projects of few MW would find any kind of financial support.

The analysis presented here focused on wave systems, but the current development stage for offshore wind in Portugal is similar, as in Portugal, only deep offshore wind installations are possible. Thus, we see as highly unlikely that the current goal for marine energies in Portugal is achieved.

These conclusions have been made upon the use of a roadmapping tool that takes into account the uncertainty of many parameters that have shown to vary significantly under the course of development of other renewable technologies. In particular, this tool uses scenarios to present different evolution storylines and presents a series of technical and economic indicators that can be easily monitored to assess the evolution of the roadmap and can be used to update it. In this way, it is easy to revise the strategy and make it more effective as a public policy instrument.

In the particular case of Portugal roadmap, it shows that the previously defined strategy has to be changed. This does not necessarily mean that the installed capacity has to be redefined, but with the level of investment required, a possibility is to change the focus from the technological development to service delivery (testing, O&M) and developing strengths in other levels of the supply chain.

Acknowledgements

The authors would like to thank to the Portuguese Foundation for Science and Technology that supported this work through the project PTDC/SEN-ENR/105403/2008.

References

1. Eurostat. Europe 2020 Indicators - Share of renewables in gross final energy consumption, 2012. <http://epp.eurostat.ec.europa.eu/portal/page/portal/eurostat/home/>
2. Directorate-General for Energy and Transport. An energy policy for Europe: Commission steps up to the energy challenges of the 21st century. European Commission - MEMO/07/7, 2007.
3. Sarmiento, A.J.N.A., “A strategy for wave energy development in Portugal”, ENER06, Figueira da Foz, September 26 to 28, 2006.
4. UK Energy Research Center. UKERC Marine (Wave and Tidal Current) Renewable Energy Technology Roadmap, 2008.
5. European Commission. Concerted Action for Offshore Wind Energy Deployment (COD), 2005
6. Distributed Generation – Future Energy Resources. Roadmapping of the paths for the introduction of distributed generation in Europe, March 2004
7. European Photovoltaic Industry Association. EPIA Roadmap, June 2004
8. D. Probert, M. Radnor. Technology roadmapping. Research Technology Management, 46 (2): 27-30, 2003.
9. C.H. Willyard, C. McClees. Motorola’s technology roadmap process. Research Management 30 (5): 13–19, 1997.
10. European Commission Project HiWays. The European Hydrogen RoadMap, February 2008.
11. California Energy Commission. Pier renewable energy technologies program, Research development and demonstration roadmap, August 2007.
12. International Energy Agency. Energy Technology Systems Analysis Programme, 2009 <http://www.etsap.org>
13. S. Lee, Y. Park. Customization of technology roadmaps according to roadmapping purposes: Overall process and detailed modules. Technological Forecasting & Social Change 72: 567–583, 2005
14. International Energy Agency. Energy Technology Roadmaps: a guide to development and implementation, 2010.
15. European Ocean Energy Association. Oceans of Energy: European Ocean Energy Roadmap 2010-2050. 2010
16. ORRECA. European Offshore Renewable Energy Roadmap. 2011
17. USA PV Industry. Solar Electric Power: The US PV industry Roadmap. 2001
18. EPIA. Solar Energy 6: Solar Photovoltaic Energy Empowering the World. 2010
19. C.A. Silva, S. Matias. Roadmapping Ocean Energies: Uncertainties Review and Assessment. Proceedings of the International Conference on Ocean Energy 2012, 2012.
20. Governo de Portugal. Plano Nacional de Acção para as Energias Renováveis ao abrigo da Directiva 2009/28/CE. 2010
21. International Energy Agency. World Energy Outlook 2009. 2009.
22. Carbon Trust. Accelerating Marine Energy. 2011
23. Grupop Lena. Energia do mar avança em Peniche com a Eneólica, 2012. <http://www.grupolena.pt/noticias.php?nid=127>

Estimation of the wave energy potential on the offshore Mediterranean Sea and propagation toward a nearshore area

V. Vannucchi and L. Cappiotti

*Dipartimento di Ingegneria Civile e Ambientale, Università degli studi di Firenze,
Via S. Marta 3, 50139 Firenze, Italy, valentina.vannucchi@dicea.unifi.it*

Abstract – This paper presents a study to quantify the availability of wave power in the Mediterranean Sea. Monthly and annual average values of powers are provided, in deep water, for the years 2010 and 2011, based on the elaboration of the data set of the model MED 6MIN - PREVIMER. Through numerical simulation, the data set was propagated from depths of 100 m to coast, taking into account the shoaling, refraction, diffraction, bottom friction and wave breaking processes. In this phase of the study, the methodology was applied only to the stretch of coast between Livorno and La Spezia.

1. Introduction

Currently in the energy sector there is an increasing interest in renewable energy sources and, within this context, the possibilities of producing energy from the waves in the sea is also emerging. The quantification of the availability of such an energy form is the first step to take and constitutes a fundamental element at the base of studies into the practicalities inherent in its conversion to usable forms through the so-called WEC - Wave Energy Converter technologies (Falnes, 2007 and Falcao, 2010).

On a European level, important contributions have been supplied in this sector such as Pontes et al. (1996), OEC (2006), but the Mediterranean has still only received little attention (Filianoti 2000, Vicinanza et al. 2011). This study adds to the knowledge of the availability of energy from the Mediterranean Sea. In addition to the analyses concerning the availability of energy from the wave motion offshore in the whole of the Mediterranean Sea, a procedure has been developed based on a numerical simulation for the detailed analysis of coastal areas with a serviceable depth of less than 100 m which can be useful in the identification of eventual focus zones.

2. Methodology

The analyses of this paper are based on wave data arising from numerical simulation models for wave generation coupled with atmospheric models. The data was provided by IFREMER that has developed a pre-operational system, called PREVIMER, aiming to provide short-term forecasts concerning the coastal environment along the French coastlines bordering the English Channel, the Atlantic Ocean and the Mediterranean Sea.

The data used in the present study arise from the numerical simulation model called MED 6MIN, a WaveWatch III model, with a third-order accuracy propagation scheme in space and time. The weather forecast conditions were provided by Météo-France and covered the twelve hours duration and the following six days. The results are provided in the NetCDF format at 3 hour intervals and the variables are, for example, wave height, period, direction.

The data set analysed covers the whole of the Mediterranean Sea with a resolution of 0.1° in latitude and longitude for a period of 2 year and 9 months, from July 2009 to March 2012. The formula used to compute the monthly and yearly mean wave power, in the case of irregular waves propagating in deep waters, is reported in eq. (1)

$$P = \frac{1}{64} \frac{g^2}{\pi} \rho H_{m0}^2 T_{m-1,0} \quad (1)$$

with ρ water density and providing that $H_{m0}=4m_0^{1/2}$ is the significant wave and $T_{m-1,0}=m_1/m_0$ is the mean spectral wave period.

This formula is computed considering, as it is well known, that in case of regular waves the specific wave power is equal to eq. (2)

$$P = \frac{1}{8} \gamma H^2 C_g \quad (2)$$

with γ specific weight [N/m³]

H wave height [m]

C_g group celerity [m/s]

The irregular waves can be considered as a superposition of an infinite number of regular components and the total power is calculated as the sum of the power associated to any component, according the eq. (3).

$$P = \sum_{i=1}^{\infty} \frac{1}{8} \gamma H^2(f_i) C_g(f_i) \quad (3)$$

In terms of the frequency spectrum, $S(f_i)$, the wave height squared, of each wave components, is expressed as in eq. (4)

$$H^2(f_i) = 8 \cdot S(f_i) \Delta f \quad (4)$$

In the case of deep water the group celerity is computed as in eq. (5)

with g acceleration of gravity [m/s²]

π Pi constant [-]

f frequency [s⁻¹]

Substituting eq. (4) and eq. (5) into eq. (3), eq. (6) is obtained:

$$P = \frac{g\gamma}{4\pi} m_{-1} \cdot \frac{m_0}{m_0} \quad (6)$$

where

$$m_k = \sum_{i=1}^{\infty} S(f_i) f_i^k \Delta f \quad (7)$$

and so finally eq.(1) is obtained.

3. Results of the wave energy characterization

The spatial distribution of the monthly mean power has been computed and reported in the form of contour maps for each month of a given year (not shown in this paper for brevity). The maximum values of the monthly mean power that resulted in the studied spatial domain have been highlighted in Figure 1 and the localization of the related points is depicted in Figure 2. Moreover, the spatial distribution of the mean power for the years 2010 (Figure 3) and 2011 (Figure 4) has been computed as the mean of the monthly mean powers.

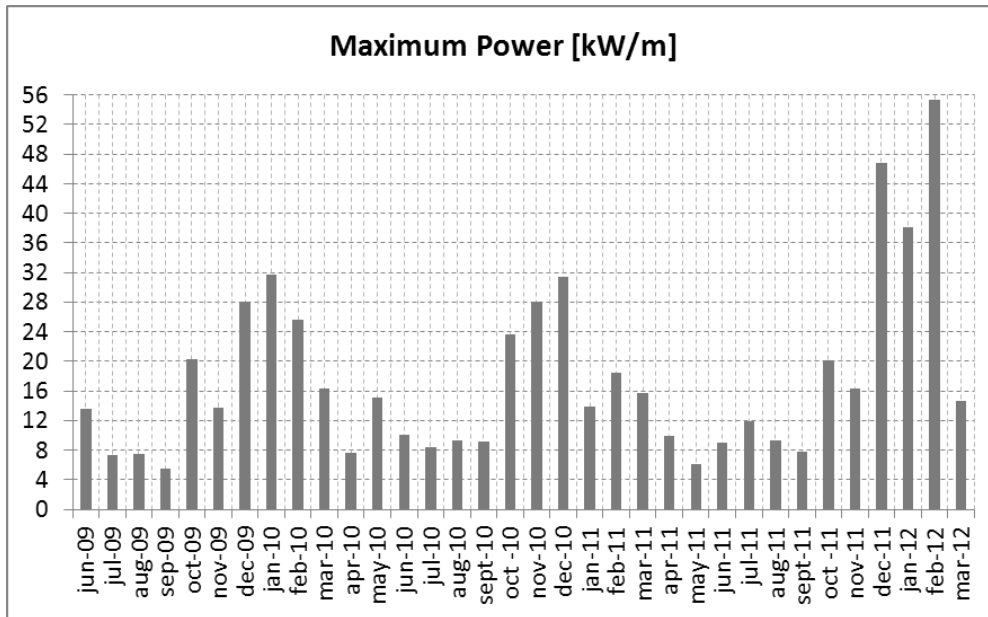


Figure 1: Maximum values of the monthly mean power and its spatial localization as reported in fig 2.

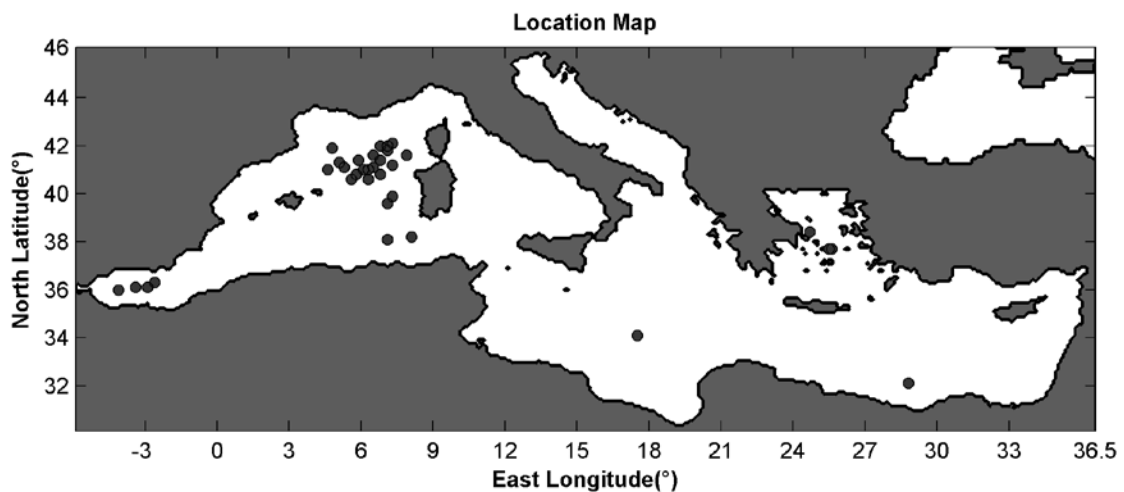


Figure 2: Location map of sea sites characterized by the maximum monthly mean power.

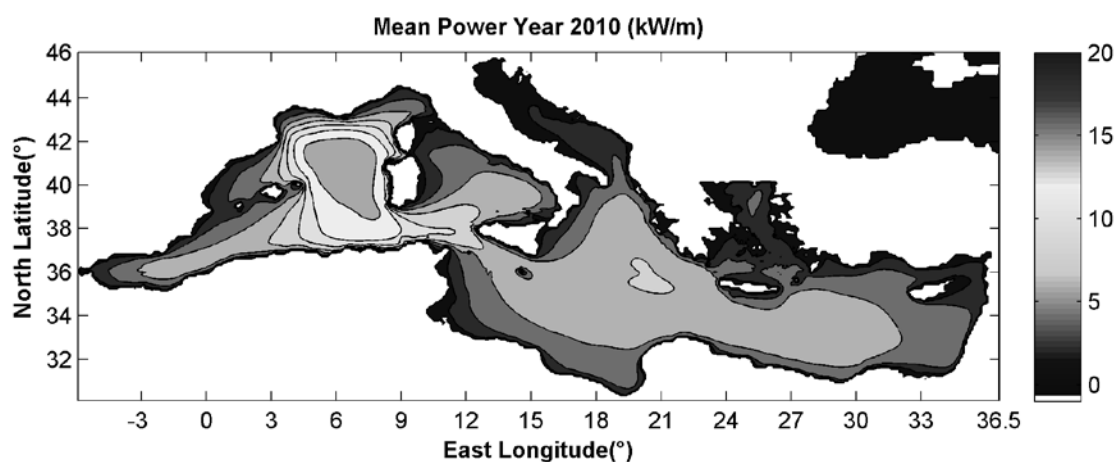


Figure 3: Spatial distribution of the Yearly Mean Power computed by using the data for the Year 2010 [kW/m].

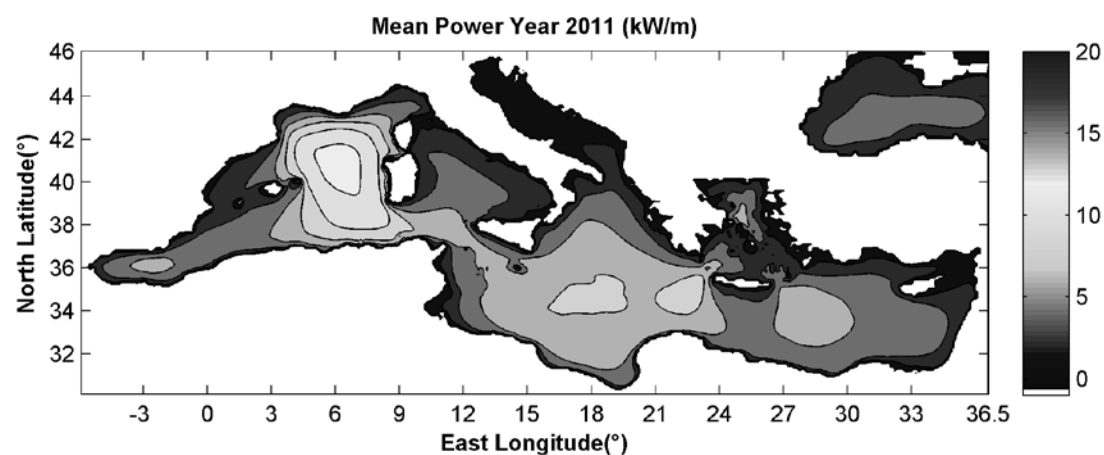


Figure 4: Spatial distribution of the Yearly Mean Power computed by using the data for the Year 2011 [kW/m].

It is worth noting that during the autumn and winter months and therefore in October, November, December, January and February, the maximum monthly mean power in the studied domain is always greater than 20 kW/m (except Nov 09, Jan11 and Feb11).

It is also evident that the most energetic parts of the northern Mediterranean are those on the Western coasts of the islands of Corsica and Sardinia. In this area the maximum annual average power, reaches values equal to 15.8 kW/m for 2010 and 12.8 kW/m for 2011.

For the exploitation of wave energy, supporting infrastructures are necessary (for examples harbours) and so to limit the cabling costs, the distance from the coast should be around 5-10km (Dalton et al., 2009). This topic is of particular interest when studying this resource in coastal waters.

Moreover, the offshore wave energy potential can easily be obtained by means of the analysis of deep water wave data, but the processes affecting waves as they propagate towards the nearshore can modify the wave energy potential, leading to reductions or, sometimes, local enhancements due to focusing mechanisms. Furthermore, due to such mechanisms, the spatial variability of wave energy potential can be remarkable, thus suggesting the need for accurate knowledge for the placing of a pilot plant in order to maximize the harvesting of wave energy.

4. The propagation model

For the numerical simulation of wave propagation, from offshore sites toward coastal sites characterized by water depths of less than 100 m, the Spectral Wave module of the MIKE21 software was used. The MIKE21-SW is a spectral wind-wave model based on unstructured mesh that allows the simulation of the following physical phenomena: non-linear wave-wave interaction, dissipation due to white-capping, dissipation due to bottom friction, dissipation due to depth-induced wave breaking, refraction and shoaling due to depth variations.

The model is used with the fully spectral formulation, based on the wave action conservation equation, where the directional-frequency wave action spectrum is the dependent variable and with the quasi-stationary mode, where the time is removed as an independent variable and a steady state solution is calculated at each time step.

As offshore boundary conditions the values of wave height, peak period, the average direction and spreading factor, of the six points extracted by the PREVIMER model on a depth of 100 m, were used. The model mesh is flexible with a triangular side of 2000 m in water depths of 100 m to 50 m, a side of 1000 m in water depths of 50 to 30 m, a side of 500 m until the water depth of 20 m and then a triangular side of 300 m (Figure 5).

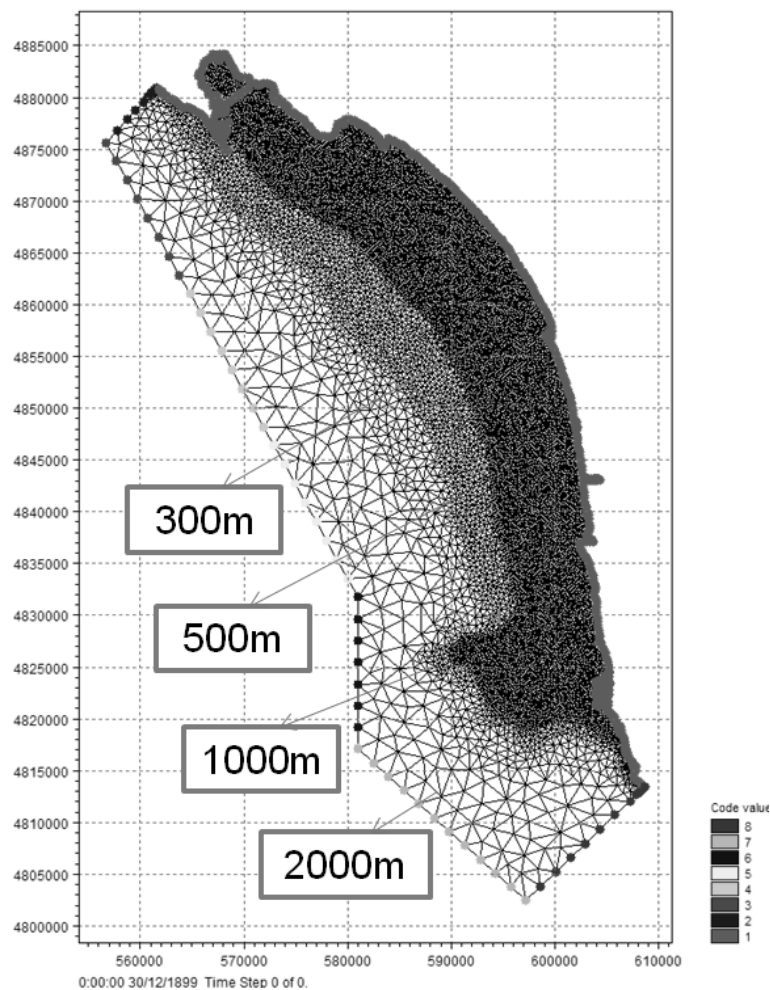


Figure 5: Boundary conditions and resolution mesh.

The model domain is about 60 km x 85 km with a maximum water depth of approximately 100 m (Figure 6).

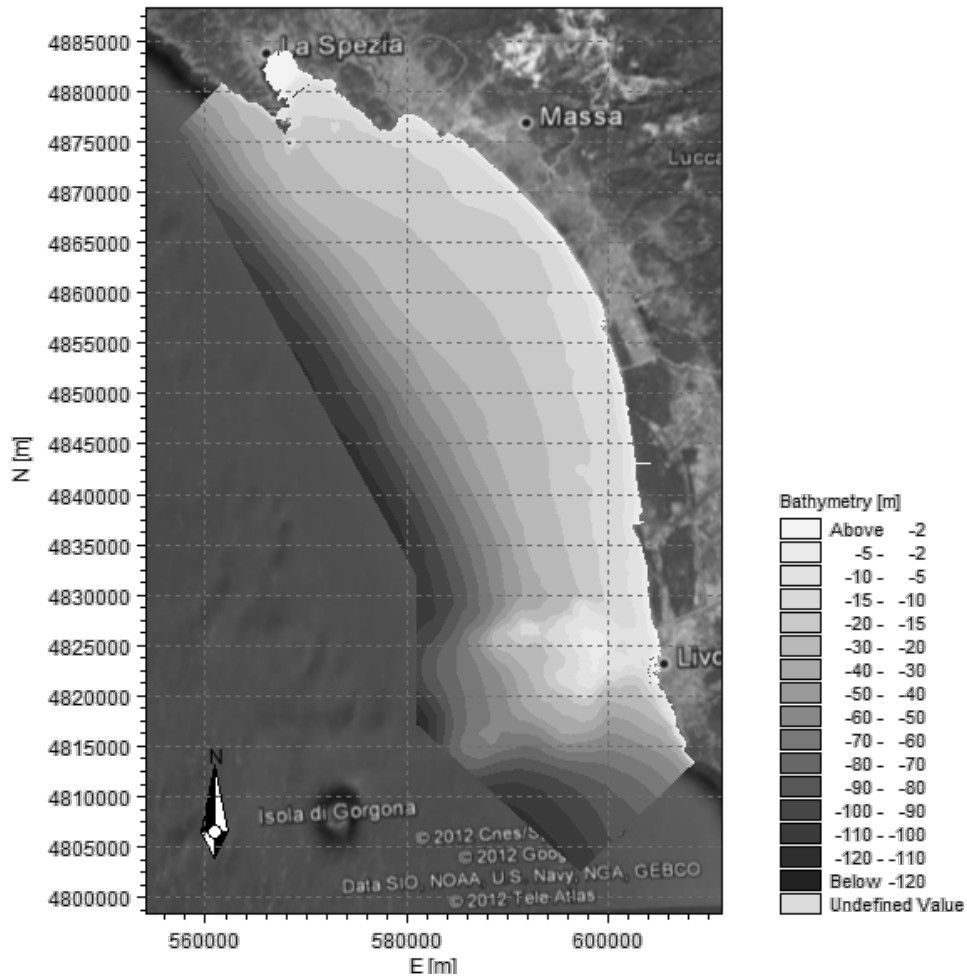


Figure 6: Propagation area bathymetry.

All the time series of the PREVIMER data set (from July 2009 to March 2012) was propagated and a constant value was assumed for the bottom friction equal to 4 cm (Nikuradse formulation) as well as a constant value representing the white capping dissipation source function, equal to 4.5. In output maps were obtained of the variation of the wave height, mean direction and wave power. In fact the MIKE21-SW allows the wave power to be obtained directly as in eq. (8)

$$P_{\text{energy}} = \rho g \int_0^{2\pi} \int_0^{\infty} c_g(f, \theta) \cdot E(f, \theta) df d\theta \quad (8)$$

where E is the energy density, c_g is the celerity group, ρ is the density of water, g is the acceleration of gravity, f is the wave frequency and θ is the wave direction.

5. Results of the propagation model

The maps of wave power were computed for each time step and fig.7 illustrates an example for one of the most energetic sea states ($H_{m0} = 4.2m$, $T_m = 7.3s$, $Dir = 240^\circ N$) on the 5th of January 2010, hour 18.00 (Figure 7).

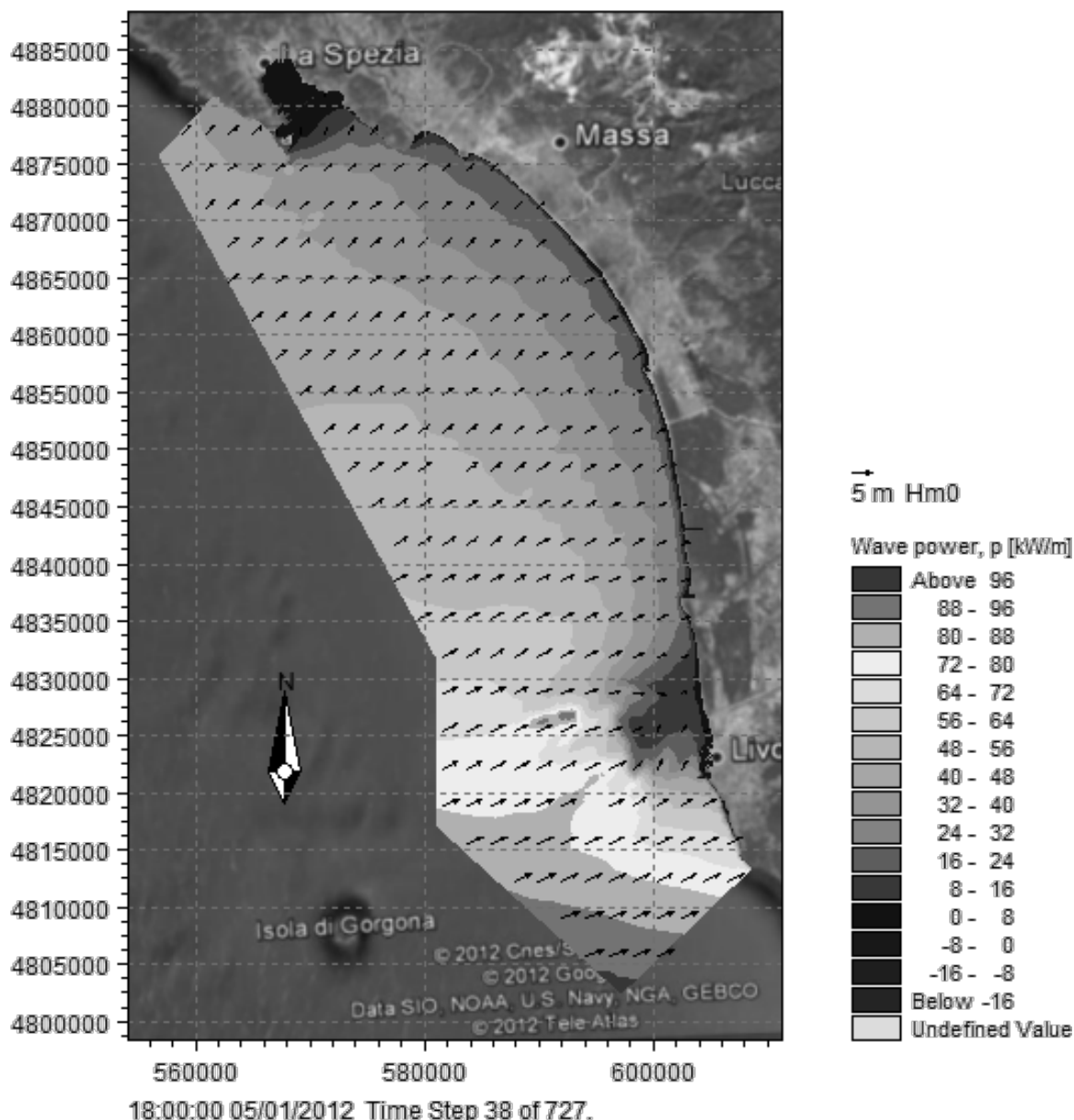


Figure 7: Spatial distribution of the wave power for the 5th of January 2010, hour 18.00 [kW/m] and wave height values (arrows).

Then the monthly mean power for each month was computed from July 2009 to March 2012, and only for the years 2010 (Figure 8) and 2011 (Figure 9), the yearly mean power.

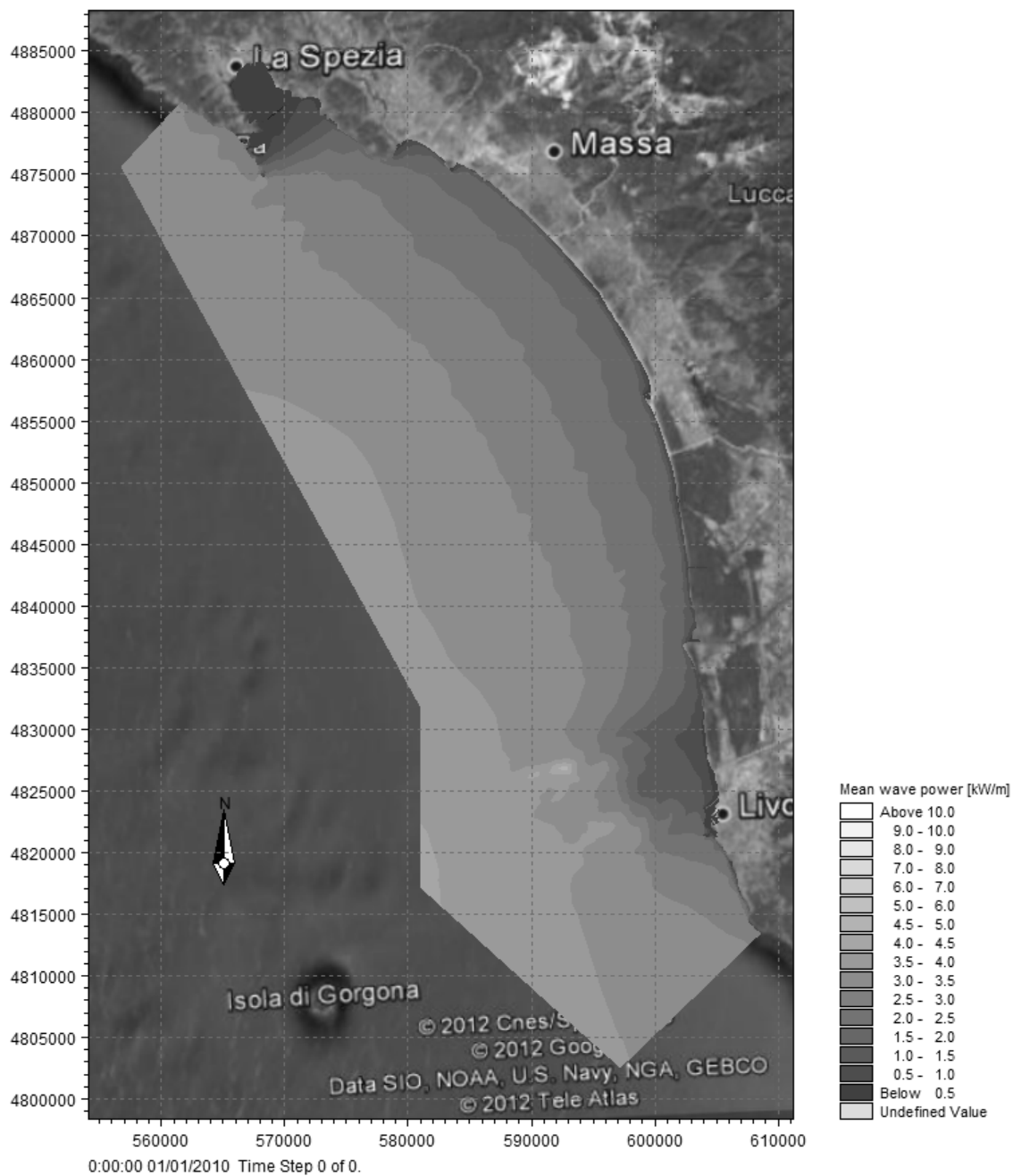


Figure 8: Spatial distribution of the Yearly Mean Power computed by using the data for the Year 2010 [kW/m].

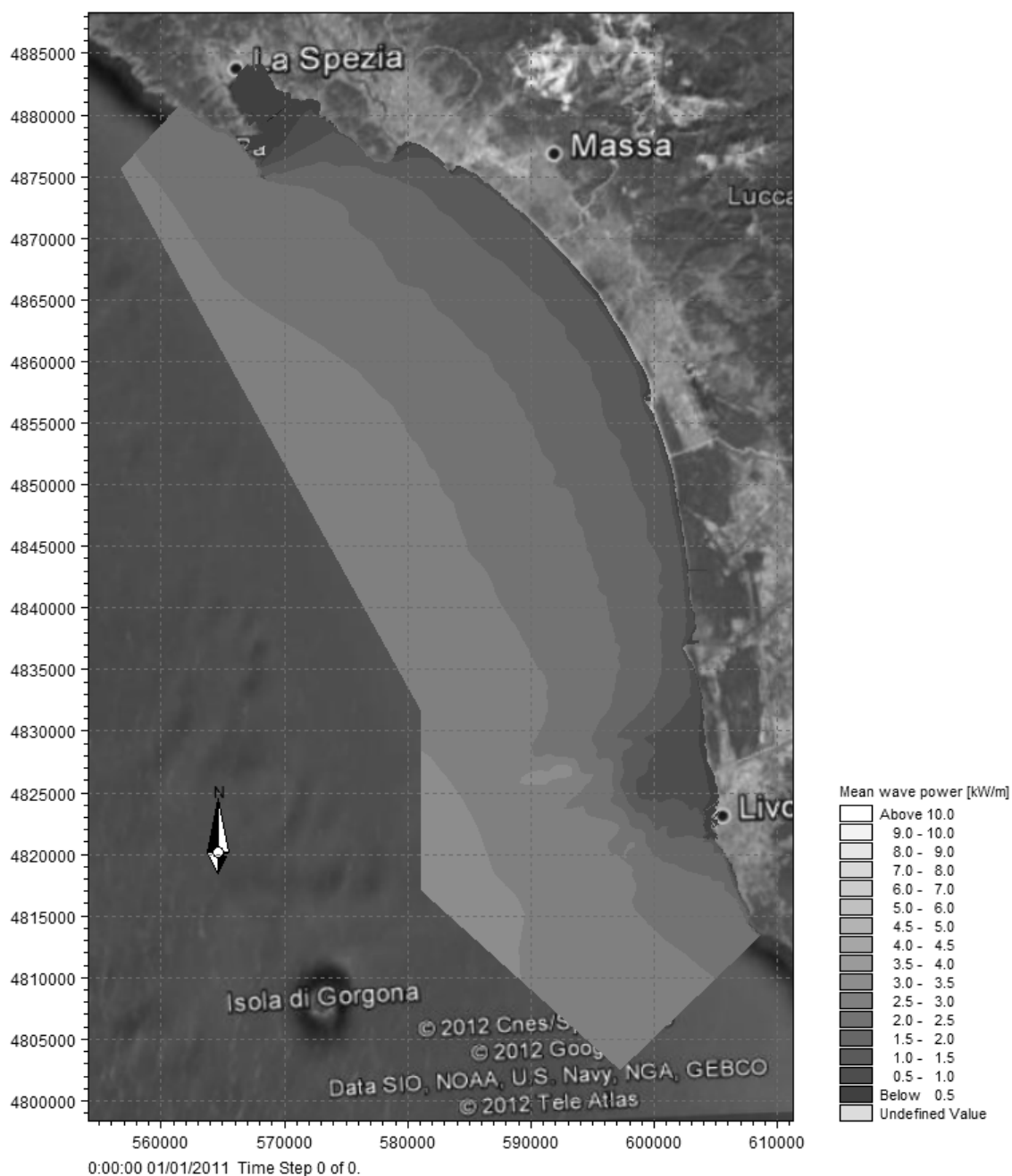


Figure 9: Spatial distribution of the Yearly Mean Power computed by using the data for the Year 2011 [kW/m].

In addition to the above analysis, it was also considered important to analyse the monthly and yearly mean power in 20 different points (Table 1), 10 located in the water depths of 15 m (from 1 to 10) and another 10 in water depths of 50 m (from 11 to 20).

Table 1: Yearly mean values of the wave power in the extracted points.

Point	Mean Power 2010 [kW/m]	Mean Power 2011 [kW/m]
1	0.97	0.72
2	2.23	1.55
3	2.23	1.61
4	2.21	1.61
5	2.06	1.48
6	2.16	1.6
7	2.28	1.71
8	2.44	1.86
<u>9</u>	<u>2.89</u>	<u>2.23</u>
10	2.1	1.6
11	3.16	2.51
12	3.16	2.5
13	3.23	2.54
14	3.33	2.61
15	3.4	2.66
16	3.38	2.65
17	3.31	2.6
18	3.36	2.65
<u>19</u>	<u>3.63</u>	<u>2.93</u>
20	3.07	2.43

At each point the wave roses are also computed (Figure 10).

It is evident that the most energetic points are the 9 in the water depths of 15 m and the 19 in the water depths of 50 m, and these points are located on the Meloria shoals (Secche della Meloria) where a focusing mechanism is affective.

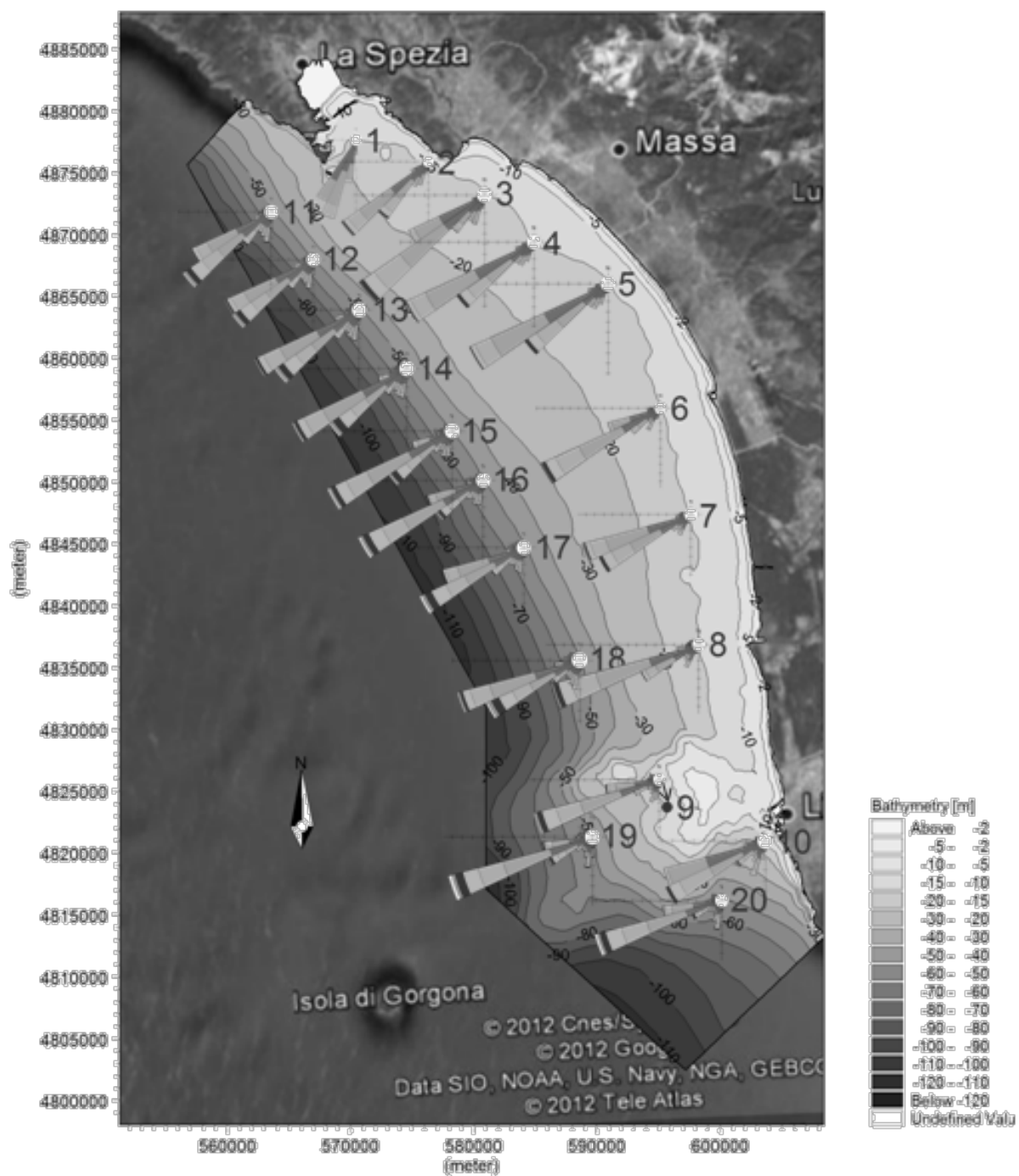


Figure 10: Location and wave rose of the points extracted.

For each month the values of the wave power were computed at all the points in the water depths of 15 m and at all the points in the water depths of 50 m.

In Figure 11 an example for February 2010 is illustrated.

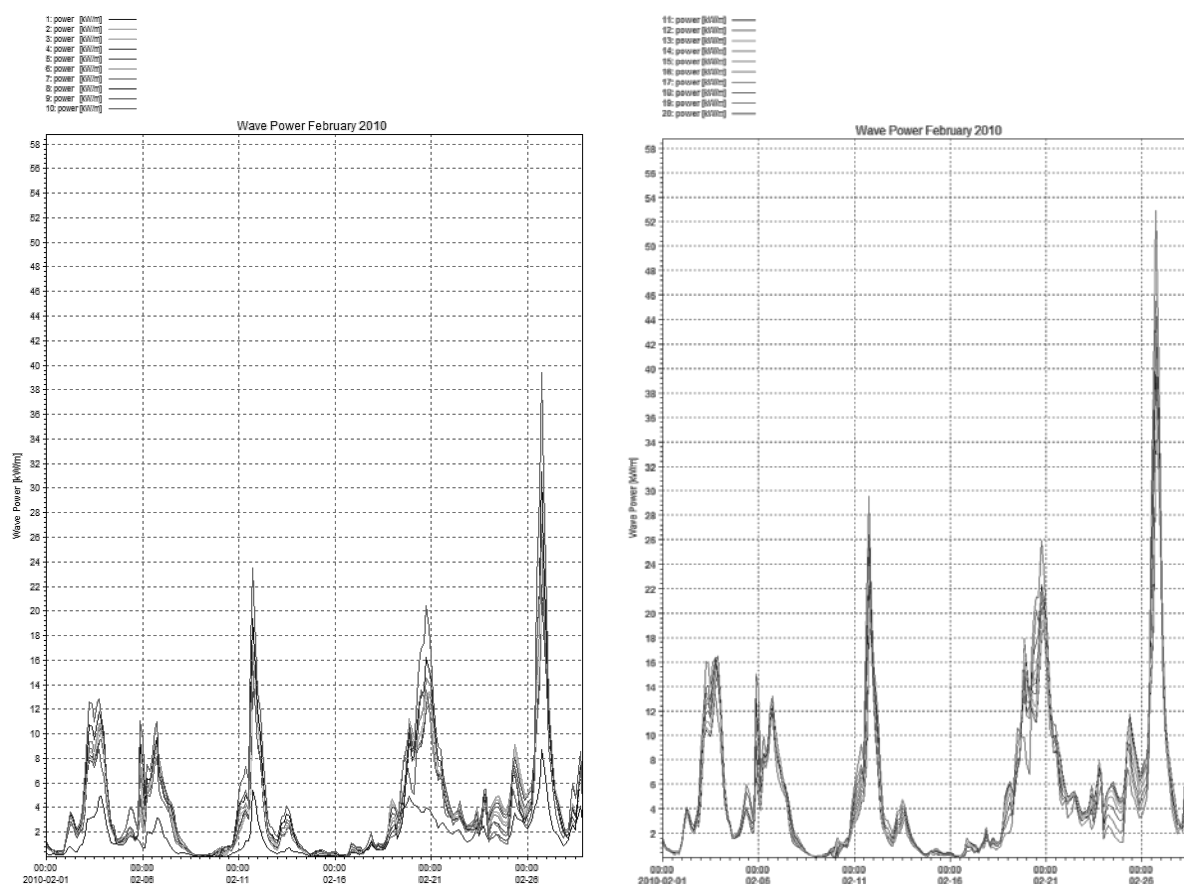


Figure 11: Monthly wave power trend of February 2010 for the points on the 15 m bathymetry (on the left) and on 50 m bathymetry (on the right).

6. Conclusions

This study presents a brief contribution to the knowledge of the availability of wave motion energy in the whole of the Mediterranean sea. The results constitute both an up-date of previous, older studies (Pontes et al. 1996) and a deeper knowledge, in terms of spatial resolution, of wave energy potentials also in respect of more recent studies (Filianoti, 2000, Vicinanza et al. 2011).

With reference to Pontes et al. (1996) it can be confirmed that the area with the most availability of average annual power is that to the West of the islands of Corsica and Sardinia. However, the maximum values supplied in Pontes et al. (1996) for the area of Alghero (5 kWm⁻¹ average annual), are much lower than those obtained from the more recent studies by Filianoti (2000) and Vicinanza et al. (2011) in the same area (9.5 kWm⁻¹ average annual).

These studies are based on data registered punctually from a few wavemeter buoys whereas the present study is based on data coming from numerical simulations (MED 6MIN-IFREMEER), something which has permitted a higher spatial resolution knowledge and so the highlighting of maximum values of up to approximately 15.5 kWm⁻¹ located in other points offshore of the same area.

The analyses are limited to the aspect of the quantitative definition of the energy availability without examining the sustainability of the use of WEC technologies.

Nevertheless, given that evident technical-economical limitations suggest that the potentially exploitable areas for supplying energy to zones inland must be located, amongst other things, between 5-10 km from the coastline, a procedure has been developed based on a second numerical model (MIKE21-SW). This takes as off-shore boundary conditions the output of the MED 6MIN model, permitting the reconstruction, with very precise location definition, of the energy availability of areas close to the coastline with sea-bed depths of less than 100 m. As a first area for testing the procedure a stretch of coastline was chosen between Leghorn and the Gulf of La Spezia. The simulations have highlighted the high spatial variability of the wave energy resource and the formation of hot-spots due to phenomena of focusing in correspondence with areas on the Secche della Meloria (the Meloria shallows). At present, other coastal areas are under examination and the results will be presented in subsequent papers.

7. Acknowledgements

This study constitutes part of the program of the Research Doctorate of Engineer V. Vannucchi, in Civil and Environmental Engineering, at the DICeA, University of Florence.

The authors wish to thank: i) IFREMER for the use of data and in particular Dr Fabrice Lecornu; ii) DHI- Italia for having supplied the availability of the software MIKE21, and in particular Engineer Andrea Pedroncini.

The support of the MARINET Project (EU-FP7, www.fp7-marinet.eu), is gratefully acknowledged.

References

1. J. Falnes. Review - A review of wave-energy extraction. *Marine Structures*, 20: 185-201, 2007.
2. A. Falcão. Wave energy utilization: a review of the technologies. *Renewable and Sustainable Energy Reviews*, 14: 899-918, 2010.
3. M.T. Pontes, G.A. Athanassoulis, S. Barstow, L. Cavaleri, B. Holmes, D. Mollison and H. Oliveira Pires. WERATLAS - Atlas of Wave Energy Resource in Europe, *Technical Report, DGXII Contract No. JOU2-CT93-0390*, INETI, Lisbon, 1996.
4. OEC2006. Ocean Energy Conversion in Europe, Recent Advancements and Prospects, European Commission, Centre for Renewable Energy Sources Ocean Energy Conversion in Europe - Recent Advancements and Prospects, 2006.
5. P. Filianoti. La disponibilità di energia ondosa su varie aree del pianeta. In *Atti del XXVII Convegno di Idraulica e Costruzioni Idrauliche*, 2000.
6. D. Vicinanza, L. Cappietti, V. Ferrante, P. Contestabile. Estimation of the wave energy in the Italian offshore. *Journal of Coastal Research*, 64: 613-617, 2011.
7. G. Dalton, N. Rousseau, F. Neumann and B. Holmes. Non-technical barriers to wave energy development, comparing progress in Ireland and Europe. In *Proceedings of the 8th European Wave and Tidal Energy Conference*, Uppsala, Sweden, 2009.

An integrated procedure for the design of a Wells turbine developed for Mediterranean operation

F. Arena¹, M. Bassetti², A. Corsini², G. Delibra², G. Faggiolati³, S. Piccinini³, F. Rispoli², G. Romani³, A. Romolo¹, M. Ruggeri³, E. Tuccimei² and P. Venturini²

¹*Mediterranea University, NOEL laboratory, School of engineering, Loc. Feo di Vito, 89122 Reggio Calabria, Italy,*

²*Dipartimento di Ingegneria Meccanica e Aerospaziale, 'Sapienza' University of Rome, Via Eudossiana 18, 00184 Roma, Italy, alessandro.corsini@uniroma1.it*

³*Faggiolati Pumps, S.p.A., Zona Industriale Sforzacosta, 62100, Macerata, Italy*

Abstract – Among renewable energy sources, wave energy has a huge potential, that in Mediterranean sea is estimated with 30 GW. In this field CRAS (Sapienza Aerospace Research Center) and *Faggiolati Pumps S.p.A.* developed a prototype of Wells turbine designed to operate under Mediterranean sea conditions. In this paper the procedure for the design of Wells turbine of 1.5 kW is illustrated. X-Foil was used to calculate lift and drag at different span sections and derive the characteristic curve of the turbine. The design IGV-OGV blades was based on flow field calculations with OpenFOAM.

1. Introduction

Among renewable energy sources, the potential of wave energy has not been fully exploited so far, even if sea wave energy features a high capacity. In fact Thorpe estimated a 2 TW/year power capacity over the total sea extension [1], with an energy density between 20 and 70 kW/m for the most favorable wave climates [2], and a more uniform daytime availability if compared to the solar radiation [3].

Among the number of wave energy converters, the Oscillating Water Column (OWC) can be considered the on-shore technology closest to maturity as it already reached the stage of full-scale prototype, with several pilot plants presently on-duty. To mention but a few, the LIMPET I and II plants on the Island of Islay in Scotland respectively started-up in 1991 [4] and 2000 [5], while the European pilot plant on the island of Pico in Portugal started-up in 1999 [6]. Other OWC devices were built in Norway [7], India and Japan. In the latter plant in Sakata, the OWC converter is integrated within the harbour breakwater structure, reducing the economical and environmental costs.

An OWC device has a chamber partly submerged, opened below the water surface to the action of the sea; in the upper part air is trapped above the free surface of the water. As the incident wave induces an oscillating motion of the free surface, wave energy is converted into low-pressure pneumatic energy by a continuous cycle of compression and expansion of the air in the chamber. The so-called Wells turbine, that is a self-rectifying turbine with symmetric blade profile and zero pitch setting, is used to convert the pneumatic power available as an alternative bi-directional airflow into unidirectional torque available to the shaft.

In this paper a procedure of design for a Wells turbine able to operate in Mediterranean Sea is described. Such device was designed for operations on shoreline near Reggio Calabria where the energy density is comprised between 7 and 8 kW/m.

2. Design specifications

In order to design a Wells turbine for Mediterranean Sea operations (labeled DIMAFP-TW1.5), an average height $H_m = 0.8\text{m}$ and a period $T=4\text{s}$ were considered to calculate nominal flow in the turbine. Geometrical constrains D_{Tip} and D_{Hub} for the turbine were chosen in order to exploit resonance inside the U-OWC chamber [8], [9] and reduce fluid dynamic losses.

Angular velocities equal to 3000 and 3600 were selected to fulfill a target of 1.5 kW for the turbine and allow direct coupling with the grid.

In Figure 1 the power available at the shaft is plotted as a function of the hub-to-tip ratio. From the same picture it is possible to deduct that in order to get the desired target of 1.5 kW the hub-to-tip ratio must be chosen equal to $\chi=0.75$.

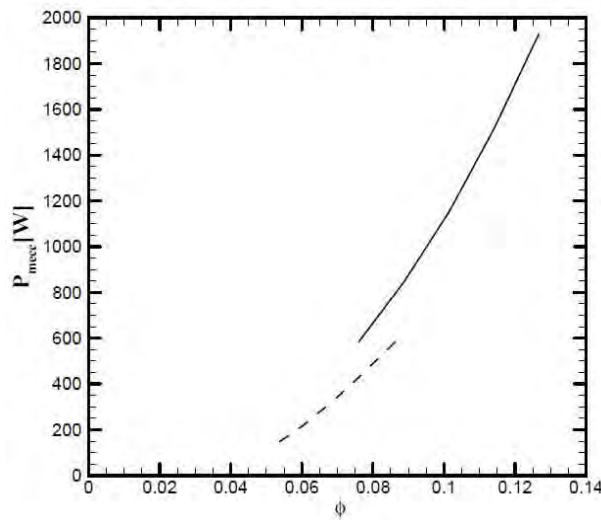


Figure 1: DIMAFP-TW1.5 power output; solid line: $\chi=0.75$, dashed line: $\chi=0.5$.

For the turbine blade, a NACA 0015 profile was selected according to the study reported in [10]. A symmetric profile was necessary in order to allow the blade to work under oscillating airflow. With the given hub-to-tip ratio $\chi=0.75$ a solidity $\sigma_h=0.64$ was selected according to the current technology [11], fixing the number of blades to 7 (Figure 2) and consequently getting a chord $c=108\text{ mm}$.

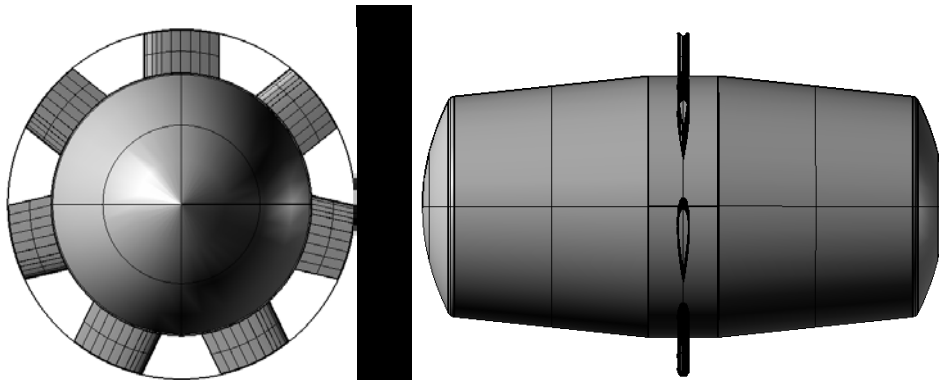


Figure 2: DIMAFP-TW1.5 rotor sketch.

Table 1: OWC and DIMAFP-TW1.5 characteristics.

Chamber			Turbine		
a	5	m	D_{cas}	500	mm
b	0.3	m	D_{Tip}	498.5	mm
H_m	0.8	m	D_{Hub}	375	mm
T	4	s	chord	108	mm
Q_{max}	0.942	m^3/s	ω	3000/3600	rpm
C_q	0.9		tip gap	0.01%	
Q_{des}	0.848	m^3/s	NACA	0015	

The entrance of the fluid in the turbine is guided by a conical nose that is connected to the shaft in order to reduce the fluid dynamic losses. As the turbine works under an oscillating airflow the same nose is present downstream, working as a diffuser. As the direction of the airflow is reversed, the second cone guide the air, while the first act as diffuser. The shape of the nose was modeled to avoid detachment of the fluid.

3. Turbine blade design with Boundary Element Method

To derive the characteristic curve of the designed turbine a methodology based on radial equilibrium flow and boundary element method was applied.

The simpler approach to model the flow in annular passage, in case of negligible radial velocity components, is commonly known as radial equilibrium flow [12], [13]. According to radial equilibrium hypothesis, it is possible to derive the velocity triangles a different radii of the blade. To this end it is necessary to compute lift and drag forces acting on the blade at each radius (Figure 4). For an isolated airfoil the axial force coefficient (C_{ax}) and the circumferential force component (C_{θ}) [13] are:

$$C_{ax0} = C_L \cos \beta_1 + C_D \sin \beta_1 \quad (1)$$

$$C_{\theta0} = C_L \sin \beta_1 - C_D \cos \beta_1 \quad (2)$$

(here the subscript θ refers to the isolate airfoil).

Following Raghunathan [12] it is possible to estimate C_{θ} and C_{ax} (and afterwards to derive the power available at the shaft) on the whole rotor through a simple proportional expression:

$$\frac{C_{\theta}}{C_{\theta0}} = \frac{C_{ax}}{C_{ax0}} \quad (3)$$

where $C_{\theta0}$ is measured in a wind tunnel for an isolated airfoil at an equivalent incidence β , C_{ax}/C_{ax0} and $C_{\theta}/C_{\theta0}$ are the ratios of the normalised aerodynamic force acting on an airfoil in a cascade with the one acting on an isolated airfoil at the same incidence angle.

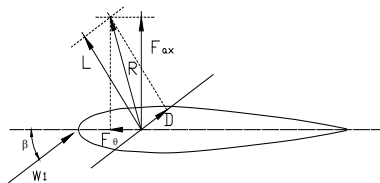


Figure 4: Force vectors acting on the blade section [14].

The actual normal aerodynamic force is then computed using the following expression, derived from the experimental dataset given in [12]:

$$\frac{C_{ax}}{C_{ax0}} = 2.7773 \cdot (\sigma^2) - 0.7106 \cdot \sigma + 1.0639 \quad (4)$$

$$\frac{C_{\theta}}{C_{\theta0}} = -4.0542 \cdot (\sigma^4) + 5.6684 \cdot (\sigma^3) + 0.3779 \cdot (\sigma^2) - 0.0715 \cdot \sigma + 0.9966 \quad (5)$$

where σ is the solidity of the turbine.

The total turbine torque, power and efficiency are computed according to the following normalized metrics:

$$C_{\theta} = \frac{T}{\rho h l Z r_{mid} \frac{(U_{mid}^2 + v_{ax}^2)}{2}} \quad (6)$$

$$C_{ax} = \frac{\Delta p Q}{\rho h l Z v_{ax} \frac{(U_{mid}^2 + v_{ax}^2)}{2}} \quad (7)$$

$$\eta = \frac{T \omega}{\Delta p Q} = \frac{C_{\theta}}{C_{ax} \phi} \quad (8)$$

The calculation of lift and drag coefficients at each blade section was carried out using X-Foil 6.94, a public domain software for the analysis of subsonic isolated airfoils by Drela and Youngren [15], [16].

X-Foil [15] is an interactive program mostly used for the design and analysis of 2D subsonic isolated airfoils. The 3D blade geometry was derived by stacking 2D blade section data using the viscous analysis option built in X-Foil [16]. This approach allows the accurate prediction of airfoil polars as a function of Reynolds and Mach numbers, taking into account the compressibility effects in the subsonic range.

For each blade geometry, the number of iterations was set to 10^3 and the turbulence transition criterion N_{crit} was set to 9 (corresponding to the free-stream turbulence of an average wind tunnel).

Coupling the results computed with X-Foil and the expressions in equations (6) to (8) it was possible to derive the torque chart of the turbine, which is showed in Figure 5. Torque at 3600 rpm is higher than at 3000 rpm at nominal rate, whereas when the flow rate decreases the opposite is true.

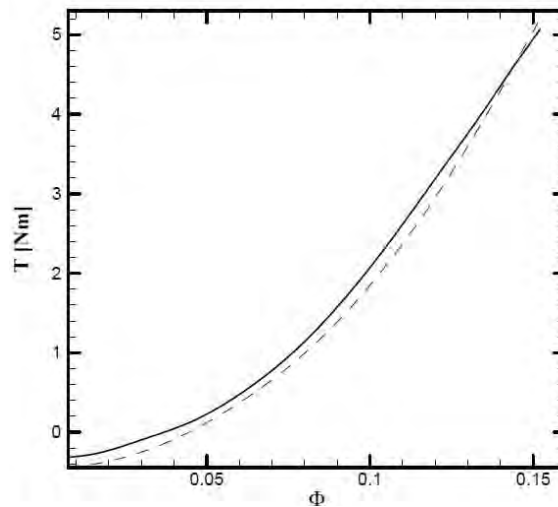


Figure 5: DIMAFP-TW1.5 torque for $c=108$ mm; solid line: $\omega=3000$ rpm, dashed line: $\omega=3600$ rpm.

As Wells turbine does not work at fixed nominal power, we selected an angular velocity of 3000 rpm in order to have the higher efficiency.

In Figure 6 we report the self-starting condition diagram as per [12]. In order to work in self-starting conditions we decreased σ_t to 0.6.

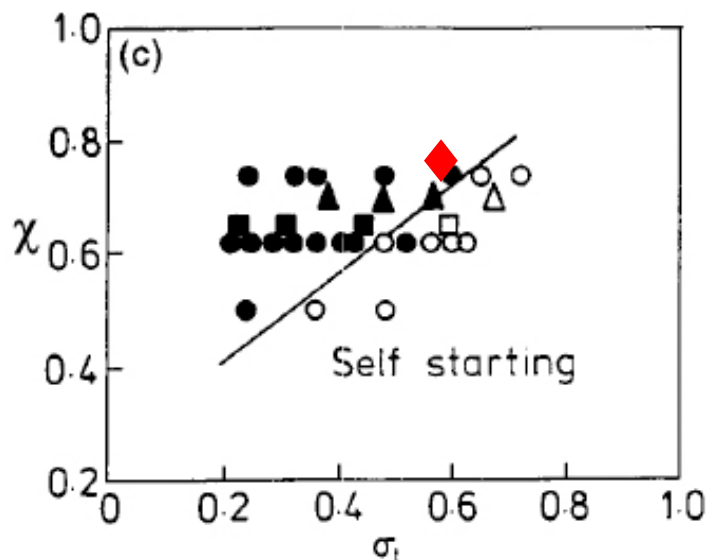


Figure 6: Self-starting diagram after Raghunathan [12]. \blacklozenge : DIMAFP-TW1.5.

Figure 7 shows torque for $c=108$ and $c=117$, respectively $\sigma_h=0.64$ and $\sigma_t=0.6$. Torque with $c=117$ is higher than torque with $c=108$, but the difference between the two decreases as the flow rate decreases.

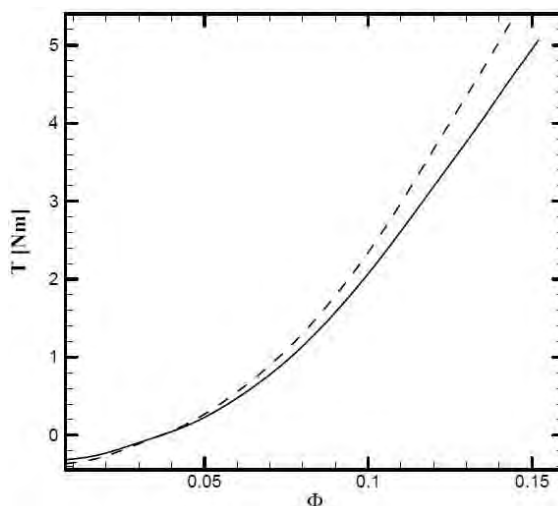


Figure 7: DIMAFP-TW1.5 torque $\omega=3000$ rpm; solid line: $c=108$ mm, dashed line: $c=117$ mm.

To verify the characteristic curve calculated from X-Foil, we derived it again following Euler work method.

Figure 8 shows that two method give similar torque output up to $0.5Q_{des}$. Below $0.5Q_{des}$ the difference increases, and Euler work method overestimates torque.

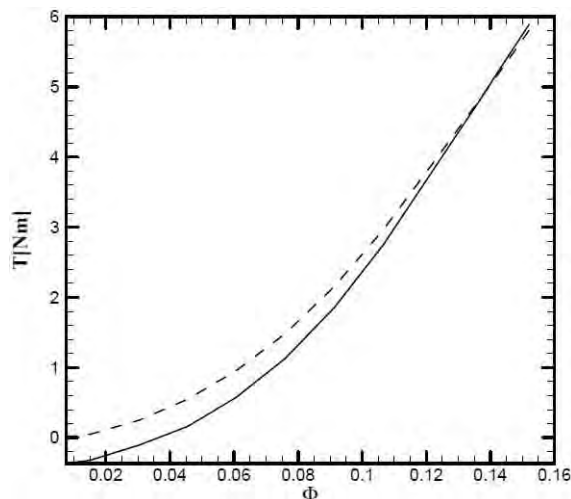


Figure 8: DIMAFP-TW1.5 torque $\omega=3000$ rpm; solid line: X-Foil data, dashed line: Euler work.

4. IGV/OGV design

A swirl component was given to the fluid that enters the Wells turbine in order to increase power and energy output; to this aim an Inlet/Outlet guide vane (I/OGV) was designed (Figure 9) following CFD computations.

Figure 10 shows the increment of torque in Wells turbine coupled with I/OGV respect Wells turbine without I/OGV. The increment of torque decreases with flow rate decrease.

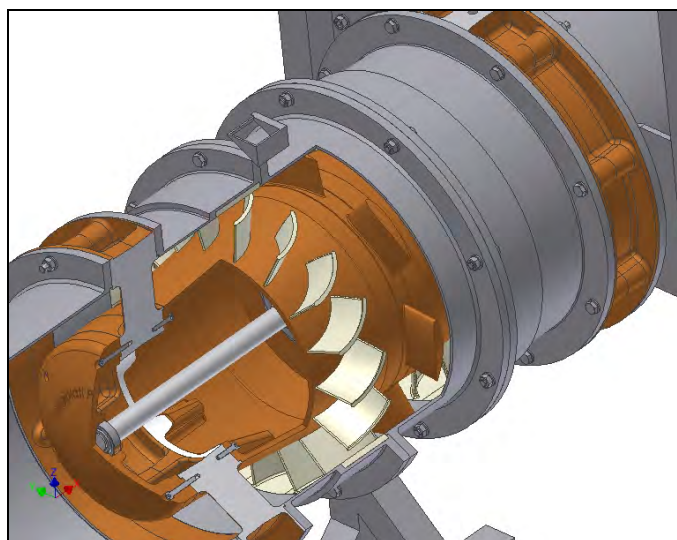


Figure 9: DIMAFP-TW1.5 rendering.

5. Acknowledgements

The authors are indebted to Stefano Minotti and Andrea Marchegiani for contributing to the studies of Wells turbine configuration.

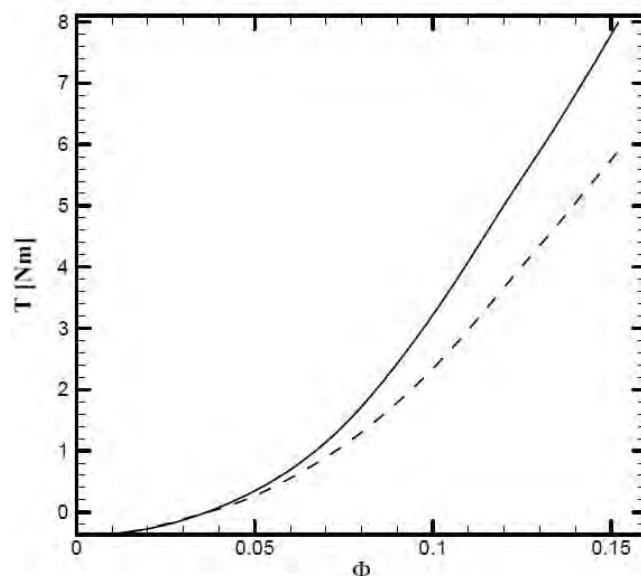


Figure 10: DIMAFP-TW1.5 torque diagram with I/OGV.

References

- [1] A. Clement et al., *Wave energy in Europe: current status and perspectives*, Renewable and Sustainable Energy Reviews, 2002, pp.405-431.
- [2] T. W. Thorpe, *A brief review of wave energy*, Report ETSU-R-120 for DTI, AEA Technology, 1999.
- [3] A. Corsini, F. Rispoli, *Modeling of wave energy conversion with an Oscillating Water Column device*, Proceedings of 6th European Seminar OWEMES, 2006, Brindisi, Italy.
- [4] T.J.T Whittaker, S.J McIlwaine, R Raghunathan, *A review of the Islay shoreline wave power plant*, Proceedings of European Wave Energy Symposium, Edinburgh, 1993.
- [5] T Heath, T.J.T Whittaker, C.B Boake, *The design, construction and operation of the LIMPET wave energy converter (Islay, Scotland)*, Proceeding 4th European Wave Power Conference, Aalborg, Denmark, paper B2, 2000.0
- [6] A.F. de O. Falcão, R.J.A. Rodriguez, *Stochastic modelling of OWC wave power plant performance*, Applied Ocean Research 2002, pp.59-71.
- [7] P. White, *Developments in Norwegian Wave Energy*, Proceedings of a Conference on Wave Energy Devices, Coventry, UK, 1989.
- [8] P. Boccotti, *On a new wave energy absorber*, Ocean Engineering 30, pp. 1191-1200, 2003.
- [9] P. Boccotti, *Caisson breakwater embodying on OWC with a small opening*, Ocean Engineering 34, pp. 806-819.
- [10] S. Minotti, *Innovative turbulence models for the simulation of air turbines in wave energy conversion system*, PhD Thesis.
- [11] Webster and Gato, *The Effect of Rotor blade sweep on the performance of the Wells Turbine*, Int. J. of Offshore and Polar Engineering, 1999
- [12] S. Raghunathan, *The Wells air turbine for wave energy conversion*, Prog. Aerospace Sci., vol. 31, pp. 335-386, 1995.
- [13] S.L. Dixon and C.A Hall, *Fluid Mechanics and Thermodynamics of Turbomachinery, 6th ed.*, Butterworth-Heinemann, Elsevier, USA, 2010.
- [14] A. Corsini, F. Rispoli, E. Tuccimei, *Development of air turbines for small power OWC Plants*, Proceeding 9th European Wave and Tidal Energy Conference Series EWTEC, Southampton, UK, 2011.
- [15] *The XFOIL 6.94 website*. [Online]. Available: <http://web.mit.edu/drela/Public/web/xfoil/>
- [16] M. Drela, H. Youngren, *XFOIL 6.94 User Primer*. [Online]. Available: http://web.mit.edu/drela/Public/web/xfoil/xfoil_doc.txt.

Session 7: Other Marine Renewable Energy and Environment issues

Chairmen: C. Borri, M. Marcelli

Experimental study of the erosion in a sand bed caused by wakes behind tidal energy extraction devices - F. Fedoul, M. Obregon, J. Ortega-Casanova, R. Fernandez-Feria (Departamento Ingenieria Mecanica y Mecanica de Fluidos, ETS de Ingenieria Industrial, Universidad de Malaga, Málaga (ES))

Aperture Plasmonic Nano-antennas in Solar Energy Harvesting - D. Ramaccia (Department of Applied Electronics, 'RomaTre' University, Rome (IT)), S. Scanu, V. Piermattei (Laboratory of Experimental Oceanology and Marine Ecology, University of Tuscia, Civitavecchia (IT)), F. Bilotti (Department of Applied Electronics, 'RomaTre' University, Rome (IT)), M. Marcelli (Laboratory of Experimental Oceanology and Marine Ecology, University of Tuscia, Civitavecchia (IT)), A. Toscano (Department of Applied Electronics, 'RomaTre' University, Rome (IT))

Small wind turbines applications in seaports: cost analysis and market potential in Italy - D. Chiaroni, V. Chiesa, F. Frattini, R. Terruzzi (Dipartimento di Ingegneria Gestionale, Politecnico di Milano, Milan (IT))

An e-Learning Platform for Off-shore Wind Energy Logistics and Infrastructures - F. Fontana, E. Cosimi, G. Ponzio (ENEA, Rome (IT))

Experimental study of the erosion in a sand bed caused by wakes behind tidal energy extraction devices

F. Fedoul¹, M. Obregon², J. Ortega-Casanova³ and R. Fernandez-Feria⁴

Departamento Ingeniería Mecánica y Mecánica de Fluidos, ETS de Ingeniería Industrial, Universidad de Málaga, C/ Dr Ortiz Ramos s/n, 29071, Málaga, Spain

¹email: fai.fed@gmail.com

²email: mariaobregon@uma.es

³email: jortega@uma.es

⁴email: ramon.fernandez@uma.es

Abstract – This work deals with an experimental fluid dynamic study of wakes generated by submerged sails used in devices of tidal energy extraction. The main aim is to study the environmental effect that these wakes could have in the sediment re-suspension from a sandy bottom located at a given distance from the sail. To that end, a 2 cm chord sail, consisting of a rectangular flat plate, is located in the center of a sediment channel of 64 mm width, whose bottom has been filled with sand of 0.3 mm mean diameter. We have characterized the effect of the sail on a sandy bottom for different angles of attack between the sail and the uniform stream flowing through the channel and different distances from the sail to the bottom for a given Reynolds number.

1. Introduction

Interest in renewable energy has increased continually over the last decades. Energy extraction using tidal current energy devices offers a sustainable alternative to conventional sources and a predictable alternative to other renewable energy technologies [1].

The airfoils and sails used in some devices to extract energy from tidal river and currents affect the marine and fluvial environments causing re-suspension of bottom sediments. Accordingly, it is important to take into consideration their potential impact on the surrounding marine and coastal environments once they are being used as a tidal energy capture device. In addition, there are many other marine and fluvial engineering devices that can also produce severe erosion on the sand bed, such as the wakes from maneuvering ship's propeller [2], and, even, on rock masses, such as the erosion phenomena downstream of spillways in large dams [3].

In this work we present an experimental fluid dynamic study of the erosion on a sand bed, and the characterization of corresponding scour, generated by wakes behind sails typically used in devices of tidal energy extraction. To that end, we have used a sediment channel where we are able to characterize the effect of the presence of a sail on a sandy bottom for different angles of attack between the sail and the uniform stream flowing through the channel, and for different distances from the sail to the bottom.

A number of different techniques are available for measuring sediment scours. Some of the current available techniques to reconstruct the scour real magnitude are, for instance, stereo photography, infrared beam, ultrasonic, depth profilers, laser 3D-scanning devices, (see [4] and [5], among others).

As it has been said previously, the main aim of this work is to study the environmental effect that wakes behind sails could have in the sediment re-suspension from a sandy bottom located at a given distance below the sail. To that end, a 2 cm chord sail, consisting of a rectangular flat plate, is located in the center of the channel of 64 mm width, whose bottom has been filled with sand of 0.3 mm mean diameter. For quantitative measurement of the scour pattern created on the sand bed, once it becomes steady, a digital camera, mounted on a side of the channel, is used to take photos of the scour illuminated by a laser sheet. These images are later digitally processed to get from them the dimensional profile of the scour. Its illumination was carried out by means of a 40 mW green laser with a wavelength of 532 nm. Similar techniques to the one used here have been previously used in [6], to characterize aeolian sand ripples, or in [5], to measure the scour created by impinging swirling jets.

The analysis of the scour properties for different values of the parameter under consideration are used to evaluate the environmental impact caused by the presence of the above mentioned devices.

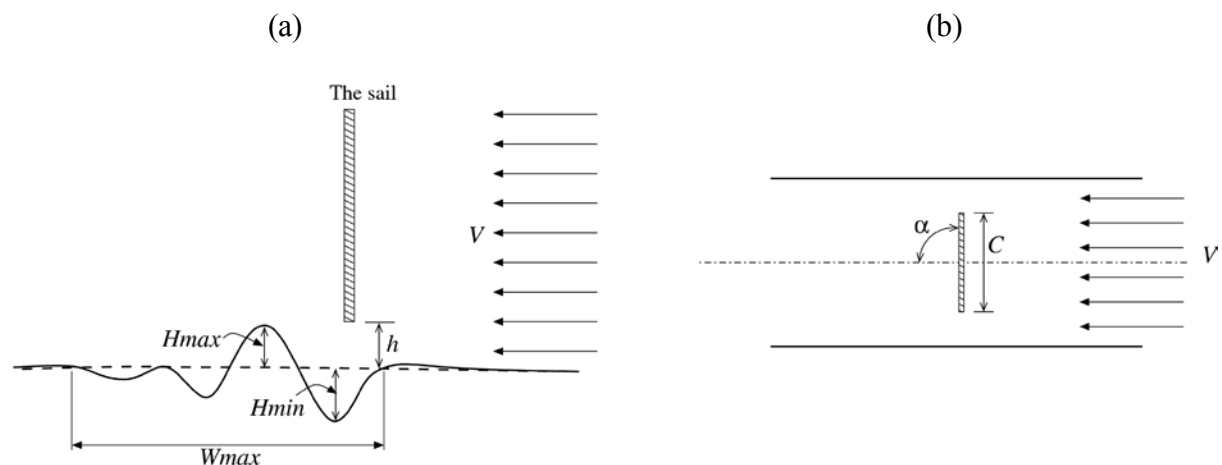


Figure 1: Sketch of the experiment. (a) Side view: the dash line is the unperturbed sandy bottom and the solid line the profile of the scour after the erosion with its main properties indicated. (b) Top view: the angle of attack and the chord are indicated. V is the mean velocity of the flow.

2. Experimental setup

The experiments have been carried out in a sediment channel where the sail is located at a known distance h above the sand (see Figure 1 with a sketch of the experiment). The measurement of the erosion on the sandy bottom around the sail is done by means of a Z-laser (with a wavelength $\lambda=532$ nm) used to illuminate the scour profile. The illuminated profile is then captured by a digital camera placed on the side of the sediment channel and, finally, the image taken is digitally processed to get the dimensions of the created scour. Figure 2 shows the different instruments and devices of the experimental setup and whose principal characteristics are described below. A sketch of the experimental setup is depicted in Figure 2 with a description of its different elements in Table 1.



Figure 2: Photograph of the experimental setup.

Element #	Description
1	Channel of rectangular section with transparent walls.
2	Storage tank.
3	Impulsion pump.
4	Input storage.
5	Flush valve.
6	Reassuring input flow.
7	Catch basin.
8	Flow control valve.
9	Flowmeter.
10	Tubing.
11	Flush valve.
12	Support.
13	Support.
14	Wheel to control the inclination of the channel.
15	Ground anchorages.
16	Orifice plate flowmeter.
17	Connecting tubes between the orifice plate and manometer tubes Panel.
18	Manometric tubes panel and hand pump.
19	Discharge pipe to the storage tank.

Table 1: Description of the elements of the setup.

2.1 Sediment channel

It consists in a channel of rectangular section (64 mm x 2.5 m) with transparent walls, made by folded transparent pieces of methacrylate, and assembled on two supports, with a system to control the inclination of the channel (which is used to set the channel horizontally).

Their different elements can be seen in Figure 3 and described in Table 1. The flow rate through the channel can be selected by means of a valve placed in the Basic Hydraulic Feed System (FME00/B).

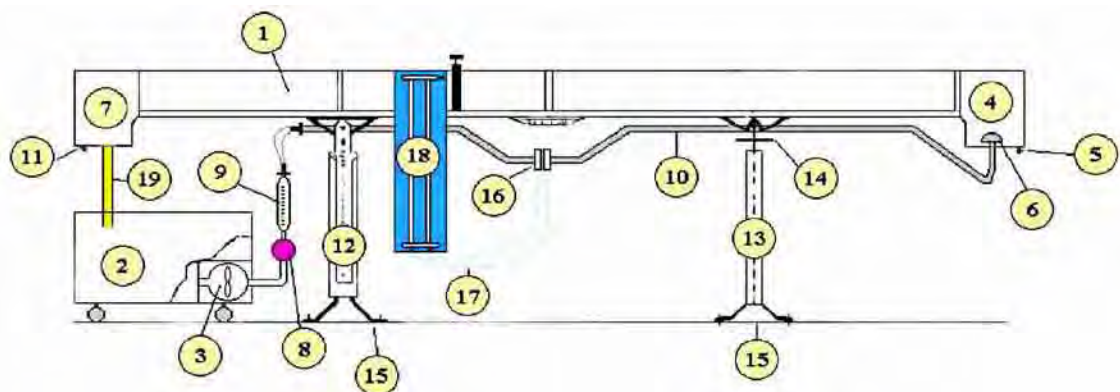


Figure 3: Sketch of Sediment channel.

2.2 The sail

The sail used was a flat plate with a 2 cm chord and a rotation angle between 0° to 360° (see Figure 4).

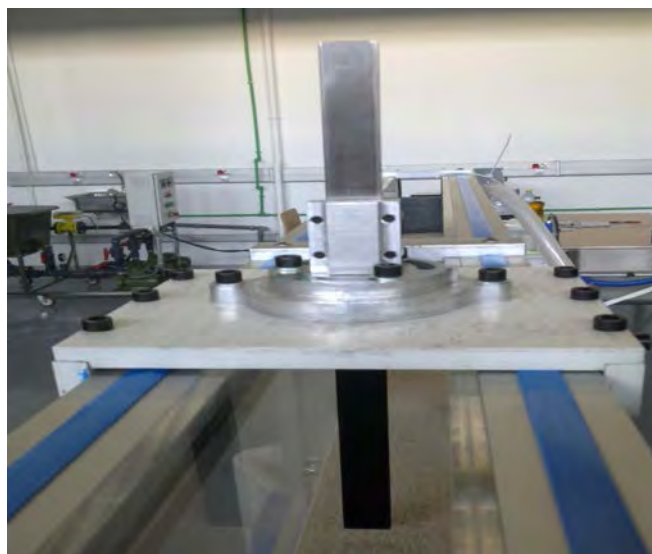


Figure 4: The sail (in black) and its support at the top of the channel of sediment.

2.3 Z-laser

For the visualization of the erosion around the sail, a Z-laser was used with the following characteristics:

- Output power: 40 m W;
- Wavelength: 532 nm; and
- Dimensions: $\varnothing 40 \times 280$ mm (11 in).

2.4 The camera

To take the photos of the illuminated scour, a camera was used with the following characteristics:

- Video camera Sony Handycam 60 GB, Model: DCR-SR37E;
- Video signal: PAL color, Specification 1.080/50i,
- Hard Disk: 60 G bytes; and
- Images per second: 25.

3. Quantitative measurements of the scour in a sandy bottom

The experimental procedure consists of several steps which can be summarized as follows:

1. An image of a target (containing an array of white concave points) inside the sediment channel with the water at rest is taken by the camera;
2. After that, the target is removed, and the sail is put in the channel at a distance h above the sand bed and with an angle of attack α with respect to the water flow (see Figure 1);
3. Then, the pump is started and a flow rate Q is selected. It works until the scour is created in the sand bed;
4. Next and once the sand bed is stabilized, the pump is switched off, the sail removed and a new picture of the scour illuminated by the laser sheet is taken; and
5. Finally, the image processing is carried out and the real magnitude of the scour is obtained.

The target contains an array of white concave points with a distance between centers of 2.5 mm. Since the real dimensions of the target and the distance between points are known, the distorted image taken in #1 (due to refraction and the misalignment between the camera and the laser sheet) will be used later to get the coefficients of a bilinear transformation between the original and distorted target (see Figure 5). Also, the ratio pixel/mm is obtained at this step. The transformation obtained will allow us to reconstruct the real magnitude not only of the target but also of the illuminated scour created.

Figure 6 shows an example of the transformation once it is applied to the illuminated scour: (a) is the distorted image of the scour pattern, as captured by the camera, and (b) is the transformed image, corresponding to its actual shape.

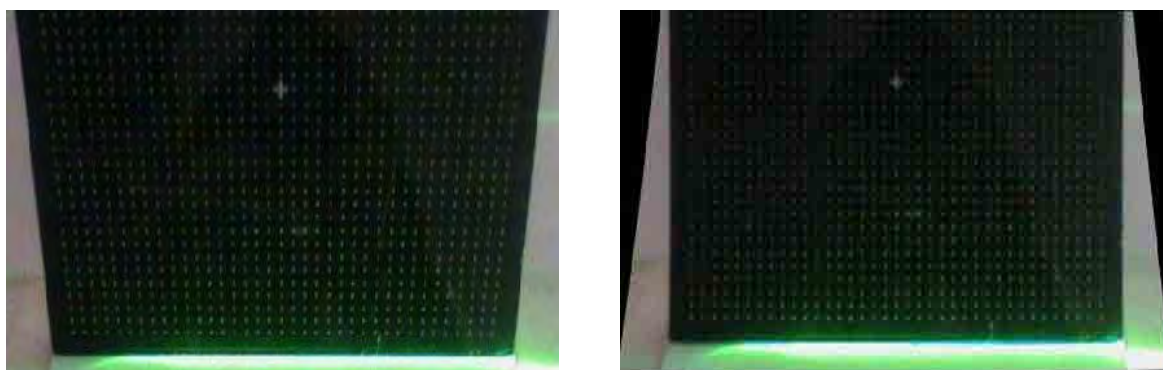


Figure 5: Image of the target before (left) and after (right) the transformation is carried out.

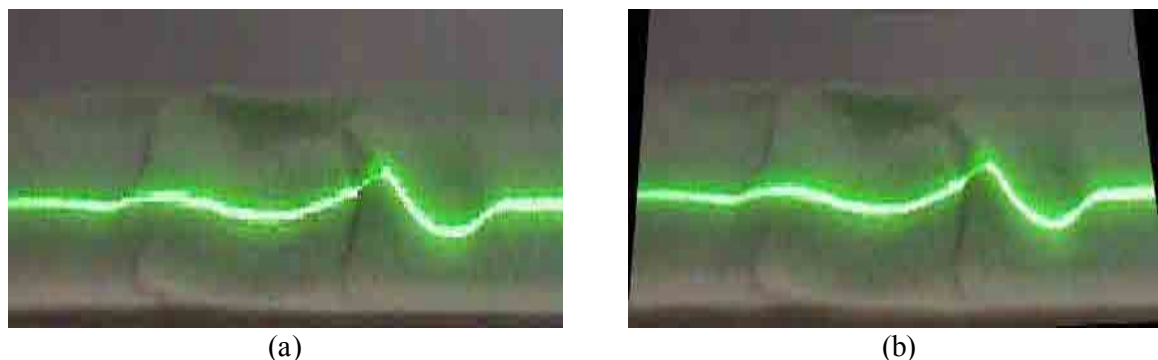


Figure 6: Images of scour illuminated with laser sheet, (a) before, (b) after transformation resulting from calibration.

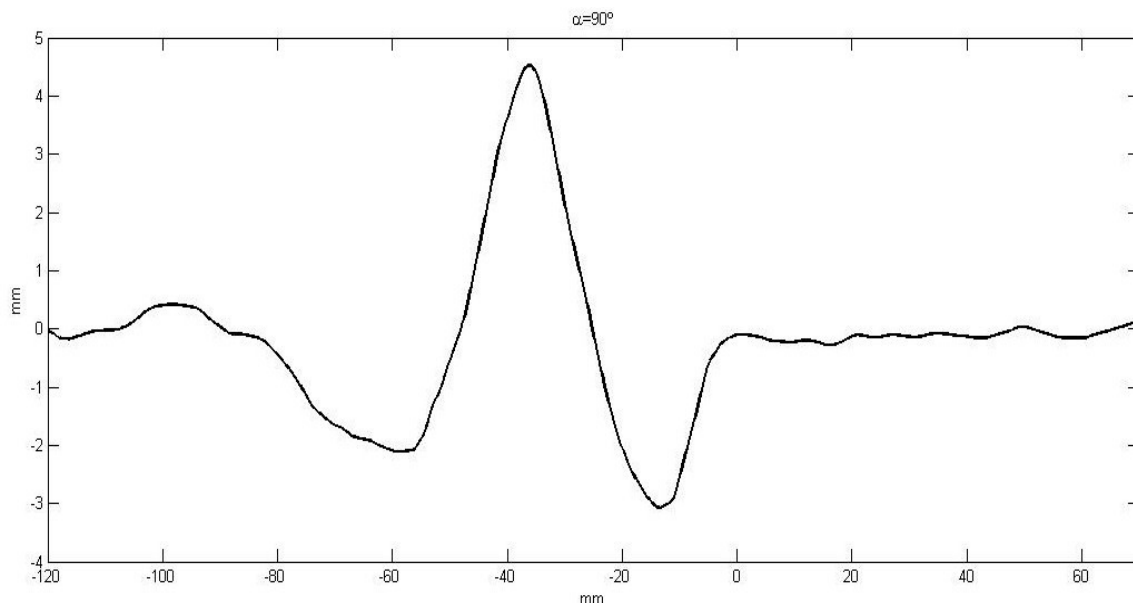


Figure 7: Dimensional digitalized profile of the scour. The flow is from right to left ($h=1\text{ mm}$, $\alpha=90^\circ$ and $Re=4500$).

In this case $h=1\text{ mm}$, $\alpha=90^\circ$ and $Q=0.0014\text{ m}^3/\text{s}$, which corresponds to a Reynolds number based on the sail chord of about 4500. Once the scour profile is transformed to its real magnitude, a threshold segmentation technique is used to select only the illuminated pixels of the image and with the known ratio pixel/mm, the real dimensions of the scour can be obtained. This can be seen in Figure 7, where the scour dimensions are shown (in mm) after the image processing is carried out.

4. Results

As it has been discussed previously, the results presented here are those obtained after the illuminated images taken of the scour are digitally processed using Matlab. We have considered three angles of attacks ($\alpha=90^\circ$, 70° y 50°), four distances h from the sail to the bottom, $h/C=0.05$, 0.1 , 0.15 y 0.2 , where C is the sail chord, and a flow rate of $0.0014\text{ m}^3/\text{s}$, being water the working fluid. From these values, and considering laboratory conditions, the Reynolds number based on the sail chord is of about 4500.

To compare all the results, we have fixed the laser sheet passing through the middle of the channel for all experiments, as shown in Figure 8, where the illuminated scour created when $\alpha=90^\circ$ and $h/C=0.05$ is shown. This image can help us to understand the process: taking into account that the flow is from right to left, with the sail located just above the first minimum in the sand bed, the fluid flows around the sail being the flow under the sail the responsible of making the first and pronounced “crater”.

Next, some of the eroded sediments are deposited just downstream the sail, giving place to a “hill”, behind which the erosion continues until a certain distance downstream where the decaying wake is not able to suspend more sediments. It is also remarkable the erosion created at both sides of the scour pattern (where the scour is actually deeper than anywhere else).

This is due to the couple of intense vortices emerging from the two lateral borders of the sail which, as can be seen in Figure 8 have high erosion capacity.

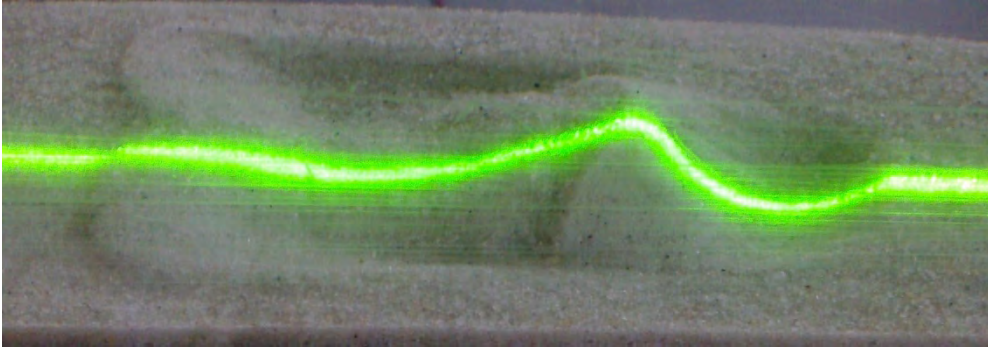


Figure 8: Image showing the scour with its central profile illuminated by the laser sheet along the middle of the channel for $\alpha=90^\circ$ and $h/C=0.05$. The flow is from right to left.

Furthermore, as one can see for this case with $\alpha=90^\circ$, the pattern created is symmetrical with respect to the laser sheet or channel symmetry line (remember the laser is passing through the middle of both the sail and channel), a fact that will not happen with other angles of attack for which the scour seems to rotate with the sail losing its symmetry with respect to the channel, as it will be shown below.

We report in what follows the non-dimensional scour profiles, as well as their most relevant features, once the images have been digitally processed.

Figures 9, 10 and 11 show the non-dimensional profiles of the scour H/C for different distances h/C between the sail and the bottom, and the three angles of attack, $\alpha=90^\circ$, 70° and 50° , respectively. Some preliminary conclusions can be drawn from their analysis: on the one hand, one can observe that the scours generated when the angle is 90° are much deeper and wider than scours generated with lower angles; that is, the higher the angle of attack, the deeper and wider the scour created. And, on the other hand, as the distance to the bed decreases both the depth and width of the scour on the sand bed increase; that is, the lower the distance from the sail to the bed, the deeper and wider the scour created.

It must be remarked that these profiles are obtained along the middle of the channel, and only when $\alpha=90^\circ$ they coincide with the symmetry line of the scour.

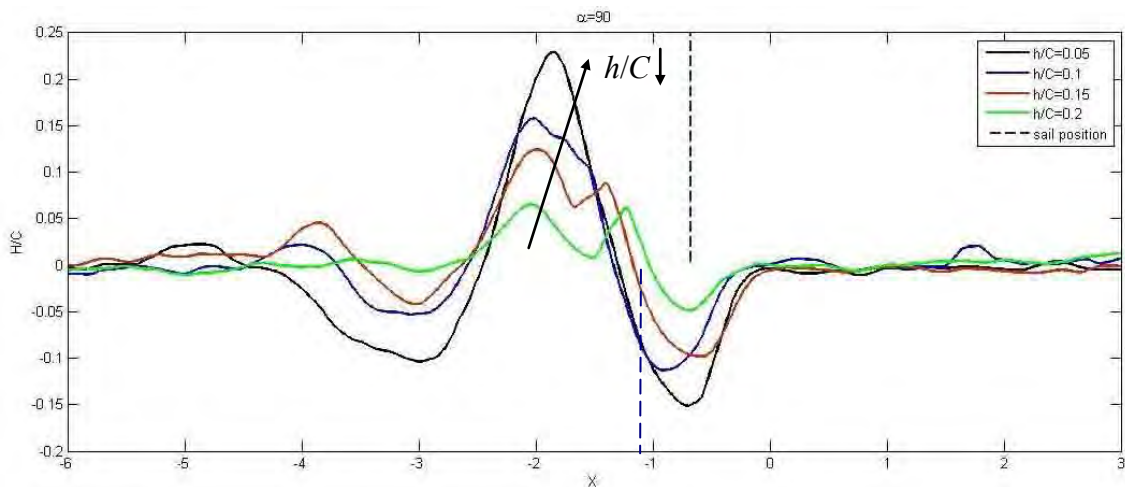


Figure 9: Non-dimensional profile of the scour for $h/C=0.05$, 0.1 , 0.15 and 0.2 with an angle of attack $\alpha=90^\circ$. The x -axis has also been made non-dimensional with the sail chord C . The flow is from right to left. The vertical dash line corresponds to the position of the sail.

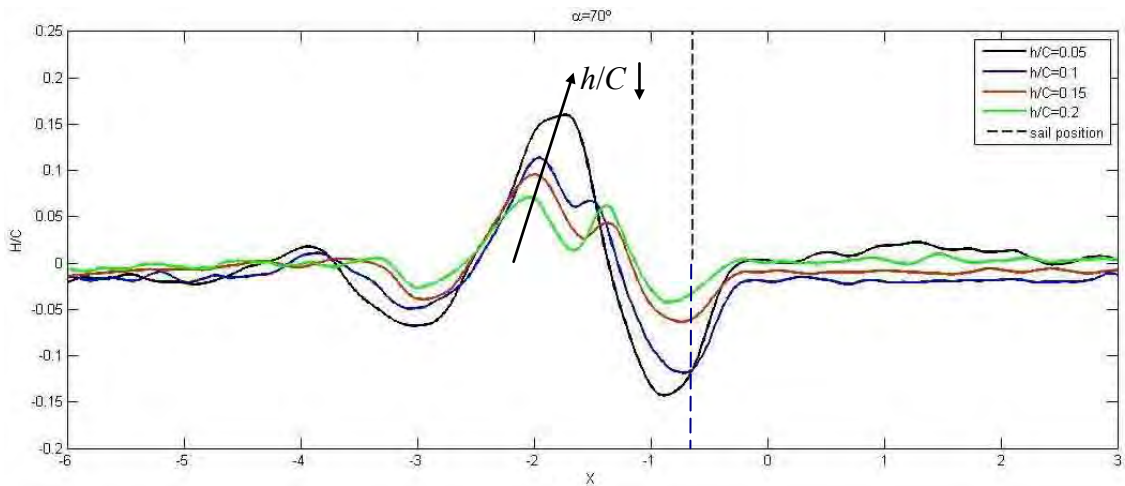


Figure 10: As in Figure 9, but for $\alpha=70^\circ$.

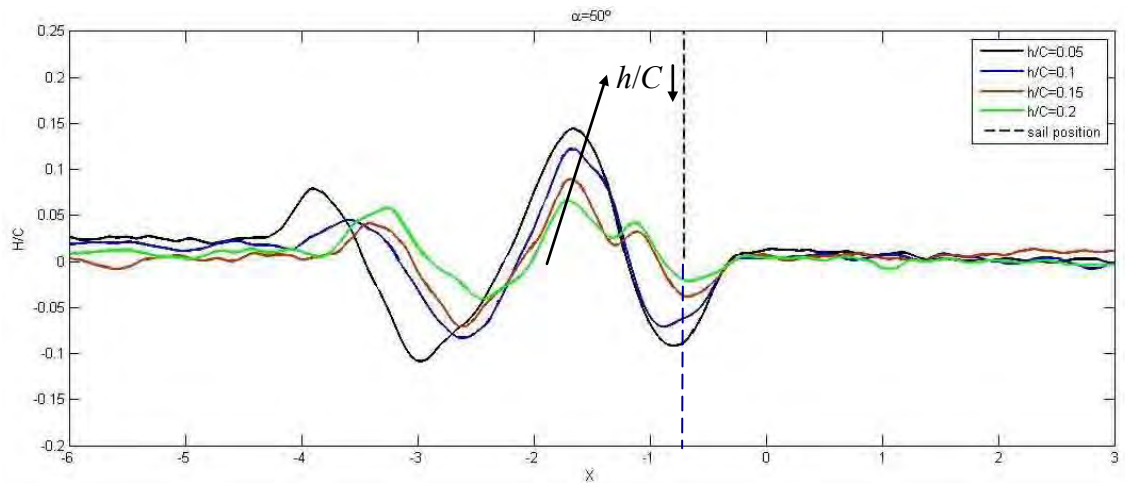


Figure 11: As in Figure 9, but for $\alpha=50^\circ$.

When the angles of attack are $\alpha=90^\circ$ (Figure 9) and 70° (Figure 10), the maximum depth along the middle of the channel is directly below the sail; i.e., it coincides with the first minimum of the measured profiles. However, when $\alpha=50^\circ$, the maximum depth is located downstream the sail and it coincides with the second minimum of the profile. This is due to the rotation of the sail having as a result a change in the main direction along which the scour develops.

This direction seems to be almost perpendicular to the sail, which means that the second minimum observed in Figure 11 is due to the lateral vortices generated by the sail, responsible of the highest erosion and deepest scour in the middle of the channel (deeper than the erosion just under the sail). To characterize the different profiles of the scours, three parameters have been used (see Figure 1): the maximum depth of the scour (H_{min}); the maximum height of the elevation due to the re-deposition of sediments (H_{max}); and the maximum width of the scour (W_{max}).

All these magnitudes can be extracted from Figures 9-11, and they are summarized in Figures 12, 13 and 14, where their non-dimensional evolution are shown as a function of the angle of attack and for the different distances h/C used. It is observed that all the mentioned parameters, H_{min} , H_{max} , and W_{max} , increase (in absolute value) when the distance to the bed decreases and the angle of attack increases.

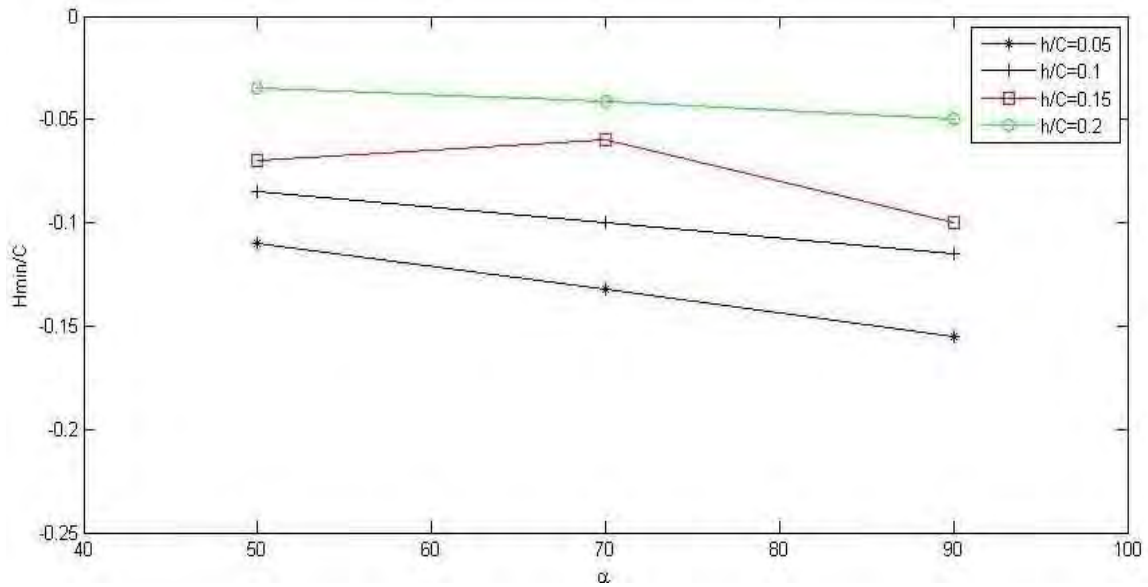


Figure 12: H_{min}/C versus the angle of attack α for the values of h/C indicated.

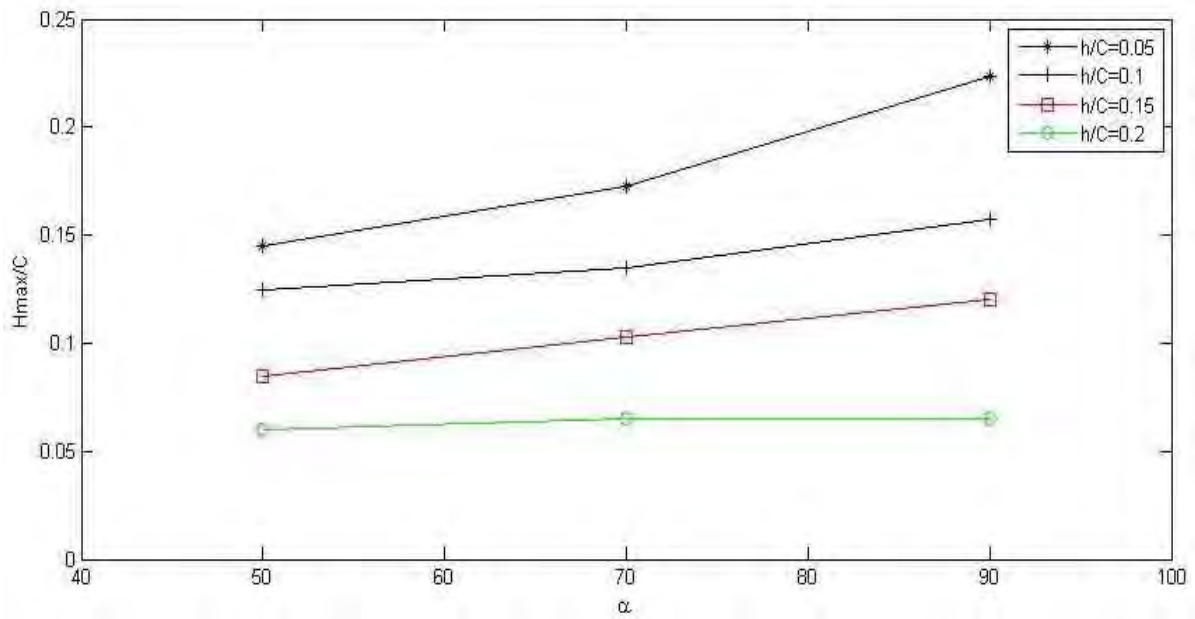


Figure 13: As in Figure 12 but for H_{max}/C .

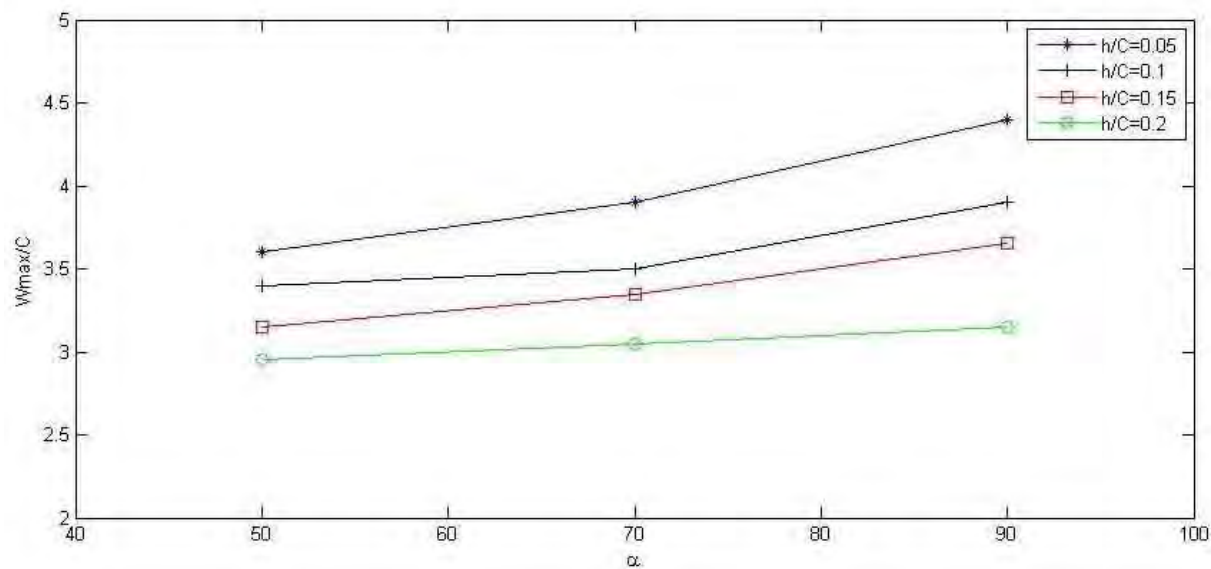


Figure 14: As in Figure 12 but for W_{max}/C .

As it was said previously, special care must be taken when *the* angle of attack is 50° , because in that case H_{min} depicted in Figure 12 is not the absolute minimum for all values of h/C .

5. Conclusions

From an environmental point of view, it is obvious that the higher the distance between the sail and the bottom, the lesser the effect on the last one. However, sometimes due to either working conditions or physical limitations, the sail have to be as close to the sandy bottom as possible. It is then when its effect on the bottom can be important and the angle of attack crucial on the final erosion created. In that sense, the results obtained show that, along the middle of the channel, the higher the angle of attack, the deeper and wider the scour on the sand bed. Nevertheless, this affirmation could be different if the whole pattern were analyzed since; in that case, the erosion due to the interaction between the leading/trailing end vortices and the sand bed could be the highest on the bottom. To answer this question, a 3D map of the scour must be obtained, being this task the authors' future work.

References

- [1] F.O. Rourke and F. Boyle and A. Reynolds, Tidal energy update 2009. *Appl. Energy*, **87**, 398-409 (2010)
- [2] G.A. Hamill, J.A. McGarvey and D.A.B. Hughes. The effect of rudder angle on the scouring action produced by the propeller wash of a manoeuvring ship. Journal of the Permanent International Association of Navigation Congresses. January 2001. No.106. pp 49-62.
- [3] R.Q. Velloso and E. A Vargas Jr. Experimental and numerical studies of erosion processes downstream of spillways in large dams. 45th U.S. Rock Mechanics / Geomechanics Symposium, June 26-29, 2011 , San Francisco, California.
- [4] R. J. Munro, S. B. Dalziel, H. Jehan. Attenuation technique for measuring sediment displacement levels. *Exp. Fluids*, **39**, 600-611 (2005).
- [5] J. Ortega-Casanova, N. Campos and R. Fernandez-Feria. Experimental study on sand bed excavation by impinging swirling jets. *J. Hydraul. Res.* **49** (5), 601-610 (2011).
- [6] B. Andreotti, P. Claudin, O. Pouliquen. Aeolian sand ripples: experimental study of fully developed states. *Phys. Rev. Letts.* **96** (2), 028001(4) (2006).

Aperture Plasmonic Nano-antennas in Solar Energy Harvesting

D. Ramaccia¹, S. Scanu², V. Piermattei², F. Bilotti¹, M. Marcelli² and A. Toscano¹

¹*Department of Applied Electronics, 'RomaTre' University*

Via della Vasca Navale 84, 00146 Roma, Italy, dramaccia@uniroma3.it

²*Laboratory of Experimental Oceanology and Marine Ecology, University of Tuscia
Molo Vespucci, 00053 Civitavecchia (RM), Italy*

Abstract – In this contribution we present a horn nano-antenna working at near-infrared frequencies which consists of a silver nano-waveguide shaped at one of its ends in such a way to increase the physical aperture and progressively transforms the guided mode into a radiated mode. Here the nano-antenna has been employed to harvest effectively the solar electromagnetic energy. The energy is guided and focused on the active area of a nano-photodiode, enhancing its performances in terms of conversion efficiency. More efficient compact solar panels can be employed for the 'green' navigation of the so-called solar-powered boats that exhibits many advantages from silent navigation, zero emissions, little wavemaking to very low-operating costs.

1. Introduction

In the last decades the renewable energy represents an interesting topic for the most of the countries around the world. Many reasons contributes to its success: first of all, the renewable energy does not deplete when we are using it because it is replenished constantly from the natural processed and does not produce a waste, secondly, the solar, wind, and marine energy are widespread on the surface of the earth and, thus, easily accessible by anyone. Although nowadays the fossil fuels still represents the most important energy source, the move towards the renewable energy is facilitated by the recent technological growth of the converting systems for the energy-harvesting.

In particular, the interest in solar electricity, also known as photovoltaics (PV), has grown rapidly from the 1950s, due to the development of more efficient and low-cost converting systems. The PV process consists of the production of an electrical current from the light energy. It take place in the PV device, such as a solar cell or a photodiode, where the electrons bound to the atoms become free to move towards the contacts due to the impinging electromagnetic energy from the sun [1]. This technology was born in 1883 when Charles Fritts fabricated the first large area solar cell with an efficiency conversion around 1% [2].

Nowadays a good compromise in terms of costs and reliability is the crystalline silicon (c-Si) technology that exhibits an efficiency conversion around 20% [3]. Different size of c-Si solar cells are manufactured in according to its specific employment in operative conditions. Typically wide solar panels are employed for the production of energy in solar plants, whereas smaller ones for powering constantly the small devices without using an electric outlet. Indeed, recently the shipbuilding industry is moving towards electric boats (Figure 1) due to the legislative framework evolved in some areas that encourages the use of less-polluting water craft and thus indirectly encouraging solar-powered boats. Moreover they exhibits many advantages from silent navigation, zero emissions, little wavemaking to, last but not least, low-operating costs [4].



Figure 1: Examples of solar-powered catamarans [4].

In fact a significant number of boat users now demand a more relaxing, quieter and cleaner approach to navigation than the one given by using the traditional diesel boats. In this scenario more efficient compact solar panels help to produce much more electric power covering the same area, that is minimal on the ships, and take advantages of more powerful electric motors. In the same time, it is possible to developed solar boat plants, i.e. fleets of boats that produce much more energy than necessary for charging other electric boats all without the use of fossil fuels.

In this framework, the electromagnetic scientific community was stimulated to propose solutions for boosting the performance of the crystalline silicon: in [5], a solar cell with a nanostructure of silicon pillars on the top was designed for increasing the light absorption, due to the multiple reflections of light between the pillars; in [6] an array of silver nanoscatterers was placed on the solar cell surface in order to enhance the localized EM field due to the plasmonic resonance of the scatterers; in [7] a study of a luminescent solar concentrators was presented.

In this paper, a different approach for the enhancement of the EM field energy in proximity of the solar cell is proposed. It starts from the horn nano-antenna concept, presented in [8], where a nano-waveguide, made of silver, has been tapered at one of its ends in order to be shaped as an horn. The aim of this contribution is to propose the horn nano-antenna as light concentrator for solar energy harvesting. The nano-antenna harvests the electromagnetic energy from the sun and collects it on the PV converter. We present the geometry and performances of the horn nano-antenna in terms of *illumination factor (IF)* and evaluate the improvement of the efficiency conversion when the nano-antenna is present.

2. Horn Nano-antennas as sunlight concentrator

A microwave horn antenna consists of a metallic waveguide shaped at one of its ends in such a way to increase the physical aperture and progressively transforms the guided mode of the waveguide into a radiated mode, matching as much as possible the wave-impedance of the waveguide to the one of free-space. Inspired from the horn antennas working at microwave frequencies, in [8] the authors present an innovative nano-antenna at near-infrared frequencies. The horn nano-antenna, shown in Fig. 2a, consist of a non-plasmonic material slab, such as just air, sandwiched between two plasmonic layers made of silver. In order to create an optical rectangular waveguide, the lateral confinement of the field is obtained inserting cylindrical silver pillars arranged in a triangular lattice (Figure 2a). The metallic parts have been modeled according to the experimental data in [9] for a realistic model in the full wave electromagnetic simulator [10].

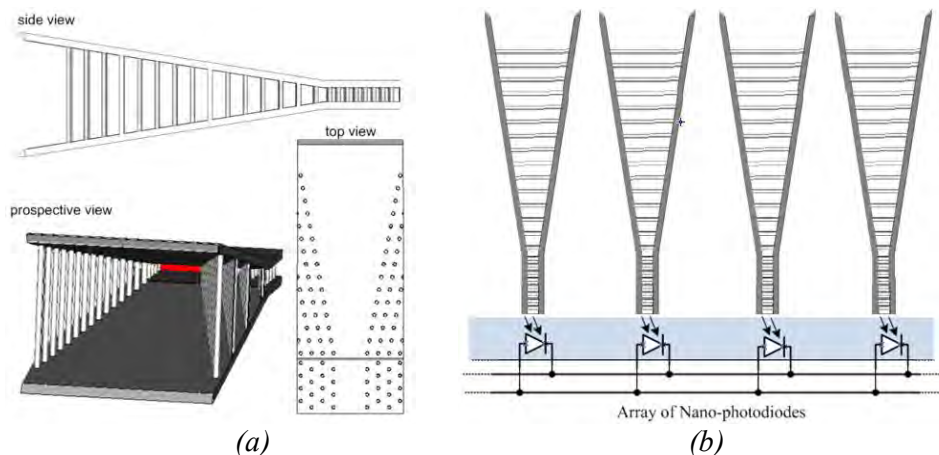


Figure 2: (a) Horn nano-antenna geometry; (b) Side-view of an array of horn nano-antennas on an array of nano-photodiodes.

In Figure 2b we show an operative configuration in which the solar cell consists of an array of horn nano-antenna placed just above on separate nano-photodiodes. Thus, the harvested and guided field is focused on the active surface of the nano-photodiodes that provide the conversion from the guided electromagnetic energy to electric energy. An electric network connects the photodiodes in a parallel connection.

For the reciprocity of the antennas, the radiation properties of the nano-antenna can be used to evaluate the amount of light energy that the antenna is able to harvest from an incident plane wave. The energy is progressively focused and guided by the nano-waveguide towards the nano-photodiode as shown in the inset of Figure 3.

The concentration ability of the component is well represented by using the key parameter *illumination factor* [1], defined as the average Poynting vector normal to the PV converting area when the concentrator is present normalized with respect to the same quantity evaluated when the concentrator is removed. Assume that the center of the detector is aligned with the center of the waveguide port, the value of the illumination factor versus frequency at the port has been numerically evaluated and is shown in Figure 3.

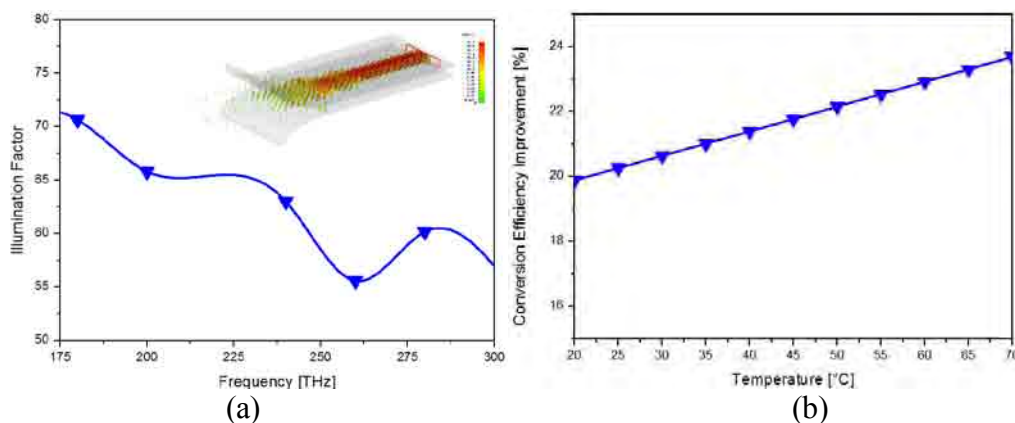


Figure 3: (a) Illumination factor at the center of the optical waveguide port as a function of frequency and (inset) 3D representation of the power flow; (b) Conversion efficiency improvement as a function of the operating temperature.

The nano-antenna increases the illumination factor up to an average value of 60 over the entire operating bandwidth and, using this value, the enhancement of the conversion efficiency as a function of the operating temperature has been evaluated as in [1] and shown in Figure 3b. The enhancement of the conversion efficiency is strongly related to the operating temperature and, thus, by using the multi-physics package in CST [10], we found that the temperature on the photodiode surface reaches the maximum value of about 49°C , assuming that the background temperature is about 30°C . At this temperature the conversion efficiency is increased of about 22%.

3. Conclusions

In this contribution, we have presented some results of our study on a novel concentrator at nano-meter scale consisting of a horn nano-antenna for photovoltaic applications. We have numerically shown the ability of the proposed antenna to concentrate and guide electromagnetic energy towards the detector. The nano-antenna increases the illumination factor up to an average value of 60 over the entire operating bandwidth.

These preliminary results are interesting for the improvement of the photovoltaic solar cell because high value of the illumination factor help to drastically reduce the dimensions of the solar panel itself. Compact and efficient solar panels are needed when the available area reserved for panels is small, such as in the case of the solar-powered boats that are widely spreading for their advantages of silent navigation, zero emissions, little wavemaking and very low operating costs. Indeed, more powerful solar panels contribute to the birth of the solar boat plants, i.e. fleets of boats employed as electrical station in the open sea for charging other boats in difficulty all without the use of fossil fuels.

References

1. A. Luque and S. Hegedus, *Handbook of photovoltaic science and engineering*, 1st ed., Wiley, 2003.
2. C. Fritts, "On a new form of selenium photocell", *Am. J. Sci.*, vol. 26, pp. 465–472, December 1883.
3. M. A. Green, A. J. Z. Wang, S. R. Wenham, "Very high efficiency silicon solar cells: science and technology", *IEEE Trans. Electron Devices*, vol. 46, pp. 1940–1947, October 1999.
4. <http://www.electric-boat-association.org.uk/>
5. C.Chen, R. Jia, H.Yue, H.Li, X. Liu, T. Ye, S. Kasai, H. Tomotsu, N. Wu, S. Wang, J. Chu, and B. Xu, "Silicon nanostructure solar cells with excellent photon harvesting", *J. Vac. Sci. Technol. B*, vol. 29, pp. 021014–021014-6, March 2011.
6. Y. A. Akimov, W. S. koh, and K. Ostrikov, "Enhancement of optical absorption in thin-film solar cells through the excitation of higher-order nanoparticle plasmon modes", *Opt. Express*, vol. 17, pp. 10195-10205, June 2009.
7. V. Sholin, J. D. Olson, and S. A. Carter, "Semiconducting polymers and quantum dots in luminescent solar concentrators for solar energy harvesting", *J. Appl. Phys.*, vol. 101, pp. 123114–123114-9, June 2007.
8. D. Ramaccia, F. Bilotti, A. Toscano, and A. Massaro, "Efficient and wideband horn nano-antenna", *Opt. Letters*, vol. 36, pp. 1743–1745, May 2011.
9. P.B. Johnson and R.W. Christy, Optical constants of noble metals, *Phys. Rev. B*, Vol. 6, pp. 4370–4379, 1972.
10. CST Studio Suite 2011 (www.cst.com).

Small wind turbines applications in seaports: cost analysis and market potential in Italy

Davide Chiaroni¹, Vittorio Chiesa², Federico Frattini³ and Riccardo Terruzzi⁴

¹*Dipartimento di Ingegneria Gestionale, 'Politecnico di Milano', Via Lambruschini 4b, 20156, Milano, Italia, davide.chiaroni@polimi.it*

²*Dipartimento di Ingegneria Gestionale, 'Politecnico di Milano', Via Lambruschini 4b, 20156, Milano, Italia, vittorio.chiesa@polimi.it*

³*Dipartimento di Ingegneria Gestionale, 'Politecnico di Milano', Via Lambruschini 4b, 20156, Milano, Italia, federico.frattini@polimi.it*

⁴*Dipartimento di Ingegneria Gestionale, 'Politecnico di Milano', Via Lambruschini 4b, 20156, Milano, Italia, riccardo.terruzzi@polimi.it*

Abstract –The paper discusses the Italian seaport potential for the adoption of small wind turbines. The paper firstly provides an overview of available technological solutions for small wind plants and discusses in depth their economics. Results about IRR (Internal Rate of Return) and PBT (Pay Back Time) are spread over a broad range of values and show however a huge potential for investments in coastal areas in Italy. Furthermore, the paper examines, through deeply analyzing and using as benchmark the recent case of the seaport of Genoa, the actual potential for small wind turbines in Italy. The analysis suggests there are 91,4 MW of economically sustainable investments at hands for small wind turbines in Italian seaports.

1. Introduction

In 2011 wind power capacity reached 238 GW, increased by 20% thanks to approximately 40 GW of new turbines. As a consequence wind power technology produced more than any other renewable technology in 2011. During this year 10 countries added about 87% of total capacity; 68 countries have more than 10 MW of reported capacity, 22 of them passed the 1 GW level. In the period between 2006 and 2011, the cumulative wind power capacity has increased at an average rate of 26%. In 2010 we could see a growth of new turbine capacity more in emerging countries than in OECD countries. As a matter of fact these are the top countries for new installations: China, USA, India, Germany, UK and Canada. The market share of European Union is about 23% of the global market and about 41% of the global capacity. Five years earlier was about 51% of the global capacity.

In 2011, the European Union reached approximately 94 GW, as the global wind capacity in 2007, with an increment of new 9.6 GW. In 2010, wind power was the third new capacity installed with a share of 21.4%, behind photovoltaic and natural gas. During the years between 2000 and 2011 wind capacity has increased from 2.2% to 10.5% because many countries installed this new technology. Germany remained the leader producer of wind European energy market: in 2011 Germany produced 46.5 TWh of electricity, and the capacity was about 29.1 GW.

In Italy the regions more suitable for the installation of wind turbines are the southern regions and the islands, especially Apulia, Calabria, Campania, Sardinia and Sicily. In Italy all the plants are installed on land, on hills or mountain sites.

In 2010 the installation of new plants decreased, with a total grid-connected wind capacity of 5,797MW, and with an increase of 948 MW over 2009. In 2010, the total number of wind turbines was 4,852, 615 of them were installed during this year, with a total capacity of 1,195 kW. The production was about 8.4 TWh, which covered about 2.6% of total electricity demand on Italian system. According to ANEV (Italian Wind Energy Association) in 2011, the Italian wind capacity reached a level of 6,747 MW, with an increase of 916.4 MW. Obviously Southern regions and islands have remained the main locations for wind production: Apulia with 1,158 MW of total power installed, followed by Sicily (1,116 MW), Campania (809 MW), Sardinia (585 MW), and Calabria (212 MW).

Vestas is the leader manufacturer in Italy, with a total installation of about 2,170 MW of Italian power, equal to 44.7% of total capacity. The second one is Gamesa (901 MW) with a share of 18.6% and the third one is Enercon (680.7MW) with a share of 14%. An emerging company is Nordex with its wind generators (116 MW installed). There are still very few, especially medium-to-large, Italian wind turbine manufacturers; in fact, only Leitwind has started to work in Italian and foreign markets so far, and with very interesting prospects (one factory in India for the Asian market).

With regard to the wind energy producers the most important are International Power, IVPC, FRI-EL, Enel Green Power, EDENS, E-ON, followed by some private companies, smaller than the previous ones, like Veronagest, Erg-Renew, Greentech, Fortore Energia, Tozzi Sud, Moncada and many more.

In Italy the development of the wind market was strongly supported by a incentives system. The main scheme for supporting RES in Italy is based on a RES quota obligation and Tradable Green Certificates (TGCs). The per kWh price for onshore wind energy is still one of the most attractive in Europe at € 0.158 per kWh for 15 years, despite the earnings reduction following the drop in value of green certificates. This price is arrived at by adding the market price for electricity to the green certificate price. This scheme is supposed to change from the next year, 2013, and in the current negotiations with the government, ANEV, the major wind association, has proposed a choice of support level between € 0.152 per kWh for 15 years or € 0.146 per kWh for 20 years. A quota system, at least equal to 650 MW per annum, could be announced to be certain of achieving the NREAP targets.

Two main issues are slowed down the development of big-size wind installations in Italy: (i) lower average wind speed than other European countries and (ii) a longer permitting and grid connection authorization procedures.

As showed in Figure 1 Italy hasn't the best wind in Europe. Countries like France and Germany have a larger availability of wind that means more production hours a year.

The second issue affecting growth came from permitting and grid connection, and from wind production curtailments ordered by the TSO. The Italian market has proven to be lively in 2011, reconfirming the technical and financial feasibility of the wind energy sector in Italy but the uncertainties of authorization procedures and the inadequacy of the information received from Public Administrations, especially at regional and local level are the main difficulties to face during the installation of a wind turbines. Another problem regards reaching the environmental requirements, in particular the Environmental Impact Assessments (EIA).

Social opposition, ranging from spontaneous neighborhood protests to professional campaigns and legal suits at national level, are an increasingly severe barrier in Italy.

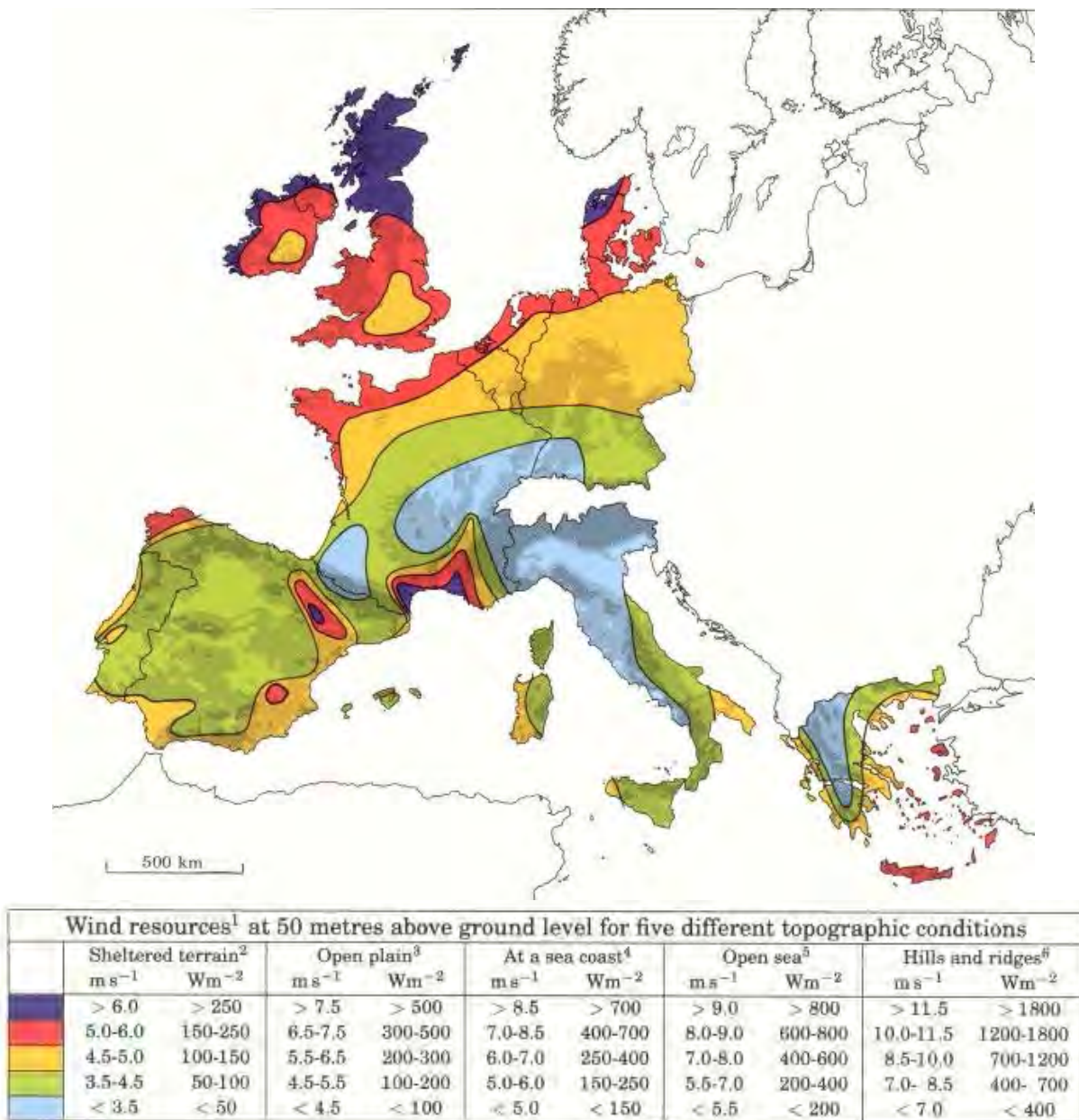


Figure 1: Wind resources at 50 meters above ground level. From: *European Wind Atlas*.
 Copyright © 1989 by Risø National Laboratory, Roskilde, Denmark.

Of course, slowing down the administrative procedures is one of the most important legal means for NIMBY groups to effectively oppose the realization of a project. A greenfield investment in wind plant in Italy could took an average of 4-5 year to be fully authorized and to start the energy production.

Small wind turbines, characterized by a lower environmental impact (with shorter authorization procedures) and a lower cut-in activation wind value, could be a solution to overcome both the issues that slowed down the big-size wind market in Italy. In next Section the economic feasibility of these small wind turbines solutions will be analyzed and then a study about the potential areas interested by this technology in Italy will be presented.

2. Methodology

This paper is composed of two different part: in the first half an economic feasibility study is presented and in the second half a study about the potential application of mini wind turbines in Italian seaport has been conducted.

The first part of the paper begins with a wind energy economic feasibility study. Technical issues include the system architecture, size of equipment, and performance of the system over a year. Economic analysis includes the extra cost of a more expensive maintenance or an extra revenue from the use of the self-produced electricity, among other standard economic parameters (IRR, PBT, ...). These kind of investment, due to the national feed in tariff (Tariffa Onnicomprensiva), in the ideal locations with adequate wind conditions can reach IRR up to 15% and PBT of just 7-8 years.

The economic issues are investigated through data simulations and through the analysis of running pilot project such as the one in Porto Corsini (Ravenna). This is a pilot project that is part of the Project Powered and that has been realized in Porto Corsini (Ravenna), thanks to the cooperation between the Province of Ravenna (which is a partner of the Project Powered), Port Authority of Ravenna, Ravenna Passenger Terminal and Tozzi Nord, that has engineered and donated the plant. The plant has been inaugurated December the 17th 2011 and has been installed on the dock of the Cruise Terminal at Porto Corsini (Ravenna). It's a small wind turbine. (rated power: 1.5 kW; rated wind speed: 13 m/s; starting speed: 4 m/s; stop speed: 20 m/s; rotor diameter: 1.78 m; hub height: 2.5 meters). Through the realization of this case study the data collected is compared and integrated with the ones from the simulations in order to obtain a "standard investment" in mini wind turbines.

Then, in the second half of the paper, a detailed inventory of seaport using different dimension such as the seaport available space for container holding, the length of the quays or the presence of a "foranea dam", a seawall. Just for instance, the hub port in Gioia Tauro has 950,000 square meters for containers holding and the gateway port in Genova has other 57,400 square meters. Regarding the seawalls, the one at La Spezia is 2,210 meters long, the one in Gela is 2,800 meters, the one in Brindisi 2,300 meters and the one in Genova is 1,800 meters.

Considering only the seawall in Genova it is been studied that can easily hold up to 39 mini wind generator with a single power of 199 kW each that can guarantee to the port an electric generation capacity of 7.7 MW from renewable energy. Based on this information a classification for the seaport is presented and then starting from this data collection about Italian seaport, a potential analysis of the application of mini wind turbines is provided. This study is conducted by a cross analysis of wind speed and land availability, among other variables of interest.

3. Small wind turbines investment analysis

This Section first describes the Italian regulations that affect the adoption of small wind turbines and then analyzes an investment in this technology.

3.1 Italian regulation on small wind turbines

In Italy there is specific scheme for supporting small-sized RES: owners of wind plants between 1 kW and 200 kW can opt for a fixed feed-in tariff, called “Tariffa Onnicomprensiva” or exchange (net-metering) contracts. Choosing the feed-in tariff means a net revenue (energy + incentive) of 300 €/kWh, instead exchange (net-metering) contracts allows a save in electricity bill variable depending on the specific contracts starting from an average value of 160 €/MWh. The feed-in tariff is managed by the energy services regulator, the GSE. One of its main objectives is to promote and to support the renewable energy production. The feed-in tariff (Tariffa Onnicomprensiva) is a national scheme applicable to RES-E plants (excluding solar ones) which have a nominal real power of less than 200 kW for on-shore wind plants. This scheme was activated in 2007. The tariff is granted over a period of 15 years, during which its rate remains fixed and based on the amount of electricity fed into the grid, for all plants commissioned by 31 December 2012. To benefit from this form of support, producers must first ask GSE to qualify their plants as RES-E (“IAFR – Impianto Alimentato a Fonti Rinnovabili”). It is differentiated by type of source: for the wind energy the feed in tariff is fixed at 300 €/MWh.

Like the previously described wind market even the regulation concerning small wind turbines is changing. New tariff and new power ranges have been proposed; Table 1 summarized the new incentives scheme. Compared to the all-inclusive rates that are still in force today (300 €/MWh), first power range, the 1-20 kW plants, could have an all-inclusive fee of 291 €/MWh (reduction of -3%) and the second range, 20-200 kW plants, a tariff of 268 €/MWh (reduction of -10%). The reduction, however, is accompanied by an extension of the incentive period from 15 to 20 years, which is consistent with the useful life of small wind turbines.

Table 1: The new incentives scheme.

Power range [kW]	Period of incentives [years]	Feed in tariff [€/MWh]
1<P≤20	20	291
20<P≤200	20	268

The impact of this change in the regulation will be discussed in the next part of the Section.

3.2 Small wind turbines investment analysis

In this Section the economic issues are investigated through data simulations and through the analysis of running pilot project such as the one in Porto Corsini (Ravenna). This is a pilot project that is part of the Project Powered and that has been realized in Porto Corsini (Ravenna), thanks to the cooperation between the Province of Ravenna (which is a partner of the Project Powered), Port Authority of Ravenna, Ravenna Passenger Terminal and Tozzi Nord, that has engineered and donated the plant. The plant has been inaugurated December the 17th 2011 and has been installed on the dock of the Cruise Terminal at Porto Corsini (Ravenna). It’s a small wind turbine. (rated power: 1.5 kW; rated wind speed: 13 m/s; starting speed: 4 m/s; stop speed: 20 m/s; rotor diameter: 1.78 m; hub height: 2.5 meters). This plant is just the first in order to test the wind availability and the profitability of similar investment in that area.

Table 2: Investment description.

	Plant A		Plant B	
Power [kW]	20		200	
Investment Cost [€/kWh]	3,000		2,500	
Construction Year	2012	2013	2012	2013
Revenue from incentives [€/kWh]	300	291	300	268
Incentives [Years]	15	20	15	20
Financing Scheme	Full equity		Full equity	

Considering now two different investment in small wind turbines such as the ones in the Table 2, in order to investigate the Internal Rate of Return (IRR) depending on: (i) the capacity factor or the yearly operating time, (ii) the power of the plant and (ii) the different incentives scheme adopted.

The two investment are similar to the one, previously described, in Porto Corsini, the only different is the power of the turbines that in our cases are higher.

The internal rate of return (IRR) is a rate of return used in capital budgeting to measure and compare the profitability of investments. In more specific terms, the IRR of an investment is the discount rate at which the net present value of costs (negative cash flows) of the investment equals the net present value of the benefits (positive cash flows) of the investment. Internal rates of return are commonly used to evaluate the desirability of investments or projects. The higher a project's internal rate of return, the more desirable it is to undertake the project. Assuming all projects require the same amount of up-front investment, the project with the highest IRR would be considered the best and undertaken first.

Figure 2 and 3 show the IRR of the investment A and B depending on the incentives scheme and on the yearly operating time.

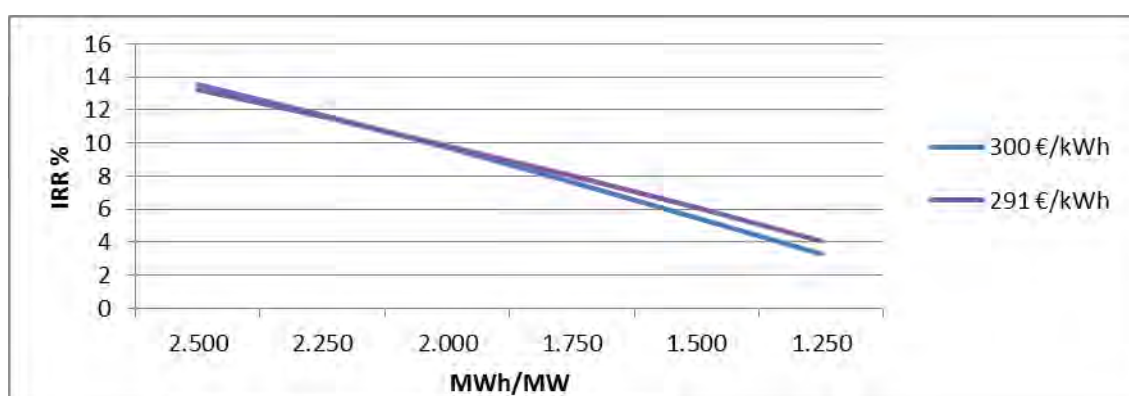


Figure 2: Comparison between different incentives schemes for the investment in plant.

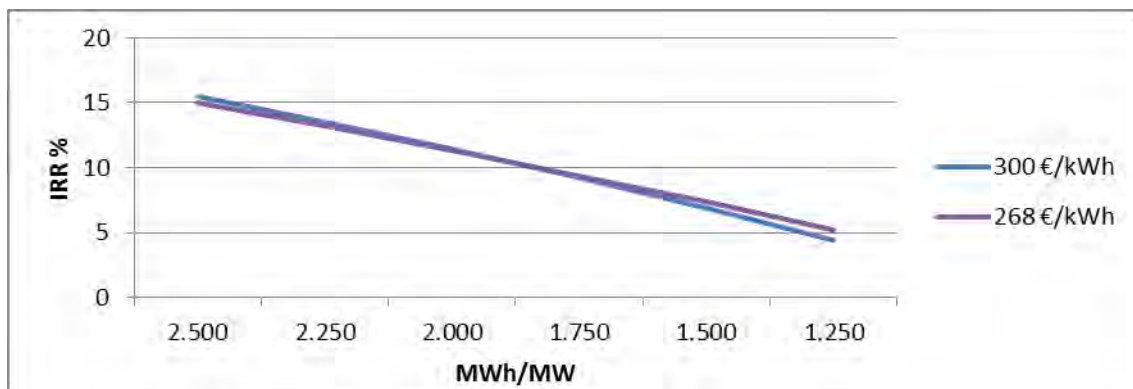


Figure 3: Comparison between different incentives schemes for the investment in plant B.

First the difference between the two incentives scheme are few, consisting in only few percentage point in the worst wind conditions. Secondly and more interesting the value of IRR at the average productivity (1,750 MWh/MW) is high enough to justify investment in small wind turbines. IRRs vary from 15% in windy and coastal areas to 5% in onshore areas. The analysis was conducted considering a full equity investment; a leverage approach to this investment can add from 5 to 10 percentage point to the IRR value.

Another interesting economic indicator is PayBack Time (PBT). PBT in capital budgeting refers to the period of time required for the return on an investment to "repay" the sum of the original investment. PBT intuitively measures how long something takes to "pay for itself." All else being equal, shorter payback periods are preferable to longer payback periods. The time value of money is not taken into account. Considering investment A and B, the PBTs range from 7-8 years in windy and coastal areas to up to 20 years in onshore areas with bad wind conditions.

Running a sensitivity analysis on investment B, depending on the initial investment price and let it varies in a range between 2,500 €/kW and 2,900 €/kW, it's possible to find a 2% point variation of the IRR, as showed in Figure 4.

According to the data there are no economic limitations to the adoption of this plants in Italy, conversely the incentives scheme seems to be generous enough support this kind of investment. The only issue is to find the ideal location for this plant to maximize the yearly operating time. In the next Section a solution to this issue is proposed.

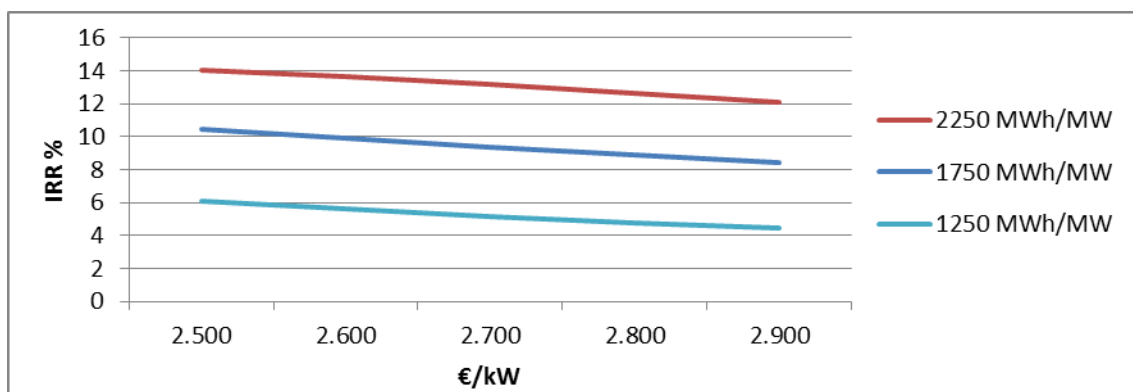


Figure 4: Sensitivity analysis on the investment in plant B.

4. Empirical test on Italian seaport

It is well known that the wind resource of the seaport areas in Italy has a very high wind potential. This has prompted many studies to be conducted on the measurement of wind speed in Italian seaport such as the project “Vento e Porti” with the aim of offer a short term forecast of wind in seaport areas or the paper from Solari et al. about the wind forecast for safety management of Italian port areas. The ideal location for small wind turbines could be a seaport. These areas usually have great availability of wind and seaports also need a lot of electricity to supply their main activity. The potential area interested in the installation of wind turbines could be different from the quays dedicated to containers to the seawalls in front of the port. Next Tables present the availability of space in some Italian seaport. Just for instance, the hub port in Gioia Tauro has 950,000 square meters for containers holding and the gateway port in Genova has other 57,400 square meters. Regarding the seawalls, the one at La Spezia is 2,210 meters long, the one in Gela is 1,150 meters, the one in Brindisi 2,300 meters and the one in Genova is 4,300 meters.

Table 3: Seaport available spaces for container holding.

Seaport location	Spaces for container holding [m ²]
Gioia Tauro	950,000
Genova	574,000
Ravenna	280,000
Trieste	270,000

Table 4: Length of the quays dedicated to containers.

Seaport location	Length of the quays [m]
Gioia Tauro	3,100
Genova	1,800
La Spezia	1,000
Ravenna	900
Livorno	600

Table 5: Length of the seawalls.

Seaport location	Length of seawalls [m]
Genova	4,300
Brindisi	2,300
La Spezia	2,210
Gela	1,150

4.1 Economics of an investment on a seawall

Analyzing an already presented project, regarding the seaport in Genova that propose the installation of 39 small wind turbines, 200 kW each, on the seawall, is possible to study deeply this kind of projects in order to extend the results to the other Italian seaport. The 39 small wind turbines will produce 12 GWh yearly and initially cost 20 million € overall.



Figure 5: Genova seaport map and seawall interested by the investment in small wind turbines.

Considering the seawall of Genova seaport that is long 4,300 m, is possible to obtain the following value for this kind of project:

- 1 turbines every 110 meters;
- total cost per 39 turbines equal to 512.000 €, meaning an average 2.500 €/kW;
- yearly production per turbines equal to 307.69 MWh, corresponding to an operating time of 1,546 hours a year.

Comparing this analysis with the previous economic results is also possible to understand the profitability of this project.

4.2 Small wind potential application in Italian seaport

The paper now shows the data collected from the other Italian seaport that have similar sea walls like the one in Genova. In the Table 6 there are 37 Italian seaports that have a seawall and potentially invest in small wind turbines project like the one in Genova.

Table 6: Main Italian seaports (listed by length of seawalls).

Seaport	Region	Length of seawalls [m]
Pescara	Abruzzo	7,300
Augusta	Sicilia	6,500
Cagliari	Sardegna	5,002
Trieste	Friuli Venezia Giulia	3,605
Gioia Tauro	Calabria	3,214
Brindisi	Puglia	2,385
Livorno	Toscana	2,256
La Spezia	Liguria	2,210
Napoli	Campania	2,042
Crotone	Calabria	1,725
Oristano	Sardegna	1,557
Salerno	Campania	1,550
Bari	Puglia	1,450
Venezia	Veneto	1,426
Crotone	Calabria	1,309
Taranto	Puglia	1,265
Monfalcone	Friuli Venezia Giulia	1,193
Gela	Sicilia	1,150
Barletta	Puglia	1,136
Ortona	Abruzzo	1,100
Trapani	Sicilia	899
Ancona	Marche	862
Porto Empedocle	Sicilia	825
Savona	Liguria	756
Margerita di Savoia	Puglia	700
Vasto	Abruzzo	631
Palermo	Sicilia	592
Marsala	Sicilia	525
Formia	Lazio	384
Reggio di Calabria	Calabria	354
San Benedetto del Tronto	Marche	345
Vibo Marina	Calabria	281
Maratea	Basilicata	204
Tropea	Calabria	200
Marina di Camerota	Campania	193
Civitanova di Marche	Marche	185

Applying to this availability of dams the same specifics of the investment in Genova. It is possible to have:

- 461 new installed turbines, 200 kW each;
- 91,4 MW cumulative amount of new wind power;
- 236 million € in investment of new wind power.

Italian seaports are the ideal location for this kind of investment. The potential applications in seaports are almost ten times bigger than the whole capacity installed today in Italy for small wind turbines.

5. Conclusion

Section 3 analyzes the main economic issues regarding investments in small wind turbines in Italy. From an economic point of view no major limitations arises from the adoption of this technology in coastal areas. This is particularly true in Italy, where incentive schemes are still rather “generous”. IRR may reach values up to 15% in windy areas and, by using financial leverage, investors may add up to 10 percentage point to this basis IRR value. Also PBT remains within 8 years, thus leaving as challenge “only” the definition of the location for maximizing the yearly operating time.

In Section 4 the Italian seaports are identified as the ideal locations for this typology of small wind turbines due to their high wind availability and to the presence of under-utilized spaces where these plants could be placed. We considered the project already under evaluation at the seaport of Genoa as a potential benchmark and estimated the entire potential of Italian seaport in 91.4 MW of small wind turbines installations.

According to these analyses, the Italian seaports have outstanding wind resource potential. The good economics of these investments make this untapped potential of great interest for companies and investors in the field.

References

1. Burlando M., Podestà A., Castino F., and Ratto C. F. (2002). *The wind map of Italy, The World Wind Energy*; Conference and Exhibition, 2-6 July, Berlin, Germany
2. Burlando M., Podestà A., Castino F., Ratto C. F., Alabiso M., Botta G., Casanova M., Lembo E. and Lusso C. (2002). *The Italian Wind Atlas*, In-Vento-2002, 15-18 September, Milan, Italy
3. Cassola F., Burlando M., Villa L., Latona P., Ratto C. F.; *Evaluation of the offshore wind potential along the Italian coasts*; Owemes 2006, 20-22 April. Citavecchia, Italy
4. EEA- European Environment Agency (2008), *Energy and Environment Report*
5. ERSE (ENEA - Ricerca sul Sistema Elettrico), *Atlante Eolico dell'Italia*
6. Hartman, J. C., and Schafrick, I. C., *The relevant internal rate of return*, The Engineering Economist 49(2), 2004, 139–158
7. Hazen, G. B., *A new perspective on multiple internal rates of return*, The Engineering Economist 48(2), 2003, 31–51
8. Italian Ministry for Economic Development (2010). *Italian National Renewable Energy Action Plan NREAP*
9. M.A.Main, *Project Economics and Decision Analysis*, Volume I: Deterministic Models, Page 269
10. Pogue, M. (2004). *Investment Appraisal: A New Approach*. Managerial Auditing Journal. Vol. 19 No. 4, 2004. pp. 565–570
11. Solari G., Repetto M., De Gaetano P., Parodi M., Pizzo M., Tizzi M.. *The wind forecast for safety management of port areas*
12. Thron, C., and Moten, J., *Efficient Estimators of Internal Rate of Return*
13. Troen, I. and Petersen E.L. (1989). *European Wind Atlas*. Risø National Laboratory, Roskilde Denmark
14. Williams, J.R. et al, 2012, *Financial And Managerial Accounting*, Mcgraw Hill, p1117

An e-Learning Platform for Off-Shore Wind Energy Logistics and Infrastructures

Flavio Fontana, Enrico Cosimi, Giangiacomo Ponzo

ENEA, Italy

flavio.fontana@enea.it, enrico.cosimi@enea.it, giangiaco.ponzo@enea.it

Abstract - In this paper an innovative e-Learning Platform for Off-Shore Wind Energy is discussed. In particular, the e-contents, course and video lessons, will be oriented to disseminate information and knowledge on “Logistics and Infrastructures” related to the Off-Shore Wind Energy. The virtual e-learning environment has been designed to manage heterogeneous multimedia contents and mobile applications. It is based on Web 2.0 technology to inquiry the e-learning platform database with an advanced mobile interface. The platform could extend the fruition in a mobile context both e-learning objects and videos of lectures and seminars for remote classrooms. The didactical program is finalized to: the new transmission infrastructure, the minimal transportation infrastructure and the installation infrastructure especially for offshore wind power plants. Moreover, a comparison of offshore wind power development in Europe and the U.S. will be presented in terms of logistic infrastructures, ports, specialized transports, impact polices and economics aspects.

The easy to use of the system will support students and teachers with new communication ways. The Usability Laboratory, ENEA Research Centre, has implemented the MATRIX platform to improve the fruition of the e-learning contents in off-shore wind energy field. The platform will be accessible also by means of smart-phones and tablets. The experimentation has been done to study, between the users, the effectiveness and satisfaction of the innovative educational tools on the renewable energies applications.

Poster Session

Chairmen: F. Cesari, A. Fiorentino

MOBI BUOY: Offshore Wind Measurements in the Sicily Channel - D. Airoidi, C. Casale, E. Lembo, C. Rosito, L. Serri (RSE SpA, Milan (IT))

A New Configuration of Vertical Axis Wind Turbine: towards the development of a highly distributed and efficient Wind Power Generation System - M.R. Chiarelli (Dept. of Aerospace Engineering, Pisa Univ., Pisa (IT)), A. Massai (AM Engineering, Florence (IT)), G. Russo, D. Atzeni, F. Bianco (Dept. of Aerospace Engineering, Pisa Univ., Pisa (IT))

New Way for Access and Maintenance of Offshore Wind Farms. The Use of Cableway to Reduce Cost and Improve accessibility. Comparison, Strengths and Limits of this Approach - M. Grecchi (Altavia Milano srl (IT)), L. Meroni (Italtel S.p.A. (IT)), P. Betteto (Vemplast S.a.S. (IT))

Levelised cost of electricity generated by offshore wind plant and other competing technologies: dynamic analysis using simulation theory - M. Gaeta, M. Rao (ENEA, Unità Centrale Studi e Strategie, Rome (IT))

TRITON - Wave Energy Converter - R. Piccinini, M. Boffini (K.I. Energy, Busan (KR))

Mapping Mediterranean Sea wind resource: state-of-the-art technologies for short term measurements and long term reference data - M. Gianni, L. Imperato (Studio Rinnovabili S.r.l., Rome (IT))

Wakes calculation in a offshore wind farm - G. Crasto (WindSim AS, Tønsberg (NO))

Overview of non destructive testing for composite materials - C. Cappabianca (AIPND, Brescia (IT))

PlasMare. Trattamento integrato eco-compatibile di Rifiuti Solidi Urbani su piattaforme navali - S. Vacante (FINCANTIERI/CETENA, Genova (IT))

New renewable energy source and its practical use in the Mediterranean and other European seas - S. Goncharenko (Kimo-Business, Kiev (UA))

Wave Energy Generation Difficulties solved by Eco Wave Power - D. Leb (EcoWavePower, Tel Aviv (IL))

A new device to produce electrical power from ocean waves: some applications to Italian coasts - F. Arena*, A. Romolo*, A. Ascanelli, A. Viviano (Dept. of Mechanics & Materials, Reggio Calabria Mediterranea Univ. (IT) and *Wavenergy.it S.r.l., Reggio Calabria (IT))

Ports for Offshore Wind Applications along the Tyrrhenian Coasts of Calabria and Sicily - F.G. Cesari, F. Taraborrelli, D. Mostacci (DIENCA Dept., Bologna Univ. (IT)), L. Milella (TRE SpA, Bari (IT)), L. Pirazzi (ANEV (Rome (IT)))

Italian Off-Shore Wave Energy Map, using Gauges and Numerical Model Data – F.M. Carli, S. Bonamano (Laboratory of Experimental Oceanology and Marine Ecology, University of Tuscia, Civitavecchia (IT)), G. Stella, M. Peviani (RSE SpA, Seriate, Bergamo (IT)), M. Marcelli (Laboratory of Experimental Oceanology and Marine Ecology, University of Tuscia, Civitavecchia (IT))

MOBI BUOY: Offshore Wind Measurements in the Sicily Channel

D. Airoidi, C. Casale, E. Lembo, C. Rosito, L. Serri

RSE S.p.A., via Rubattino, 54 - 20134 Milan – Italy

tel. +39 02 39925285, fax +39 02 39925626, e_mail: laura.serri@rse-web.it

Introduction

Significant offshore wind capacity has already been installed in the North of Europe and offshore wind plant deployment is going to be considered also in many other countries in the world, such as the U.S.A., China etc. Installation and operation costs are higher than on land, but offshore wind regimes are generally less turbulent and the specific power production can exceed 4000 MWh/MW. Moreover the visual impact is strongly reduced by going farther and farther from the coast. For these reasons also Italy and other Mediterranean countries are looking at the challenge of offshore wind energy production even if their resource is lower and the water is deeper than in the North Sea. Accurate offshore wind assessment is required for the evaluation of the most suitable sites and for a preliminary economic evaluation of the projects under consideration. Many wind maps are available at present, but all of them are based on very few direct offshore measurements. Particularly in the Sicily Channel, where water depth and wind resource seem to be suitable for future development of offshore wind plants, no direct data are available.

RSE is at present carrying out a campaign for offshore wind measurement together with the development of dedicated tools [1] e [2].

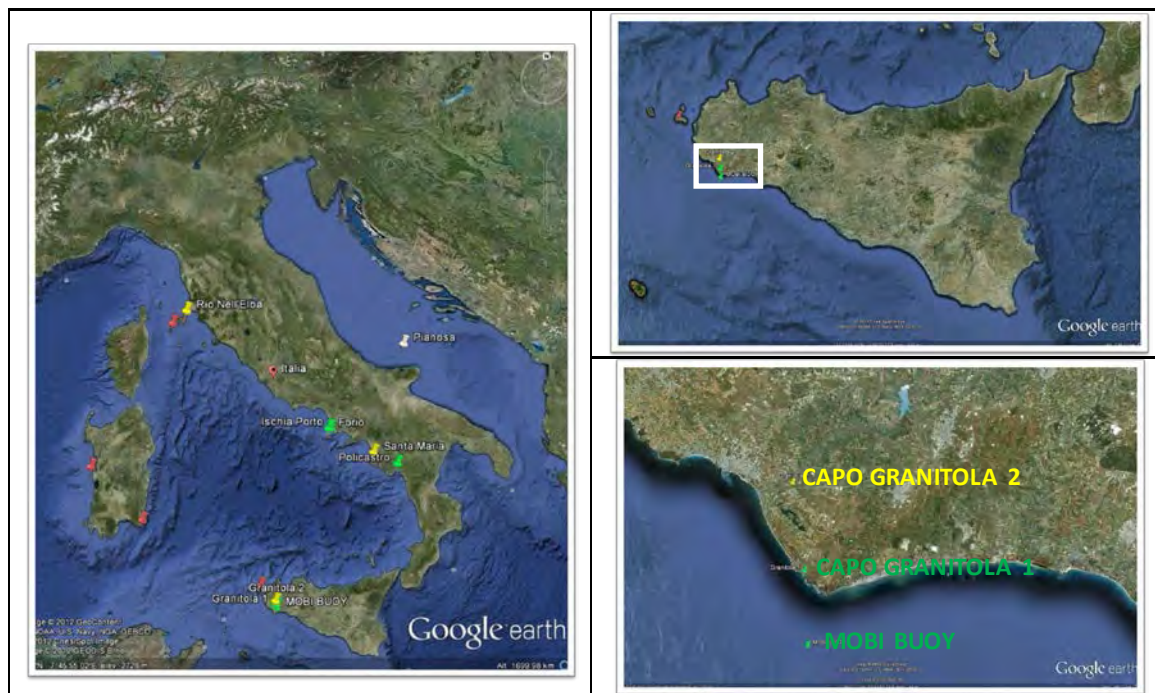


Figure 1: Map of RSE wind measurement stations with zoom on Sicily and on the MOBI buoy area. (Legend: green: installed, yellow: advanced permitting stage, red: permitting process too long, white: disinstalled).

Some coastal and island sites are already under investigation by means of wind measurement stations, and other similar suitable sites are under consideration and could enrich the database of measurements. A map of RSE wind measurement stations is shown in Figure 1.

Moreover, RSE has recently installed a buoy named MOBI (Marine Offshore Buoy for Investigation) 5 km off the coast of Mazara del Vallo (South-West Sicily) in order to monitor offshore wind resources and other meteo-marine quantities. MOBI is an elastic beacon and the wind measurements will be performed at a height of about 10 m a.s.l.

In its preliminary configuration, it is equipped with two cup anemometers, two wind vanes, a sonic two-dimensional sensor, an air temperature sensor and an air pressure sensor. The whole data acquisition system is powered by batteries fed by PV panels and by a small wind turbine. The whole dataset acquired by MOBI is transmitted daily to a remote PC located at the RSE headquarters in Milan.

After a first test period, the buoy will also be equipped with an inertial platform suitable for measuring its angular movements. The latter measurements will be used for the correction of the measured wind direction and, eventually, of the wind speed intensity.

At the same time, a coastal station has been installed near the port of Capo Granitola and another is going to be installed in the surroundings in order to acquire data suitable for correlation analysis. A map with the position of the MOBI buoy and Capo Granitola stations is shown in Figure 1 too.

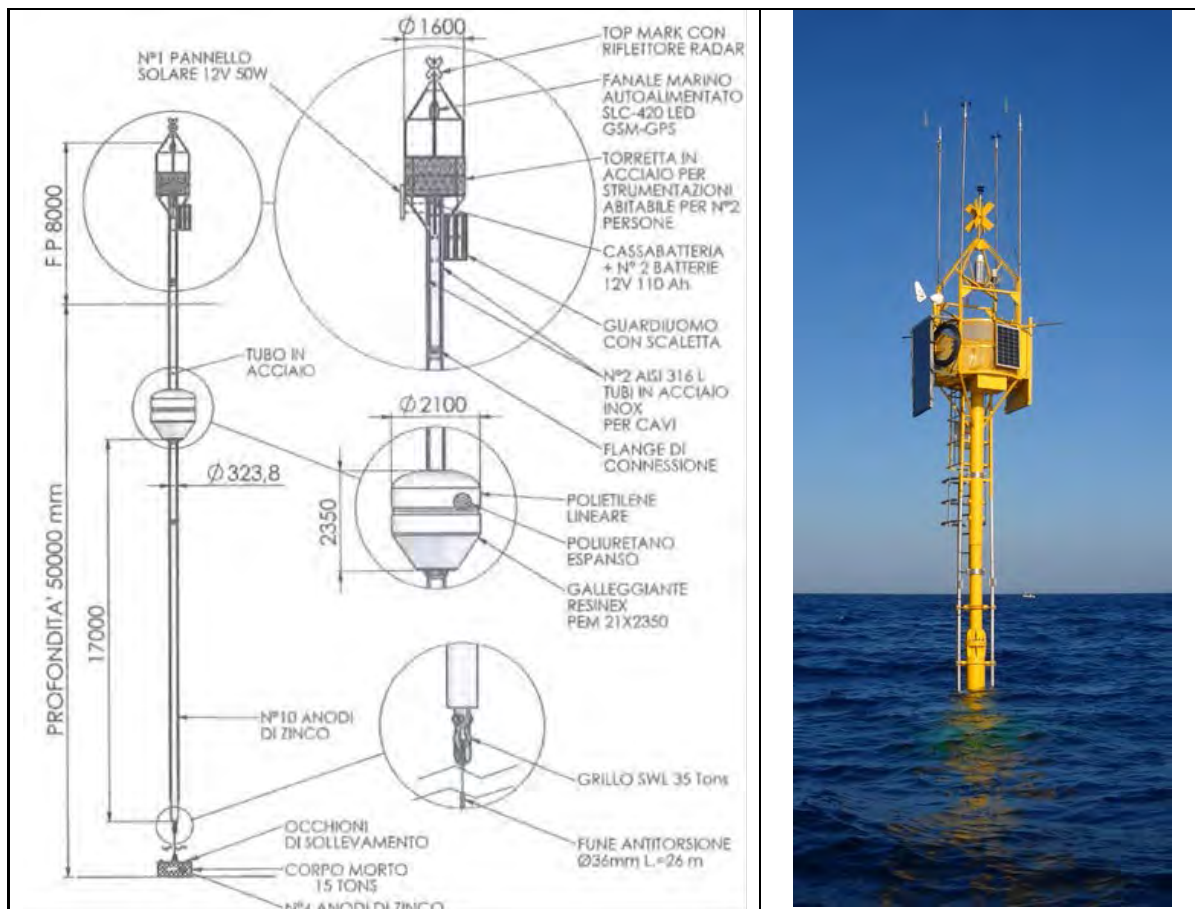


Figure 2: Scheme of MOBI buoy and an image of the buoy after installation (taken on 19th June 2012).

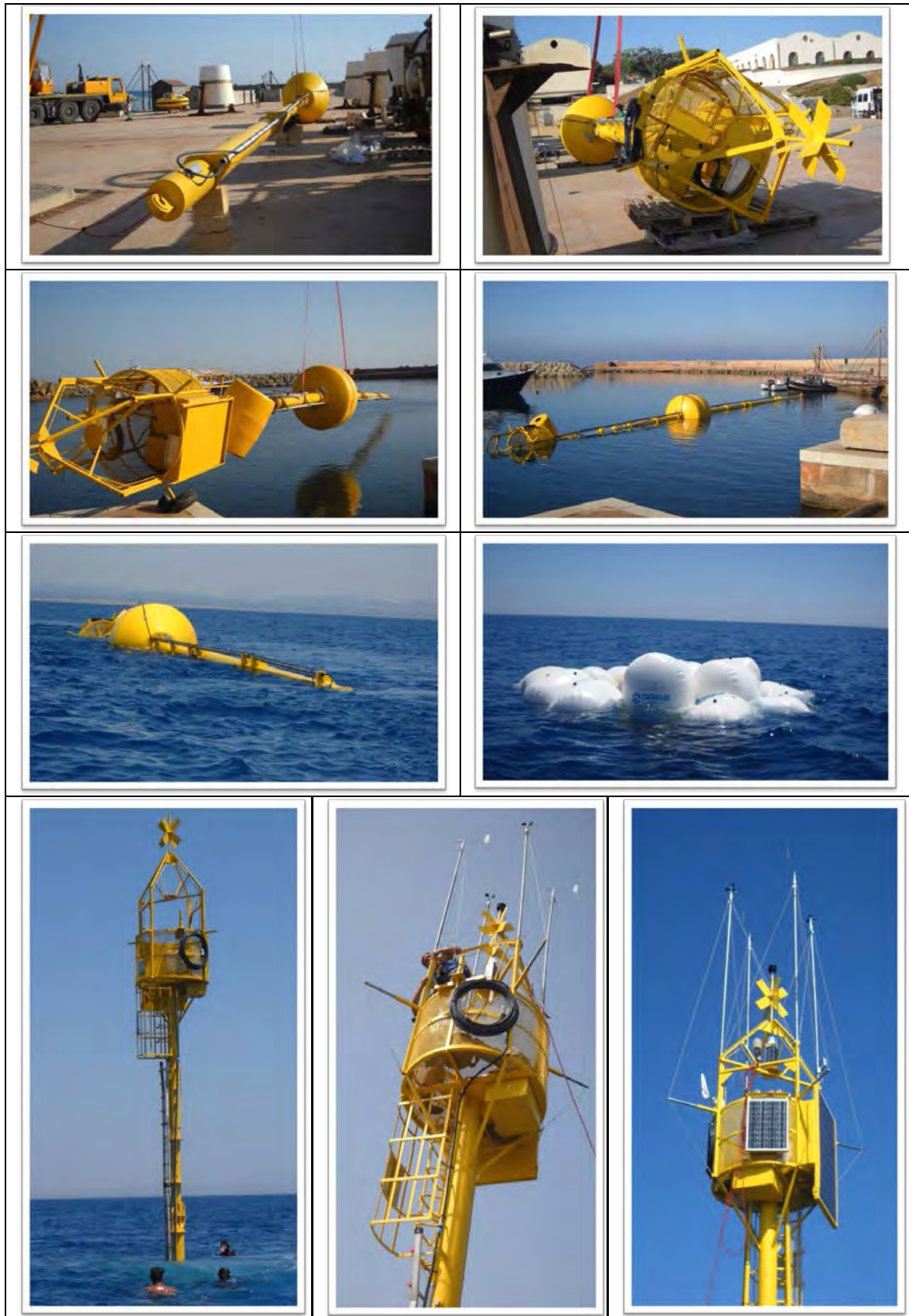


Figure 3: Images of different installation phases of MOBI buoy in the Sicily Channel.

Conclusions

A buoy for offshore wind measurements has been installed in the Sicily Channel by RSE in June 2012 and will be completely equipped with instruments before Autumn 2012. The system, based on the concept of elastic beacon, is very cheap in comparison with “traditional” offshore wind measurement stations based on fixed foundations, and also with recently proposed wind LIDARs installed on floating platforms [3][4][5]. Conversely, the height of the anemometers is only 10 m a.s.l. and their measurements also have to be corrected in order to take into account the angular motions of the buoy. After having checked the reliability of the buoy and its measurement system, and having gathered a significant period of data, a correlation analysis with contemporary and historical wind data available in that marine and coastal area will be undertaken. The results of this analysis should address the quality of the buoy measurements and give an evaluation of the long-term annual mean wind speed expected at the measurement point. The full measured data will be published on the Wind Atlas Website [6] and will be freely available for download as is generally allowed for all the other datasets of measurements performed by RSE stations.

This work has been financed by the Research Fund for the Italian Electrical System under the Contract Agreement between RSE (formerly known as ERSE) and the Ministry of Economic Development - General Directorate for Nuclear Energy, Renewable Energy and Energy Efficiency stipulated on July 29, 2009 in compliance with the Decree of March 19, 2009.

References

1. D. Airoidi, C. Casale, E. Lembo, L. Serri, “Italian Offshore Wind Potential Evaluation through GIS Tools and Data”, *EWEA Offshore 2011*, 29 Nov.-1 Dec. 2011, Amsterdam
2. C. Cavicchioli, R. Marazzi, S. Maran, “A Web GIS support for ICZM and Marine Spatial Planning”, *EWEA Offshore 2011*, 29 Nov.-1 Dec. 2011, Amsterdam
3. M. Smith, “An insight into lidars for offshore wind measurements”, January 2012, http://www.sintef.no/project/Deepwind%202012/Deepwind%20presentations%202012/C2/Smith_M.pdf
4. “North Sea floating LIDAR wind measurement trials, a huge success” www.flidar.com
5. G. W.-Möhlmann., H. Lilov, B. Lange, “Simulation of motion induced measurement errors for wind measurements using LIDAR on floating platforms”, 2011, <http://www.enecafe.com/interdomain/idfukyo/lidar/paper/2011/Simulation%20of%20motion%20induced%20measurement%20errors%20for%20wind.pdf>
6. <http://atlanteolico.rse-web.it/viewer.htm>

A new configuration of vertical axis wind turbine: towards the development of a highly distributed and efficient wind power generation system

M.R. Chiarelli¹, A. Massai², G. Russo¹, D. Atzeni¹ and F. Bianco¹

¹*Dipartimento di Ingegneria Aerospaziale, University of Pisa, Via Caruso 8, 56122 Pisa, Italy, chiarelli@dia.unipi.it, giovanrus@alice.it, atzeni.dav@gmail.com, bianco.fran@yahoo.it*

²*AM Engineering, Firenze, Italy, andrea.massai@libero.it*

Abstract – Preliminary results obtained for a new configuration lift based vertical-axis wind turbine are shown. The turbine rotor is a cross flow fan type made with high curvature aerodynamic profiles. A reduced scale model of the turbine rotor has been designed and preliminary tested at the Department of Aerospace Engineering of the University of Pisa (rotor diameter = 250 mm, rotor height = 210 mm). The reduced scale model shows an efficiency of about 18%. The rotor is of a self-starting type. Two-dimensional CFD analyses have been performed applying both the Moving Reference Frame and the Moving Mesh conditions to the grid which surrounds the rotor blades (Fluent® Rel. 6.3 and STAR-CCM+® Rel. 6.04 have been used). Noticeable scale effects have been found numerically, so, the efficiency of a full scale lift based vertical axis multi-blades optimized wind turbine is expected to be comparable with lift based horizontal-axis wind turbines.

1. Introduction

At the Department of Aerospace Engineering of the University of Pisa a research activity has been carried out concerning the development of a high efficiency vertical axis wind turbine in order to demonstrate the feasibility of a diffuse and competitive (low cost) electrical energy system generation.

Example of traditional configurations of vertical axis wind turbines are represented in the Figure 1. Recently new configurations of these machines assume, more and more, the shape of a cross flow fan. As an example see the work of Klemm et al. (2007). These vertical axis wind turbine configurations, studied also by the authors of the present paper, start substantially from an early idea of machine: the *Lafond turbine* (Champly, 1933) that, from a practical point of view, can be classified as a cross flow fan without the casing.

As it is well known in literature, the efficiency values of traditional vertical axis machines are, in general, lower than the efficiency values of horizontal axis machine as shown in Figure 2 (Patel, 1999).

The substantial difference of the turbine configuration described and studied in this paper consists on the aerodynamic shape of the blades. Promoting several studies, thanks to the contribution of students in Aerospace Engineering course, e.g. Di Filippo (2007), the authors of present paper observed that two-dimensional CFD analyses, carried out on a Lafond turbine with $D=10$ m having 24 blades, provided high values of the aerodynamic efficiency of the rotor (Figure 3a). CFD analyses were carried out with the commercial code Fluent® and applying the steady MRF method (Fluent Inc., 2006). The numerical simulated flow agrees very well with an experimental visualization (Figure 3b) which is available in the work of Gabi et al. (2004).

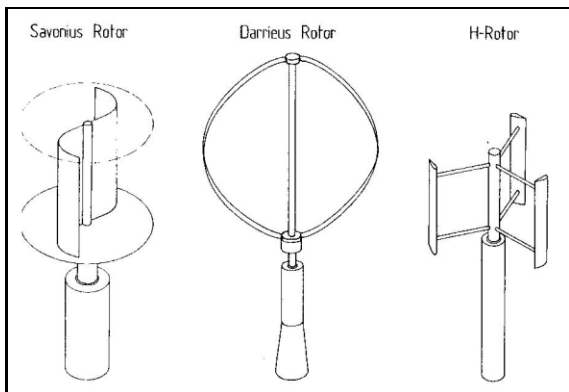


Figure 1: Conventional vertical axis wind turbine configurations.

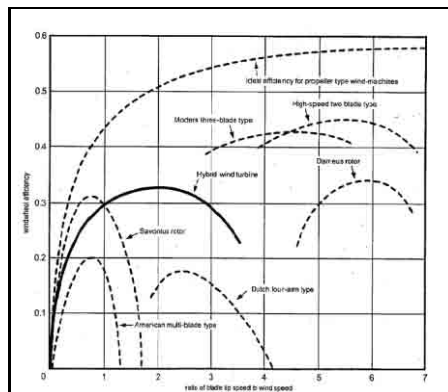


Figure 2: Wind Wheel Efficiency vs λ , data available from literature (Patel, 1999).

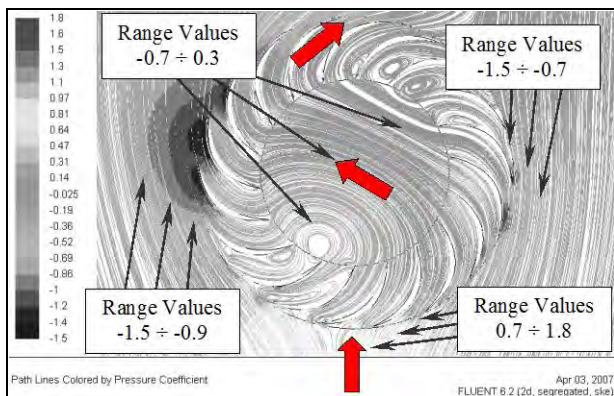


Figure 3a: Path Lines and pressure coefficient distribution - 2D CFD analysis of a 10 m Rotor
(Method MRF: $V=10$ m/s , $\Omega = 1$ rad/s).

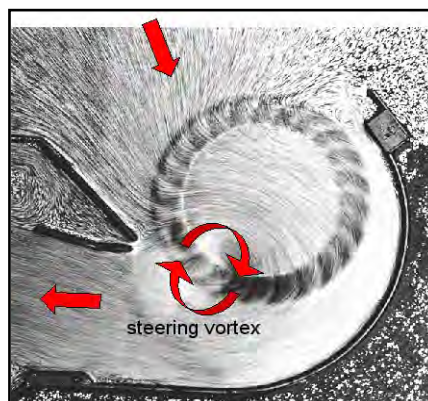


Figure 3b: View of fluid flow for a cross-flow fan in Gabi et al. (2004).

In the work of Di Filippo (2007) several configurations of stator blades, which favorably deviate the asymptotic flow in front of the wind wheel, also were examined (Figure 4). These kind of stator have a shape similar to configurations examined in a recent work (Colley et al., 2010).

The simulated flow field (Di Filippo, 2007) shows typical behavior of turbines or pumps (Cornetti, 1993): that is the asymptotic flow undergoes two different deviations (Figure 3a). The repeated variation of the fluid momentum, due to the effects of blades, generates a torque around the wind wheel axis.

The preliminary numerical results encouraged further studies and finally a reduced scale model of rotor has been designed and numerically simulated (Russo, 2008). The rotor model has been designed using high curvature aerodynamic profiles in order to increase the variation of the fluid momentum. Starting from the layout examined by Russo (2008), represented in Figure 5, a carbon fiber model of the rotor has been manufactured (Figure 8) and preliminarily tested in the wind tunnel available at the Department of Aerospace Engineering of Pisa. The dimensions of the reduced scale rotor model are: $D=250$ mm, $H=210$ mm. The shape and the external dimensions of the aerodynamic profile of blades are shown in Figure 6.

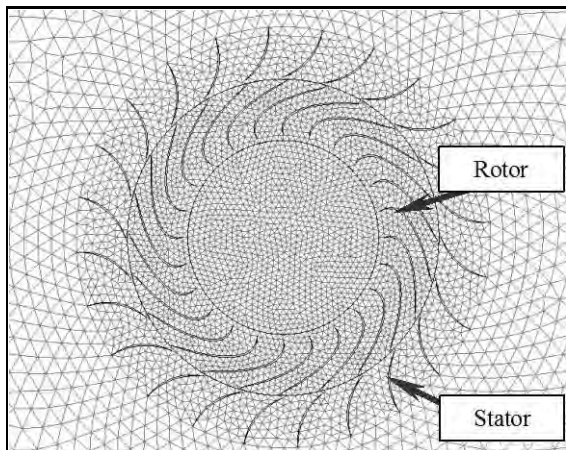


Figure 4: Grid of a Stator-Rotor configuration, (Di Filippo, 2007).

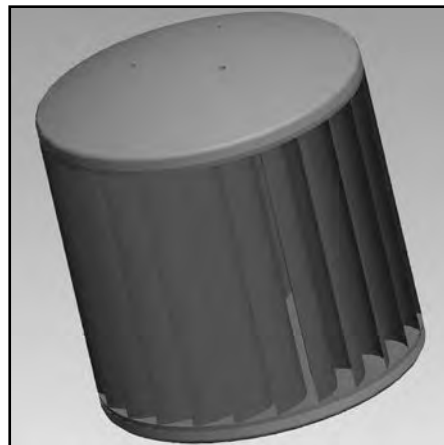


Figure 5: CAD model of the rotor, (Russo, 2008).

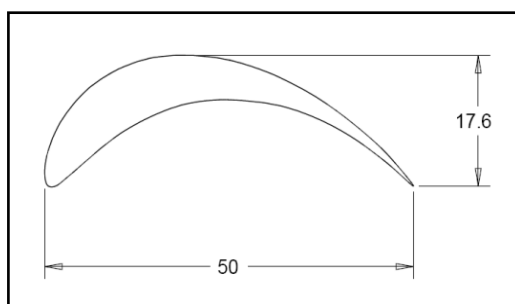


Figure 6: Sketch of the high curvature blades profile used in the reduced scale rotor model (units: mm) (Russo, 2008).

As it can be seen from the same figure, the geometry of blades profile is unconventional if compared with other technical applications relevant to a vertical axis wind turbine. Moreover, in the present configuration, the trailing edge of the profiles lies along the external diameter of the rotor (Figure 7 and Figure 8).

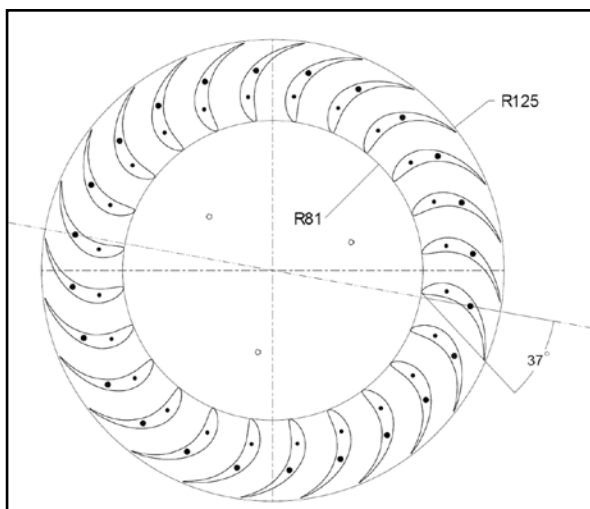


Figure 7: Sketch of blades arrangement in the rotor model (units: mm; Russo, 2008).



Figure 8: View of the blades arrangement in the reduced scale rotor model.

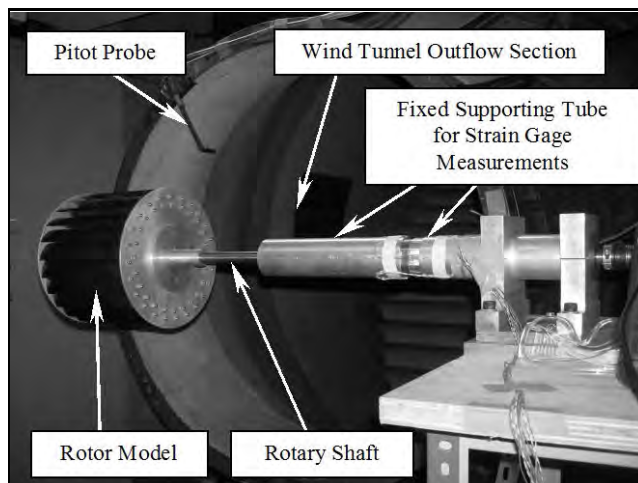


Figure 9: Sketch of the wind tunnel test arrangement at DIA.

Test results have shown that maximum values of reduced scale rotor efficiency is about 18%, on the other hands, during tests non-negligible vibration effects have been observed (Figure 9 shows a view of the test arrangements).

In the Figure 10 and in the Figure 11 a comparison between the test results and preliminary numerical results is shown. The Fluent[®] code has been used.

The numerical values of torque have been obtained using a first level grid refinement (Figure 16) and using only the MRF method applied to the blading zone (the rotor) of the grid. This type of analysis provides results which are in a good agreement with the experimental ones.

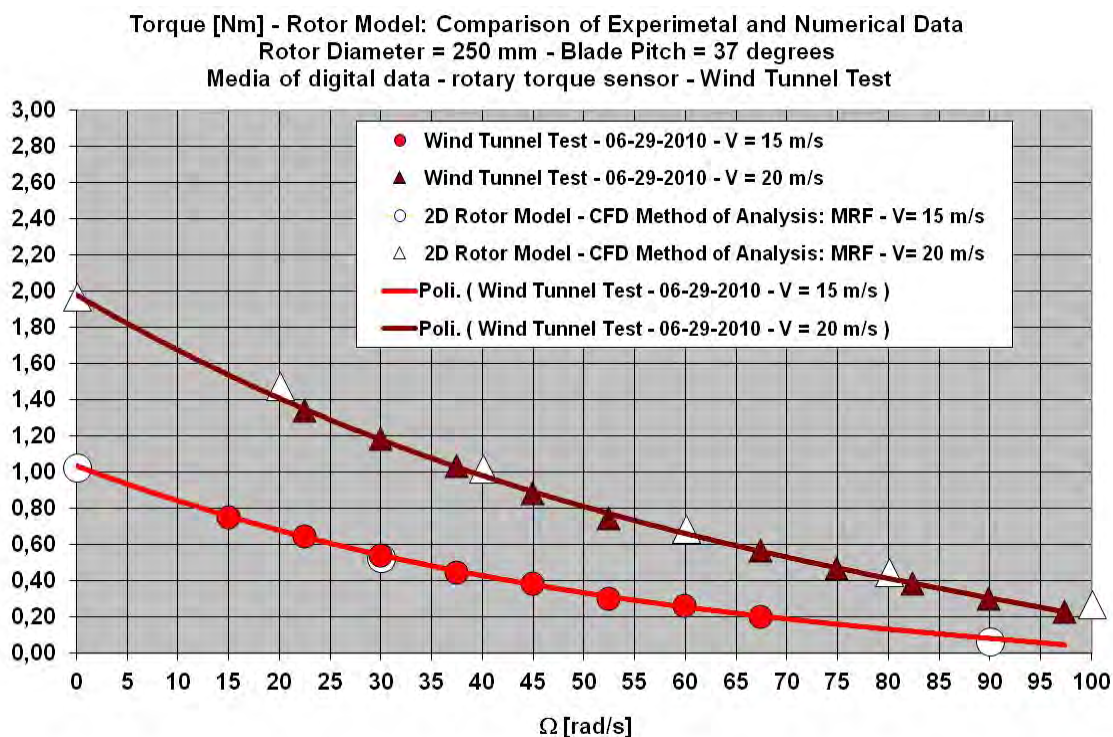


Figure 10: Comparison of measured and computed Torque (Reduced Scale Rotor Model).

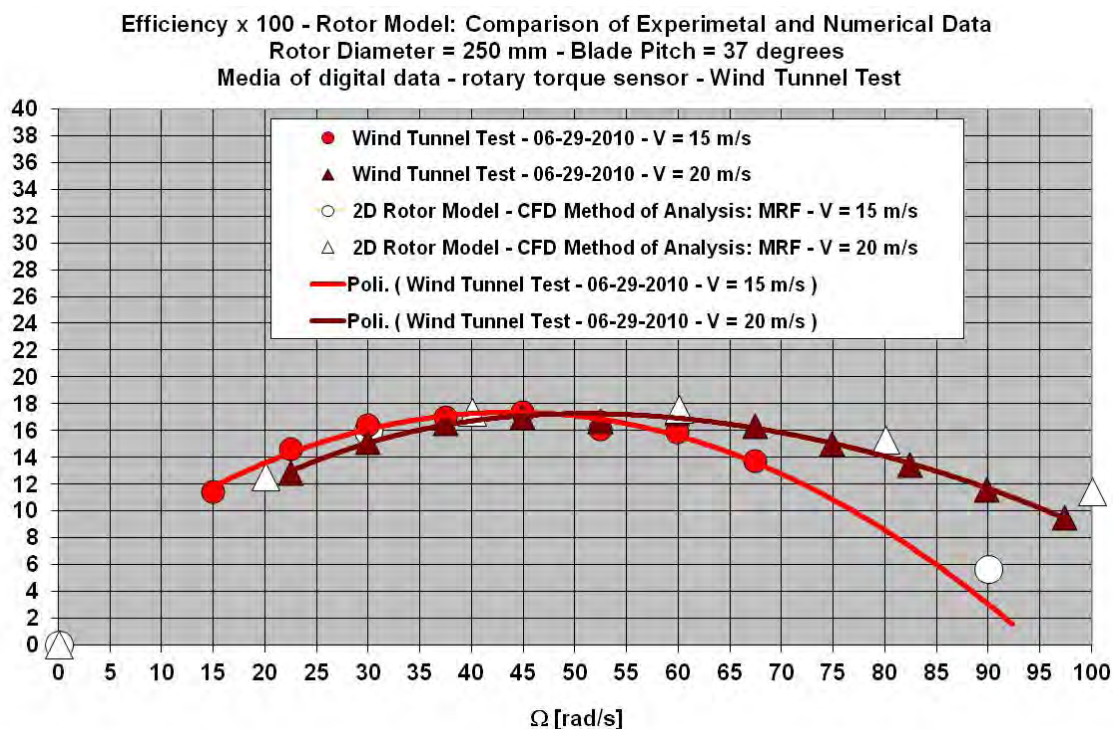


Figure 11: Comparison of measured and calculated efficiency vs Ω .

But as will be observed in the next, from a numerical point of view the grid refinement and the restart sequential method of analyses (MRF + MM) influences the converged numerical data while, from experimental point of view, the vibration effects, which developed during the test, have, probably, reduced the values of the torque measured. In any case, the value of efficiency measured at DIA agrees with some results available in the literature relevant to small scale rotor models. As an example in the recent work of Colley et al. (2010) two-dimensional numerical simulations of a rotor with a tip radius of 0.7 m provide maximum values of efficiency between 15% and 25%. But it must be taken into account that these results have been obtained using a stator-rotor configuration which modifies the performances of the rotor alone.

In the case of present rotor type the number of blades, blades shape, blades dimensions with respect to the rotor diameter and blades pitch can be optimized in order to achieve higher efficiencies even when the wind has a low speed (2-3 m/s). In this way the average energy produced can be further increased. In addition, taking into account the scale effect, the efficiency of full scale wind generators based on the present type of rotor, is expected to be higher than the efficiency of any type of the actual vertical-axis wind generators. In fact, the existing vertical-axis wind generators have efficiencies that do not exceed 35-40% (Darrieus Rotor), while the latest horizontal-axis wind generators can achieve efficiency values around 45-50% (Figure 2).

Starting from the preliminary results obtained during the test activity (which has been influenced by the effects of vibrations) and preliminary numerical analyses, further and more accurate analyses have been carried out which show the effect of the grid refinement (both the adapt boundary methodology has been used at the interfaces of the blading zone and the restart of the analyses changing the method of solution from MRF to MM) and the effects of scale (increasing values of the rotor diameter).

In this case the grid topology is of the same type adopted, as an example, in a recent paper (Lain et al., 2010): that is a strip of very thin elements has been inserted near the wall of the profiles to better simulate the effect of the boundary layer (Figure 17). The results of these analyses are shown in the Figure 18 and in the Figure 19. As can be seen from Figure 19, in the present case of two-dimensional simulations, assuming the peaks value of the torque converged solution to evaluate the efficiency, values greater than 40% has been obtained for the rotor model with a diameter of 4 m.

2. Wind tunnel test of the wind-rotor scaled model

As anticipated, following the computational results described in Russo (2008), the fabrication of a reduced scale prototype of the rotor was decided in order to get experimental confirmations. A specialized company manufactured suitable moulds in order to obtain the designed blades made with a foam core covered with thin carbon fiber laminates (blades skins). Suitable thin steel bars have been inserted in the moulds to realize metal pins necessary to fix blades pitch, and to join the blades ends to the upper and lower closing plates. The closing plates of the rotor were done with worked aluminum alloy sheets with a thickness of 3 mm. As said, Figure 6 shows the geometry of the high curvature aerodynamic profile designed for the blades. In the Figure 7 a transversal section of the rotor is represented. The pitch angle of blades considered during the test campaign is equal to 37° , as shown in the figure, the external radius of rotor is equal to 125 mm ($D=250$ mm) while the internal radius, which defines the boundary of the inner vane of the rotor, is equal to 81 mm. The rotor has been assembled in a 24 blades configuration. Figure 8 shows a photo of the reduced scale rotor model during a pre assembling phase: in the photo are also visible the metal pins inserted in the foam core of blades and one of the two aluminum terminal plate joined to the blades row

The test equipment is shown in the Figure 9. The wind tunnel available at the DIA is of Göttingen type with an open and circular test section with a diameter equal to 1.1 m and length equal to 1.5 m. The test velocities range between 15 m/s and 40 m/s. In the wind tunnel, the following values of the nominal flow velocity measured in the test section were considered: 15 m/s, 18 m/s and 20 m/s. The test temperature T was about 28°C .

The rotor has been attached to a rotating steel shaft supported by commercial rotating bearings inserted into a fixed aluminum beam with an hollow section. On the external surface of the fixed beam four strain gauges have been glued to execute real time measurements of the support beam deformation during the rotating motion of the wind rotor scaled model.

The torque produced by the aerodynamic pressure acting on the rotor has been measured by a dynamic torque sensor and the rotating motion has been imposed to the rotor using an hydraulically driven variator.

Suitable elastic joints have been inserted along the rotation control chain to avoid failure of the rotary torque sensor.

The results of the torque measurements are shown in the Figures 10 and 11 ($V=15$ m/s and $V=20$ m/s). From these figures a value of about 18% for the maximum efficiency of the scaled rotor model can be estimated.

Strain gauges measurements have been recorded and analyzed to evaluate dynamic effects due mainly to the elasticity of the support frame of the test equipment and due to the dynamic behavior of the rotating shaft (a 20 mm diameter steel rod) and of the fixed aluminum beam.

In the Figures 12, 13, 14 and 15 (Atzeni, 2012) the electrical signals of the strain gauges are shown: the data, which depend on the whole mechanical system frequency content and on the rotational frequency, are relevant to the wind tunnel velocity 15 m/s and 18 m/s.

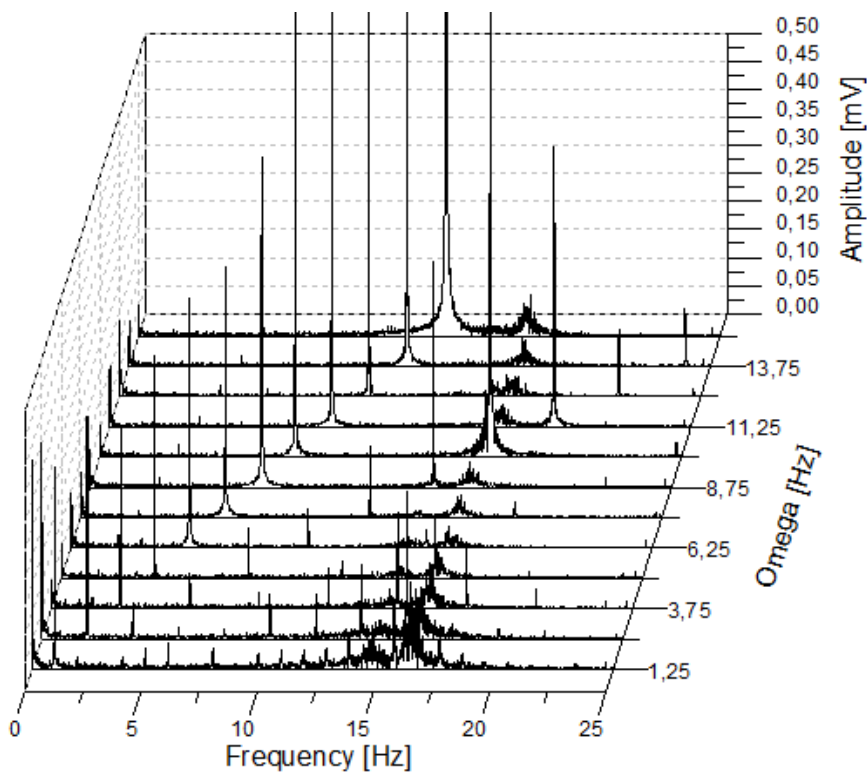


Figure 12: Strain gauges data ($V=15$ m/s – cross flow direction – vertical plane) signal units: mV.

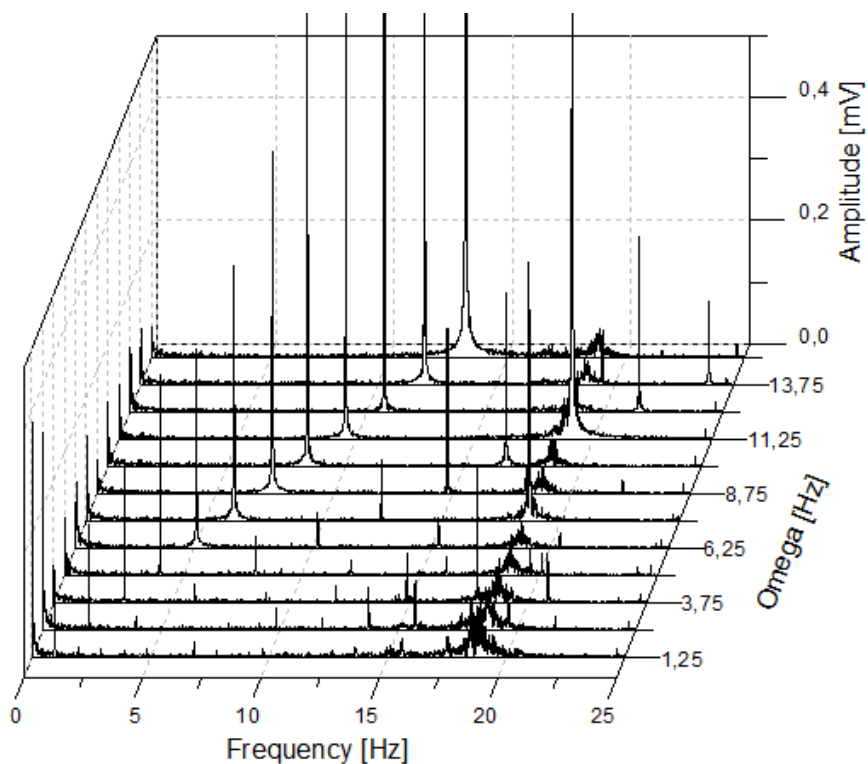


Figure 13: Strain gauges data ($V=15$ m/s – in line direction – horizontal plane) signal units: mV.

Two strain gauges were positioned in the vertical plane (cross flow direction) and two strain gauges were positioned in the horizontal plane (in line direction) on the supporting beam. From the figures the first two bending natural frequency (simple bending modes) of the system can be observed: the in line first bending frequency equal to about 18 Hz and the cross flow first bending equal to about 15 Hz. The difference in these values depends on the “elasticity” of the support frame of the test equipment (made of little thickness steel joined trusses). These frequencies do not depend on the rotational velocity of the rotor (Ω in the figures). On the other hand first basic harmonics ($1 \times \Omega$, $2 \times \Omega$ and $3 \times \Omega$) interact with the natural bending mode of the rotor system: an important increase of the signal amplitude (which correspond to bending deformations of the support beam and then to lateral oscillations of the rotor) can be observed in the bending frequency graph for a rotational velocity of about 11 Hz (660 rpm). The vibration phenomena have affected the torque measurements and then the experimental measurements of the rotor aerodynamic efficiency, that is, the per cent ratio between the actual mechanical power of the rotor, $\mathbf{M} \times \Omega$, being M the torque, and the available asymptotic flow power, $\frac{1}{2} \rho \mathbf{D H V}^3$.

As can be seen from the Figure 11, the unwanted vibration effects develop just in the range of rotational velocity which corresponds to the maximum values of the efficiency curves (45÷65 rad/s). It would be necessary to execute wind tunnel tests making use of a more expensive equipment to avoid the described dynamics effects because of the limit in the lower velocity field (operational minimum velocity = 15 m/s) due to the cooling of the electric motor of the wind tunnel.

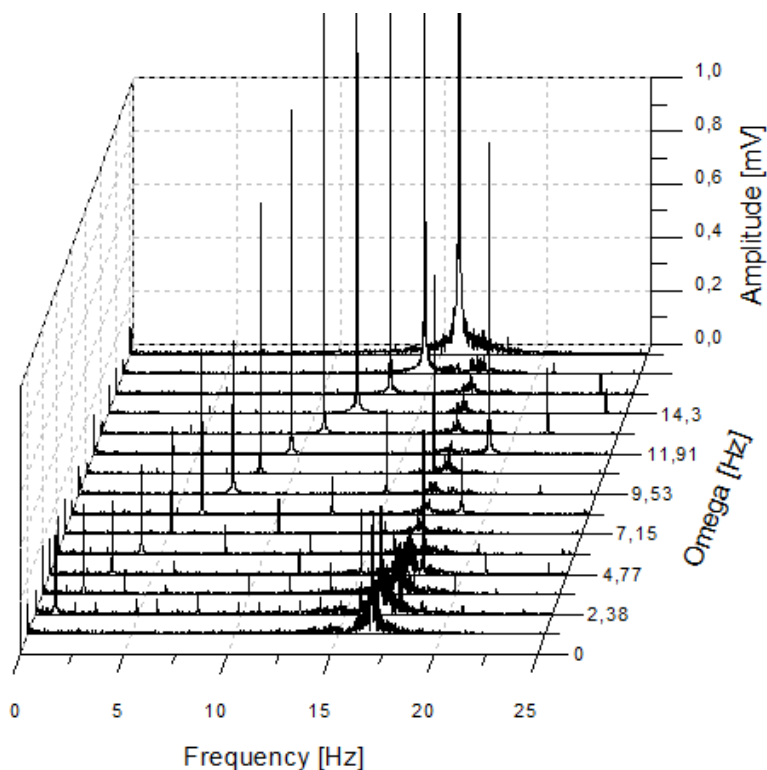


Figure 14: Strain gauges data ($V=18$ m/s – cross flow direction – vertical plane) signal units: mV.

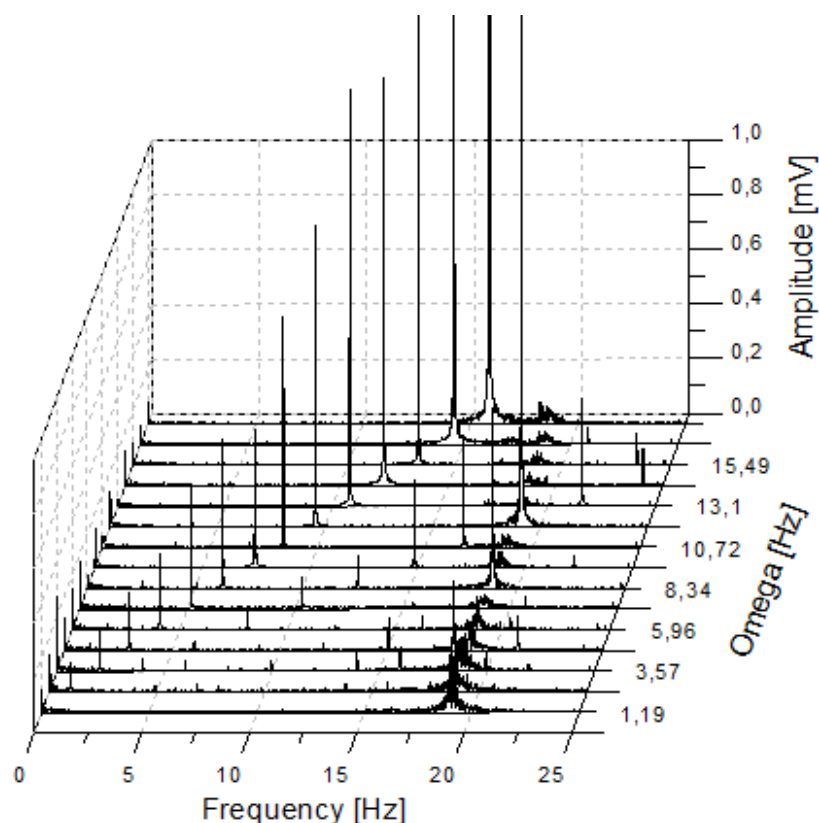


Figure 15: Strain gauges data ($V=18$ m/s – in line direction – horizontal plane) signal units: mV.

3. Two-dimensional CFD analyses executed with Fluent®

A first set of two-dimensional numerical analyses have been executed using the commercial code Fluent Re. 6.3. In the Figure 16 the first type of grid, made of about 300.000 cells, used in the research is shown. A stationary MRF method of analysis and a standard k- ϵ turbulence model has been adopted.

The results of these first set of analyses are shown in the abovementioned Figure 10 and Figure 11. A good agreement between numerical and experimental data has been obtained.

On the other hand to take into account the effect of rotor motion a second type of analyses have been executed: the Moving Mesh method (with the relative formulation applied only for the rotor grid) applied sequentially to the MRF method and the adapt boundary procedure available in the Fluent code have been used to better simulate the physics of the motion and to increase the grid refinement along the interface between the rotor crown (the mobile part of the grid) and the internal and external fields of the grid. In this case starting from the previous grid a new grid made of about 1.000.000 cells has been defined: this grid has been used to execute analyses on different geometry of the rotor; in particular they have been analyzed three different rotor model with same aerodynamic profiles and different diameters ($D=250$ mm, $D=1$ m and $D=4$ m) scaling the same refined grid.

The results of these analyses are shown in the Figure 18 and Figure 19. In the Figure 18 the average of the numerical data of the converged solution are shown and in the Figure 19 the peaks of the numerical data of the converged solution are shown.

Both a grid refinement effect and also an important scale effect can be highlighted. In this case the estimated efficiency for smaller models of the rotor increases to about 27%÷28% (averaged data).

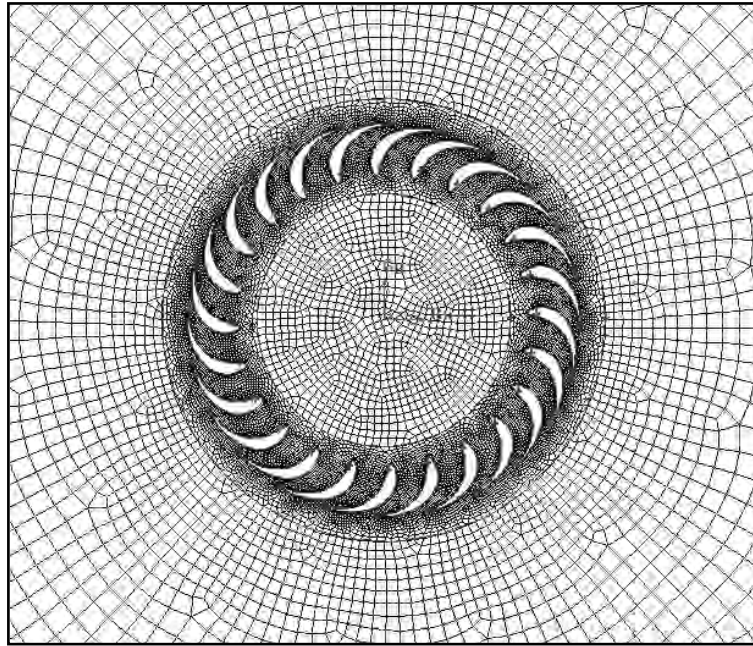


Figure 16: View of the two-dimensional grid (first level refinement) used for the study of reduced scale rotor model. The picture shows the first level grid without refinements (Atzeni, 2008).

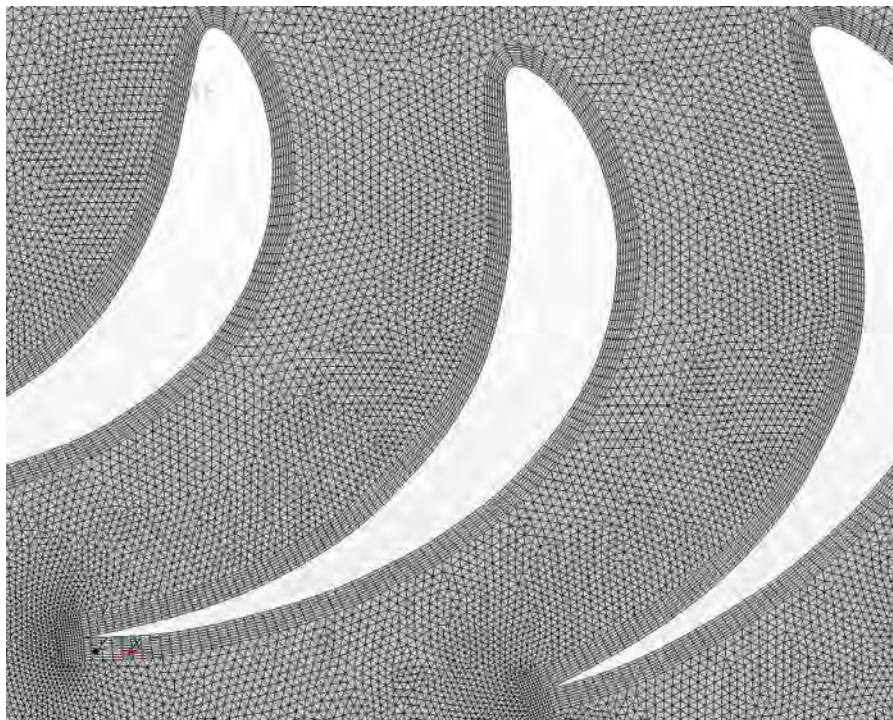


Figure 17: Local view of the two-dimensional grid used for the study of the rotor model (strips of structured grid has been inserted to better simulate the boundary layer effects) (Atzeni, 2008).

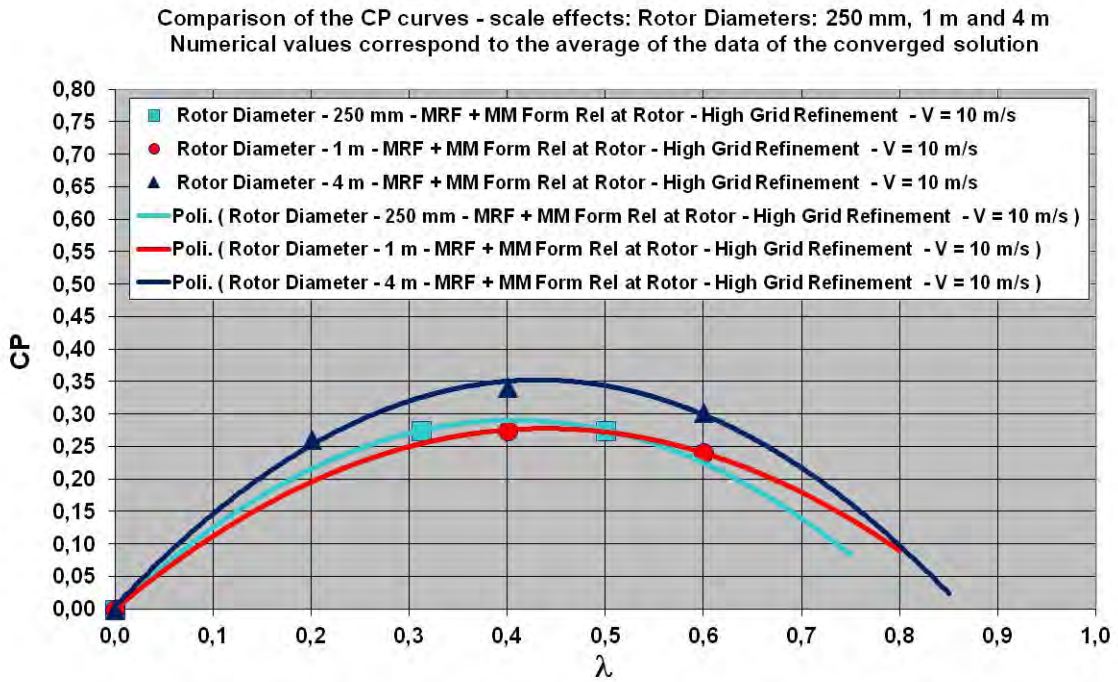


Figure 18: Comparison of the efficiencies of different rotors (Power Coefficient) – scale effects and grid effects (Fluent results, 2D numerical analyses: average data of the converged solutions).

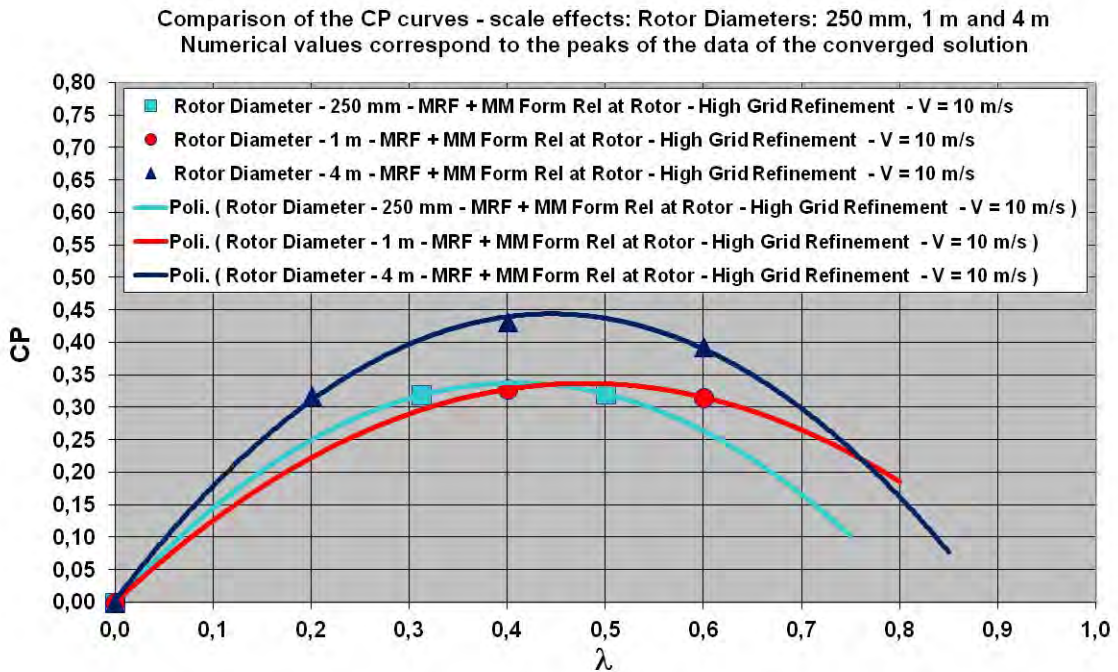


Figure 19: Comparison of the efficiencies of different rotors (Power Coefficient) – scale effects and grid effects (Fluent results, 2D numerical analyses: peaks data of the converged solutions).

For the rotor model with an external diameter equal to 4 m a maximum efficiency of about 34%-35% has been estimated (averaged data). Taking into account the peaks value of torque, a maximum of the efficiency greater than 40% can be observed for the 4 meter rotor model. It is well known that scale effects are very important in the turbine and in the pumps fluid mechanics as shown as an example in Cornetti (1993), so on the basis of the present numerical results the authors of the paper advance the hypothesis that the proposed multiblades wind-turbine rotor behaves like a pump or a turbine, for this reason, to better investigate the scale effects of the multiblades rotor model a second set of analyses have been carried out at DIA using a different code and a different method of analysis.

4. Two-dimensional CFD analyses executed with STAR-CCM+[®]

The CFD analyses carried out in the last part of the research are based on the use of the commercial code STAR-CCM+[®] Rel. 6.04 available at the DIA. The grid has been constructed starting from the geometry of the smaller rotor model ($D=250$ mm) and then the same grid has been scaled up to simulate the effects of the increase of the diameter dimension.

The topology of the grid around the blades is shown in Figure 17. The grid has been constructed with 233.432 cells for the blading zone, 35.034 cells for the inner zone of the grid and 34.814 cells for the external zone of the grid. The external region of the grid has a circular boundary with a diameter which is 24 times the rotor diameter. The inlet condition has been imposed to the lower half external boundary of the grid. The runs have been executed on a personal computer adopting the parallel option (2 or 4 active processes).

The analyses has been carried out adopting the MRF method and the Implicit Unsteady solution methodology; as in the previous cases a Reynolds-Averaged Navier-Stokes mathematical model with Segregated Flow option has been set; moreover, in this case, the standard turbulence Spalart-Allmaras model has been used. A time step of 0.01 s has been adopted with a number of *50 Iterations* for each time step.

The diameter dimensions examined are: $D=250$ mm, $D=2$ m, $D=4$ m, $D=10$ m and $D=20$ m.

As an example, in the Figure 20 is shown the time history of the moment about the axis of the rotor evaluated with a STAR-CCM+ implicit unsteady MRF analysis (in the figure is shown the case with a rotor diameter $D=4$ m, $V=10$ m/s, $\Omega=2$ rad/s).

In the Figure 21 are shown the estimated values of the maximum efficiency for the cases analyzed: these numerical data confirm the scale effects phenomena for the multiblades rotor model proposed. The values of the efficiencies were calculated using the averaged data of the converged solution (as indicated also in Figure 20). In all the cases the grids used have been obtained just scaling the basic grid constructed for the smaller model ($D=250$ mm): for this reason also all the dimensions of the cells increase and then during these analyses the grid refinement effects have not been taken into account.

In the Figure 22, Figure 23 and Figure 24 some views of the velocity field around the blades are shown.

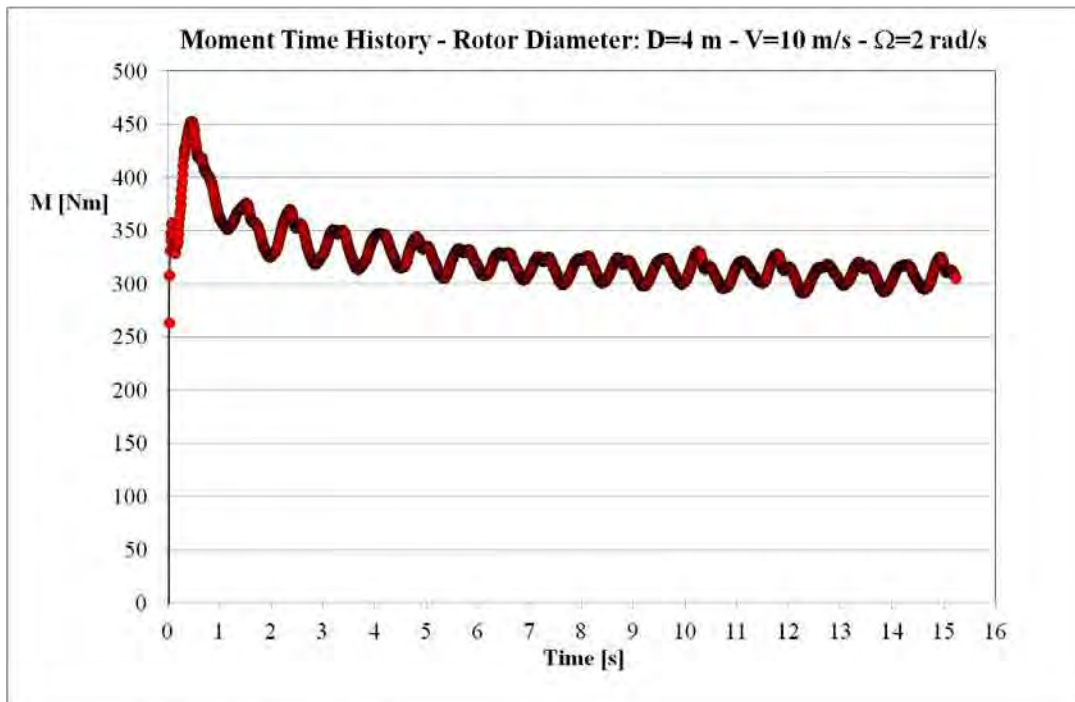


Figure 20: Time history of the moment about the rotor axis (asymptotic average data 310 Nm).



Figure 21: Scale effects: Rotor Efficiency vs. Rotor Diameter (STAR-CCM+ results).

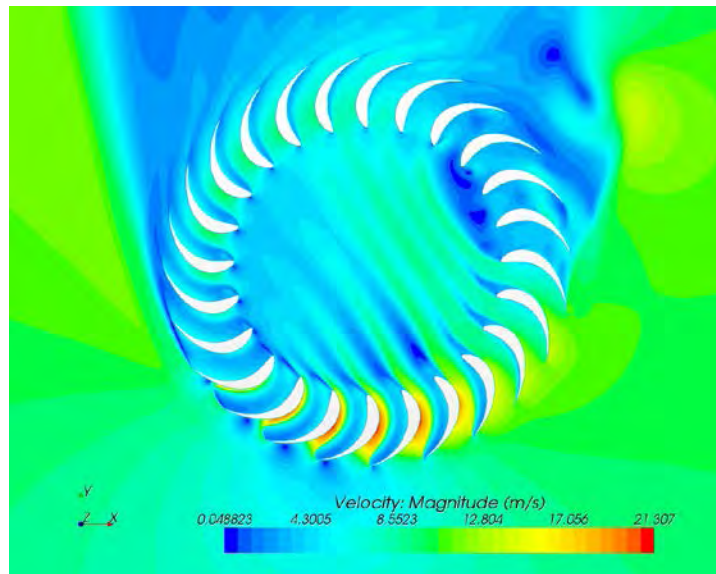


Figure 22: Sketch of the velocity field around the blades row (STAR-CCM+ unsteady analysis results: Rotor Diameter 4 m, $V=10$ m/s (Y direction), $\Omega=2$ rad/s).

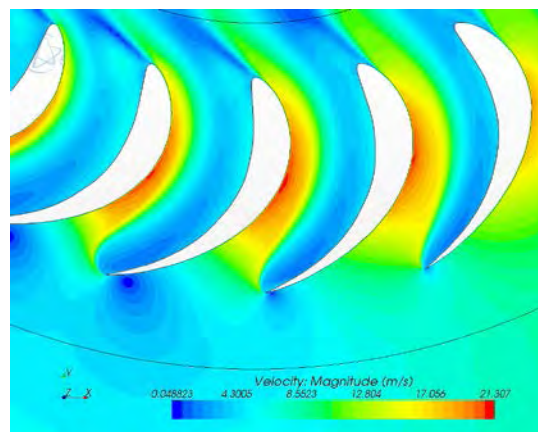


Figure 23: Sketch of the velocity field around the blades (STAR-CCM+ unsteady analysis results – rotor lower part: Rotor Diameter 4 m, $V=10$ m/s (Y direction), $\Omega=2$ rad/s).

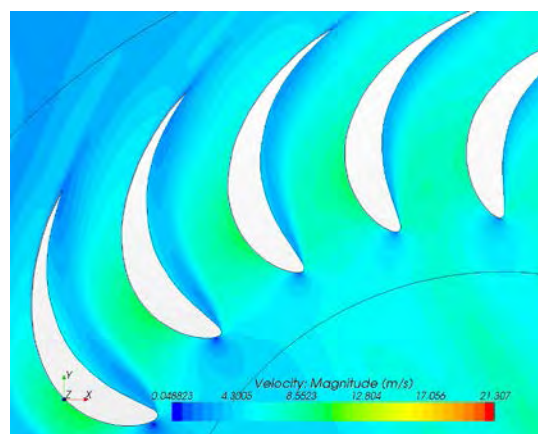


Figure 24: Sketch of the velocity field around the blades (STAR-CCM+ unsteady analysis results – rotor upper part: Rotor Diameter 4 m, $V=10$ m/s (Y direction), $\Omega=2$ rad/s).

5. Conclusion

A multiblades vertical axis wind-rotor model has been studied. Preliminary experimental tests have been carried out at the Department of Aerospace Engineering of Pisa on a small scale rotor model (the diameter of the small scale rotor = 250 mm). At the same time a campaign of two-dimensional numerical analyses has been executed to estimate the behavior of the rotor model both in small scale and real scale dimensions.

Even if the experimental tests have been affected by unwanted vibration phenomena numerical and experimental results are in a good agreement. The comparison has been carried out using the Fluent® code (Moving Reference Frame method of analysis applied only to the grid around the blades) with a first level refinement grid. The maximum value of the estimated efficiency is equal to 18%.

In a second phase of the research, scaling the grid and adopting the adapt boundary option available in the Fluent® code (applied along the interfaces between the blading zone and the inner and external zone of the grid) and a sequential method of analysis based on a MRF run plus a steady Moving Mesh run, a greater value of the efficiency (about 35%) have been found for a scaled rotor model. In particular an important scale effect has been found scaling a basic grid type to a rotor with a diameter of 4 m. To confirm these results a second campaign of numerical analyses has been executed using the commercial code STAR-CCM+®. A basic grid of about 300.000 cells has been constructed and a number of runs for different rotor models have been carried out adopting the MRF method and the Implicit Unsteady procedure available in the code.

These analyses confirm qualitatively the scale effects for the rotor model (Figure 21) and suggest that the proposed multiblades vertical axis wind-rotor, with a suitable optimized configuration, can provide efficiency's values comparable with modern lift based horizontal-axis wind turbines.

6. Appendix I: nomenclature

D rotor external diameter

H rotor height

R rotor external radius

Ω angular velocity of the rotor

V asymptotic flow velocity

CP power coefficient

λ tip speed ratio ($R \cdot \Omega / V$)

T atmospheric temperature

ρ air density

η Efficiency of the rotor

CFD Computational Fluid Dynamics

MRF Moving Reference Frame method

MM Moving Mesh method

DIA Department of Aerospace Engineering (University of Pisa, Italy)

Acknowledgements

The authors wish to thank Dr. Valerio Iungo and the technicians Gabriele Adorni Fontana, Luca Lombardi, Claudio Lippi and Fabio Pioli for their contribution.

References

1. T. Klemm, M. Gabi, J.N. Heraud. Application of a cross flow fan as wind turbine, *Journal of Computation and Applied Mechanics*, Miskolk University Press, Vol. 8, No. 2, pp. 123-133, 2007.
2. R. Champly. *Les moteurs a vent: théorie, construction, montage, utilisation au puisage de l'eau et à la production de l'électricité*, Dunod, Paris, 1933.
3. M.R. Patel. *Wind and Solar Power Systems*, CRC Press, NY, 1999.
4. A. Di Filippo. Two-dimensional numerical simulation to calculate and to optimize the efficiency of a vertical axis wind turbine, *First Level Degree Thesis in Aerospace Engineering, Department of Aerospace Engineering, CD-ROM n. 193 2005/2006, University of Pisa, Italy, 2007.*
5. Fluent Inc. *Fluent 6.3 Tutorial Guide*, Centerra Resource Park, 10 Cavendish Court, Lebanon, NH 03766, 2006.
6. M. Gabi , T. Klemm. Numerical and Experimental Investigation of Cross-Flow Fans, *Journal of Computation and Applied Mechanics*, Miskolk University Press, Vol. 5, No. 2, pp. 251-261, 2004.
7. G. Colley, R. Mishra, H.V. Rao, R. Woolhead. Effect of rotor blade position on Vertical Axis Wind Turbine performance, *International Conference on Renewable Energies and Power quality (ICREPQ'10)*, Granada, Spain, 2010.
8. G. Cornetti. *Macchine a fluido*, ISBN 978-88-4266015-6, Il Capitello, Torino, 1993.
9. G. Russo. Three-dimensional modeling and preliminary fluid dynamic study of a vertical axis wind turbine prototype, *First Level Degree Thesis in Aerospace Engineering, Department of Aerospace Engineering, CD-ROM n. 281 2006/2007, University of Pisa, Italy, 2008.*
10. D. Atzeni. Estimation of the aerodynamic efficiency of a vertical axis wind turbine by means of two-dimensional and three-dimensional CFD simulation, *First Level Degree Thesis in Aerospace Engineering, Department of Aerospace Engineering, CD-ROM n. 300 2006/2007, University of Pisa, Italy, 2008.*
11. S. Lain, C. Osorio. Simulation and evaluation of a straight bladed Darrieus-type cross flow marine turbine, *Journal of Scientific & Industrial Research Engineering*, Vol. 69, December 2010, pp. 906-912, 2010.
12. D. Atzeni. A numerical study and a preliminary experimental analysis of the dynamics of a vertical axis micro wind turbine, *Master Degree Thesis in Aerospace Engineering, Faculty of Engineering, University of Pisa, Italy, 2012.*

New Way for Access and Maintenance of Offshore Wind Farms. The Use of Cableway to Reduce Cost and Improve Accessibility. Comparisons, Strengths and Limits of this Approach

Massimo Grecchi¹, Luigi Meroni², Piergiorgio Betteto³

¹ Geologist and Physicist – University of MI, University of MI-TS Firm: Altavia Milano s.r.l. Activities: Project Manager. Offshore Engineering and Cable Car System
Via Lomellina 25 - 20133 MILANO Tel +39.02320625290
Website www.altaviamilano.it e-mail geomon@tiscali.it m.grecchi@altaviamilano.it

² Electronic Engineer – Politecnico of Milan Firm : Italtel S.p.A Activities : Project Manager. TLC expert , Senior SW Testing Expert, Smart Grid. Energy Management, Renewable Energy Expert Address : Via Reiss Romoli, Settimo Milanese 20019 MI Italy Tel. +39024388708
Mobile +39335592044 e- mail Luigi.meroni@italtel.it lmero@tin.it

³ Study:IUAV Architecture Venice University Firm : Vemplast S.a.S.Tel. +39 049 659174
Mobile +39 3937357779 e-mail vemplast@email.it - giorgioxt@gmail.com

Abstract - The work proposes a new method in order to deploy an affordable and reliable way for maintenance when it is necessary to access to offshore wind farms. The new system, based on cableway infrastructure is aimed to allow a lower cost of maintenance compared to other system for the same kind of operation but also to improve the reactivity and accessibility compared to them. Maintenance activities are taken into consideration in term of cost, period, nature,(e.g. in term of dimension of part to be carried / changed), accessibility of wind farm, kind of maintenance we want/need to use in order to ameliorate the availability/reliability of the wind farm.. Five different configurations with related cableway system are analyzed in order to demonstrate that facing a reasonable increasing of Capital Cost, sizable saving and extra revenue can be obtained if projected on the expected life of future Wind Farm.

1. Wind Energy Deployment

Wind sector, and in particular offshore, is going to grow reaching a high level of penetration in energy, but in particular, in electricity market. Forecasts show the increasing relevance of this source in absolute and relative term. In EU many research programs are devoted to Wind sector in order to study the technical, regulatory, financial aspect that can boost this sector. Wind energy is developing offshore facing new challenges as demonstrate by the trends in recent years. Deeper sea installation and farer from shore site are investigated in order to propose new investment in the sea. Many countries in Europe have widely installed wind park on and offshore but other country, notably Great Britain are aimed to increase to rate of deployment to reach ambitious targets (Figure 1).

Moreover Round 3 was launched with 9 zones around Great Britain in order to reach a target of 25% of electricity (Figure 2). With the help of ATLAS of UK Marine Renewable Resources it is possible to see the characteristic of the different zones. In particular it is possible to know sea level, wind speed, wave and tidal condition. Jointly to distance from shore these are fundamental data in order to show the how the proposed cableway system can be usefully used.

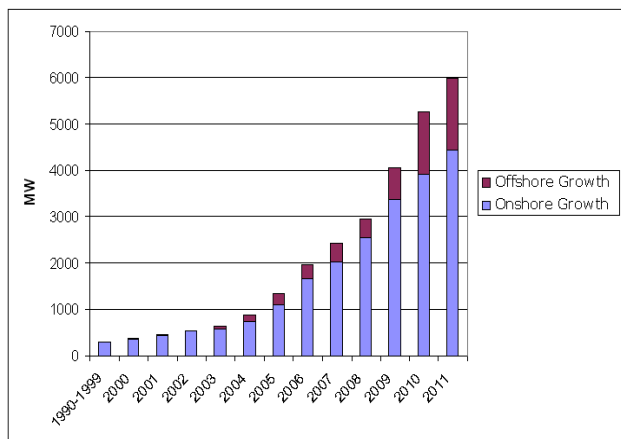


Figure 1: UK Installed wind power capacity 1990-2011.



Figure 2: UK Round 3 Zones.

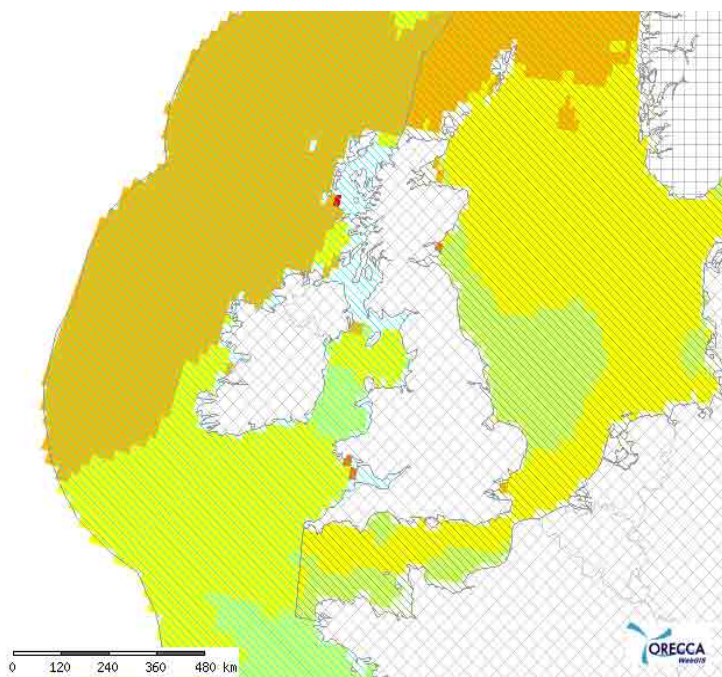


Figure 3: Wind Assessment in UK from ORECCA WEBGIS.

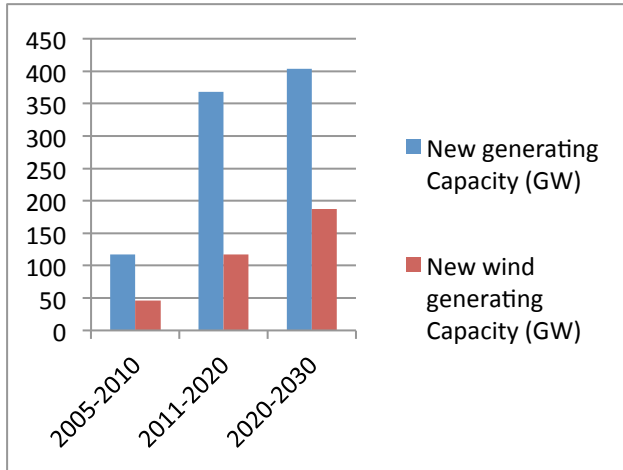


Figure 4: New and Wind Generating capacity in EU Source EWEA.

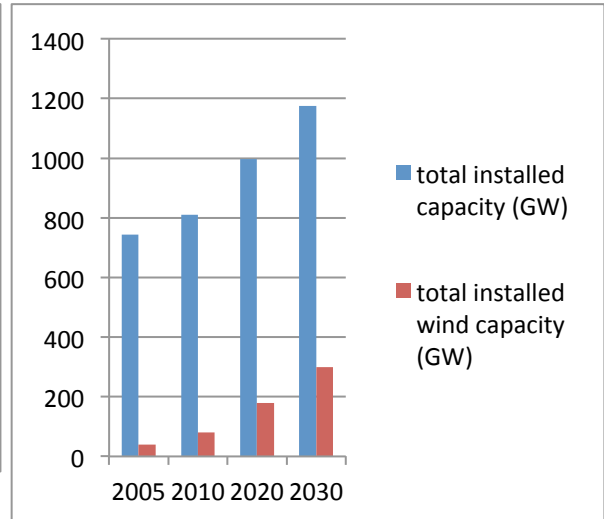


Figure 5: Total and wind installed power capacity in EU. Source EWEA.

Figure 5 show the forecasted new generating capacity in EU till 2030 and in parallel is possible to appreciate the effort for wind generation. Ambitious targets are also supported by European industry that is facing a fierce concurrence by China's manufacturers. The new wind installed capacity cumulated in the next 20 years and summed with the capacity already installed will attain the level of 300 GW.

This forecast was created by EWEA 5 years ago, In parallel it is worthwhile understand the dynamic of wind field worldwide. Figure 7 show the market comparing EU and the rest of the world. In 2009, following a very high rate of increase EU was surpassed. New installation in China, India, South America, USA, will in the future increase due also to the energy request in many of these regions. Offshore will play a major role in this trend.

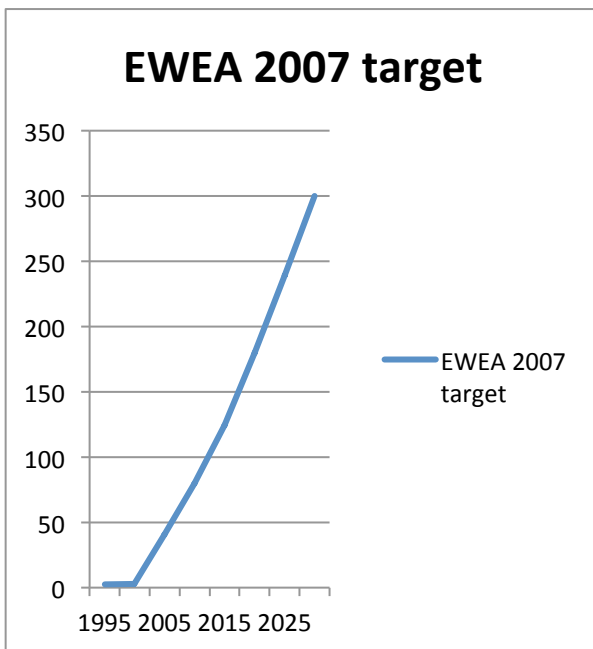


Figure 6: EWEA 2007 Target.

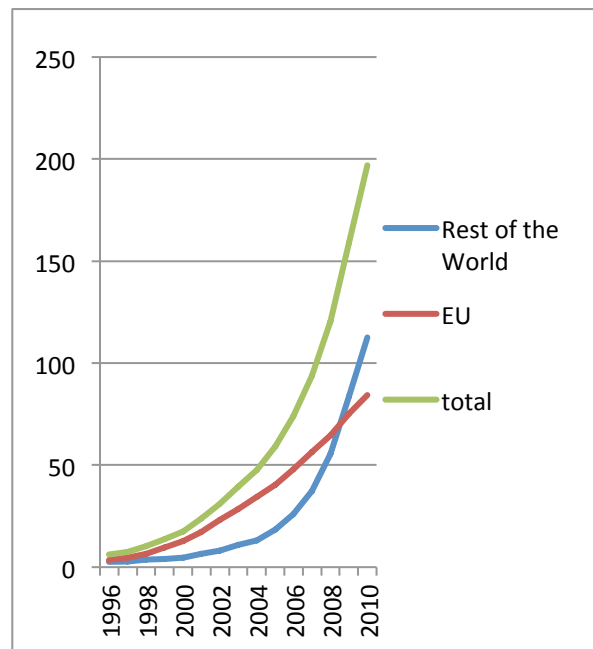


Figure 7: Cumulated wind power capacity (GW).

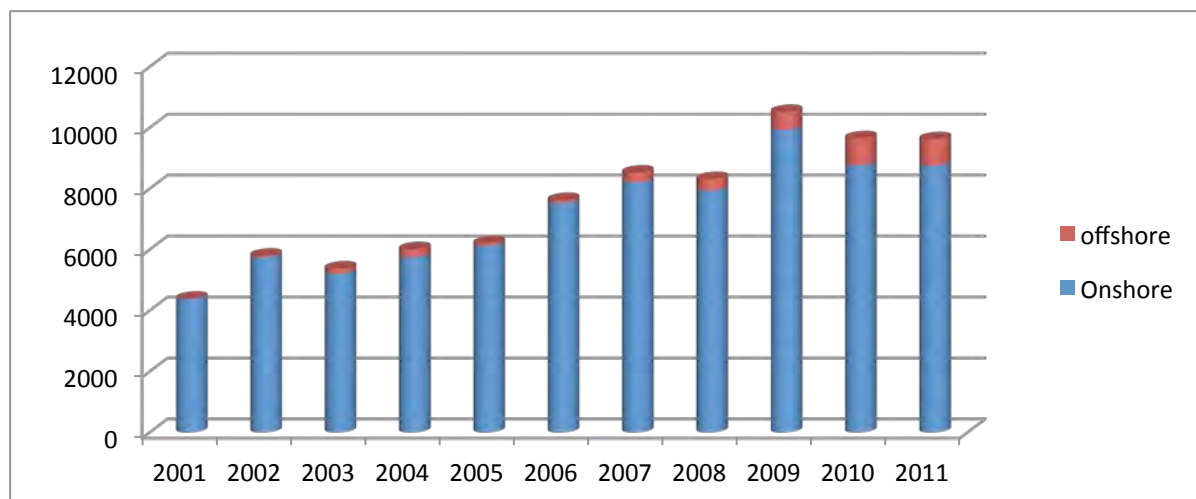


Figure 8: EU Onshore and Offshore total installation in MW.

On the contrary, in Europe, in the last year, onshore and offshore installation lost their momentum mainly due to crisis situation started in 2009. If we look after 2030 we can today see the data at 2050. In particular we can obtain this data from the Final Report of ORECCA Project www.orecca.eu.

For 2050 a total offshore wind capacity of about 1200 GW a 420 GW in Europe are expected. But in connection with these there is also the forecast of all the oceanic energy. Moreover is investigated the possibility to have at least 2 of even more sources of energy which share the same site or platform creating energy factory offshore or near shore or on the coast Starting also from these results one of our proposals takes advantage of the combination of other sources and in particular of the structure that they must build.

2. Cost of Energy

Levelised Cost of Energy (LCOE see Formula 1 at the end of the chapter) is one of the most important value, if not the most important in order to verify how and when a source of energy is competitive related to the others. Comparison with “carbon – energies” is very important. In order to do this it is possible to use tools which calculate the financial indicators. EWEA provided a tool to perform this comparison.

On EWEA site (<http://www.ewea.org/index.php?id=201>). The methodology was presented at a webinar held on 16 February 2012 and presentation can be retrieved at <http://www.ewea.org/index.php?id=2158>

IEA provides a spreadsheet for some country taking in account the specific situation. It is possible to find them at http://www.ieawind.org/task_26.html.

The files contain no comparison.

Briefly we want present the result obtained from the EWEA web site.

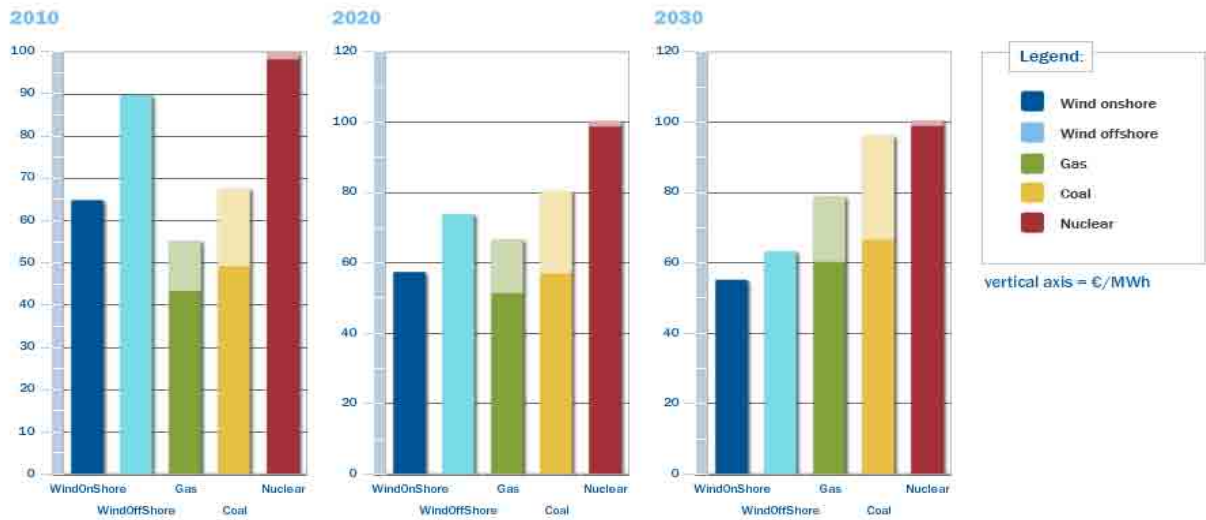


Figure 9: Cost of Energy comparison performed with EWEA calculator.

Category	Cost Component	Unit	2010	2020	2030
Energy Calculations	Installed Capacity	MW	40	40	40
	Load factor	%	35	35	35
	Energy Produced	MWh	122,640	122,640	122,640
	Inflation	%	2	2	2
	Nominal Discount rate dn	%	7.5	7.5	7.5
	Real Discount rate d	%	5.39	5.39	5.39
	Years of Operation (Lifetime)	y	20	20	20
	Total Capacity installed (Europe)	GW	2.9	40	150
Technology Cost	Learning Rate	%	5	5	7
	Capital Cost	€/kW	2,500	2,058.75	1,792.69
	Percentage of Total Cost	%	75.45	75.45	76.59
O&M	O&M	€/kWh	0.02	0.02	0.01
	Percentage of Total Cost	%	24.55	24.55	23.41
Result	Levelised Cost of Electricity	€/MWh	89.62	73.8	63.31

Figure 10: Hypothesis for Offshore Wind Energy.

The three main factors included in this calculation are :

- Capital Cost
- O&M
- Energy produced

Discount rate is also another important variable but we want to focus on the other elements. Capital cost must be shared between the cost of Wind turbine and the installation (without forgot the decommissioning). For offshore installation there are some parameters that can change dramatically the investment and we are speaking about sea level and distance for shore. By the way, German Energy Law, aware of this fact, at Par. 31 of EEG (Erneuerbare Energie Gesetz) specifies both parameters in the calculation of incentives.

O&M is a item that is assuming an increasing importance and is linked to theoretical methodology and practices that also affect the third factor: energy produced. In EWEA's analysis the calculation take into account and separate the fuel costs from operation and maintenance and adding the carbon emission costs.

$$(1) LCOE = \frac{LI+DO\&M+DCf+DCCo2}{E}$$

Where:

- **LI (€/year):** levelised investment cost which is the annual breakdown of the capital cost.
- **DO&M (€/year):** discounted operation and maintenance costs, including the fixed (€/kW) and variable €/kWh) costs which are associated with land renting, insurance and operation and maintenance costs.
- **DCf (€/year):** discounted fuel cost which represents the present value of the annual expenditure related to fuel.
- **DCCO₂ (€/year):** discounted carbon cost which represents the present value of the annual expenditure related to carbon emissions.
- **E (MWh/year):** annual energy Production

The future cost will depend on the present cost and is linked to the total installed capacity by the Learning Rate that is typical of every power technology.

$$C_{future} = C_{present} \left(\frac{P_{future}}{P_{present}} \right)^{\frac{\ln(1-LR)}{\ln 2}}$$

Where:

- **C_{future}, C_{present}:** future and present value for a specific cost component
- **P_{future} :** total installed capacity of the respective power plant [GW]
- **P_{present} :** total installed capacity of the respective power plant [GW]
- **LR :** represents the learning rate applied to each power technology [%]

3. Operational Availability

We must compose a clear view of all the items that appear in the Figure 11 starting from reliability. We could use this definition: “Reliability is the probability of successful operation or performance of systems and their related equipments, with minimum risk of loss or disaster or of system failure. “ But a more complex definition can be found in the USA Military Standard (MIL-STD-721B). “Reliability is the probability that an item will perform its intended function for a specified interval under stated conditions”. The conditions must be clearly taken in account, so we can regard the real condition.

Starting with the definition. “Availability is the item’s capability of being used over a period of time”, the measure of an item’s availability can be defined as “that period in which the item is in a usable state”. But this is not enough because we can have different kinds of availability defined starting from design to operational condition.

Inherent availability, A_{in} can be defined as “the prediction of expected system performance or system operability over a period which includes the predicted system operating time and the predicted corrective maintenance down time”.

$$A_{in} = \frac{MTBF}{(MTBF + MTTR)}$$

where

MTBF = Mean time between failure

MTTR = Mean time to repair

Source DoD RAM guide 2005

Actual Availability, A_{ac} , also defined Operational Availability, A_{op} , can be defined as “the evaluation of potential equipment usage in its intended operational environment, over a period which includes its predicted operating time, standby time, and active and delayed maintenance down time”. This is the final result of a design strategy and real environment condition of operation. On this definition there is the convergence of all the other items taken into account in this simplified but meaningful picture.

$$A_{ac} = \frac{MTBM}{(MTBM + MDT)} = \frac{Uptime}{Total Time}$$

Where:

MTBM = Mean time between maintenance

MDT = The mean or average time that a system is not operational due to repair or preventive maintenance. It includes logistics and administrative delays.

Availability is that aspect of system reliability that takes equipment maintainability into account. Designing for availability requires an evaluation of the consequences of unsuccessful operation or performance of the integrated systems, and the critical requirements necessary to restore operation or performance to design expectations.

Maintainability is that aspect of maintenance that takes downtime of the systems into account. Designing for maintainability requires an evaluation of the accessibility and ‘reparability’ of the inherent systems and their related equipment in the event of failure, as well as of integrated systems shutdown during planned maintenance. Maintainability is primarily a design parameter, and designing for maintainability defines how long the equipment is expected to be down.

Serviceability implies the speed and ease of maintenance, whereby the amount of time expected to be spent by an appropriately trained maintenance function working within a responsive supply system is such that it will achieve minimum downtime in restoring failed equipment. In designing for maintainability, the type of maintenance must be considered, and must have an important role in considering serviceability.

Finally, with the result of Operational Availability we reach our aim to know the Actual availability as defined in the Figure 11.

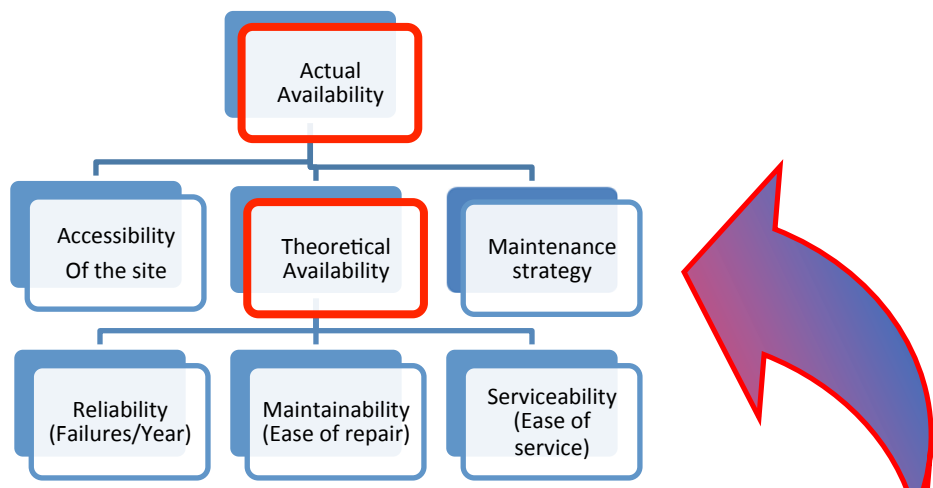


Figure 11: Elements concurring to actual availability.

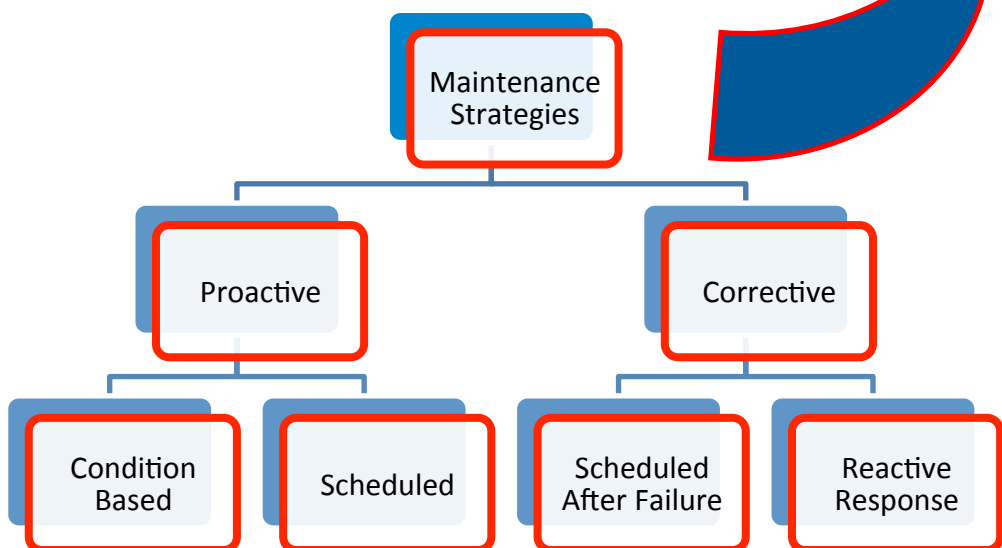


Figure 12: Pyramid of Maintenance Strategies.

4. Maintenance Strategies which trade-off between accessibility and availability?

In this chapter we will analyze the maintenance strategies in relationship with the needs of WT and the accessibility of the wind farm itself. This evaluation is necessary in order to compare the proposed system. The first and unavoidable question is: “which kind of maintenance and how long it will takes”. Many studies were realized in order to answer. These were coupled to project (e.g. DOWEC) in order to analyze all the aspects of a Wind Project. Model about cost of system, and forecast was proposed. The starting point is the division between categories of maintenance.

Maintenance Categories for the DOWEC reference turbine	
Cat. 1	Heavy components, external Crane
Cat. 2	Large components, internal crane
Cat. 3	Small parts 2 days repair time
Cat .4	Small / no parts 1 day repair time

Table 1: Maintenance Categories from Dowec Project.

Proposed projects must evaluate the needs of maintenance, and related costs because on these can be based the decision of the stakeholders, mainly the investors, which decision on resources to be used is very important. The problem of maintenance must be addressed not only on the side of the burden of costs but also on the side of “loss of income” during the life of the wind farm. Awareness of maintenance is not ubiquitous in new energy sectors, or better is not an issue if feed in premium/ feed in tariff levels are high. DOWEC documents contain a very detailed explosion of the four categories. Moreover it is necessary to evaluate the frequency for each of them as it is in the Table 2.

Maintenance Category	Required action on	Offshore Equipment required	% of all action
Cat. 1	Heavy components	Vessel + Jack-up	1
Cat. 2	Large components	Vessel + build up internal crane	7
Cat. 3	Small parts	Vessel + permanent internal crane	23
Cat .4	Small or no parts	Vessel or Helicopter	69

Table 2: Category and percentage from DOWEC Project.

Basing our estimation on NREL studies it is possible to use, on average, during Wind farm life time, a value of 200h/Turbine/year for maintenance that for a wind farm of 100 WT (5MW) means an amount of 20.000 hours. Some tasks really require every year more or less the same amount of hours and in other case these values are averaged (Blade replacement, gearbox replacement...).

Using these values and the values of the two Tables previously seen we can share the burden for every category as showed in the subsequent Table 3. But maintenance requires accessibility that is strictly connected to the availability of a wind farm that is the goal of our effort due to the impact on Capacity Factor and finally on annual revenue. The issue related to accessibility can be addressed imaging the maintenance needs and the environmental condition which impact on accessibility.

Category	Hours / task	People	%	Index	Hours for every category
Cat. 1	336	8	1	2688	4164
Cat. 2	168	4	7	4704	7286
Cat. 3	48	2	23	2208	3420
Cat .4	24	2	69	3312	5130

Table 3: Hours of maintenance for every category - 100 WT 5MW – 20000 hours.

This can be done, regarding the condition of the site where the wind farm is installed and composing the so-called scatter diagram that crossed which Vessel's characteristic can say us if the site can be accessed, but, moreover we must take into account that "when is possible" due to condition doesn't matches necessary with "when we need" and in any case can impact on "how long we must access" in order to perform the maintenance's operation. So the first point is to build an access way in order to overcome these difficulties and allow accessibility even if the condition prevent to access with other means, in particular this will be done with maintenance's category 3 and 4. The Figure 13 clearly say us way we need to improve accessibility to the site with the independence from sea condition (tide, wave and wind).

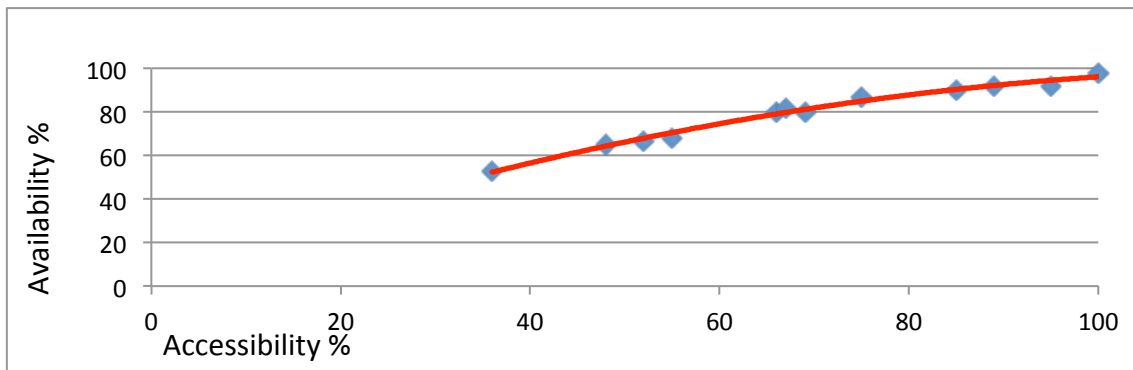


Figure 13: Accessibility Vs. Availability from Dowec Project.

5. Wind Farm Costs

In this paragraph we will insert 2 graphs related to the trend of MEuro/MW and total rated capacity Vs capital costs for selected Wind farm in the last 10 years. Wind farm capital cost will be used in order to calculate the cost of cableway system in term of percentage of capital cost of the wind farm without this system.

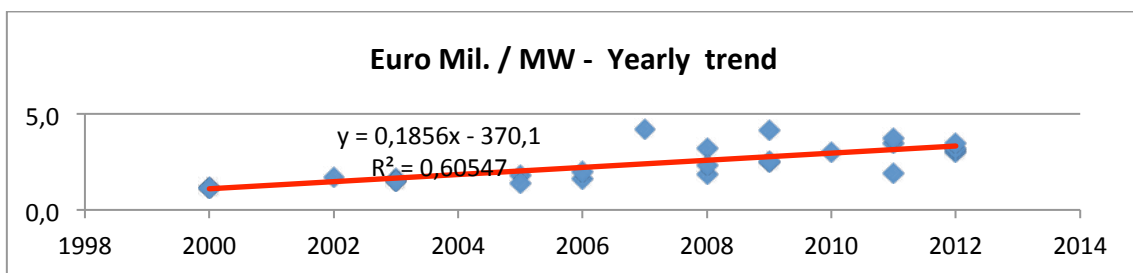


Figure 14: Trend of Costs for installed Wind Turbines.

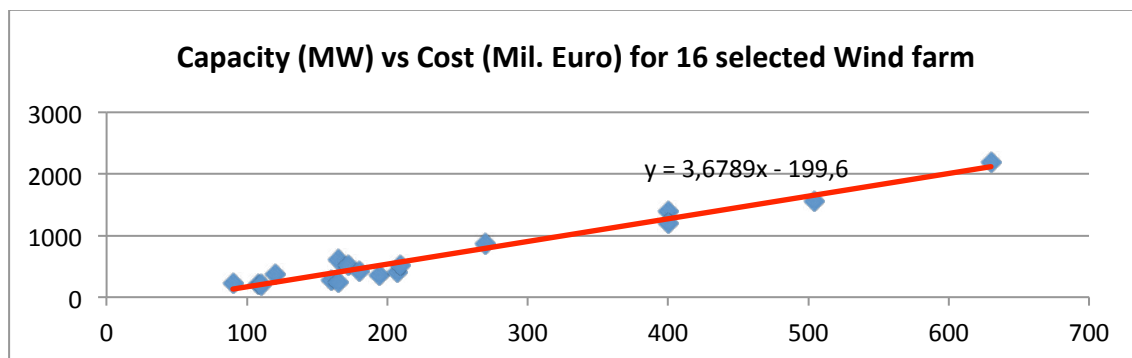


Figure 15: Relationship Capacity / Cost For Real Wind Farm.

For our purpose we will consider a wind farm of 500 MW and a Capital Cost of 1500 Mil. euro. The wind farm, if not differently written, is considered composed by 100 Turbines.

6. From real case to real solution

We can consider now the parameters for designing the cableway system related to WT dimensions. We take into account Diameter “D” and Hub Height “H” (on sea level). This means that the margin “Mrg” between the minimum point of blade and the sea level is:



Figure 16: WT with relevant dimensions.

$$Mrg = H - D/2 \quad (1)$$

But we must subtract to “Mrg” the value of other parameters and in particular:

- Tidal wave height “Tw” (max value)
- Sea Wave height “Hs” or Significant wave
- Arrow of cableway system with no load “Ac”
- Extra Arrow with Cable-railway car “EAc”

This means that we want:

$$H - D/2 - (Tw + Hs + Ar + EAc) > 0 \quad (2)$$

This in order to be sure that the system will always work even if the Hs and Tw assure a margin in the worst condition and not in normal condition. The value Ar is function of the distance of the point where the cable is connected and EAc is a function of weight and in this case is 6 meter.

In the Table 4 we assume that the distance between the Turbines is equal to 7 Diameter. So we can list the arrow “Ar”. We can see that in order to assure a margin “Mrg” of 20 meter we must have the Hub Height listed in the table. The real Hub Height is not always enough to assure what we want in (2). We assume for example Tw = 2m, Hs=6m and EAc=6m .

We have 6 meters more in order to face worst condition in particular for Tw and Hs. We can note that in three out of six situations we can assure a margin level enough for our purposes and this is representative of real deployment. If we take into account bigger WT we can note that the necessary Hub height is normally not in use for offshore deployment because is not necessary.

Technical and economic reasons forbid to ask to augment the Hub Height to the necessary level, so in these cases other solutions will be used.

Diameter	Power	Hub height	Spacing 7D	Arrow	Margin
138	6	125	959	36	20
126	5	113	875	30	20
106	3,6	99	742	26	20
98	3	91	678	22	20
88	2,5	84	619	20	20
80	2	77	553	17	20

Table 4: Margin as function of Diameter and Hub Height

7. Solution layout with Cableway Systems



Figure 17: Solution Layout 1 – Short Distance and Margin enough to install cableway system.

In this case we have:

- Short Distance
- Low Cost
- Simple architecture
- Useful for Repower of wind farm of 2-3 MW without change of layout



Figure 18: Solution Layout 2 with intermediate pile.

In this case we have:

- Large distance
- Higher costs that Solution 1
- Foundation and pile are necessary and this add complexity to layout
- Useful for WT of > 5 MW

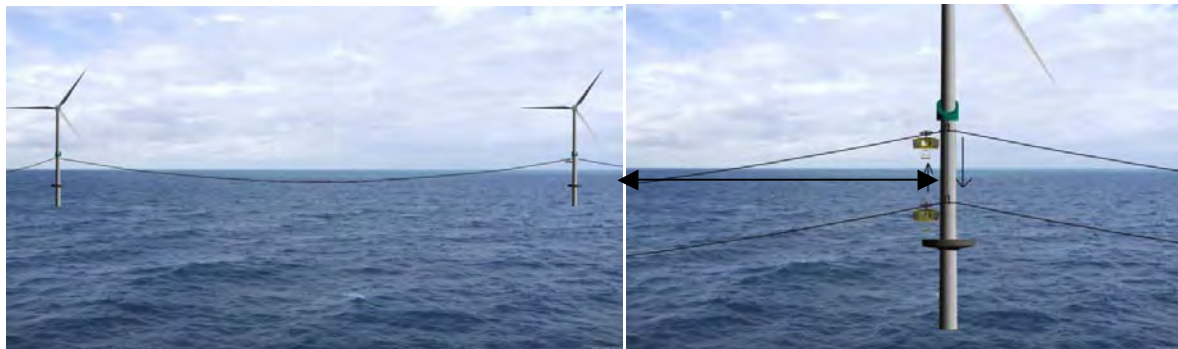


Figure 19: Solution Layout 3 – Margin not enough so the cableway position is not fixed.

In the Solution Layout 3 there is not enough margin for a “pure” deployment like in Solution Layout 1 but we can add a mechanism in order to elevate the cableway system when necessary. This must be done with the block of yaw mechanism in order to avoid interference. This can save money but add more complexity to the system which requires a synchronization of operations.

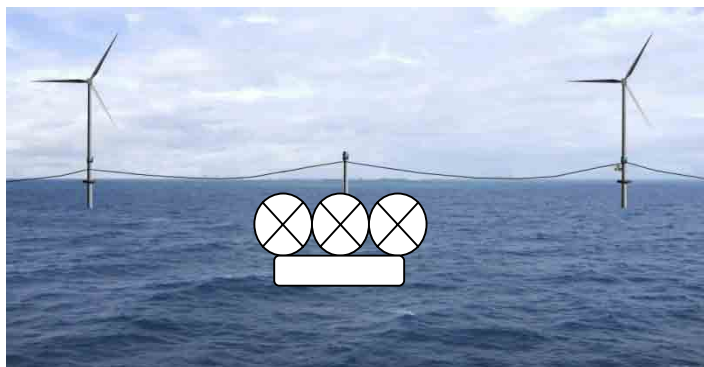


Figure 20: Solution Layout 4 – Use of structure of other renewable energy present in the wind farm.

In Solution Layout 4 inside the wind farms are located the structures of another marine renewable energy that are used. In particular there is the saving of foundation that has a relevant cost if referred to Solution Layout 2.



Figure 21: TITAN foundation and cableway system.

TITAN platform for foundation can be used, due to the particular form in order to deploy a cableway system to cover larger distance because the concept of “margin” is changed. The system is not connected to the tower but to one of the 3 piles of the foundation.

Which are the advantages of the cableway system? In the next chapter the economic issues are showed but we want to stress now that accessibility is guarantee by the fact that the system can work absolutely till a wind speed of 20 m/s but some cableway systems assure stability till 25 meter /s of wind speed.

Lighting is another point of strength because the cable-railway-car is a faraday’s cage. Moreover we can assure an extra margin when we consider severe conditions (the extreme) for tidal and sea wave. We can assure service continuity and immediate response to every task without compromise availability. Category 3 and 4 maintenance are always and completely guaranteed.

Only for Solution Layout 3 we have the complication that an extra mechanism must be added because the “margin” previously defined is not enough.

Also, the particular geometry of TITAN system can assure the margin we need even if the distance is high. The margin, due to the fact that the pile is 33-35 m far from the tower is augmented without the need to have a higher tower, need that for some reasons cannot be asked to reach the margin that we prefer.

8. Costs and Saving

In this chapter we will perform some calculation in order to demonstrate the advantages of cableway system. Firstable we will consider a wind farm of 100x5 MW Turbine with a capital cost of 1500 Mil. Euro. For solution layout 1 was necessary to taken into account a layout of same power dimension but with 16x16=256 wind turbine. Capital costs are listed in Table 5 for the different solution layout.

Solution Layout	Capital cost cableway Mil. Euro	% Total related to Capital Costs of the Wind Farm
1	41	2,73
2	67	4,47
3	57	3,80
4	52	3,47
5	39	2,60

Table 5: Capital cost of Cableway system as percentage of capital cost of Wind Farm Solution layout 1 was calculated with a wind farm of 256 Turbines of 2 MW each in order to have the possibility to apply this layout due to the short distance between WT.

But this is not enough. It is necessary to analyze what extra revenue is possible to obtain from the augmented availability. We want consider a 1% more of Capacity Factor. We can use the data from EEG (Erneurbare Energie Gesetz) which for Germany decides the incentives for Offshore Wind Energy.

EEG Par 31	
See level meter	30,0
Distance from Coast (miles)	70
Year	15,8
Feed in premium Euro	0,15

Table 6: Data from EEG (Germany) for a wind farm 70 miles from coast and 30 m of sea level.

Turbines	100
MW	5
Year	15,8
Capacity factor = 34% --> 35%	35%
Hours	3066
Euro / kWh	0,15
Extra Revenues	€ 104.025.000

Turbines	100
MW	5
Year	9,2
Capacity factor = 34% --> 35%	35%
Hours	3066
Euro / kWh	0,1
Extra Revenues	€ 40.150.000

TOT	€ 144.175.000
-----	----------------------

Table 7: Extra revenue for 1% more of Capacity Factor.

We can consider that with 9000 hours (see Table 3 adding the hours for Cat. 3 and Cat. 4) we have:

Technicians on site = $9000/1800 = 5$

But we, using people on-site without transport between the coast and the wind farm we can discount the cost of some item listed below.

- We can save 1 vessel for 1 year
- We can save about 90 extra day of vessel for bad condition (+25%) that will enlarge the time for maintenance action
- We can save about 90 extra day of 5 technicians for bad condition (+25%) that will enlarge the time for maintenance action
- We can save the cost of the time for travel from cost to the wind farm for vessel and people for every travel that is necessary to perform.

The sum for this items is calculated as optimistic in 5 M euro / year. Considering 25 years of life for the wind farm we have 125 M euro of saving on maintenance activities.

9. Conclusion and further works

Cableway system was taken into account in relationship to 5 different Wind Farm layouts. Precise calculations were derived in order to demonstrate potentialities and limits of this system. The different alternatives are critically analyzed demonstrating the benefits for the double effects of cost reduction of the maintenance activities related to alternative methods and due more revenue due to the improvement of availability (boosted by augmented accessibility) On one side cost reduction can be estimated between 30% and 50 and annual revenue can be increased greatly. Another benefit of the system is that a standard solution can be used when we decide to adopt this system so that all technology trends and results of cableway system are at this moment ready in order to be used.

Further works are related to new geometric layout of Offshore Wind Farm and their integration with other Sea energy. This will allow the creation of isle connected with cableway systems. Studies will be necessary in order to synchronize maintenance with yawing system for “Solution Layout 3”. We will propose also to describe the cableway system in term of IEC specification including them into IEC 61400-25 written specifically for Wind System in order to integrate the maintenance of the global system. This info model and in particular his “ontology” will be integrated with Webservices for maintenance. Moreover due to the fact there is an increasing complexity in such Wind Farm including Cableway system it is necessary to extend geohazards analysis and the monitoring system. Application to floating Wind Farm, as emerging technology for deep oceanic installation must be addressed.

10. Acknowledgements

We want to thank the people that supported us to write this article. Moreover we want to thank ALTAVIA for the deep background in cableway systems which help us for this work.

11. References

1. Report Wind Power R&D Seminar – Deep Sea Offshore Wind Power Trondheim, Norway 20-21 January 2011 John Olav Tande (Editor)
2. Model For Comparing And Projecting The Levelized Cost Of Electricity Generated By New Gas, Coal, Nuclear Power Stations And Wind Energy (On- And Offshore) Athanasia Arapogianni, Gloria Rodrigues, Nicolas Fichaux, Arthouros Zervos, George Caralis
3. BWEA Guidelines for the Selection and Operation of Jack-ups in the Marine Renewable Energy Industry guidance aimed at jack-up operators, developers and contractors
4. Report Wind Power R&D Seminar – Deep Sea Offshore Wind Power Trondheim, Norway 20-21 January 2011 John Olav Tande (Editor)
5. EWEA Wind In Power 2011 European Statistics – February 2012
6. The European offshore wind industry key 2011 trends and statistics - January 2012
7. GWEC global wind statistics 2011 - 07.02.2012
8. ORECCA European Offshore Renewable Energy Roadmap September 2011 www.orecca.eu . See also ORECCA WEBGIS <http://map.rse-web.it:8082/orecca/map.phtml> offshore renewable in Europe
9. NREL - Development of an Operations and Maintenance Cost Model to Identify Cost of Energy Savings for Low Wind Speed Turbines NREL/SR-500-40581 January 2008
10. Model-based operations and maintenance for offshore wind Trinh Hoang Nguyen, Andreas Prinz, Trond Friisø
11. Report Wind Power R&D Seminar – Deep Sea Offshore Wind Power Trondheim, Norway 20-21 January 2011 John Olav Tande (Editor)
12. EWEA Wind In Power 2011 European Statistics – February 2012
13. The European offshore wind industry key 2011 trends and statistics - January 2012
14. ORECCA European Offshore Renewable Energy Roadmap September 2011 www.orecca.eu . See also ORECCA WEBGIS <http://map.rse-web.it:8082/orecca/map.phtml> offshore renewable in Europe
15. NREL - Development of an Operations and Maintenance Cost Model to Identify Cost of Energy Savings for Low Wind Speed Turbines NREL/SR-500-40581 January 2008
16. Work Package 1 Final Report IEA Wind Task 26 Multi-national Case Study of the Financial Cost of Wind Energy. Authors Paul Schwabe: National Renewable Energy Laboratory- Sander Lensink: Energy Research Center of the Netherlands - Maureen Hand: National Renewable Energy Laboratory
17. ECN - Optimization of maintenance strategies for offshore wind farms. A case study performed with the OMCE-Calculator R.P. van de Pieterman H. Braam T.S. Obdam L.W.M.M. Rademakers T.J.J. van der Zee Presented at: The Offshore 2011 conference, 29 November – 1 December 2011, Amsterdam, The Netherlands
18. ECN - Installation, operations and maintenance We@Sea research area 5 L.W.M.M. Rademakers
19. NREL Definition of a 5-MW Reference Wind Turbine for Offshore System Development J. Jonkman, S. Butterfield, W. Musial, and G. Scott Technical Report NREL/TP-500-38060 February 2009
20. Overall Cost-Modeling of the DOWEC Lifecycle in a Wind Farm. Work package 1, Task 18 Ir. M.B.Zaaijer (TUDelft,editor) 10 March, 2003 DOWEC-F1W1-MZ-01-037/02-P DOWEC 037 rev. 2

21. ECN Operation and Maintenance Cost Estimator (OMCE) Final Report L.W.M.M. Rademakers H. Braam T.S. Obdam R.P. v.d. Pieterman
22. ECN - Implementation of a Probabilistic cost model into OWECOP – S. A. Herman
23. TITAN platform Offshore wind power system of Texas
<http://www.offshorewindpowersystemsoftexas.com/>
24. ATLAS of UK Marine Renewable Energy Resources <http://www.renewables-atlas.info/>
25. Round 3 Offshore Windfarm Zones www.thecrownestate.co.uk
26. RSE – CESI RICERCA Studio di fattibilità e progetto di massima di un’installazione eolica galleggiante e analisi dei costi. Silvano Viani, Claudio Casale, Ettore Lembo, Laura Serri Febbraio 2009
27. RSE – CESI RICERCA Documento di sintesi di Progetto “Produzione di energia da fonte eolica con particolare riferimento ai sistemi offshore” Anno 2008
28. The German Wind Turbine Reliability Database WMEP Wind Power R&D Seminar – Deep Sea Offshore Wind Power Trondheim, Norway 20-21 J. Bard, S. Faultisch, P. Lyding IWES
29. http://www.nrel.gov/analysis/tech_lcoe.html
30. EWEA online Energy Cost calculator <http://www.ewea.org/index.php?id=201>
31. Ampelmann Development of the Access System for Offshore Wind Turbines – Thesis - David Julio CERDA SALZMANN – University of Delft vedi bibliografia primo capitolo + 15
32. DNV Access to offshore wind facilities – What can we learn from other industries BWEA Health & Safety Conference 2010
33. The DOWEC Offshore Reference Windfarm: analysis of transportation for operation and maintenance, Wind Engineering Volume 27, No. 5, p 381-392 Bussel, G. van and W. Bierbooms (2003)
34. O&M Aspects of the 500 MW Offshore Wind Farm at NL7 – Optimization Study, DOWEC 10090 rev 1 Rademakers, L, and H. Braam (2003)
35. DOWEC wind and wave conditions Wim Bierbooms (ed.) Section Wind Energy Delft University of Technology DOWEC 47 rev. 2
36. www.altaviamilano.it
37. <http://altaviamilano.it/plesk-stat/webstat/> Altavia’s statistics
38. EWEA pure power - Wind energy targets for 2020 and 2030

Levelised cost of electricity generated by offshore wind plants and other competing technologies: dynamic analysis using simulation theory

M. Gaeta¹, M. Rao¹

¹ENEA Agenzia per le nuove tecnologie, l'energia e lo sviluppo economico sostenibile, Lungotevere Grande Ammiraglio Thaon di Revel 76, 00196 Roma, Italy,

maria.gaeta@enea.it marco.rao@enea.it

Abstract – This work is focused on the offshore wind technology's economic performance in power generation, compared with other technologies among those of greatest interest (ASC coal FGD with CCS, Nuclear EPR 3, onshore wind and gas CCGT). The present analysis is based on a DECC study (2011), integrated with other works (RAE, 2004 and others). Comparing results in power generation costs from different technologies is far from simple. The LCOE approach is a standard recognized tool in literature, despite several limitations. In this work, that methodology is used in conjunction with the Monte Carlo technique, in order to take into account the uncertainty and the variability of most significant cost components and, in presence of forecast data, to elaborate possible cost scenarios.

1. Introduction

The aim of this work is to evaluate under what conditions the electricity generation from offshore wind plants could become economically competitive with a representative set of other technologies. The method chosen for comparison is the *Levelised Cost Of Energy* (LCOE); moreover, simulation theory was used to measure the likelihood of the competitiveness conditions above mentioned.

Technologies from renewable energy sources are becoming increasingly important and more widespread (RES) in power generation. In recent years, wind generation has become more relevant, especially from wind offshore plants, due to its higher generation capacity and lower environmental impact, compared to other traditional technologies. Over the past 10 years offshore wind power cumulative capacity in EU has grown more than 1GW per year [28]. However, the basic problem of RES technologies arises from the market distortions brought about by the presence of strong incentives granted to them, as a result of mitigation policies. [9] In order to make sensible decisions about energy policy, policy makers need to be able to compare the costs and benefits of different types of power generation plants in the most efficient and accurate way. Quoting one of the most relevant studies that reference the following analysis, despite the complexity of defining and calculating generation costs, is crucial to “*compare like with like*” to increase meaning and usefulness of this kind of work. [7] In determining generation costs, results are subject to high unpredictability: this is especially true for those, like offshore wind, that fall in the field of less proven, FOAK (First Of A Kind)¹ type of technologies. [8]

The constant-money levelised lifetime cost method was adopted to estimate the generation cost in this work. The Levelised Cost Of Energy (LCOE) approach represents a standard in measuring economic performance for energy plants and it allows comparisons across different technologies in a meaningful way [1].

¹ It is used in engineering economics where the first item or generation of items using a new technology or design can cost significantly more than later items or generations.

LCOE is the average price that would have to be paid by consumers to repay exactly the investor/operator for the capital, operation and maintenance and fuel expenses, with a rate of return equal to the discount rate [17].

It's generally not simple to obtain the necessary data to calculate the LCOE, especially using a detailed cost model that accounts for uncertainty; the LCOE equation can be specified in lesser or greater detail on the basis of available data and on the trade-off between accuracy and complexity. Furthermore, there are cost components potentially not captured by this type of approach (e.g. externalities) [3,10,13]: LCOE is only one of the indicators available to evaluate investment options, a sort of "first order assessment of project viability" [5]. Simulation methods (here, the basic Monte Carlo approach), allow to estimate measures for generating costs that account for variability connected to their main components.

This report is structured in five sections, besides the introduction: Section 2 outlines the technologies considered and presents the key assumptions on plant costs and their performance; Section 3 discusses our definition of levelised costs, with a focus on the financial part of the model; the Section 4 shows the simulation techniques adopted and Section 5 presents the key results of the study, including some sensitivity tests while the Section 6 summarizes the main conclusions.

A list of acronyms and abbreviations used in this work, is given in Appendix I.

2. Technical and economic data of technology

The power generation technologies chosen to compete with Wind Off-shore plants (W-Off), are: Wind On-shore (W-On), Gas fired Combined Cycle Gas Turbine (CCGT), Advanced Supercritical (ASC) coal plant with Flue Gas Desulphurization (FGD) and with post-combustion Carbon Capture and Storage (CCS), and nuclear European Power Reactor (EPR) 3. Such a set include two types of traditional technologies considered in an "innovative variant": nuclear EPR 3 and coal FGD with CCS, one "mature" technology (CCGT, without CCS to take account of a relative less "advanced" but economically competitive characteristics) and the Wind Onshore.

The choice made takes into account the level of innovation and the economic competitiveness, so as to harmonize the different main comparison factors among technologies to improve the significance of the results.

Assumptions on these technologies are based on reference studies [2,5,6,7,8] combined with other sources [24,25,29]. About specifications on the chosen technologies we assume the following:

- a Wind Onshore plant (100 MW) located 10 km from a MV substation;
- a Wind Offshore (200 MW) located 25 km from shore in 20 meters of water, using monopole foundations;
- gas CCGTs type: in a very wide range of GTs that can be employed in open cycle operation ranging we selected a configuration based on a twin block installation with a gross capacity of 830 MW, hence comparable with the coal and nuclear plants examined;
- ASC Coal FGD with CCS: assumptions chosen are in accordance with the EU directive implemented in April 2009 and selected size is 1600 MW;
- Nuclear EPR third generation: plant size is 1600 MW and technology is pressurised water reactors (PWR).

The cost and performance parameters selected take into account are:

- timing (development, construction, operational and decommissioning period),
- technical data (plant heat and power output, efficiency and forward profiles for availability, load factor and changes in efficiency due to degradation),
- capital costs (design and development, regulatory and licensing, construction, infrastructure and phasing of each technology across the appropriate time period)
- operational and maintenance costs (fixed and variable maintenance costs, use of system charges and insurance).

The model also contains input assumptions for the cost of CO₂ disposal, waste disposal, decommissioning, fuel price projections, exchange rates and CO₂ price projections, following the approach and the dataset used by DECC.

The availability of reliable and accurate data is crucial. This work encountered data availability limitations and it has been based, where possible, on data from reference plants or on main components of total costs time series from the literature or institutional data sources [2,5,6,14,17,18,24,28].

For offshore wind, special attention was paid by using a set of reference studies focused on key factors affecting the final cost and its main components (see Figure 1) [11,12,15,16,17,22, 24,27,29].

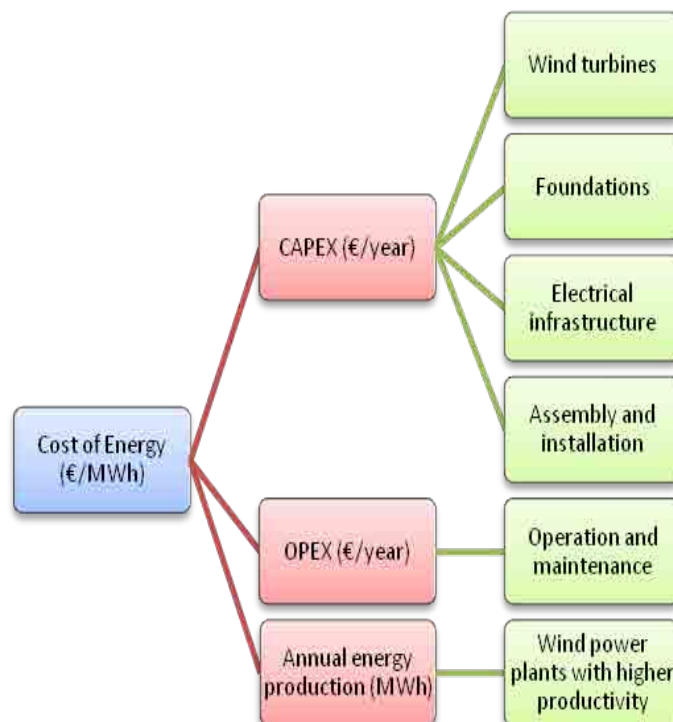


Figure 1: LCOE costs structure for Wind Offshore power plants, Rao, Gaeta 2012.

Operators of offshore wind farms have to solve several critical issues to ensure that the cost of energy will be reduced and that their investments are cost-effective: lower investment costs: today's cost of wind farms (about 3.1 M€/MW) are not sustainable in the long run; higher reliability, to maximize availability and minimize operation and maintenance costs (e.g. the utilization of advanced materials to design wind turbines that can withstand harsh marine environments); innovative Operation & Maintenance concepts, to contribute to significant reductions in O&M costs.

Europe is the world leader in offshore wind, which will be key to Europe's energy future. In 1991, Denmark built the world's first offshore wind farm, with eleven 450-kW turbines. Since then, offshore generation has grown considerably. In 2007, the European Union set itself the target of producing 20% of its final energy demand from renewable sources. Denmark has a primary role in the above scenario and a variant of some forecasts from Denmark wind industry have been used as a benchmark for some sensitivity analysis performed and discussed in chapter 5.

Research, development and demonstration in lowering construction and installation costs (CAPEX), comprised in the four areas "wind turbines", "foundations", "electrical infrastructure" and "assembly and installation", are estimated to contribute significantly and equally to reducing cost per installed MW. A reasonable target for players is to reduce CAPEX by approximately 40% of current costs [22], an indication taken into account in this study.

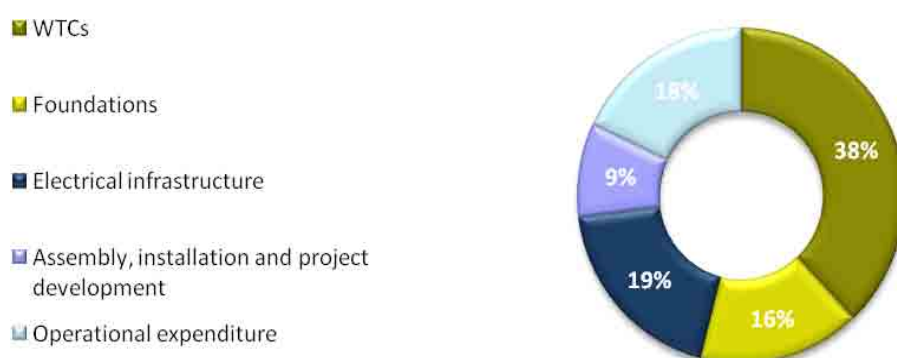


Figure 2: Main cost components for wind offshore power plant, Danish Wind Industry Association, 2010.

As said, the methodology to estimate the power generation cost is LCOE, calculated for the plant lifetime and given in currency units per megawatt-hour (€/MWh). So, each technology has a set of variables and parameters necessary to calculate the LCOE standard expression. All parameters and variables are given by appropriate expressions for each reference technology. For instance, fuel costs reflect (under functional form) the η value. Table 1 show a selection of such a parameter's set.

In order to compare mature and innovative technologies is useful to operate a distinction between two cases: the first of a kind (FOAK) and the nth of a kind (NOAK) plant. If a project activity is "first-of-its-kind", it is clear that implementation of the specific technology is not yet "common practice" [31]. The definition of the (NOAK) plant is somewhat arbitrary, although it is often taken as the fifth or higher plant. [30] CCGT technology is already at the NOAK level, as is onshore wind.

All assumptions about FOAK and NOAK values for all parameters were made following the main reference studies [7,8,17]. Variation between sites and general uncertainty (represented through the variation of values across the high, medium and low levels) was integrated in the simulation phase of work.

The treatment of FOAK and NOAK is very relevant when considering the capital cost and forward price adjustments of new technologies.

Table 1. Key parameters for technologies examined [2,8].

	m.u.	Wind Offshore	Wind Onshore	Gas - CCGT	ASC Coal with CCS	Nuclear EPR 3
Key Timings						
Construction period	years	1.5-3	2-2.2	2.5-3.2	4.8-6	5-7
Plant operation period	years	21	22	28	36	60
Technical data						
Gross power output	MW	200	100	830	1600	1600
Gross Efficiency	%	100	100	58	35	100
Average Degradation	%	0	0	3,5	2,5	0
Average Load Factor	%	39	28	78	78	90
Capital costs						
EPC cost	€/kW	3000-3850	1450-1900	700-780	2900-3400	3100-4000
Pre-licensing cost, Technical and Design	€/kW	50-72	55-110	31-44	66-130	55-110
Regulatory + licensing + public enquiry	€/kW	50-71.5	38.5-77	27.5-39	66-130	55-110
O&M costs						
O&M fixed fee	'000€/MW	125.4-141.9	34-41.3	22.2-31.6	92.4-134	85.8-106.7
O&M variable fee	€/MWh	0	0	2,4-2.5	14.8-15.8	2-2.75

For the fossil power plant the variability of the fuel price and the carbon price is very important to establish a realistic value of electricity production cost. The fuel prices have been based on DECC's [2] projections until 2030 and they are shown in Table 2.

Table 2. Average fuel prices in 2015-2030 [2, 7, 8,].

Scenario	Unit	Gas	Coal
Low	€/GJ	4.3	1.5
Mid	€/GJ	8.1	2.4
High	€/GJ	11.2	4.0

Three different scenarios of projected costs were considered, depending on varying global energy demand levels. The price of nuclear fuel includes the uranium enrichment and fabrication of fuel elements [20] (average 3-5 €/GJ). A high fossil fuels price may be justified even in the presence of strong policies for climate mitigation and therefore with higher carbon prices. The influence of greenhouse gas restrictions is realized through the emission price. In this work we have relied on the central hypothesis of DECC's study [7] where the CO₂ price starts from 14 €/t in 2010 and rises to 18 €/t by 2020 and to 77 €/t in 2030.

3. LCOE model and financial analysis

The adoption of a standardized methodology for cost calculations is a prerequisite for a fair comparison between different electricity generation options.

The levelised cost of electricity generation (LCOE), for IEA [17], is “*the ratio of total lifetime expenses versus total expected outputs, expressed in terms of present value equivalent. This cost is equivalent to the average price that would have to be paid by consumers to repay exactly the investor/operator for the capital, operation and maintenance and fuel expenses, with a rate of return equal to the discount rate*”. The LCOE is adopted to compare the different technologies because among other things it takes into account the various amounts of energy produced over the different technical lifetimes [29]. So *the levelized cost of energy (LCOE) allows to compare alternative technologies when there are different scales of operation, different investment and operating time periods, or both. For example, the LCOE could be used to compare the cost of energy generated by a renewable power plant with that of a conventional fossil fuel power plant.* [1]

The main components, factored into the calculation of LCOE, are: capital costs, fuel cost, O&M costs (variables and fixed), waste management and decommissioning costs, carbon costs and any cost for meeting emissions regulations, data like plant lifetime (economic), plant load factor (technical), discount rate and others (e.g. shape of the learning curve). There are many components not captured by levelised costs [5] like the externalities, the system factors (e.g. transmission costs) and every component that provides some kind of “business impacts” (e.g. revenue volatility). Indeed it is possible to incorporate some of these factors by adjusting one or more of the elements described above, so that they act as a proxy for the ‘missing’ elements.

In fact, not even only differentiating the risk of prediction which have some flows of costs (volatility price), the result is to underestimate the costs of generation technologies with relatively risky future cost streams (e.g. fossil fuel plants) and to overestimate the costs of technologies with lower risk future cost streams (e.g. wind turbines). Nevertheless, the simplicity of the calculation makes it attractive for use in comparisons between generating technology options, as shown by the large number of existing works that use LCOE, which makes this approach of calculating the costs an international standard. However you should be aware that, in estimating the components of LCOE, we use a wide range of specific assumptions, each of which is far from being unanimously accepted.

Therefore, for the present work, the LCOE is defined by the following formula as:

$$LCOE = TLCC / \left\{ \sum_{n=1}^N [Q_n / (1 + d)^n] \right\} \quad 1)$$

where:

LCOE	levelized cost of energy
TLCC	total life-cycle cost
Q_n	energy produced or saved in year n
d	discount rate
N	analysis period

The extended standard equation used in this work is:

$$LCOE = \frac{INV + \sum_{n=1}^N \frac{O\&M}{(1 + DR)^n} + \sum_{n=1}^N \frac{FC}{(1 + DR)^n} + \sum_{n=1}^N \frac{CO_2}{(1 + DR)^n} - \frac{RV}{(1 + DR)^N}}{\sum_{n=1}^N \frac{hours * \sum_{n=1}^n (P * LF)}{(1 + DR)^n}} \quad 2)$$

Where:

INV	Investment cost
N	Economic Lifetime
O&M	Total Operation and maintenance costs, fixed and variable (O&M)
DR	Real discount rate
FC	Annual fuel cost
CO ₂	Annual cost of carbon emissions
RV	Residual Value (possible)
P	Power (in MW)
LF	Load factor

The choice of real or nominal LCOE depends on the purpose of the analysis. For long-term studies the LCOE is better computed in real currency to take into account inflation. Hence, our choice was a constant-euro analysis to define with more accuracy the actual cost trends. [1,17] The choice of a common currency unit, euro, is convenient for presentation purposes but the bias introduced by converting currencies through exchange rates from the various data sources should not be overlooked. In this case, most of this work was done using reference studies. [1,8,18] Each component of the simplified model above had required an ad-hoc treatment for every technology: for example, the discount rate is expressed both using a fixed value and simulated through a model. The model used in this study is developed in an Excel spreadsheet and it allows the calculation and comparison of the levelised cost of electricity generation for each of the technology options, to make a number of sensitivity scenarios and to upload input data in a standard template form for each technology.

3.1 Financial part of the model

The discount rate (DR) is a crucial component of cost model.

The levelised cost methodology discounts the time series of expenditures to their present values in a specified base year by applying a discount rate value. The discount rate considered is appropriate for the power sector may differ from country to country, and, in the same country, from utility to utility. Applying a discount rate takes into account the time value of money, i.e. a sum earned or spent in the past or in the future does not have the same value as the same sum (in real terms) earned or spent today. The discount rate may be related to rates of return that could be earned on typical investments; it may be a rate required by public regulators incorporating allowance for financial risks and/or derived from national macroeconomic analysis; or it may be related to other concepts of the tradeoff between costs and benefits for present and future generations [17].

The capital intensive technologies are very sensitive to discount rates, and some technologies may be associated with higher discount rates because they are perceived to be riskier. DR should incorporate or reflect in some way the risk profile associated to the riskier technologies: this is especially difficult using LCOE approach [5]. Furthermore, due to a complex financial structure of commercial projects, it is often impossible to compare the capital costs of power plants in a meaningful manner [7].

In LCOE approach, the major problem is overestimating the risk profile of such type of technologies because the traditional methods take account of the same DR in comparison with the low capital intensive technology. Remembering IEA approach, differences in the cost of capital, between debt finance versus equity finance reflect the indirect assumption that equity is riskier than debt, so high risk technologies will require higher discount rates.

Another important issue reflects the need to take account of market structure. [5,17]. Each cost stream should be associated to an appropriate DR. Typical case of different kind of cost,

speaking of that, is represented by Operation and Maintenance (O&M) and fuel cost dynamic profiles (the second, more unpredictable than the first).

In this work, we have used a discount rate model obtained from the classical theory of the CAPM to consider a rather low randomness of the equation parameters (like β), in order to verify a compromise solution to one of the limitations in the estimation of LCOE: this approach doesn't take account of different rates of discount to be applied to the various components of cost (typically the distinction between operations and maintenance costs and fuel costs above mentioned). The simple DR model chosen is fit for this type level of analysis, like other works demonstrate [18].

In the present study, the levelised generation costs use a discount rate at 10% per annum, a value representative of those adopted in most works upon which are based the costs analyzed in this report (sensitivity analysis shown a DR variability among the range 2.5% and 12.5% per annum) [5,6,8,17]. Discounting is applied over the economic life of power plants, which are assumed to be somewhat longer than the typical financing terms. We have used both a fixed discount rate that a model based DR.

The discount rate for capital budgeting (WACC - weighted average cost of capital) is the rate that a company is expected to pay on average to all its security holders to finance its assets. WACC equation is as follow:

$$WACC = w_d * k_d(1 - t) + w_s * k_s \quad 3)$$

where:

- w_d weight of debt proportion to total capital
- w_s weight of equity proportion to total capital
- k_d cost of debt
- k_s cost of equity
- t corporate tax rate

In order to calculate the discount rate (WACC) for capital budgeting, we need to identify at least six different parameters. The fundamental assumptions and parameters are variables of depending reference economic systems, and they involve Cost of debt, Debt fraction, Risk free rate, Market Risk Premium, equity Beta (last three for cost of equity) and nominal WACC.

We assumed that projects will be financed by both debt and equity and they will return the expected interest payments to creditors and the expected dividends to shareholders. Therefore, the after-tax weighted average cost of capital is an appropriate discount rate for evaluating investment opportunities.

The cost of debt is relatively simple to calculate. In practice, the interest-rate paid by the company can be modeled as the risk-free rate (the rate of interest with no risk, typically based on public bond, e.g. the State treasury yield curve) plus a risk component (risk premium), which itself incorporates a probable rate of default (and amount of recovery given default). For companies with similar risk or credit ratings, the interest rate is largely exogenous (not linked to the company's activities).

Using Capital Asset Pricing Model (CAPM) it needs to compute a cost of equity (the return, often expressed as a rate, that firm theoretically pays to its equity investors, i.e., shareholders, to compensate for the risk they undertake by investing their capital). which is an implied investor's opportunity cost or the required rate of return of any risky investment.

The model for such a cost is:

$$k_{st} = k_{RFRt} + (EMRP * \beta_{equity}) \quad 4)$$

where

k_{st}	cost of equity at year t
k_{RFt}	risk-free rate at year t
EMRP	expected market risk premium (constant)
B_{equity}	equity beta (constant)

Assumptions on the DR model's variables reflect the author's evaluation on their behavior in EU region.

4. Dynamic analysis and simulation

Monte Carlo simulation is a numerical method used to find the solutions to mathematical problems, which have many variables not easily solved, simulating different probability distributions of main parameters. In fact, it performs uncertainty analysis through the substitution of a probability distribution for any factor that has a huge uncertainty [32].

The efficiency of this method increases compared to other methods when the size of the problem grows. In the LCOE calculation, the unpredictability of main parameters and the life times of power plants necessitate the use of Monte Carlo method.

Taking into account the complexity and the vastness of the calculation here required, can quite easily see how appropriate the words of Mark Kac, "*you use Monte Carlo until you understand the problem*": and such a horizon, that still seems pretty far.

The method chosen is basic Monte Carlo: very often other numerical methods of resolution are the most recommended and effective, this work has been made a deliberate choice of compromise in which the basic Monte Carlo was considered competitive due to various considerations: the difficulty of establishing boundary that delimits the domain of integration; the variables to be integrated on average not exhibit peaks concentrated in very restricted regions and, finally, it was found a trade-off between accuracy and simplicity acceptable.

For purposes of this work, it was chosen to maintain the random variable Uniform as a model of the probability distribution for each variable simulated.

This choice was based, partly on lack of reliable time series for the variables, which does not allows for a homogeneous methodological approach in the simulation. Another motivation resides in the fact that the standard methodology LCOE was partially interpreted with some assumptions, such as that relating to the choice of modeling the discount rate according to the theory of the CAPM instead of using a fixed value. This means that, in the application of simulation methods LCOE approach, the use of a single model of the probability distribution can also be considered as a compromise between uniformity of the calculation assumptions between different technologies and different components of the cost model and the desire to characterize the same to more closely match the true. The variables and parameters of respective LCOE calculated reflect an average of the present available values of chosen technologies.

In each calculation, one value is selected randomly according to preset probability distribution for each variable and LCOE is calculated. Calculation is repeated 10000 times, results are rounded to the nearest full euro. The number of times LCOE calculations resulted in certain value is presented as LCOE frequency and is displayed in charts.

5. Results

In this chapter some results are presented in various graphics. They show LCOE comparison among the five technologies described in chap. 2.

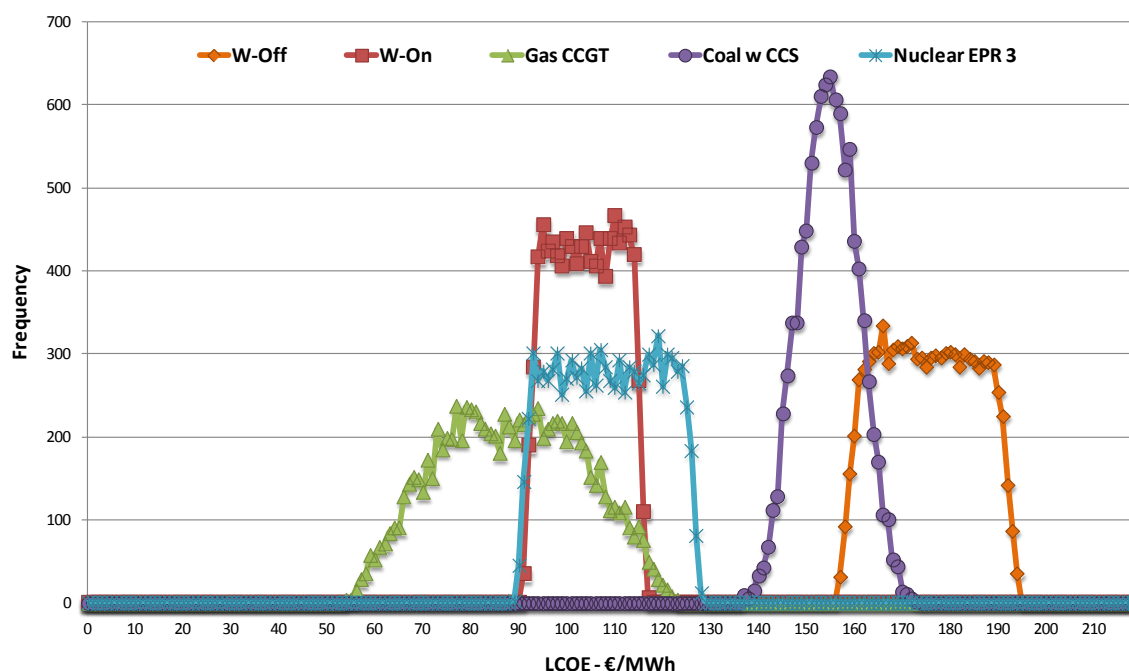


Figure 3: Probability distribution for LCOE (discounted rate: 10%), Rao, Gaeta 2012.

As Figure 3 shows, the average cost of a megawatt hour generated by Wind-offshore plant is centered around a cost of just over 175 €/MWh, a value significantly higher than that of competing technologies, according to the current technological and cost parameters. In fact Gas fired CCGT is the existing technology able to achieve the lowest cost of generation (89 €/MWh) under the assumptions made (e.g. in particular about the dynamics of gas prices adopted).

The calculations relating to the CCGT plants show more competitiveness, in terms of production costs, compared to values for the other power plants. Offshore wind energy is therefore not highly competitive with conventional systems such as CCGT, but this technology isn't the first target to achieve for future technological and economical advances of the offshore. The main target to reach could be (remaining in a comparable size of the required investments) the LCOE of CCS coal plant and, maybe, the nuclear EPR 3. The investment costs and important boundary conditions (such as changes in financing conditions but especially in the costs of greenhouse gas emissions) can impact deeply to get the future target.

The average LCOE, total and main components, is shown in Figure 4.

Analyzing the weight of the different cost components of the technologies examined we can affirm that the competitive games for the offshore wind plants, in the baseline scenario, are based mainly on the investment costs. The complete independence of wind technologies from the carbon cost and fuel cost also clarifies that, in a scenario of capital costs abatement, even technologies as CCGT, now unattainable, could become a realistic target.

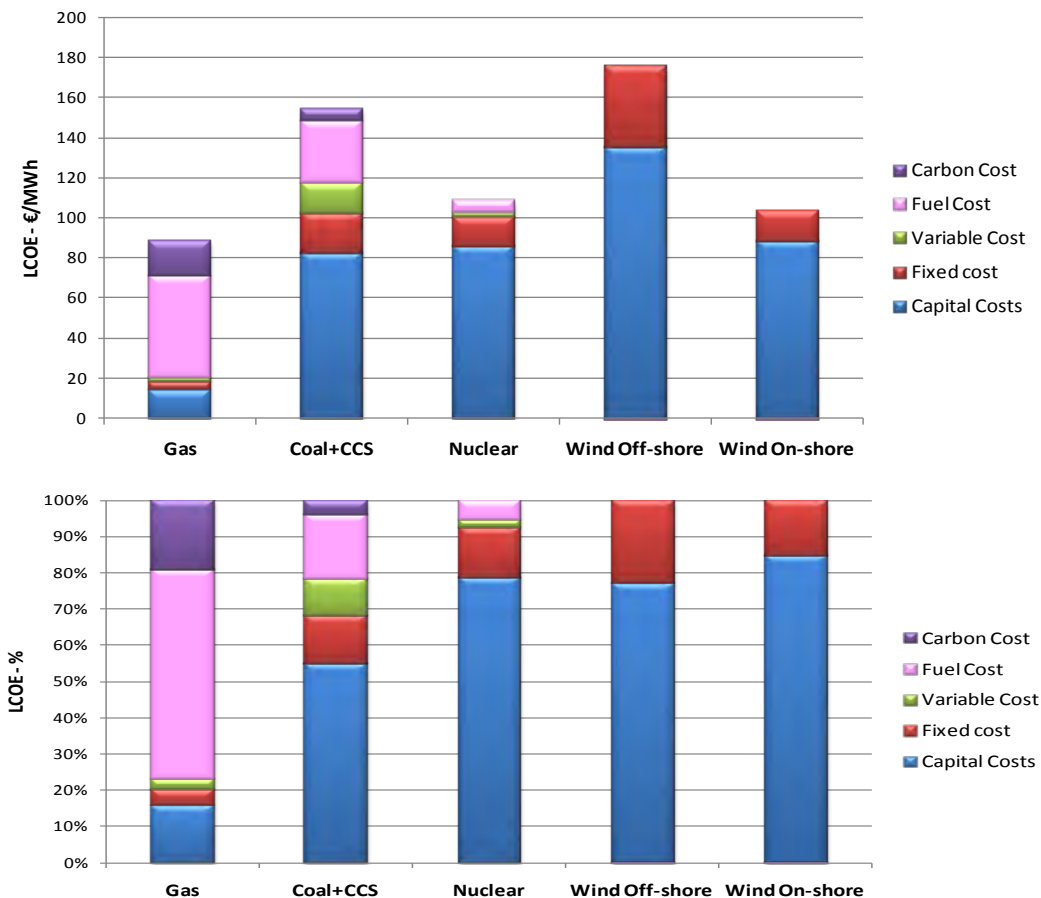


Figure 4: Average LCOE (total and main components) for power plants examined, Rao, Gaeta 2012.

In fact the capital cost component is dominating in the nuclear and in the wind generation costs (~80%). The capital cost of wind offshore power plants is 60% higher than nuclear plants. As a consequence of the emission trading the electricity generation costs will grow of 18 €/MWh for CCGT and 6 €/MWh for plants coal based. The minor increase in the coal plants is due to the presence of a carbon capture and storage.

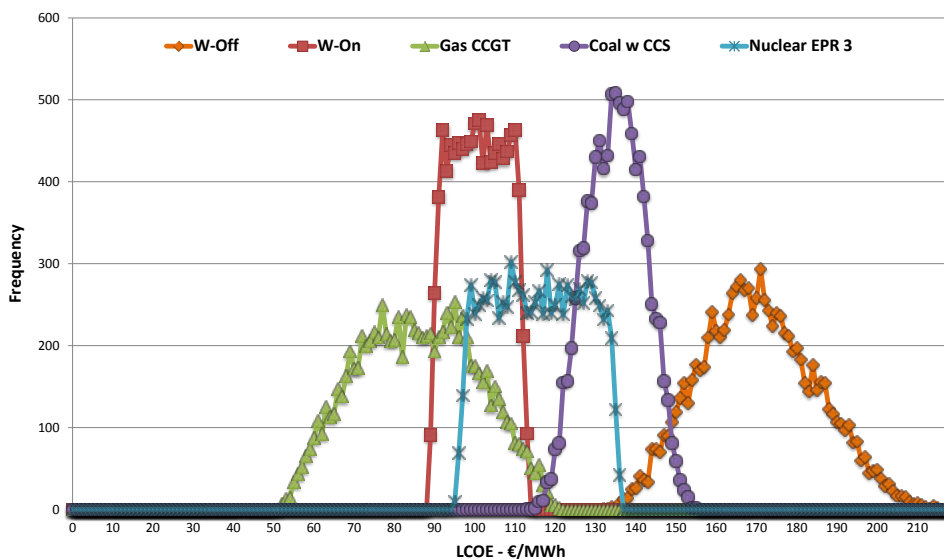


Figure 5: Probability distribution for LCOE (using the discounted rate model), Rao, Gaeta 2012.

Compared with the case of fixed discount rate, using the model described in section 3, the costs curves of nuclear, onshore and offshore are moved forward by 10 €/MWh circa, as a result of strong dependence from investment and fixed costs: it is notable that offshore distribution becomes very similar to normal distribution, with a remarkable change of skewness and range of variation (155-195 to 135-205€/MWh). The impact of changes in the input data has been studied in a sensitivity analysis by setting one value of the parameter at a time, while the others parameters remains the subjects of a Monte Carlo simulation. The main results of analysis performed are shown in the following section. This section will focus on the effect of varying the investment cost, the discount rate, the fuel costs and the CO₂ price [20]. In order to estimate conditions to make competitive the Wind Offshore power plant with conventional plants analyzed, it will be presented an analysis focused on best perspective of abatement investment and fixed cost (key factor to get Wind Offshore competitive), based on future improvement expected for this type of technology (Figure 6).

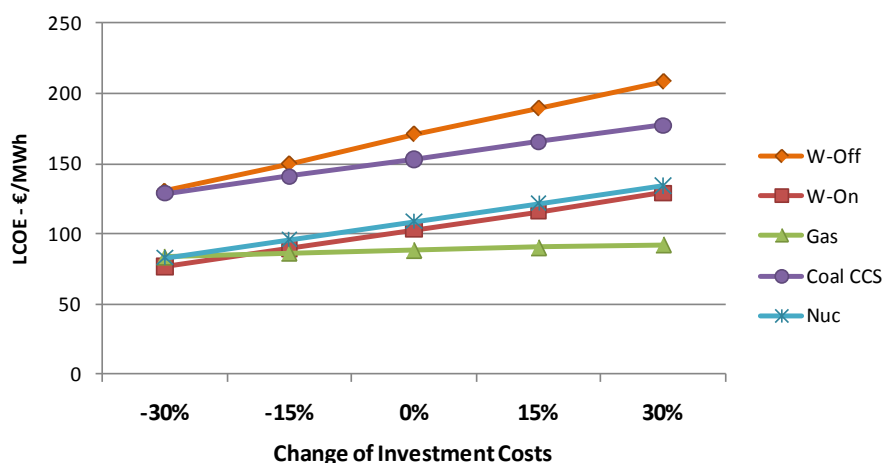


Figure 6: Effects of the change of the investment cost, Rao, Gaeta 2012.

When the capital cost of wind offshore plants is reduced by 30%, compared to average value considered, the electricity generation cost would decrease to 40 €/MWh. In the Figure 6 it is possible to see that even just a reduction of 15% of the investment cost allows wind offshore plants to become competitive with Coal CCS plant.

The impact of discount rate on electricity generation is illustrated in Figure 7. The nominal discount rate varies in the range of 2.5% to 12.5% [26].

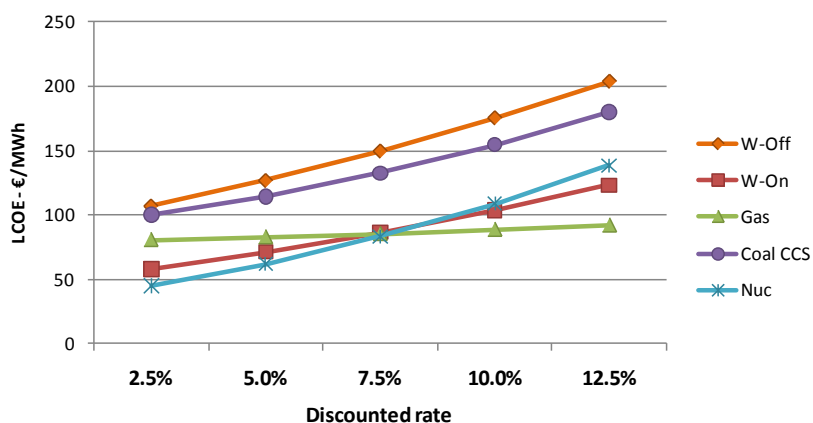


Figure 7: Sensitivity of levelised costs to discount rate variation, Rao, Gaeta 2012.

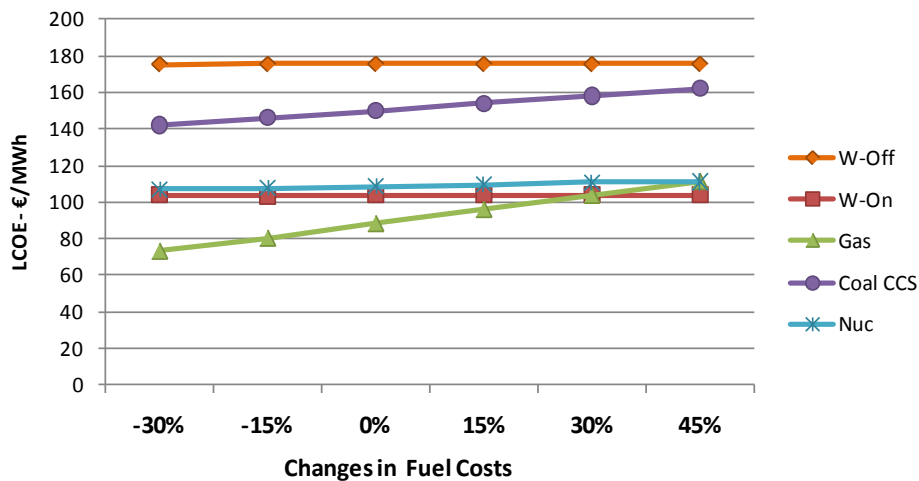


Figure 8: Sensitivity of levelised costs to fuel price variation, Rao, Gaeta 2012.

The impact of the growth of the discount rate is greatest for the capital intensive plant as wind, nuclear and CCS (nuclear and offshore have the highest slope).

As for the sensitivity to fuel price changes, the technologies that are naturally more vulnerable, are the CCGT and the CCS, and, with a much lesser degree of dependence, the nuclear plant.

From Figure 8 we can see that if the fuel price increases of 30%, the nuclear generation cost increases of 2%, the coal CCS cost of 5% while the gas based plant of 18%.

Moving to the costs of emissions, the situation change, becoming also nuclear power essentially neutral to changes simulated (Figure 9).

In fact the emission trading improves the competitiveness of carbon free power production compared to the fossil fuel power plants [20].

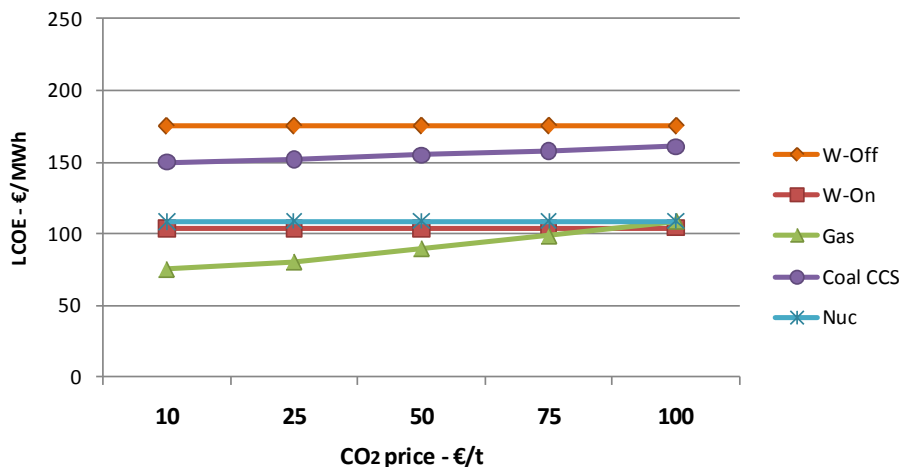


Figure 9: Sensitivity of levelised costs to fuel price variation, Rao, Gaeta 2012.

6. Main Conclusions

Using LCOE approach to determine the generation cost and performing Monte Carlo simulations, it follows that wind Offshore technologies are currently still not really competitive. In fact, the electricity generation cost of the Wind Offshore Plant could seem relatively high: 175 €/MWh, mainly due to high capital cost. At the present state the fossil plants appear to be an appealing investment, experiencing low levelized cost. In the sensitivity analysis we can see that with a reduction of capital cost it is possible to make competitive wind technology with the conventional plants. In addition the wind plants are not vulnerable in front of fluctuations and volatility of the fuel price on the market and of carbon price. The impact of this kind of variables is great and it affects the final LCOE of conventional and nuclear plants and the cost components associated with fuel and carbon emissions [29].

Therefore the Wind Offshore will be preferable in the near future if will be an investment that would not suffers from high and unpredictable cost in the era of mitigation of climate change.

References

1. W. Short, D. J. Packey and T. Holt- A Manual for the Economic Evaluation of Energy Efficiency and Renewable Energy Technologies, National Renewable Energy Laboratory, NREL/TP-462-5173, pp. 47-50, march 1995
2. JC. Palacios, G. Alonso R. Ramirez A Gomez, J Ortiz, L. Longoria levelized costs for nuclear, gas and coal for electricity, under the Mexicano scenario, Instituto nacional de investigaciones nucleare
3. R. D. Rowe, C. M. Lang, L. G. Chestnut - Critical factors in computing externalities for electricity resources, Resource and Energy Economics 18 (1996), USA
4. A contribution to technology forecasting from a technology dynamics perspective, Universiteit Twente, 6 november 1998
5. Phil Heptonstall - A REVIEW OF ELECTRICITY UNIT COST ESTIMATES, UK Energy Research Centre (2006 upd. 2007) UKERC/WP/TPA/2007/2006
6. The Cost of Generating Electricity - A study carried out by PB Power for The Royal Academy of Engineering, 29 Great Peter Street, Westminster, London, SW1P 3LW, March 2004
7. Electricity Generation Cost Model - 2011 Update Revision 1 Department of Energy and Climate Change, August 2011
8. Mott Macdonald. UK Electricity Generation Costs Update. June 2010
9. K. Gillingham, J. Sweeney - Market Failure and the Structure of Externalities - Stanford University, Precourt Energy Efficiency Center, Department of Management Science and Engineering, Stanford, CA 94305, USA
10. F. Roth, L. L. Ambs - Incorporating externalities into a full cost approach to electric power generation life-cycle costing Energy 29 (2004), University of Massachusetts Amherst, USA
11. Twidell, J. et al (2006) - Renewable Energy
Resources <http://books.google.de/books?id=pVmZPI3cfuEC&printsec=frontcover>
12. M. A. Lackner, C.N. Elkinton - An Analytical Framework for Offshore Wind Farm Layout Optimization, Wind Engineering, Vol. 31, n. 1, Jan 2007 UK
13. Peter Rafaj, Socrates Kypreos - Internalisation of external cost in the power generation sector: Analysis with Global Multi-regional MARKAL model, Energy Policy 35 (2007) 828–843,
14. A Brief Characterization of Gas Turbines in Combined Heat and Power Applications – EPA 2002
15. Hisham Khatib - Review of OECD study into “Projected costs of generating electricity 2010 Edition Global Energy Award Laureate, Elsevier

16. IEA - Electricity information, 2009 edition, International Energy Agency 9, rue de la Fédération, 75739 Paris Cedex , France
17. IEA International Energy Agency - Projected cost of generating electricity, 2005 update
18. EIA - The Electricity Market Module of the National Energy Modeling System Model, NEMS Documentation Report, U.S. Department of Energy Washington, DC 20585
19. Nikola Čavlina, Comparison of different options for base load production, University of Zagreb, Croatia
20. Tarjanne Risto, Kivisto Aija – Comparison of electricity generation cost, Lappeenranta Universty Technology, 2008
21. Denmark - supplier of competitive offshore wind solutions - Megavind's Strategy for Offshore Wind Research, Development and Demonstration – MegaVind – Danish Wind Industry Association, 2010
22. Danish Energy Agency, Technology data for energy plants, June 2010.
<http://www.ens.dk/da-DK/Info/TalOgKort/Fremskrivninger/Fremskrivninger/Documents/Teknologikatalog%20Juni%202010.pdf>
23. Department of Energy (DOE), 2009 Wind Technologies Market Report. Washington 2010.
http://www1.eere.energy.gov/windandhydro/pdfs/2009_wind_technologies_market_report.pdf
24. EWEA, The European offshore wind industry – key trends and statistics 2009. January 2010.
25. EWEA, The European offshore wind industry, key trends and statistics 2010, EWEA, January 2011
<http://www.ewea.org/fileadmin/emag/statistics/2009offshore/pdf/offshore%20stats%2020092.pdf>
26. Danish Energy Agency, Technology data for energy plants, June 2010. <http://www.ens.dk/da-DK/Info/TalOgKort/Fremskrivninger/Fremskrivninger/Documents/Teknologikatalog%20Juni%202010.pdf>
27. EWEA (2009) Operational Offshore Farms 2009
28. W. Musial, B. Ram, Large-Scale Offshore Wind Power in the United States, National Renewable Energy Laboratory (NREL)
29. A. Arapogianni, G. Rodrigues, N. Fichaux, A. Zervos, G. Caralis, Model for comparing and projecting the levelised cost of electricity generated by New Gas, Coal, Nuclear Power Stations and Wind Energy (On and Offshore)
30. M. Matuszewski, M. Woods Quality guidelines for energy systems studies - Technology Learning Curve (FOAK to NOAK) NETL/DOE-341/042211, Mar 2012
31. UNFCC, CDM – Meth Panel- Thirty-fourth meeting – Report Annex 10
32. S.B. Darling, F.You, T.Veselka, A. Velosa, Assumptions and the Levelized cost of energy for photovoltaics. Energy & Environmental Science, January 2011

Acronyms

Capex	Capital expenditure
CCGT	combined-cycle gas turbine
CCS	Carbon Capture and Storage
CHP	combined heat and power
CO ₂	carbon dioxide
DECC	Department of Energy and Climate Change
EIA	Energy Information Administration
EPC	engineer, procure and construct
EPR	European Pressurised water Reactor
ETS	Emissions Trading Scheme
EU	European Union
FGD	Flue Gas Desulphurisation
FGD	flue gas desulphurisation
FOAK	First Of A Kind
GJ	gigajoules
GT	Gas Turbine
GT	gas turbine
IEA	International Energy Agency
IGCC	integrated gasification combined cycle
KW	kilowatt (power)
KWh	kilowatt hour (energy)
MW	megawatt
MWe	megawatt electric
MWth	megawatt thermal
MWth	megawatt thermal
NOAK	Nth Of A Kind (as opposed to first)
NPV	net present value
O&M	Operation and Maintenance
O&M	operation and maintenance
OCGT	Open Cycle Gas Turbine
OCGT	open-cycle gas turbine
OECD	Organisation for Economic Co-operation and Development
Opex	Operating expenditure
PC	Pulverised Coal

TRITON - Wave Energy Converter

R. Piccinini, M. Boffini

K.I. Energy, Busan (KR)

K.I. Energy's TRITON is Wave Energy Converter system, which absorbs and transforms energy from the waves into "grid ready" electrical energy.

The system is divided in three functional groups:

- Absorber group: includes surface buoy (floats), Chain and Ballast. The main function is to transmit the gravitational energy of the wave, to the Generator group.
- Generator group: includes patented unidirectional gear train, electric generators, control and safety units, submarine cable junction box, all included in a watertight structure.
- Foundation group: also called "Mooring group" includes mooring wires and concrete structure (tetrapod).

The working principle is rather simple. The gravitational energy of the waves is transferred to the generator unit. A patented mechanism directly converts bidirectional linear motion of the link chain in unidirectional rotational motion.

The correct sizing of the absorber group and the real-time feedback from the control unit, allow the surface float to follow the wave crest thus optimizing energy harvesting.

The main benefits of TRITON unique design are:

- Direct energy conversion, no power is lost on hydraulics or pneumatics systems
- Active control of the surface buoy, to maximize energy harvesting
- Technology and solutions already available for marine and offshore industry.
- TRITON is tailored to match installation site specifications, thus maximize efficiency.
- TRITON is a modular design, so large farms can be created connecting several units together.



Mapping Mediterranean sea wind resource: state-of-the-art technologies for short term measurements and long term reference data

M. Gianni¹ and L. Imperato²

¹Studio Rinnovabili Srl, Via G.L. Lagrange 1, 00197 Rome, Italy,
m.gianni@studiorinnovabili.it

²Studio Rinnovabili Srl, Via G.L. Lagrange 1, 00197 Rome, Italy,
l.imperato@studiorinnovabili.it

Abstract – Legal and technological concerns won't succeed in avoiding offshore wind farms to develop in the Mediterranean sea, mainly in deep waters. Environmental concerns will push projects far offshore, thus wind mapping of open sea can't rely on traditional on-shore met stations. Two kinds of data are needed: in situ measurements, typically short term, and long term references. Only the correlation of these inputs will provide a low-uncertainty assessment of the wind resource at a specific site. This paper reviews the state-of-the-art technologies for short-term measurements and the available long term data sources, discussing the related issues in terms of reliability, consistency and costs.

1. Introduction

The high sensitivity of wind turbines to wind speed is a known issue, therefore an accurate evaluation of the wind resource is a constraint for a successful financing of a large offshore farm. In a large part of the Mediterranean Sea, environmental concerns will push projects far offshore, thus wind mapping of open sea can't rely on traditional on-shore met stations. Two kinds of data are needed: in situ measurements, typically short term, and long term references. Only the correlation of these inputs will provide a low-uncertainty assessment of the wind resource at a specific site. This paper reviews the state-of-the-art technologies for short-term measurements and the available long term data sources, discussing the related issues in terms of reliability, consistency and costs.

2. In situ measurements in marine environment

For offshore projects, in situ measurements of the wind resource may be carried out with traditional anemometry, typically cup sensors on masts, or modern solutions, i.e. remote sensing systems.

2.1 Offshore mast

The typical approach for offshore wind measurements is that of setting up a lattice mast equipped with high quality traditional cup anemometers and vanes. The mast may be a stand-alone tower, typically with monopile foundation, or can be mounted on an existing offshore platform.

The advantage of this approach is straightforward: this solution will provide a robust and bankable database, provided that the mounting requirements of the IEC 61400-12-1 are fulfilled, first of all a top measuring altitude at least 2/3 of the hub height.

However, such solution also presents significant concerns: offshore towers are un-guyed, and need therefore to be much wider than onshore. This aspect, combined with all the technical effort required for offshore foundations, result in a very high cost, about 100 times higher than onshore [1]. The cost is in the order of 1-5 m EUR, also depending on the water depth. Although in the marine environment one single station may be sufficient for a very large wind farm, and the percentage cost of the mast with respect to the wind farm cost is far below 1%, such expense may be anyway a big limit, given the high development risk.

2.2 Remote sensing

An alternative solution for offshore monitoring of the wind resource is represented by remote sensing, that is Lidar and Sodar devices.

The main advantage is the flexibility of this approach, because the small dimensions of such devices (see Figure 1) make it easy to install them on any existing structure like platforms and rigs. Lidar systems are the most compact, they are insensitive to any background noise (e.g. waves), and they can be installed right beside any existing physical obstacle (like a tower or an existing structure). Therefore they are being extensively used for offshore wind mapping in the North Sea [2]. Sodar systems, especially the new generation with 3-antenna configuration, although more sensitive to environmental conditions like obstacles and background noise, have been also successfully tested in offshore campaigns [3] and offer advantages in terms of costs and power consumption.

In general, the use of remote sensing devices benefits from installation and operations costs which are only a fraction of those related to the mast solution.

With regard to the accuracy of remote sensing, it is significantly increased over the last decade, and is now comparable with traditional anemometry [4, 5]. Measurements are typically available at hub height and over the whole area swept by the rotor. The general feeling in the scientific community is that data from Lidar and Sodar devices are now getting ready to be bankable, provided that the measurement protocol follows the international guidelines [6], especially regarding the accuracy verification before and after the campaign.

Finally, it should be highlighted that floating solutions are also becoming available for remote sensing, and a floating Lidar (FLIDAR) has been successfully tested in the North Sea [7]. This approach could be particularly interesting in the Mediterranean Sea, as it would be suitable for stand alone measurement systems in deep waters.

In Figure 1, the aforementioned solutions for in situ offshore measurements are summarized.

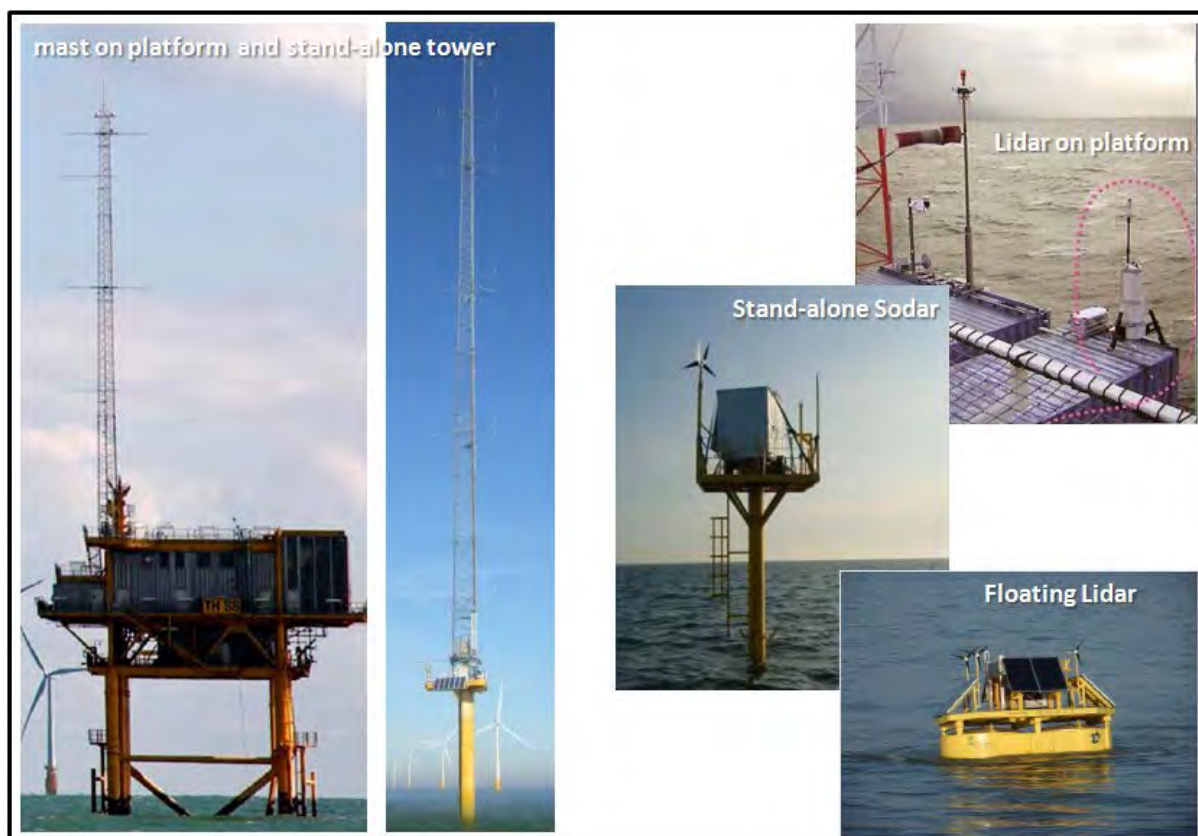


Figure 1: Summary of possible solutions for in situ offshore measurements. Traditional approach (left side) and remote sensing (right side).

3. Long term wind references

In situ offshore measurements will be typically available for short periods, because of technical and economic constraints. Therefore, given the well known annual variability of the wind speed and the related uncertainty, a sensible approach requires correlation with long term reference data, in order to calculate representative statistics of the wind resource on site.

In the following the typical sources of long term data will be reviewed, evidencing the related advantages and disadvantages.

3.1 Onshore stations

The spatial variability of the wind resource offshore is reduced with respect to onshore sites, where orography can play a significant role. As a result, onshore stations installed on the coast, even if located several km away from the site, may be potentially useful for correlation.

The network of onshore met station is usually the largest available, because there can be both publically funded and private met stations, with long time series of data. These stations can be operated by universities, research institutions, Military, national ministries, or private developers. With regard to the Italian case, one may cite the “Aeronautica Militare”, the “ISPRA”, and “CNR-ISMAR” as the main public institutions providing wind data from onshore stations located along the Italian coasts. The most important advantage of these data is the good spatial and temporal availability at a relative low price.

On the other side, the consistency of data is the major concern, as the operational history of these stations is often variable and difficult to track; there can be height changes, re-positioning, variable obstacles affecting the wind flow etc which are not fully detailed, thus compromising data consistency and the possibility to use them for long term correlation.

3.2 Offshore stations

Offshore fixed stations would perhaps be the most reliable sources of data for correlation, especially in terms of accuracy. However the network of such stations is relatively small, as only few public stations are installed; An example is given in Figure 2 (second from left), showing a meteo station of the CNR-ISMAR research institute. Private offshore stations are even more difficult to get, also because of the few offshore projects currently developed in the Mediterranean Sea. Another option would be meteo stations installed on oil and gas platforms, though availability is still a concern.

Again, consistency of data should be evaluated, due to possible movements or changes in the configurations of the platform, and their difficult traceability. Also, in the case of met stations for offshore projects, data may become inconsistent when the wind farms are built.

3.3 Moored buoys

Another possible source of long term data is that of moored buoys. These are mainly deployed by institutional bodies like national research institutes, or by meteo agencies. Data are generally rather convenient, available for long time intervals, and no obstacles are normally present. However they may have some disadvantages: the low measurement altitude and the buoy oscillations result into poor data accuracy, and direction data may be also unreliable.

3.4 Ships, Radiosonde stations and satellite measurements

Other possible sources of offshore wind data include meteo stations installed on ships, Radiosonde stations and satellite measurements. Radiosonde stations refer to rubber or latex balloons periodically launched, and carrying meteorological sensors. Satellite measurements consist of radar pulses or microwave pulses transmitted by satellites and reflected back from the sea surfaces, allowing estimation of wind speed.

The mentioned sources present the general disadvantage of poor accuracy and low sampling rate. Conversely, especially when referring to satellite measurements, they cover large areas, and they are generally consistent over time.

3.5 Reanalysis data

Reanalysis models are complex numerical representations of the equations of motion for the atmosphere. They are run assimilating a number of different sources of data, including satellites, aircraft and radiosonde. They have the advantage of a global coverage, long historical period, and are generally available for free. However, consistency is difficult to confirm, given the wide range of data sources, and resolution is rather low. Among the most commonly used, the reanalysis models from NCEP/NCAR, available from 1948 with 2.5 degs resolution, and the Merra model from NASA, available from 1979 with a finer resolution of $\approx 0.67 \times 0.5$ degs.

3.6 Mesoscale models

Mesoscale models are numerical weather predictions elaborating a wide range of meteorological inputs, typically from reanalysis. They normally use massive computer resources to accomplish downscaling of input data, also accounting for orography and roughness. They can be open sources or proprietary, and present a typical resolution of 1-3 km. As reanalysis models, they are available globally, but present higher resolution and are have user friendly formats. However, as reported in [8], consistency is a significant concern, and can be even lower than reanalysis models. Conversely, their reliability during the concurrent period with in situ measurements (usually the latest years) has proved fine performances in terms of absolute and relative wind speeds and direction. This imply that, although they can't be regarded yet as a certain reference for long term prediction, these models can be valuable tools in the initial phase of an offshore wind project, when evaluating the suitability of a site.

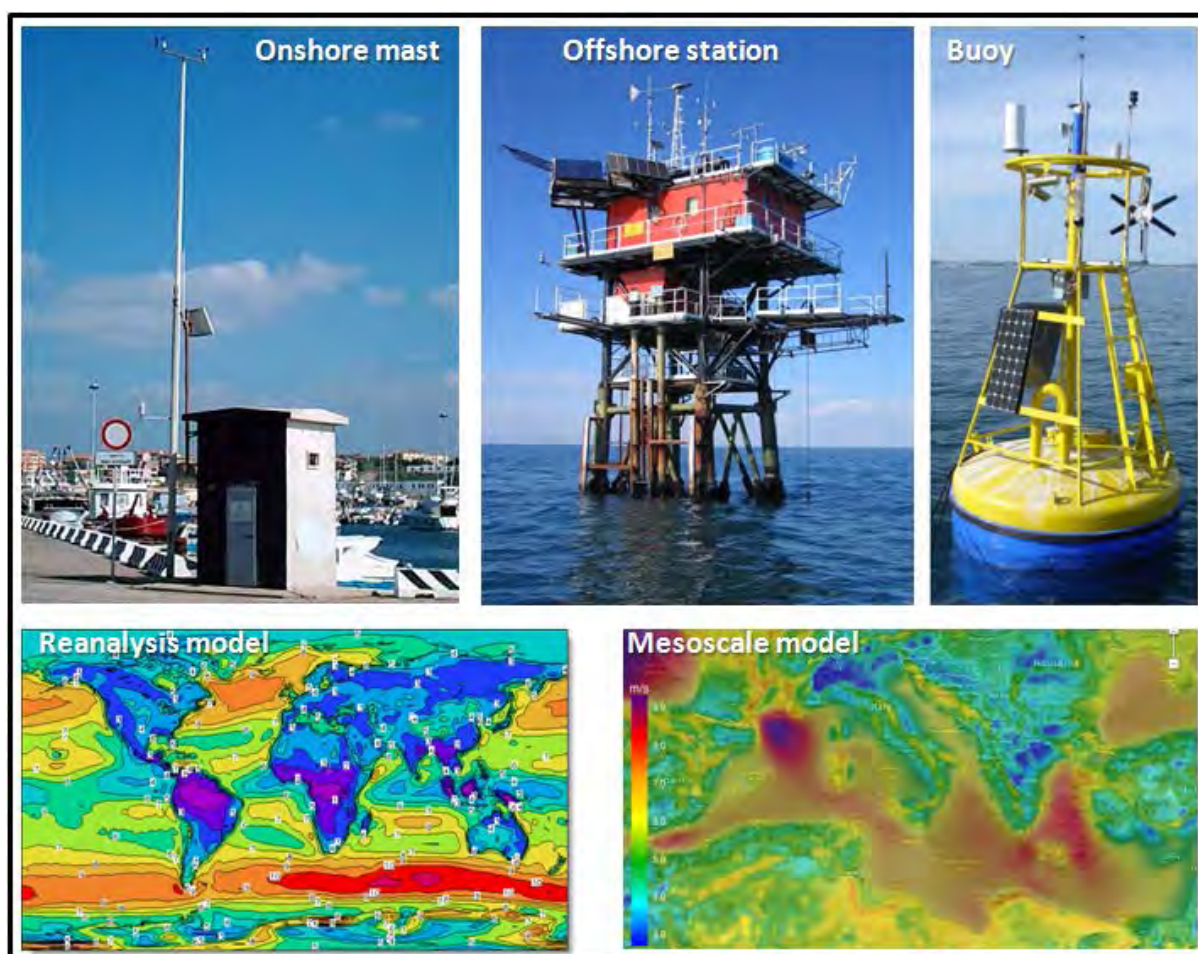


Figure 2: Summary of long term references, showing physical measurements (onshore stations, offshore stations, buoys) in the upper part, and numerical data (Reanalysis, Mesoscale) in the lower one.

4. Concluding remarks: a sensible approach for offshore wind assessment

Given the features of the aforementioned data sources, both in situ and long term, a sensible approach for offshore wind assessment could be arranged as follows; for an initial scan of the wind resource, mesoscale models (preferably 2-3) could be run to evaluate the average wind conditions on site, and therefore the feasibility of a wind project. Then, in situ measurements should be performed. In shallow waters, a fixed mast would be suggested, or a remote sensing device installed on a fixed platform or structure. In deep waters, a floating remote sensing solution could be implemented as an alternative to fixed systems. After few months of the measuring campaign (minimum 4-6 months), correlation could be attempted for long term wind prediction; it is suggested to collect as many data sources as possible, including onshore and offshore stations (if any) and to run both reanalysis models and mesoscale. In this way it will be possible to have a clear picture of possible inconsistencies of some input data, and increase the accuracy of long term prediction.

References

1. Garrad Hassan. Wind resource assessment offshore In *Wind Energy, The Facts*, EWEA, 2009.
2. D. Kindler et al. Testing and calibration of various Lidar remote sensing devices for a 2 years offshore measurement campaign. In *Proceedings of EWEC'09 Marseille*, 2009.
3. I. Antoniou et al. Offshore wind profile measurements from remote sensing. In *Proceedings of EWEC'06 Athens*, 2006
4. Clive et al. The Myres Hill remote sensing intercomparison study: preliminary results. In *Earth Environ. Sci.* 1, 2008
5. A. Oldroyd. Ground Based Remote Sensing. In *Proceedings of the Wind Resource Assessment Conference, London*, 2012
6. IEA. Recommended Practices for the Use of Sodar in Wind Energy Resource Assessment. 2012
7. JM. Thevenoud et al. Lidars for offshore applications. In *Proceedings of EWEC'12 Copenhagen*, 2012.
8. C. Murray. Offshore long term references. In *Proceedings of the Wind Resource Assessment Conference, London*, 2012

Wakes calculation in an offshore wind farm

G. Crasto

WindSim AS, Fjordgaten 15, N-3125 Tønsberg, Norway, giorgio.crasto@windsim.com

Abstract – This paper is focusing on the wake modeling in large offshore wind farms. Over the sea the ambient turbulence is much lower than onshore, wakes persist for long distances, mixing in a complex pattern. Hence an accurate evaluation of the wakes becomes crucial in the estimation both of the production and loads. Regarding loads the main effect of the turbines wakes is an increase of turbulence compared to the ambient one. A careful assessment of the wakes is therefore required when analyzing offshore wind farms.

The approaches in estimating the wake losses go from simple theoretical or empirical laws to full rotor aerodynamic calculations; in between there is a range of intermediate calculations.

Two approaches will be presented: the use of relative simple equations (also called analytical models) which are the standards in the wind resource assessment and a more accurate, but computationally more demanding, the actuator disc technique.

1. Introduction

Analytical models, thanks to their speed of execution, allow testing several layouts in relative short time. The speed of execution makes for example these models ideal for optimization tools.

The actuator disc in this case consists in the resolution of Reynolds Averaged Navier-Stokes equations, including a two equations turbulence model, where the turbine rotor is simplified with a disc exerting forces on the flow, in our model computed from the thrust coefficient curve of the turbine. A more advanced actuator disc modeling could be obtained by calculating the distributed forces over the swept area from the lift and drag laws of the airfoils use to design the blades of the turbines rotors.

2. Analytical wake models

Wake losses can be estimated also using analytical models to post-process the CFD solutions of the simulated wind without turbines. In this case the wind field CFD calculations are performed firstly disregarding the turbines and only in a following step the results are post processed for wakes. This methodology allows testing very quickly a large number of wind farm layouts, with different models of turbines. In WindSim there are implemented three analytical wake models:

- Jensen (Wake Model 1) [1]
- Larsen (Wake Model 2) [2]
- Ishihara (Wake Model 3) [3]

2.1 Jensen single wake model

$$\delta u(x) = U - V \tag{1}$$

$$\frac{\delta u(x)}{U} = \frac{1 - \sqrt{1 - C_T}}{\left(1 + \frac{2kx}{D}\right)^2} \tag{2}$$

Where:

C_T thrust coefficient
 k wake expansion factor
 D rotor diameter

The wake expansion factor k is computed by:

$$k = A \cdot \ln(h / z_0) \quad (3)$$

Where:

A constant, $A = 0.5$
 h hub height
 z_0 aerodynamic roughness length

2.2 Larsen single wake model

$$\frac{\delta u(x)}{U} = \frac{1}{9} \sqrt[3]{C_T A_r x^{-2}} \left(r^{3/2} (3C_1^2 C_T A_r x)^{-1/2} - \left(\frac{35}{2\pi} \right)^{3/10} (3C_1^2)^{-1/5} \right)^2 \quad (4)$$

Where:

C_T thrust coefficient
 A_r rotor swept area
 D rotor diameter
 C_1 model parameter

The model parameter C_1 is computed by:

$$C_1 = \left(\frac{D}{2} \right)^{\frac{5}{2}} \cdot (C_T A_r x_0)^{-\frac{5}{6}} \quad (5)$$

$$x_0 = \frac{9.5 D}{(2 R_{95} / D)^3} - 1 \quad (6)$$

$$R_{95} = 0.5 (Rnb + \min(h, Rnb)) \quad (7)$$

$$Rnb = \max(1.08D, 1.08D + 21.7D(Ia - 0.05)) \quad (8)$$

Where:

Ia ambient turbulent intensity at hub height

2.3 Ishihara single wake model

$$\frac{\delta u(x)}{U} = \frac{1}{32} \sqrt{C_T} \left(\frac{1.666}{k_1} \right)^2 \left(\frac{x}{D} \right)^{-p} \exp\left(-\frac{r^2}{b^2} \right) \quad (9)$$

Where:

$$b(x) = k1 \left(\frac{C_T^{1/4}}{0.833} \right) D^{1-\frac{p}{2}} x^{\frac{p}{2}} \quad (10)$$

$$p = k2(Ia + Iw) \quad (11)$$

$$Iw = k3 \cdot \left(\frac{C_T}{\max(Ia, 0.03)} \right) \left(1 - \exp \left(-4 \cdot \left(\frac{x}{10 \cdot D} \right)^2 \right) \right) \quad (12)$$

C_T	thrust coefficient
D	rotor diameter
Ia	ambient turbulence intensity at hub height
Iw	wake induced turbulence intensity
$k1$	constant, $k1 = 0.27$
$k2$	constant, $k2 = 6.00$
$k3$	constant, $k3 = 0.004$

2.4 Multiple wakes

When wakes are overlapping the wake deficit is obtained with a sum of squares of wake deficits as in the following equation:

$$\delta u(x) = \sqrt{\sum_i \delta u_i^2(x)} \quad (13)$$

Being δu_i the single wake wind speed deficit produced by the i -th turbine.

3. The actuator disc technique:

Numerical actuator disc consists in a number of computational cells covering the swept area of the rotor. The cells provide a resistive force to the flow which is computed directly from the thrust coefficient curve of the turbine. The result is the generation of a wake with a reduction of mean kinetic energy and a higher production of turbulence due to velocity gradients. A description of the methodology as implemented in the code WindSim is given in Crasto & Gravdahl [4].

In order to estimate the power production an integral method is instead used, this has been presented in Crasto *et al.* [5].

4. Comparison against production at Horns Rev

Horns Rev is an offshore wind farm located 13 km from the Danish coastline consisting of 80 wind turbines (Vestas V80), arranged in a skewed array of eight east-west rows of ten turbines. For this site a study with both actuator disc and analytical wake models has been carried out. The actuator disc technique has been tested only for a few cases: 6 and 10 m/s at hub height for a direction of $270^\circ \pm 1^\circ$, and 10 m/s for the directional sector $270^\circ \pm 5^\circ$. The behavior of the analytical wake models is much more illustrated by the good number of cases tested, especially for wake model by Katic *et al.* [1], also known as Jensen model, and the one from Larsen [2]. In Figure 1 it's plotted a sketch for the wind farm layout and the positioning of three reference masts named M2, M6 and M7.

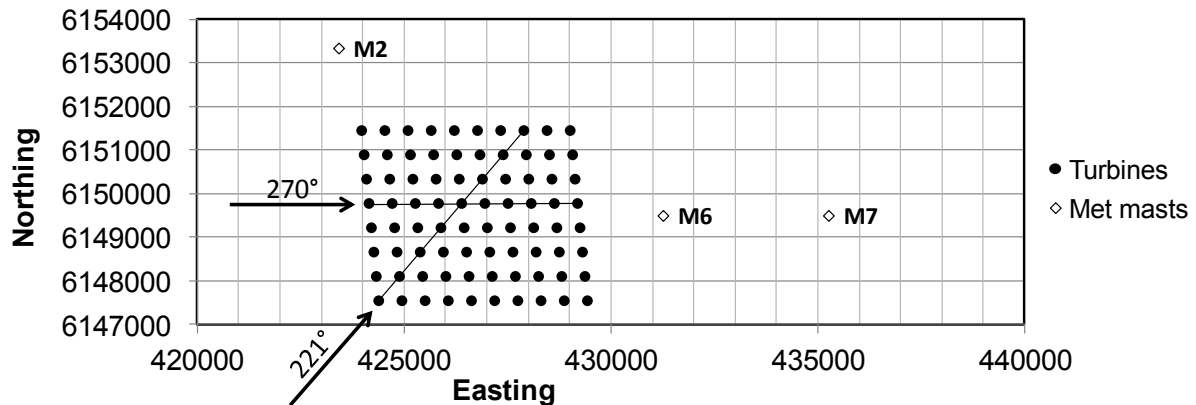


Figure 1: Horns Rev layout, 80 turbines and 3 met masts.

Some production data in Horns Rev has been disclosed for studying of the performance of the wind farm and better prediction for future similar projects. In Figure 2 the power production for a very narrow sector ($\pm 1^\circ$) is plotted. It can be noticed as the power output at first column (approx north-south) of turbines is over predicted, the power drop from column 1 and 2 it is also over predict by all models, leading to power outputs at second column lower than the one recorded at site. Probably from column 3 down to the 8th also the multiple wake models become important so the effects of the single wake models are significant for the prediction of the power drop between the first two columns.

For this study only the wind direction 270° is analyzed. For other two wind directions, 221° and 312° some production data are also available.

In Figure 3 the power production is presented for a wider sector $270^\circ \pm 5^\circ$ and increasing in the following Figures 4 and 5 which are respectively for sectors of $270^\circ \pm 10^\circ$ and $270^\circ \pm 15^\circ$. In Figure 6 it has been sketched the ratio of the power to the average power at first column for sector $270^\circ \pm 15^\circ$, the normalized plot allows to highlight a different trend compare to Figure 5, because there is a not negligible overestimation of power production for those wind turbines which are not under wake conditions.

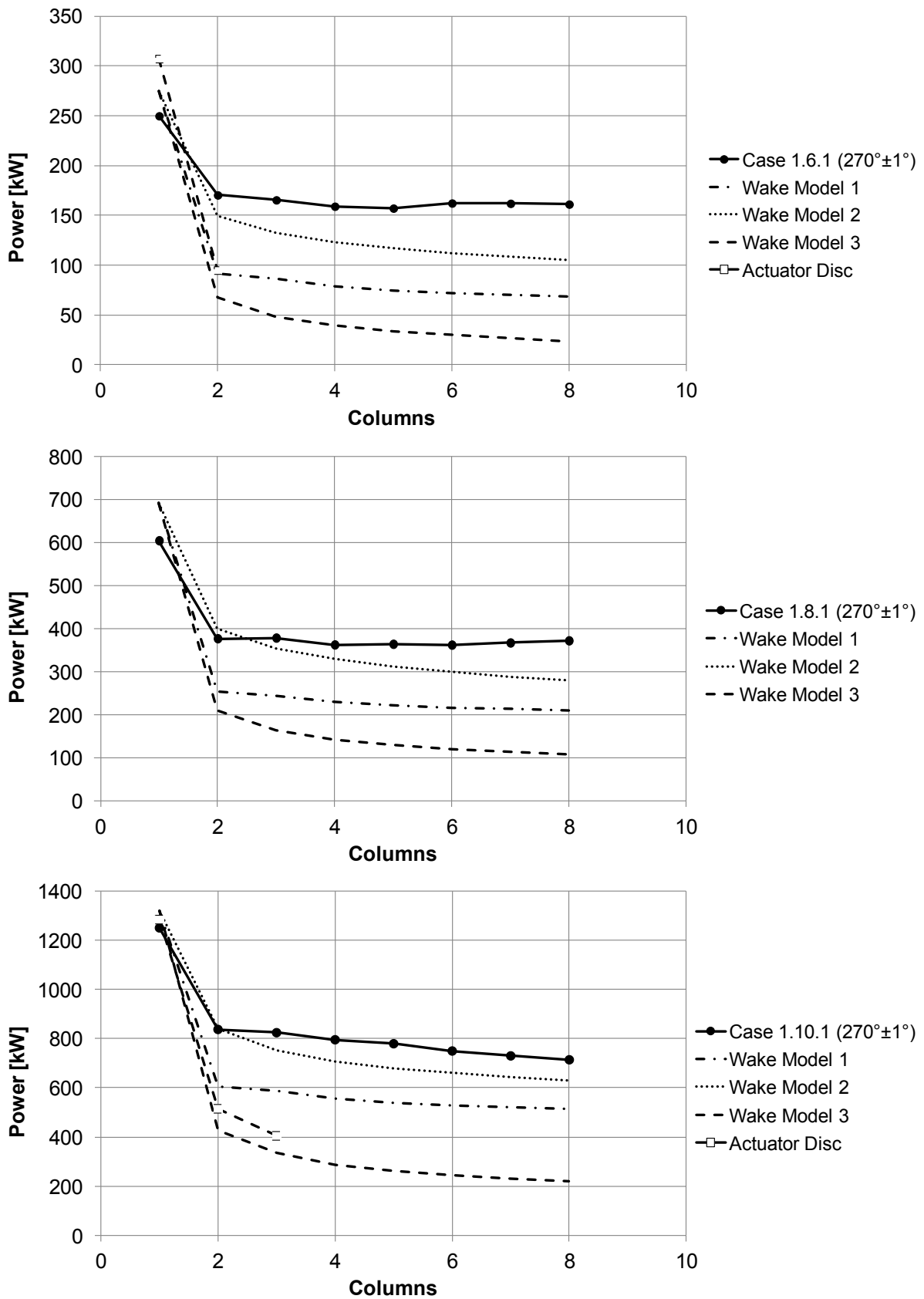


Figure 2: Evaluation and real power production at Horns Rev, with use of wake models [1,2,3] and Actuator Disc. Wind sector $270^\circ \pm 1^\circ$.

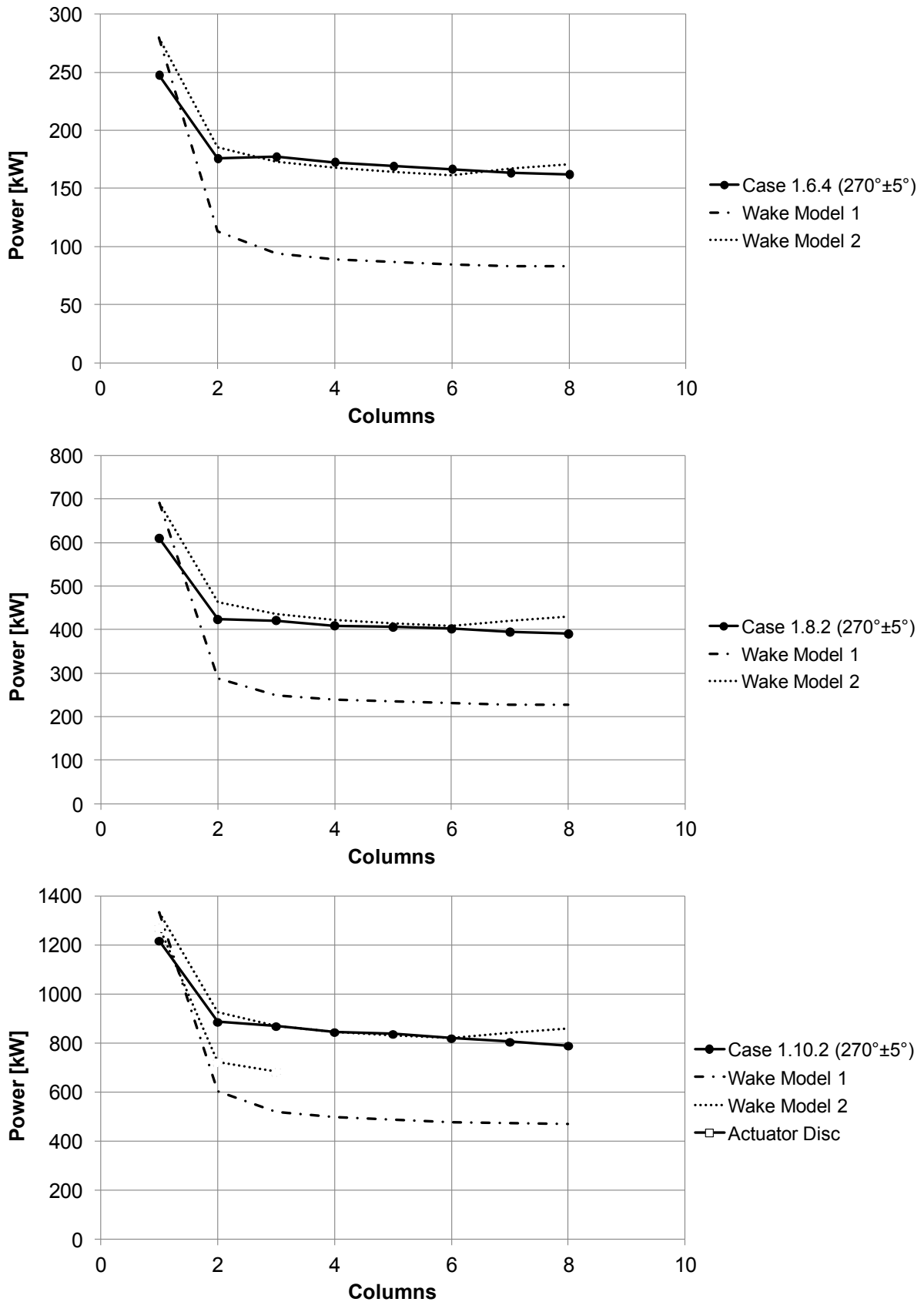


Figure 3: Evaluation and real power production at Horns Rev, with use of wake models [1,2]. Wind sector $270^\circ \pm 5^\circ$.

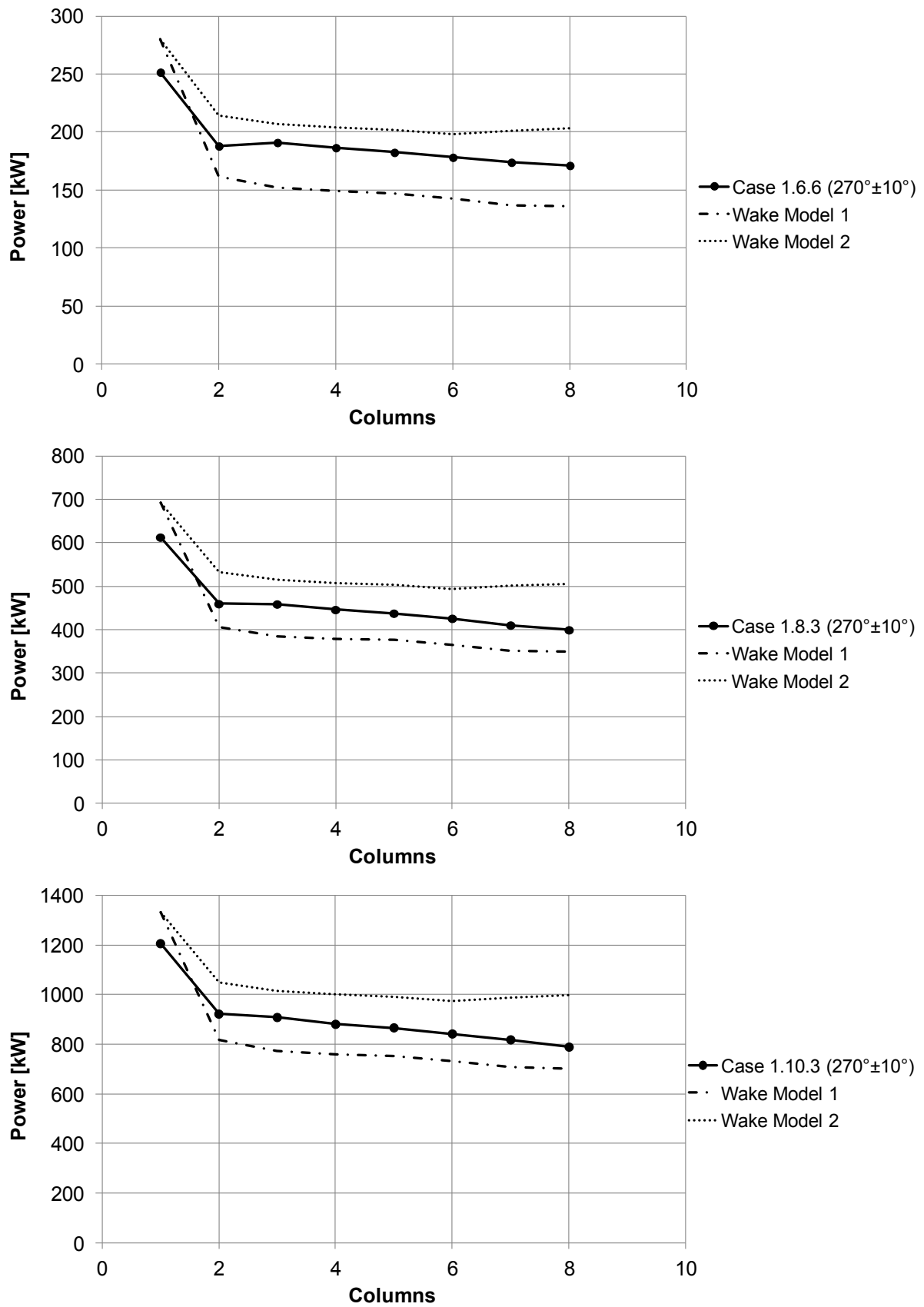


Figure 4: Evaluation and real power production at Horns Rev, with use of wake models [1,2]. Wind sector $270^\circ \pm 10^\circ$.

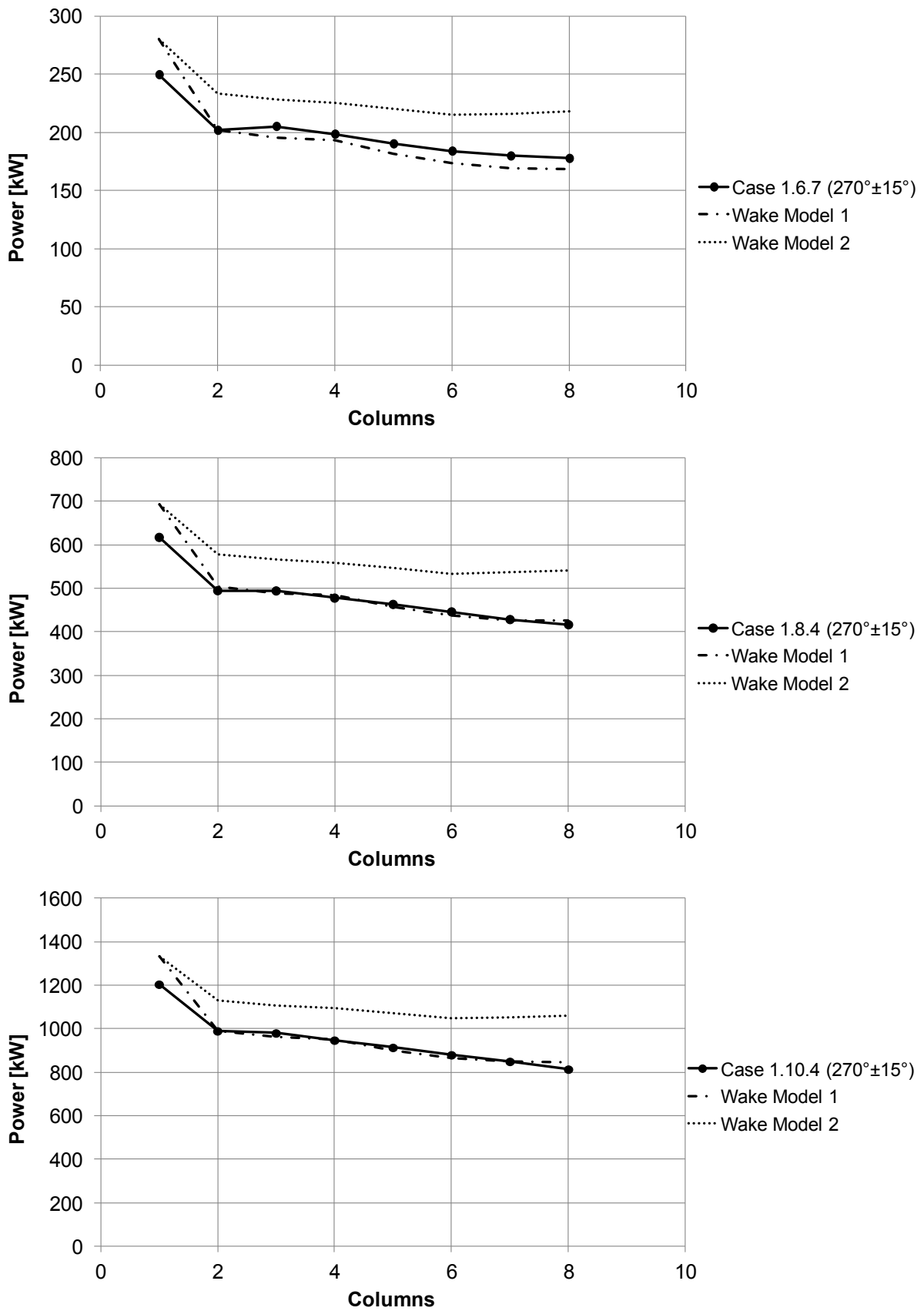


Figure 5: Evaluation and real power production at Horns Rev, with use of wake models [1,2]. Wind sector $270^\circ \pm 15^\circ$.

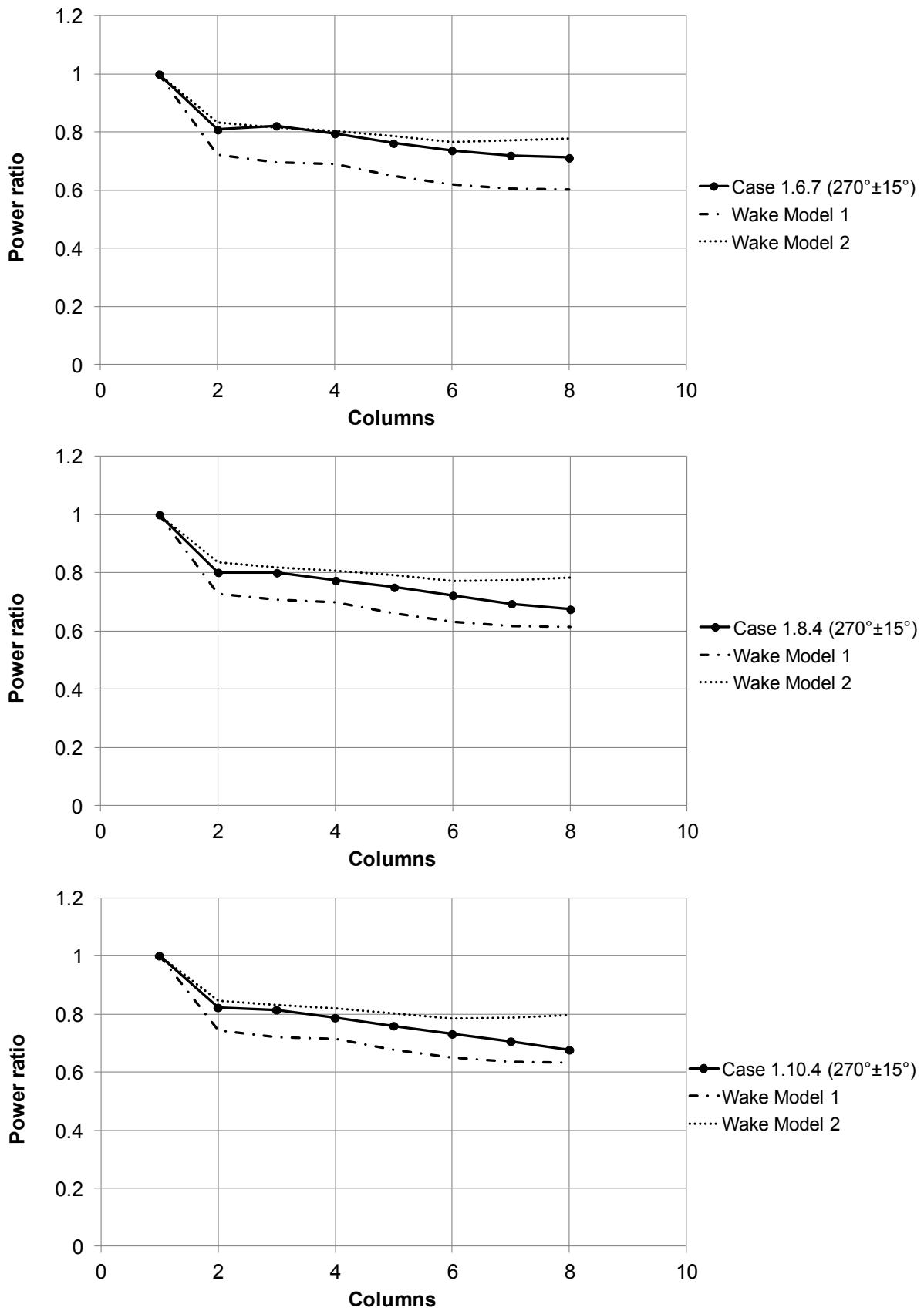


Figure 6: Evaluation and real power production at Horns Rev, with use of wake models [1,2]. Wind sector $270^\circ \pm 15^\circ$

Conclusions

A series of RANS simulations are carried out over the sea and analytical wake models are then applied to mimic the wake behavior in the wind farm of Horns Rev. Another series of RANS simulations is carried out with numerical technique of the Actuator Disc. Results from both the techniques are compared against real wind farm production.

The three wake models show all a different behavior, the wake model which is causing less wake losses is the wake model 2, by Larsen [2], in many cases this has been also the closest to the production data of reference. Wake model 1 by Katic *et al.* [1] and 3 by Ishihara *et al.* [3] instead are predicting generally a lower production compared to Larsen [2]. It is interesting to notice that the power production at wind turbines not under wake influences, first north-south column for 270° wind direction, is systematically over predicted., this could be due to a not exact match between the power curve used in the computation and the one at the site, another reason could come from the different the wind shear at the site and the one present during the calibration of the used power curve.

The Actuator Disc technique employed does not show a clear improvement compared to analytical wake models. Both the methodologies have room for improvements, the meandering of the wakes is not taken into account in both the approaches. This is probably one of the reasons why models are not that precise for narrow sectors up to 10° width. Moreover the swirling of the wakes is not included in the model, forces are computed from the thrust coefficient and not the lift-drag laws.

The power output for the different wake models is computed extracting the wind speed at the hub position and applying the power curve. It can be that for a better prediction an equivalent hub height wind speed should be computed by scanning the whole wind speed distribution over the swept area.

Acknowledgements

The author wishes to thank the owners Horns Rev wind farm, DONG Energy and Vattenfall, that provided a selection of production data of Horns Rev.

References

1. I. Katic, J. Højstrup, N.O. Jensen. A Simple Model for Cluster Efficiency. *EWEC Proceedings, 7-9 October 1986, Rome, Italy.*
2. C.G. Larsen. A Simple Wake Calculation Procedure. *Risø-M-2760, 1988.*
3. T. Ishihara, A. Yamaguchi, Y. Fujino. Development of a New Wake Model Based on a Wind Tunnel Experiment. *Global Wind Power 2004.*
4. G. Crasto, A. R. Gravdahl. CFD wake modeling using a porous disc. *EWEC2008 Proceedings, 30 March – 3 April 2008, Brussels, Belgium*
5. G. Crasto, F. Castellani, A. R. Gravdahl, E. Piccioni. Offshore wind power prediction through CFD simulation and the actuator disc model. *EWEA Annual Event 2011 Proceedings, 14-17 March 2011, Brussels, Belgium.*

Overview of non destructive testing for composite materials

Claudio Cappabianca

Direttore Tecnico AIPND, via Foresti 5 25127 Brescia, claudiocappabianca.cc@gmail.com, www.aipnd.it

Abstract - We describe in this paper the most used methods and the possible developments to expedite controls on composite components for the blades of wind turbines.

1.0 Summary

Composite materials, due to their characteristics of lightness and mechanical properties have always more applications in the most diverse sectors. Here are described various non-destructive methods used or usable for testing on composite materials and components, using glass or carbon reinforced fibers and honeycomb structures. For each of these methods are described limits and analysis capabilities, bearing in mind that the typical defects to be revealed are: delaminations, cracks of fibers, no-bonding fiber/matrix, breaks from impact matrix (typical defects in components for Aeronautics).

Body parts, spoilers, truck boxes, doors, panels and instruments. Present denomination *composite materials* identifies those materials based on fibers like *silicon, boron, carbon, aramid or also wires*, incorporated in a resin matrix having no essential tasks of mechanical strength but function of cohesion among fibers and among the various layers of the artifact.

Field of application	Use
Aeronautics	Parts of wings, tails, fuselages, Interior panels, helicopter blades
Energy	Blades for eolic generators
Automotive	Body parts, spoilers, truck boxes, door panels instruments
Costruction civil	Pipelines, reinforcing elements for recovery, fences
Nautical	Nautical boats, sails, bridges, structural profiles, trees, cordage
Sports	Fishing rods, golf clubs, bicycles, skis, canoes, tennis racquets

Table 1

There is also a third component: *interface* whose function is to promote the coupling between the fibers and the matrix. In some cases, fibers are coated for compatibility issues with the array. In summary, the functions which are the individual components are:

- Fibers:
 - support workload
 - prevent any movement of dislocations and prevent the spread of cracks, cracks, delaminations, which occur within the array
 - give the required stiffness composite

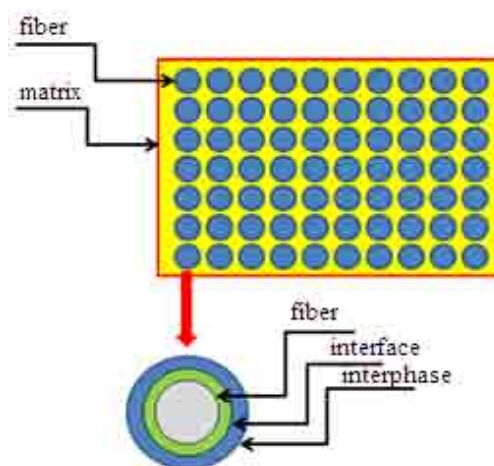


Figure 1

- Interphase:
 - allow the wettability between fiber and matrix
 - ensure no dispersion of components
 - ensure the positioning of the fibres preventing direct contact
- Interface:
 - guarantees the coupling fiber/matrix
 - transfer the efforts of matrix to fibres
- Matrix:
 - transfer the loads and stresses fibers. Transmission is the effect of tangential stress.
 - space out and keep together the fibers
 - protection against external agents or prevent any flaws to propagate in the various layers and between fibres.

Main characteristics of composites are to have high values of:

- tensile stress
- modules longitudinal elasticity both in absolute value is especially in relation to their density

The classification of composites generally takes place according to the type of fibers and matrix:

- Fibres:
 - long or continuous
 - orientation (unidirectional, bidirectional, random)
- Array:
 - unidirectional
 - multidirectional

The study of the behavior of a composite component under load, and where you are experiencing the growth of a failure is very complex. From experimental data, it was found that interesting matrix cracks propagate to nearby fibres, causing damage, breakage and finally putting out. The characteristics of fibers are therefore decisive factor for the tensile strength of the component or favoring the propagation delay of the crack. Breaks can be so divided:

- fiber breakage due to excessive load
- fibre matrix with posting more or less widespread

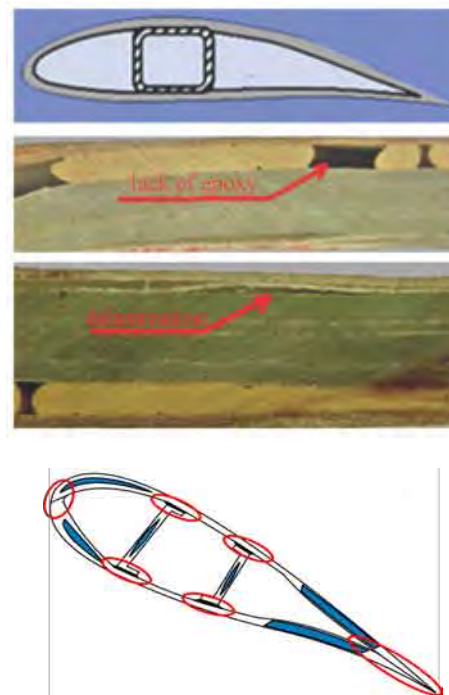


Figure 2: Cross-section and typical defects and critical areas in wind turbine blades.

This brief description is indicative and certainly not exhaustive of the complexity of the issues relating to the qualification of composite components by non destructive testing both during production and maintenance.

In particular, the blades for wind turbines due to their complexity, curved surfaces and varying thickness with variety of materials present significant difficulties for non-destructive testing. Figure 2 shows a cross-section of a wing blade in GFRP critical areas and its typical defects: lack of epoxy and delaminations.

1.1 Non Destructive methods

The most commonly used control methods is the realization of basic materials and components are:

- radiography and tomography
- ultrasound
- mechanical impedance
- eddy current
- shearography
- thermography
- acoustic emission.

2.0 Radiography and computer tomography

As is well known, the detection of defects in radiography is a function of the difference in absorption of incident radiation component inspection and in the areas affected by defects; in

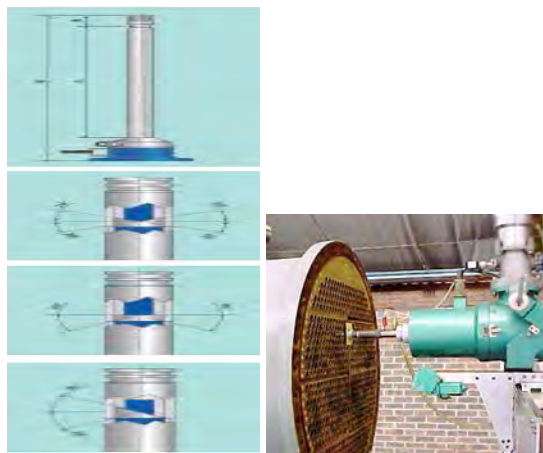


Figure 3: Left: head of microfocus x-ray, on right heat exchanger inspection with rod

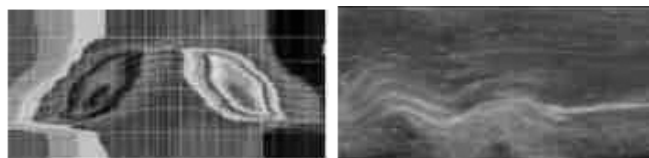


Figure 4: Fiber failure.

composites because the difference in absorption between the polymer matrix and fibers is very low, you will need to use low energy to have a good contrast. The detection of delaminations need to dispose of a very little focal spot, in some cases micron: so basically, delaminations are unlikely to be identified with traditional x-ray machines. The use of micro-focus, high resolution depends on one spot lower emissions to 10 μm . For inspection of pipes or hollow road anodes can be used with diameters of about 10 mm and length up to 500 mm; the x-ray beam can be directional or circular. Defects are detectable as empty, if large enough, broken glass, fibers as they have absorption coefficient of radiation higher than the surrounding matrix are detectable. In some cases, it is possible use contrast media such as tetrabormoethane (TBE), which has a much higher absorption coefficient compared to composite materials.

The defect, for example, impact damage, must be open to the surface. The TBE is applied before the x-ray examination for about 30 minutes and then be easily removed. The contrast between area with defects and not is greatly improved. This methodology is able to reveal even delaminations.

Digital radiography: this method uses array of detectors; use of film is abolished.

Other systems that may be used for special purposes are *tomographic systems* for the detection of tangential defects. Tomography can reveal the following defects in composite structures:

- cracks in fiber
- delaminations and decoupling
- aging cracks
- gaseous inclusions
- non-uniform distributions of fiber and matrix
- fractures in the array and deformations
- incorrect assembly.



Figure 5: Radial crack.

In the case of corrugated structures with high loads, the fibers are designed to withstand the load just in case they are aligned in the same direction; otherwise, or if the stresses are different direction the array must be able to sustain the effort: result, causing it to bend matrix with every probability the bending of fiber and their eventual breakup.

The detection of any cracks or fiber breakages with tomographic method is mainly a function of the x-ray emission spot so it is necessary very low spot x-ray (few microns) and the size of the detectors. The x-ray can reveal defects, such as voids, just in case they have a difference of absorption, as compared to the surrounding area, of 2%. Synthesizing, Tomography to produce images with good contrast should use low-energy x-ray systems, in relation to the

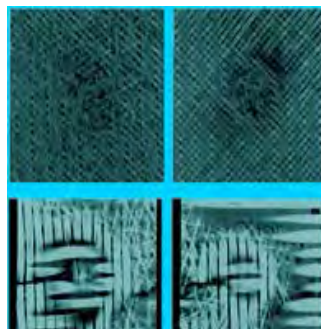
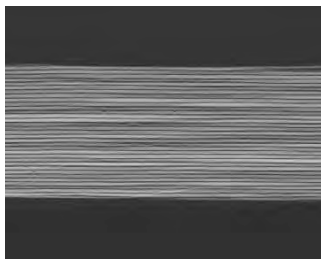


Figure 6: Left: CT dislocation fibre composites, on right composite with damage by impact.

thickness and characteristics of the composite, high dynamic and detectors, high-resolution, parallel beam; tomography can reveal delaminations, which is not possible with the other application of radiography, tomography is the study of dislocation of fibres and their alignment.

3.0 Ultrasound

Ultrasonic methods that can be used for inspection of composites are different: contact, immersion, squirters, mating in the air, reflection, transmission, A-B-C scan, measurement of mechanical impedance, etc. Inspection in transmission (Figure 7) is used to verify even very large components and complex geometries with help of anthropomorphous robot to move ultrasonic probes.

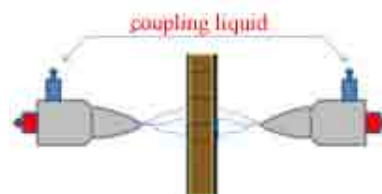


Figure 7: Inspection on aeronautical component with squirters and anthropomorphous robot.

The measurement of mechanical impedance is particularly useful for detecting delaminations between honeycomb structure and the outer strips (honeycomb); the C-scan immersion, hardly usable in the field, is particularly suitable for the detection of very small defects.

$$F_r = \frac{0.47h}{r^2} - \frac{E}{\rho(1 - \vartheta^2)}$$

where:

h = defect depth

r = defect radius

E = Young module of material on defect

R = material density

ϑ = Poisson ratio of material on defect

The measurement of mechanical impedance using a dual probe, a transmitter and receiver, with a bandwidth of 1 MHz in order to induce a forced oscillation in the composite.

The signal receiver is filtered and operates on a wavelength of approximately 1/2 than the resonance frequency of the component free from defects; in the presence of the stiffness decreases and then reduced the frequency of resonance, in addition to the decrease of eco. The sensitivity of the method is particularly effective for detecting parallel to the

surface defects, such as defects in the skin-core honeycomb structures.

The signal can be in: **Pitch-catch** (RF, impulse and swept), **MIA** (Mechanical Impedance Analysis), resonance. Pitch catch mode is used to inspect composite honeycomb. The spacecraft transmitter sends acoustic energy in the receiving probe and it registers the echo attenuated by the components of the structure. When there is a defect area, the amount of energy returned to the receiver is greater and therefore the visible result is the increase of the amplitude. In literature, it mentions that a no-bonding of approximately 25x25 mm can be found at the bottom of a honeycomb structure.



Figure 8: Pitch Catch method.

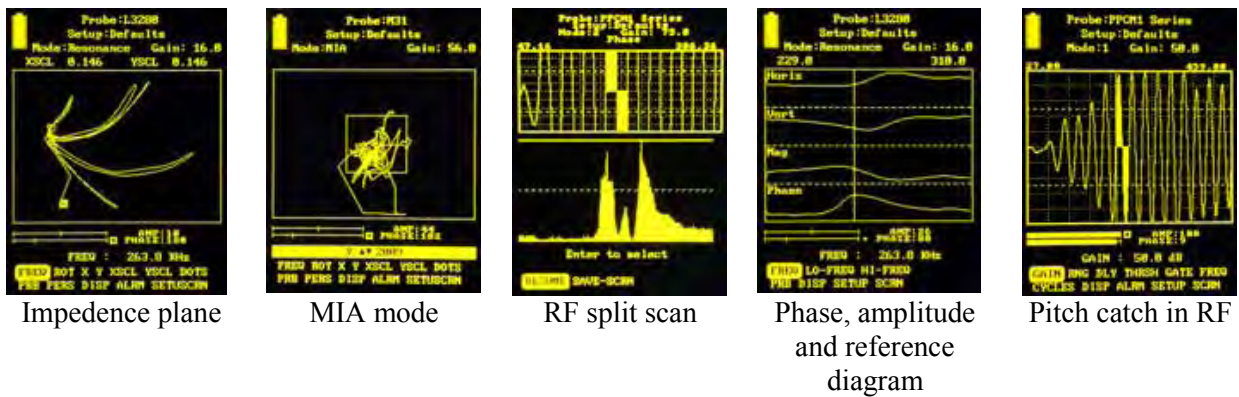


Figure 9: Display of various modes in resonance.

3.1 Testing with Phased Array probes

In inspections of small items or with complex geometries with individual tests and contact probes are still very widespread; the use of Phased Array Probes, in recent years, is greatly increased thanks to the ability of the method: possibility of displaying signals A, B, C, and S-scan for processing and analyzing the information arising from complex structures. Phased array method allows the generation of a bundle of ultrasound. The beam can also be multiplexed onto large arrays. In the composite control, scanning angle 0° runs exciting items in succession. The advantages of using this type of probes are manifold: speed, inspection of the area coverage, inspection resolution. The stored data can be analyzed and then display them in A, B, and C-scan.

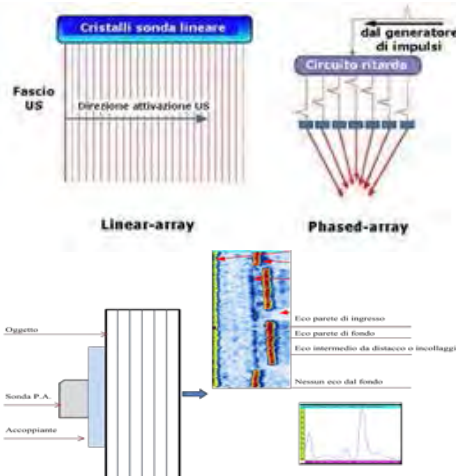


Figure 10: Phased Array inspection.

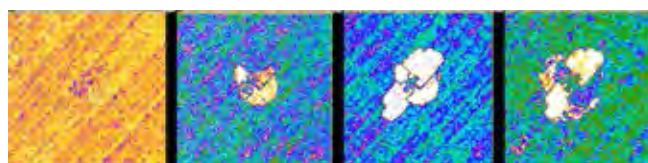


Figure 11: Impact defects.

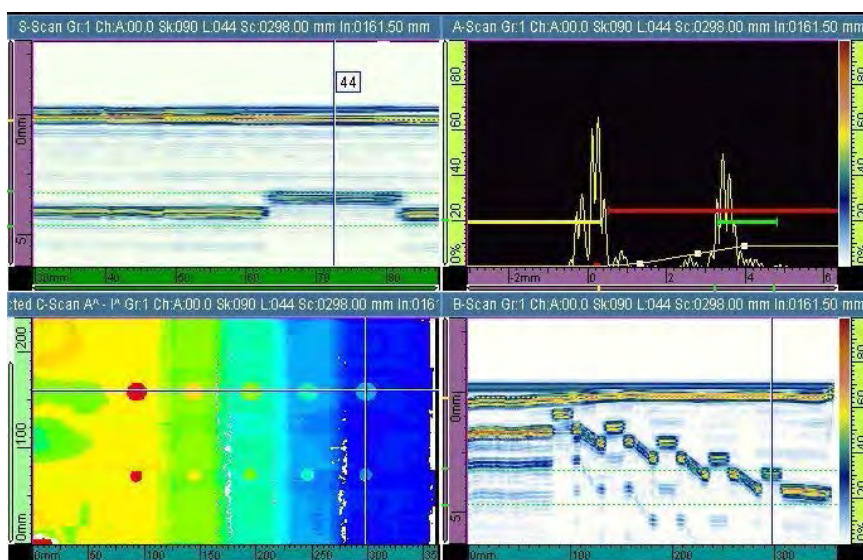


Figure 12: Different types of viewing: A,B,C-Scan and Phased Array.

3.2 Measurement of mechanical impedance (MIA)

Using a dual probe, transmitter receiver, the signal is analyzed in amplitude and phase measurement and reveals the stiffness of the component under consideration. The probe applies a localized forced oscillation in the area under consideration. The analysis is the comparison type, so you must have test-pieces with known defects. The method is more usable for the detection of defects on the surface of the parallel structure and does not require coupling media.

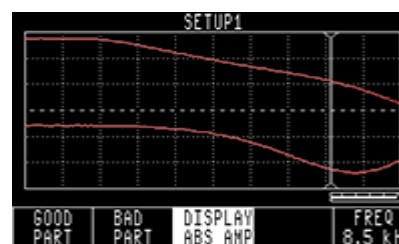


Figure 13: MIA.

3.3 Resonance

The ultrasonic probe is excited at the resonance frequency of the component inspection. Finding defects is done by analyzing electrical impedance changes in the sensor. In some cases, the depth of any posting can be correlated to signal phase rotation

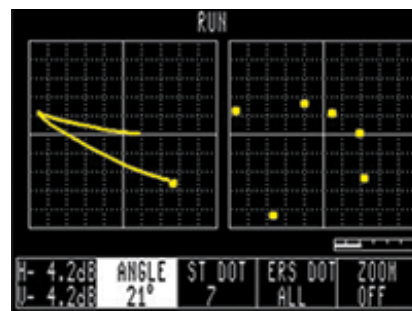


Figure 14: Resonance method.

4.0 Shearography

Holography is a method that involves registering an optical front comprising both amplitude data that phase of light reflected from the object under examination. Data logging is called "hologram" and derives from Greek holos (body). The shearography is an optical method that makes it possible to reveal any deformation of the surface of the object under consideration in relation to the load of the structure; in fact this method is attributed to holographic interferometry. The load may be caused by heat, pressure or vibration. Any defects are highlighted for different deformation than surrounding areas do not lack. In the context of non-destructive testing is used a laser, monochromatic light source, which produces a spherical front to illuminate the surface to be inspected; the result for a flat surface without deformation or defects, is an interferogram which shows a series of concentric white and black.



Figure 15: Shearographic system.

The sherographic system, see Figure 15, is composed of:

- laser component inspection
- interferometer (shearing interferometer) having the task to display the interference due to collimation of two bundles not coincident
- computer for processing, data storage, system control.

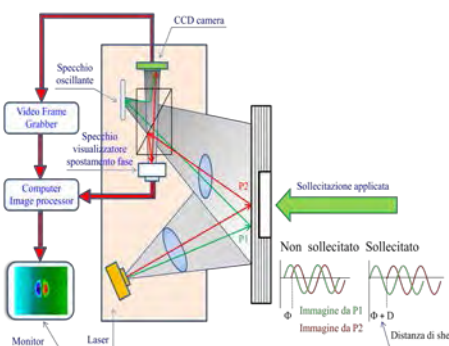


Figure 16: Shearograph diagram.

The principle of system, see Figure 16, by modernising the A.A. Michelson Interferometer, is as follows: a beam of light generated by a laser, with a capacity of about 150 mW strikes, "illuminates" the area to be examined; oscillating mirror captures the image, "image" sheared "and move into phase with the original still image. The amount of shift determines a vector whose angle is related to the displacement and is an important factor, among others, influencing the sensitivity of measurement; the two laser images resulting from stress of the area concerned, in the carrier's move offset, will interfere with side fringes on the surface of the object; a CCD camera will record the reflected light of the interferometric image (speckle).

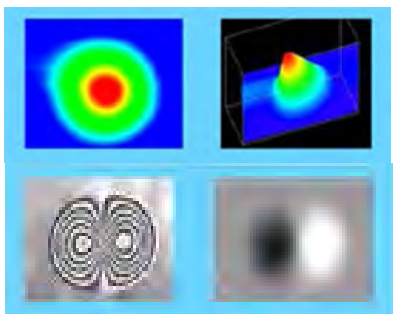


Figure 17: Viewing of defects.

In optics, the term speckle defines the image point formed when a beam of coherent light is passed through a half messy. The image produced is derived from a random phase variation of beam incident. The camera will record a series of waves, pictures, consistent but with random phase for some directions that will be constructive and destructive: so here's the formation of an interferometric image with light and dark rings. In fact, the two images speckles, moved into phase are focused on a sensitive element CCD camera. Each frame is the complex sum of two speckles can be subtracted from a pre-recorded image and reference; the result is directly observed on the monitor.

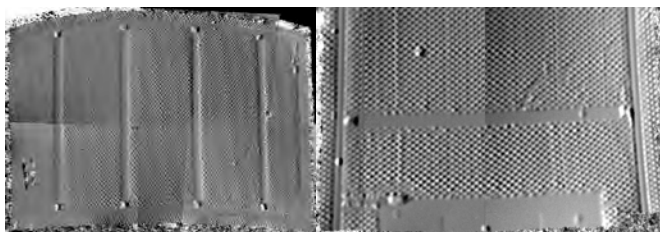


Figure 18: Structure in Honeycomb 700x500 mm, inspection time about 20 sec. Pressurizing from inside.

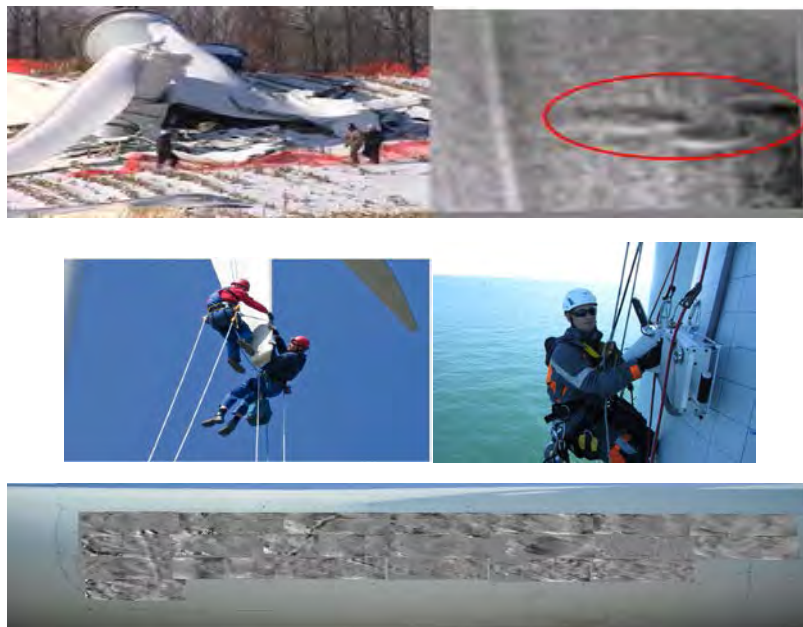


Figure 19: Effects of wrinkling, in field inspection, below mosaic of 5x1,5 m.

Solicitation	Detectable defects
Thermal with $\Delta = 1\div 40$ °C	Impact damage – delamination- disbonding
Vacuum	Disbonding in Honeycomb – core damage – disbonding inside core
Vibration	Disbonding – delamination inside solid plate or inside core of honeycomb components
Pressure	Impact damage – fiber delamination delle fibre in pressure vessel

Table 2: Shearografia - Methods of solicitation and detectable defects.

In the case of inspection of wind blades with shearography it is possible to detect presence of water inside the sandwich structure.

5.0 Termography

Critical points for the blades are the ends: thermography is to help verify the possible defects in these areas both in construction and operation.

5.1 Transient thermography

Transient temperature variation allows you to identify, through comparative measures, the amount of carbon fibers in composite.

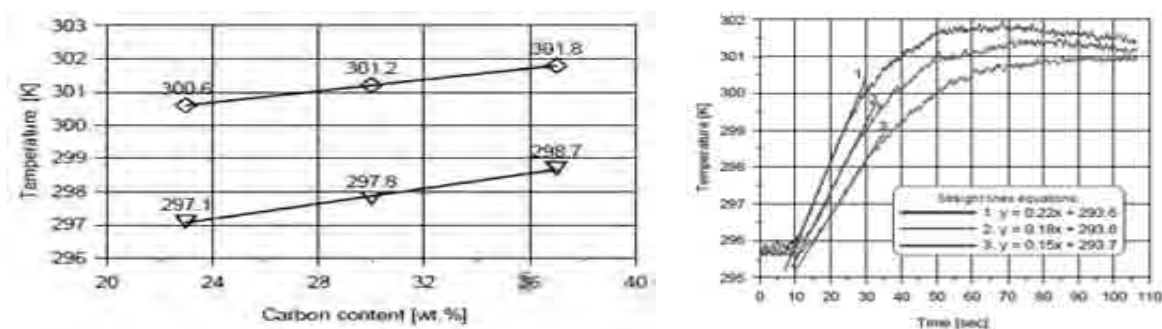


Figure 20: Temperature variation as a function of fiber content.

5.2 Flash thermography

In the case of flash thermography method the heat pulse is applied with xenon flash lamp or bulb, but having composites low thermal conductivity it is possible the detection only of surface defects. But the method has proved effective for stress defects such as corrosion under paint: in this case were used by lamps with pulse 6 kJ at 2 msec.

5.3 Termography lock-in

It is a technique based on the generation of thermal waves inside the component to try in steady state. The object is heated with sine waves, typically modulated intensity halogen lamps, modulated at a frequency ω giving rise to heat wave greatly attenuated. The acquisition of the phase retardation of wave heat generated provides information on non-uniformity of thermal structure and present defects.

This is particularly suitable for the detection of:

- inclusion of air or water (Figure 21)
- damage from impact, delaminations, lack of bonding
- characterization of large components.

In some cases, the thermal excitation can be generated by high energy ultrasound transducers piezo-ceramic type with frequency of 40 Hz $20 \div 4$ and about kW. Defects are detected by high-sensitivity cooled cameras with analysis of high-speed data, or if you require more sensitivity with lock-in. It is possible to inspect components very thick and the orientation of the defect is irrelevant. Another possibility to induce thermal energy are induced currents, eddy-current. Inspection depth depends on the conductivity of the object and the probe frequency exciter, and analysis of phase angle reveals flaws. The frequency of the probe is approximately $10 \div 40$ Hz with power up to 10 kW (Figure 21).

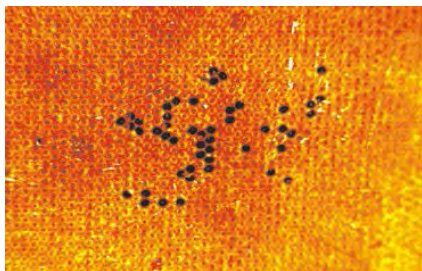


Figure 21: Water inclusion.

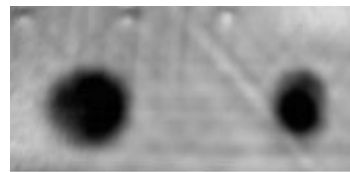


Figure 22: Impact damage.

6.0 Acoustic Emission

The method is based on elastic wave detection when a transient object is subjected to stress; waves generated thereby release energy and if you can identify the source using piezoelectric sensors. “Microphones” sensors are positioned properly to monitor the areas to inspect and analyze:

- *amplitude*
- *count*, number of times the signal exceeds the threshold set
- *rise time*, time that the signal employs to achieve maximum
- *energy*, energy revealed by the sensor.

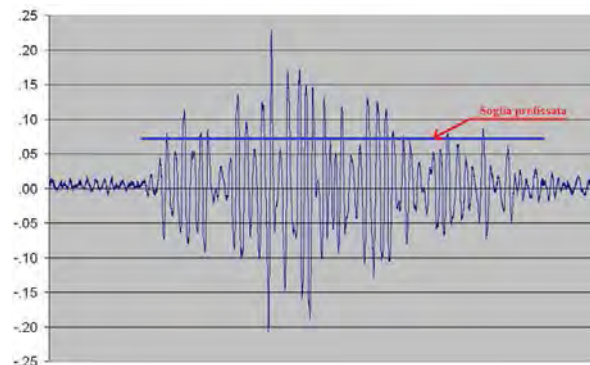


Figure 23: Typical AE signal.

Analysis of signal amplitude, time, distance in linear 2D or 3D mode allows the detection of the defect and its dislocation. The sensors are attached to the wheel with low attenuation and hill can also used in monitoring the bearing reducer. It required experimentation to determine the positioning of the sensors and the number of sensors to obtain the required results.

7.0 General considerations and conclusions

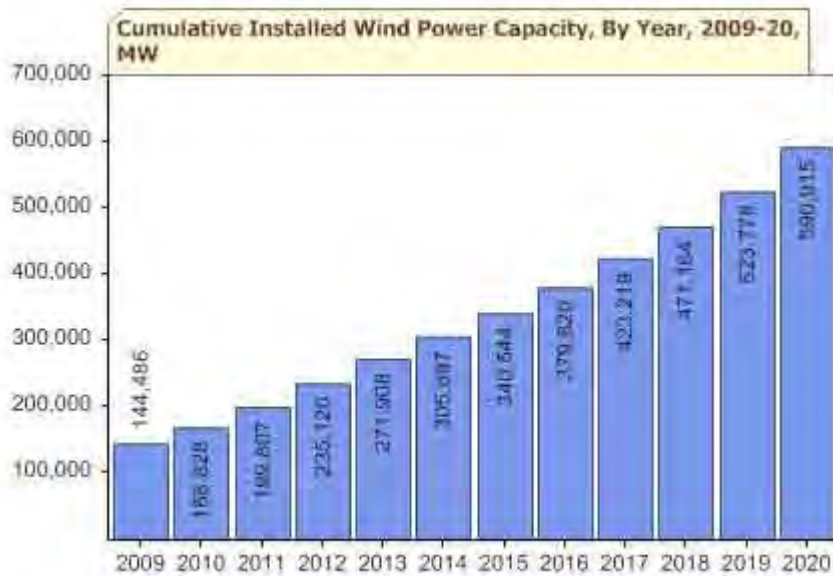


Figure 24: Cumulative installed wind power capacity years 2009-2020.

The Green Power Review.

Currently the production capacity in Italy is about 6747 MW and so Italy is in the 4th place in Europe, after Germany 29060 MW), Spain 21674 MW, and Denmark 6800 MW.

Exploitation of wind energy with off-shore platforms, today as near-shore 3810 MW, is increasingly used. Still, the construction of rotor blades in length up to 100 m is in early phase development.

For the above question it is very important to have in all phases project, construction, use and maintenance testing that guarantee the reliability and security of installations, but with costs that are not they grow the final cost: so reliability, velocity. Composite wind turbine blades are designed to last for 20 years in the field. Every defect on the surface of a wind blade disrupts its aerodynamic efficiency and, as a result, reduces the turbine's power production. Operating maintenance is a serious problem: test must be performed to considerable heights, and then require the use of scaffolding designated equipment inspection must therefore be easy to carry and use, resistant, possibly with autonomous power supply, transmit data via web for remote review and storage. During operation/maintenance optical methods will be preferred and those methods that do not involve contact, not excluding a priori methods widely used such as ultrasound.

Ultrasound methods are suitable for detecting flaws within the bonding areas below several centimeters of composite laminate.

Shearography currently used in aerospace and marine industries is proving a reliable and capable of providing information in rapid times. As described above shearography can identify subsurface defects, such as wrinkles, delaminations, disbonds, porosity, crushed core and core displacements in sandwich laminates. Certainly, such methods will use shearography as the method does not require any coupling means, equipment with low weight and speed of use. In conclusion, only research and experience can determine the choice of method or methods to be used.



Figure 25: Blade failure.

In table 3, summarizes the peculiarities of the individual methods.

Method	Detectable defect	Reliability	Sensitivity	Velocity	Ease of use	Cost
Ultrasound	Delaminations, inclusion, porosity, cracks, distribution fibers alignment	Good species in automatic systems	Typically high	Low	Low	Low in manual, high in automatic test
Radiography	Delaminations, inclusion, porosity, cracks, distribution fibers alignment			Good	Medium	Low in manual, high in automatic test
Termography	Delaminations, bonding, inclusion	Good	Medium for delamination or inclusions	Good	Medium	Medium/high
Shearography	Delaminations, bonding, inclusion	Good	Good	High	Medium	Medium/high
Acoustic emission	Cracks, delaminations, propagation of crack	Good	Good	High	Medium	High

Table 3: Peculiarities of the individual methods.



PlasMare

Trattamento integrato eco-compatibile di Rifiuti Solidi Urbani su piattaforme navali

Scenario

Forti di un'esperienza pluriennale nella concezione di impianti navalizzati per il trattamento di Rifiuti Solidi Urbani (RSU), FINCANTIERI/CETENA hanno condotto uno studio di fattibilità per rinnovare radicalmente l'attuale sistema di gestione dei RSU, basato in misura preponderante su compattamento e stoccaggio in discarica. Al fine di ridurre l'impatto ambientale, si è perseguito l'obiettivo di trasformare gli RSU in una risorsa energetica in modo da uniformarsi alla normativa comunitaria in tema.

Non solo si è individuata e valutata una nuova tecnologia di trattamento e recupero energetico dai RSU, efficiente ed eco-compatibile, ma si è anche sviluppato il concetto di installazione dell'impianto innovativo su una piattaforma navale, rivoluzionando al contempo l'intera catena logistica (raccolta, conferimento, trattamento dei RSU; sfruttamento dei prodotti e dei sottoprodotti del trattamento): al centro dell'attenzione, la baricentricità dell'impianto rispetto al bacino di utenza e il superamento della sindrome *NIMBY (Not In My Back Yard)*.

Gestione del ciclo dei rifiuti:
dall'approccio tradizionale ad un approccio innovativo

Rifiuto	Costituenti	Metodi di trattamenti tradizionali	Logistica tradizionale
Rifiuti solidi urbani	tutte le specie di rifiuti domestici quali: rifiuti organici, carta, plastica, metalli, prodotti chimici, oli, ecc.	<ul style="list-style-type: none"> • Differenziazione e riciclo • Discarica • Incenerimento con produzione di rifiuti pericolosi (in particolare ceneri e incombusti) e recupero parziale di energia • Biodigestione di rifiuti organici • Compattamento e granulazione • Produzione di CDR 	<ul style="list-style-type: none"> • Via terra
↓ ↓			
Rifiuto	Costituenti	Metodo di trattamento innovativo	Logistica innovativa
Rifiuti solidi urbani	tutte le specie di rifiuti domestici quali: rifiuti organici, carta, plastica, metalli, prodotti chimici, oli, ecc.	<ul style="list-style-type: none"> • Alta differenziazione e riciclo di metalli • Triturazione, asciugatura, separazione, bricchettatura in CDR dei componenti combustibili dei RSU • Trattamento bricchette CDR in impianto al Plasma con produzione di energia e a residui solidi inerti utilizzabili in edilizia 	<ul style="list-style-type: none"> • Via mare • Via terra

Prodotto e elaborato da CETENA S.p.A. - Contrasto

a FINCANTIERI COMPANY

Descrizione della tecnologia

FINCANTIERI/CETENA - a fronte di uno screening tecnologico condotto in ambito nazionale, europeo ed extraeuropeo - hanno individuato nell'accoppiamento della tecnologia di trasformazione degli RSU in CDR-Q (Combustibile Derivato dai Rifiuti di alta Qualità) alla tecnologia del recupero energetico tramite gassificazione al Plasma la nuova frontiera del trattamento e recupero energetico dei RSU.

New renewable energy source and its practical use in Mediterranean and other European seas

Sergey Goncharenko

Kimo-Business, Avtoparkovaya str., 5, Kiev, 02121, Ukraine
sp@kimo.com.ua

Introduction

Renewable or **regenerative energy** is energy of sources which are inexhaustible by people's standards. The main principle of renewable energy use is its extraction from processes continuously happening in the environment and further provision for technical application. The most known renewable energy sources are wind, river flow, sea flow, sea waves, breaking waves, high and low tides. Despite of different reasons of generation, all the renewable energy sources specified above, including the main renewable energy source – solar radiation, have the common characteristic: they all constitute a fluid flow, they all are in constant movement, and they all have **kinetic energy**. Kinetic energy of air flows is converted into electric energy with the help of propeller-type converters. At the present time there are no effective converters of water flows kinetic energy into electric energy. Growing needs in electric energy and low efficiency of existing plants used for generation of electric energy from renewable energy sources make inventors to look for new technologies and to develop new devices for obtaining of ecologically clean energy. Propeller-type energy converters have high loss of kinetic energy due to the flow turbulization (up to 85 %) and related ecological problems. Oscillation-type converters do not have these disadvantages. Besides that, if certain conditions are created during the oscillation process, it is possible to obtain significant amount of additional energy (condition of resonance [1] and condition of self-oscillations of "flutter" type [2]).

Main part

Theoretical substantiation of the possibility of appearance and control of effective work of unsteady aerodynamic forces and moments arising due to the interaction with a fluid flow of working elements oscillating in mode of self-oscillations of "flutter" type.

"Self-oscillations" is a term used for oscillating objects that get energy from the fluid flow (air, water), maintaining continuous oscillation. If energy is got from the uniform flow, such process of self-oscillations is called "flutter". A term "flutter" is generally used for wings of aircrafts and blades of turbo machines. Later this term has been used in studies of tubular masses of heat-exchange apparatuses.

In aviation flutter is considered to be especially dangerous comparing to other oscillations and various types of vibrations having influence on aircrafts; these intensive oscillations cause dynamic stresses in aircraft structures, these stresses can increase dangerously in seconds that will lead to the aircraft destruction during flight [3]. That is why occurrence of any form of flutter is inadmissible.

In studies of interaction between oscillating objects and the fluid flow the flutter condition has always been considered as a harmful condition appearing only in technical equipment and leading to deterioration of an object. The flutter should be avoided.

That is why all studies, tests, and calculations connected with the flutter condition have been come to determination of boundary conditions of flutter appearance and recommendations how to avoid these conditions [2, 4]. Authors of these works do not consider the possibility of use of additional energy that is generated during appearance of the flutter condition and may be used for obtaining of electric energy.

The main types of flutter of oscillating objects in the fluid flow in case of subsonic flow are stall flutter, lattice flutter, and the most simple bending-torsion flutter [2]. Theoretically conditions of appearance and analysis of bending-torsion flutter of a single wing (working element) are described in this work [5]. If there were only bending or only torsion oscillations they would fade due to aero dampening (as well as due to mechanical dampening). Appearance of combined bending-torsion oscillations drastically changes the situation. The fact is that as bending, so torsion oscillations of a working element will cause appearance of unsteady aerodynamic forces and moments (unsteady aerodynamic influences – UAI), work of which can be as positive, so negative depending on the angle of phase displacement between bending and torsion oscillations. If added and derived energy are balanced, continuous harmonic oscillations occur. As long as aerodynamic forces and moments depend on the main flow speed, the balance of energies will be achieved at specific speed that is called critical. If speed exceeds the critical value, there will be oscillations with increasing amplitude.

Under certain conditions (which depend not only on the working element oscillations phase displacement) it may be seen that additional influences change their direction, the unsteady aerodynamic force (moment) caused by the working element oscillations changes its sign, i.e. acting in the phase at the working element speed. Depending on parameters determining the oscillating process there may be cases when direction of the considered UAI coincides with direction of the working element oscillations. Then these influences execute effective work. If in this case positive work of UAI in absolute magnitude exceeds always negative work of mechanical damping forces, the working element self-oscillations of type flutter will occur. Actually, in case of flutter the aerodynamic damping changes its sign and total damping possesses negative values. Appearance of the working element flutter is characterized by loss of dynamic stability of forced oscillations of the working element.

A scheme of interaction between a single-module device and a fluid flow when kinetic energy of the fluid flow theoretically can be converted into effective work is specified on figure 1.

Designations: 1 – working element; 2 – air flow; L – angle of phase displacement between movement and force; P – force of the flow influence on the side surface of the working element, normal to reciprocating movement of the working element; P_n – normal component of force of the P flow influence on the side surface of the working element, coinciding with direction of reciprocating movement of the working element; P_c – resultant component of P force, normal to the side surface of the working element; P_{HAB} – total UAI of unsteady aerodynamic forces and moments; A – initial time; B – 90 degrees phase displacement relative to the initial time; C – 180 degrees phase displacement relative to the initial time; D – 270 degrees phase displacement relative to the initial time.

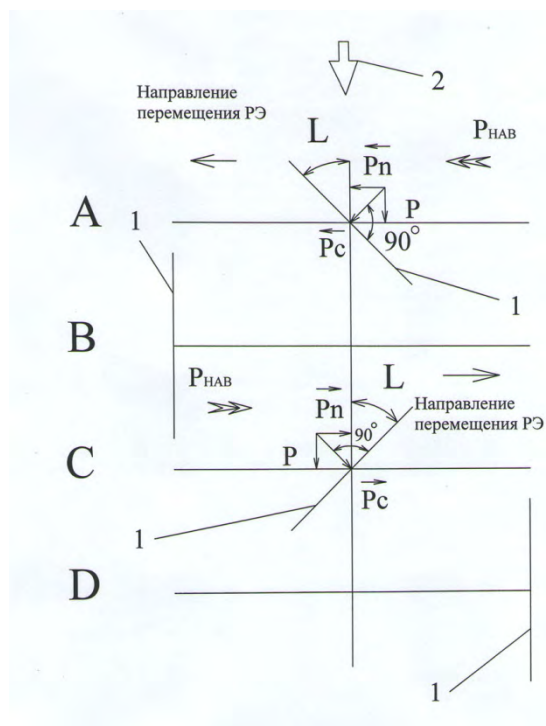


Figure 1: A scheme of interaction between a single-module device and a fluid flow.

Arrows indicate directions of reciprocating movements of working elements 1, occurring due to influence of the flow 2 and total influence of UAI on working elements 1.

In this work [1] formula 42 shows that at steady-state forced oscillations the biggest work per oscillation cycle will appear during 90 degrees phase displacement between the movement and the force.

$$W = \pi AP \sin L \quad (1)$$

where W – work executed by disturbing force per cycle in the process of steady-state forced oscillations; π – dimensionless mathematical constant expressing relation between perimeter of circle and length of the circle diameter; the constant equals 3,14; A – amplitude of oscillations; P – disturbing force; L – the angle of phase displacement between the movement and the force.

That is why reciprocating movement of the working element in the proposed device should be organized normal to the fluid flow direction. In this case the normal component of P_n force of P flow influence on the working element side surface coincides with the working element displacement, and the resultant component P_c is normal to the working element side surface.

At the same time the working element will perform harmonic rotatory movements around axis of its fixation. Angle of attack L (angle between the working element side surface and the flow direction) will change at any specific time, reaching its maximum approximately in the middle of reciprocating movement and possessing zero values in case of change of the working element reciprocating movement direction.

According to the theoretical substantiation [5], interaction of the working element performing bending-torsion oscillations with air flow leads to occurrence of bending-torsion flutter. As a result, unsteady aerodynamic forces and moments occur, total UAI of which (P_{UAI}) can coincide (under specific conditions) with direction of the working element displacement.

In case of realization of the proposed scheme of the working element reciprocating and rotatory movements in the fluid flow under condition of interaction with the fluid flow, the work of the normal component of P_n force of P flow influence on the working element side surface and total UAI of unsteady aerodynamic forces and moments (P_{UAI}) will always be maximum at the specified moment of time (except cases of reversal change of reciprocating movement directions, when the work of the normal component of P_n force of P flow influence on the working element side surface according to formula 42 [1] will equal zero; total UAI of unsteady aerodynamic forces and moments (P_{UAI}) will also possess zero value, because UAI value depends as on the flow speed [1], so on intensiveness of interaction between the working element and the flow; zero angle of attack is passed by the working element due to inertia forces).

According to the scheme of the device interaction with the fluid flow, specified on Figure 1, the device functions like the following.

Working element 1 is placed in the fluid flow 2 at an angle L relative to the flow 2 direction with a possibility to perform reciprocating movements in direction normal to the flow 2 direction, and rotatory movement around axis 6 relative to which the working element 1 is fixed on a connecting rod 3, when geometric axis of axis 6 is located in the plane of the working element 1 (Figure 2, 3). The fluid flow 2 (Figure 1) influences on the working element 1 in position "A" and creates force moving the working element 1 in direction normal to the flow 2 direction (direction of the movement is shown by arrow) and rotating the working element 1 around the axis 6 (Figure 2, 3). At the same time unsteady aerodynamic forces and moments occur, total UAI (P_{UAI}) of which coincide with the flow force. These forces and moments also move the working element 1 in direction normal to the flow 2 direction (direction of the movement is shown by arrow) and rotate the working element 1 around the axis 6 (Figure 2, 3).

In this case vector of the normal component P_n of the flow P moving force and vector of total UAI (P_{UAI}) (Figure 1) coincides with direction of displacement of the working element 1, and resultant component P_c of the flow P moving force is directed normal to the working element 1 side surface. Angle L between the working element 1 and the flow direction decreases, as well as value of the flow 2 influence on the working element 1. In position "B" the working element 1 changes the movement direction reversely, when L angle = 0, there is no influence of the flow 2 on the working element 1, there is no total P_{UAI} , and "B" position is passed by the working element through inertia due to energy of the crankshaft 8 (Figure 2, 3). After passing "B" position (Figure 3) L angle becomes different from zero, as a result forces P_n and P_{UAI} occur, coinciding with inertia force of the crankshaft 8 influence (Figure 2, 3) and moving the working element 1 to position "C" (Figure 1), L angle increases, vector of the normal component P_n of the flow P moving force and vector of total UAI coincide with direction of displacement of the working element 1, and resultant component P_c of the flow P moving force is directed normal to the working element 1 side surface. Maximum influence of the flow 2 and P_{UAI} on the working element 1 is in positions "A" and "C", when L angle reaches its maximum and equals 45 degrees (in this specific case). After passing "C" position L angle decreases, as well as value of the flow 2 and total UAI influence on the working element 1.

In position “D” the working element 1 changes the movement direction reversely, when L angle = 0, there is no influence of the flow 2 on the working element 1, there is no total P_{UAI} , and “D” position is passed by the working element through inertia due to energy of the crankshaft 8 (Figure 2, 3). After passing “D” position (Figure 1) L angle becomes different from zero, as a result a force coinciding with inertial force of the crankshaft 8 influence (Figure 2, 3) occurs and moves the working element 1 to position “A” (Figure 1), L angle increases, vector of the normal component P_n of the flow P moving force and vector of total P_{UAI} (P_{UAI}) coincide with direction of displacement of the working element 1, and resultant component P_c of the flow P moving force is directed normal to the working element 1 side surface. Then the process repeats.

Device converting energy of self-oscillations of type flutter into electric energy

Hypothesis of possible appearance and control of effective work of unsteady aerodynamic forces and moments arising due to the interaction with a fluid flow of working elements oscillating in mode of self-oscillations of "flutter" type was realized with the help of a modular device consisting of a crank-and-rod mechanism with a working element located on the fixed base. With the help of such device the working element could perform harmonic bending-torsion oscillations in the form of reciprocating and rotatory movements with constant amplitudes, when phase displacement between the flow influence force and the working element reciprocating movement is 90 degrees. The working element was executed in the form of rectangular plate. Reciprocating and rotatory movements of the working element were performed with the help of a crank-and-rod group fixed on the immovable base in the form of a single-module device.

Longitudinal view of this device with one working element and a view of the device from the side of the working element are schematically shown on Figure 2 and Figure 3.

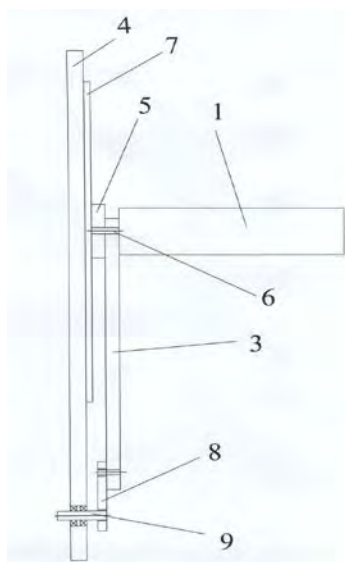


Figure 2: Longitudinal view of this device with one working element.

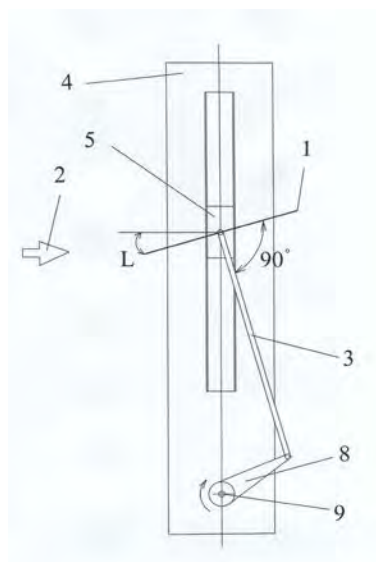


Figure 3: View of the device from the side of the working element.

The device contains the working element 1 that can be placed in the fluid flow 2. The working element is rigidly fixed in cantilever fashion on the connecting rod 3 installed on the fixed base 4 of the crank-and-rod mechanism, the slider 5 of which is connected with the connecting rod 3 with the help of the axis 6 and has a possibility of reciprocating movement along the guide 7. The opposite end of the connecting rod 3 is pivotally connected with the crankshaft 8 kinematically connected with one end of the shaft 9 established on the same fixed base; the second end of the shaft is meant for transmission of the crankshaft 8 rotation energy to the power extraction device (not specified on the figure). Amplitude of reciprocating movements of working elements 1 depends on geometric parameters of the crankshaft 8. The slider stroke length will be equal to two lengths of the crankshaft. The working element 1 is installed at angle of 90 degrees relative to the connecting rod 3 with angle of attack L relative to the flow 2. The working element 1 is installed with a possibility of fixed turn and rotatory movement around axis 6, relative to which it is fixed on the connecting rod 3, and geometric axis of axis 6 is located in plane of the working element 1. This gives a possibility to establish a fixed angle of phase displacement between rotatory and reciprocating movements of working elements 1 required for starting of the device and its effective work.

A pilot laboratory wind-hydro device WHD-1 constituted a platform executed in the form of a rectangular plate on which it was possible to locate 1 to 8 modules with studied working elements. Dimensions of the platform: 180 mm * 320 mm. 8 modules were located along the length of the platform. The crankshaft length was $L_{cr} = 22$ mm and determined the amplitude of reciprocating movements of "A" working elements.

$$A = 2 * L_{cr} = 44 \text{ mm.}$$

Working elements were executed in the form of rectangular plates with the following parameters: width $b = 64$ mm; height $h = 172$ mm; plate thickness $t = 1,0$ mm

$$\text{Working element area} \quad spe = b * h = 0,29 \text{ sq.m.}$$

Working elements were located in two rows, four elements in each row. Angle of phase displacement between adjacent working elements in each row was 90 degrees. Angle of phase displacement between adjacent rows was 180 degrees.

All tests on investigation of interaction between the pilot laboratory plant and air flow were conducted on aerodynamic stand ADU-2 (certificate No. 4/89, National Academy of Science of Ukraine, Institute for Problem of Strength). The aerodynamic stand ADU-2 is meant for investigation of unsteady aerodynamic characteristics of objects oscillating in the gas flow with excitation frequency of 0 – 1000 Hz and speed of no more than 300 m/sec.

A scheme of the aerodynamic stand is shown on Figure 4.

With the help of a high-pressure compressor (not shown on the figure) air flow 1 was supplied through the air line 2 and the honeycomb 3 to the prechamber 4, then through the damping screen 5, the acceleration nozzle 6, and Vitoshinsky nozzle 7 to the working chamber 8, interacting with studied working elements 9 located in the working chamber 8, and then the air was discharged into the atmosphere through the diffuser 10.

All these components of the aerodynamic stand (the honeycomb 3, the prechamber 4, the damping screen 5, the acceleration nozzle 6, and Vitoshinsky nozzle 7, the diffuser 10) provided uniformity of the flow and a laminar flow in the working chamber of the plant not filled with working elements.

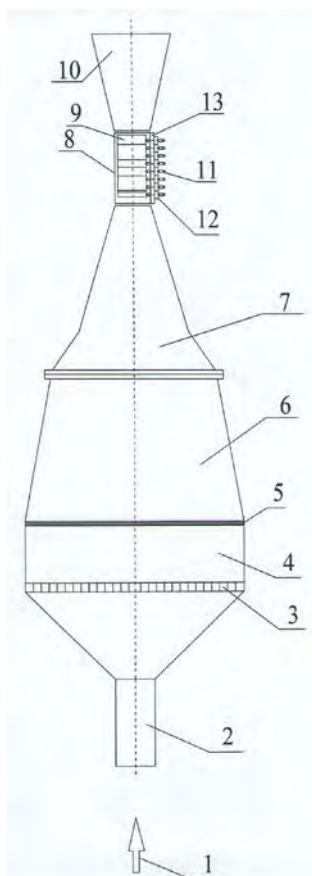


Figure 4: A scheme of the aerodynamic stand.

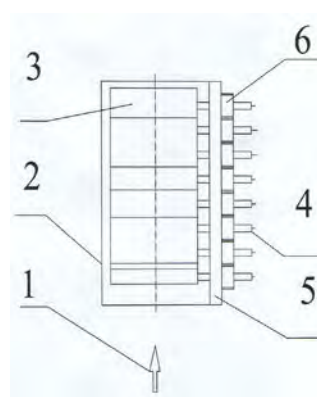


Figure 5: Location of the working element.

The working chamber 8 constituted a closed part of the aerodynamic stand with inner cross section of 150*180 mm and length of 320 mm, with removable walls. Measurements of the air flow pressure were carried out with the help of static pressure sensors located along the length of the working part in direction of the flow at distance of 23 mm to the air inlet into the working chamber, 50 mm, 200 mm, 315 mm from the beginning of the working part in direction of the working flow, and 26 mm behind the working part in direction of the air flow. One of the side walls in the working chamber of the aerodynamic stand ADU-2 was replaced by a platform of the laboratory wind-hydro device WHD-1 that was installed together with working elements inside the working chamber. Connecting gears 6 and crankshaft ends were located outside.

Location of the laboratory wind-hydro device WHD-1 working elements within the working chamber of the aerodynamic stand ADU-2 is shown on Figure 5.

Working elements 3 interacting with air flow 1 in the working chamber 2 start to move, transmitting energy of movement through connecting rods and crankshaft (are not specified on Figure 5) to shafts 4 installed on the platform 5. Toothed gears are installed on shafts 4 outside the platform 5.

In this situation working elements were located inside the working chamber, the connecting gears – outside the working chamber, that gave a possibility to change the angle of phase displacement between adjacent working elements or to install a direct current generator for extraction of electrical power from the crankshaft of any module (Figure 2, 3).

The plane of a working element installed in cantilever fashion was located normal to the connecting rod axis with possibility of an angle change relative to the connecting rod axis. In this series of tests the angle between the connecting rod axis and the plane of the working element was 90 degrees (Figure 3).

At the initial moment of interaction between the working element that can perform reciprocating and rotary movements and air flow the unsteady aerodynamic forces and moments (UAI) equal zero. Due to interaction of the working element with the air flow it starts to move along the trajectory preset in the device structure, overcoming forces of mechanical dampening (friction at joints of transmission gears and toothed gears) and forces of aerodynamic dampening, performing reciprocating and rotary movement that is a condition of UAI occurrence. Unsteady aerodynamic forces and moments (UAI) occur and increase from zero to their maximum value determined by kinetic energy of the flow and intensiveness of interaction between the working element and the flow. Mechanic energy of reciprocating and rotary movements of the working element in the pilot laboratory plant WHD-1 is converted into mechanical energy of the crankshaft rotation with the help of additional mechanisms. Further conversion of energy of the crankshaft rotation into electric energy with the help of a generator installed on the crankshaft is not difficult. The only condition to obtain effective work in this scheme is that initial rotation of the crankshaft (or generator shaft) should proceed without load. When UAI reach their maximum value and the crankshaft reaches its maximum revolution speed, it is allowed to load the generator and to obtain effective work due to conversion of kinetic energy of the flow into electric energy.

Drawings showing connection between extracted power, net efficiency and air flow speed V and number of investigated working elements n are shown on Figure 6 and 7, respectively.

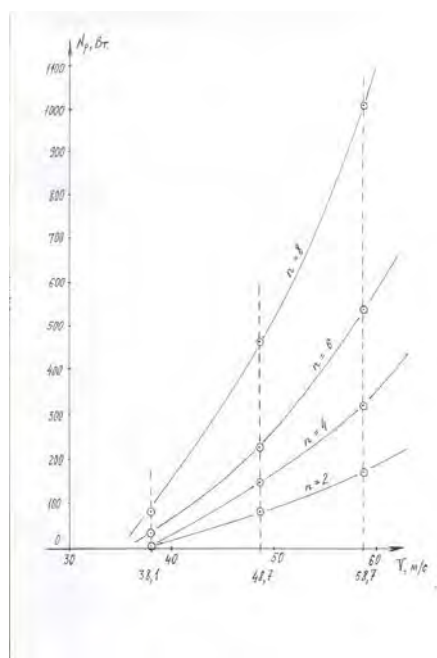


Figure 6: Schedule power change.

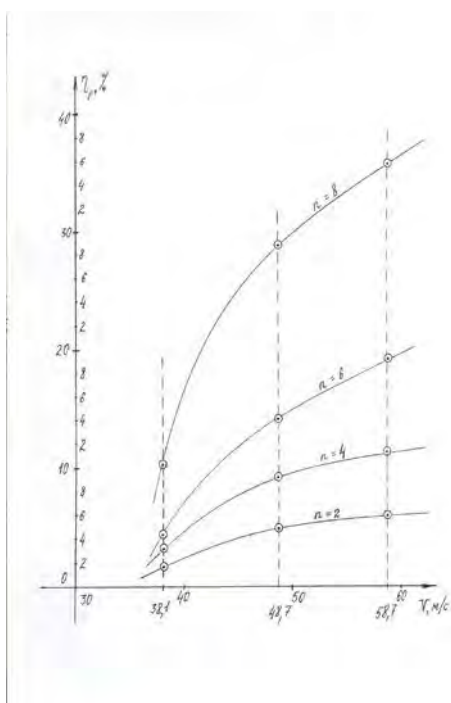


Figure 7: Schedule of changes in efficiency.

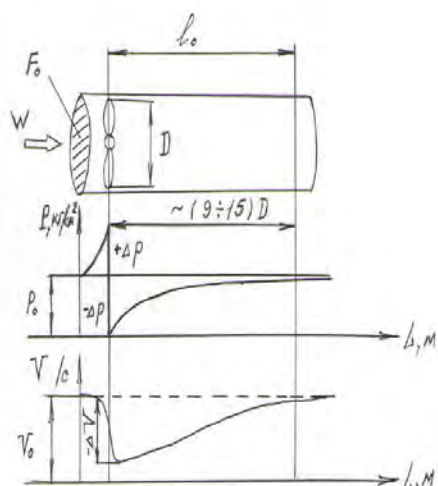


Figure 8: Drawings showing changes of the air flow speed and pressure in cases when the working element is represented by a usual screw.

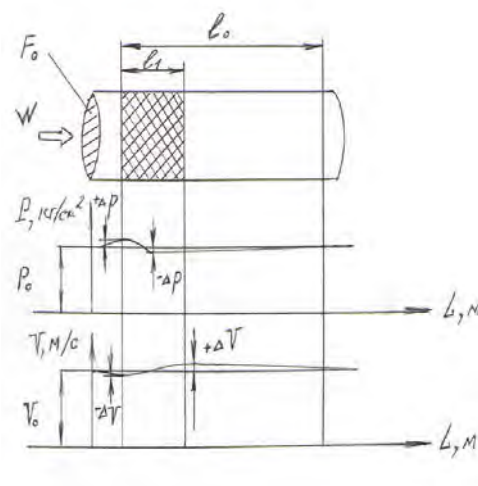


Figure 9: Drawings showing changes of the air flow speed and pressure in cases when the working element is represented by a investigated plant.

Extracted power and net efficiency increase proportionally to the increase of the flow speed and number of investigated working elements.

Drawings showing changes of the air flow speed and pressure in cases when the working element is represented by a usual screw and the investigated plant are shown on Figure 8 and 9, respectively.

On the drawings we can clearly see differences in change of the air flow pressure and speed during interaction with a usual screw and the investigated plant located in the same working chamber of an aerodynamic tunnel. In the investigated device there are practically no pressure and speed drops at the input, while at the output of the device there is insignificant increase of the air speed. Besides that, lack of the pressure drop at the input of this device indicates lack of overturning moment on the device. Behind the wind motor screw (Figure 8) there is a so called dead zone at a distance of (9-15) D (where D – screw diameter), i.e. the distance necessary to restore the air flow power, while in the investigated device (Figure 9) there are no such dead zones. Behavior of silk threads in the air flow (the threads were placed into the working chamber filled with working elements of the investigated devices WHD-1) confirms the presence of the air flow laminar motion along the whole length of the working chamber. In case of turbulization of the flow before the working chamber of the investigated devices WHD-1 the flow laminarization occurs directly after the first working element. Besides that the silk threads were also attached to a probe executed in the form of a needle that was inserted into the working chamber along the whole length of the working chamber and at different cross-sections.

Results of aerodynamic investigations:

- 1) manufacturing of a laboratory plant that can generate self-oscillations of flutter type and unsteady aerodynamic influences (UAI);
- 2) confirmation of possible control of UAI;
- 3) confirmation of hypothesis of conversion of air flow kinetic energy into effective work;

4) obtaining of practical results of investigation of UAI influence on working elements oscillating in the air flow:

- a) there are practically no pressure and speed drops at the input of the investigated devices WHD-1 that indicates lack of overturning moment on the device;
- b) constant laminar flow during interaction of air flow with the working element side surface, as well as along the length of the working part and behind the working elements with any number of working elements, even if the flow before the investigated plant is turbulized;
- c) increase of the air flow speed behind the working elements comparing with the air flow speed before the working elements indicates to occurrence of UAI total positive work of which coincides with direction of working elements displacement and normal component of moving force of the flow that leads to increase of the flow kinetic energy;
- d) increase of the air flow kinetic energy behind the working elements comparing with the air flow speed before the working elements is observed even at partial removal of effective work from the generator shaft installed on the shaft of one of the rotating crankshafts of the working element; as a result, value of kinetic energy removed from the generator shaft can regulate the flow speed at the output of the device that will make process of conversion of the flow kinetic energy into electric energy absolutely ecologically safe;
- e) extracted power and net efficiency increase proportionally to the increase of the flow speed and number of investigated working elements;
- f) conducted tests confirm the possibility of the device power growth by adding of additional working elements along the length of the device;
- g) comparing with widely-spread screw blades used for conversion of kinetic energy of air or water flow into electric energy, the investigated working elements have no turbulent flow behind the working elements that indicates more effective conversion of the flow kinetic energy into electric energy.

Hydraulic tests of the laboratory wind-hydro device WHD-1 were conducted at treated water outlet of Bortnichskaya aeration plant (city of Kiev, Ukraine).

Mooring tests of the WHD-1 device were conducted on the special hydrodynamic stand. Working elements of the WHD-1 device were used as propulsion devices instead of propellers. Working elements were located in two rows along the length of a ship model. Maximum number of working elements was 16.

Hydraulic tests and mooring tests of the laboratory wind-hydro device WHD-1 confirmed all regularities obtained during tests in the air flow on the aerodynamic stand.

According to results of the conducted tests a model of the pilot industrial WHD-2 device was designed and manufactured; the model consisted of two independent modules located on the common platform. Design of the pilot industrial plant modules was similar to design of the laboratory plant modules (Figure 2, 3). Each module consisted of a crankshaft, a connecting rod, and a slider. A working element executed in the form of a rectangular plate was cantilever fitted on the end of the connecting rod so that the axis connecting the slider with the connecting rod coincided with the geometric axis of the working element plane and the working element had a possibility to perform rotatory movement around this axis (axis connecting the slider with the connecting rod). The slider movement was restricted by guides fitted on the platform. The crankshaft was also fitted on the platform.

Each shaft ended with a gear playing role of a flywheel in order to simplify passing of “dead” points during change of direction of reciprocating movements (angle $L = 0$). All the gears were connected between each other through toothed gears. A shaft of one module was longer than others and had a possibility of direct connection with a generator shaft. On the same shaft there was installed an additional gear used to increase revolutions and to transfer total force of all working elements to an independent gear, which shaft was fixed on the platform and also had a possibility of direct connection with a generator shaft.

Dimensions of the working platform: 2.2 m * 1.5 m. 8 modules were located along the length of the platform according to a scheme similar to the scheme of the laboratory plant location. Working elements were executed in the form of rectangular plates with the following parameters: width $b = 410$ mm; height $h = 710$ mm; during conduction of aerodynamic tests, $h = 510$ mm, during conduction of hydrodynamic tests $h = 510$ mm; thickness $t = 2.0$ mm. The platform together with modules was installed on the base of frame design.

Design of the pilot device WHD-2 allowed conduction of tests for one, two, three, four, five, six, seven, and eight working elements by removal of the working element from the connecting rod. In this case all connecting gears are engaged or unnecessary gears are disengaged. In this way total work performed by working elements oscillating in the fluid flow consists of effective work removed on the generator shaft, as well as of work on overcoming of forces of aerodynamic (or hydrodynamic) damping and mechanic damping (friction at joints of transmission gears and toothed gears). During investigation of performance of the pilot device WHD-2 with one and two gears in the fluid flow not only remain working elements were removed from connecting rods, but six toothed gears were also disengaged. So, total work performed by the investigated working elements (one or two) oscillating in the fluid flow consists of effective work removed on the generator shaft, as well as of work on overcoming of forces of aerodynamic (or hydrodynamic) damping and mechanic damping (friction at joints of transmission gears (one or two) and friction at two toothed gears).

Design of the pilot industrial plant WHD-2 allows changing the angle of phase displacement between oscillations of adjacent working elements that gave a possibility to investigate different kinematics of working elements interaction in the fluid flow. Silk threads were fixed on the side edges (surfaces) of working elements (near the side edges along the height of working elements) in order to monitor the flow turbulence (or laminar movement of the air flow).

General view of the WHD-2 device during conduction of hydraulic tests at treated water outlet No. 2 of Bortnichskaya aeration plant (city of Kiev, Ukraine) is shown on Figure 10.

Tests of the pilot plant as a generator for conversion of the fluid flow kinetic energy into electric energy were conducted in the air flow and in the water flow (river Lyubich, Ukraine, speed 0.7 m/s, treated water outlet of aeration plant, city of Kiev, Ukraine, speed 0.9 m/s). Maximum coefficient of efficiency in the air flow and in the water flow in case of use of 8 working elements is 21%. There is no overturning moment. Power removed from generator and coefficient of efficiency of the device increase with increase of number of working elements.



Figure 10: General view of the WHD-2 device.

Conclusions

The main difference of the device using effective work of UAI from traditional wind generators and hydraulic generators of propeller type is that **it has no overturning moment**. As a result, there is no need to construct complicate hydraulic facilities (dams, dikes) for hydraulic plants or to lay solid foundations to strengthen masts of wind plants. The plant is simply placed into the water flow or air flow and that is it, the plant produces electric energy. The plant is simply installed on the roof of the house, low rise or high rise, or on a dike or a dam, or on a ship deck, and that is it, the plant functions. At the same time there is no hazard of deterioration of the roof of the house or of the dam, dike, or the ship deck; electric energy is produced safely.

Results of conducted mooring tests confirmed a possibility of **proportional** increase of tractive force due to increase of the power plant capacity or increase of a sea craft speed due to increase of the driven shaft speed. In this situation the sea craft consumes less fuel or moves faster with the same fuel consumption.

Unlike generally accepted screw propellers these propellers do not turbulize water flow, as a result 85 % of the ship engine power is used not for the flow turbulization, but for effective work on creation of additional traction necessary for movement. Lack of overturning moment during interaction of the propeller with water environment allows to count on significant increase of the ship speed. Location of working elements along the length of the ship hull will make it possible to exclude (or to significantly decrease) coefficient of friction between the ship hull and the water flow due to creation of dynamic pressure negative gradient along the length of the ship hull.

Areas of effective use of this product have been determined basing of the conducted tests:

1. Hydraulic generator for conversion of kinetic energy of rivers, channels, sea streams, tides, breaking waves into electric energy.
2. Wind generator on a stationary base (shoreline, masts, lighthouses, dams, dikes) and on sea craft decks.
3. Propellers on floating crafts (instead of screws): sea vessels, yachts, boats, submarines.

References

1. Timoshenko S.P., Fluctuations in engineering. Publ. "Science", 1967, pp. 78-84.
2. G.S. Pisarenko, A.A. Kaminer, Aerodynamic damping vibrations of turbomachinery blades - Kiev: Naukova Dumka, 1991, p. 9-15, 19-22.
3. Aviation: An Encyclopedia. - M.: The Great Russian Encyclopedia. Editor in Chief G.P. Svishev. In 1994.
4. Paydussis, Curling, Gegnon, Experimental investigation hydroelastic instability bundles of cylinders in the longitudinal flow fluid, Theoretical Foundations, 1982, Vol 104, n. 3, p. 164-174.
5. Samoilovich G.S. Unsteady flow and turbomachinery aeroelastic oscillation of lattices. - Publishing House "Nauka", Moscow, 1969, from 26-27.

Wave Energy Generation Difficulties solved by Eco Wave Power

D. Leb

EcoWavePower, Tel Aviv (IL)



Wave Energy
Generation
Difficulties
Solved by
Eco Wave Power



David Leb, Founder

15.05.2012

Eco Wave Power

- ✔ Established in March, 2011.
- ✔ Young and innovative company in the field of ocean energy.
- ✔ We believe in a fast, yet reliable, progress. Our competitors in the ocean energy sphere had spent 5 to 15 years researching the ocean energy field, resulting with no commercial scale devices available for sale and implementation. We want to be different. We want to be able to offer our commercial scale devices within the shortest time frame, and for the most attractive prices.

As said by John Henry Newman: *"Nothing would be done at all if a man waited until he could do it so well that no one could find fault with it."*

The Challenges

- ✔ The greatest challenge of the wave energy industry is to find the "golden middle" between producing maximum amount of KW, while still insuring the reliability and the long life span of the system.
- ✔ On the one hand high waves enable the greatest KW production, but also put the highest risk to the system. On the other hand, low waves do not endanger the system, yet they also do not produce sufficient KW amounts. Another problematic issue that was important to address is the cost of such system.

High Waves	➔	High Energy Amounts
High Waves	➔	Highest Risk to the System
Low Waves	➔	Low Energy Amounts
Low Waves	➔	Lowest Risk to the system

Eco Wave Power's Solution

We chose to put an emphasis on 4 main ingredients, which enable us to reach the golden middle:

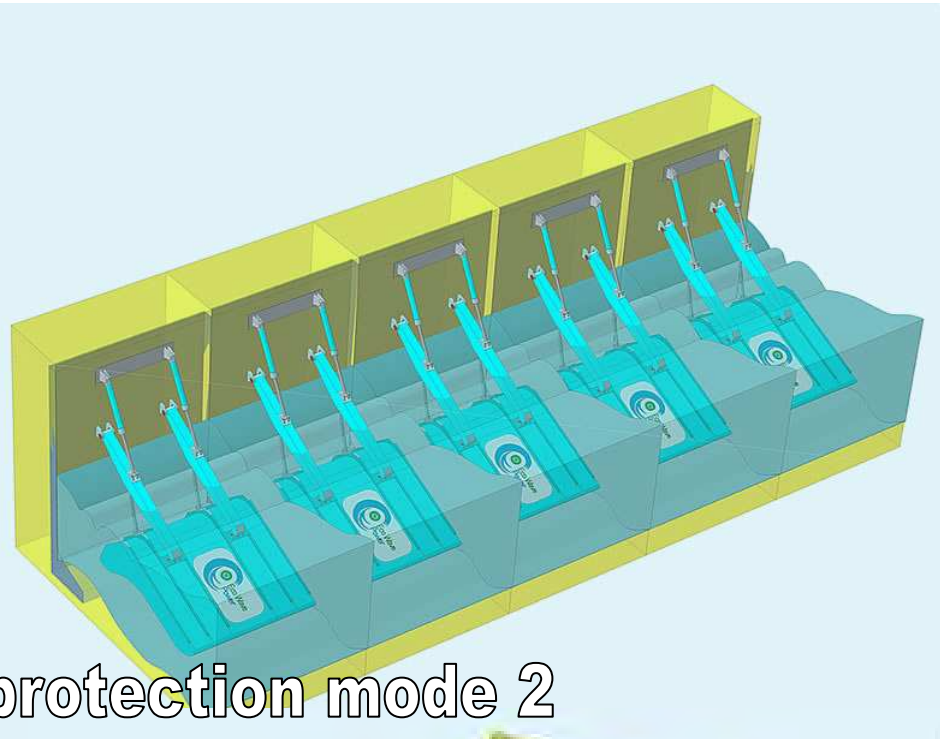
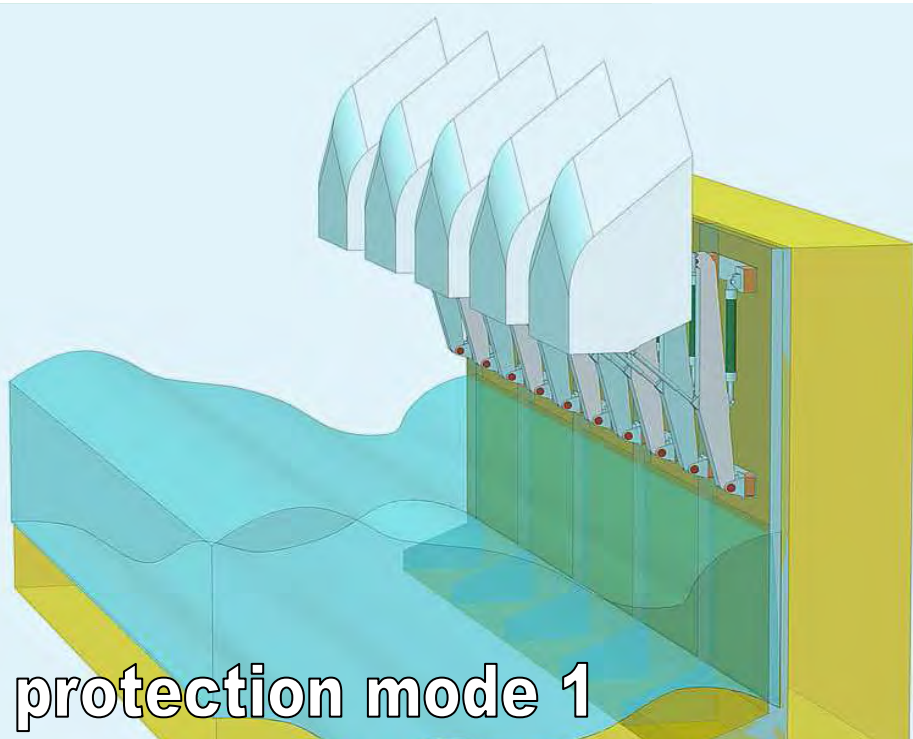
- ✔ Reliability
- ✔ Compatibility
- ✔ Sufficient Energy Production
- ✔ Cost

Reliability

We have invested efforts in making our wave energy generation system adjustable to different waves, locations, and weather conditions.

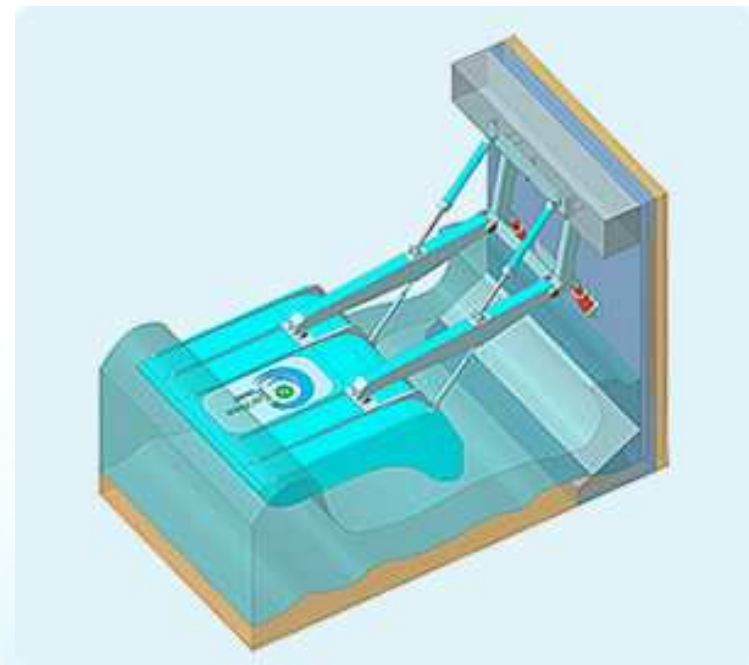
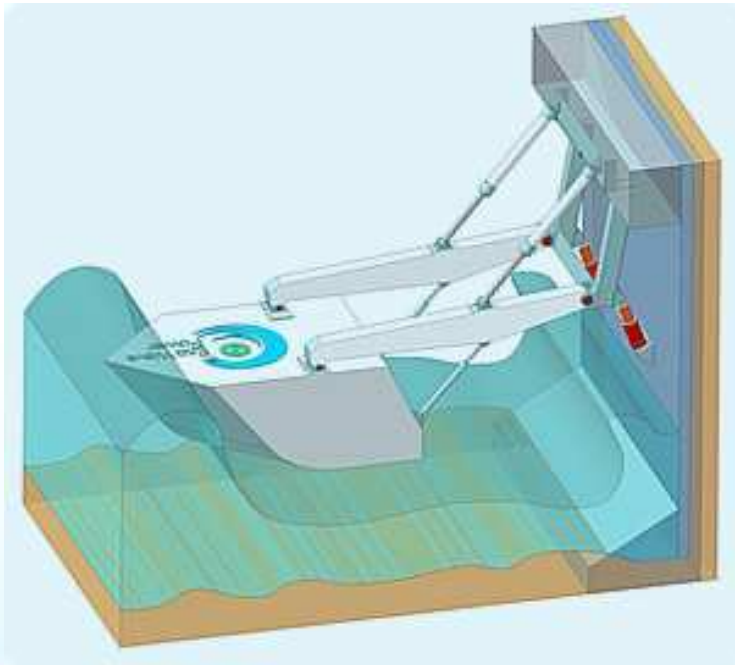
Our system has:

- ✔ Different Storm-Protection Mechanisms (in some cases we found that it is better to raise the floaters above the water level, whereas in others submersion is the best option)
- ✔ An easy and efficient maintenance process
- ✔ Corrosion Protection which enables a floater's life span of at least 30 years
- ✔ a shock-wave protection Mechanism
- ✔ a Lever Regulation Mechanism
- ✔ a Float Position Regulation Mechanism
- ✔ and an innovative Energy Control System and a Flexible Modular Structure.



Compatibility

- ✔ we do not believe in a “one size fits all” approach. Our policy is to tailor the float to the region in question. This way our clients get better results, and we lower the risk of damages.



Sufficient Energy Production

- ✔ Eco Wave Power came to the conclusion that it is not sufficient to use traditional floater forms such as: cylinder shaped floaters, square or simple round floaters.
- ✔ When we examined the operational principles of wave energy convertors with regular floaters, we came to the conclusion that they only generate a small amount of power compared to their lifting force. However, they didn't recover well from an incident flow. As a result, we improved the floater shape so they generate power both at change of water level and from an incident flow.
- ✔ When the "Wave Clapper" and "Power Wing" are operating at different wave heights, their buoyancy remains stable. A triumph of design over the elements.

Cost

- ✔ Although, the world's electricity market is at \$800-billion-a-year and rising. It has been estimated that there are at least 1.6 billion people still living without electricity today, and the world demand in developing countries is doubling every eight years.
- ✔ By the end of the 20th century the developing countries have spent \$40 to \$60 billion a year on electricity (G8, RETF, 2001), and still approximately 40% of the population in these countries remains without access to electricity. This means that the number of people throughout the world who have no electricity has hardly changed since 1970 (UNDP, 2000, p. 374).
- ✔ These countries need a reliable, yet cost-efficient solution to their energy needs, and therefore one of the biggest emphases in our development process was the price.

Our system is being developed to produce electricity for cheaper prices than traditional energy generation methods such as: coal, gas, oil , as well as green energy generation methods such as wind and solar.

Their Difficulties & Our Solutions

The main difficulties of the wave energy field can be divided into:

- a. Environmental Difficulties
- b. Location-based Difficulties
- c. Design-related Difficulties
- d. Reliability

Environmental Difficulties

- ✔ The Difficulty : The environment provides difficulties such as saltwater (which is very corrosive)

Our Solution: Due to our experience in the Sea Wave Energy field, EWP's anti-corrosion protecting process includes: optimum application of protective coatings and an advanced cathode protection. As a result, protection of metal constructions can be provided up to 30 years, until their complete overhaul is needed .

- ✔ The Difficulty: The surface of the world's oceans is a hostile environment, highly unsuitable for mechanical and electrical equipment. Under severe weather conditions, the ocean surface becomes even dangerous for ships .today severe storms rarely sink ships because of improvements in weather prediction and in communications. In contrast, wave-energy equipment sitting in a stationary position on the ocean surface typically has no way of avoiding storms.

Our Solution: EWP's unique wave energy devices are not stationary, "The Wave Clapper" and the "Power Wing", have an automatic control system that takes care of the floats' rise and submersion process in case of stormy weather conditions.

Location-based Difficulties

✔ The Difficulty: The ocean floor is a difficult and expensive location for building equipment foundations, particularly if they must resist harsh and stormy conditions.

Our Solution: EWP chose to install its' energy convertors on existing, stable structures such as breakwaters, piers and floating and fixed platforms. As a result, no underwater high-cost works are needed. Moreover, EWP's systems, that operate as wave energy absorbers may reduce shoreline and breakwater erosion and extend their life-span significantly.

✔ The Difficulty: Some companies place their floaters in the middle of the ocean, and therefore are not capable of providing service to the floaters while on site, and have the necessity to bring all their equipment to a suitable maintenance facility.

Our Solution: The EWP's system proximity to the shore provides flexibility in the programming of the work and the ability to minimize installation costs. EWP puts an emphasis on the development of a maintenance strategy, which will enable servicing the floaters on site.

✔ The common belief is that deep water systems actually work more efficiently than those closer to shore. But efficiency gains on these systems is given up to power losses through long distances of expensive underwater transmission lines that have to be ran to bring the power to shore.

Our Solution: EWP's proximity to the shores enables an easier transmission.

Design-related Difficulties

- ♥ The Difficulty: energy devices can extract significant amounts of electricity when the waves hit the buoy directly, which is usually not the case. As a result, the traditional wave energy techniques do not yield their energy continuously .

Our Solution: EWP is applying a floater regulation mechanism, which automatically directs the buoy to the exact directions of the wave, which in turn maximizes the KWh production.

Reliability

✔ The Difficulty: there are some systems being tested that are underwater and out of sight. However, If they are shallow enough such that they become navigation hazards, they will have to have marker buoys – lots of marker buoys.

Our Solution: In EWP's case, the chosen areas will not have the risk of endangering any marine traffic, due to the fact that ocean vessels are always avoiding proximity to ocean structures such as breakwaters

✔ The Difficulty: Storms may cause ocean wave generators to occasionally dislodge from their anchors and become serious navigation hazards.

Our Solution: Eco Wave Power's generators and all technical equipment are located on land, just like a regular power station. This prevents the occasional dislodging from anchors and any further navigation difficulties

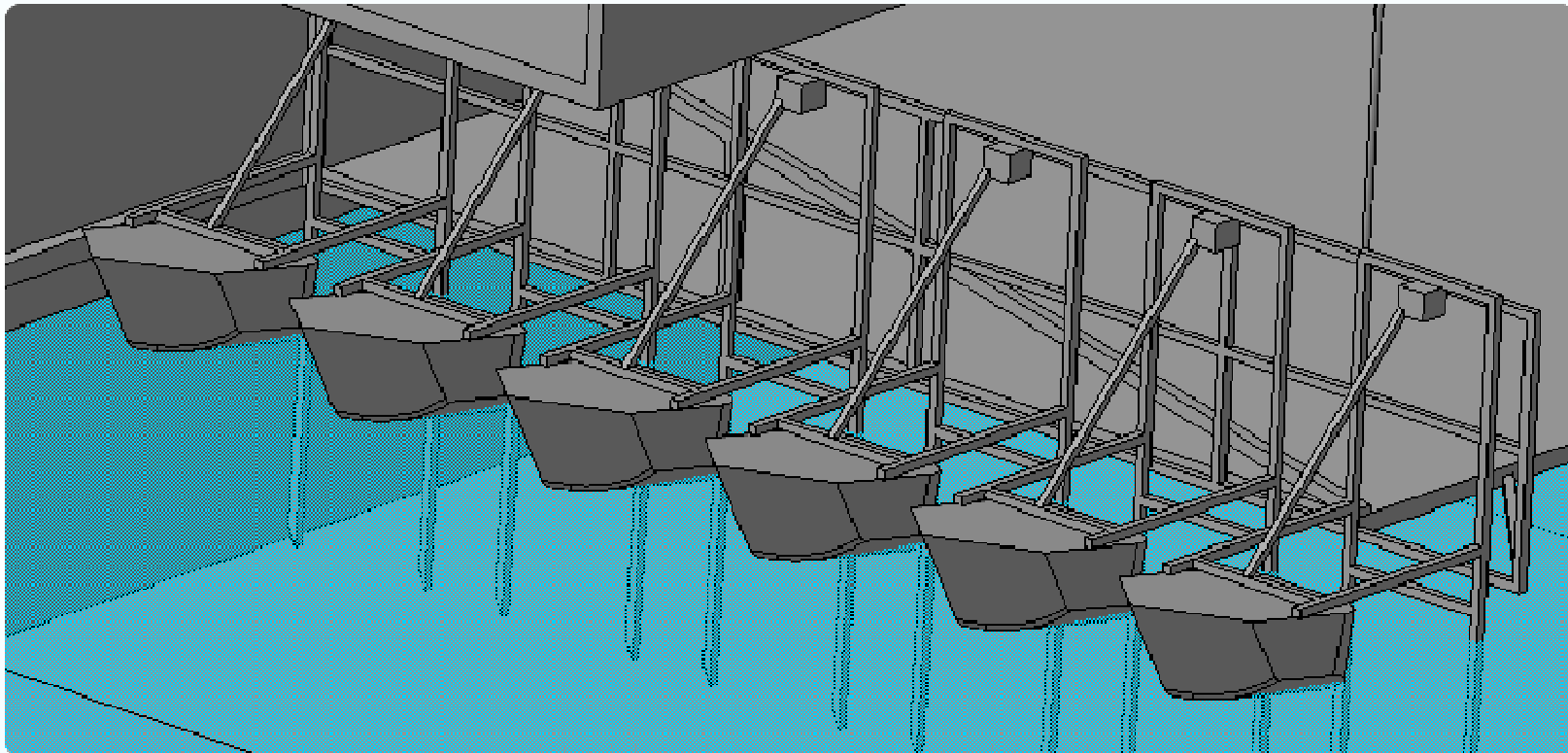
✔ Another difficulty of traditional sea wave power convertors is that the pollution of ocean waters by the release of foreign matter is no longer being tolerated. When such pollution happens, it is difficult and expensive to clean up .

Our Solution: EWP's "Wave Clapper" and "Power Wing" oil tanks, and hydro pneumatic equipment is located on land, just like a regular power station, which significantly minimizes the risk of hydraulic fluid pollution, as well as the risk of mechanical failures. In addition, EWP uses hydraulic fluid that is biodegradable in the marine environment, and therefore is not harmful to it.

Mile-Stones

- ✔ Eco Wave Power is testing its' solutions through the construction of various wave energy systems.
- ✔ EWP has already secured funding for the construction of three sea wave power plants:
 - A. Small-scale power plant, with the purpose of proving the efficiency of the unique floater shapes of Eco Wave Power.
 - B. Medium-scale power plant, was built to examine all the technical components as well as the floaters in larger scale.
 - C. Full size, commercial-scale, sea wave power plant with the ability to supply energy to at least 1000 households.

Modeling



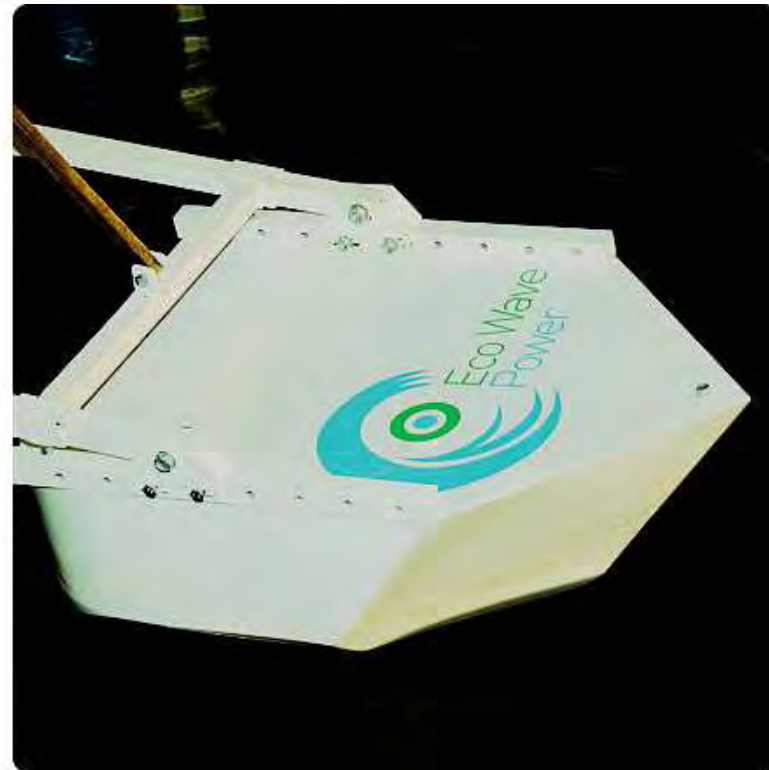
Here is an illustration of our fast progress from basic concept to fully operational models.

Small-Scale Power Plant



This is our small-scale power plant, developed and tested in cooperation with the Kiev Hydro Mechanical Institute. The Protocol submitted to Eco Wave Power, by the Institute, has concluded the experiments as following: "All floaters of Eco Wave Power Company have proved their workability... According to the results of the tests, we have reached a decision to recommend continuing the development of the **green energy generation system** that is based on such principles, and enlarge the model to greater sizes".

The “Wave Clapper” and “Power Wing”



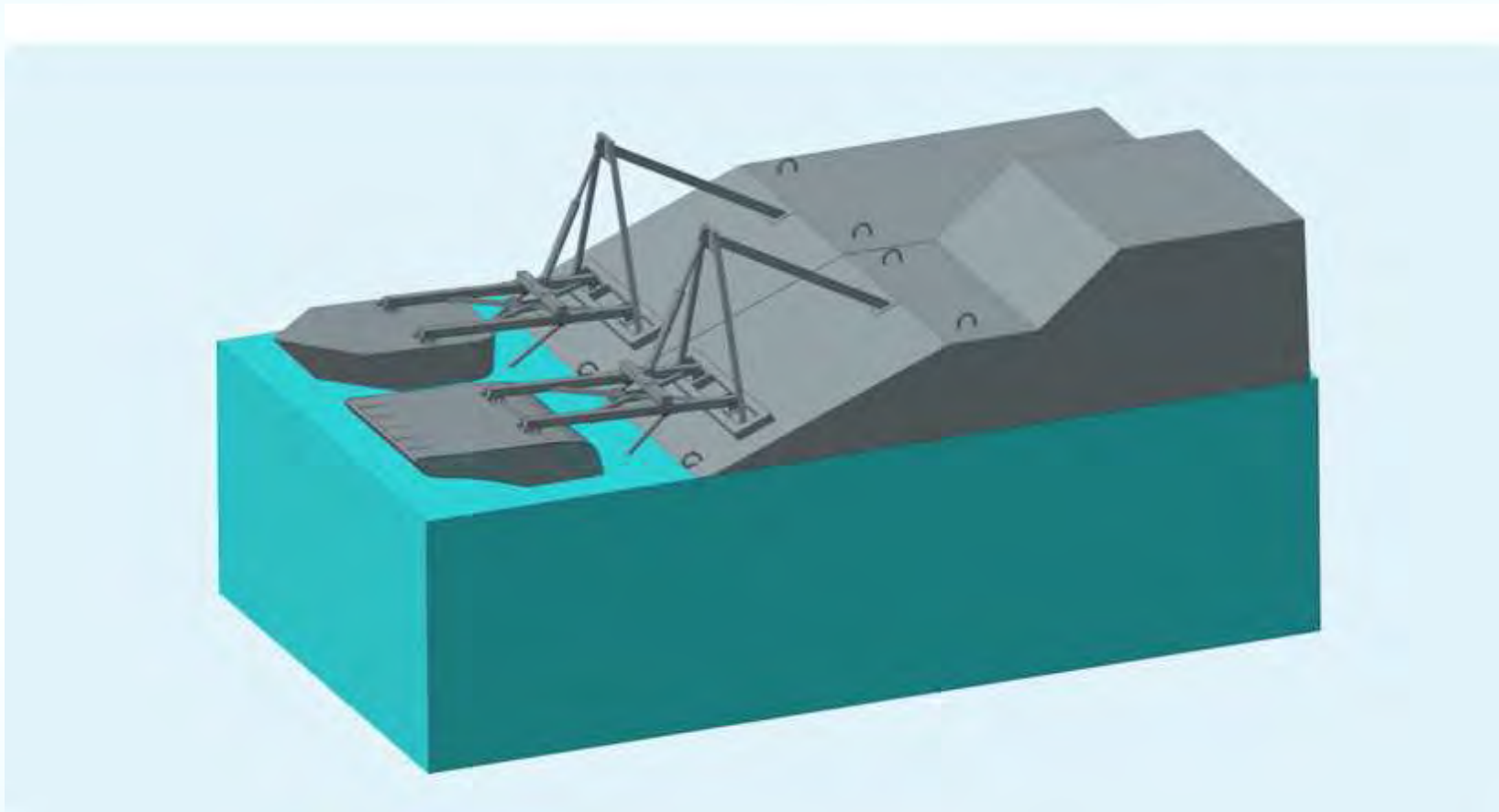
We examined 8 different shapes, and chose the 2 that had the best performance.

Construction



Then, we started the enlargement process of such floaters

Modeling



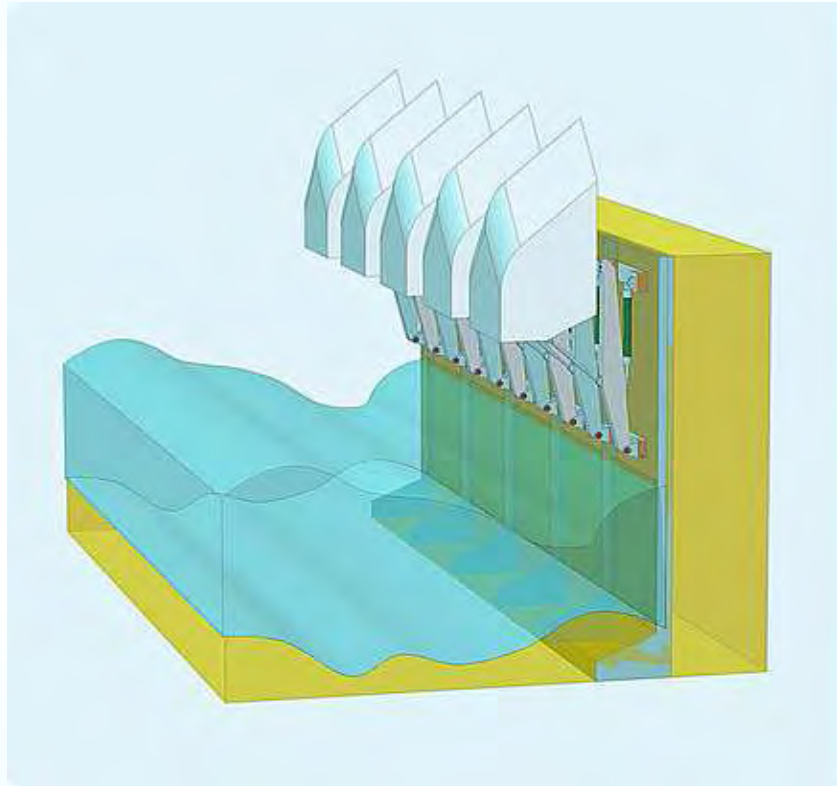
We designed connections that were specific to the location of implementation

Implementation



And eventually tested the fully operational system, that produced 5KW from each floater

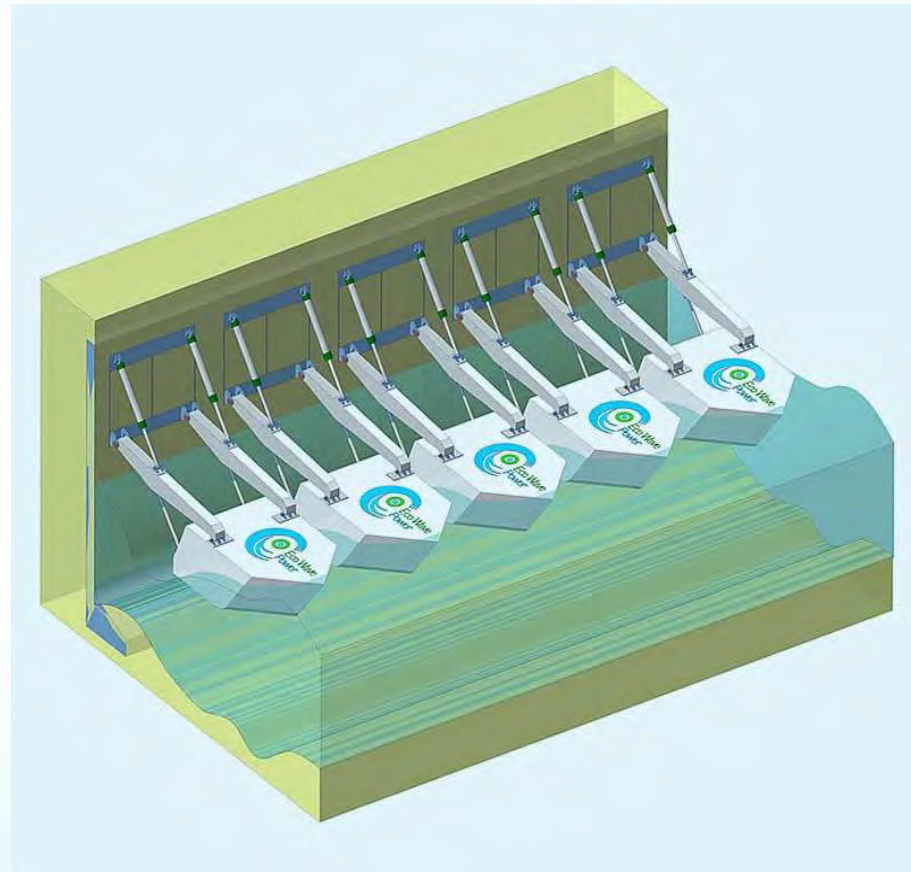
From Concept to Realistic Product



We also tested our storm-protection mechanisms. In this slide, you can see how our modeling came to a realistic product.

Next Phase

Commercial Scale
wave energy generation
system, capable of
providing electricity for
600 to 1000 households.





For Further info:

Please do not hesitate to contact us, at:

www.ecowavepower.com

info@ecowavepower.com

Eco Wave Power
Energy Re-Invented

A new device to produce electrical power from ocean waves: some applications to Italian coasts

Felice Arena^{1,5}, Alessandra Romolo^{2,5}, Alfredo Ascanelli³, Antonino Viviano⁴

^{1,2,3,4} *Department of Mechanics & Materials, Faculty of Engineering, 'Mediterranea' University of Reggio Calabria, Italy*

⁵ *Wavenergy.it s.r.l., Via F. Baracca trav. De Salvo, Reggio Calabria, Italy*
E-mail: 1 arena@unirc.it, 2 aromolo@unirc.it, 3 alfredo.ascanelli@unirc.it, 4 antonino.viviano@unirc.it

In the last decades, the research has directed its efforts and resources towards the possibility to incorporate wave energy converters, for the exploitation of wave energy, into the traditional maritime breakwaters to combine classical use with new opportunities and developments (for example, the Green Ports). Since the nineties, the OWC (Oscillating Water Column) plants were developed at full scale to produce electrical power from ocean waves (see Falcao, 2010 for a complete review).

A prototype was built into a caisson breakwater of the Sakata Port, in Japan (Takahashi et al., 1992); other plants were built in India (Raju and Neelamani, 1992), in Scotland at Islay (Heath et al., 2000), in Portugal at the Azores (Falcao, 2000). A new plant was built in Mutriku (Spain) recently. A new kind of OWC caisson, named U-OWC or REWEC3, which has the advantage to obtain an impressive natural resonance without any device for phase control, has been patented by Boccotti in 2002. This new device UOWC gives performances better than those of a conventional OWC either with small wind waves or with high waves (Boccotti, 2007). The properties of REWEC3 have been verified with two small-scale field experiments carried out in the natural ocean engineering laboratory NOEL of Reggio Calabria off the eastern coast of the Straits of Messina (Boccotti, 2003; Boccotti et al 2007; Arena et al. 2007).

In the paper, a general description is given on the U-OWC devices, and some applications are proposed to the Italian coasts.

Ports for offshore wind applications along the Tyrrhenian coasts of Calabria and Sicily

F.G. Cesari¹, F. Taraborrelli¹, D. Mostacci¹, L. Milella², L. Pirazzi³

¹ (DIENCA Dept., University of Bologna, via Dei Colli n.16 – 40100 Bologna, Italy),

cesfranco@libero.it; ² TRE SpA, Bari, luigi.milella@tozziholding.com

³ (ANEV, V. Palestro 1, 00100 Roma, segreteria.scientifica@anev.org).

Abstract: Ports are necessary for offshore wind farms. We proposed two solutions: dock-yard port and reference port. The dock-yard port has enough areas available for construction, assembling, offshore installation of wind turbines and electrical devices. The reference port could be any port having enough space for the loading and unloading of wind plant components; the aforesaid components could be produced by manufacturers located or not near the boarding sites.

Some ports, in the southern Tyrrhenian sea were considered to clarify the requested needs.

Some examples of dock-yard ports are Gioia Tauro in Calabria and Trapani in Sicily, while Palermo is a typical commercial port to be used for arrival/departures of components. These ones could also arrive/be sent far from Mediterranean area.

1. Introduction

The existing infrastructural plan and its development along major part of Italian coasts offers one of the critical devices to generate new installations and the growth of offshore wind parks. Yet we need new ideas to overcome the actual difficulties in view of a drastic reduction of costs. Traditional approaches could be simply not working or not completely acceptable in this perspective. We need to rethink our policies, embrace new opportunities offered by technology and rethink how to finance them.

In any case we have firstly to re-examine the marine facilities operating along our coasts to select accurately the available solutions, secondly to individuate their main improving for the next future. In an optimistic forecast this attempt should involve policy-makers, business men and technical experts from transports, energy and digital communications, to explore new approaches to infrastructure and the opportunities at present or in a short period of time. It is evident that the main solicitation should be addressed to Governmental organizations like Ministries of Environment, Finance, Interior, Economic Development and Infrastructures/Transport.

The last one does administrative and other tasks related to: protection of the sea from the ship caused pollution; sea ports, maritime property and definition of borders of maritime property, marine insurance and maritime agencies; inland waterways ports; shipping centres on land; airports; means of transport except the tasks which are responsibility of other ministries; telecommunications and post; definition of technical prerequisites and terms of use of facilities, technical equipment and installations of telecommunications and radio communications; legislation of subordinated laws and regulations about concessions for providing public telecommunication services; broadcasting and distribution of radio and television programmes; international coordination for utilization of radio frequency ranges, domestic utilization of radio frequency ranges; issuing of permits for radio stations to domestic and foreign persons; inspection duties; safety of maritime shipping, domestic and international road traffic and roads, except the tasks which are the responsibility of Ministry of Interior, rail traffic safety, air traffic safety, inland waterways traffic safety, telecommunications and post, domestic and international postal and telecommunications traffic and regulation of radio frequency ranges; tasks of Coast Guard (port authorities).

2. Wind farm and infrastructures

Power concentration is coherent with actual technical practice towards cheaper investment costs. Economies of scale achievable through high power wind-plants are evident.

A modern wind-farm requests unit power not less than 3 MW, because of the cost of infrastructures and some components, (commercial turbines are up to 7 MW power today, as V164-7 Vestas in final development), and total wind-farm power is up to several hundreds MW (London Array is the most powerful wind-farm which is being carried out, up to 1 thousand MW, located just outside the estuary of Thames, while it's projected to perform 2 or 3 thousands MW offshore wind plants).

Large Wind-farm projects, to be located especially in Northern Europe seas (North Sea, Irish Sea), have some advantages: high productivity of the site, due to high average wind speeds up to 10 m/s; sea-bed depth lower than 20-30 m; availability of sandbanks or other low depth seabeds at long distances from the shore (up to tens of kilometres from the shore). Composition of the seabed made of sand, silt, clay. These advantages give a competitive benefit to Great Britain and Germany sites, which are attracting wind energy investments in Europe.



Figure 1: Gioia Tauro harbor.

As well as seabed depth determines typology and costs of foundation structures for wind turbines, high distance from the shore determines high costs for electrical connections and energy transmission. It's obvious that the more the distance from the shore increases, the more the length of electric cables increases, and probably also the depth of installation. If distances are not longer than a few miles, the economical weight of cables should be kept down.

Economical weight of cables/electrical devices could be lower in a sandbank having depths lower than 40-50 m, even if at long distance from the shore. Installation could be possible at tens of kilometres from the coast, as the Offshore Bard I plant, which is installed about one hundred kilometres from the Borkum island.

Electrical connections inside the wind-farm are achieved by 20-30 kV alternating current. Alternating current has to be transformed in direct current by an electrical station, to be transmitted onshore. At land, electrical current must be transformed again to alternating current for onshore distribution.

3. Port characteristics for offshore wind applications

The Italian peninsula with its strategic position in the center of the Mediterranean sea could represent a reference country as a starting point, through its ports, for offshore wind installations, not only in Italian sites but in other countries of the basin.

The Italian ports, and particularly those located on the southern coasts, must satisfy a series of requirements in order to meet the offshore wind farm needs. Two of them have to be considered to determine the purpose of each facility. They could be summarized as follows:

- support for all the operations requested by the installation of an offshore wind farm. This is the case of the so called *dock-yard port* for a wind farm to be placed at a relatively short distance from the coast and from the port. The surface of the service space on ground level should be available inside the port area and dimensioned on the basis of the turbines number and the global power of the wind farm. Usually from some hundreds square meter per MW to one thousand is the range considered for actual wind plants. The correct definition of the surface, has to be a compromise with needs envisaged and possibilities offered in reality;
- storage and partial or total assembling in a functionally equipped area of the main components necessary to a wind plant located also in a far offshore site. Due to the size of some components, this area has to be selected with a sufficient surface to allow all the requested operations. This case is corresponding to the situation conventionally named as a *reference port*. This could be also placed as far as from the wind farm site. The actual aim consists in commercial activities based on charge and discharge of components from Italian manufacture industries, for wind farm installations in a port conveniently located and equipped to answer rapidly and efficiently to the requests.

Before describing in detail all the characteristics of the ports it is important to highlight the difference between the first situation –ports, devoted to support the operation of an offshore wind farm located at a short distance- and the second one. In this last approach, the materials will be received and sometimes partially or totally assembled before to be transported towards offshore wind farms located also very far and probably in other countries of the Mediterranean Sea, not too distant like Egypt or Morocco.

In order to satisfy any requirement of the reference port, the logistic infrastructures must be adequate for carrying out all the task requested in terms of support to near and distant offshore wind plants. So, in addition to the analysis of functionality of the harbor (basin depth, operational surface, numbers/dimensions of wharfs, quay-crane availability, etc.) the needs to support the operations of a wind farm (like infrastructures of territory and system of roads in the port zone, known as intermodular connections) has to be preliminary examined. It is of fundamental importance to have a quite large area and the availability of equipment for moving and climbing heavy pieces, and to reach information more exactly as possible on performance of technical equipment existing (and operating) in the port.

The site accessibility is a fundamental aspect in defining the adequate work program for the on land and offshore operations and for the following maintenance activities. The main elements conditioning the connection to the site are:

- national/international airports equipped for cargo system too;
- harbors for the commercial maritime transportation, requested for the arrival of components by sea;
- shipyard and reference port system for goods movement and personnel towards the sea site;
- local/regional road/railways system and transportation connection to the harbor.

A very important issue, which must be considered as a challenging question, depending on the technology used (fixed foundation or floating platform), is the water depth of the harbor. In case of floating platform the water depth could be much higher than in the traditional system.

4. Ports to be selected in support of wind farm construction along the South-Tyrrhenian coast

On the basis of these aspects and also taking into account the geographical position, a series of ports located in the south and main islands of Italy, have been individuated and in particular some detail shall be presented for Gioia Tauro, located in Calabria region, and Palermo and Trapani, sited in northern Sicily. Their main characteristics are shortly presented in manner to have a landscape of all main equipment sufficient to respond to the technical requirements. It is evident that only the port of Gioia Tauro can operate as a dock-yard port for a wind farm construction.

4.1. Gioia Tauro harbor

It is the busiest and largest container terminal in Italy and in the Mediterranean Sea. The Gioia Tauro Port Authority is responsible for managing and operating the port.

Gioia Tauro Harbour contains hundreds meters of quays with alongside depths up to 18 meters. It covers about 440 hectares of land area for containing 1.8 millions square meters of stocking yards. It is connected by road and rail to inland Italy.

In the 1970s, the harbor was initially supposed to serve the iron and steel industry. Declines in the industry, however, led to abandonment of those plans, and the harbor was a “ghost port” from 1973 until the 1990s. In 1994, the Contship Group undertook an effort to convert the port into a container terminal. The first container vessel anchored at the Medcenter Container Terminal in 1995.

Located in the Province of Reggio Calabria at the tip of the Italian “boot,” Gioia Tauro Harbour is the seventh biggest container port in Europe, handling 3.7 millions TEUs of containerized cargo on over three thousands vessels in 2007. The port handles over one-third of Italy’s national traffic, and it is specialized in trade with USA and Far East.

On the busy route between the Suez Canal and Gibraltar, the harbor is on one of the world’s busiest maritime corridors. Traffic increased from 50 ships and 17.000,00 TEUs in 1995 to over three thousands ships and 2.6 million TEUs in 2003. Gioia Tauro Harbour has added over one thousand jobs for the local economy.

The Harbor Terminal contains quays of 280 and 436 meters and surface area of 270 hectares. The terminal offers three deep-water and two short-sea berths sectors (as represented in Figure 2) with alongside depths from 13.5 to 15.5 meters. The terminal includes three state-of-the-art Vehicle Processing Centers spread over the terminals to handle cars before delivery to the end customer. The Terminal’s regular roll-on/roll-off service handles new and used cars.

Continuing investments will assure the position of the harbor in the future. Plans include enlarging the basin and harbor entrance, dredging to 18 meters, lengthening the wharves, and providing facilities for manufacturers and logistics firms with refrigerated goods.



Figure 2: Gioia Tauro Harbour.



Figure 3: Quay in the Port of Gioia Tauro.

4.2. Trapani harbor

Trapani, thanks to its position that is at the same distance from the channel of Suez and from the strait of Gibraltar, can be considered a port “in the center of the Mediterranean center”. Further, the port is located between the traffics that move from North to South and from East to West. This baricentric position gives to the Sicilian port great potentialities, necessary for the development of short sea shipping traffics and all other traffics like general cargo, container and bulk and also cruise and yacht traffic. The port, whose coordinates are lat. 38° 01' 36" N and long. 12° 30' 49" E, has about 1650 m of piers used for:

- Ro/Ro ships, Lo/Lo ships, Cruise Ships and Multipurpose ships for commercial operations,
- Passenger traffic to the Egadi Islands, to Pantelleria and to other ports.

In the port there is a Customs base that is about 90.000 sqm large. This customs instrument is very important for the port. It is located close to the commercial piers and is easily reachable. Thanks to this Customs base, Trapani has been several times appointed as operative base, by many companies.

The works inside port basin are:

- Construction of piers with 12 m draft in Ronciglio area and in the Eastern area, dedicated to commercial traffics.
- Construction of wide areas close to the aforesaid piers;
- Completion of other piers;
- Construction of buildings dedicated to port services;
- Dragging of sea floor in order to reach 12 m draft;
- Improvement of fishing port.

The port of Trapani (2nd category, 1° class; Figure 5), has 1.650 m quays totally available for Ro/Ro, Lo/Lo ships and Multipurpose commercial activities. They are used for passenger lines from and to islands (Pantelleria, Egadi, Ustica), northern Africa, cruises, and for thousands of passengers; actual issue is to reach new destinations in western Sicily, such as Castellamare del golfo, S.Vito Lo Capo, Marsala, Mazara del Vallo, Selinunte.

Quay Sanità and Garibaldi are located in front of the ancient Customs building and of the Historical city centre, together the new Maritime station, in the northern sector of the port you can also see boardings for touristic ferry-boats and hydrofoils.

Passenger traffic is about one million tourists per year. The port is a great stop off for cruise ships passing for Trapani, thanks to its natural structure and available services, as well as an ideal place to receive yachts having different typology and dimensions (Figure 4).

The Trapani outer harbor is limited in the western direction by the Lazzaretto reef and by the Colombaia Quay reef (Figure 6), 240 m long, having quays and bollards for head berthing of cruise ships and waiting ships.

The port has a cove shape, oriented in E-W direction, large from 225 m between the two navigation lights, to 450 m along the East side of the entrance.

It's limited in the northern side by quays Garibaldi, Marinella, and by the slipway, in the southern side by Ronciglio Quay and in the Western side by Sanità wharf.

We can distinguish three zones in the harbour area, as it is also said in the writings taken by the “Pagine Azzurre”. The first one is reserved to passengers' traffic, and it is the one that is perfectly inserted in the historical centre of the city. The second area is reserved to goods traffic, while the eastern area is open to the fishing boats harbor, containing 522 medium-small sized boats. There is also a touristic harbour for 200 boats.

Two graving docks and eight slipways are located inside the port.

The port was constituted in “Port Authority” (DPR 2/04/2003) until the year 2009. It’s a base for Customs and Port Authority. Railway terminal is nearby the port.

We are now giving some information we got by “Pagine Azzurre” (p. 370 and following), the Italian pilot’s book of seas.

The port is made of an outer port (Colombaia quay in West direction, Ronciglio quay in East direction, reef in South direction), a commercial harbour, a fishing boats harbour, and of a touristic harbour. The touristic one extends in the sea area in front of Regina Elena Street. It is protected by a 275 m. reef equipped with some floating wharves, lying parallel to the aforesaid street.

To have a more precise description of the maritime characteristics could be useful to recall the following requirements in manner to have a detailed picture on technical properties of the port (this should be done only for Trapani harbour).

<i>Geographical coordinates:</i> 38°00',39 N 12°30',03 E.
<i>Danger:</i> low sea-depth from 1,5 m up to 10 m extend for 1,5 miles towards south direction from the port, starting from the green entrance light.
<i>Access time:</i> continuous.
<i>Access:</i> it is dangerous to enter into the port in presence of strong SE, SW e NW winds.
<i>Lighthouse and headlamps:</i> 3138 (E 1970) white light lighthouse, for 5 s, 12 miles range, on the Palumbo rock.
<i>Seabed:</i> muddy.
<i>Seabed depth:</i> inside the port and next to the quay from 1 up to 8 m.
<i>Radio:</i> Vhf channel 16 vhf; 2182 HF/SSB; C.B. channel 09 (h. 24).
<i>Boats parking:</i> 450 units.
<i>Prohibitions:</i> it’s forbidden entering into the port and berthing without Portual Authority permission.
<i>Winds:</i> II,III, and IV quadrant.
<i>Ordeal:</i> southwest wind.
<i>Shelter:</i> I and IV dial.
<i>Local experts:</i> pilots by Trapani’s Harbour.
<i>Nearest safe creek:</i> Cala Rossa (Favignana) in presence of SE winds.

4.2.1. Areas reserved to pleasure boats

Marinella Quay is reserved to pleasure boats and it is managed by the Portual Authority of Trapani. In the Eastern zone of the port, some floating wharves are located, managed by the shipyard, as well as next to fishing boats harbor which are managed by Italian Lega Navale and by the shipyard. In addition, you can find two more buoy areas managed by Portual Authority: first one is in North direction from the new green headlight lying on the reef, while the second one is located in North direction from the Colombaia Quay, for pleasure boats berthing.

4.2.2. Services and Facilities

Petrol and gas oil Station on the quay; supply also by tank truck for large quantities – electrical and water devices for supply- quay lighting – slide – slipway – fixed crane – two mobile cranes ranging up to 80 Tons – travel lift up to 250 Tons – open/covered garaging – engines repairs – electrical and electronical repairs – repairs of wooden or steel or fiberglass made hulls – piloting – persons for berthing/mooring – scuba diver – fire services – refuse

collection – meteorological services – hygienic services at the Maritime station – food supply – ice reseller at the fishing boats harbor – car parking out of the port with fee – booth. Ligny tower, you can see in Figure 7, was erected in 1671 on the Trapani cape, as you can read on the inscription present on the main building prospect. This tower was built to defend the town by Saracenic attacks, and it derives its name by Don Claudio Moraldo prince of Lignè. In recent years the tower was used as a headlight station, while today the Prehistory museum is located in this site.



Figure 4: Trapani Port – Cruises.

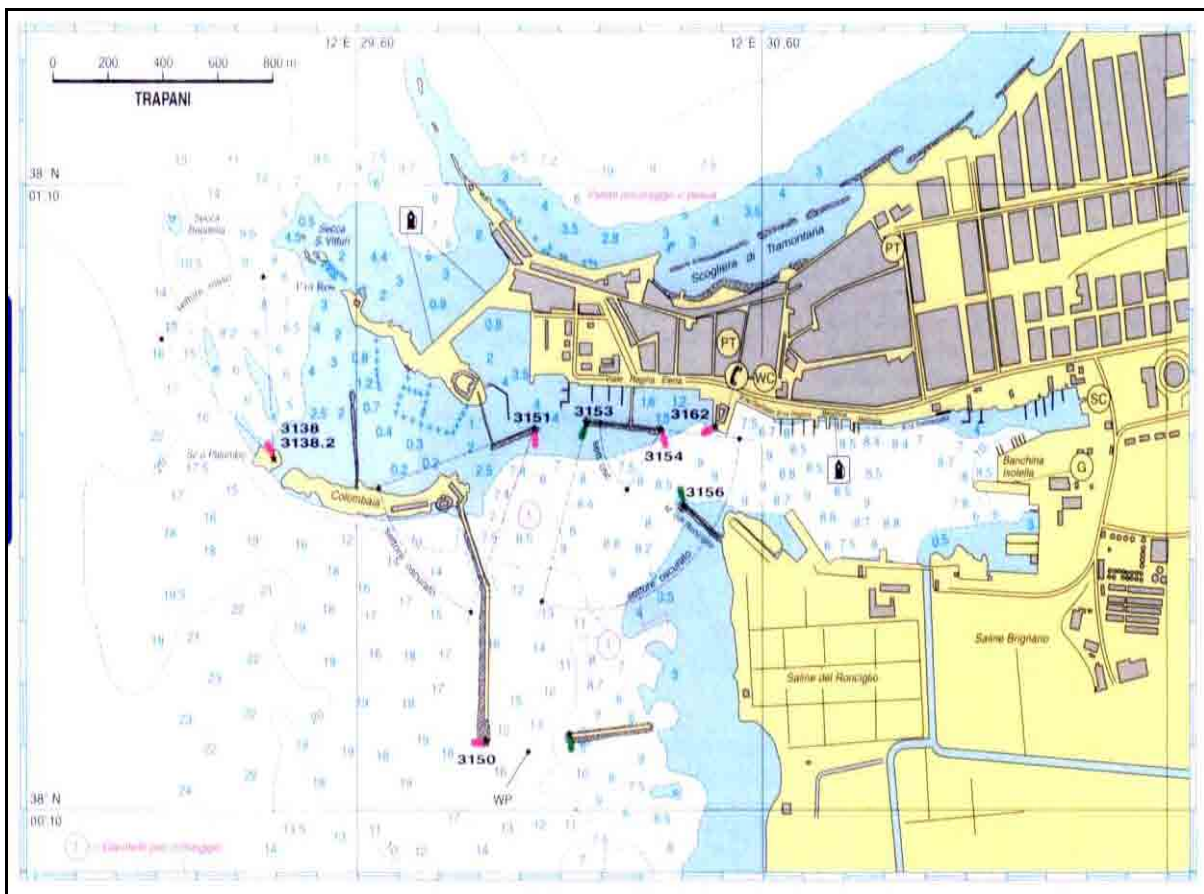


Figure 5: Trapani Port – Map.



Figure 6: Trapani port - Colombara quay reef.



Figure 7: Trapani Port - Ligny tower.

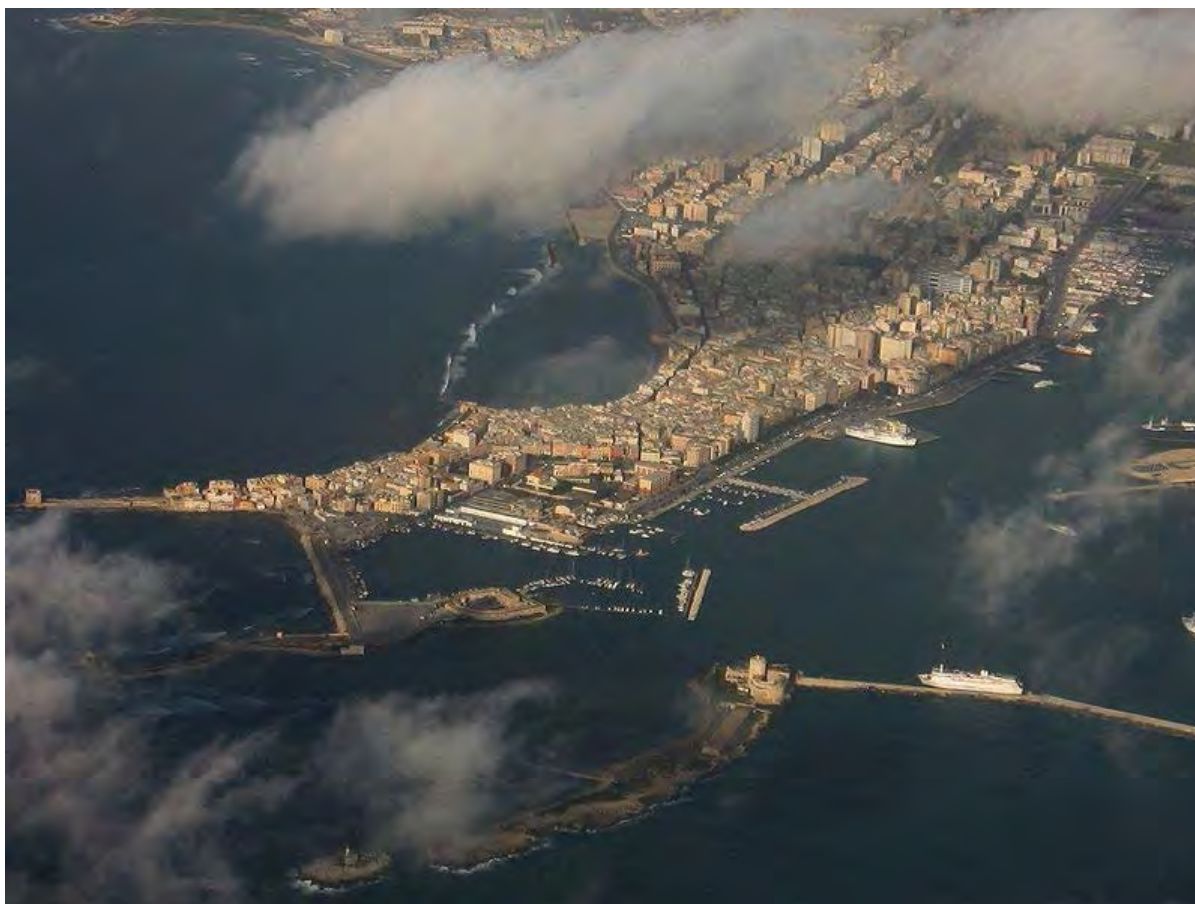


Figure 8: Trapani Port – skyview.

4.3. Palermo harbor

The port of Palermo (geographical coordinates 38°07'41"N - 13°22'10"E), working as a commercial and touristic port, is one of the most important port of call for passenger traffic south of Naples (Figure 9). It's connected by hydrofoil to Eolian islands and to Ustica island, while it's connected by passenger vessels and cruise ships respectively to Genova, Naples, Livorno, Cagliari, Tunisia, and to other Mediterranean places.

The port gives services for commercial traffic (container), passing for Gioia Tauro Harbour and directed all over the world. Fourteen berthing points are available on the 4.000 m quays, different operational landing place are available (six of them for big tonnage ships, two for feeders ships, eight for medium tonnage ships and one of them for large capacity containers). Inside the port you can find working shipyards (Figure 10), which are one of the few examples in the southern-central Mediterranean Sea. Palermo's shipyards (having two dry dock and two floating dock) are owned by Fincantieri, which is working upon construction and repair of cargo and passenger ships (up to 160.000,00 TDW).

Shipyards are also equipped by light and heavy carpenter's shops able to produce precast products, sandblast plant, pipes workshop, electrical workshop, quality control service, equipments for ultrasound and X-Ray checks.

In addition the shipyard is able to organiza a staff for mantainance and emergency works, all over the world.

The global system of Palermo’s landing places is made of S.Erasmo’s small port, which is not fit for industrial uses because of the short depth (2.5 m), laying 1 km far from commercial port, of industrial port, of Commercial port and of Acquasanta Port, last one is the touristic port of the town.

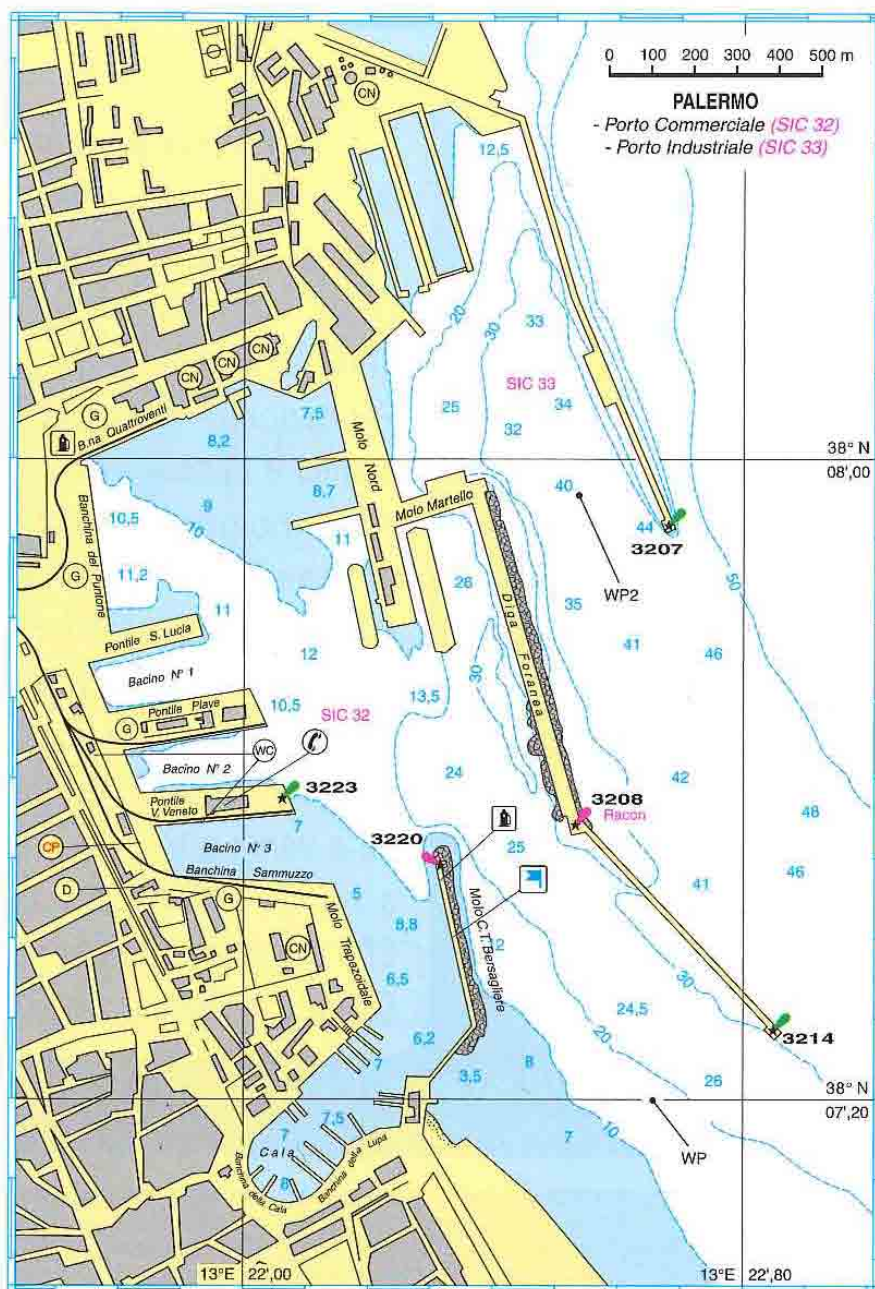


Figure 9: Palermo Harbor – map (Pagine Azzurre).

Conclusions

At the end of this work it is quite clear that several activities must be arranged in order to use the Italian South Tyrrhenian ports for offshore wind bases. A general problem, with the exception of Gioia Tauro, is the shortage of available space for storage of large quantities of main components like nacelles, towers, foundations and blades. In particular the Trapani and Palermo harbours are very close to downtown, which makes the potential acquisition of further areas very difficult or impossible.

However, Italy with its peninsula shape has a very long coastline and other opportunities for offshore wind applications can be found along the Adriatic Sea, while at the same time, could be interesting to investigate the Sardinia Island, where some commercial and industrial ports are located.



Figure 10: Palermo Harbor – Shipyard having a ship in the dry basin.

It is evident that Gioia Tauro and Trapani Harbour are suitable to be used as a dock-yard port for a wind farm to be installed nearby, while Palermo is a harbour for commercial activities. It is important to remember:

- either the yard is located in a harbor area, this is the case of Gioia Tauro;
- or the yard must be connected to a harbor, or to an equipped area able to permit the access and use of marine equipments (adequate seabed depth for marine crafts and boats of different characteristics, jack up, tugs and others), and the loading/unloading of goods as in Trapani harbour.

Then, it is necessary to have docking quays for naval crafts and for transport to the offshore site of components and lifting tools, to have available space for vehicles movement and for marine crafts repair.

In addition to operational needs of land and sea crafts, an accurate review of land logistics should be done especially for direct connection to the yard.

When you use a port, you have to examine the access to permit the mobility of land means carrying the components of the turbines. Blades, more than other turbines' components, need space (for storing and turning of vehicles on the road), due to their dimensions.

As well as the blades, towers need space, while nacelles need less space. These areas are conditioned by installation methods to be used, because of land installation or sea installation.

Our hypothesis would consider the most important regional ports for the aforesaid reasons, and not for the administrative importance. So, for the Calabrian region Gioia Tauro harbor was considered and Palermo for Sicily.

References

1. F.G.Cesari, Maritime and ground logistics of Adriatic and Tyrrhenian ports for windfarm requirements, (*in publication*), 2012.
2. AA.VV., Pagine Azzurre - Il Portolano dei mari d'Italia, Roma, 2007.

Italian off-shore wave energy map, using gauges and numerical model data

Filippo M. Carli ⁽¹⁾, Simone Bonamano ⁽¹⁾, Giuseppe Stella ⁽²⁾, Maximo Peviani ⁽²⁾, Marco Marcelli ⁽¹⁾

⁽¹⁾ *Laboratory of Experimental Oceanography and Marine Ecology
DEB – Tuscia University
Molo Vespucci, Port of Civitavecchia, Italy
phone: +39/0766 366945*

⁽²⁾ *RSE SpA., Via Pastrengo, 9, 24068 Seriate (BG), Italy,
phone: +39/0239927776; fax: +39/0239925440*

*e-mails: fmcarli@unitus.it, simo_bonamano@unitus.it, giuseppe.stella@rse-web.it,
maximo.peviani@rse-web.it, marcomarcell@unitus.it*

Introduction

Marine Energy is one of the most promising resources among the emerging renewable energies. Italy, with his more than 7000 kilometres of coasts could be one of the leading countries, as far as research, development and implementation of this technology is concern. But, at the time Italy presents few initiatives looking to marine energy production.

If compared to North Sea and Atlantic Ocean, Mediterranean Sea shows consistently lower energy levels, but it does not mean that Italy has no possibilities to produce energy from marine renewable resources; it just means that a supplementary effort in scientific research have to be done. Moreover, the lack of an appropriate assessment of the energy trapped in coastal waves and currents, does not permit stakeholders to have a clear vision of the real possibilities of these new technologies along the Italian coasts. In this framework, the implementation of studies concerning non-technological barriers is an urgent need as much as facing technological ones.

In this paper a survey on wave power distribution along Italian coasts is presented. The study is based on the analysis of the wave climate records from the National wave gauges network (RON) and from the wave gauges of the National electricity board (ENEL) and, where measured data were not available, from the numerical data produced within the MEDATLAS Project. The operation leads to the elaboration of the “Wave energy potential map” along the Italian coast. The map describes Italian coasts by dividing them into coastal bands, on the basis of the wave power. It will permit public administrations, involved in energy planning, to have a first estimation of the wave energy availability for electrical power generation. In addition, it allows the private sector to perform cost/benefit analysis and rise to the convenience to invest in wave energy power plants.

1. Background

1.1 Wave energy development: most advanced projects and state-of-the-art of potential assessment studies

Energy converters development

Since the first pioneering designs of a wave energy converter carried out by Yoshio Masuda and Stephen Salter (1974), many progresses have been made. Nevertheless, nowadays only very few attempts have reached the commercial scale.

The most remarkable projects, meaning the most mature technologies, are the Pelamis Wave Energy Converter and the Wavegen Oscillating Water Column (Figure 1). The first one is a 180 meters long articulated pipe, able to convert wave energy into electricity through hydraulic pumps disposed at the junctions of the device.

The successive crossings of wave crest and wave trough forces the pumps producing electrical energy on the vertical axes. Three 750 kW grid connected Pelamis devices were installed off the coast of Aguçadoura, Portugal, for a total installed capacity of 2.25 MW and further modules should have to be deployed. Nevertheless, few months after the installation economical issue brought to a temporary lay-off.

As far as the Wavegen Oscillating Water Column is concern, several years of experiments brought to the implementation of of LIMPET project in at the Islay Island, in UK (Figure 2); while, most recently, a new breakwater equipped with 16 Wavegen turbines, with a rated power of almost 300 kW was built in Mutriku (Spain). The Wavegen device is a typical oscillating water column, made of an air chamber open to the incoming waves. Crests and trough determine continuous compression and decompression of the contained air which is constrained to flow through an upper hole forcing a Wells turbine inside of it.

Anyway, as many different technologies were proposed at an experimental phase, in order to exploit the enormous potential of wave energy, the most versatile classification of devices is the one proposed by the European Ocean Energy Association, with three categories depending upon the installation distance from the coast.



Figure 1: SDE's wave energy converter (Jaffa, Israel).



Figure 2: Overtopping wave energy converter (Wave Dragon project)

By this subdivision the converters are classified as follow:

Shoreline: technologies conceived to be fixed or incorporated along the coastline. They present the great advantage of an easier installation and maintenance, which allows a strong depletion of the costs, although the energy potential can be consistently lower than in deep waters.

Nearshore: these devices are usually installed within 20-25 m from the coastline, at a distance not beyond 500 m. They have the advantage of reducing costs of grid connection and operating and maintenance procedures, while they can catch wave usually higher than in the shoreline. As an example, the Wavegen device has the possibility to be installed both in the shoreline and the nearshore mode.

Offshore: they can exploit the highest possible potential, as wave fronts are totally unaltered. Obviously there is a very higher expense in all the installing phases as grid connection and mooring involve a steep rising of the costs; the same is true in relation to the maintenance costs which are pushed by the necessity of carry out every operation through vessels and boats. Pelamis converters fit this category, Aguçadoura plant was standing on a seafloor exceeding 50 meters.

Wave potential energy assessment

Taking into account the available potential energy assessment along the Italian coasts, some studies have been already carried out. Different approaches have been employed, mostly depending on whether experimental data or model data are the mean source of information.

A measure-based method consists on the elaboration and computing of data produced by wave gauge buoys, usually deployed in deep water but not very far from the littoral. A model-based method is usually settled on basin-scale numerical models, often considering the entire Mediterranean Sea, dealing with nesting processes in order to enhance the spatial resolution.

Pros and cons of the two approaches categories are self-evident. Measured-based ones provide a very accurate evaluation of wave climate in the zone of installation of the wave gauge buoy; presenting data in a punctual way, but the information tends to get inadequate moving far from the instrument. On the other hand, model-based approaches can present a geographical wide spread description of wave parameters, but the results can be partly affected by the unavoidable approximation needed to run the models. Without system malfunctioning, measured data are always more reliable than computed ones, but they are not always available on an adequate temporal and spatial scale.

As regards measure-based approaches, the most important studies carried out in Italy are the "*Italian Wave Atlas - Analysis of 12-year wave measurements by the Italian Wave Network*" (Piscopio et al. 2002, APAT) and "*Assessment of Wave Energy around Italy*" (Vicinanza et al., 2009). Both of these projects evaluated the wave potential on the basis of the data produced by the Italian Wave Network (RON), the first analysing eight buoys for a twelve years time series, the second using all the fifteen buoys installed until 2008.

With respect to the model-based approaches, MEDATLAS and WERATLAS are particular noteworthy. MEDATLAS is a joint project involving Italy, France and Greece which have developed a Mediterranean Atlas based on the average distribution of spectral parameters computed through the European Centre for Medium-Range Weather Forecasts (ECMWF) WAM model. It provides information on wave climate, not directly computing the associated wave power. WERATLAS is the result of an EU funded research project involving Italy, Greece, Norway, Ireland, Scotland and Portugal. It has produced wave power distribution maps for European seas, including the Mediterranean Sea.

The largest part of the data is derived via ECMWF's WAM model.

1.2 Available data

The main source of data on wave climate in Italy is undoubtedly the Italian Wave Network (RON) which operates an array of 15 wave gauge buoys installed along the Italian coasts. The first eight buoys were deployed in 1989 and then added with further seven devices, for this reason the time series is not the same for all the measurement sites. Wave height, peak and mean period, direction and the other spectral parameters are computed in a continuous way providing a constant monitoring of wave climates. Data are freely available on the RON website www.idromare.com.

Because of the high variability of Italian coasts, integration to the spatial and temporal season in some zones is required, in order to provide a better coverage and more comprehensive analyses of wave power distribution. For this reason in this work the RON database was integrated with information provided by the National energy board (ENEL) which since the seventies began to install monitoring buoys in deep waters, mostly corresponding to fossil fuel power plants or electrical infrastructures. Thanks to this integration, a comprehensive assessment of wave power along the Italian coast has been possible, both under the spatial and temporal scale.

The distribution of the wave gauge buoys used to generate the necessary database is presented in the map of Figure 3.

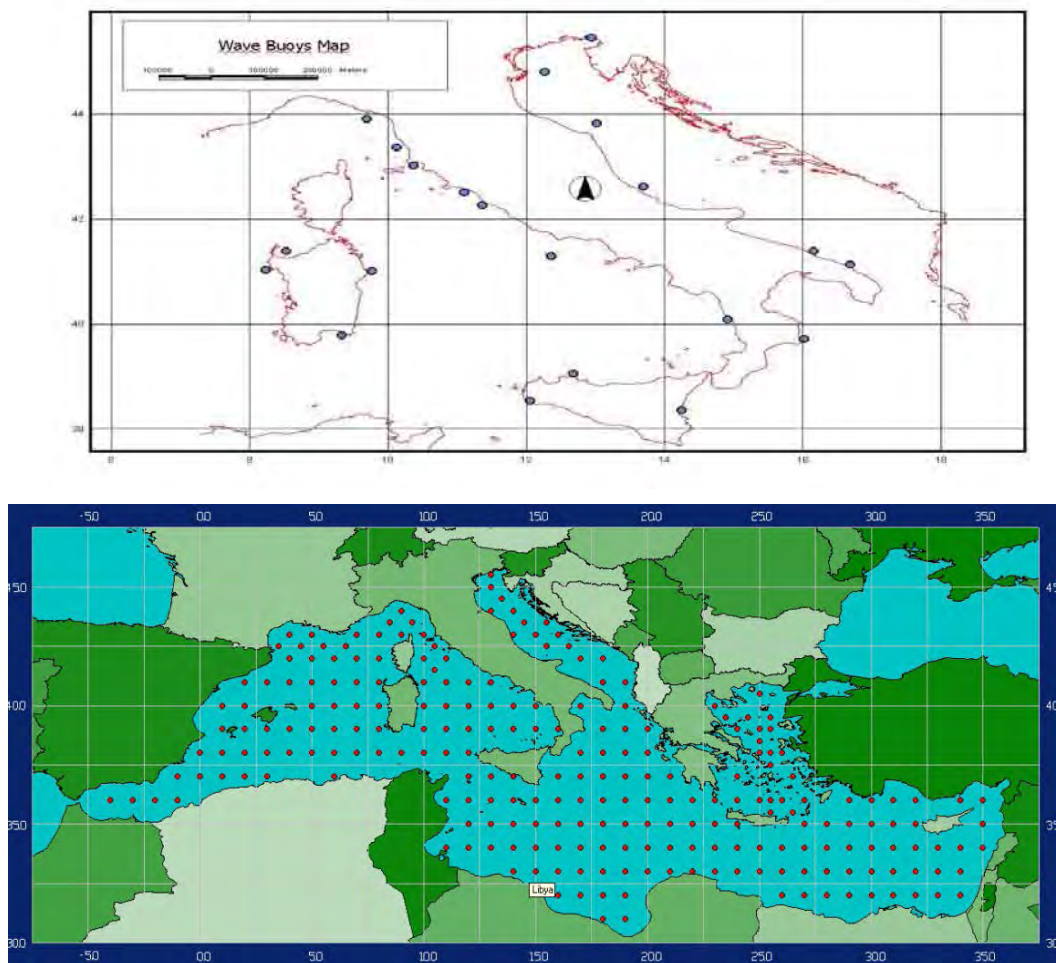


Figure 3: Map of the wave gauge stations used in the present work and of data points in MEDATLAS.

After the integration of databases, some traits of coast still resulted uncovered by data distribution. Lacks in direct measures were overcome through the statistical analyses carried out with numerical models in the MEDATLAS Project. The result is an array of 30 data points along the whole Italian coastline. As stated above, it was led between 1999 and 2004 by a consortia of six companies located in France, Italy and Greece. The main objective was to provide reliable long term wind and waves statistics at specified points of the Mediterranean Sea at practically every offshore location (at about 50 km intervals). This atlas presents the results of the statistical analysis carried out on wind and wave data, spanning a ten year period collected and analysed by the participants. For further information on MEDATLAS should be found in the references section.

2. Wave potential computing

2.1 Data elaboration

The amount of data collected for the scope of this work needed to be screened and selected before its use in wave power computing. To have a clear view of the real wave climate in the area of the buoy, some operations have been carried out, such as spikes erasing and functioning time percentage evaluation.

Once out of scale data are examined and eventually corrected, it is very important that the observing time series is made coherent by assessing the lacks of information. Malfunctioning wave gauge buoys, problems with mooring, communication obstacles, and extreme weather conditions can bring to a lack in the spectral parameters acquiring. For this reason obtaining a continuous and complete assimilation of data is practically impossible. The absence of some information was weighed and analysed and differential distribution of the seasonally missing data has been analysed. In this way, a reasonable distribution of data along the year has been possible to obtain.

Another issue to be considered is the different acquisition time range of the wave gauge buoys. As regards the RON devices, it has to be noted that they registered wave parameters every three hours until 2003, while this time step was lowered to half an hour, after the 2003 modernization of the network. For this reason, has been chosen to work with event frequencies rather than with total number of events.

After data normalization, the wave power evaluation procedure consisted of a series of five matrixes. The first matrix is the double parameters table, in which for every sea state, identified by significant wave height and peak period ranges, the number of events registered is given. The second matrix presents the above mentioned frequency occurrence of these sea state, expressed in terms of n° events of a sea state (H_s, T_p) /total n° events; the third one is the generic wave power for every sea state. The fourth one presents the effective wave power, computed by multiplying the frequency by the generic waved power, for every cell of the matrix. In the last one, additional information is given, describing the annual energy in each of the cells, considering the total number of hours in one year.

2.2 Computing formula

From a theoretical point of view, in the field of wave climate assessment studies, several variances on the definition of the wave power were proposed. Differences are mainly due to the different interpretation of the spectrum and the associated approximation. In this work has been adopted the methodology used in the *"Wave Data Catalogue for Resource Assessment in IEA-OES Member Countries"* (2009), published by the Ocean Energy System – International

Energy Agency (OES-IEA). In deep water, when depth is higher than half wavelength ($d > L/2$), wave power P can be computed in terms of significant wave height and energetic period:

$$P = \frac{\rho \cdot g^2}{64 \cdot \pi} \cdot H_s^2 \cdot T_e [W / m]$$

Seawater density is assumed to be $\rho = 1025 \text{ kg/m}^3$, and the gravity acceleration is $g = 9.81 \text{ m/s}^2$. Consequently wave energy flux for length unit of wave front is computed as follow:

$$P = 0.49 \cdot H_s^2 \cdot T_e [kW / m]$$

Where, H_s is expressed in meters and T_e in seconds.

In oceanography dataset, energetic period is usually not specified so, when the spectrum shape is unknown, it has to be derived on the basis of other known parameters. For example, in the drawing of “*Atlas of UK Marine Renewable Energy Resources*” (2004), the energetic period was assumed to be $T_e = 1.14 T_z$, where T_z is the average period of the spectrum.

In the present study, the energetic period is evaluated following the criterion described by A. M. Cornett in the work “*A Global Wave Energy Resource Assessment*” (Canadian National Research Council, 2008), that is in function of peak period T_p as follows:

$$T_e = \alpha \cdot T_p$$

α coefficient depends on the shape of the wave spectrum: $\alpha = 0.86$ for a Pierso-Moskowitz one, with α tending to 1 with the narrowing of the spectrum. For example, Hagerman (2001) assumed $T_e = T_p$ in evaluating wave potential in southern New England. In the work of Cornett a more conservative assumption was made, for which $\alpha = 0.90$, meaning $T_e = 0.9 T_p$, corresponding to a standard JONSWAP spectrum, considering a peak factor $\gamma = 3.3$.

For the evaluation of every sea state (i) associated energy, wave power, function of $H_s(i)$ and $T_e(i)$, was multiplied by its specific occurrence frequency $f(i)$, and afterwards by the duration associated to that specific sea state. The energy summation of every sea state represents the average annual available energy $E [kWh/m]$, expressed by the following formula:

$$E = \sum P_i \cdot f_i \cdot 8760 [kWh / m]$$

where P_i is the associated power for every sea state and $f_i = n_{event} / n_{total}$ is the corresponding frequency. In the same way, the average annual available power $P [kW/m]$ is obtained from the summation of the multiplication of single sea state's power P_i with its own frequency f_i .

3. Results

By repeating the above described methodology for every data point (both measured and computed), a global evaluation for Italian coasts was made possible. In the following Figure 4 synthetic results are presented the, for both wave power and wave energy, computed at each data point.

<i>Data Point</i>	<i>Database</i>	<i>Yearly Power (kW/m)</i>	<i>Yearly Energy (Mwh/m)</i>
Sant'Antioco	MEDATLAS	12.09	105.91
Alghero	RON	11.74	102.86
Marettimo	MEDATLAS	7.88	69
Capo Passero	MEDATLAS	6.92	60.61
Golfo di Genova	MEDATLAS	6.31	55.31
Mazara del Vallo	RON	5.49	48.13
Siracusa	MEDATLAS	4.61	40.37
Stromboli	MEDATLAS	4.44	38.94
Capo Palinuro	MEDATLAS	4.22	36.95
Golfo di Taranto	MEDATLAS	4.05	35.51
La Spezia	RON	3.85	33.71
Ponza	RON	3.77	32.98
Palermo	RON	3.65	31.98
Fiume santo	ENEL	3.46	30.34
Crotone	RON	3.37	29.49
Cetraro	RON	3.15	27.63
Civitavecchia	RON+ENEL	3.12	27.33
Piombino	ENEL	3.08	27
Punta della Maestra	RON	2.75	24.05
Ancona	RON	2.6	22.82
Monopoli	RON	2.57	22.5
Catania	RON	2.43	21.27
Ortona	RON	2.33	20.44
Montalto	ENEL	2.28	19.97
Marina di Cecina	ENEL	2.18	19.09
Siniscola	RON	2.02	17.7
Brindisi	ENEL	1.49	13.02
Cagliari	RON	1.44	12.58
Bibione	MEDATLAS	1.12	9.81
Punta Sdobba	ENEL	0.17	1.47

Figure 4: Yearly wave power and energy associated to each data point along the Italian coast.

3.1 Map of wave energy potential along the Italian coast

A wave energy potential map was drawn by assigning a portion of coast to each data point, where the wave climate can be considered representative. As a starting approach, it has been used the APAT (Italian Environmental Protection and Technical Services Agency) geographical zoning presented in the work “*Coasts atlas: wave motion off Italian coasts*” (2006), that uses data from only the RON network. Considering that in the present study, seven additional wave gauges from ENEL has been used, the APAT zoning was integrated and the qualitative zones were slightly modified in order to obtain a better resolution of the assessment.

Nevertheless, when some parts of the Italian coastline are not covered by any wave gauge buoy, MEDATLAS data filled the lack.

The following Figure 5 reports the map of the mean annual wave power potential distribution along the Italian coast.

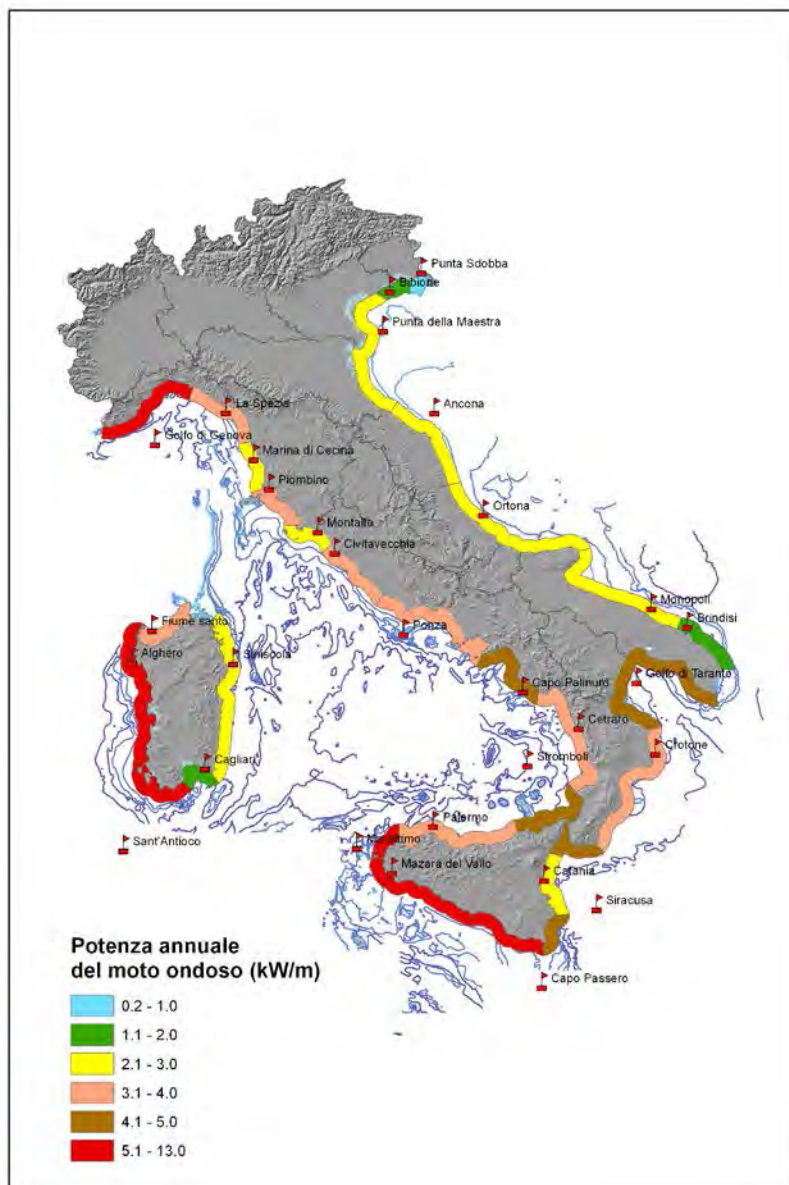


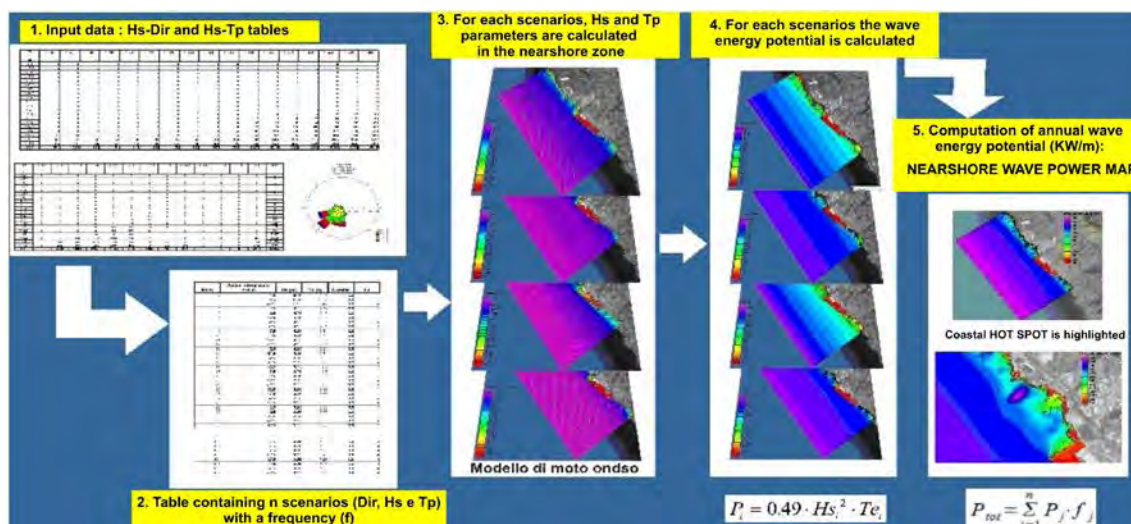
Figure 5: Map of the mean annual wave power distribution along the Italian coasts [kW/m].

When analysing the previous map, has to be underlined that wave height, from which power distribution depends, is tightly linked to the available dataset, which is valid for offshore conditions where the buoy are located. This means that features such coast line orientation, buoy's distance from the shoreline, see bottom bathymetry and coastal morphology, will certainly affect the evaluation of the available wave power along the Italian shoreline. For this reason, the values reported in the map have to be considered as indicative mean annual power level for that zone, making clear that still strong differences in the effective wave potential can easily take place within each sector.

4. Work in progress

The map shown in the present study has to be considered as the first step in a process leading to the evaluation of the wave potential in the Italian coastal waters. Indeed, for the Italian typical wave climate, most suitable wave energy converters seem to be those conceived for the installation on breakwaters, coastal protection works or other marine structures. Considering that these kinds of infrastructure are usually located close to the shoreline, shallow waters effect on wave propagation needs to be considered. Future developments will bring to the realization of an atlas of the nearshore wave energy potential along the Italian coast.

At present, a methodology for the investigation of shallow waters wave power, through numerical models, has been set up. Simulations on wave propagation through coastal zones in a study area are currently undergoing, and will bring to the definitive tuning of a stable methodology. Last step will be the drawing of an Italian wave power in coastal zone atlas.



5. Conclusions and future developments

From the analyses of the results of the survey on wave power distribution it is possible to draw some conclusions on the offshore availability of the resource.

If results of wave power computing are compared to fetch direction and length at each data point, the atlas looks coherent with the awaited wave power values. As it was predictable, the two sites in western Sardinia shows the higher levels (up to 12.09 kW/m), consistently above the first data point outside that region. Northern and southern Tyrrhenian Sea are quite energetic, and can be considered as the second most intense regions in Italy, with 7.88 kW/m in Marettimo (northern Sicily) and 6.31 in Genova's gulf. Proceeding from boundary sites to central Tyrrhenian Sea wave power levels go down for the shading effect of the Corsica-Sardinia barrier; wave power in this region usually ranges from 3 to 4 kW/m. Adriatic Sea is always less energetic than western waters, with wave power levels that never exceed 2.6 kW/m, and values never differs so much anyway. Ionian Sea shows wave fields comparable to southern Tyrrhenian with the Taranto's gulf data point standing on levels above 4 kW/m.

Future developments on this work are directed to the nearshore wave power map. Offshore data, presented in this work, will be used as input for wave propagation numerical models, in order to obtain a qualitative classification of Italian coasts in shallow water. This will help the stakeholders involved in marine energy sector to focus their efforts, by promoting the nearshore technologies suitable for Italian wave climates.

As coastal zone are very sensitive areas, the future of studies on non-technological barriers will also be focused on the possibility of integration of wave energy devices with the ecological equilibrium of coastal systems.

References

1. ABP Marine Environmental Research Ltd.: "Atlas of UK Marine Renewable Energy Resources: Technical Report", Report No. R.1106 prepared for the UK Department of Trade and Industry (2004)
2. APAT – Dipartimento di Tutela delle Acque Interne e Marittime - Servizio Difesa delle Coste: "Atlante delle coste: Il moto ondoso a largo delle coste italiane" (2006)
3. Bedard R. et al.: "Offshore Wave Power Feasibility Demonstration Project, Project Definition Study, Final Summary Report" EPRI Report E21 EPRI Global WP 009 – US Rev 1, Electric Power Research Institute Inc. (EPRI), Palo Alto (USA) 2005
4. Cornett A. M.: "A Global Wave Energy Resource Assessment" (Canadian National Research Council, (2008)
5. Franco L., Piscopia R., Corsini S., Inghilesi R., L'Atlante delle onde nei mari italiani - Italian Wave Atlas, Full Final Report by APAT-University of Roma Tre, sponsored by AIPCN Italian Section and Italia Navigando, Roma 2004. , APAT
6. Vicinanza, D., Cappiotti, L., Contestabile, P. (2009). "Assessment of Wave Energy around Italy", 8th European Wave and Tidal Energy Conference, Uppsala, Sweden.
7. Carli F.M.: "Stato dell'arte della produzione di energia rinnovabile da fonti marine, analisi delle soluzioni tecniche adattabili alle coste italiane e caratterizzazione energetica del litorale laziale" – Tesi di Laurea, Facoltà di SS.MM.FF.NN. Università della Tuscia (2009)
8. Carli F.M., Bonamano S., Marcelli M., Peviani M.A.: "Existing Technologies for Marine Energy Production and Potentialities of Development Along the Italian Coasts" OWEMES (2009)
9. Contini P., De Girolamo P.: "Caratterizzazione climatica e modellistica litoranea delle coste laziali" - Convenzione di ricerca tra l'Assessorato alle opere e reti di servizi e mobilità della Regione Lazio e il Dipartimento di idraulica, trasporti e strade dell'università di Roma "La Sapienza" (2001)
10. Guandalini R., Peviani M., et al.: "Indagini per la valutazione del potenziale di producibilità energetica dal moto ondoso e dalle correnti marine, lungo la fascia di acque territoriali italiane" – RdS 10000264 (2010)
11. Guandalini R., Agate G, Peviani M., Carli F.: "Valutazione del potenziale di producibilità energetica dal moto ondoso e dalle correnti marine dei mari italiani" – RdS 11000312 (2011).
12. Masuda Y.: Wave-activated generator. Int. Colloq Exposition Oceans. France: Bordeaux (1971)
13. Meghella M., Peviani M., Carli F., et al.: "Roadmap della ricerca e dell'innovazione in materia di fonti energetiche rinnovabili "emergenti" in Italia"- RdS 08005964 (2009)
14. Ocean Energy System – International Energy Agency (OES-IEA): "Wave Data Catalogue for Resource Assessment in IEA-OES Member Countries" (2009)
15. Piscopia et al. : "Italian Wave Atlas - Analysis of 12-year wave measurements by the Italian Wave Network" (APAT, 2002)
16. Salter, S.H.: Wave Power. Nature (1974)

Special Session: Mediterranean Marine Energy Technologies Perspective

Chairmen: A. Lazzari, C. Borri

Presentations by:

- GSE: G. Montanino, *IT RES Support Mechanisms*
- IEA Wind: W. Popko, F. Vorpahl, J. Jonkman, A. Robertson, *OC3 and OC4 projects - Verification benchmark exercises of the state-of-the-art coupled simulation tools for offshore wind turbines*
- IEA OES: A. Brito e Melo, *Implementing agreement on Ocean Energy Systems*
- MARINET: T. Lewis, *Marine Renewables Infrastructure Network*
- OMC: E. Titone, *Renewable and Fossil Resources: Opportunity for Synergy and Integration*
- IET: M. Fiorini, *On the European Union Maritime Spatial Planning: are EU oceans and seas shrinking?*

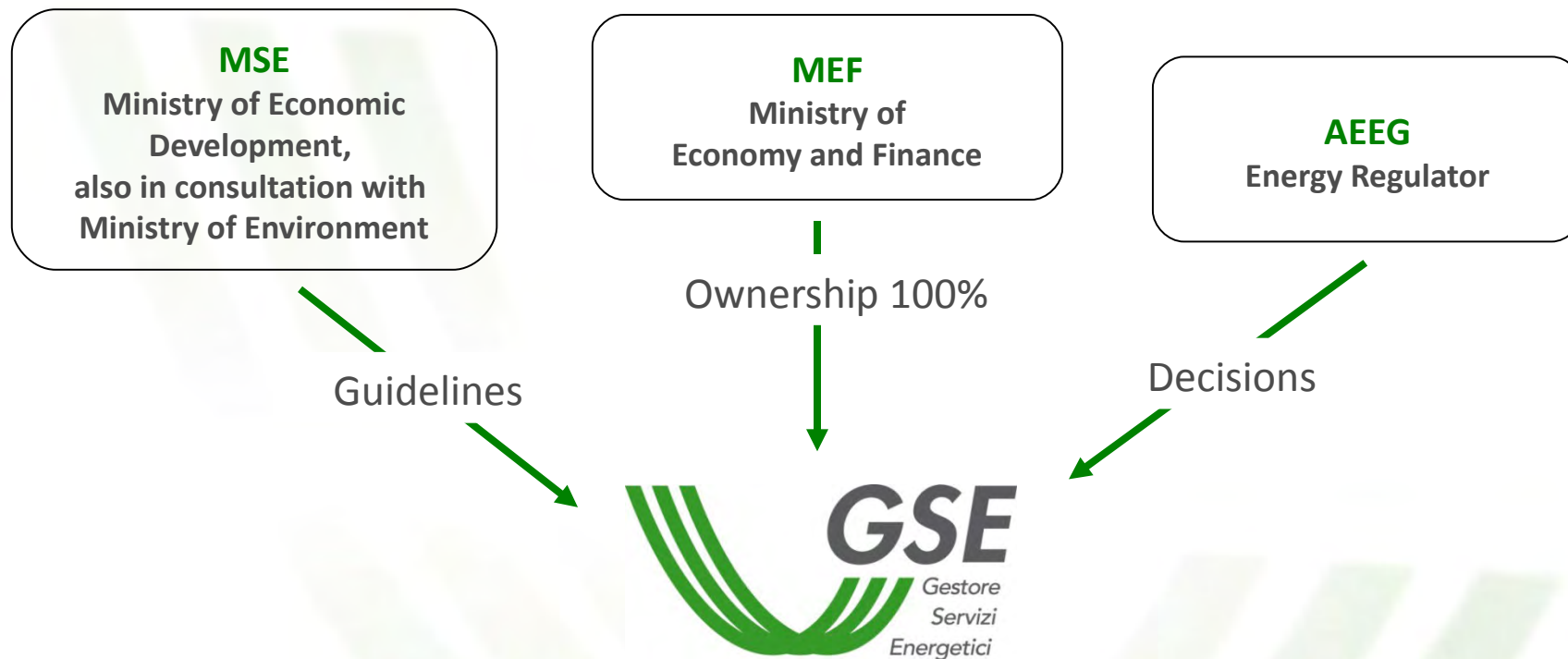
IT RES Support Mechanisms

Gerardo Montanino

GSE, Head of Operational Division

1. **GSE – the Energy Services Operator**
3. **Italian RES targets and results**
4. **Current RES Support Mechanism and Updating**

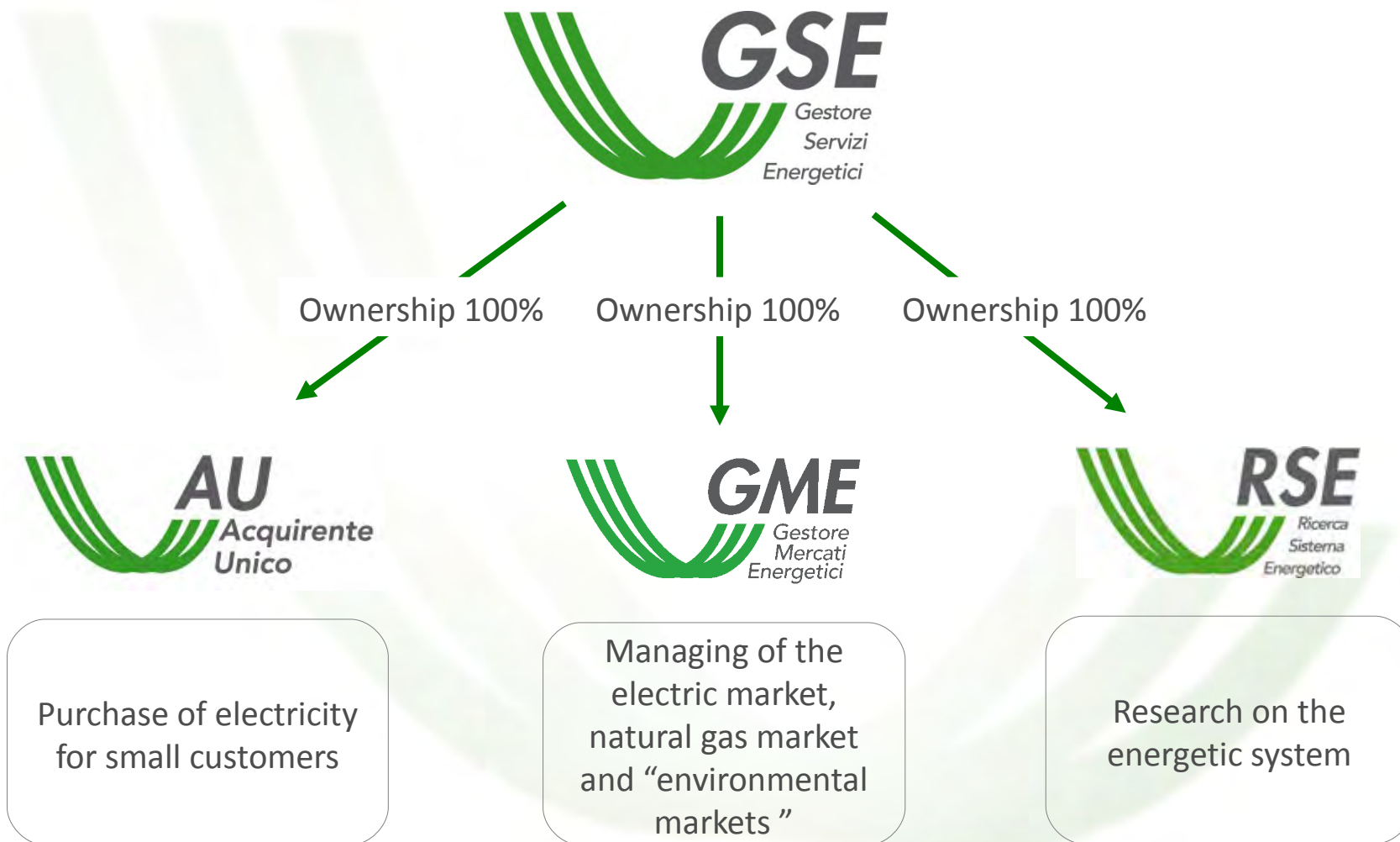
The organization



MISSION

GSE promotes the development of renewable energy sources in Italy, by granting economic incentives, supporting the policy makers and organizing awareness campaigns on sustainable use of energy

The group



Managing of different systems for the promotion of RES, CHP and Energy Efficiency

(qualifying plants, carrying out technical inspections on plants, incentives granting, re-selling in the market of the RES-electricity sale, collecting different types of data from plants through a satellite system, etc.)

▪ **Support schemes for RES electricity**

- **Green Certificates:** issuing GC and monitoring compliance of producers and importers obligated;
- **Feed-in Tariff** for small plants (up to 1 MW);
- **Fixed Feed-in-premium** (“Conto Energia”) for PV and thermodynamic solar plants;
- **Sliding Feed-in premium** for all RES plants since 2013 (Min. Decree 2012.07.06)

▪ **Energy Services for RES and CHP electricity**

- **Net-metering** system for electricity generated by RES and CHP plants up to 200 kW;
- **Dedicated Electricity Intake:** purchase at average market price of electricity from RES and other plants (producers opting for electricity sale through GSE).

▪ **Support schemes for thermal RES and Energy Efficiency**

- **White certificates** and other **specific incentives** (work in progress).

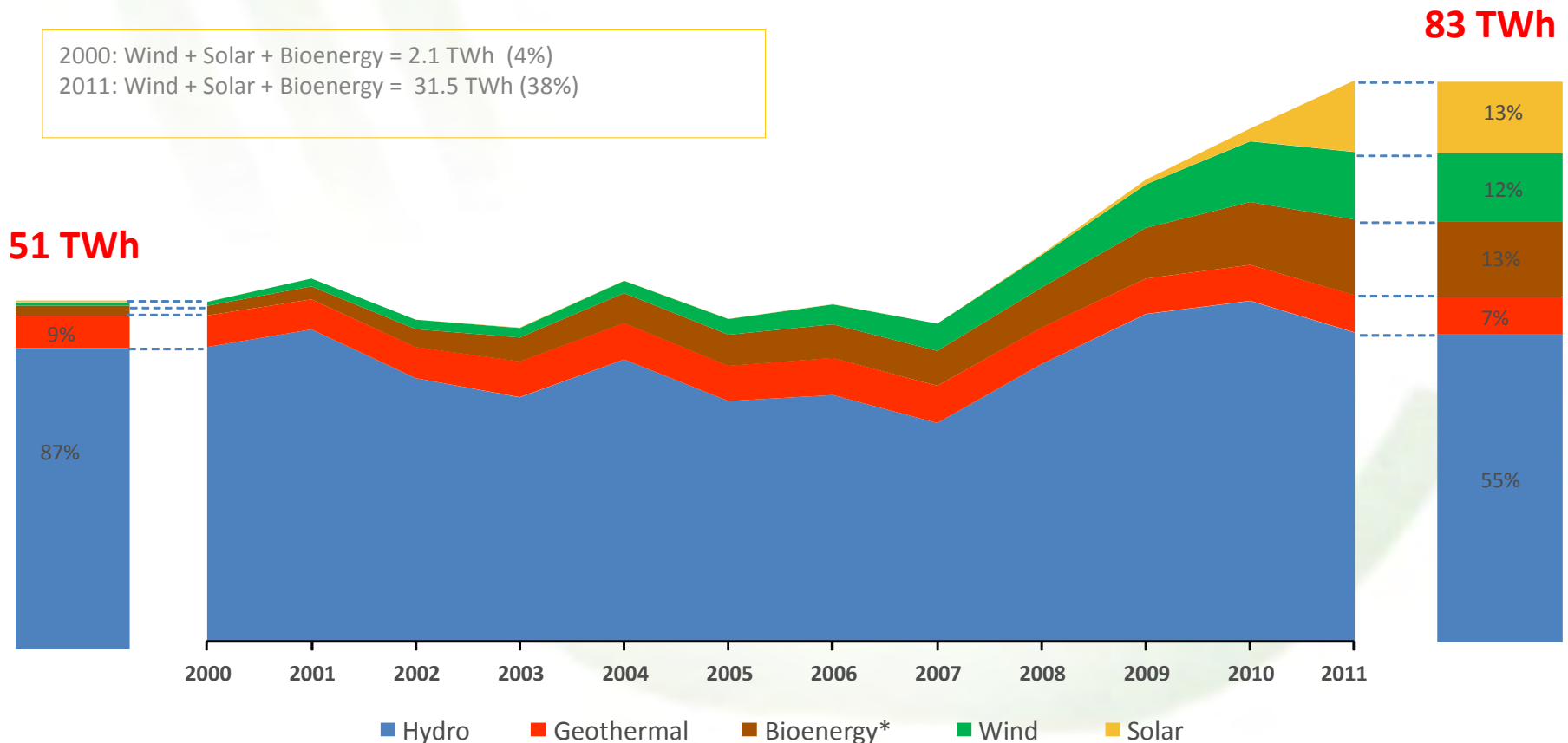
Not only economic support for RES: many other activities

- **International activities:** international relations; participation in the energy projects funded by EU as well as in the main international associations of the sector (IEA, OME, AIB, etc.)
- Support to the **institutional policy makers**
- **Studies** on energy topics (costs and incentives at international level, supply chains and jobs creation, environmental impacts, forecasts and predictions, certification schemes for biofuels, etc.)
- **Statistical monitoring** of RES in the electric, thermal and transport fields, at national and regional level, to follow the approach to the Italian national and regional energy targets
- Support to the **Public Administration**, by supplying specialist services in the energy sector
- **Information** and **training:** promotion of RES and EE (workshops, reports and guides, training, dedicated web-page on incentives, authorization procedures and best practices, etc.)

Growth of total gross RES electricity production

In 2000: **51 TWh** => in 2011: **83 TWh**
Total increase of around 32 TWh (+62%) due to new RES

2000: Wind + Solar + Bioenergy = 2.1 TWh (4%)
 2011: Wind + Solar + Bioenergy = 31.5 TWh (38%)



* Bioenergy: solid biomass, biodegradable part of waste, biogas and bioliquids

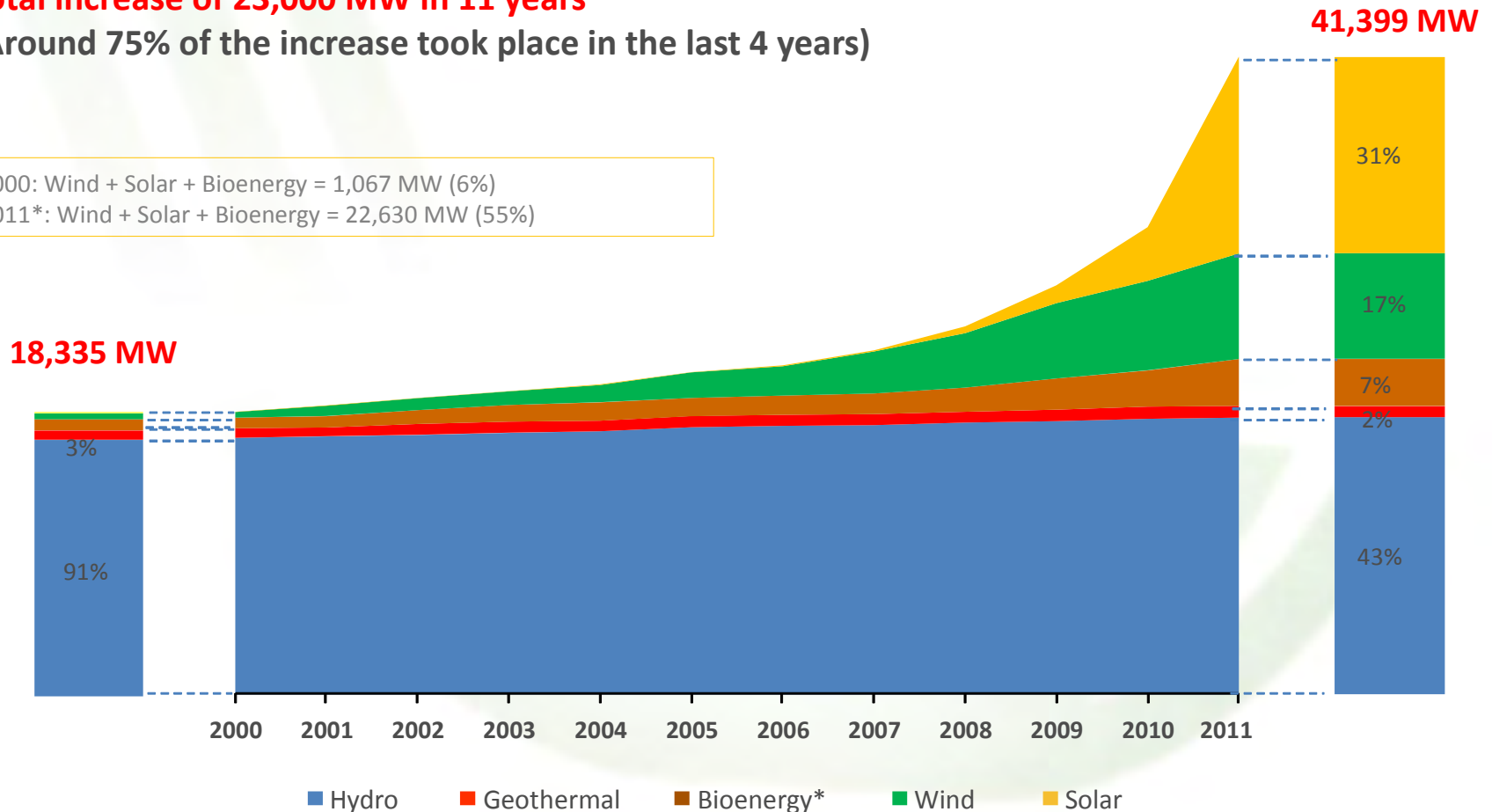
Growth of RES capacity

In 2000 : **18,335 MW** => in 2011 : **41,399 MW**

Total increase of 23,000 MW in 11 years

(Around 75% of the increase took place in the last 4 years)

2000: Wind + Solar + Bioenergy = 1,067 MW (6%)
 2011*: Wind + Solar + Bioenergy = 22,630 MW (55%)



* Bioenergy: solid biomass, biodegradable part of waste, biogas and bioliquids

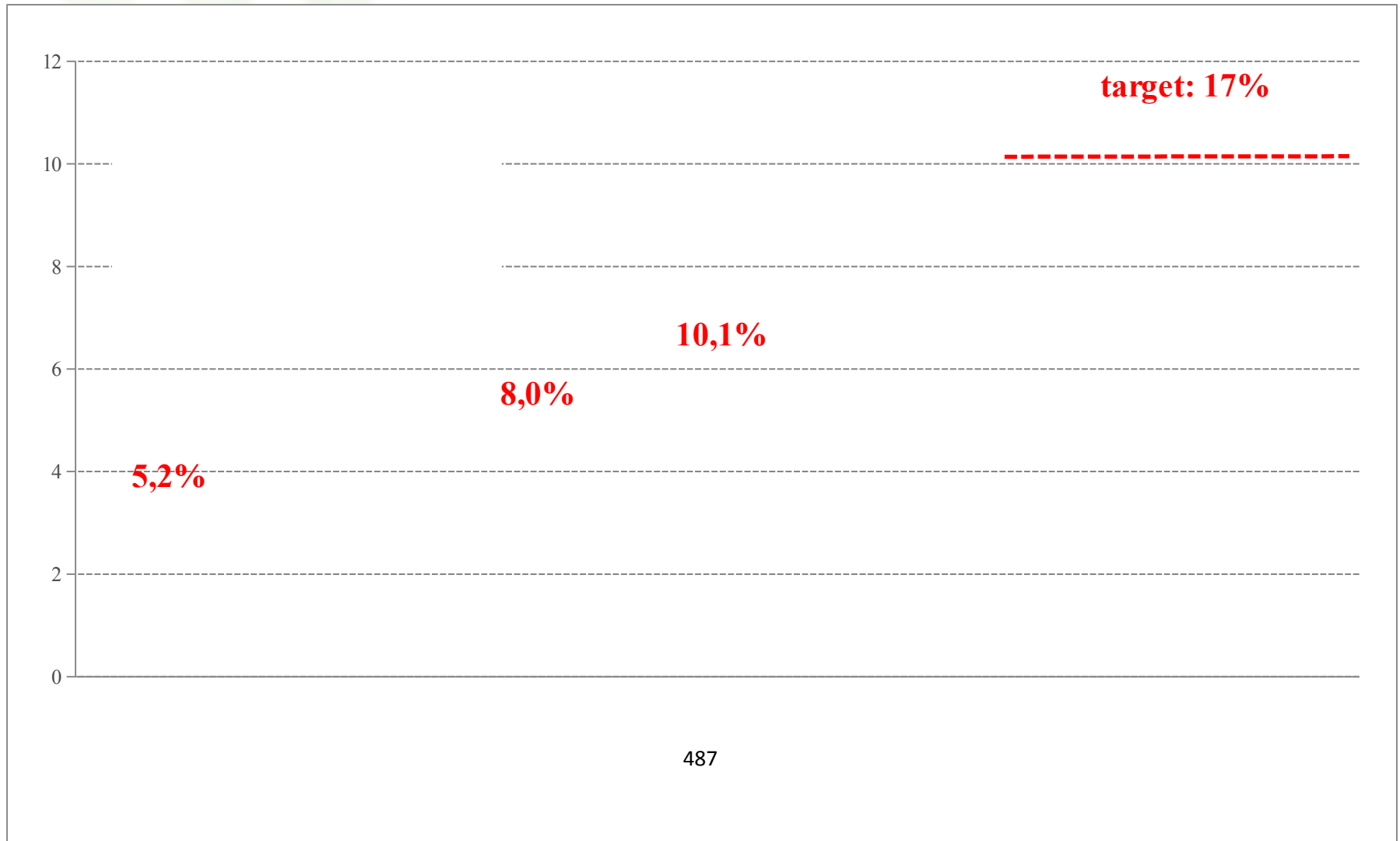
Total and sectorial RES consumption (Mtoe)

Statistics 2008 and forecasts to 2020

	2008			2020		
	RES consumption	Gross final consumption	RES / consumption	RES consumption	Gross final consumption	RES / consumption
	[Mtoe]	[Mtoe]	[%]	[Mtoe]	[Mtoe]	[%]
Electricity	5,026	30,399	16,53%	8,504	32,227	26,39%
Heating	3,238	58,534	5,53%	10,456	61,185	17,09%
Transports	0,723	42,619	1,70%	2,530	39,630	6,38%
From cooperation mechanism	-	-	-	1,127	-	-
Gross final consumption	8,987	131,553	6,83%	22,617	133,042	17,00%

Directive 2009/28/EC sets up national targets for EU countries by 2020

Italian Renewable Energy Action Plan (NREAP 2010) vs Progress Report (2011)



Feed-in tariff



Feed-In Tariff (TO)

- ✓ Energy's Purchase at incentivized prices

RECOGNITION OF THE INCENTIVE

On energy injected into the grid

PRODUCER'S REVENUE

Sell energy to the GSE

INCENTIVE COVER CHARGE

Directly to end users through tariff component A3

Quota obligation



Green Certificate (GC)

- ✓ Producers and importers must feed into the grid an amount of renewable energy equal to the x % (6,80 % for 2011) of conventional energy produced or imported the year before

RECOGNITION OF THE INCENTIVE

On energy produced

PRODUCER'S REVENUE

Selling GC + value of energy sold

INCENTIVE COVER CHARGE

Indirectly by end users through market energy price

The Feed-in tariff system (TO)

- ✓ **Small plants** may obtain an “All-inclusive Tariff”, **alternatively** to Green Certificates
- ✓ Renewable power plants with a total capacity < 1MW (< 200kW for wind plants), **except for PV**, may be incentivized through the feed-in tariff system
- ✓ The amount of tariff is **differentiated by source** and will be **updated every three years** through specific ministerial decrees
- ✓ The support is granted over **15 years**
- ✓ **Power Plants Qualification**: to get TO, RES power plants must request and obtain the qualification (positive assessment concerning the source and the technical characteristics of the p.p.). The Qualification is awarded by a Technical Commission and the process is ruled by a specific procedure, published on GSE web site, and it is based on silence approval
- ✓ **Granting of TO**: GSE transfer the support (*ex post, on monthly basis*) on demand of the producers. The producers during the support period can only once switch to the GC mechanism and viceversa

The Feed-in tariff system (TO)

Source	Tariff (euro cent/kWh)
Wind < 200 kW	30
Solar	-
Geothermal	20
Wave & Tidal	34
Hydro	22
Biomass, biogases and bioliquids (vegetal oil) when complying with EU Regulation 73/2009	28
Landfill gas, sewage treatment plant gas, biogases and bioliquids	18

- The incentive is granted for the net electricity produced and injected into the grid
- GSE manages the related production on the power exchange

The new IT PV support scheme under M. Decree 5 July 2012

V Conto Energia

Main items

- Started on 27-08-12, 45 days after achieving the yearly cumulative cost of **6 billion euro**
- Incentives **will cease** on reaching the yearly cumulative cost of 6,7 billion euro Cap for the new scheme: 700 million euro
- 2 different ways to access in order** to get the support scheme:
 - Direct access M 12 kW
 - Registries mechanism >12 kW
- Support granted over **20 years, for the electricity injected** into the grid
- Premiums for self consumption, for modules produced in EU and EEA, for asbestos removal are recognized

≤ 1 MW	> 1MW
Feed-in tariff	Feed-inPremium
Value banded on Technology and Size	Value of Feed-in MINUS Hourly zonal price

The Green Certificates mechanism: Key elements of the system

- It is based on a **quota obligation** on electricity from conventional sources **for each producer/importer** (EE produced/imported above 100 GWh of each producer/importer)
- Producers and importers **must feed into the grid an amount of renewable energy** equal to the x % (6,80 % for 2011) of conventional energy produced or imported the year before
- GC mechanism will decrease to \emptyset up to 2015
- Producers and importers can fulfill their obligation by means of GC issued in favor of their own renewable electricity production or purchased from other producers
- The support is granted over **15 years**
- Green Certificates have a validity of **3 years**
- 1 GC is issued for each **MWh produced** multiplied for a **“k” factor** related to the source used
- The producers during the support period can only switch once to the **TO mechanism** (if power < 1MW) **and viceversa**
- Green Certificates can be sold or purchased through: **Bilateral agreements and GME trading platform**

The Green Certificates mechanism: Key elements of the system

	Source	K
1	Wind > 200 kW	1
1- bis	Wind off-shore	1,5
2	Solar	-
3	Geothermal	0,9
4	Tidal & Wave	1,8
5	Hydro	1
6	Biodegradable wastes and biomass other than that ones at point 7	1,3
7	Biomass and biogases obtained from agriculture, animal husbandry and forestry on a short supply-line basis	1,8
8	Landfill gas, sewage treatment plant gas and biogases (other than the ones indicated in the previous point)	0,8

The new RES support scheme under Ministerial Decree 6 July 2012

Application to Plants ≥ 1 kW into operation from 1 January 2013



**3 ways of access to incentives
based on capacity**

Directly	Registries	Auction
Very small plant* & other marginal cases	<ul style="list-style-type: none">• RES ≤ 5 MW• Hydro ≤ 10 MW• Geothermal ≤ 20 MW	<ul style="list-style-type: none">• RES > 5 MW• Hydro > 10 MW• Geothermal > 20 MW

*Tidal and Waves ≤ 60 kW

Yearly cumulative cost for the support schemes: **not more than 5.8 billions €/year**

Milestones of the new system

- **RES Power Capacity Caps (MW)** to be supported based on **Registries** are as follows:

Source	New power plants			Rebuilt power plants		
	2013	2014	2015	2013	2014	2015
Wind on shore	60	60	60	150	150	150
Wind offshore	0	0	0	0	0	0
Hydro	70	70	70	300	300	300
Geothermal	35	35	35	40	40	40
Biomass, biogas, sewage gas,, landfill gas and sustainable bioliquids	170	160	160	65	65	65
Other biomass	30	0	0	70	70	70
Oceanic (tides and waves)	3	0	0	0	0	0

- All incentives **decrease yearly by 2%** and are granted **over all the life of the plant**
- Plants which are admitted to the support mechanisms (positive ranking after the GSE assessment) must **enter into operation** within the foreseen **deadlines** (penalties in terms of **incentive reduction** are foreseen)

Incentives for registries system

$P \leq 1\text{MW}^*$		$1\text{ MW} < P < \text{max registry size}$
Feed-in Tariff	Kind of intervention	Feed-in Premium
A fixed tariff (technology and size banding incentive) PLUS any applicable premium	New power plants	Feed-in tariff MINUS Electricity hourly zonal price
Application of an intervention reduction factor to the fixed rate (premium included) for new plants	<ul style="list-style-type: none"> • Rebuilt • Reactivated • Empowered 	Application of an intervention reduction factor to the Feed-in Premium for new plants

*also for direct access

Auction system

- The system is a **Dutch Auction** which awards the lowest prices
- Auctions are on **annual basis** (some exception are foreseen for wind on shore) with **source/technology cap** (see in the table below)
- Reductions admitted are between **2%** and **30%** of the auction base (**fixed tariffs**)

	2013	2014	2015
Wind on shore	500	500	500
Wind off shore	650	0	0
Idro	50	0	0
Geothermal	40	0	0
Biomass	470	0	0
Tides& waves	0	0	0

Thank for your attention

gerardo.montanino@gse.it

Phone: +39 06 8011 4469

www.gse.it

OC3 and OC4 projects – Verification benchmark exercises of the state-of-the-art coupled simulation tools for offshore wind turbines

W. Popko¹, F. Vorpahl¹, J. Jonkman² and A. Robertson²

¹*Fraunhofer Institute for Wind Energy and Energy System Technology IWES, Am Seedeich 45, 27572 Bremerhaven, Germany, wojciech.popko@iwes.fraunhofer.de*

²*National Renewable Energy Laboratory, Golden, CO 80401, United States of America, jason.jonkman@nrel.gov*

Abstract – This document briefly presents the activities of the Offshore Code Comparison Collaboration (OC3) and Offshore Code Comparison Collaboration Continuation (OC4) projects under the International Energy Agency (IEA) Wind Tasks 23and30, focused on advancing the overall accuracy of the coupled simulation tools for offshore wind turbines (OWT). These two projects focus on the verification of simulation tools performed by direct code-to-code benchmarking exercises. A methodology of the verification process and its outcome are briefly described. Also an introduction to the state-of-the art simulation of OWT is given.

1. Introduction

The enormous potential of offshore wind power and financial support from the European Union and its individual member states drive the offshore wind industry business. Offshore wind turbines (OWT) are becoming a significant source of renewable energy in Europe and also worldwide. However a large-scale development is hampered by dissimilar offshore conditions at diverse sites, which make the standardization of OWT design difficult. Offshore sites differ in terms of wind and wave conditions, water depth, seabed properties etc. This creates a need for the utilization of different types of sub-structures like bottom-fixed monopiles, gravity bases, space frames or floating structures. The price of an entire OWT can be significantly reduced by an appropriate choice of such a sub-structure and its cost-effective design, to which a robust load analysis is the key.

The analysis of OWT relies on aero-hydro-servo-elastic simulation tools and is performed in the time domain, as only this approach can incorporate non-linear dynamic effects and transient events of importance. The coupled tools take into account an interaction of various environmental conditions and the entire structural assembly of the turbine with its control system as shown in Figure 1. This includes various models describing: aerodynamics (aero), control systems (servo), hydrodynamics (hydro) and structural-dynamics of a wind turbine and its offshore support structure (elastic). The coupled approach is required by design standards and guidelines (e.g. International Electrotechnical Commission (IEC 2009) and Germanischer Lloyd (GL 2005)) for an accurate prediction of the system dynamic response and the extreme and fatigue loads of an OWT. Dynamic interaction should not be disregarded as it may result in a considerable loss of accuracy. As for example the aerodynamic damping coming from a rotor can, in some cases, significantly reduce hydrodynamic load effects on a support structure, which can only be captured in the coupled analysis.

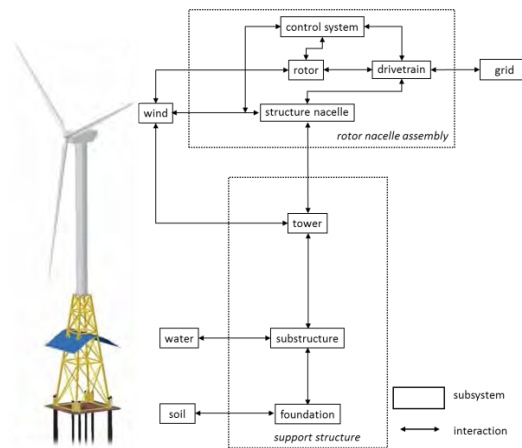


Figure 1: Schematic of interactions between different OWT components in an aero-hydro-servo-elastic simulation tool.

Due to the high complexity and sophistication of these simulation tools, their verification and validation is required. The validation is currently impeded by the limited availability and high uncertainty of full-scale measurement data. However, the verification can be done by a direct code-to-code comparison, which is an effective way to identify inaccuracies and errors that may persist in numerical models and simulations. The first international approach dedicated to the verification of simulation tools for OWT, including hydrodynamic loads, was undertaken within the Offshore Code Comparison Collaboration (OC3) project (Jonkman and Musial, 2010) operated under the International Energy Agency (IEA) Wind Task 23 Subtask 2. The cooperation was focused on coupled simulations of an OWT with sub-structures like a monopile, a tripod and a floating spar buoy. Further research needs triggered a follow-on project, the Offshore Code Comparison Collaboration Continuation (OC4) project formed under the IEA Wind Task 30 (Musial et al. 2009) in 2010, where the focal points of coupled simulations are a jacket sub-structure and a semi-submersible platform. In both projects the “NREL 5-MW Offshore Baseline Turbine” defined by Jonkman et al. (2009) was utilized. A number of academic and industrial partners from multiple countries were involved in the OC3 and OC4 projects. Those actively involved, who delivered the simulation results are listed in Table 1.

Table 1: Active participants of the OC3 or OC4 project.

Country	Institution
China	China General Certification
Denmark	Technical University of Denmark - Department of Wind Energy (former Risø DTU), Det Norske Veritas, Vestas Wind Systems, Siemens Windpower, DONG
Germany	Fraunhofer Institute for Wind Energy and Energy System Technology IWES, Endowed Chair of Wind Energy at the University of Stuttgart, Institute of Steel Construction at the Leibniz Universität Hannover, REpower Systems SE
Greece	National Technical University of Athens
Korea	Pohang University of Science and Technology
Norway	Fedem Technology AS, Institute for Energy Technology, Centre for Ships and Ocean Structures, Norwegian University of Science and Technology, Marintek
Spain	National Renewable Energies Center, AccionaEnergia
The Netherlands	Knowledge Centre WMC, Energy Research Centre of the Netherlands
UK	Garrad Hassan & Partners Ltd.
USA	National Renewable Energy Laboratory, American Bureau of Shipping

Each one of the participants has their own area of expertise, and therefore, their own unique contribution to the projects.

2. Objectives and Methodology of Verification Exercises

The OC3 and OC4 projects are focused on verification and benchmarking exercises for OWT simulation tools, with emphasis on different sub-structures. The following goals are within the scope of both projects:

- assessment of simulation accuracy and reliability,
- investigation of capabilities of implemented theories,
- refinement of analysis methods,
- identification of further R&D needs,
- training of new analysts how to run tools correctly.

The fulfillment of these goals involves discussion of modeling strategies, development of benchmark models and simulations, running the simulations, post-processing and comparison of the results.

For each Phase of the projects, detailed definitions of different support structures in terms of geometry, structural properties, hydrodynamic coefficients etc. are disseminated to the project participants for the implementation in their simulation tools.

Different groups of load cases are defined for each single Phase of the OC3 and OC4 projects. Each set consists of load cases of increasing complexity allowing for

- (1) stepwise comparison of results and
- (2) tracing back possible errors coming from different models and methods implemented in the simulation tools. Different subsystems of an OWT are modeled as flexible or rigid depending on the actual load case.

Additionally, environmental loads such as wind and wave are applied independently or simultaneously depending on the complexity of a given load case. Load cases with deterministic environmental loads (e.g. constant wind, regular wave) are directly compared in terms of time-series outputs, whereas those with stochastic environmental loads (e.g. turbulent wind, irregular sea state) are examined in terms of probability density functions, power spectral densities, and damage-equivalent loads. For each load case, the outputs are recorded at a number of nodal points denoted as sensors, spread over the rotor-nacelle assembly and different support structures. The location of outputs is chosen in a way that allows capturing a global response of the entire OWT, as well as its local dynamics (e.g. local vibration of a jacket).

The results obtained are the outcome of several revisions, which were necessary due to the complexity of models, user errors, the ongoing development of some of the codes etc. These account for corrections at all stages of OWT modeling, its simulation and post-processing of the data. Project participants put some effort into ensuring that their models:

- (1) are implemented according to the provided specification of the OWT,
- (2) initial conditions of the simulations are fulfilled and simulation start-up transients are eliminated,
- (3) use proper coordinate systems for the data outputs. The results of the OC3 project are published in Jonkman (2010), whereas the results of the OC4 project, Phase I with the jacket sub-structure are shown in Popko et al. (2012).

Some exemplary results for one of the load cases of Phase I of the OC4 project are shown in Figure 2.

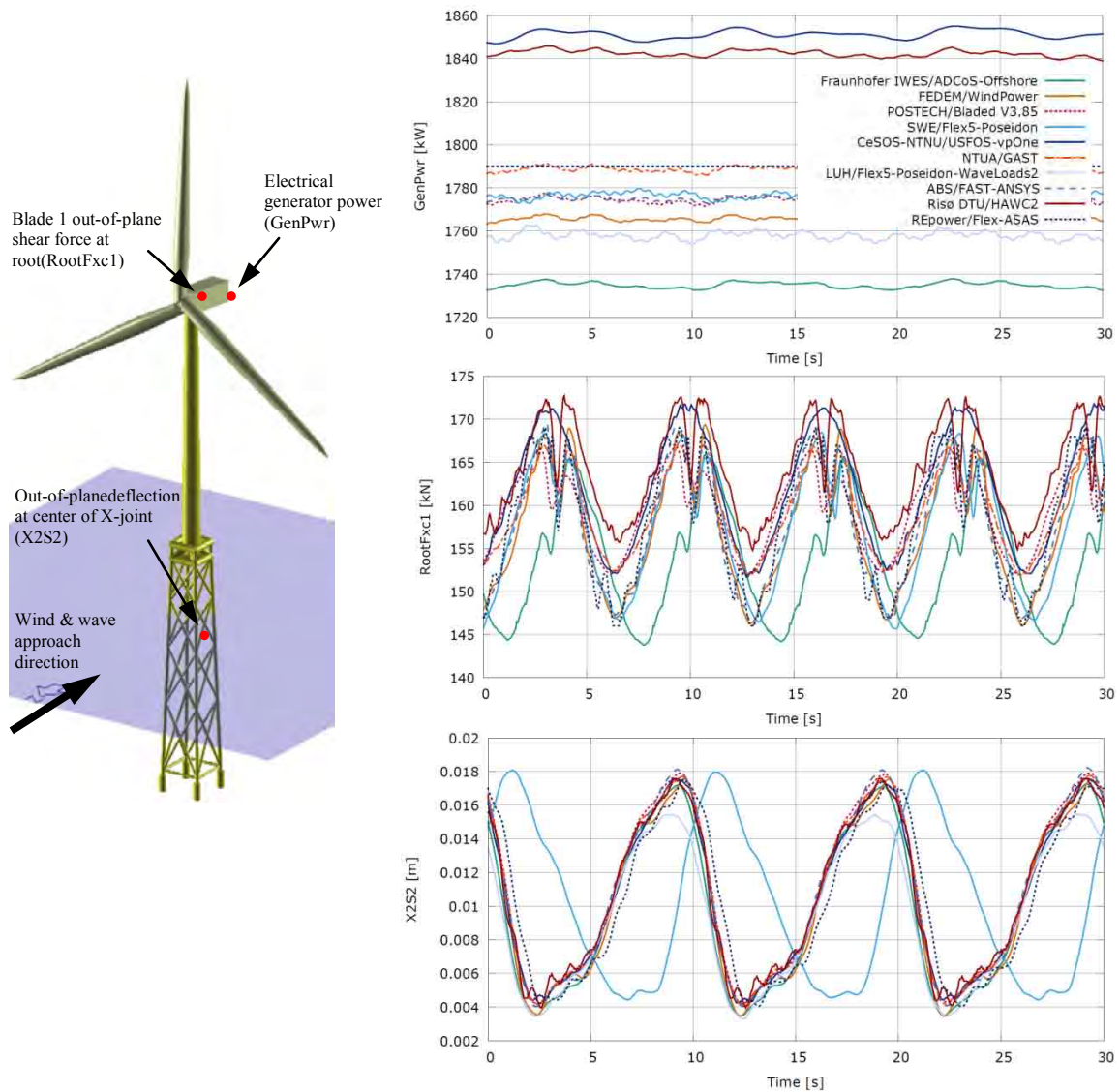


Figure 2: The OWT assembly (left) and the exemplary outputs (right) of: generator power, root out-of-plane shear force and out-of-plane deflection of the X-brace located in the splash zone.

Herein the entire OWT is modeled as flexible and excited by deterministic wind and wave that act simultaneously. A very good match of the electrical generator power is achieved for the majority of codes. The tower blockage effect is captured by most of the tools as small fluctuations of the generator power (corresponding to 3P frequency) and peaks in the out-of-plane shear force at the blade root (corresponding to 1P frequency). Also the agreement of out-of-plane deflection of the X-brace located in the splash zone is remarkably good between the simulation tools, though the peak-to-peak amplitude is very small.

Phase II of the OC4 project dealing with a semi-submersible platform is currently under work.

3. Outcome

The coupled simulation of OWT is an elaborated process that involves multidisciplinary knowledge within the fields of aerodynamics, aeroelasticity, hydrodynamics, mechanics, control, software development etc.

The OC3 and OC4 projects provide an excellent platform for the exchange of knowledge between specialists within all these engineering fields, through which a better understanding of model complexity and limitations of some theories was achieved. Both projects led to significant improvements of simulation tools. Many of the participants were able to verify their codes and methodologies developed for the dynamic analysis of an OWT with various support structures. Some inconsistencies and errors in models were detected in a direct code-to-code comparison of the results. Furthermore, the comparison with other codes has provided the first sanity checks for the newly developed tools. These results are very important because the advancement of the offshore wind industry is closely tied to the development and accuracy of coupled simulation tools. The results already obtained within the OC3 and OC4 projects received the international recognition in the academic and industrial sectors. Furthermore, the Experts Meeting on Computer Code Validation for Offshore Wind System Modeling, in the scope of the OC4 project, was hosted by National Renewable Energy Laboratory, where issues regarding the prospect of validation of coupled simulation tools against model-scale and full-scale measurements were discussed.

Acknowledgements

Walt Musial from NREL and the International Energy Agency are acknowledged for setting up the OC3 and OC4 projects. All the participants of the OC3 and OC4 projects are acknowledged for sharing their expertise and tremendous work. Without their active participation and true engagement, the success of both projects would not be achieved.

References

1. GL. Guideline for the Certification of Offshore Wind Turbines. Germanischer Lloyd, Hamburg, 2005.
2. IEC. Wind turbines - Part 3: Design requirements for offshore wind turbines. IEC 61400-3, 1.0 edition, 2009.
3. J. Jonkman and W. Musial. Offshore Code Comparison Collaboration (OC3) for IEA Task 23 Offshore Wind Technology and Deployment. NREL/TP-500-48191, Golden, CO: National Renewable Energy Laboratory, 2010.
4. J. Jonkman, S. Butterfield, W. Musial, G. Scott. Definition of a 5-MW Reference Wind Turbine for Offshore System Development. NREL/TP-500-38060, National Renewable Energy Laboratory, 2009.
5. W. Musial, J. Jonkman, F. Vorpahl, L. Quesnel. Annex 30 Task Proposal Comparison of Dynamic Computer Codes and Models Offshore Code Comparison Collaboration Continuation (OC4) Project. International Energy Agency, 2009.
6. W. Popko, F. Vorpahl, A. Zuga, M. Kohlmeier, J. Jonkman, A. Robertson, T. Larsen, A. Yde, K. Sætertrø, K. Okstad, J. Nichols, T. Nygaard, Z. Gao, D. Manolas, K. Kim, Q. Yu, W. Shi, H. Park, A. Vásques-Rojas, J. Dubois, D. Kaufer, P. Thomassen, M. de Rooter, J. Peeringa, H. Zhiwen, H. von Waaden, Offshore Code Comparison Collaboration Continuation (OC4), Phase I – Results of Coupled Simulations of an Offshore Wind Turbine with Jacket Support Structure. In *Proceedings of the 22nd International Ocean and Polar Engineering Conference*, 2012.

Implementing agreement on Ocean Energy Systems

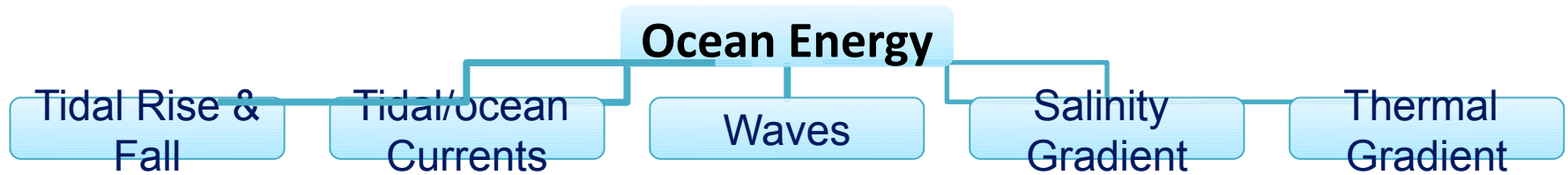
Ana Brito e Melo

IEA OES



Implementing Agreement on Ocean Energy Systems

Ana Brito e Melo



- OES covers all forms of ocean energy, including submarine geothermal, but NOT offshore wind - seawater must be the motive power
- Products can include: electricity, heat, cooling, water (drinking and pressurized), biofuels, chemicals
- Ocean energy is a nascent but truly international industry

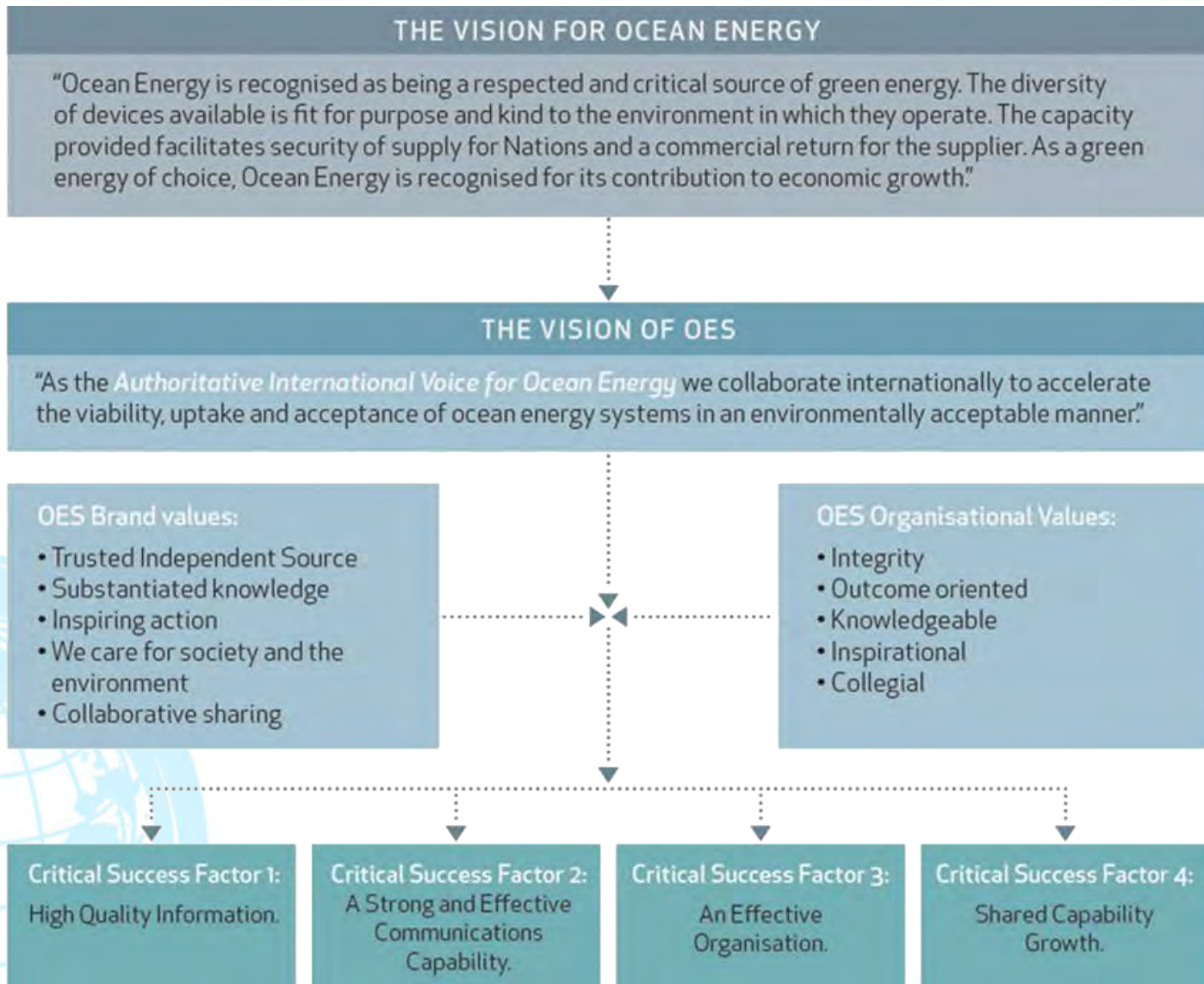
The Ocean Energy Systems Implementing Agreement (OES):

- Intergovernmental collaboration between countries
- Operating under a framework established by the International Energy Agency (IEA) in Paris.
- OES was founded by three countries in 2001 and has grown to its present 19 country governments.



2012 – 2016 VISION

As the **Authoritative International Voice on Ocean Energy** we collaborate internationally to accelerate the viability, uptake and acceptance of ocean energy systems in an environmentally acceptable way



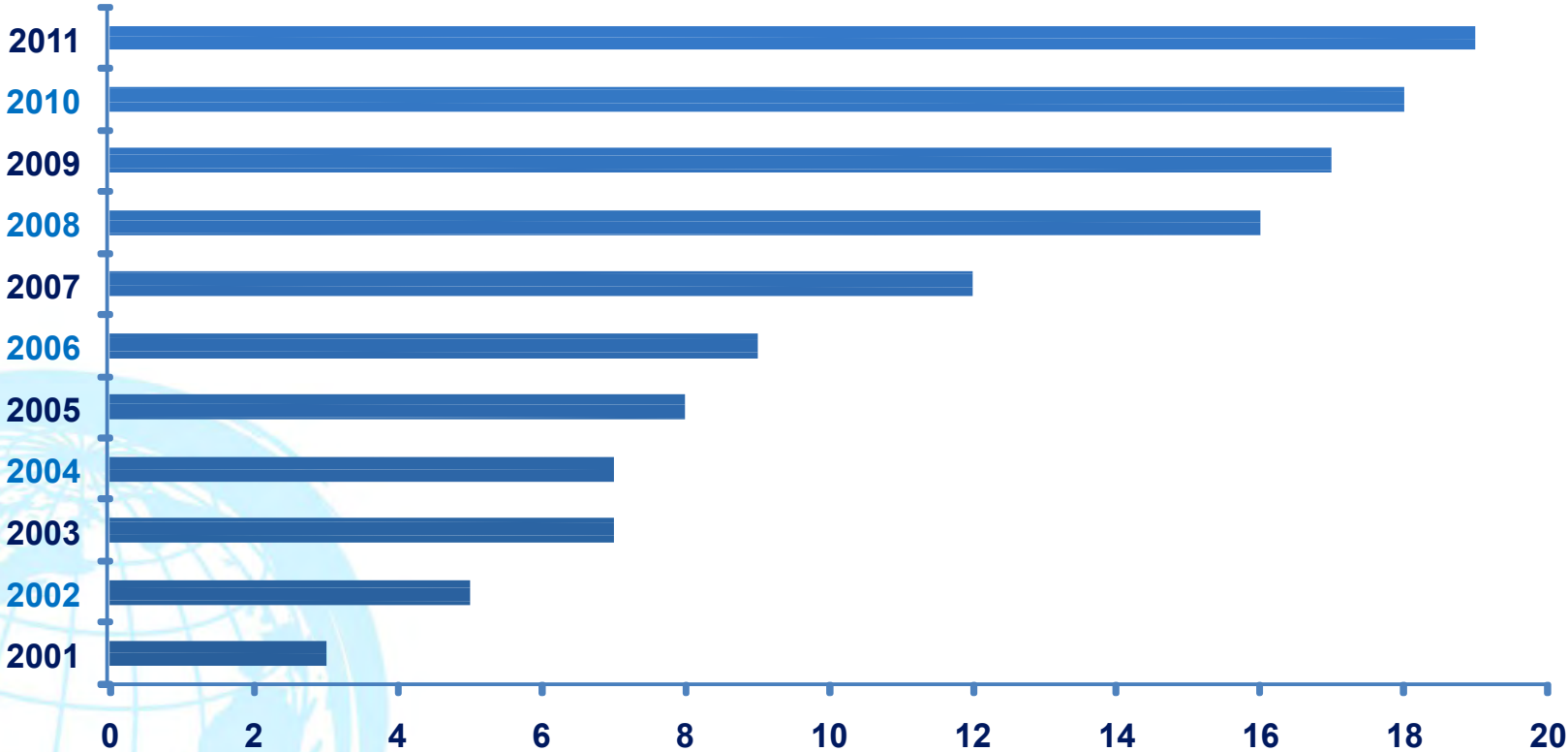
Connect organisations and individuals working in the ocean energy sector to accelerate development and enhance economic and environmental outcomes.

Educate people globally on the nature of ocean energy systems, the current status on development and deployment, and the beneficial impacts of such systems, improve skills and enhance research.

Inspire governments, agencies, corporate and individuals to become involved with the development and deployment of ocean energy systems.

Facilitate education, research, development and deployment of ocean energy systems in a manner that is beneficial for the environment and provides an economic return for those involved.

Present Membership



19 Members with a wide range of Contracting Party roles and interests:

- Government departments USA, UK
- Government resource agencies Canada, Korea, China
- National energy agencies Sweden, Ireland, South Africa, Denmark
- Universities Japan, Belgium, Mexico
- Research organizations Spain, Portugal, Germany
- Device/project developers Australia, Norway, Italy
- Industry associations New Zealand

Key Strengths:

- Diverse membership
- Collaborative efforts between countries
- Pooled capital, resources and effort
- Transfer of experience and knowledge

An International Vision for Ocean Energy

Society Goal

By 2030 ocean energy will have created 160,00 direct jobs and saved 5.2 billion tonnes of CO2 emissions.



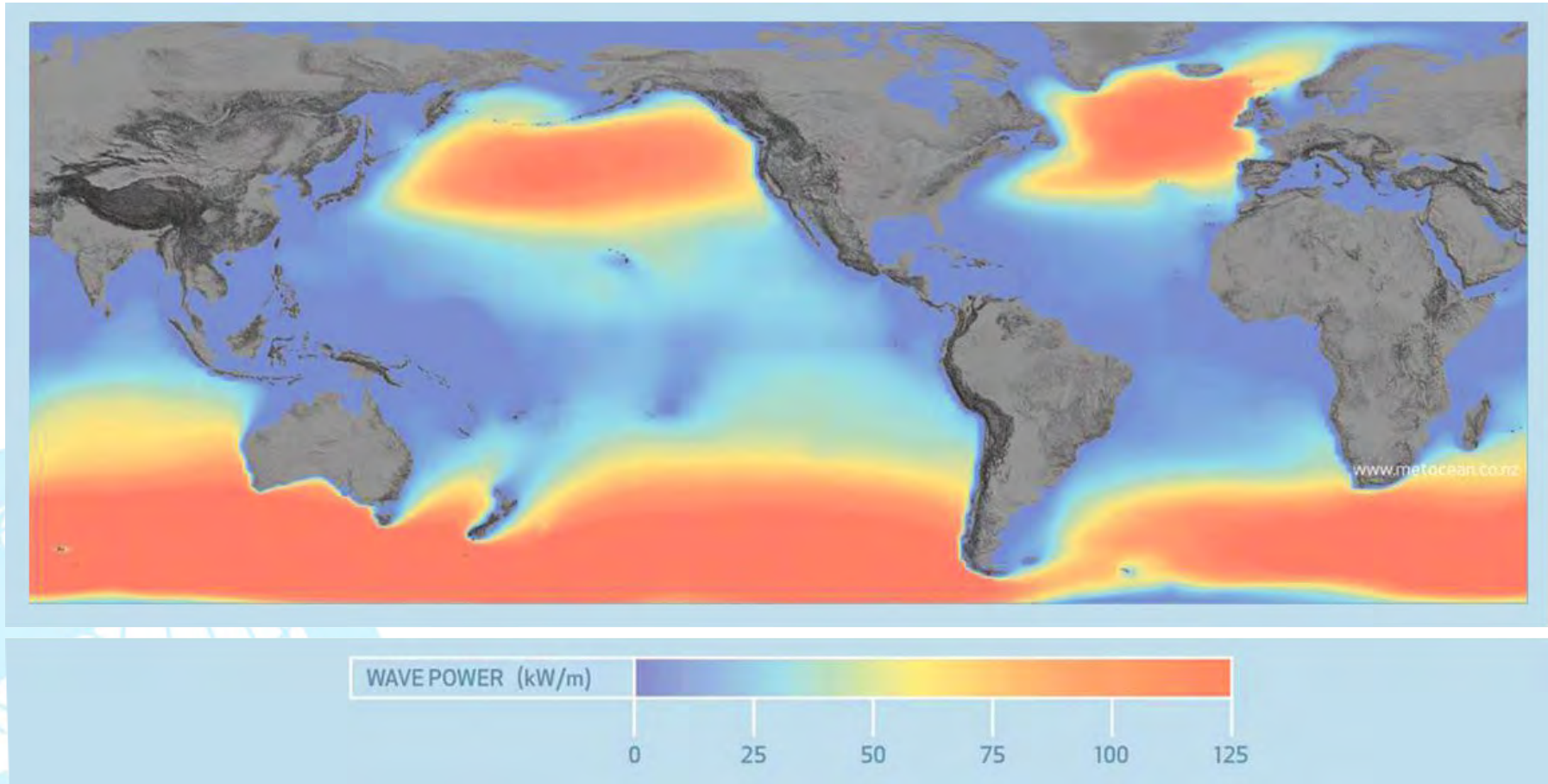
An International Vision
for Ocean Energy

- 20-page full-colour brochure
- Facts and figures as well as scenarios to 2050
- All forms of ocean energy in proportion to their present status
- Updated costs figures and 'iconic figures'
- People, water and energy nexus




Phase II (2012): Market Development

- Simple, contestable scenarios for market growth
- MARKAL modelling with IEA Modelling Group in Paris

Wave Power







Classification of tidal current devices

DEVICE TYPE	HORIZONTAL AXIS TURBINES	VERTICAL AXIS TURBINES	OSCILLATING HYDROFOIL
DESCRIPTION	<p>These devices have two or three blades mounted horizontally to form a rotor; the kinetic motion of the water current creates lift on the blades causing the rotor to turn driving an electrical generator.</p>	<p>These devices generally have two or three blades mounted along a vertical shaft to form a rotor; the kinetic motion of the water current creates lift on the blades causing the rotor to turn driving an electrical generator.</p>	<p>This device operates like an aeroplane wing but in fluid; control systems alter their angle relative to the water current, creating lift and drag forces that create device oscillation; this physical motion from this oscillation feeds into a power conversion system.</p>
DIAGRAM			

Turbina Kobold ad asse verticale



Classification of wave energy devices

DEVICE TYPE	ATTENUATOR	OVERTOPPING	OSCILLATING WATER COLUMN (OWC)	POINT ABSORBER	OSCILLATING WAVE SURGE CONVERTER (OWSC)
DESCRIPTION	Attenuator devices are generally long floating structures aligned in parallel with wave direction, which then absorbs the waves. Its motion can be selectively damped to produce energy.	Overtopping devices are a wave surge/focusing system, and contains a ramp over which waves travel into a raised storage reservoir.	In an OWC, a column of water moves up and down with the wave motion, acting as a piston, compressing and decompressing the air. This air is ducted through an air turbine.	A point absorber is a floating structure absorbing energy from all directions of wave action due to its small size compared to the wavelength.	An OWSC extracts energy from the surge motion in the waves. They are generally seabed-mounted devices located in nearshore sites.
DIAGRAM					



Motivation

- OES is the only international intergovernmental organization
- Contribution of ocean energy remains unclear
- Available ocean energy resources are not well understood
- Timing of technological maturity is uncertain

Opportunity

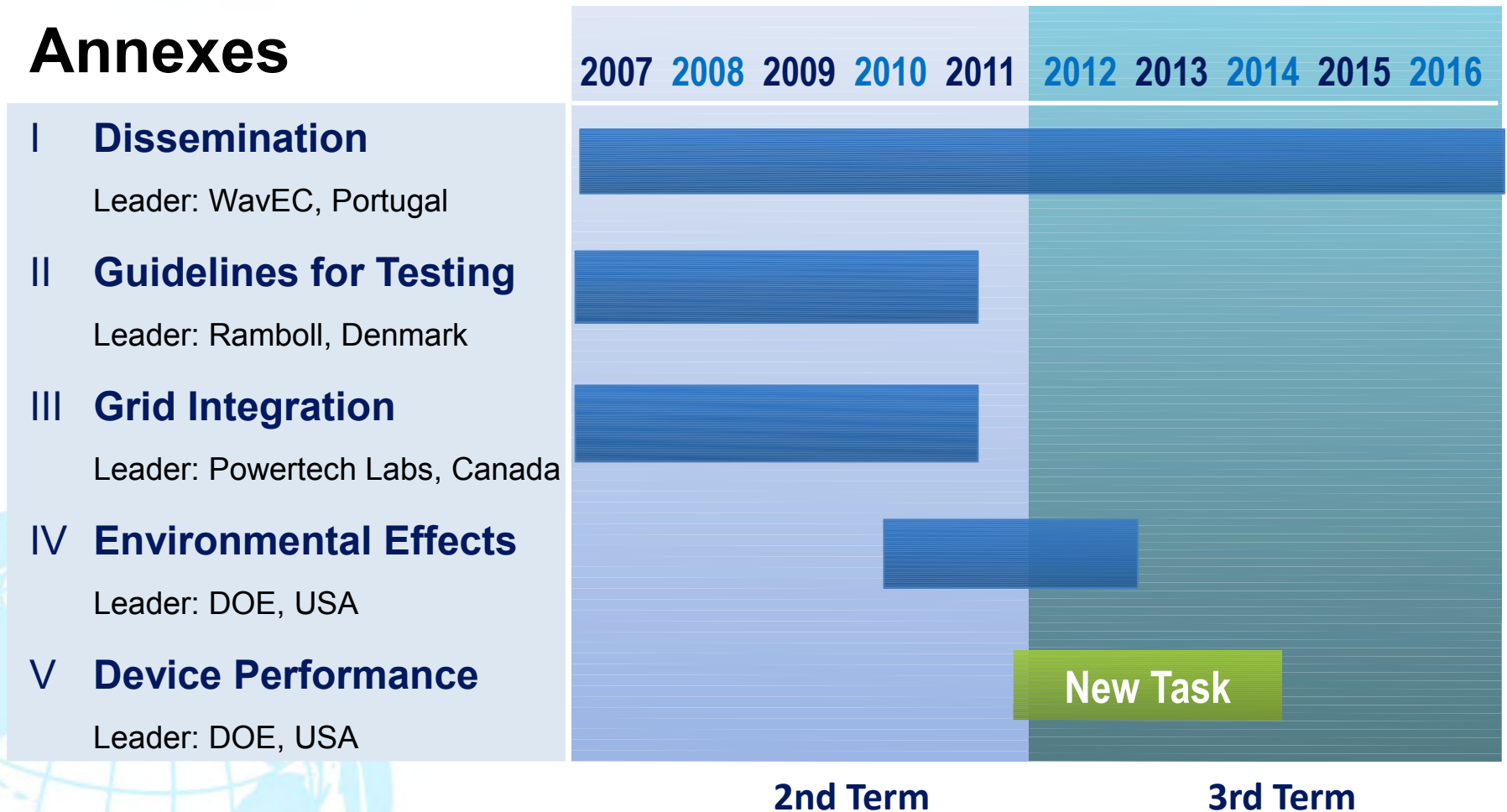
- OES members include most active countries in terms of R & D, policy implementation and device deployments
- Representatives can access national figures and databases
- OES has publishing/broadcasting role

Audience

- Governments, policy makers, regulators and planners
- Industry participants, supply chain and general public

By 2030 ocean energy will have generated 160,000 direct jobs and savings of 5.2 billion tonnes of CO₂

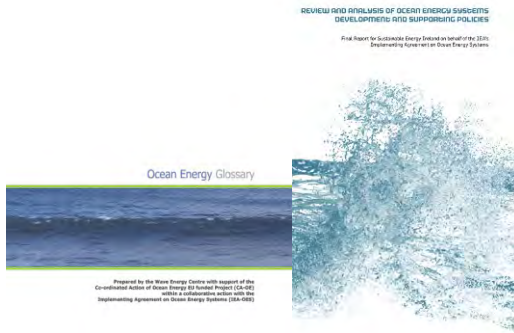
Annexes



Strategic Planning has led to several other Annex proposals – under development

**Central information collation and dissemination
Annex on the technical, economic, environmental
and social aspects of ocean energy systems.**

**Contribution to the definition of future priorities for
the Implementing Agreement as a whole.**



● Review and Analysis of Ocean Energy Systems
Development and Supporting Policies | **2006**

● Ocean Energy Glossary | **2007**

● Wave Data Catalogue for Resource Assessment | **2007**

● Ocean Energy: Global Technology Development
Status | **2009**



OES Annual Report: Single, detailed, authoritative reference source



Country Reports:

- Ocean Energy Policy
- Research & Development
- Technology Demonstration

Special Themes:

2011 Annual Report

Marine Spatial Planning & Ocean Energy

2010 Annual Report

Key facilitators of ocean energy

2009 Annual Report

Technical and non-technical barriers to ocean energy

2008 Annual Report

Present status of ocean energy

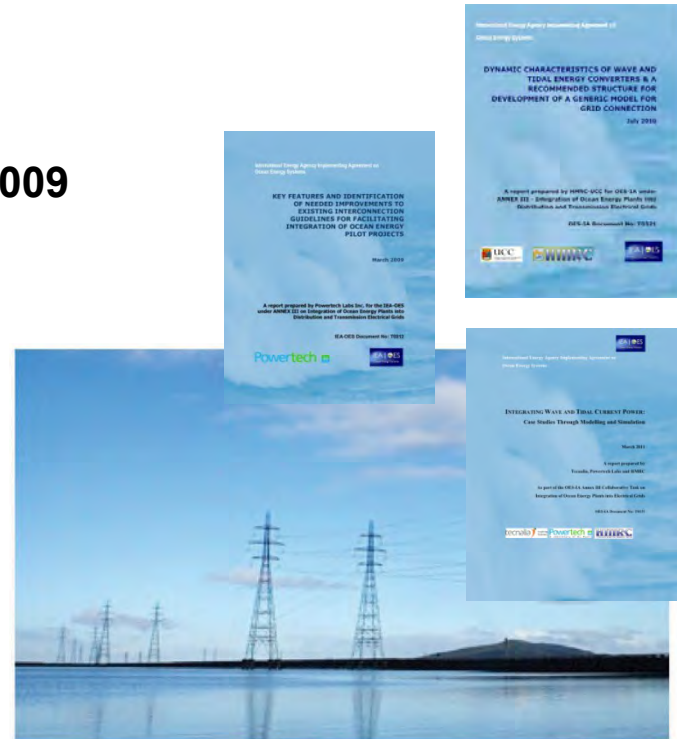
Development of Recommended Practices for Testing and Evaluating Ocean Energy Systems

- Development of Recommended Practices for Testing and Evaluating Ocean Energy Systems – SUMMARY | **2011**
- Generic and Site-related Wave Energy Data | **2010**
- Guidelines for the Development & Testing of Wave Energy Systems | **2010**
- Guidelines for the Design Basis of Marine Energy Converters | **2009**
- Guidance for Assessing Tidal Current Energy Resource | **2008**
- Tidal Energy Development Protocol | **2008**
- Energy Device Performance Protocol | **2007**
- Preliminary Tidal-current Energy Device Performance Protocol | **2007**



Integration of Ocean Energy Plants into Distribution and Transmission Electrical Grids

- **Report:** Key Features and Identification of Needed Improvements to Existing Interconnection Guidelines for Facilitating Integration of Ocean Energy Pilot Projects | **2009**
- **Report:** Potential Opportunities and Differences Associated with Integration of Ocean Wave and Marine Current Energy | **2010**
- **Report:** Dynamic Characteristics of Wave and Tidal Energy Converters & a Recommended Structure for Development of a Generic Model for Grid Connection | **2010**
- **Report:** Integrating Wave and Tidal Current Power: Case Studies through Modelling and Simulation | **2011**



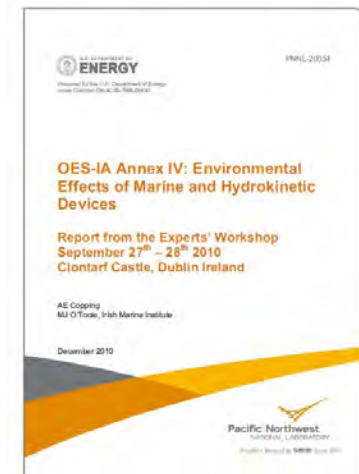
Assessment of Environmental Effects and Monitoring Efforts for Ocean Wave, Tidal, and Current Energy Systems

Objectives:

- Expand knowledge of environmental effects and monitoring methods
- Increase accessibility of information
- Make available proven mitigation strategies
- Foster efficient and timely government oversight and public acceptance

Mechanism for information sharing: Publicly accessible database

http://mhk.pnnl.gov/wiki/index.php/Annex_IV



Exchange and Assessment of Ocean Energy Device Project Information and Experience

Objectives:

● Develop computational models capable of:

- projecting the cost of electricity for MHK energy conversion
- evaluating the opportunities for device cost reduction

● Develop and validate tools and techniques for industry use

- ...build better devices

● Establish:

- benchmarks and standardized methods to evaluate new technologies
- government sanctioned device assessment methods

THANK YOU FOR THE ATTENTION



Chair

Dr. John Huckerby
AWATEA, New Zealand
international@awatea.org.nz

Vice-Chair

Mr. Jose Luis Villate
TECNALIA, Spain
joseluis.villate@tecnalia.com

Vice-Chair

Mr. Eoin Sweeney
SEAI, Ireland
Eoin.Sweeney@seai.ie

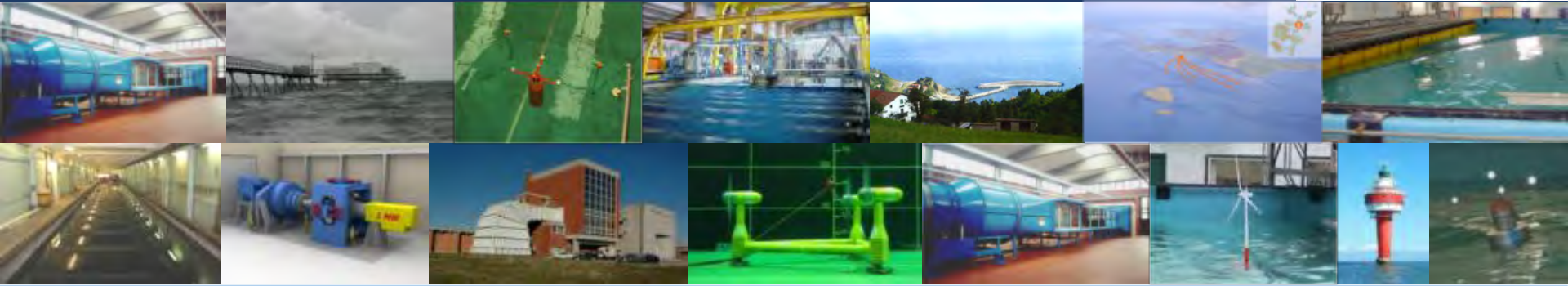
Secretary

Dr. Ana Brito Melo
WAVE ENERGY CENTRE, Portugal
ana@wavec.org

Marine Renewables Infrastructure Network

Tony Lewis

MARINET - Marine Renewables Infrastructure Network



MARINET

Marine Renewables Infrastructure Network



What is MARINET?

- Initiative to coordinate Europe's marine renewable energy test infrastructure (facilities)
- Network of world-class marine renewables testing facilities at all scales
- Funded by the EC (FP7) to:
 - Offer periods of **free access** to all
 - Coordinate **research**
 - **Standardise** testing
 - Organise **industry networking**

Aim is to accelerate the commercialisation of marine
 Provide training in testing techniques



MARINET in numbers

- 29 world-class research institutions
- 12 countries
- 42 test facilities providing free test access in:
 - Wave energy
 - Tidal energy
 - Offshore-Wind Energy & Environmental Data
 - Cross-Cutting areas (electrical, moorings etc.)
- 48 month duration: April 2011 – March 2015

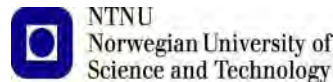
Who is involved?

- 29 Partners – 28 EC, 1 ICPC (Brazil)
- Coordinator: UCC-HMRC



Who is involved?

- 29 Partners – 28 EC, 1 ICPC (Brazil)
- Coordinator: UCC-HMRC



What does MARINET offer?



Facility Access: Test technology at one of the 42 facilities...free-of-

charge

- 42 test infrastructures providing EC-funded access
- Facility costs are paid by the EC
- Open to all, and is aimed at users outside the network – companies of any size, research groups etc.
- Facilities available at all scales



Focus Area	Wave	Tidal	Offshore-Wind and Environmental Data	Common Aspects e.g. Electrical/ PTO/ Materials etc
Scale				
Small Lab	<ul style="list-style-type: none"> ▶ AAU – Wave Basin ▶ AAU – Nissum Bredning Test Site ▶ UCC HMRC – Wave Basin ▶ UEDIN – Curved Wave Tank ▶ UNI_STRATH-Kelvin Hydrodynamics Lab 	<ul style="list-style-type: none"> ▶ UNI_STRATH – Kelvin Hydrodynamics Lab ▶ DTU – Current Flume (with carriage) ▶ USTUTT – Laminar Wind Tunnel 	<ul style="list-style-type: none"> ▶ UNIFI-CRIACIV – Small Boundary Layer Wind Tunnel ▶ UNI_STRATH – Kelvin Hydrodynamics Lab ▶ USTUTT - Laminar Wind Tunnel ▶ DTU – Current Flume with a Carriage 	<ul style="list-style-type: none"> ▶ UCC HMRC – Rotary Test Rig ▶ TECNALIA – Electrical PTO Lab ▶ SINTEF – Renewable Energy Lab - SmartGrids ▶ USTUTT – Turbine Test Rig
Large Lab	<ul style="list-style-type: none"> ▶ IFREMER - Wave Basin of Brest ▶ IFREMER – Current Circulation Tank ▶ NAREC – Wave Flume (marine test site) ▶ CNR-INSEAN – Wave Tank ▶ ECN – Hydrodynamic and Ocean Engineering 	<ul style="list-style-type: none"> ▶ IFREMER – Recirculation channel with waves ▶ CNR-INSEAN – Circulating Water Channel 	<ul style="list-style-type: none"> ▶ ECN – Hydrodynamic and Ocean Engineering ▶ CNR-INSEAN – Wave Tank 	<ul style="list-style-type: none"> ▶ NAREC – Grid Integration ▶ NAREC – Nautilus Rotary Rig ▶ IFREMER – Materials and Structures Group ▶ DTU – PowerLabDK ▶ NAREC – CPTC Energy Link Lab ▶ DTU – Mechanical Test Facilities
Medium-Scale Site	<ul style="list-style-type: none"> ▶ AAU – Nissum Bredning ▶ SEAI_OEDU – Galway Bay ▶ SEAI_OEDU - Belmullet ▶ EMEC- Nursery Site Wave ▶ QUB – Shallow Water Wave Tank 	<ul style="list-style-type: none"> ▶ QUB – Portaferry Tidal Site ▶ TTC – Den Oever Tidal Site ▶ EMEC – Nursery Site Tidal 	<ul style="list-style-type: none"> ▶ SEAI_OEDU – Wave Site Data Galway ▶ SEAI_OEDU – Wave Site Data Belmullet ▶ AAU – Nissum Bredning ▶ QUB – Portaferry Tidal Test Centre 	<ul style="list-style-type: none"> ▶ UNEXE - Moorings
Large-Scale Site	<ul style="list-style-type: none"> ▶ EVE – Biscay Marine Platform ▶ SEAI_OEDU – Belmullet Test Site 		<ul style="list-style-type: none"> ▶ DTU – National Wind Test Site ▶ QUB – Portaferry Data ▶ DTU – Mobile Offshore Wind Measuring ▶ ECNeth – Database of Measurements on OWEZ ▶ USTUTT – Offshore Nacelle LiDAR ▶ PU – HF Radar ▶ Environmental Monitoring Facility ▶ NTNU – Full-scale wind measurement station ▶ DTU - Database of wind 	<ul style="list-style-type: none"> ▶ FH_IWES – Offshore Field Test Site ▶ WavEC – OWZ Pico ▶ EVE - Mutriku

How to apply for access

- Organised through at least 4 calls for access
- Apply at www.fp7-marinet.eu
- Eligibility
 - Participants must be working in Europe (or country associated to FP7)
 - Facility accessed must be outside Applicant's home country
- Conditions
 - Must produce a publishable report for website

More than just free-of-charge access...

- Organised industry networking
 - User workshops – possible collaboration leading to joint ventures
- Common-test standards
 - To move seamlessly from one facility to the next

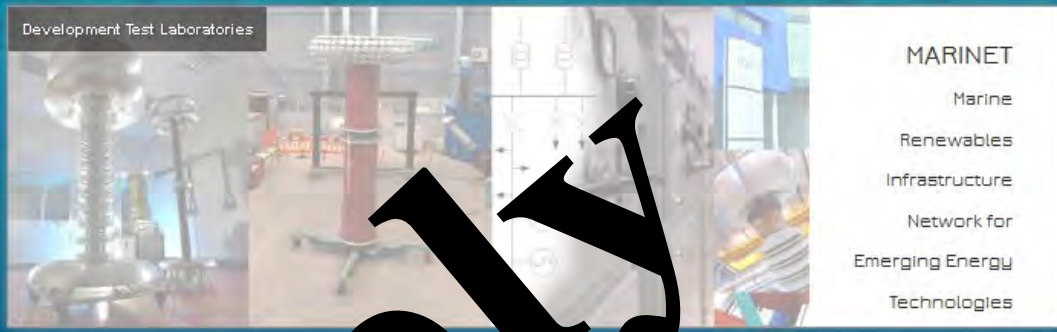


• Coordinated research

Main Project News

- Facility access
 - 1st Call underway
 - >60 applications from 12 countries
 - Expert panel (internal & external) made selections:
~ 50% selected
 - Successful users accessing facilities up to Feb 2013
 - 2nd Call – open July 16th to 30th Sep
 - For access Feb-July 2013
 - 3rd Call to follow





Development Test Laboratories

MARINET

- Marine
- Renewables
- Infrastructure
- Network for
- Emerging Energy
- Technologies

MARINET is an EC-funded network of research centres and organisations that are working together to accelerate the development of marine renewable energy - wave, tidal & offshore-wind - by offering periods of free access to their world-class test facilities, standardising testing, coordinating research, providing training and Industry networking.

FREE-OF-CHARGE ACCESS TO TIDAL AND OFFSHORE-WIND TESTING FACILITIES OPEN TO COMPANIES OF ANY SIZE, RESEARCH GROUPS, ACADEMIC GROUPS ETC.**Call for Applications - Free-of-Charge Transnational Access to Test Facilities - Now Open**

After the first call which granted 29 projects free-of-charge access to marine renewable energy testing facilities, the MARINET consortium has announced that the 2nd call is now open for applications for transnational Access to these 42 world-class test facilities located throughout Europe.

Opportunity is open to any group with one or more individuals from the group leader and majority of group members are based in the EC or a country associated to the EC FP7 programme, i.e. companies or research groups, academic groups etc. Free-of-charge access is available to facilities which are based outside the country where the applicant works.

The deadline for applications is 30th September 2012. Applications will be announced on the 20th of December 2012.

For further information and to apply online, please go to [Access](#).

MARINET Information

Find out more [About](#) MARINET and the opportunities for free facility [Access](#) open to companies, research groups etc. See the [28 MARINET partners](#) and their [42 world-class test facilities](#) which are available for periods of free access.

Updates

Subscribe [here](#) to receive MARINET notifications and announcements by email.



Apply Now!

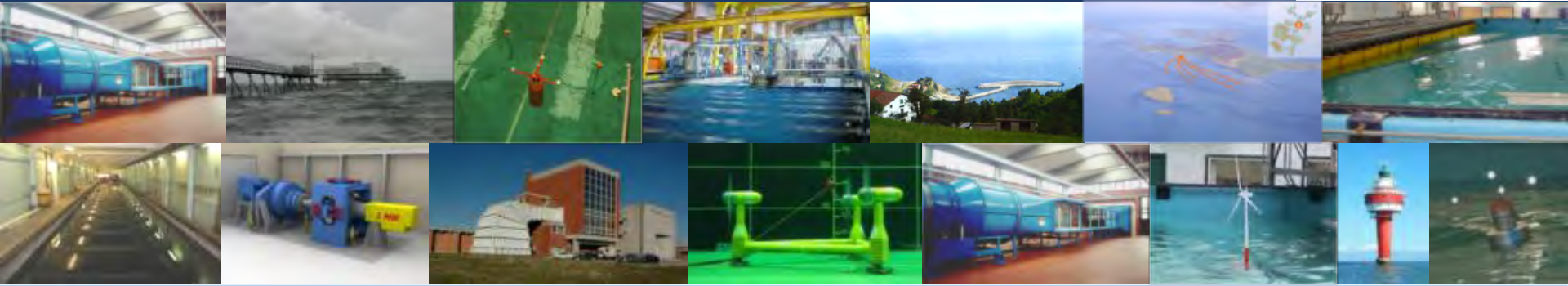
www.fp7-marinet.eu

[Login](#)[Apply](#)

Workshop area for project services and draft applications | [Apply for free-of-charge access to world-class test facilities](#)

NEWS
2012 - 2nd MARINET Call - Now Open!
Apply for free-of-charge access to test facilities - see

Jun 13, 2012 - Next All-Partner Meeting
Ifremer Boulogne-sur-Mer, France.
21-25 October, 2012



MARINET

Coordinator Contact: Marine Renewables Infrastructure Network

Test for Success...

Hydraulics and Maritime Research Centre, University College Cork

Prof. Tony Lewis (HMRC), Project Coordinator

Mark Healy (HMRC), Project Manager

info@fp7-marinet.eu

+353 21 425 0021



Renewable and Fossil Resources: Opportunity for Synergy and Integration

Innocenzo Titone

Managing Director OMC

Let me first of all introduce **OMC** (Offshore Mediterranean Conference) Scrl. The Company was established in 1992 by the Ravenna Chamber of Commerce, the Ravenna Offshore Contractors Association (ROCA) and Assomineraria (Italian Petroleum Industry Association). It organizes a biannual oil&gas conference in Ravenna. In the last edition (March 23-25, 2011) 240 technical papers were submitted and the conference witnessed the attendance of over 1200 delegates.

Following recent and significant changes in the international energy scenario, the Company decided to set up an event to reflect and debate the energy market evolution with respect also to the stringent measures introduced by European Community to combat GHG emissions and the climate change.

As a result of these considerations, **REM** (Renewable Energy Mediterranean Conference) was organized in Ravenna on February 29 and March 1, 2012.

The theme of the Conference was focused on the EU “20-20-20 objective” in order to discuss the binding targets set by the European Community. Compared to other pure renewable events the Conference also involved oil&gas upstream companies in the discussion, given the relevant role they are playing in the energy scenario, the sizeable amount of investments they are undertaking in the renewable sector and the significant role gas is and will be playing in the future as the most environmental friendly fossil fuel.

The Conference aimed at creating a framework for knowledge sharing in the context of renewable energies, emissions cuts and energy efficiency with an important contribution from the projects presented by North African delegations.

The EU targets are a challenge as well as an opportunity for the Energy Companies to contribute to a new energy mix. The discussion highlighted the contribution that all Energy resources can give to reduce emissions, improve efficiency and reach a balanced energy mix.

Today I am pleased to present some highlights of the conference sessions including contributions both from pure renewable companies and from the oil&gas upstream industry, some case histories and interesting ideas to prove the benefit that can derive to the energy industry from a close cooperation between the oil&gas industry and the renewable sector.

For those who are interested in more details, the individual papers can be retrieved from www.remenergy.it

The dynamics of the energy market is heavily influenced by non-OECD countries which are responsible for about 90% of demographic growth, 70% of the economic cycle and 90% of the increase in energy demand (World Energy Outlook 2011 AIE).

China, India and Africa alone will cover 68% of the total energy demand, with China overtaking USA and becoming the first energy consumer by 2035 (ExxonMobil “The Outlook for Energy: A View to 2040”).

Fuelled by economic and demographic growth, energy consumption by 2020 will go up by a 39% (but only 4% in the OECD countries).

In this panorama, fossil resources still maintain a leading role (81% of world demand) thanks to the development of non-conventional resources (shale gas, oil sands, shale oil and new technologies) with a more and more significant contribution of natural gas, gradually replacing coal. Gas is probably destined to play an important role as “enabler” for a high share of renewable energy.

The electricity will grow by 80% with the contribution of renewables (biomass, hydroelectric, solar, wind, biofuels) in strong growth too but covering only 15% of energy needs.

Investments in the development of energy infrastructures in the period 2011-2035 will be 38.000 billion \$ (\$ 2010) out of which petroleum and natural gas account for 20,000 billion \$, mainly allocated in non-OECD countries.

A recent discussion paper *"Oil: The Next Revolution - Upsurge of Oil Production Capacity, What It Means for the World"**, based on a bottom-up analysis of the world wide upstream activity foresees that the net additional production capacity by 2020 could be 17.6 Million of barrel of oil equivalent per day (Mboed), yielding a world oil production capacity of 110.6 Mboed. This is the most significant increase since the 80s. This could lead to a glut of overproduction and a steep dip in oil prices. * *Leonardo Maugeri – Harvard Kennedy School – Belfer Center for Science and International Affairs*

This scenario may entail GHG emission levels not compatible to an average temperature increase of 2 °C. We could expect something between 3.5 and 6 °C increase. Avoiding 1 \$ investment before 2020 will require, in the following years, investing 4.3 \$ to counterbalance GHG emissions increase.

Moving to the Italian contest, the National Action Plan of 2010 assigned to nuclear a coverage of 24% of electricity needs (90 of 375 TWh), which ought now to be developed from renewable and fossil sources.

It can be assumed that renewable sources from an assigned 26% (98 TWh) will now have to develop at least 52 of the 90 TWh of nuclear power, or 40% of the national demand (150 TWh). The remaining 38 TWh could be produced with a more efficient and effective use of fossil fuels.

From the foregoing we may understand how unpredictable is the energy sector, exposed sometime to dramatic changes. In order to be ready to face the future we need research and technological innovation, improved energy efficiency, a new and more efficient legislative and regulatory framework and a strategic redefinition of the whole chain from research to production and distribution.

A combination of the hydrocarbons and renewables technologies can positively contribute to a solid and balanced growth in the energy sector by making use of the know-how and competences of the oil&gas industry in the research, design, construction and installation of hydrocarbon facilities.

To start with, I will briefly mention the feasibility study on carbon capture and storage to reduce emissions from process operations and some applications of the integration of solar technology in oil fields in operation in North Africa. E&P business is a relatively low energy intensive industry, but there are a lot of opportunities.

The technique of capture and storage of CO₂ (CCS) consists of three main stages: CO₂ capture at fossil fired plants, transmission of CO₂ to the site of injection and underground injection at high pressure to attain a supercritical state, similar to gas (to penetrate rapidly through the porous geological strata) and similar to liquid in terms of density and stockability.

The project is part of a Strategic Cooperation Agreement between Eni and Enel to realize the first integrated pilot project in Italy, combining Enel's CO₂ post-combustion capture pilot plant at Brindisi coal fired power station and Eni's pilot CO₂ injection project in an exhausted gas field at Cortemaggiore. The know-how deriving from this experience will be used for feasibility studies on large integrated projects to inject CO₂ into hydrocarbon fields or saline aquifers, as well as to boost the productivity via EOR (Enhanced Oil Recovery) and EGR (Enhanced Gas Recovery).

The North Africa belt is characterized by high intensity direct solar radiation. The solar Atlas shows that the average direct normal solar radiation is 2000 – 3200 kWh/m²/year. That favours the installation of an Integrated Solar Combined Cycle (ISCC), a combination of two proven technologies in a single plant: combined cycle gas fired turbine technology (CCGT) and the parabolic trough solar concentrators (CSP Concentrated Solar Power).

Examples of application were brought by Sitep of Tunisia in El Borma, NREA of Egypt in Kuramayat and NEAL of Algeria in Hassi Rimal showing a substantial saving of fuel and reduction in GHG emission.

An example of the synergy between the two industries is the research study of Eni that has developed an innovative Power Management System (PMS) able to couple and manage the electric power production by a common diesel generator and a photovoltaic plant (PV), in order to overcome the need of energy storage. The system allows sharing power production between the PV plant and the diesel generator, balancing the continuous alternate current from the fossil fuel generator with the discontinuous direct current of the photovoltaic plant. This new configuration guarantees power reliability with reduced diesel oil consumption (close to 30%) and a decrease of GHG emissions

But is the offshore wind energy one of the most interesting and perspective industries both from the point of view of technology and business opportunity.

In Europe, in 2011, nine offshore plants for 235 turbines and 866 MW power installed were completed and UK and Germany have already started new projects worth 2.3 GW within the next 5 years. In Italy exists a significant potential of 10 GW in 1,600 km² of sea, but all projects in recent years have been rejected or stranded in the authorization phase.

However an assessment of the technological development status shows that R&D in this area requires making technologies more reliable and profitable.

The highly developed infrastructure and technology of the oil&gas industry can contribute to the offshore wind industry with interesting solutions. I will briefly describe some projects and initiatives, currently under development that will help in overcoming some of the criticalities associated to the offshore wind sector.

The design of wind towers in deep-water environments is a great challenge because of the combined effects of environmental loads and the loads from the turbine itself. The Hywind concept, developed by Statoil, is based on the use of advanced tools, developed in house, for detailed analyses of wave, wind and structural response combining in a new setting the proprietary technologies, result of their extensive offshore oil&gas experience. Hywind opens up the possibility for capturing wind energy in deep-water environments.

Hywind Demo is in operation since 2009 with a 2.3 MW wind turbine installed on a floating steel cylinder (buoy) filled with a ballast extending 100 metres beneath the surface in a water depth of approximately 220 metres and attached to the seabed by a three-point mooring spread, 10 km off the western coast of Norway. No negative effects were observed as a consequence of being installed on a floating foundation. The average capacity factor during the first 11 months in 2011 exceeds 49%. The demonstration has given proof to the technology, and based on the experiences gained, the concept as well as the installation methods are being optimised.

One of the major criticality of the renewable resources is the intermittency. As a result we might have available electricity from a wind farm when there is no demand from the market and vice versa.

An example of the statistical distribution of the instantaneous power over one year shows that the average full power is reached for 900h, 50% of the time the power is less than 250MW and there is no power during 1000h. The year average capacity factor is 44% of the rated capacity. Similarly the seasonal capacity factors are: 57% in winter and 29% in summer.

To overcome the problem of intermittency several potential energy storage techniques can be envisaged: fly-wheels, capacitors, batteries, pumped hydro storage, compressed air storage. Each of them has its own limitations: the first three offer a small storage capacity whilst for the last two there are very few available suitable sites.

There is need therefore of an innovative approach to offer a TWh range of energy storage capacity.

To achieve that a radical re-design of the entire cycle production-transportation-distribution system will be required. It is not a simple task. It might require decades to create the legislative, normative and technical framework basis and to build-up the new infrastructure.

The oil&gas industry, with its highly developed infrastructure and technology, can contribute with interesting solutions to stabilize the intermittency. Some initiatives are currently under development.

The Power to Gas technologies presented by Rosetti envisage, at low market demand, the utilization of the electric energy produced in a wind farm for the production of hydrogen through electrolysis or electric decarbonisation or the production of Synthetic Natural Gas (SNG). The renewable electric energy can in this way stored as hydrogen or SNG. To that purpose can be utilized a dedicated storage (capacity of GWh) or utilizing the natural gas grid up to 10% (storage capacity of TWh).

A closer integration of the electric and the natural gas grid could become a credible option for mitigating the problems of intermittency of renewable energy.

The sea is a demanding place. Design and installation of offshore wind turbines or other marine energy equipment require the skills of knowledgeable specialists. The experience gathered along the development of the offshore oil&gas industry can be utilized to materialize sound renewable energy projects.

Examples are given of the various factors which must be taken into account when building offshore systems and how beneficial the experience can be at sea.

In Italy, in recent years, the authorization for all the projects relevant to the installation of wind farm offshore have been rejected notwithstanding the significant potential of 10 GW in 1,600 km² of sea.

In the European project POWERED several Italian and international partners are joining experience and knowledge in order to:

- define a clear and quick authorization procedure for public and private investors involved in Adriatic offshore wind farm realizations;
- define a shared normative framework in the form of international guidelines taking into account all the environmental problems in order to preserve marine nature and biodiversity and the exiting economic activities (i.e. fishing) with respect to offshore wind farm installations;
- to verify the real energy potential with respect to the sea floor depth over the entire Adriatic basin by means of a numerical procedure and by an experimental meteorological network and produce the relevant maps.

The numerical procedure involves the use of two codes (MM5 and AWRF), in order to estimate the wind history, over the entire Adriatic basin, for the period 2002-2012. The MM5 code is used for the back-casting analysis in order to realize wind energy maps having a horizontal spatial resolution of 1km x 1km and a time interval of 4 minutes; this very fine mesh resolution is essential to take in account the fundamental interactions between coast lines and open sea. In some cases, as example for the Croatian islands or for very complex orography, it is necessary to increase the mesh resolution up to some hundred meters; this research group solved this problem by modifying the MM5 terrain pre-processor so to collect and use high resolution digital terrain models (SRTM database).

The met mast network includes onshore towers, at least one for each project partner, and one offshore tower; the experimental data, collected by the network, will be used to tune and verify the numerical codes and also to input local data for a forecasting procedure that will be implemented before the project end.

On the European Union Maritime Spatial Planning: are EU oceans and seas shrinking?

Michele FIORINI

Fellow

The Institution of Engineering and Technology (IET) - ITALY Network

e-Mail: mfiorini@theiet.org

Abstract — As stated in the invitation to the international conference “The case for Maritime Spatial Planning: efficient resource management for sustainable growth” hosted by Ms Maria Damanaki, European Commissioner for maritime affairs and fisheries, the Maritime Spatial Planning (MSP) is crucial for creating an environment in which the maritime economy can grow in harmony with the surrounding ecosystem. Transparency, stability, predictability and reduced transaction costs are the factors that encourage and accelerate investments – and are among the benefits that MSP can bring. The author present the risks and the challenges being faced in the maritime domain with examples of possible use of the MSP as a tool and process for Members States to organize and optimize their sea space according to national objectives, highlighting trends and the progress made from the EU Blue book dated October 2007.

I. Introduction

On March 2012 Ms Maria Damanaki, European Commissioner for maritime affairs and fisheries starts her keynote speech [1] at the European Commission in Brussels with the following sentences: “Today the oceans and seas around the European Union are shrinking. They are not becoming smaller, but more and more users are racing to develop their activities there, and to compete with those who’re already there”. The MSP as promoted by the EU integrated maritime policy, is crucial for creating an environment in which the maritime economy can grow in harmony with the surrounding ecosystem. Transparency, stability, predictability and reduced transaction costs are the factors that encourage and accelerate investments. And the potential growth of “blue economy” could be amazing in the near future.

Maritime Transport grows at an average rate of over 8.5 percent every year – consider that over 90% of world’s trade is carried by sea (IMO source, 2009) for a total of 23 million tonnes of cargo and 55,000 cruise passengers travelling by ship every day. Cruise alone has tripled its size between 1999 and 2009 carrying now over 6,000 passengers on ultra-large cruise ships and neither the anniversary of the *Titanic*’s tragedy (14th April 1912) nor the *Costa Concordia* accident (13th January 2012) seems to slow down this trend.

Renewable wind energy or aquaculture are only at the beginning. Offshore wind energy is expected to grow from 4 GW capacity this year to 150 GW in 2030 – this is 4000 percent! And we are still understanding the potential of tidal energy, deep sea mining, maritime tourism and dredging. Dredging companies have increased their turnover by 150 percent in less than a decade.

Ms Damanaki continue saying “One thing that all these activities have in common is where they take place: They all use maritime space”, [1].



Figure 1. Pictorial manifesto of the International Conference “The case for Maritime Spatial Planning: efficient resource management for sustainable growth” hosted by EU Commissioner Maria Damanaki, Brussels, March 2012.

It is not a case that even the European Union decides to formalize, from 2008, the “European Maritime Day”, May 20th each year, to celebrate the potential of Europe’s seas. It has been established by a joint tripartite declaration signed by the three presidents of the European Parliament, the Council of the European Union and the European Commission recalling that Europe is a maritime continent with almost 70.000 km coastline with 22 of 27 member States with direct access to the sea. Recalling that over two thirds of the Union’s boundaries are maritime and that marine space under the jurisdiction of its Member States are larger than their terrestrial territory, [2].

II. Maritime Transport

Global shipping, maritime safety and security and the movement of goods by sea have seen substantial changes during recent decades in an increasingly interconnected global economy, with the consequence that the traditional techniques are often no longer sufficient to satisfy the needs of the maritime stakeholders. As reported in the introduction session the great majority of world’s trade is carried by sea and in Europe, EU Parliament Member Ms Gesine Meissner, stated that it is possible to reach 40% of EU Gross Domestic Product (GDP) generated by maritime industries and services excluding raw materials such as oil, gas or fish.

As well known, according to the Safety Of Life At Sea (SOLAS) convention - hold for the first time in London in 1914 after the *Titanic*’s tragedy and then in 1929, 1948, 1960 and 1974 – modern large vessels have to be equipped with the Automatic Identification System (AIS) as follows:

- all ships of 300 gross tonnage and upwards engaged on international voyages (since 1 July 2004);
- cargo ships of 500 gross tonnage and upwards not engaged on international voyages (since 1 July 2008);
- passenger ships irrespective of size (since 1 July 2003).



Figure 2. Container routes in the Baltic Sea, [3].



Figure 3. Baltic Sea, one week recording AIS data, 2008. Source: HELCON AIS.



Figure 4. Satellite AIS worldwide coverage, courtesy exactEarth, [4].

Observing the distribution of real-time vessels worldwide comes quite obvious the idea of creating Sea’s Motorways based on the matter of fact that the great majority of global shipping follows almost fixed path. This is due mainly to safety and efficiency and are on the basis of various projects such as the Mona Lisa under develop by the Swedish Maritime Administration with a number of partners, co-financed by the European Union according to the EU Strategy for the Baltic Sea Region, [8].

Traffic density is unfortunately synonymous of emissions and pollutions, 70 percent of the vessel emissions are released with 400 km from the shore line. With reference to the Baltic, at any time around 2000 ships are operating in the Baltic Sea emitting approximately 400 kt NO_x/year where the largest contributing category is passenger ships resulting 20% of NO_x emitted by 6% of the fleet, [5].

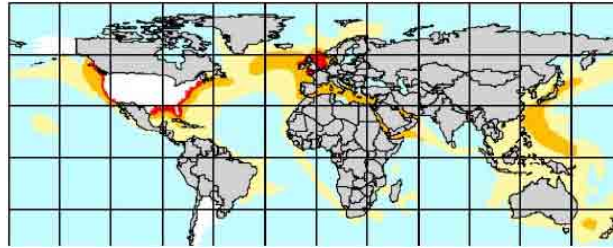


Figure 5. Vessel emissions: sky-blue, low; yellow, medium; orange, high; red, extra high, [6].

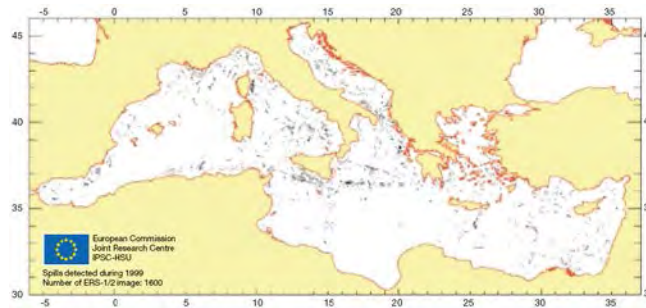


Figure 6. Fingerprints of illicit vessel discharges detected on ERS-1 and ERS-2 SAR images during 1999 in the Mediterranean Sea, [7].

Piracy also – fortunately out of EU – continue to threaten shipping having an economic impact estimated to be around \$ 7 bn in 2011. Two main initiatives related to maritime traffic are reported hereafter. They are complementary each other and aims to harmonize the further technology developments in the maritime context.

A. e-Navigation

The International Maritime Organization (IMO) adopted the following definition of e-Navigation: “e-Navigation is the harmonized collection, integration, exchange, presentation and analysis of maritime information onboard and ashore by electronic means to enhance berth to berth navigation and related services, for safety and security at sea and protection of the marine environment”, [9], [10].

Within the e-Navigation definition, IMO recall that “the overall goal is to improve safety of navigation and to reduce errors. However, if current technological advances continue without proper coordination there is a risk that the future development of marine navigation systems will be hampered through a lack of standardization on board and ashore, incompatibility between vessels and an increased and unnecessary level of complexity” (MSC85-report, Annexes 20 and 21).

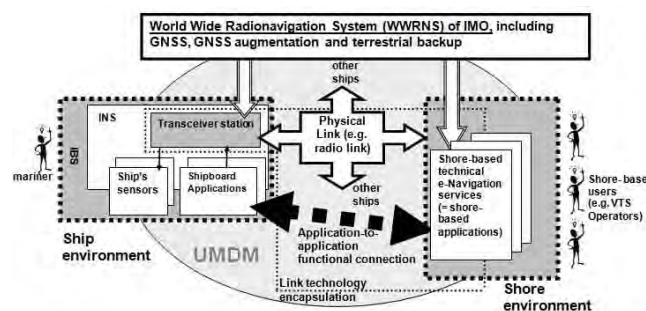


Figure 7. e-Navigation architecture Source: IALA e-NAV140, [11].

B. e-Maritime

The European Union (EU) e-Maritime has been defined as “the EU initiative aims to foster the use of advanced information technologies for working and doing business in the maritime transport sector”. On the 21st January 2009, the Commission adopted the EU Maritime Transport Strategy 2018, COM(2009) 8; and the establishment of the European Maritime Space without barriers, COM(2009) 11. In addition COM(2005) 589 amending Directive 2002/59/EC establishing a Community vessel traffic monitoring and information system of the 3rd maritime safety package was adopted by the European Parliament - 11th March 2009, [12].

The European Commission organised a public online consultation on the EU e-Maritime initiative. The consultation lasted two months and finished on Sunday 27 June 2010. The aim of the consultation was to gather stakeholders' opinions on e-Maritime initiative in order to assess the possible actions that could help meet the e-Maritime objectives. As a result, consensus on EU e-Maritime has been gained and there is widespread support and agreement that maritime reporting data should be submitted electronically and only once. Therefore the technical standardization process and the implementation of the *National Single Window* emerge as measures receiving the highest support. There was also a mention that the level of investment in Europe is low compared to that in Asia. There is a general recognition that the lack of common data structure, established procedures and lack of data sharing and interoperability causes unnecessary reporting duplications (such as Administrative and Port applications), wastes resources and increases the probability of errors, [13]. In short a key element of the consultation has been that the maritime reporting data should be submitted electronically and only once, “Single Window” concept. A ‘Single Window’ can be described as “a system that allows traders to lodge information with a single body to fulfil all import- or export-related regulatory requirements” (UN/CEFACT International Trade Procedure Working Group, ITPWG).

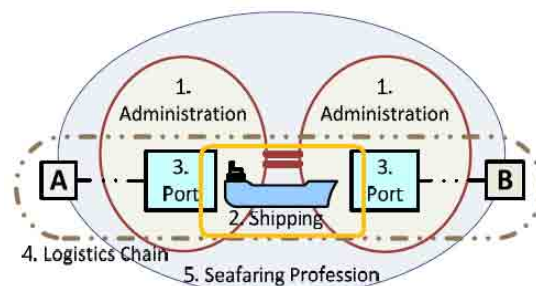


Figure 8. e-Navigation vs. e-Maritime. Source: EU Commission, Directorate for Mobility and Transport, Nov. 2010.

The place of IMO e-Navigation into the EU e-Maritime initiative is highlighted with the yellow box: the scope of e-NAV covers berth-to-berth voyage.

III. Renewable Energy

A. Wind energy

The world's first offshore wind turbine was commissioned in 1990 in Sweden. It was built as a test plant "in order to examine the influence of birds, fish and fishing, shipping, public opinion, maintenance and the effects on foundations from wind and ice". It lies about 250 m out to sea, in 6m of water, from the fishing village of Nordersund southern Sweden. It consists of a single 3-bladed Danish wind turbine with a hub height of 37.5m and rated output of 220 kW.

One year later, 1991, the first commercial offshore wind-farm was commissioned in Denmark. It is in the Baltic Sea, North-West of the island of Lolland, near the village of Vindeby, in Denmark. It was built by SEAS, has a capacity of 4.95 MW and consists of 11 Bonus 450 kW stall controlled wind turbines in two parallel rows.

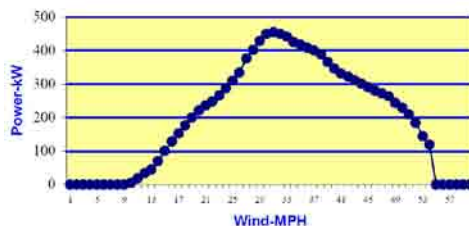


Figure 9. Bonus 450 kW Power Curve. Source: Refurbished Specs.

Nowadays the European offshore wind energy market in 2011 has been composed by 53 wind farm installed in 10 countries for 3.8 GW offshore wind capacity using around 2,400 km² of sea space. It's worth € 2.4bn annual investments with more than half, 59% to be exactly, of the installed capacity have been in the North Sea.

Forecast is 40 GW by 2020 and 150 GW by 2030. This allows realizing respectively 4% and 14% of total electricity demanded in EU in 2020 and 2030. Sea space occupied in 2020 would be 25,000 km².

B. Tidal energy

There are two quite distinct categories of tidal resource: tidal stream and tidal range. The tidal stream resource is the kinetic energy contained in fast-flowing tidal currents, which are generally found in constrained channels. The tidal range resource refers to the gravitational potential energy that can be found in estuarine areas that exhibit a large difference in water height (their ‘tidal range’) between high and low tides.

The technology used to exploit each of these resources is quite different. Tidal stream devices rely on capturing some of the energy contained in the currents passing by them, whereas tidal range devices seek to impound large volumes of water at high tide, and then release the water through turbines at low tide. Put another way, tidal stream devices make use of the kinetic energy of tidal currents, whereas tidal range devices rely on the gravitational potential energy created when water at high tide is kept behind an artificial impoundment.

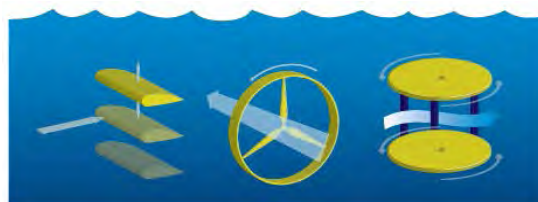


Figure 10. Pictorial representation of tidal stream devices.

Efficiency on a tidal device is remarkable, just to consider the following simple equation to calculate the output power (P):

$$P_{\max} = 0.5 \cdot R \cdot A \cdot V^3 \quad (1)$$

Where A is the swept out area of the propeller [m^2], R is the density of the fluid [seawater is 1024 kg/m^3], V is the stream velocity. For a 20 m propeller, a sea device in a 3.5 m/s current can generate 2 MW. On the contrary, a 2 MW wind generator would require a wind speed of 360 km/h!

iv. Maritime Spatial Planning

Before to approach the MSP it is convenient to briefly recall the following considerations. More than 70% of Earth's surface is covered by water. The marine and maritime economic sectors forming the EU's 'blue economy' represent roughly 5.6 million jobs and account for a Gross Value Added (GVA) of €495 billion [14]. The European Commission is seeking to identify and eventually counter bottlenecks and barriers to sustainable growth and to devise the most appropriate policy responses.

The Blue growth study started from the perspective of six global maritime functions, Figure 11. , each of them with a broader socio-economic value that could be rephrased as follows: maritime trade and transport; food, nutrition and health; energy and raw materials; living, working and leisure in coastal regions and at sea; coastal protection, and nature development; and maritime security, [16].

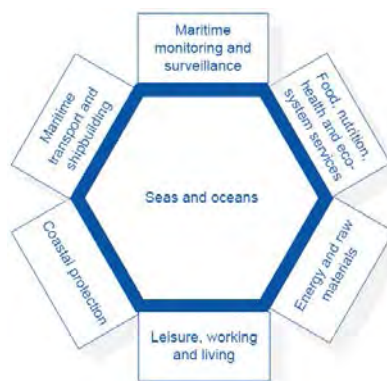


Figure 11. Six initial global maritime functions, [16].

Those above functions are then subdivided in sub-functions and work-packages and the study is still undergoing. The list of sectors relevant from a maritime perspective is sheer endless and recently various Europe 2020 Flagship initiatives (see for instance the EC's Flagship on 'Integrated New Industrial Policy in the Globalisation era', COM 2010-614) grow attention on value chains with assessment of functions across sectors and world-wide, pointing out synergies and risks. These chains have to be considered on to the MSP.

Largely owing to the difficult of obtaining biological data with a good spatial coverage maps for marine environments are almost not applicable as the information available are generally restricted to a few points in space that in most cases cover only a tiny fraction of the area of interest. As a result a prerequisite for an MSP is an in-deep analysis and classification of the surrounding environment.

Maritime spatial planning is about planning and regulating all human uses of the sea, while protecting marine ecosystems. It focuses on marine waters under national jurisdiction and is concerned only with planning activities at sea. It does not cover management of coastal zones or spatial planning of sea-land interface. MSP remains a prerogative of individual EU countries. However, plans for shared seas should be compatible, to avoid conflicts and support cross-border cooperation and investments.

Common principles agreed at EU level can ensure that national, regional and local maritime spatial plans are coherent. MSP aims to balance frequently competing sector-based interests in order to use marine space resources efficiently and sustainably, and make possible to take decisions based on in-depth knowledge of the sea. This will encourage economic development and attract investors that should have sound data on the area of interest and legal certainty, [15].

A. *The Baltic experience: BaltSeaPlan*

The Baltic Sea is a brackish shallow sea of approximately 377,000 km², as reported in [16].

It is connected to the Atlantic Ocean only via the small entrances of the Sound and the Belt Sea. Water exchange is extremely limited and water can remain in the Baltic for up to 30 years prior to exchange, resulting in a highly eutrophic marine environment with substantial areas of oxygen depletion throughout.

The depth average water of 55 m.



Figure 12. *European sea basin and catchments. Source: DGMare.*

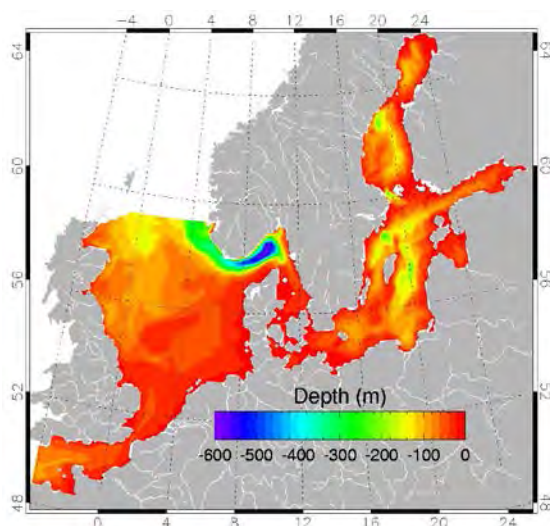


Figure 13. *Baltic depth (bathymetry), [17].*

The most crucial feature of the Baltic Sea is that the salinity is low, making the Baltic the world's second largest brackish-water basin after the Black Sea. The salinity decreases in eastward and northward directions into the Baltic. The low salinity is of tremendous importance to life in the Baltic and is the key to understanding and managing the sensitive marine ecosystem. Only a few marine animals and plants are able to tolerate the low salinity, rendering them irreplaceable in the Baltic ecosystem. A system made up of so few species is not very stable, and is very susceptible to such pressures as fishing, habitat destruction, and pollution.

Fourteen partners from seven countries around Baltic Sea are working together from 2009 on the BaltSeaPlan programme (www.baltseaplan.eu) to develop, introduce and implement Maritime Spatial Planning (MSP) throughout the Baltic sea region in a coherent manner with the challenge to create a joint understanding, to learn together from pilot initiatives and to base new regulations on transnational and coherent principles.

Pilot project involves the following areas as reported in Figure 14.

- Pomeranian Bight (DE/PL/SE/DK)
- Western Gulf of Gdansk (PL)
- Middle Bank (PL/SE)
- Western Baltic T-Route (DK)
- Pärnu Bay (EE)
- Hiiuma & Saaremaa Islands (EE)
- Western Coast of Latvia (LV)

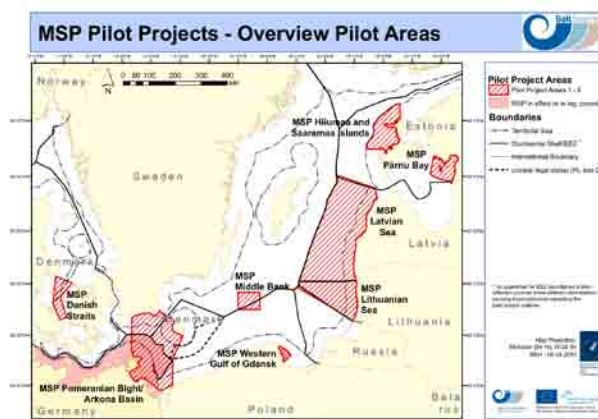


Figure 14. Selected areas on the Baltic Sea for MSP pilot project. Source: BaltSeaPlan website.

For a sack of brevity let consider one region only. The approach should be the same in all regions even if local consideration and result may vary from case-to-case. The choice was on Pomeranian Bight because that area involves four countries: Germany, Poland, Sweden and Denmark.

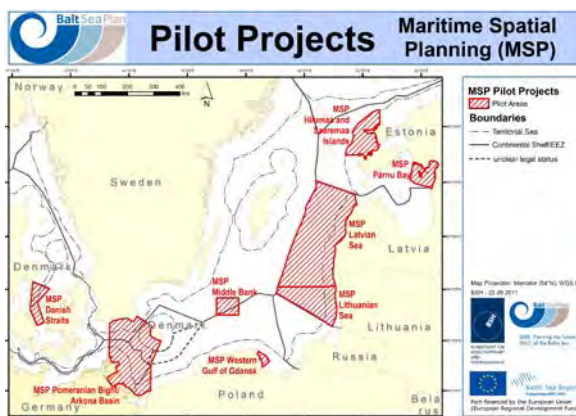


Figure 15. Project area of the Pomeranian Bight, [19].

It was one of the two transnational pilot project within BaltSeaPlan involving a number of countries with respective planning systems, authorities and legislation. Stakeholders were involved by means of a joint questionnaire and physical meetings and analysis of planning context, spatial regulations and socio-economic environment were taken into account. Demography in recent years was also considered: German, Polish and Danish population decrease in the project area while Sweden population increase resulting in a higher population density in the Malmö area compared to DE/PL/DK.

An very important land-sea relation in that area is the maritime transport and traffic on both East-West direction and North-South link via ferry lines and ports. Tourism is strong and economically very significant on various forms from coastal and island tourism to water sports and leisure sailing. On the contrary, fishery and fish processing, as well as agriculture and food processing industries, declining.

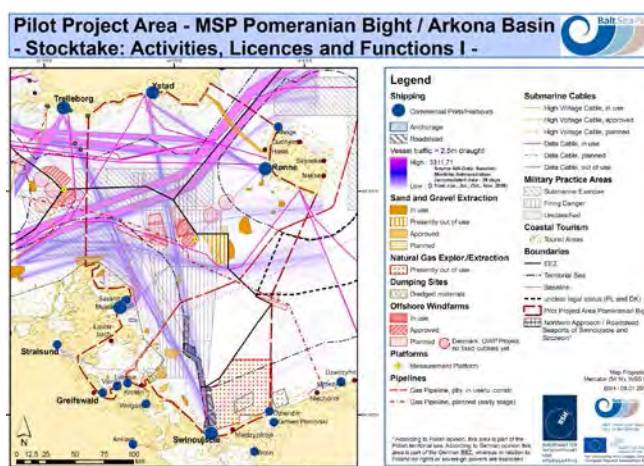


Figure 16. Selected human activities such as shipping, offshore wind energy, sand and gravel extraction, submarine cables and pipeline on the Pomeranian Bight area, [19].

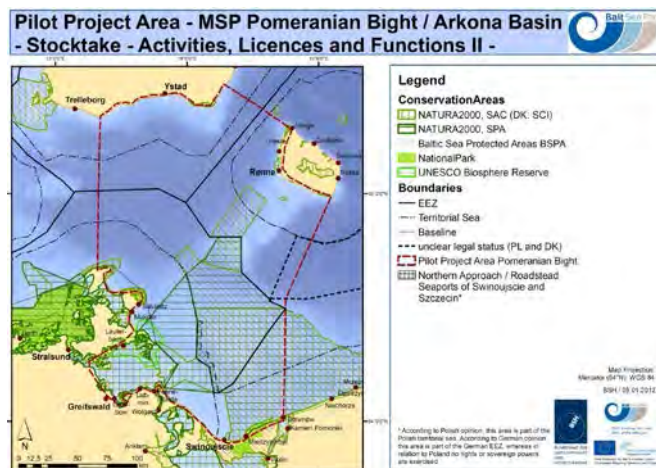


Figure 17. Relevant nature constraints such as nature conservation areas, bird migration, abundance of sea birds or mammals and physical conditions like bathymetry and wind conditions in the Pomeranian Bight area, [19].

The analysis of data collected is not concluded but an important conclusion could already be pointed out as follows. There are a lot of conflicting activities and interests almost in every area, Shipping conflict with Offshore Wind-Energy that in some case conflict itself with Nature Conservation. Nature Conservation conflict with Fishery and with Tourism or Leisure Sailing as well. For a visual representation of main conflicts so far highlighted in the area of interest please refer to Figure 18.

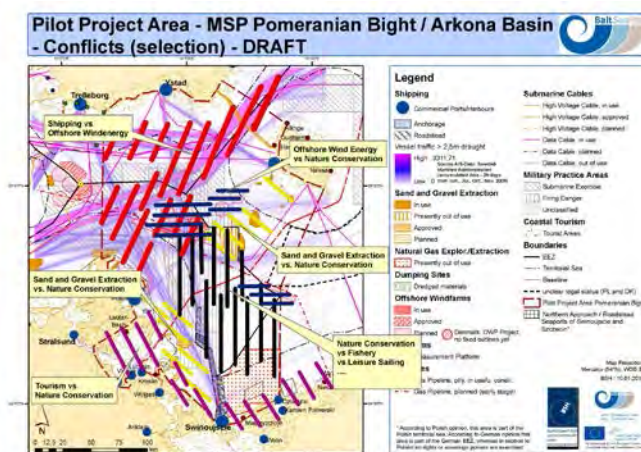


Figure 18. Main conflicts in the Pomeranian Bight area, [19].

It is clear from Figure 18. that only working towards minimization and mitigation of conflicts between human activities and interests and between human uses and natural environment that could be possible to reach a sustainably future.

Similar approach is now going to be transferred to the rest of EU's seas including the Mediterranean, [18].

CONCLUSION

Maritime Spatial Planning is a valuable tentative to organise, harmonise, regulate and standardise a fast growing business area that affect a fundamental resource of our World, the Maritime Space. For most of us MSP may be seen as an abstract concept well far away from our digital life however this could not be further from the true. Maritime resources are limited and an harmonised and sustainable use of them is imperative. This could be achieved only by means of coordinate policies, agreements and regulations that cross geographic borders and political boundaries involving all maritime domain stakeholders in an increasingly interconnected global economy.

It is challenging and maybe ambitious too but for the old continent (worldwide an increasing dominance of Asia will probably be unavoidable) the EU should drive this process with an open and innovative political approach inviting all Community Members, at transnational level, to consider for all their maritime and coastal activities and the land-sea interaction their global impact. And of course this is only the beginning as the most difficult part should be to convince and to support countries turning the MSP into reality.

To conclude in one sentence: Maritime Spatial Planning cannot be learned from books, it must be practiced !

ACKNOWLEDGMENT

Useful discussions with Dr Gaetano Gaudiosi, President OWEMES Association, Rome, Italy; Ms Anne-Bénédicte Genachte, Regulatory Affairs Advisor Offshore Wind Power, EWEA, Brussels and Ms Joanna Łukaszewska, Environmental Analysis Consultant, Gdynia, Poland, are grateful acknowledged.



Michele Fiorini, *PhD, CEng, FIET*, is principal engineer at SELEX - Sistemi Integrati, a Finmeccanica company, in Rome, Italy where he is currently Technical Head for the “*Zautomatyzowanego Systemu Radarowego Nadzoru (ZSRN) polskich obszarów morskich / Automatic National System of Radar Control (ZSRN) for Maritime Areas of Poland*”. Work which has taken him often to Gdańsk, Poland, in the past few months. He is also as a member of the architecture technical working group (WG5) e-Navigation committee at the International Association of marine aids to navigation and Lighthouse Authorities (IALA), Paris and has served in London on different committees and boards of the IEE and IET from 2003 to 2009 including Council and Qualification Board where he was the first non-UK member elected ever. He is now Chairman of the IET Italy Network.

REFERENCES

- [1] M. Damanaki, “Maritime spatial planning: the right answer to secure and support Blue growth for the European Union” EU International Conference *The case for Maritime Spatial Planning: efficient resource management for sustainable growth*, Brussels, speech 12/224, pp. 1–3, 26 March 2012.
- [2] European Commission (EU), European Maritime Day website, http://ec.europa.eu/maritimeaffairs/maritimeday/about/background_en.htm
- [3] J. Anselmo, white paper 2011 – TENT & MoS 2012 and beyond, Proc. Smart Cities Need Intelligent Ports, European Parliament Seminar, February 2012.
- [4] R. Tremlett, “Satellite based AIS”, Proc. IALA Workshop on Global Sharing of Maritime Data, IALA HQ, St. Germain en Laye, France, 12-16 September 2011.
- [5] K. Andersson, “Towards cleaner shipping” available online at www.cleanshippingproject.se
- [6] S. Sköld, “Clean Shipping Project” available online at www.cleanshippingproject.se
- [7] P. Pavlakis, D. Tarchi, A. J. Sieber, G. Ferraro, G. Vincent, “On the monitoring of illicit vessel discharges. A reconnaissance study in the Mediterranean Sea”. European Commission, Ispra, Italy, 2001.
- [8] U. Svedberg, “MONA LISA, Motorways & Electronic Navigation by Intelligence at Sea”, Proc. IALA Workshop on Global Sharing of Maritime Data, IALA HQ, St. Germain en Laye, France, 12-16 September 2011.
- [9] M. Fiorini, “Verso e-Navigation”, Rivista AEIT (seguito de L’Elettrotecnica, edita dal 1914), Federazione Italiana di Elettrotecnica, Elettronica, Automazione, Informatica e Telecomunicazioni, No. 9, September 2011, pp. 48-53 (*in Italian*).
- [10] M. Fiorini, “e-Navigation: a Systems Engineering Approach”, Proc. MAST 2010, 5th Maritime Systems and Technology conference, palazzo dei congressi, Rome, Italy, 9-11 November 2010
- [11] e-NAV 140 “The e-Navigation Architecture – the initial Shore-based Perspective” Ed.1.0, IALA Recommendation, December 2009.
- [12] European Commission, Mobility & Transport website, http://ec.europa.eu/transport/maritime/index_en.htm
- [13] European Commission, Directorate General for Mobility and Transport, “Summary report of the contributions received to the e-Maritime public online consultation” available online at http://ec.europa.eu/transport/maritime/consultations/doc/2010_06_27_emaritime_summary_report.pdf
- [14] ECORYS, Working Document, Blue Growth: Scenarios and drivers for Sustainable Growth from the Oceans, Seas and Coasts, p. 9, 22 December 2011.
- [15] European Commission, Maritime spatial planning website, http://ec.europa.eu/maritimeaffairs/policy/maritime_spatial_planning/index_en.htm
- [16] European Commission, DG MARE, Third Interim Report of the on-going Blue Growth study “Scenarios and Drivers for Sustainable Growth from the Oceans, Seas and Coasts”, Rotterdam/Brussels, 13 March 2012.
- [17] E. Buch, J. She: Operational forecasting at the Danish Meteorological Institute. - Environmental Research, Engineering and Management, 3(33): 5 - 11, 2005.
- [18] European Commission, Directorate-General for Maritime Affairs and Fisheries, framework contract FISH/2007/04, “Exploring the potential of Maritime Spatial Planning in the Mediterranean Sea” final report, February 2011.
- [19] B. Käppeler, “MSP in transboundary areas – the case of Pomeranian Bight (DE, PL, SE, DK)”, conference proceedings on Advancing Maritime Spatial Planning: results from the BaltSeaPlan project and beyond, Berlin, 12th January 2012.

Published by ENEA
Relations Central Unit, Communication Service

Lungotevere Thaon di Revel, 76 – 00196 Rome
www.enea.it

Editorial review and digital version: Giuliano Ghisu
Cover design: Cristina Lanari

February 2013



ISBN 978-88-8286-283-1